

# **Evolution of an Artificial Allylic Alkylase based on the Biotin-Streptavidin Technology**

**Inauguraldissertation**

zur

Erlangung der Würde eines Doktors der Philosophie

vorgelegt der

Philosophisch-Naturwissenschaftlichen Fakultät

der Universität Basel

von

**Fabian René Schwizer**

aus Nesslau-Ennetbühl SG, Schweiz

Basel, 2018

Originaldokument gespeichert auf dem Dokumentenserver der Universität Basel

[edoc.unibas.ch](https://edoc.unibas.ch)

Genehmigt von der Philosophisch-Naturwissenschaftlichen Fakultät  
auf Antrag von

Prof. Dr. Thomas R. Ward

Prof. Dr. Andreas Pfaltz

Basel, den 12.12.2017

Prof. Dr. Martin Spiess  
Dekan

# Acknowledgements

A special thanks goes to my supervisor Prof. Dr. Thomas R. Ward for hosting me in his group for several years and giving me the opportunity to conduct exciting studies on the design and evolution of artificial metalloenzymes.

I would like to thank Prof. Dr. Andreas Pfaltz for his commitment of being the co-examiner.

A thanks goes to Prof. Dr. Sven Panke for being the external expert and to Prof. Dr. Cornelia G. Palivan for being the chairman of my PhD defense.

A big thank you goes to Dr. Tillmann Heinisch. Thank you very much for your help and the nice team-work on the *in vivo* catalysis project. Thank you for your great efforts and the proof-read of this manuscript.

I would like to thank all the people who have actively contributed to this thesis: Dr. Tillmann Heinisch, MSc Philipp Rottmann, Dr. Tsvetan Kardashliev, Dr. Christine Tinberg, MSc Eleonore Schmidt, Dipl.-Biol. Juliane Klehr, BSc Brett Garabedian, Dr. Vincent Lebrun and MSc Maxime Barnet.

I would like to thank PD Dr. Daniel Häussinger (NMR analysis), Dr. Heinz Nadig (HRMS analysis), the Werkstatt-team as well as Esther Stalder, Isa Worni and Beatrice Erismann (secretary office) for their precious support.

I would like to thank all actual and former members of the Ward group and the Creus group (Alexandria, Boris, Coentin, Fadri, Isabel, Jaicy, Jingming, Joan, Johannes, Jonas, Juliane, Martina, Miriam, Roxanne, Ryan, Sascha, Shuke, Tillmann, Valentin, Valerio, Yasunori, Yi, Yoann, Esther, Anamitra, Christian, Christian, Eleonore, Emeline, Ewa, Hendrik, Maxime, Michela, Raphael, Vincent, Anna, Aping, Charlotte, Fabien, Elisa, Gaetano, Hermeto, Julian, Livia, Marc, Marc, Mark, Maurus, Narasimha, Noah, Nobutaka, Praneeth, Seraina, Stefan, Tommaso, Victor, Yvonne). I really enjoyed the time we spent together.

Zum Schluss möchte ich meiner Familie und meinen Freunden danken für die tolle Unterstützung, die ich über all die Jahre hinweg erfahren durfte. Vielen lieben Dank.

# Summary

The PhD thesis presented here summarizes the work and the scientific effort done in the research group of Prof. Dr. Ward at the University of Basel during the years 2013 – 2017. The Ward group has a long-term knowledge in the design and evolution of artificial metalloenzymes capable of catalyzing reactions including transfer hydrogenation, ring-closing metathesis, C-H activation, Suzuki-coupling and many more. Artificial metalloenzymes are formed by the incorporation of a catalytically active transition-metal complex into a host protein. This allows combining the advantageous features of both homogeneous catalysis and enzyme catalysis. The protein forms a defined reaction environment (i.e. a second coordination sphere) around the metal cofactor. Thus, artificial metalloenzymes can be evolved by chemical modification of the metal cofactor or by genetic engineering of the host protein. In the Ward group often the biotin-streptavidin technology is applied to generate artificial metalloenzymes. This system relies on the ultra-high affinity of the protein streptavidin for the small molecule biotin. Attachment of a biotin-anchor to a transition-metal complex ensures its incorporation into the streptavidin scaffold.

In this thesis the design, expression and evolution of an artificial allylic deallocase based on the biotin-streptavidin technology is described. A biotinylated ruthenium complex was synthesized, incorporated into streptavidin and a crystal structure of the resulting artificial metalloenzyme was determined. The activity of the hybrid catalyst in a deallocation reaction was investigated. An O-allyl carbamate caged pro-fluorescent coumarin derivative was deprotected in the presence of the artificial metalloenzyme. The *in vitro* performance of the artificial allylic deallocase was evolved by genetic modification of the host protein. In a next step, the artificial metalloenzyme was displayed on the surface of *E. coli* cells. The activity of the hybrid catalyst was further evolved by *in vivo* screening of several single-site saturation mutagenesis libraries. It was aimed to further increase the throughput of the screening assay by application of a microfluidic system in combination with fluorescence-activated droplet sorting. In a third step, a biogenetic switch based on O-allyl carbamate caged inducer molecules was designed. By the action of the artificial allylic deallocase, the caged inducer was deprotected and subsequently induced the expression of a green fluorescent protein (GFP)-reporter. By substitution of the GFP with another natural protein, a cascade reaction can be envisioned. In parallel, a series of streptavidin mutants with lid-like amino acid structures on top of the biotin-binding vestibule was designed. This approach aimed gaining a better control of the second coordination sphere of the metal cofactor in order to increase the activity and selectivity of the artificial metalloenzyme.

In summary, these efforts should allow a straightforward design, expression and evolution of new artificial metalloenzymes for *in vivo* applications. During the time in the Ward group a deeper knowledge on protein design and expression, molecular biology, synthesis of organometallic cofactors, *in vivo* catalysis and high-throughput screening based on microfluidics was garnered.

# Contributions

The following persons contributed with their work to this thesis:

**Dr. Tillmann Heinisch (Ward group, University of Basel):**

Tillmann Heinisch determined the crystal structure in chapter 2.1.4 (Figure 9). He cloned the pBAD33 and the pCD353 plasmid (Figure 13 and Figure 22) and performed *E. coli* strain screening in Figure 23. He performed the streptavidin-antibody staining in Figure 15 and the subsequent mutant screening with the *E. coli* surface displayed streptavidin constructs in chapter 2.3.2. The cell experiments in Figure 16 and Figure 24 were performed in collaboration.

**Dr. Tsvetan Kardashliev (Panke group, DBSSE ETH Zürich):**

Tsvetan Kardashliev designed and cloned the DmpR/GFP reporter system and performed the corresponding cell experiments (chapter 2.4.5, Figure 25 and Table 8).

**MSc Philipp Rottmann (Panke group, DBSSE ETH Zürich):**

Philipp Rottmann designed, produced and operated the microfluidic device (Figure 19).

**Dr. Christine Tinberg (Baker group, University of Washington, Seattle):**

Christine Tinberg designed the circular permuted streptavidin constructs Cp1 – Cp4 (Figure 28c/d and Table 9, entries 37-40).

**Dr. Vincent Lebrun (Ward group, University of Basel):**

Vincent Lebrun prepared the protein-ligand docking of  $[\text{CpRu}(\text{QA-Biot})(\text{H}_2\text{O})]\text{PF}_6 \cdot \text{Sav}$  (Figure 10, Figure 18, Figure 31 and chapter 4.2.1).

**PD Dr. Daniel Häussinger (University of Basel):**

Daniel Häussinger measured and analyzed the NMR spectra in chapter 2.1.2 (Figure 5 and Figure 7).

**MSc Maxime Barnet (Ward group, University of Basel):**

Maxime Barnet prepared the protein-ligand docking of  $[\text{CpRu}(\text{QA-Biot})(\text{Allyl})]\text{PF}_6 \cdot \text{Sav}$  and of  $[(\text{Biot-Cp})\text{Ru}(\text{QA-NMe}_2)(\text{Allyl})]\text{PF}_6 \cdot \text{Sav}$  (Figure 4).

**MSc Eleonore Schmidt (Ward group, University of Basel):**

Eleonore Schmidt produced, purified and analyzed 11 streptavidin mutants (Table 9, entries 25-35) and tested them in catalysis (Figure 11, Figure 12).

**MSc Jaicy Vallapurackal (Ward group, University of Basel):**

Jaicy Vallapurackal optimized the primer design and the reaction conditions for the “22-codon trick” PCR performed in chapter 4.2.4.

**Dipl.-Biol. Juliane Klehr (Ward group, University of Basel):**

Juliane Klehr cloned the pBAD33 and the pCD353 plasmid (Figure 13 and Figure 22).

**BSc Brett Garabedian (Ward group, University of Basel):**

Brett Garabedian helped to perform the streptavidin-antibody staining in Figure 15 and the subsequent mutant screening with the *E. coli* surface displayed streptavidin constructs in chapter 2.3.2.

# Table of Contents

Acknowledgements .....	i
Summary.....	ii
Contributions.....	iii
1 Introduction.....	1
1.1 Artificial metalloenzymes .....	1
1.2 The biotin-streptavidin technology .....	3
1.3 Transition metal-catalyzed allylic substitutions .....	5
1.4 Ruthenium-catalyzed uncaging reactions in living cells .....	9
1.5 Caged inducer systems .....	11
1.6 Aims of the thesis .....	12
2 Results and discussion .....	13
2.1 Design of an artificial allylic deallocase .....	13
2.1.1 Synthesis of a biotinylated ruthenium cofactor .....	15
2.1.2 NMR studies of the designed ruthenium complexes .....	18
2.1.3 Assembly of the artificial allylic deallocase .....	23
2.1.4 Crystal structure determination .....	25
2.2 <i>In vitro</i> catalysis with an artificial allylic deallocase .....	26
2.2.1 Catalysis with a caged coumarin substrate .....	26
2.2.2 <i>In vitro</i> screening of streptavidin mutants .....	28
2.3 Catalysis on the surface of <i>E. coli</i> cells .....	31
2.3.1 Design of a surface displayed streptavidin construct.....	31
2.3.2 Screening of surface-displayed streptavidin libraries .....	36
2.3.3 Micro-droplet system for ultrahigh-throughput screening.....	39
2.4 Design of a caged inducer system .....	43
2.4.1 Self-immolative linkers .....	43
2.4.2 Design and synthesis of caged IPTG substrates.....	45
2.4.3 <i>In vitro</i> evaluation of the best IPTG substrate.....	47
2.4.4 Catalysis in the presence of GFP reporter cells .....	50
2.4.5 Design of a caged DmpR inducer system .....	53
2.5 Streptavidin loop mutants.....	56
2.5.1 Design of streptavidin loop mutants .....	56

2.5.2	Expression of streptavidin loop mutants.....	58
2.5.3	3D-model printing.....	64
3	Conclusion and Outlook .....	66
4	Experimental part.....	71
4.1	Instruments and material.....	71
4.2	Methods .....	72
4.2.1	Protein-ligand docking.....	72
4.2.2	HABA titration.....	73
4.2.3	Catalysis procedure for the coumarin substrate .....	74
4.2.4	Screening of <i>E. coli</i> surface Sav libraries.....	75
4.2.5	Microfluidics and droplet production.....	77
4.2.6	Catalysis procedure for caged IPTG substrates .....	78
4.2.7	Cloning of Sav loop mutants.....	80
4.2.8	Expression and purification of Sav mutants .....	86
4.2.9	Preparation of a 3D-printing model .....	90
4.3	Synthesis.....	93
4.3.1	Biotinylated ruthenium cofactor: main synthesis route .....	93
4.3.2	Biotinylated ruthenium cofactor: alternative synthesis routes .....	100
4.3.3	Non-biotinylated ruthenium complex.....	114
4.3.4	Caged coumarin substrate.....	115
4.3.5	Caged IPTG substrates .....	118
4.3.6	Caged 2`-Amino-IPTG substrate .....	129
4.3.7	Caged aniline substrate .....	134
4.3.8	Urea test substrate .....	135
4.4	Table of compounds .....	137
5	Abbreviations.....	148
6	References .....	150
7	Annexes .....	171
7.1	Additional screening results .....	171
7.2	NMR and mass spectra .....	173
8	Curriculum Vitae.....	214



# 1 Introduction

## 1.1 Artificial metalloenzymes

Artificial metalloenzymes are formed by incorporation of a catalytically active metal cofactor into a host protein.<sup>1-9</sup> This strategy was first introduced by Whitesides *et al.*<sup>10</sup> and Kaiser *et al.*<sup>11</sup> in the 1970's. They designed hybrid catalysts by the modification of avidin with a biotinylated diphosphine rhodium (I) moiety and by the exchange of a Zn(II) with a Cu(II) in carboxypeptidase A, respectively. The concept of hybrid catalysts allows combining the advantageous features of both homogeneous catalysis and enzyme catalysis.<sup>12</sup> Homogeneous catalysts typically reveal a wide substrate scope, can contain a variety of different transition metals and show a high tolerance towards organic solvents. The activity and selectivity of these catalysts can be optimized by chemical modification of the ligand. However, their performance (i.e. the turnover number) is often limited. On the other hand, enzymes typically reveal high activities and selectivities. At the same time, the substrate scope of natural enzymes is often narrow and reactions are mostly limited to water as solvent. In artificial metalloenzymes, the high selectivity of natural enzymes and the wide substrate scope of homogeneous catalysts can be combined and new-to-nature reactions can be implemented.<sup>13-14</sup> Embedding of an abiotic metal cofactor into a host protein creates a new reaction environment (i.e. a second coordination sphere)<sup>6</sup> around the active metal center. It allows the installation of a catalytic acid/base or a coordinating residue at the correct spatial place, or the creation of a hydrophobic pocket – features which are often difficult to provide with small molecule ligands. In this way, the activity and especially the selectivity of the artificial metalloenzyme can be engineered by genetic modification of the host protein. In combination with the tools of directed evolution<sup>15-17</sup>, highly active and selective hybrid catalysts can be created. Artificial metalloenzymes with kinetics and catalytic efficiencies (i.e. high  $k_{cat}/K_M$  values and high turnover numbers) similar to native enzymes have been created, as reported by Hartwig *et al.* for a reconstituted cytochrome P450 performing C-H insertion reactions<sup>18</sup> or by Baker *et al.* for an artificial hydrolase.<sup>19</sup> In addition to natural proteins, also DNA and small peptides have been utilized as hosts for transition metal catalysts.<sup>20-21</sup> Furthermore, a variety of *de novo* proteins have been designed for the creation of artificial metalloenzymes.<sup>22</sup> This was done, amongst others, by Tezcan *et al.* for an artificial  $\beta$ -lactamase<sup>23</sup>, by De Grado and Kaplan as well as by Lombardi *et al.* for an artificial phenol oxidase based on the due ferri protein family<sup>24-25</sup> and by Pecoraro *et al.* for an artificial hydrolase based on the TRI peptide family.<sup>26</sup> The incorporation of unnatural amino acids<sup>27</sup> into the host proteins completes the toolbox for the design of artificial metalloenzymes. Schultz *et al.* introduced the metal-chelating unnatural amino acid (2,2'-bipyridin-5-yl)alanine (Bpy-Ala) into the *E. coli* catabolite activator protein (CAP) and upon binding of Fe(II) or Cu(II) DNA-cleavage activity was observed.<sup>28</sup>

Incorporation of the abiotic metal cofactor into the host protein can be performed in four different ways, including (i) covalent linkage, (ii) supramolecular anchoring, (iii) dative anchoring, or (iv) metal substitution (Figure 1).<sup>29</sup> The metal cofactor can be covalently linked to the host protein by selective reaction of a nucleophilic residue of the host protein (e.g. serine, lysine or cysteine) with an electrophilic moiety in the cofactor (e.g. maleimide or  $\alpha$ -halocarbonyl). Covalent linkage can also be achieved by formation of a disulfide bond or by a “click reaction” involving an unnatural alkyne or azide residue.<sup>30</sup> The supramolecular assembly relies on a high affinity between the host protein and an anchoring moiety attached to the metal cofactor (e.g. biotin-streptavidin; see chapter 1.2). This high affinity may be realized by an extended hydrogen-bond network between the host protein and the anchor and/or strong hydrophobic interactions. The dative anchoring involves direct coordination of a residue of the host protein (e.g. histidine, serine, aspartate, glutamate or cysteine) to the metal center of the abiotic cofactor. Finally, the metal center of a natural metalloenzyme (e.g. iron or zinc) can be exchanged for other transition metals (e.g. copper, iridium or rhodium).<sup>31-33</sup>

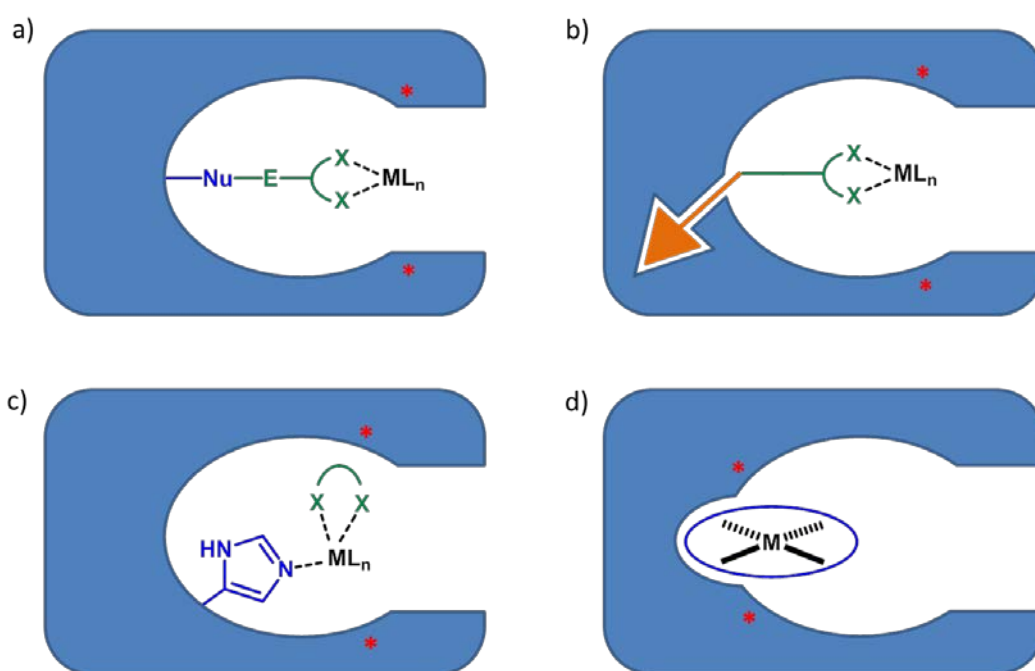


**Figure 1: Anchoring strategies of abiotic metal cofactors for the creation of artificial metalloenzymes.**

The four anchoring strategies include: a) covalent linkage, b) supramolecular anchoring, c) dative anchoring, d) metal substitution. The host protein is illustrated as blue cartoon shape. Natural residues/cofactors in blue. Artificial metal in black. Ligand and linkers in green. Supramolecular anchor in orange. Possible mutation sites in close proximity of the metal cofactor are displayed as red stars.

## 1.2 The biotin-streptavidin technology

The biotin-streptavidin technology is a supramolecular anchoring strategy relying on the ultra-high affinity of the protein streptavidin for the small molecule biotin (also known as vitamin H).<sup>34</sup> With a dissociation constant  $K_d$  of approximately  $10^{-13}$  M, it is one of the strongest non-covalent interactions known in nature.<sup>35</sup> Streptavidin is a homotetrameric  $\beta$ -barrel protein (dimer of dimers with a  $D_2$ -symmetry) with an approximate molecular weight of 65 kDa.<sup>36-37</sup> Every monomer consists of eight antiparallel  $\beta$ -sheets with seven interconnecting loops (Figure 2b; see also chapter 2.5 and Figure 26a). Streptavidin is derived from the bacterium *Streptomyces avidinii* and is closely related to the protein avidin from chicken egg white (32% sequence homology).<sup>38</sup> The tight biotin binding of streptavidin originates from an extended hydrogen bond network and several hydrophobic interactions. This includes hydrogen bonds between the urea moiety of biotin and the residues Asn<sub>23</sub>, Ser<sub>27</sub>, Tyr<sub>43</sub>, Ser<sub>45</sub> and Asp<sub>128</sub> as well as a hydrogen bond between the thioether and Thr<sub>90</sub> and hydrogen bonds between the valeric acid of biotin and the residues Asn<sub>49</sub> (backbone NH) and Ser<sub>88</sub> (Figure 2a). The residues Trp<sub>79</sub>, Trp<sub>92</sub>, Trp<sub>108</sub>, and Trp<sub>120</sub> (from the adjacent monomer) form a hydrophobic binding pocket.<sup>36, 39-41</sup> Furthermore, the loop 3,4 (Ser<sub>45</sub>...Arg<sub>53</sub>) adopts a closed position when biotin is bound.<sup>42-43</sup> In terms of tetramer stability, residues in the subunit interfaces (including Val<sub>55</sub>, Thr<sub>76</sub>, Thr<sub>90</sub>, Leu<sub>109</sub>, Trp<sub>120</sub>, Val<sub>125</sub>, His<sub>127</sub> and Asp<sub>128</sub>) play a critical role.<sup>44-47</sup> In addition, there is an important inter-subunit salt-bridge between Asp<sub>61</sub> and His<sub>87</sub> (at physiological pH).<sup>48</sup> Overall, streptavidin is stable at a wide pH-range (pH 3 - 11), at elevated temperatures (up to 110 °C), in mixtures with organic solvents (e.g. DMSO or ethanol) and in the presence of chaotropic agents (e.g. sodium dodecyl sulfate) or high concentrations of guanidinium hydrochloride (6 M) or urea (8 M).<sup>49-52</sup> The stability of streptavidin, in terms of melting temperature  $T_m$ , increases from 75°C to 112°C upon binding of biotin.<sup>53</sup> Building on this robustness, streptavidin is an ideal template for the creation of artificial metalloenzymes. Streptavidin can bind up to four molecules of biotin, in which each  $\beta$ -barrel of the tetramer hosts one guest in its center. Thereby, non-cooperativity was observed for individual binding events.<sup>54</sup> The core of biotin is deeply buried inside of the  $\beta$ -barrel, whereas the valeric acid side chain points towards a half-open vestibule (Figure 2b). Functionalization of the carboxylic acid of biotin (e.g. formation of an amide) allows to covalently attach a metal cofactor. Due to the  $D_2$ -symmetric structure of the streptavidin tetramer, two metal cofactors are located in close proximity to each other, which can potentially cause steric clashes (see chapters 2.1 and 2.1.4).<sup>55</sup> Furthermore, mutations within the binding site of one monomer are reflected by symmetry in the adjacent monomer. Streptavidin can be expressed in high yields in *E. coli*. Up to 35% of the total protein amount in the cells can be the protein of interest.<sup>56-57</sup> Cells can be lysed and the streptavidin can be purified by affinity column chromatography (2-iminobiotin coated sepharose beads; see chapter 4.2.8). This allows a simple production of medium-sized streptavidin mutant libraries.

Various avidin and streptavidin variants have been created and genetically engineered.<sup>58</sup> Some of them display very high stability towards harsh chemical conditions (e.g. high concentrations of methanol, ethanol, acetone or DMF).<sup>49</sup> Engineered (strep)avidins were utilized in biotechnological applications, ranging from purification and labeling methods to drug targeting and formation of nanostructures.<sup>59</sup> In the Ward research group, several artificial metalloenzymes based on the biotin-streptavidin technology have been designed. These hybrid catalysts are able to perform reactions such as transfer hydrogenation<sup>60-63</sup>, ring-closing metathesis<sup>64</sup>, C-H activation<sup>65</sup>, anion- $\pi$  catalysis<sup>66</sup>, Suzuki-coupling<sup>67</sup>, dehydrogenation of olefins<sup>68</sup> and more.<sup>69</sup> Artificial metalloenzymes based on the biotin-streptavidin technology were also successfully applied in cascade reactions.<sup>70-71</sup>

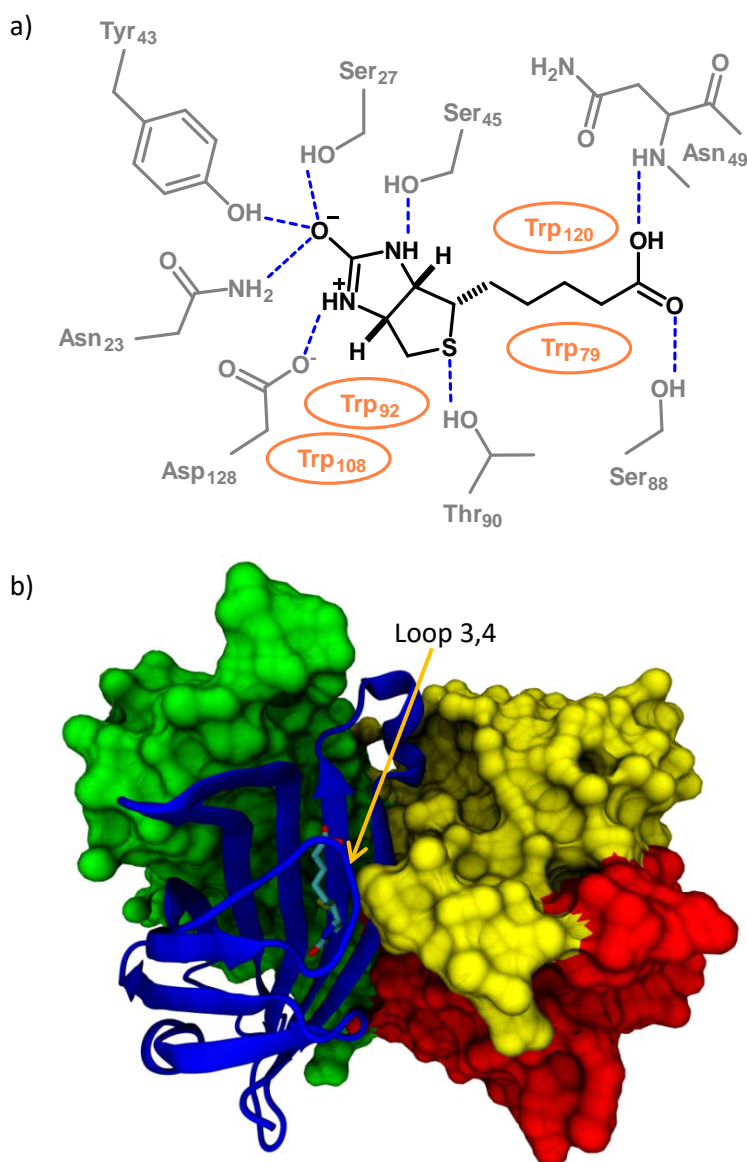
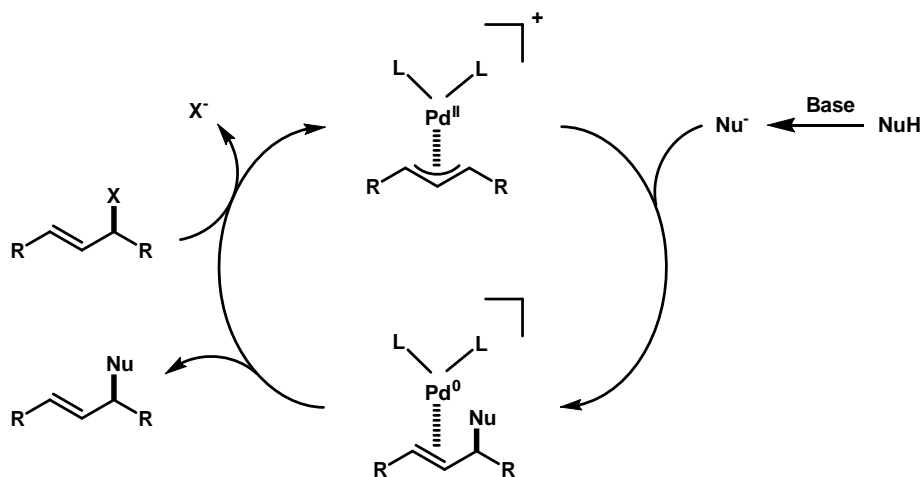


**Figure 2: Structure of streptavidin and interactions with biotin.**

a) Hydrogen bond interactions between biotin and streptavidin (residues Asn<sub>23</sub>, Ser<sub>27</sub>, Tyr<sub>43</sub>, Ser<sub>45</sub>, Asn<sub>49</sub>, Ser<sub>88</sub>, Thr<sub>90</sub> and Asp<sub>128</sub>) as well as hydrophobic interactions including the residues Trp<sub>79</sub>, Trp<sub>92</sub>, Trp<sub>108</sub> and Trp<sub>120</sub> (from the adjacent monomer). Protein in grey, biotin in black, hydrogen bonds as dotted blue lines, tryptophane residues in orange. b) Structure of biotin-bound streptavidin (PDB ID 1STP).<sup>36</sup> The streptavidin monomers are displayed as surface representation (green, red and yellow) or in cartoon style (blue). Biotin is displayed as sticks (atom color code: C = cyan, N = blue, O = red, N = blue, S = yellow).

### 1.3 Transition metal-catalyzed allylic substitutions

Transition metal-catalyzed allylic substitution reactions are nowadays a common tool in organic synthesis and catalysis.<sup>72-77</sup> Most often, palladium complexes are utilized to catalyze such reactions.<sup>73, 78</sup> Beside palladium, also iridium<sup>79</sup>, ruthenium<sup>80</sup>, rhodium<sup>81</sup>, molybdenum<sup>82</sup>, nickel and tungsten<sup>83</sup> complexes have been reported to catalyze nucleophilic allylic substitutions. The general mechanism of a palladium-catalyzed allylic substitution includes: 1) oxidative addition of the allylic substrate to form an  $\eta^3$ -allyl palladium(II) complex with the simultaneous release of the leaving group (e.g. allyl carbonates release alkoxides, which can act as base to activate a nucleophile), 2) attack of the nucleophile (often carbanions) on one of the allyl-termini to form an olefin-palladium(0) complex (attack on the central carbon has however also been reported<sup>84</sup>), and 3) release of the product, followed by the oxidative addition of another substrate molecule (Scheme 1).<sup>73</sup> The  $\eta^3$ -allyl palladium(II) complex is typically surrounded by two additional ligands (or one bidentate ligand) and adopts a square-planar coordination geometry. At this stage, the  $\eta^3$ -allyl palladium(II) complex is highly dynamic and can undergo ligand dissociation-association processes or  $\pi$ - $\sigma$ - $\pi$  isomerization. In the later process, the  $\eta^3$ -coordination of the allyl ligand is temporarily disrupted to form a short-lived  $\eta^1$ -intermediate. In this stage, a rotation along the C-C single bond of the allyl ligand is possible, which can result in different isomers. Furthermore, the stereoselectivity of the formed product is influenced by the (chiral) ligands.



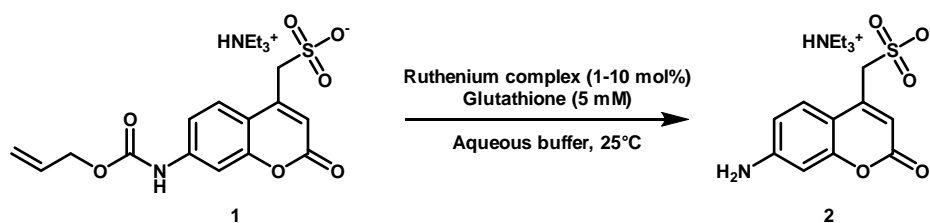
Scheme 1: Mechanism of a palladium-catalyzed allylic substitution.<sup>73</sup>

In this thesis, we focused on the deprotection of O-allyl carbamate-caged fluorophores (e.g. caged allyl-coumarin **1**; see Scheme 2 and chapter 2.2) and inducers (e.g. caged allyl-IPTG **58**; see Figure 20 and chapter 2.4). Since the used allyl moiety does not bear any substituents, an achiral allyl-transfer product results. It should be emphasized here that we are mainly interested in the liberated leaving group, rather than in the allylic substitution product.

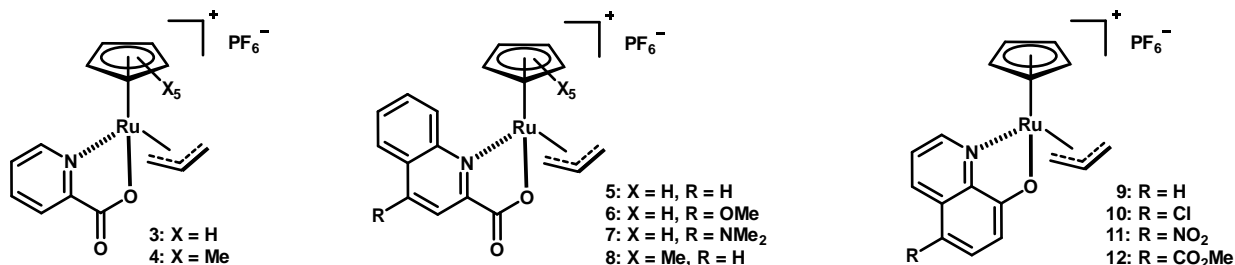
The formation of an artificial allylic dehalocase and its *in vivo* application requires that the incorporated metal cofactor is stable under air in aqueous solutions and maintains activity in a cellular environment (e.g. in the presence of millimolar concentrations of thiols). A transition metal catalyst for allylic substitutions which fulfill these requirements is, amongst others, the ruthenium complex [CpRu(QA)(Allyl)]PF<sub>6</sub> (**5**) (see Scheme 2 and chapter 1.4). This complex was first described by Kitamura *et al.* for the allylation of alcohols, using a 1:1 mixture of 2-propen-1-ol and the alcoholic substrate as solvent.<sup>85</sup> The same complex was also applied for the deprotection of allyl ethers<sup>86</sup> and the cleavage of allyl esters and allyl carbonates.<sup>87</sup> The structure of such ruthenium complexes and the kinetics of the deallylation of allyl methyl carbonate were described by Bruneau and Waymouth.<sup>88-89</sup> Most of these allylation/deallylation reactions were performed in organic solvents (often in methanol). The cleavage of allyl phenethyl carbonate however also proceeded with high yields in a 1:1 mixture of methanol/water.<sup>87</sup> Kitamura *et al.* subsequently anchored the ruthenium complex **5** onto magnetic particles (Fe<sub>3</sub>O<sub>4</sub>@SiO<sub>2</sub>) to construct a heterogenous catalysts, which can be easily separated after completion of the reaction.<sup>90</sup> With the ruthenium complex [CpRu(QA)(Allyl)]PF<sub>6</sub> (**5**), as well as with the related complex [Cp\*Ru(cod)Cl] (**13**), also allylation of thiols was performed.<sup>91-92</sup>

The research group of Meggers applied such ruthenium complexes in the deprotection of O-allyl carbamates (e.g. caged pro-fluorescent coumarin derivative **1**; Scheme 2 and Table 1).<sup>93-95</sup> The reactions were performed in water and in the presence of thiols. Furthermore, activity of these complexes in HeLa cells was observed (see chapter 1.4).

Meggers *et al.* tested a variety of Cp/Cp\*-ruthenium complexes for the deprotection of the O-allyl carbamate caged coumarin **1**. Complexes bearing acetonitrile, 2,2'-bipyridine or 1,5-cyclooctadiene ligands only revealed moderate activities (Table 1, entries 1-4). 2-quinolinecarboxylate (QA) or 2-pyridinecarboxylate (PA) ligands increased to activity of the corresponding ruthenium complexes (Table 1, entries 5-8). However, ruthenium complexes bearing a Cp\*-ligand performed slower than their corresponding Cp analogues. Complexes bearing electron donating groups at the 4'-position of the QA-ligand revealed elevated activities: H < OMe < NMe<sub>2</sub> (Table 1, entries 9-11). In contrast, the opposite trend for the allylation of alcohols and the cleavage of allyl ethers with the ruthenium complex [CpRu(PA-4'X)(Allyl)]PF<sub>6</sub> was observed (-OMe < -H < -Cl < -CF<sub>3</sub> < -NO<sub>2</sub>).<sup>96</sup> Exchange of the 2-quinolinecarboxylate (QA) ligand by 8-hydroxyquinolines (HQ) further increased the activity of the ruthenium complex (Table 1, entries 12-17).<sup>95</sup>



Ruthenium complexes:



**Scheme 2: Ruthenium-catalyzed deprotection of allyl-coumarin 1.**<sup>94-95</sup>

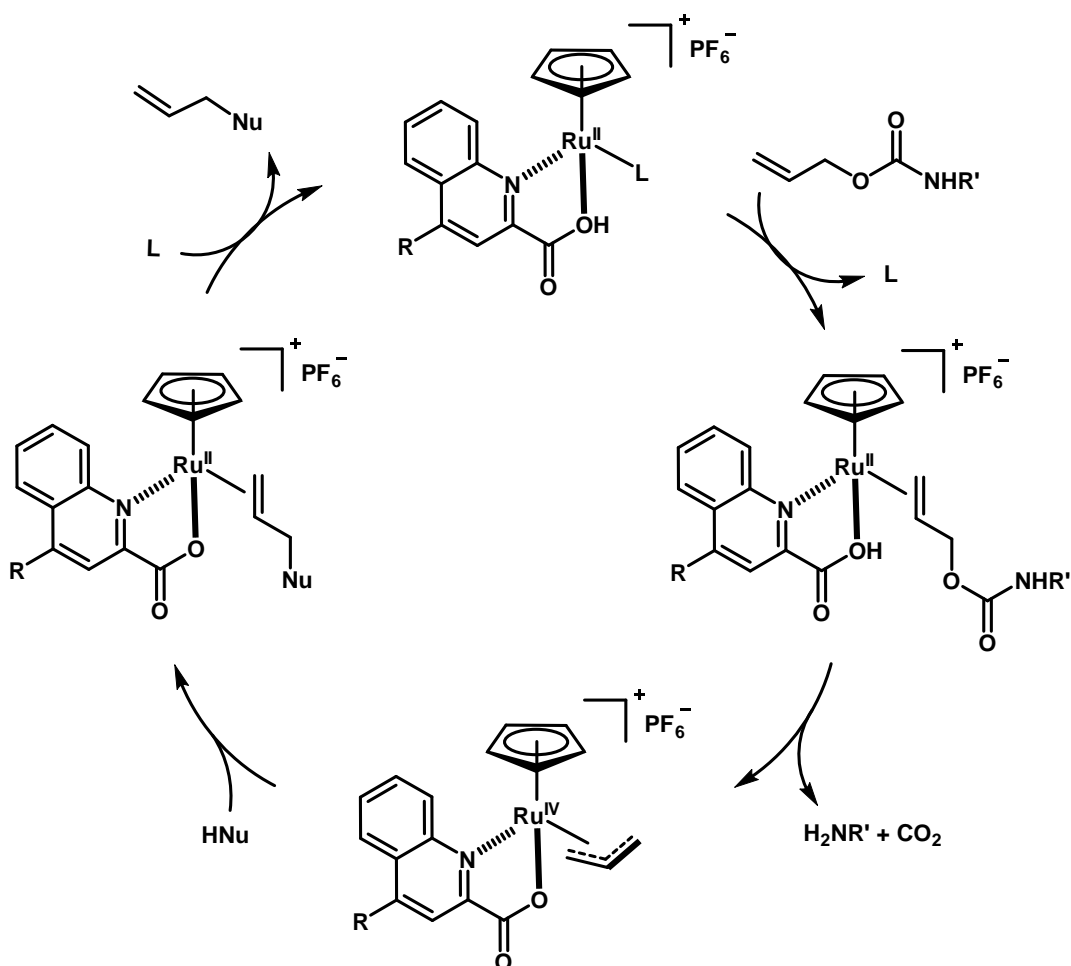
Reaction conditions: see Table 1.

**Table 1: Catalytic performance of ruthenium complexes in the cleavage of an *O*-allyl carbamate protected coumarin (1).**<sup>94-95</sup>

Entry	Complex	Catalyst loading	Reaction time	Yield [%]
1 <sup>a</sup>	[CpRu(MeCN) <sub>3</sub> ]PF <sub>6</sub>	5 mol%	4 h	< 10
2 <sup>a</sup>	[Cp <sup>*</sup> Ru(MeCN) <sub>3</sub> ]PF <sub>6</sub>	5 mol%	4 h	< 10
3 <sup>a</sup>	[CpRu(bpy)(MeCN)]PF <sub>6</sub>	5 mol%	4 h	~20
4 <sup>a</sup>	[Cp <sup>*</sup> Ru(cod)Cl] ( <b>13</b> )	5 mol%	4 h	~20
5 <sup>a</sup>	[CpRu(PA)(Allyl)]PF <sub>6</sub> ( <b>3</b> )	5 mol%	4 h	80
6 <sup>a</sup>	[Cp <sup>*</sup> Ru(PA)(Allyl)]PF <sub>6</sub> ( <b>4</b> )	5 mol%	4 h	10
7 <sup>a</sup>	[CpRu(QA)(Allyl)]PF <sub>6</sub> ( <b>5</b> )	5 mol%	4 h	>99
8 <sup>a</sup>	[Cp <sup>*</sup> Ru(QA)(Allyl)]PF <sub>6</sub> ( <b>8</b> )	5 mol%	4 h	38
9 <sup>a</sup>	[CpRu(QA)(Allyl)]PF <sub>6</sub> ( <b>5</b> )	1 mol%	4 h	47
10 <sup>a</sup>	[CpRu(QA-OMe)(Allyl)]PF <sub>6</sub> ( <b>6</b> )	1 mol%	4 h	79
11 <sup>a</sup>	[CpRu(QA-NMe <sub>2</sub> )(Allyl)]PF <sub>6</sub> ( <b>7</b> )	1 mol%	4 h	91
12 <sup>b</sup>	[Cp <sup>*</sup> Ru(cod)Cl] ( <b>13</b> )	10 mol%	2 h	1
13 <sup>b</sup>	[CpRu(QA-NMe <sub>2</sub> )(Allyl)]PF <sub>6</sub> ( <b>7</b> )	10 mol%	2 h	30
14 <sup>b</sup>	[CpRu(HQ)(Allyl)]PF <sub>6</sub> ( <b>9</b> )	10 mol%	2 h	56
15 <sup>b</sup>	[CpRu(HQ-Cl)(Allyl)]PF <sub>6</sub> ( <b>10</b> )	10 mol%	2 h	75
16 <sup>b</sup>	[CpRu(HQ-NO <sub>2</sub> )(Allyl)]PF <sub>6</sub> ( <b>11</b> )	10 mol%	2 h	67
17 <sup>b</sup>	[CpRu(HQ-CO <sub>2</sub> Me)(Allyl)]PF <sub>6</sub> ( <b>12</b> )	10 mol%	2 h	89

Reaction conditions: a) Entries 1-11: Allyl-coumarin **1** (500 μM), ruthenium catalyst, glutathione (5 mM) in water/DMSO (200:1), room temperature, air. For [Cp<sup>\*</sup>Ru(cod)Cl] thiophenol (2.5 mM) was added to the reaction mixture. Conversion determined by fluorescence intensity measurements. b) Entries 12-18: Allyl-coumarin **1** (50 μM), ruthenium catalyst, glutathione (5 mM) in potassium phosphate buffer (pH 7.4), room temperature, air. Conversion determined by HPLC analysis. Cp = η<sup>5</sup>-cyclopentadienyl, Cp<sup>\*</sup> = η<sup>5</sup>-pentamethylcyclopentadienyl, bpy = 2,2'-bipyridine, cod = η<sup>4</sup>-1,5-cyclooctadiene, PA = 2-pyridinecarboxylate, QA = 2-quinolinecarboxylate, HQ = 8-hydroxyquinolate.

The proposed mechanism of the ruthenium-catalyzed deallylation of O-allyl carbamates includes the same steps as the mechanism for palladium-catalyzed allylic substitutions (Scheme 1). First, the allyl moiety of the substrate coordinates to the ruthenium(II)-complex. Upon ionization of the allyl carbamate, decarboxylation and release of the leaving group, an  $\eta^3$ -allyl ruthenium(IV) intermediate is formed. Attack of the nucleophile and decomplexation of the formed olefin-ruthenium(II)-complex finally releases the allylic product (Scheme 3).<sup>97</sup>



Scheme 3: Proposed catalytic cycle for the ruthenium-catalyzed deprotection of allyl-coumarin 1.<sup>94</sup>



## 1.4 Ruthenium-catalyzed uncaging reactions in living cells

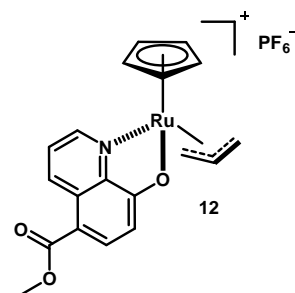
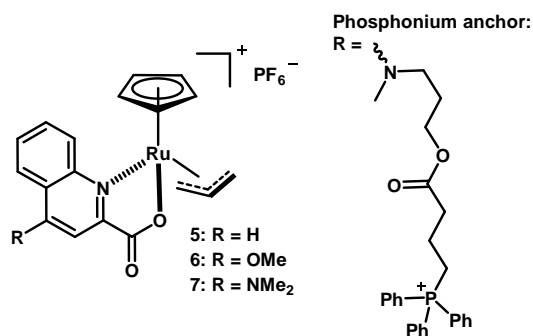
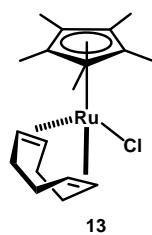
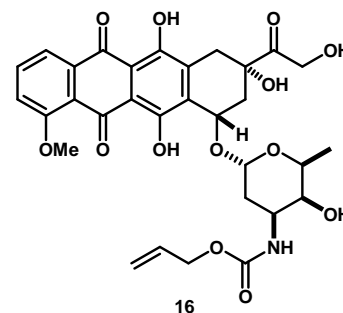
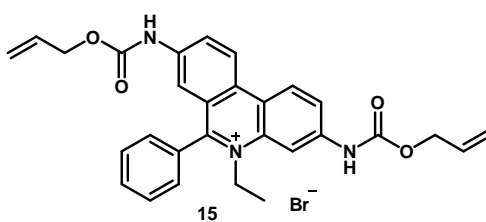
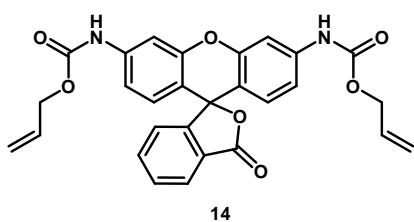
Bioorthogonal bond cleavage reactions have developed into an important tool in biochemical applications.<sup>98-</sup>

<sup>99</sup> One of these reactions is the deprotection of O-allyl carbamate caged compounds. The groups of Meggers<sup>93-94</sup>, Mascareñas<sup>100-101</sup> and Rotello<sup>102</sup> have demonstrated that such substrates can be deprotected inside of cells, applying different ruthenium complexes (Scheme 4).

Meggers *et al.* deprotected an O-allyl carbamate caged rhodamine 110 derivative (**14**) inside of HeLa cells using the ruthenium complex [Cp\*Ru(cod)Cl] (**13**).<sup>93</sup> By the addition of thiophenol, a higher rhodamine 110 fluorescence intensity was obtained. The ruthenium catalyst was subsequently further optimized. Complex [CpRu(QA)(Allyl)]PF<sub>6</sub> (**5**) revealed a highly increased activity for the same reaction.<sup>94</sup> The performance of the catalyst could even be further increased by an exchange of the substituent at the 4'-position of the quinoline carboxylate ligand (complexes **6** and **7**). The same trend was observed for the *in vitro* deprotection of the caged coumarin **1** (see Table 1, entries 9-11). Recently, Meggers *et al.* have further increased the catalytic activity of their ruthenium complex by substitution of the 2-quinolinecarboxylate ligand with an 8-hydroxyquinolate ligand (see Table 1, entries 12-17).<sup>95</sup> Both optimized ruthenium catalysts, complex [CpRu(QA-NMe<sub>2</sub>)(Allyl)]PF<sub>6</sub> (**7**) and complex [CpRu(HQ-CO<sub>2</sub>Me)(Allyl)]PF<sub>6</sub> (**12**), were able to deprotect a caged doxorubicin derivative (**16**) in HeLa cell cultures. The released active drug then decimated the number of living HeLa cells. Thus, ruthenium complexes in combination with caged drugs might also be applied in anti-cancer treatment. Furthermore, the catalysis rate of the ruthenium complex [CpRu(QA)(Allyl)]PF<sub>6</sub> (**5**) is independent of the glutathione concentration (tested between 0 – 10 mM).<sup>94</sup> As shown by Ward *et al.*, artificial metalloenzyme containing precious metal cofactors (e.g. artificial transfer hydrogenases containing piano-stool iridium complexes) were strongly inhibited by thiols (e.g. glutathione).<sup>103</sup> Thus, the zero order rate dependency of the ruthenium complex [CpRu(QA)(Allyl)]PF<sub>6</sub> (**5**) for glutathione represents an important feature for the design of potential artificial metalloenzymes for *in vivo* catalysis.

Mascareñas *et al.* attached a phosphonium anchor to the ruthenium complex [CpRu(QA-NMe<sub>2</sub>)(Allyl)]PF<sub>6</sub> (**7**). The resulting catalyst preferentially accumulated in the mitochondria of the HeLa cells.<sup>101</sup> In addition, they demonstrated that a DNA-binding agent (**15**) can be uncaged inside of chicken embryo fibroblast cells, applying [Cp\*Ru(cod)Cl] (**13**).<sup>100</sup>

The research group of Rotello designed gold nanoparticles, in which they embedded the ruthenium complex [Cp\*Ru(cod)Cl] (**13**).<sup>102</sup> The intracellular catalytic activity of this construct towards the deprotection of caged rhodamine 110 (**14**) was controlled by the interaction with a supramolecular cucurbit[7]uril “gate-keeper”. Finally, Wender *et al.* implemented a cellular luciferase reporter system.<sup>104</sup> A caged probe (O-allyl carbamate protected D-aminoluciferin) was deprotected by the ruthenium complex [CpRu(QA-OMe)(Allyl)]PF<sub>6</sub> (**6**). The released luminophore (D-aminoluciferin) was then used up by the luciferase in order to produce an optical readout. However, studies varying the order of addition of catalyst and substrate as well as ICP-MS experiments suggested that the catalysis occurred extracellularly.

**Ruthenium catalysts:****Caged substrates:**

**Scheme 4:** *In vivo* deprotection of *O*-allyl carbamate caged substrates applying different ruthenium complexes.

Beside the ruthenium mediated deprotection, also palladium(0)-microspheres<sup>105</sup> and various palladium-salts (e.g.  $\text{Allyl}_2\text{Pd}_2\text{Cl}_2$ )<sup>106</sup> were successfully applied in the uncaging of *O*-allyl carbamate-protected species. In addition, Meggers *et al.* demonstrated that natural enzymes (e.g. cytochrome P450-BM3) are able to uncage allyl ether-protected compounds.<sup>107</sup> However, the natural enzymes revealed higher activities for the corresponding propargyl-derivatives.

Based on the high activity and the *in vivo* compatibility of the presented ruthenium complexes (see Scheme 4 and Table 1), we envisioned the design of an artificial allylic deallocase based on the biotin-streptavidin technology. Therefore, we planned to attach a biotin anchor to the ruthenium complex [CpRu(QA-NMe<sub>2</sub>)(Allyl)]PF<sub>6</sub> (**7**) with subsequent incorporation of the cofactor into streptavidin (chapter 2.1). The designed artificial allylic deallocase can then potentially be evolved and applied in catalysis in the presence of *E. coli* cells (chapters 2.2 and 2.3). By the design of caged inducers (chapter 1.5), the expression of a protein of interest could be triggered with an artificial metalloenzyme (chapter 2.4).

## 1.5 Caged inducer systems

Biogenetic switches allow the regulation of genes and the expression of proteins in cells. In bacteria, often systems depending on small molecule inducers such as isopropyl- $\beta$ -D-thiogalactopyranoside (IPTG) or L-arabinose are employed for this task. However, once one of these inducers has been added to the cell culture, the gene expression cannot be longer controlled by an external stimulus. This control can be gained back by attachment of a protecting group to the inducer. The protected inducer can then be added to the cell culture and later on be activated when desired. Often photo-labile protective groups are used to “cage” the active inducer.<sup>108</sup> This was applied for the protection of IPTG and arabinose using photo-cleavable 6-nitropiperonyl caging groups.<sup>109-111</sup> Another caged IPTG inducer was chemically released by an RNA-templated Staudinger reaction followed by a 1,6-elimination.<sup>112</sup> Alternatively, not the inducer molecule itself but the required T7 RNA polymerase can be caged.<sup>113</sup>

In this thesis, we envisioned the design of an *O*-allyl carbamate/carbonate protected IPTG derivative, which can be uncaged by the action of our artificial allylic deallocase (chapter 2.4). The liberated IPTG can then induce the expression of a GFP reporter protein.

## 1.6 Aims of the thesis

The Ward research group has designed a variety of different artificial metalloenzymes based on the biotin-streptavidin technology. The performance of these hybrid catalysts has been optimized by chemical modification of the biotinylated metal cofactor or by genetic engineering of the host protein. The resulting active artificial metalloenzymes have then been successfully applied in catalytic transformations, including transfer hydrogenation, C-H activation, ring-closing metathesis, Suzuki-coupling, anion- $\pi$  catalysis and many more (chapters 1.1 and 1.2). In parallel, highly active allyl transfer catalysts based on palladium, iridium and ruthenium complexes have been developed, and some of them have been successfully applied in *in vivo* catalysis (chapters 1.3 and 1.4). Based on this knowledge, the following aims were formulated for this PhD thesis:

- Creation of an artificial allylic deallocase by incorporation of a biotinylated ruthenium cofactor into streptavidin isoforms.
- Optimisation of the catalytic performance of the artificial allylic deallocase by genetic modification of the host protein.
- Design of streptavidin variants containing a lid-like structure on top of the solvent exposed biotin binding vestibule, in order to increase the influence of the host protein on the metal cofactor. In this way, the catalytic activity and selectivity of the artificial metalloenzyme can be further evolved.
- Application of the artificial allylic deallocase in an *in vivo* catalysis reaction in *E. coli*.
- Design of an ultrahigh-throughput assay for the *in vivo* evolution of the artificial allylic deallocase.
- Design of *O*-allyl carbamate protected inducer molecules (IPTG) for the creation of a biogenetic switch, which can be triggered by the action of the artificial allylic deallocase.

## 2 Results and discussion

### 2.1 Design of an artificial allylic deallocase

Inspired by the previous results of Meggers *et al.*<sup>94</sup> (chapters 1.3 and 1.4) and the knowledge of the Ward group on artificial metalloenzymes based on the biotin-streptavidin technology, a new artificial allylic deallocase was designed. Incorporation of the catalytically active transition metal complex into streptavidin required the covalent attachment of a biotin anchor to the ruthenium cofactor. This linkage could be done either (i) via the cyclopentadienyl (Cp) ligand or (ii) via the 2-quinolinecarboxylate (QA) ligand (Figure 3, b and c).

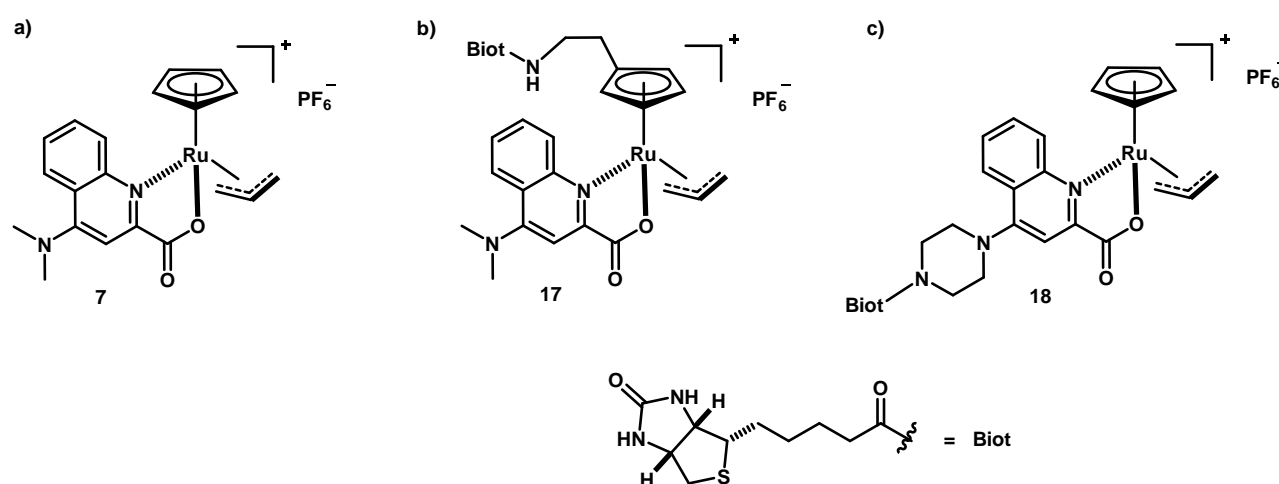


**Figure 3: Designed biotinylated ruthenium complexes for the construction of an artificial allylic deallocase.**

a) Ruthenium complex  $[\text{CpRu}(\text{QA-NMe}_2)(\text{Allyl})]\text{PF}_6$  (**7**) reported by Meggers *et al.*<sup>94</sup>; b) Ruthenium complex  $[(\text{Biot-Cp})\text{Ru}(\text{QA-NMe}_2)(\text{Allyl})]\text{PF}_6$  (**17**) with a biotin anchor attached to the cyclopentadienyl ligand; c) Ruthenium complex  $[\text{CpRu}(\text{QA-Biot})(\text{Allyl})]\text{PF}_6$  (**18**) with a biotin anchor attached to the 2-quinolinecarboxylate ligand.

The first strategy, linkage via the cyclopentadienyl ligand (**17**), allows a simple and fast exchange of the second coordination partner.<sup>62</sup> Thus, the chemical diversity of the system could be explored by testing a variety of ligands (e.g. substituted 2-quinolinecarboxylates, 2-pyridinecarboxylates or 8-hydroxyquinolines; Scheme 2 and Table 1).<sup>94-95</sup> However, ruthenium complexes bearing a Cp\*-ligand perform slower in the catalytic cleavage of an *O*-allyl carbamate protected coumarin (**1**) than their corresponding Cp analogues (Table 1, entries 5-8; Scheme 2).<sup>94</sup> It is believed that this is caused by the steric hindrance of the five methyl groups. Thus, attachment of a bulky biotin anchor might decrease the catalytic efficiency of the complex as well.

In the second strategy, the biotin anchor is attached to the 2-quinolinecarboxylate ligand (**18**). An increased catalytic efficiency for ruthenium complexes  $[\text{CpRu}(\text{QA-4}^{\text{X}})(\text{Allyl})]\text{PF}_6$  bearing electron donating groups at the 4'-position was detected:  $-\text{H} < -\text{OMe} < -\text{NMe}_2$  (Table 1, entries 9-11; Scheme 2).<sup>94</sup>

The beneficial effect of the electron donating dimethylamino group on the catalytic activity should be kept when the biotin anchor is attached. To simultaneously increase the rigidity of the ligand, a piperazine linker was selected to connect the biotin anchor to the ligand (Figure 3, c). For both strategies a protein-ligand docking was performed using GOLD (Figure 4).

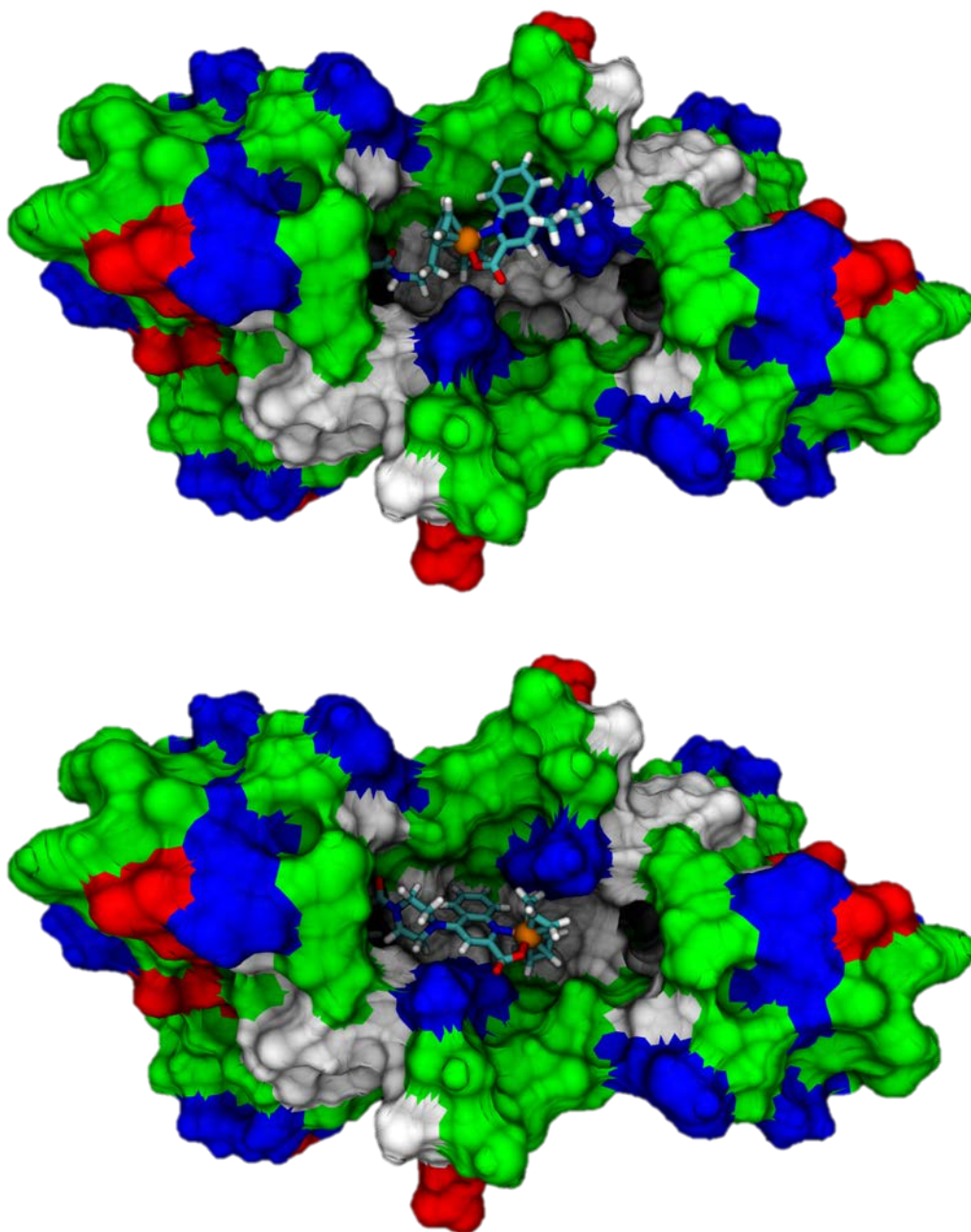


**Figure 4: Protein-ligand docking of [(Biot-Cp)Ru(QA-NMe<sub>2</sub>)(Allyl)] (17, top) and [CpRu(QA-Biot)(Allyl)] (18, bottom) in Sav-WT.**

A biotin anchor was modelled into a crystal structure of [CpRu(QA)(Allyl)]PF<sub>6</sub> (5) (Cambridge Structural Database Refcode: NAJLUG)<sup>85</sup> and the complete ruthenium cofactor was docked into a crystal structure of streptavidin (Protein Database entry: 3PK2).<sup>60</sup> The docking was performed with the dimer of streptavidin. Protein in surface representation (color code for the residues: white = apolar, green = polar, red = acidic, blue = basic), biotinylated ruthenium complex represented as sticks (elements: H = white, C = cyan, N = blue, O = red, S = yellow, Ru = orange ball). The docking procedure is described in details in chapter 4.2.1. Docking was done by MSc Maxime Barnet (University of Basel).

For both strategies the designed biotinylated ruthenium complexes would potentially fit into the host protein. The docking furthermore suggested that two adjacent biotin-binding sites provide only the required space to host one cofactor. Due to the promising catalysis results presented in Table 1 it was decided to proceed with the second strategy, the attachment of the biotin anchor to the 2-quinolinecarboxylate ligand.

### 2.1.1 Synthesis of a biotinylated ruthenium cofactor

Synthesis of the desired biotinylated ruthenium complex [CpRu(QA-Biot)(Allyl)]PF<sub>6</sub> (**18**) required the covalent attachment of a piperazine linker and a biotin anchor to the 2-quinolinecarboxylate ligand (Scheme 5). The synthesis was started from the commercially available kynurenic acid (**19**). Esterification with sulfuric acid in refluxing methanol led to the formation of methyl ester **20**, which was further brominated at the 4'-position to form compound **21**. The *tert*-butyloxycarbonyl (Boc) protected piperazine linker was attached via a Buchwald-Hartwig amination using Pd<sub>2</sub>(dba)<sub>3</sub> and racemic BINAP in refluxing 1,4-dioxane. Compound **22** was the starting point for a variety of synthetic routes. However, at this point, two central questions arose: (i) What type of biotin or biotin-analogue should be used as an anchor? (ii) At which step of the synthesis should this anchor be installed?

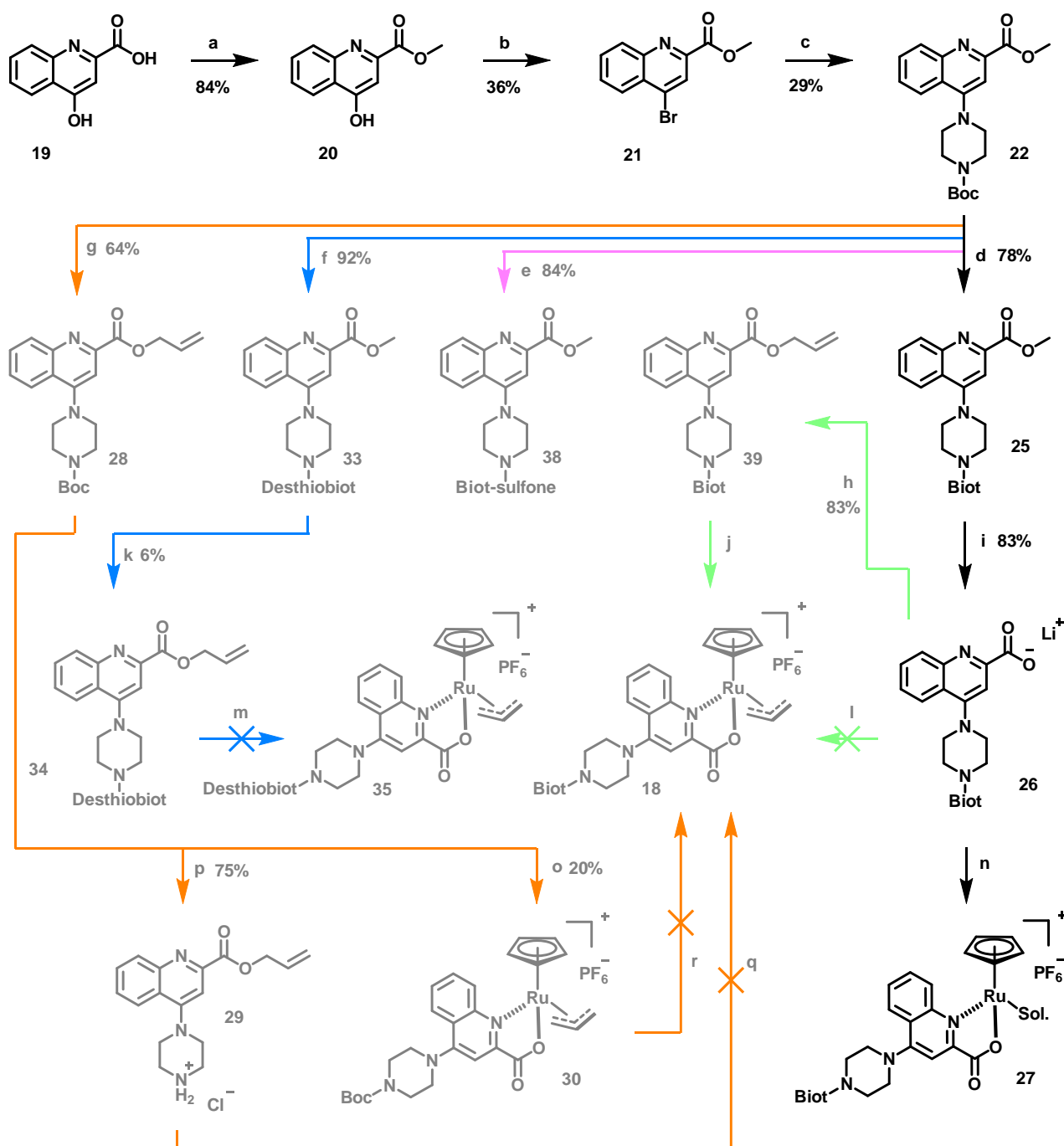
Using D-biotin as an anchor might cause problems, since its thioether group could potentially interact with the ruthenium center. On the other hand, a part of the affinity for (strept)avidin is lost when D-biotin is exchanged for desthiobiotin or its sulfone analogue (Table 2).<sup>35</sup> However, since the interactions with avidin remain high ( $K_d \sim 10^{-13}$  M), D-biotin, D-biotin sulfone and desthiobiotin anchors were tested for the synthesis of the ruthenium complex.

Table 2: Affinities of biotin derivatives towards avidin.<sup>35</sup>

Entry	Biotin analogue	$K_d$ [M] <sup>a</sup>
1	D-Biotin	$10^{-15}$
2	D-Biotin sulfone	$>10^{-13}$
3	Desthiobiotin	$5 \cdot 10^{-13}$
4	2'-Iminobiotin	$3.5 \cdot 10^{-11}$
5	2'-Thiobiotin (pH 9)	$5 \cdot 10^{-13}$
6	<i>N</i> -3'-methoxycarbonyl biotin methyl ester	$10^{-8}$ - $10^{-9}$
7	<i>N</i> -1'-methoxycarbonyl biotin methyl ester	$4 \cdot 10^{-7}$

<sup>a</sup>Determined in aqueous solution at pH 7.

The biotin anchors were in general attached to the 2-quinolinecarboxylate moiety prior to complexation with ruthenium. The conditions to remove the Boc protective group or the correspondingly formed secondary amine might not be compatible with the ruthenium complex. Nevertheless, the other strategy was attempted as well in case of the D-biotin anchor. All the synthetic strategies and their success are summarized in Scheme 5.



**Scheme 5: Synthetic strategies for the synthesis of a biotinylated ruthenium catalyst.**

Reaction conditions: a)  $\text{H}_2\text{SO}_4$ , MeOH (dry), reflux, 20 h; b)  $\text{P}_2\text{O}_5$ ,  $\text{Bu}_4\text{NBr}$ , toluene,  $90^\circ\text{C}$ , 1 h; c) *N*-Boc-piperazine,  $\text{Pd}_2(\text{dba})_3$  (6 mol%), *rac*. BINAP (6 mol%),  $\text{Cs}_2\text{CO}_3$ , 1,4-dioxane (dry), reflux, 15 h; d) 1.) 50% TFA in DCM, TIS, r.t., 1 h. 2.) Biotin-PFP (**24**), DIPEA, DMF, r.t., 24 h; e) 1.) 50% TFA, TIS, DCM, r.t., 1 h. 2.) Biot-sulfone-PFP (**37**), DIPEA, DMF, r.t., 20 h; f) 1.) 50% TFA, TIS, DCM, r.t., 1 h. 2.) Desthiobiotin-PFP (**32**), DIPEA, DMF, r.t., 20 h; g) 1.)  $\text{LiOH}\cdot\text{H}_2\text{O}$ , MeOH, r.t., 48 h. 2.) Allyl bromide (2.0 eq.),  $\text{NaHCO}_3$ , DMF,  $50^\circ\text{C}$ , 18 h; h) Allyl bromide (1.5 eq.),  $\text{NaHCO}_3$ , DMF,  $50^\circ\text{C}$ , 15 h; i)  $\text{LiOH}\cdot\text{H}_2\text{O}$ , MeOH, r.t., 22 h; j) Ligand **39** +  $[\text{CpRu}(\text{MeCN})_3]\text{PF}_6$ , test reactions with different dry solvents (acetone, DCM, MeCN), r.t., 15 min, glovebox (see also chapter 2.1.2); k) 1.)  $\text{LiOH}\cdot\text{H}_2\text{O}$ , MeOH, r.t., 24 h. 2.) Allyl bromide (2.0 eq.),  $\text{NaHCO}_3$ , DMF,  $50^\circ\text{C}$ , 18 h; l) 1.) Ligand **26**/ $[\text{CpRu}(\text{MeCN})_3]\text{PF}_6$  (1:1), acetone (dry), r.t., 15 min, glovebox. 2.) Allyl alcohol (1 eq.), r.t. 15 min, glovebox; m) 1.)  $[\text{CpRu}(\text{MeCN})_3]\text{PF}_6$  (1 eq.), acetone (dry), r.t., glovebox. 2.) Ligand **34** (1 eq.), r.t., 45 min; n)  $[\text{CpRu}(\text{MeCN})_3]\text{PF}_6$  (1.0 eq.), DMF, r.t., 15 min, used for catalysis *in situ*; o)  $[\text{CpRu}(\text{MeCN})_3]\text{PF}_6$ , acetone (dry), r.t., 45 min; p) HCl in 1,4-dioxane (10 eq.), 1,4-dioxane, r.t., 2.5 h; q) Ligand **29**/ $[\text{CpRu}(\text{MeCN})_3]\text{PF}_6$  (1:1), MeOH (dry), r.t., 15 min, glovebox; r) 1.) HCl (gas), DCM, r.t., 3 h. 2.) DCM, r.t., stirring overnight. 3.) Biotin-PFP (**24**),  $\text{NEt}_3$ , DMF, r.t., overnight; Biot = D-biotin; Desthiobiot = Desthiobiotin; Biot-sulfone = D-biotin sulfone; Boc = *tert*-butoxycarbonyl.



In the first synthetic route (Scheme 5, orange arrows), quinoline **22** was trans-esterificated to the corresponding allyl ester **28**, which was then mixed with  $[\text{CpRu}(\text{MeCN})_3]\text{PF}_6$  in dry acetone to form the ruthenium complex  $[\text{CpRu}(\text{QA-Boc})(\text{Allyl})]\text{PF}_6$  (**30**). This complex was treated with  $\text{HCl}_{(\text{g})}$  in DCM to remove the Boc protective group, followed by addition of an activated biotin ester (**24**) in DMF to install the biotin anchor. However, according to NMR and MS analysis, the desired biotinylated ruthenium complex  $[\text{CpRu}(\text{QA-Biot})(\text{Allyl})]\text{PF}_6$  (**18**) was not formed. Alternatively, allyl ester **28** was deprotected first to form the corresponding piperazine hydrochloride salt (**29**). Due to its limited solubility (insoluble in acetone, MeCN, DCM, THF), MeOH was selected as solvent for complexation. NMR analysis of the ruthenium precursor  $[\text{CpRu}(\text{MeCN})_3]\text{PF}_6$  in methanol- $d_4$  revealed that the Cp ligand had been displaced. Therefore, no complexation with the biotinylated ligand was attempted.

The second synthetic route (Scheme 5, blue arrows) includes the use of a desthiobiotin anchor. Quinoline **22** was deprotected and treated with pentafluorophenyl desthiobiotin (**32**) to yield methyl ester **33**. After transesterification to the corresponding allyl ester (**34**), complexation with  $[\text{CpRu}(\text{MeCN})_3]\text{PF}_6$  in dry acetone was attempted. However, according to NMR analysis, the desired biotinylated ruthenium complex  $[\text{CpRu}(\text{QA-Desthiobiot})(\text{Allyl})]\text{PF}_6$  (**35**) was not formed.

In the third synthetic route (Scheme 5, pink arrow) a D-biotin sulfone anchor was successfully attached to the quinoline frame. The formed product (**38**), however, had very limited solubility (product precipitated during the synthesis from DMF), which rendered its use in subsequent synthesis very challenging.

In a final synthetic route (Scheme 5, black arrows), D-biotin was introduced as an anchor for streptavidin. Quinoline **22** was deprotected and biotinylated to afford methyl ester **25**, which was saponified to yield carboxylate **26**. This ligand was mixed with  $[\text{CpRu}(\text{MeCN})_3]\text{PF}_6$  in DMF (1:1 ratio) and the formed ruthenium complex  $[\text{CpRu}(\text{QA-Biot})(\text{Sol.})]\text{PF}_6$  (**27**) was used *in situ* for catalysis. Detailed structural analysis (NMR studies, crystal structure analysis) and its performance in catalysis are discussed in chapters 2.1.2, 2.1.4 and 2.2.

Based on the proposed mechanism (Scheme 3), it should be independent at which step of the catalytic cycle the reaction starts. This means that bearing an allyl fragment is not a requirement for the initial ruthenium complex to act as an allyl transfer catalyst. Nevertheless, synthesis of the allylated ruthenium complex  $[\text{CpRu}(\text{QA-Biot})(\text{Allyl})]\text{PF}_6$  (**18**) was attempted in two different ways (Scheme 5, green arrows). Direct complexation of ligand **26** with  $[\text{CpRu}(\text{MeCN})_3]\text{PF}_6$  in dry acetone followed by the addition of allyl alcohol (formation of the allyl ligand) failed. Therefore, allyl ester **39** was prepared and subsequent complexation with  $[\text{CpRu}(\text{MeCN})_3]\text{PF}_6$  was attempted using different organic solvents (acetone, MeCN or DCM), different ligand:metal ratios and different orders of addition (see chapter 2.1.2). Complexation with a 1:1 mixture of ligand **39** and ruthenium precursor  $[\text{CpRu}(\text{MeCN})_3]\text{PF}_6$  in dry DCM resulted in the successful formation of the desired ruthenium complex  $[\text{CpRu}(\text{QA-Biot})(\text{Allyl})]\text{PF}_6$  (**18**) as revealed by HRMS analysis. However, the crude product contained a fraction of the initial ruthenium precursor  $[\text{CpRu}(\text{MeCN})_3]\text{PF}_6$ .

Purification of this mixture by chromatography (reverse phase TLC) proved to be challenging. Based on the good catalysis results with  $[\text{CpRu}(\text{QA-Biot})(\text{Sol.})]\text{PF}_6$  (**27**) (chapter 2.2), the synthesis and isolation of the allylated analogue  $[\text{CpRu}(\text{QA-Biot})(\text{Allyl})]\text{PF}_6$  (**18**) was not further pursued.

In summary, a biotinylated 2-quinolinecarboxylate ligand (**26**) was synthesized in five steps (Scheme 5, black arrows), with a Buchwald-Hartwig amination as the key step. The synthesis started from the commercially available kynurenic acid (**19**). Moderate to good yields (29-84%) were obtained for the individual steps. The efficiency of the aromatic bromination and the Buchwald-Hartwig amination (Scheme 5, steps b and c) could be further increased. Synthetic transformations in presence of biotin derivatives proved to be challenging and the desired products could not always be obtained in pure form. However, an *in situ* mixture of the biotinylated ligand **26** with the ruthenium precursor  $[\text{CpRu}(\text{MeCN})_3]\text{PF}_6$  in DMF was successfully applied in catalysis (chapter 2.2).

### 2.1.2 NMR studies of the designed ruthenium complexes

#### $[\text{CpRu}(\text{QA-NMe}_2)(\text{Allyl})]\text{PF}_6$ (**7**): Effect of DMSO on the allyl ligand

Based on the catalytic performance of  $[\text{CpRu}(\text{QA-NMe}_2)(\text{Allyl})]\text{PF}_6$  (**7**) for the deprotection of the coumarin derivative **1** (Scheme 6, Table 4), in which significantly higher yields were obtained if the catalyst stock solution was prepared in DMSO compared to MeCN, a set of 2D-NMR spectra of the ruthenium complex in these solvents were investigated. Only a single species (complex  $[\text{CpRu}(\text{QA-NMe}_2)(\text{Allyl})]\text{PF}_6$  (**7**)) was detected in the  $^1\text{H}$  NMR spectrum using  $\text{MeCN-d}_3$  as solvent. Two species were detected in  $\text{DMSO-d}_6$  (Figure 5). In addition to the initial ruthenium complex  $[\text{CpRu}(\text{QA-NMe}_2)(\text{Allyl})]\text{PF}_6$  (**7**), the allyl ester **40**, in which the  $\eta^3$ -coordinated allyl fragment was transferred to the carboxylate of the quinoline ligand, was detected. The signals at 5.91 ppm and at 5.19 + 5.02 ppm show typical chemical shifts and coupling patterns for an allyl ester. There was no HMBC cross-peak between the 1'-carbon and the 12'-protons detectable. It is thus believed that there is a fast exchange between the two species **7** and **40**. In the  $^1\text{H}$  NMR spectrum using  $\text{DMSO-d}_6$  as solvent, the two species were obtained in the ratio **7/40** = 1.5:1. In addition, a set of NOE cross-peaks between the Cp ligand and the 2-quinolinecarboxylate/allyl ligand was detected, which supports the proposed arrangement of the ligands around the metal center. Whether DMSO coordinates to the ruthenium center in complex **40** could not be clearly established in this NMR study. However, complex **40** contains a potentially free coordination site at the ruthenium center, which might explain the increased activity of the complex if DMSO is used as the co-solvent.

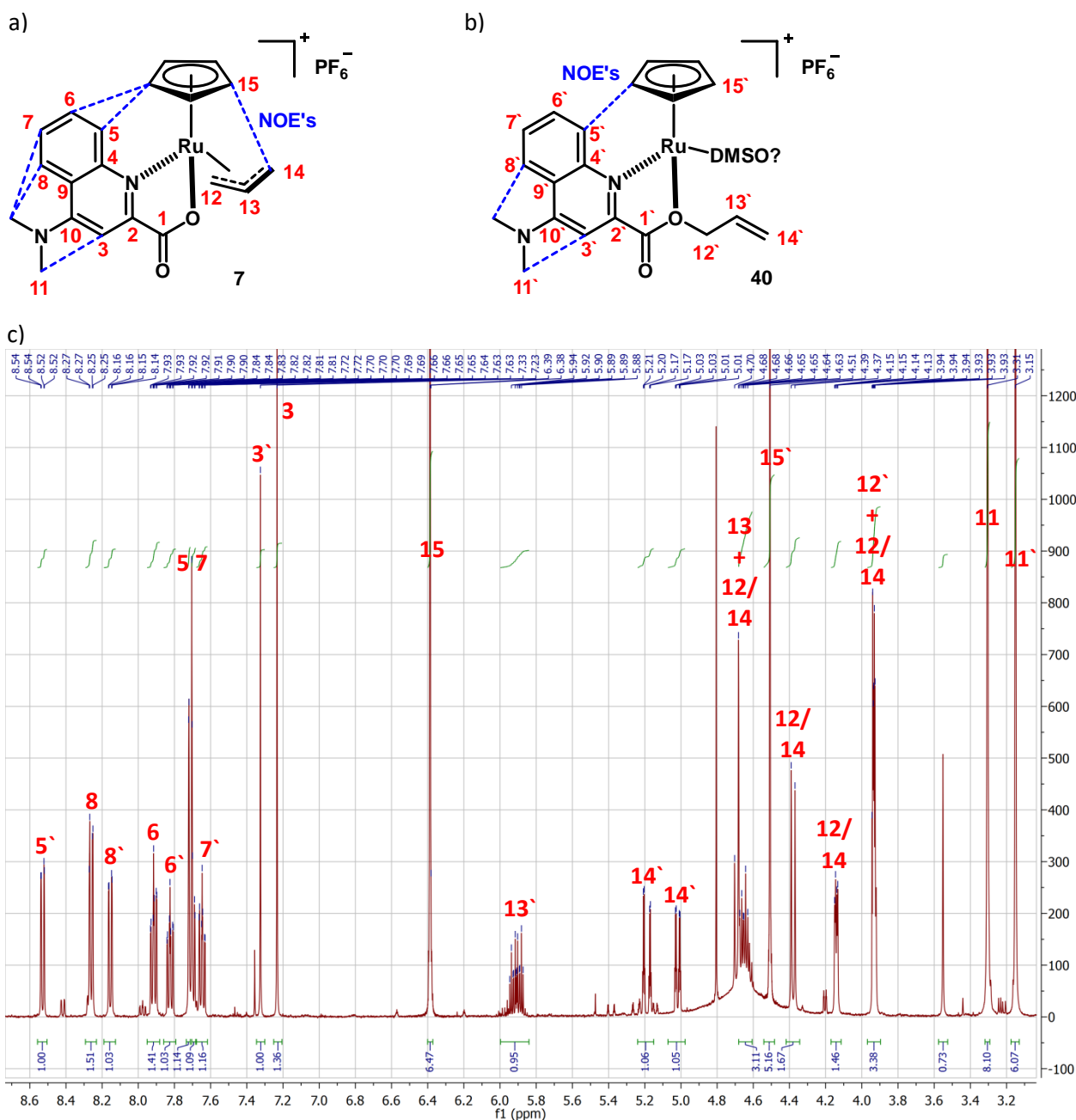


**Figure 5:**  $^1\text{H}$  NMR spectrum of  $[\text{CpRu}(\text{QA-NMe}_2)(\text{Allyl})]\text{PF}_6$  (**7**) in  $\text{DMSO-d}_6$ .

a) Structure of the ruthenium complex  $[\text{CpRu}(\text{QA-NMe}_2)(\text{Allyl})]\text{PF}_6$  (**7**). b) Proposed structure of its analogue bearing an allyl ester and a potentially free coordination site instead of an  $\eta^3$ -coordinated allyl fragment. c)  $^1\text{H}$  NMR spectrum of complex  $[\text{CpRu}(\text{QA-NMe}_2)(\text{Allyl})]\text{PF}_6$  (**7**) in  $\text{DMSO-d}_6$ . The two species were obtained in the ratio **7/40** 1.5:1. Dashed blue lines indicate the obtained NOE peaks. Complete assignment of the spectrum:  $^1\text{H}$  NMR (500 MHz,  $\text{DMSO-d}_6$   $\delta$ /ppm): 8.53 (dd,  $J = 8.7, 1.2$  Hz, 1H, **5'**), 8.29 – 8.24 (m, 1H, **8**), 8.15 (dd,  $J = 8.5, 1.3$  Hz, 1H, **8'**), 7.92 (ddd,  $J = 8.8, 6.9, 1.5$  Hz, 1H, **6**), 7.82 (ddd,  $J = 8.5, 6.8, 1.4$  Hz, 1H, **6'**), 7.73 – 7.71 (m, 1H, **5**), 7.70 – 7.68 (m, 1H, **7**), 7.65 (ddd,  $J = 8.3, 6.8, 1.3$  Hz, 1H, **7'**), 7.33 (s, 1H, **3'**), 7.23 (s, 1H, **3**), 6.39 (s, 5H, **15**), 5.91 (ddt,  $J = 17.2, 10.5, 4.7$  Hz, 1H, **13'**), 5.19 (dd,  $J = 17.2, 2.1$  Hz, 1H, **14'**), 5.02 (dd,  $J = 10.4, 2.1$  Hz, 1H, **14'**), 4.68 – 4.60 (m, 2H, (**12 or 14**) + **13**), 4.51 (s, 5H, **15'**), 4.38 (d,  $J = 10.4$  Hz, 1H, **12 or 14**), 4.14 (dd,  $J = 6.2, 2.7$  Hz, 1H, **12 or 14**), 3.97 – 3.87 (m, 2H, (**12 or 14**) + **12'**), 3.31 (s, 6H, **11**), 3.15 (s, 6H, **11'**). Unknown species: 7.71, 4.81, 4.70, 3.55. Solvents: DMSO (2.50), acetone (2.08). Standard: TMS (0.00). The spectra were measured and assigned with the help of PD Dr. Daniel Häussinger (University of Basel).

### Formation of [CpRu(QA-Biot)(Allyl)]PF<sub>6</sub> (**18**): Effect of different solvents

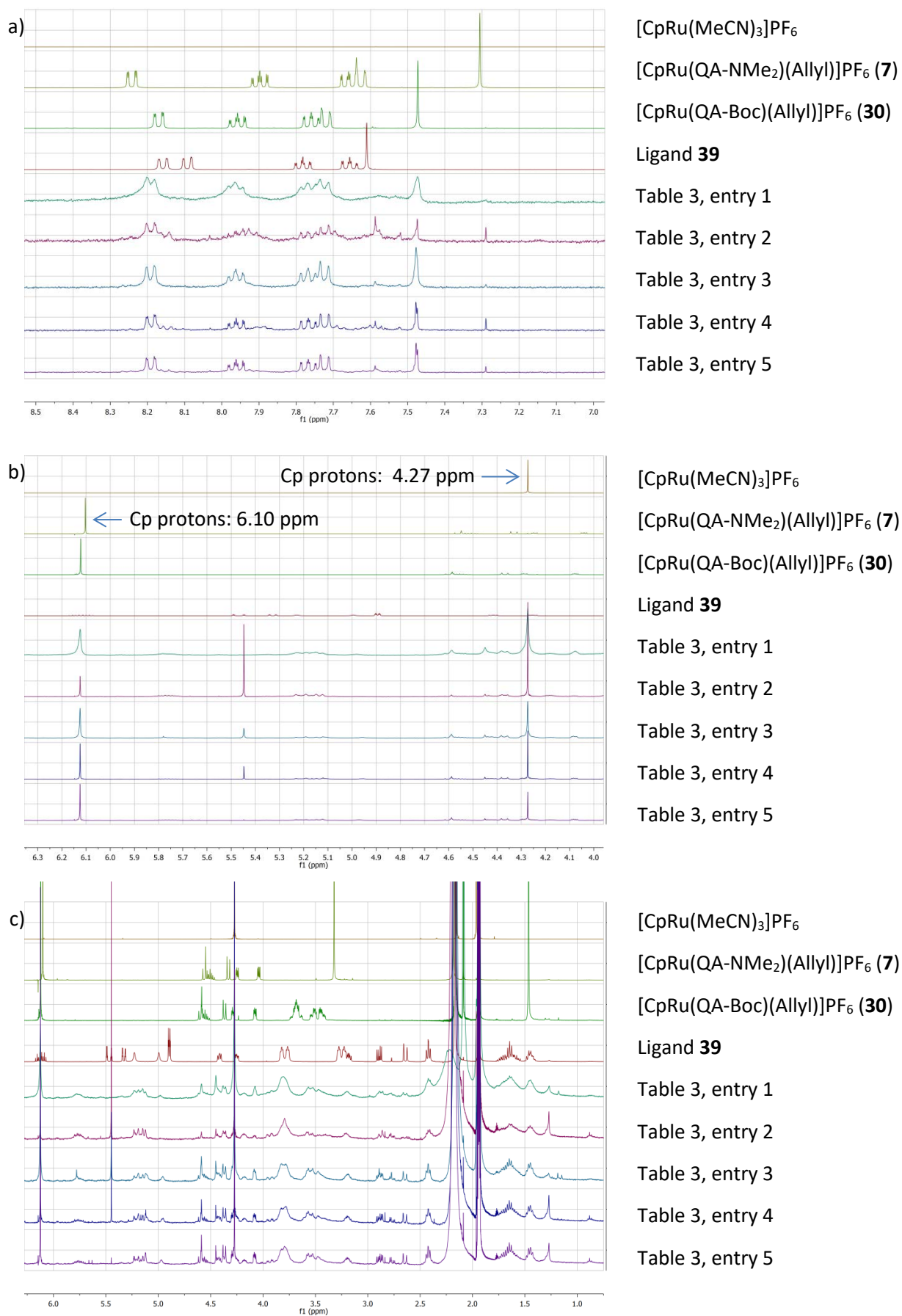
Formation of the complex [CpRu(QA-Biot)(Allyl)]PF<sub>6</sub> (**18**) from [CpRu(MeCN)<sub>3</sub>]PF<sub>6</sub> and biotinylated ligand **39** (Scheme 5, green arrows) was tested in different solvents with different ligand:metal ratios and orders of addition. Synthesis of the non-biotinylated metal complexes [CpRu(QA-NMe<sub>2</sub>)(Allyl)]PF<sub>6</sub> (**7**) and [CpRu(QA-Boc)(Allyl)]PF<sub>6</sub> (**30**) were performed in acetone.<sup>94</sup> A summary of all experiments is collected in Table 3 and a comparison of the determined <sup>1</sup>H NMR spectra is presented in Figure 6.

Table 3: Formation of [CpRu(QA-Biot)(Allyl)]PF<sub>6</sub> (**18**) from [CpRu(MeCN)<sub>3</sub>]PF<sub>6</sub> and biotinylated ligand **39**.<sup>a</sup>

Entry	Solvent	Ligand:Metal	Added first	Obtained product
1	Acetone (dry)	1:1	[CpRu(MeCN) <sub>3</sub> ]PF <sub>6</sub>	Brownish solid
2	MeCN (dry)	1:1	Ligand <b>39</b>	Dark red-brown solid
3	DCM (dry)	1:1	[CpRu(MeCN) <sub>3</sub> ]PF <sub>6</sub>	Yellow-ochre solid
4	DCM (dry)	2:1	[CpRu(MeCN) <sub>3</sub> ]PF <sub>6</sub>	Yellow-orange solid
5	DCM (dry)	1:1	Ligand <b>39</b>	Yellow-orange solid <sup>b</sup>

<sup>a</sup>Reaction, stoichiometry and conditions: see Scheme 5. <sup>b</sup>HRMS analysis confirmed the presence of the desired ruthenium complex [CpRu(QA-Biot)(Allyl)]PF<sub>6</sub> (**18**), annex spectrum on page 189.

In the aromatic region of the spectra (Figure 6, a), the five reactions show peaks (and peak splitting) with very similar chemical shifts compared to the ruthenium complex bearing the Boc protected piperazine linker ([CpRu(QA-Boc)(Allyl)]PF<sub>6</sub> (**30**)). The peaks are clearly shifted compared to the ones from the free ligand (**39**), thus indicating a change in the chemical environment (i.e. coordination to the ruthenium). However, besides a singlet peak at 6.12 ppm, which is very close to the one arising from the Cp protons of [CpRu(QA-Boc)(Allyl)]PF<sub>6</sub> (**30**), all spectra also display a singlet at 4.27 ppm, which was detected for the Cp protons of the metal precursor [CpRu(MeCN)<sub>3</sub>]PF<sub>6</sub> as well (Figure 6, b). This result suggested that all of the test reactions still contain a fraction of the initial metal precursor. The peaks at 6.12 ppm and 4.27 ppm were integrated. The reactions in DCM (Table 3, entries 3 – 5) revealed ratios 6.12/4.27 ppm > 0.8, whereas for the reactions in acetone (Table 3, entry 1) and MeCN (Table 3, entry 2) ratios of 0.6 and 0.4 were obtained, respectively. Formation of the complex [CpRu(QA-Biot)(Allyl)]PF<sub>6</sub> (**18**) seems therefore to be slightly favored in DCM. Indeed, the presence of the desired complex [CpRu(QA-Biot)(Allyl)]PF<sub>6</sub> (**18**) for the reaction in DCM (Table 3, entry 5) could be detected by HRMS analysis. However, no pure product was obtained using the conditions collected in Table 3.



**Figure 6: Comparison of <sup>1</sup>H NMR spectra for the reactions collected in Table 3.**

The three pictures display different parts of the spectra: a) 8.5 – 7.0 ppm, b) 6.3 – 4.0 ppm and c) 6.1 – 0.7 ppm. All spectra were determined in MeCN-d<sub>3</sub>. Intensities of the individual spectra were adjusted for better visibility.

In addition, DOSY spectra were determined for the reaction mixture in MeCN (Table 3, entry 2) as well as for the metal precursor and the free biotinylated ligand. With DOSY NMR measurements, the diffusion coefficient ( $D$ ) of a molecule in the considered solvent can be determined, which allows to estimate the molecular weight (MW) of the compound.<sup>114</sup> Often the Einstein-Stokes equation ( $D = k \cdot T / (6 \cdot \pi \cdot \eta \cdot R_h)$  with  $k$ : Boltzmann constant,  $T$ : absolute temperature,  $\eta$ : solvent viscosity,  $R_h$ : hydrodynamic radius) or an empirically derived power law ( $D = K \cdot MW^\alpha$  with  $K$ : molecule dependent constant,  $\alpha$ : coefficient depending on the shape of the particle) are applied.<sup>115</sup> Approximating the molecules as spherical objects, the diffusion coefficient depends on the molecular weight as follows:  $1/MW \propto D^3$ . For the metal precursor  $[\text{CpRu}(\text{MeCN})_3]\text{PF}_6$  a diffusion coefficient of  $1.92 \cdot 10^{-9} \text{ m}^2/\text{s}$  and for the ligand **39** a diffusion coefficient of  $1.26 \cdot 10^{-9} \text{ m}^2/\text{s}$  were determined. For the reaction mixture a smaller diffusion coefficient of  $1.15 \cdot 10^{-9} \text{ m}^2/\text{s}$  was determined, suggesting that this species has a larger hydrodynamic radius, and therefore in a first approximation, a larger molecular weight. The ratio of the cubed diffusion coefficients  $(D_{\text{ligand}}/D_{\text{reaction}})^3$  with a value of 1.315 is in good agreement with the ratio of the molecular weights  $MW_{\text{complex}}/MW_{\text{ligand}} = 1.317$ . Thus, the DOSY NMR experiments strongly indicate that a complexation of the biotinylated ligand **39** with the metal precursor  $[\text{CpRu}(\text{MeCN})_3]\text{PF}_6$  has taken place.

#### **Analysis of $[\text{CpRu}(\text{QA-Biot})(\text{Sol.})]\text{PF}_6$ (**27**) in DMF**

Formation of the complex  $[\text{CpRu}(\text{QA-Biot})(\text{Sol.})]\text{PF}_6$  (**27**) in DMF from a 1:1 mixture of metal precursor  $[\text{CpRu}(\text{MeCN})_3]\text{PF}_6$  and biotinylated ligand **26** (Scheme 5, black arrows) was followed by DOSY NMR analysis. From the spectra, the following diffusion coefficients were extracted:  $D_{\text{metal precursor}} = 4.35 \cdot 10^{-10} \text{ m}^2/\text{s}$ ,  $D_{\text{ligand}} = 3.00 \cdot 10^{-10} \text{ m}^2/\text{s}$  and  $D_{\text{reaction}} = 2.70 \cdot 10^{-10} \text{ m}^2/\text{s}$ . Again here, a smaller diffusion coefficient was obtained for the reaction mixture compared to the free biotinylated ligand, indicating an increase in molecular weight. The ratio of the cubed diffusion coefficients  $(D_{\text{ligand}}/D_{\text{reaction}})^3$  with a value of 1.372 is in proximity of the ratio of the molecular weights  $MW_{\text{complex}}/MW_{\text{ligand}} = 1.509$ , keeping in mind that these molecules are not spherical. A complexation of the ligand **26** with the metal precursor  $[\text{CpRu}(\text{MeCN})_3]\text{PF}_6$  most likely took place, although no unique ruthenium complex was formed as highlighted by  $^1\text{H-NMR}$  analysis (Figure 7). However, when this mixture was applied to an aqueous solution of streptavidin, a crystal structure of the defined complex  $[\text{CpRu}(\text{QA-Biot})(\text{H}_2\text{O})] \cdot \text{Sav S112M-K121A}$  was determined (chapter 2.1.4).

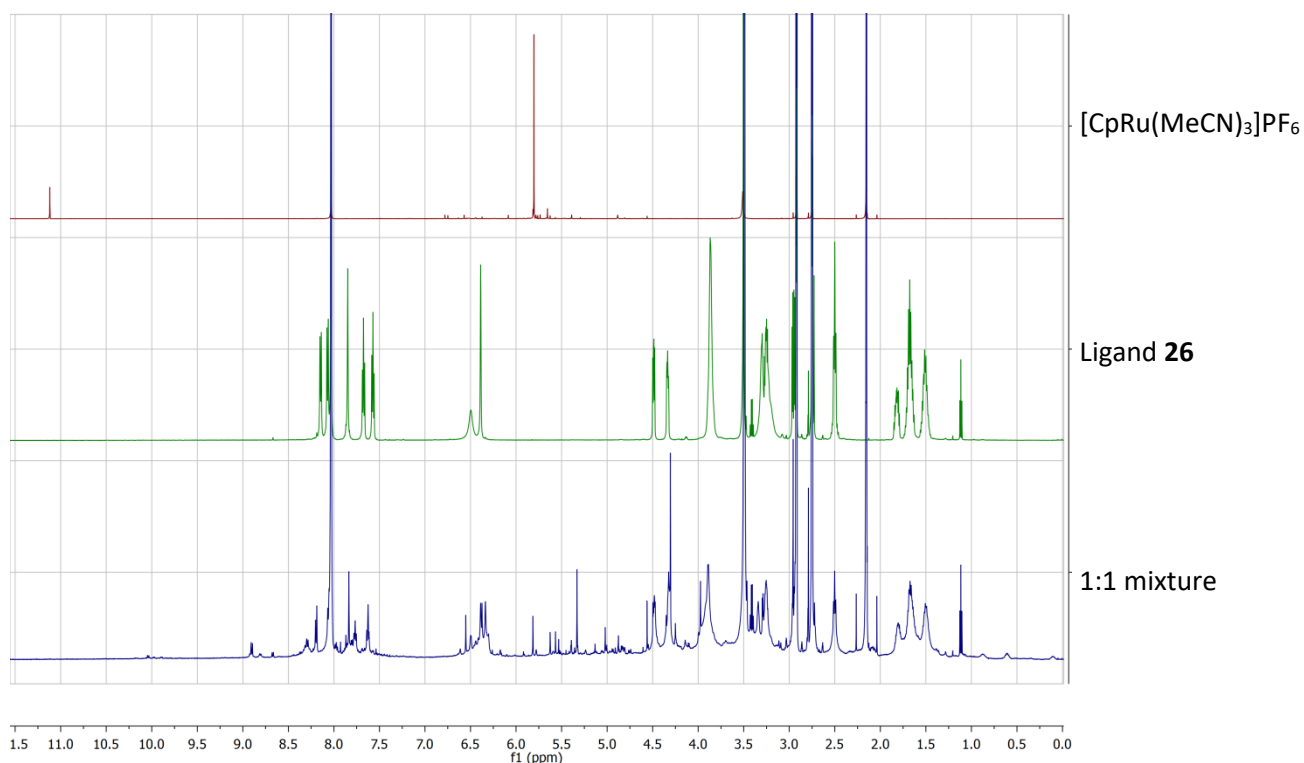


**Figure 7: Comparison of the  $^1\text{H}$  NMR spectra of  $[\text{CpRu}(\text{MeCN})_3]\text{PF}_6$  (red), ligand **26** (green) and a 1:1 mixture of both (blue).**

All spectra were determined in  $\text{DMF-d}_7$ . Intensities of the individual spectra were adjusted for better visibility. The spectra were measured with the help of PD Dr. Daniel Häussinger (University of Basel).

### 2.1.3 Assembly of the artificial allylic deallocase

In a next step, the catalytically active artificial allylic deallocase was assembled by incorporation of the ruthenium complex  $[\text{CpRu}(\text{QA-Biot})(\text{Sol.})]\text{PF}_6$  (**27**) in wild-type streptavidin. Binding of the biotinylated cofactor to streptavidin was highlighted by HABA-titration. In this titration assay 2-(4'-hydroxybenzeneazo)benzoic acid (HABA), a small streptavidin-binding molecule ( $K_d \approx 10^{-4} \text{ M}$ )<sup>39, 116</sup>, is displaced by the biotinylated ruthenium cofactor with a higher affinity. This process is accompanied by a color change from red (HABA bound to avidin,  $\lambda_{\text{abs., max}} = 496 \text{ nm}$ ) to yellow (HABA free in solution,  $\lambda_{\text{abs., max}} = 439 \text{ nm}$ )<sup>117</sup>, which leads to a decrease in absorption at 506 nm. Titration curves were determined for D-biotin, the biotinylated ligand (**26**) and the biotinylated ruthenium complex  $[\text{CpRu}(\text{QA-Biot})(\text{Sol.})]\text{PF}_6$  (**27**). All results are summarized in Figure 8.

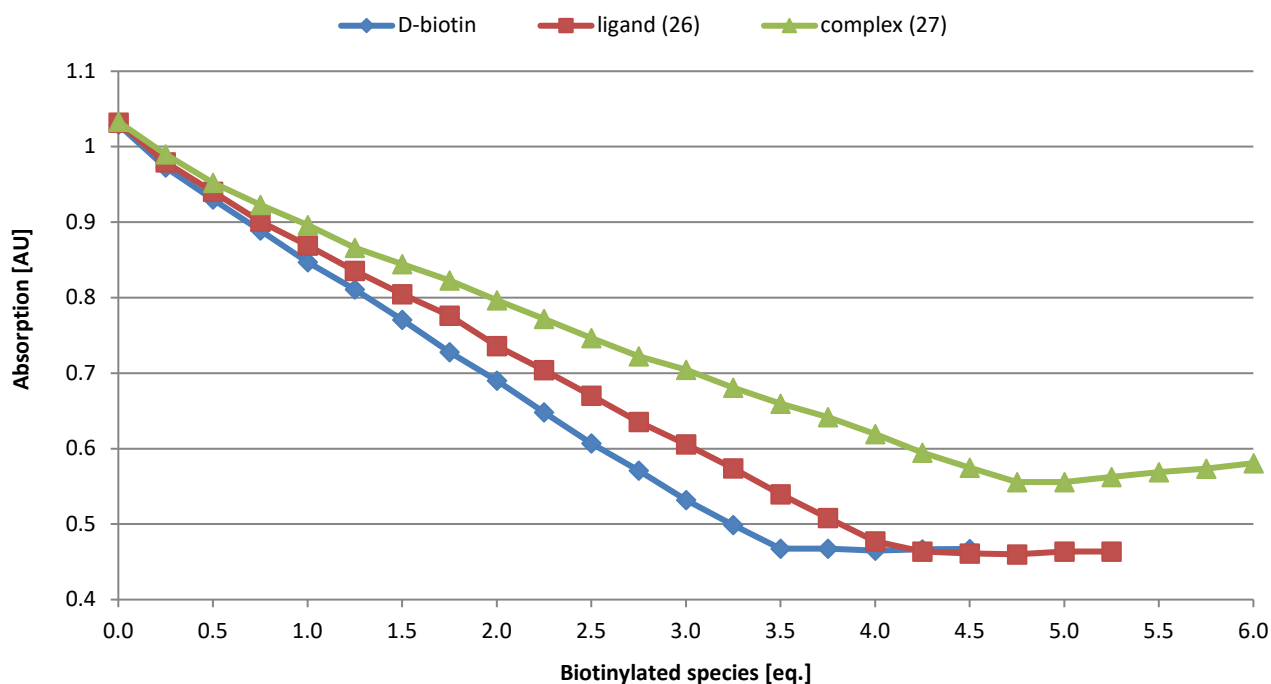


**Figure 8: HABA-titration for a designed artificial allylic deallocase.**

Conditions: 7.1  $\mu\text{M}$  streptavidin wild-type (tetramer), 1.1 mM HABA in phosphate buffer (20 mM, pH 7.4). Absorption determined at 506 nm.

For all compounds tested (D-biotin, ligand **26**, and complex **27**) a linear decrease in absorption was obtained upon titration, indicating that these molecules are able to displace HABA and bind to streptavidin. Thus, the affinities of these compounds for streptavidin are significantly higher than HABA ( $K_d < 10^{-4}$  M). The titration curves for D-biotin and the biotinylated ligand **26** (Figure 8, blue and red curves) stay at the same absorption level as soon as all streptavidin-bound HABA molecules are released. In case of complex **27** (Figure 8, green curve), a small increase in absorption was determined after the addition of more than 4.7 eq. of the biotinylated species. This is caused by the complex **27** itself, which has an absorption band around 506 nm. For D-biotin, the equivalence point was reached at 3.5 eq. of biotinylated species per streptavidin tetramer, which is in good agreement with the B4F-assay (3.4 biotin binding sites per tetramer; see chapter 4.2.8). Ligand **26** and complex **27** revealed equivalence points at 4.2 and 4.7 eq. of biotinylated species, respectively. These too high values are potentially caused by impurities (e.g. traces of water) in those samples, leading to a smaller concentration of the active biotinylated species than actually calculated. In general, concentrations of solutions should be directly determined by photospectrometric methods rather than by weighing and dissolving a certain amount of the compound. However, the binding of the biotinylated ruthenium complex [CpRu(QA-Biot)(Sol.)]PF<sub>6</sub> (**27**) was established by determination of its streptavidin-bound X-ray crystal structure (see chapter 2.1.4).



### 2.1.4 Crystal structure determination

A crystal structure of the streptavidin mutant S112M-K121A with the bound biotinylated ruthenium cofactor [CpRu(QA-Biot)(H<sub>2</sub>O)]PF<sub>6</sub> (**27**) was determined (Figure 9, PDB entry 6FH8)<sup>118</sup>. The protein as well as the biotinylated 2-quinolinecarboxylate ligand are clearly resolved in the crystal structure and there is a unique electron density for the ruthenium ion. The cyclopentadienyl ligand however can adopt two positions, indicated by the smeared electron density. The crystal structure revealed that two biotinylated ruthenium cofactors fit well into two adjacent binding sites. The methionine residue at position 112 is oriented on top of the aromatic rings of the 2-quinolinecarboxylate ligand. Thus, potentially a C-H... $\pi$  interaction is formed which could stabilize the ruthenium complex. Replacement of the lysine residue at position 121 by an alanine removes a positive charge and generates more space in the biotin binding vestibule (i.e. the substrate coordinated to the ruthenium cofactor might better fit). The observed higher catalytic activity of the artificial allylic deallocase bearing the mutations S112M and K121A might be explained by these two features. A more detailed analysis of the crystal structure is published elsewhere.<sup>118</sup>

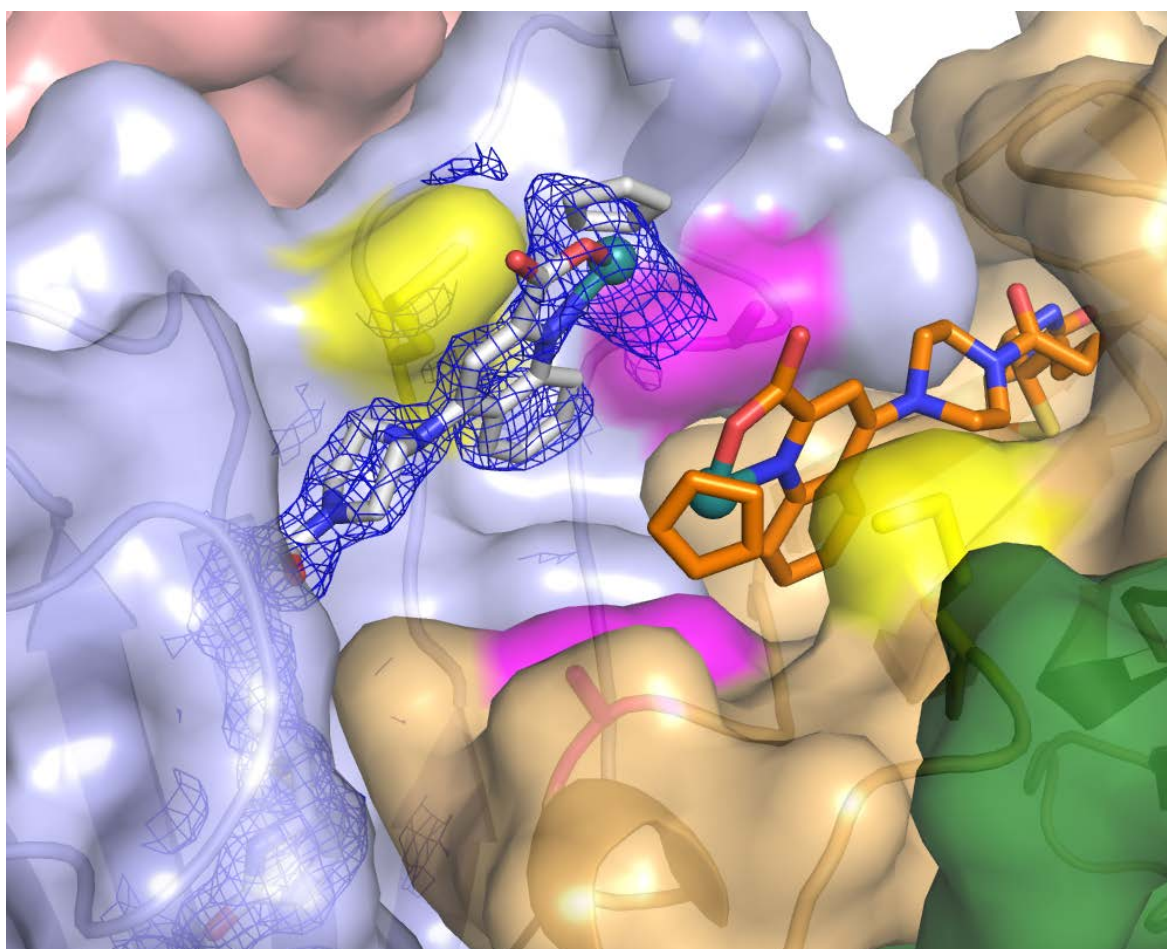


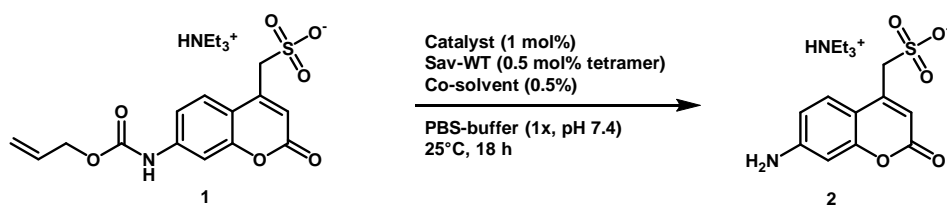
**Figure 9: Crystal structure of the artificial allylic deallocase [CpRu(QA-Biot)(H<sub>2</sub>O)]PF<sub>6</sub> (**27**) · Sav-S112M-K121A.<sup>118</sup>**

The four monomers of streptavidin are displayed in cartoon style with half-transparent surface (blue, red, brown, green). Mutations S112M and K121A are highlighted in yellow and pink, respectively. The electron density map of one cofactor is displayed as fine blue wires. The biotinylated ruthenium cofactors are displayed as stick (element color code: C = grey/orange, N = blue, O = red, S = yellow, Ru = turquoise ball). The crystal structure was determined by Dr. Tillmann Heinisch (Ward group, University of Basel) and deposited in the Protein Data Base (PDB entry 6FH8).<sup>118</sup>

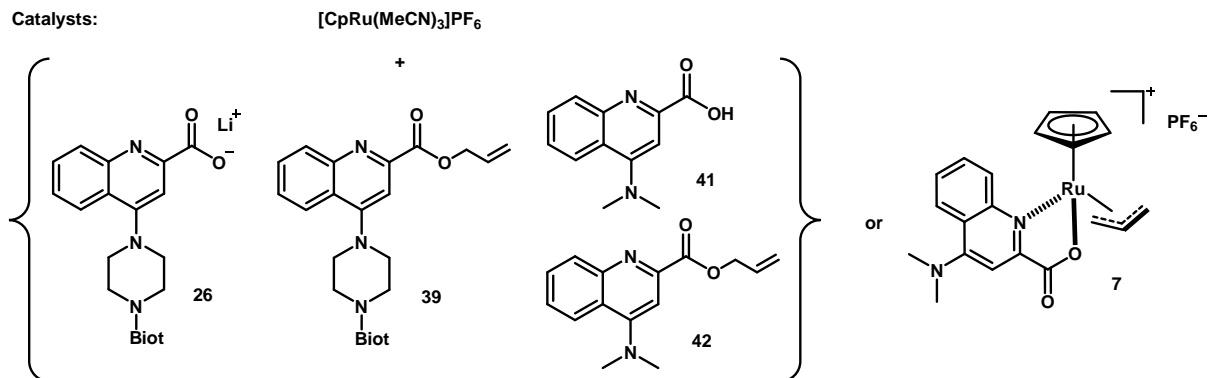
## 2.2 *In vitro* catalysis with an artificial allylic deallocase

### 2.2.1 Catalysis with a caged coumarin substrate

The activity of the designed artificial allylic deallocase was tested for the cleavage of an *O*-allyl carbamate protected coumarin (**1**, Table 4). The substrate was synthesized according to literature procedures from Kanaoka *et al.*<sup>119</sup>, Ryckelynck *et al.*<sup>120</sup> and Meggers *et al.*<sup>94</sup> The catalytic activity of the ruthenium complex [CpRu(QA-NMe<sub>2</sub>)(Allyl)]PF<sub>6</sub> (**7**) designed by Meggers *et al.*<sup>94</sup> was tested for the uncaging of the *O*-allyl carbamate protected coumarin **1** (Scheme 6). Thereby, a catalyst concentration of 5 μM (= 1 mol%) was applied. High reactivity was obtained when this complex was prepared in DMSO (Table 4, entry 1). In sharp contrast, the activity dramatically dropped if other solvents such as MeCN, DMF or EtOH were used (Table 4, entries 2 - 4). However, the reactivity could be restored if DMSO was added to a solution of complex **7** in MeCN (Table 4, entry 5). This phenomenon is discussed in more details in chapter 2.1.2. Mixtures of the ruthenium precursor [CpRu(MeCN)<sub>3</sub>]PF<sub>6</sub> with the biotinylated ligand **26** were tested (Table 4, entries 6 - 10). The best results were obtained with DMF as co-solvent, in which a 2.5-fold increase in conversion of the artificial metalloenzyme compared to the free cofactor was obtained (9% conv. with free cofactor vs. 25% conv. with Sav-WT). A biotinylated ligand containing an allyl ester group (**39**) and the non-biotinylated analogues (**41** and **42**) were tested as well, leading to no improvement in activity (Table 4, entries 11 - 13). Low yields and no protein acceleration were obtained. Finally, the catalytic activity of the individual components (ruthenium precursor and ligands) was investigated separately (Table 4, entries 14 - 19). The results unambiguously demonstrated that neither the ruthenium precursor [CpRu(MeCN)<sub>3</sub>]PF<sub>6</sub> nor one of the (biotinylated) ligands alone is catalytically active. A 1:1 mixture of [CpRu(MeCN)<sub>3</sub>]PF<sub>6</sub> and ligand **26** in DMF performed best. The 2.5-fold increase in activity in combination with Sav-WT vs. free ruthenium cofactor represented an ideal starting point for a screening campaign of different streptavidin isoforms.



Catalysts:



Scheme 6: Deprotection of caged coumarin **1** catalyzed by artificial allylic deallocases (Table 4).

Table 4: Catalytic performance of artificial allylic deallocases towards the deprotection of coumarin **1** (Scheme 6).<sup>a</sup>

Entry	Catalyst (1 mol%)	Co-solvent	Conversion [%] <sup>b</sup>	
			No protein	Sav-WT
1	<b>7</b>	DMSO	96	94
2	<b>7</b>	MeCN	7	9
3	<b>7</b>	DMF	9	9
4	<b>7</b>	EtOH	3	3
5	<b>7</b>	MeCN + DMSO <sup>c</sup>	87	n.d.
6	[CpRu(MeCN) <sub>3</sub> ]PF <sub>6</sub> + <b>26</b>	DMSO	5	3
7	[CpRu(MeCN) <sub>3</sub> ]PF <sub>6</sub> + <b>26</b>	MeCN	12	7
8	[CpRu(MeCN) <sub>3</sub> ]PF <sub>6</sub> + <b>26</b>	DMF	9	25
9	[CpRu(MeCN) <sub>3</sub> ]PF <sub>6</sub> + <b>26</b>	EtOH	3	8
10	[CpRu(MeCN) <sub>3</sub> ]PF <sub>6</sub> + <b>26</b>	Allyl alcohol <sup>d</sup>	14	25
11	[CpRu(MeCN) <sub>3</sub> ]PF <sub>6</sub> + <b>39</b>	DMF	13	3
12	[CpRu(MeCN) <sub>3</sub> ]PF <sub>6</sub> + <b>41</b>	DMF	12	10
13	[CpRu(MeCN) <sub>3</sub> ]PF <sub>6</sub> + <b>42</b>	DMF	7	4
14	[CpRu(MeCN) <sub>3</sub> ]PF <sub>6</sub>	DMF	1	1
15	[CpRu(MeCN) <sub>3</sub> ]PF <sub>6</sub>	Allyl alcohol <sup>d</sup>	1	1
16	<b>26</b>	DMF	1	1
17	<b>39</b>	DMF	1	1
18	<b>41</b>	DMF	1	1
19	<b>42</b>	DMF	1	1

<sup>a</sup>Reaction conditions: 500  $\mu$ M substrate **1**, 1 mol% catalyst, 0.5 mol% Sav-WT (tetramer), PBS-buffer (1x, pH 7.4), 0.5% co-solvent, 25°C, 18 h. The catalyst was dissolved in the co-solvent and added to the aqueous buffer containing the protein and the substrate.

<sup>b</sup>The conversion was determined by fluorescence of the product **2** from single reactions. <sup>c</sup>Complex **7** was dissolved in MeCN followed by the addition of an equal amount of DMSO, resulting in a total co-solvent concentration of 1.0% in the reaction mixture. <sup>d</sup>Reaction time = 29 h.

### 2.2.2 *In vitro* screening of streptavidin mutants

In order to identify promising residues for mutagenesis, the optimized biotinylated ruthenium cofactor [CpRu(QA-Biot)(Sol.)]PF<sub>6</sub> (**27**) was docked into streptavidin (Figure 10). The docking revealed that the catalytically active ruthenium center is most likely closely surrounded by the residues S112, K121 and L124. Other residues in close distance to the cofactor include, amongst others, the amino acids P64, A65, D67, R84, H87, T114, N118, H127 and D128 (see also chapters 2.3.2 and 2.5). In an initial screen, a nearly complete site-saturation library at the positions S112 and K121 was tested (all mutants except S112I, K121I and K121T). For the other positions, a selection of mutants available within the Ward research group was tested. Finally, double and triple mutants as well as elongated loop constructs and combinations of loops with promising single mutants were tested. The results of this screening campaign are summarized in Figure 11.

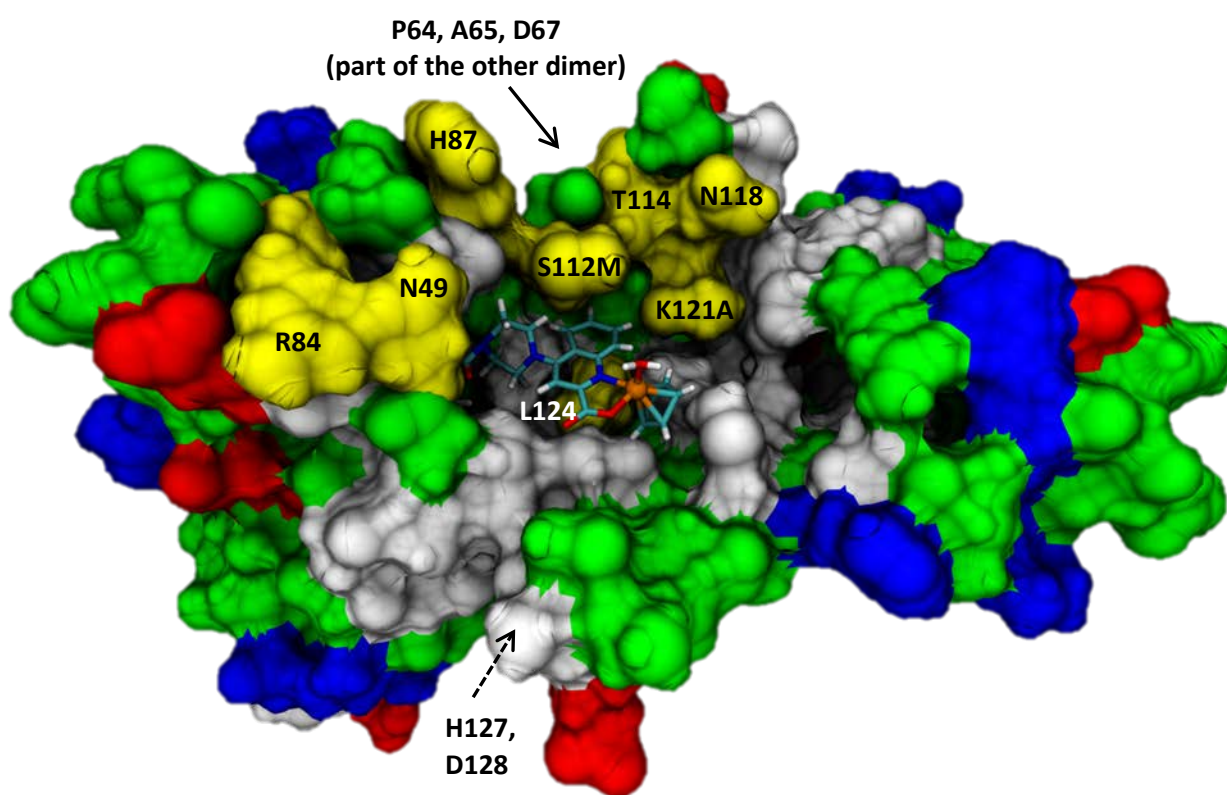


**Figure 10: Protein-ligand docking of [CpRu(QA-Biot)(H<sub>2</sub>O)] (**27**) in Sav S112M-K121A (dimer).**

A biotin anchor was modelled into a crystal structure of [CpRu(QA)(Allyl)]PF<sub>6</sub> (**5**) (Cambridge Structural Database Refcode: NAJLUG)<sup>85</sup> and the complete ruthenium cofactor (allyl ligand was replaced by a water molecule) was docked into a crystal structure of streptavidin (Protein Database entry: 3PK2).<sup>60</sup> The docking was performed with the dimer of streptavidin. Protein in surface representation (color code for the residues: white = apolar, green = polar, red = acidic, blue = basic), biotinylated ruthenium complex represented as sticks (elements: H = white, C = cyan, N = blue, O = red, S = yellow, Ru = orange ball). Residues targeted for mutagenesis (see: Figure 11) are highlighted in yellow. For clarity, only residues from one of the two adjacent binding sites are labelled. For details of the docking procedure see chapter 4.2.1. Docking was done by Dr. Vincent Lebrun (University of Basel).

Good catalytic activities were obtained for single mutants at the positions S112 (S112A, S112L, S112M), K121 (K121A, K121L, K121R) and L124 (L124G). Especially the mutants S112M, K121R and L124G displayed significant increase in catalytic activity compared to Sav-WT or the free ruthenium cofactor.

However, no general trend for preferred side chains at the positions S112 and K121 was identified, except that negatively charged amino acids such as aspartate or glutamate as well as cysteine residues or structure breaking prolines performed poorly. Surprisingly, the mutant containing a methionine at position S112 showed an increased catalytic activity (see also chapter 2.1.4). At position L124, small amino acids proved beneficial, which may be caused by the limited free space underneath the ruthenium cofactor (Figure 10).

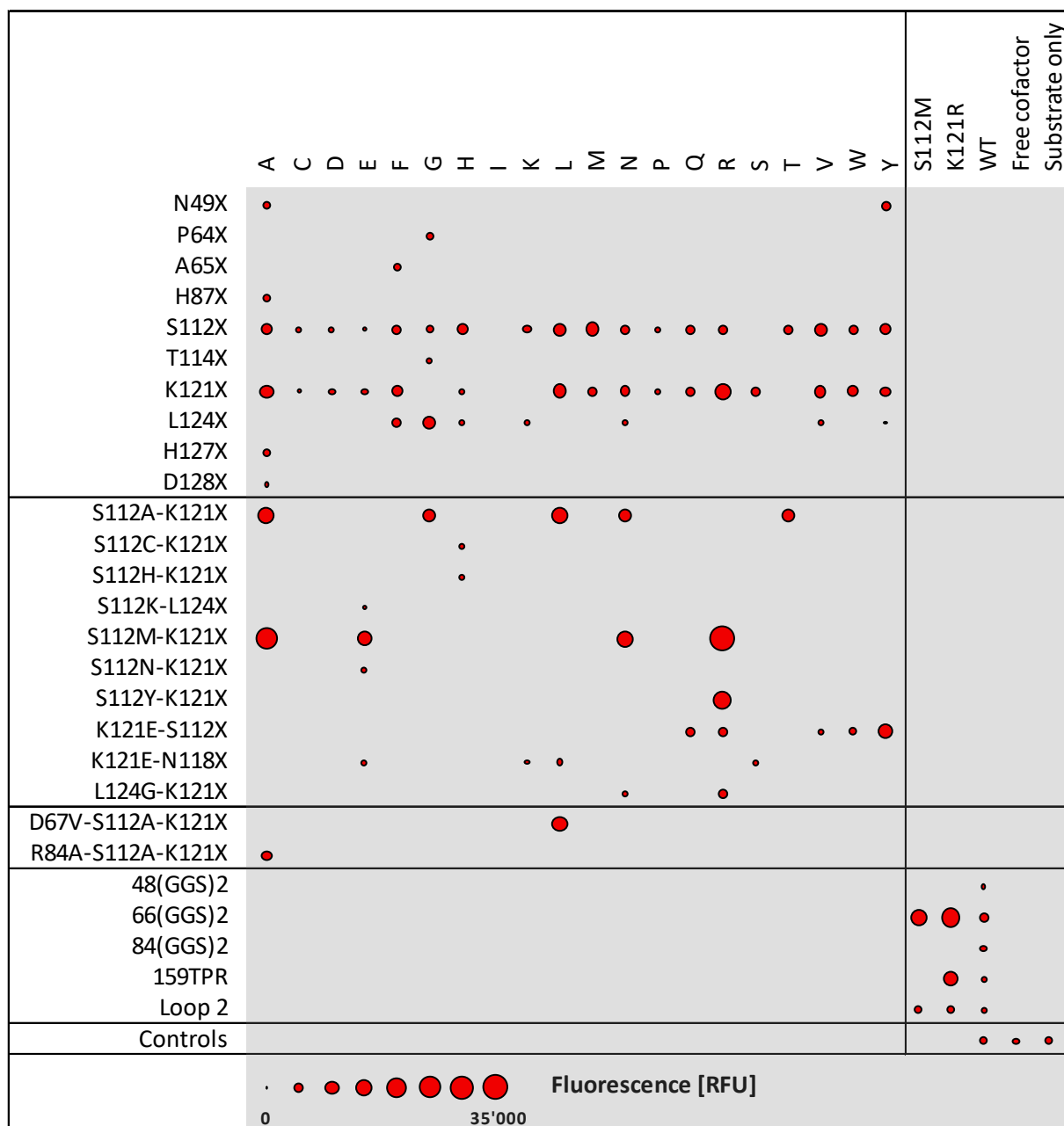


**Figure 11: Screening of streptavidin mutants for the uncaging of coumarin 1.**

Activities of the mutants are displayed as “bubble chart”, in which the size of the bubbles corresponds to the determined fluorescence of the product. Reaction: see Scheme 6. The reaction conditions were adapted in the following way: 500  $\mu$ M coumarin substrate **1**, 2  $\mu$ M ruthenium cofactor **27** (in DMF), 4  $\mu$ M streptavidin (free biotin binding sites), PBS-buffer (1x, pH 7.4), 0.5% DMF, 30°C, 300 rpm shaking, 18 h. Fluorescence of product **2** was determined at  $\lambda_{ex.} = 395$  nm and  $\lambda_{em.} = 460$  nm from single reactions. List with all the numerical values: see Annexes, Table 15. The following proteins showed a reduced solubility in the used reaction buffer: N49Y, S112P, K121N-L124G, K121R-L124G, 66(GGS)<sub>2</sub>-K121R, 159TPR and 159TPR-K121R.

Having obtained these promising results for streptavidin single mutants, selected double mutants at positions S112X-K121X, N118X-K121X and K121X-L124X were tested (see also Table 9, entries 25-30). Thereby, a synergetic effect was obtained for the combinations of activated single mutants such as S112A, S112M, K121A and K121R. Especially the combination S112M-K121R revealed a highly increased catalytic activity. For the single mutant S112M a 2.9-fold and for the single mutant K121R a 3.7-fold higher fluorescence compared to streptavidin wild-type was obtained, respectively. The combined double mutant S112M-K121R exhibited a 7.1-fold higher overall fluorescence. Compared to the free cofactor, the double mutant S112M-K121R yielded a 16.3-fold higher fluorescence. The double mutant S112Y-K121R, displayed almost the same activity (15.6-fold increase in fluorescence compared to the free ruthenium cofactor). Inspired by these results, elongated streptavidin loop mutants including 66(GGS)<sub>2</sub>, 159TPR and Loop2 were tested (Table 9, entries 31-35). Promising results were obtained for the 66(GGS)<sub>2</sub>-loop mutant, revealing a 1.3-fold higher conversion than Sav-WT. Combination with activated single mutants led again to a further increase in catalytic activity (66(GGS)<sub>2</sub>-S112M: 4.1-fold, 66(GGS)<sub>2</sub>-K121R: 4.7-fold). A selection of the best performing mutants was rescreened in triplicate to highlight the increased catalytic activity (Figure 12). The best performing double mutant, Sav-S112M-K121R, was finally combined with additional single mutations in an *in vivo* screen (chapter 2.3.2).

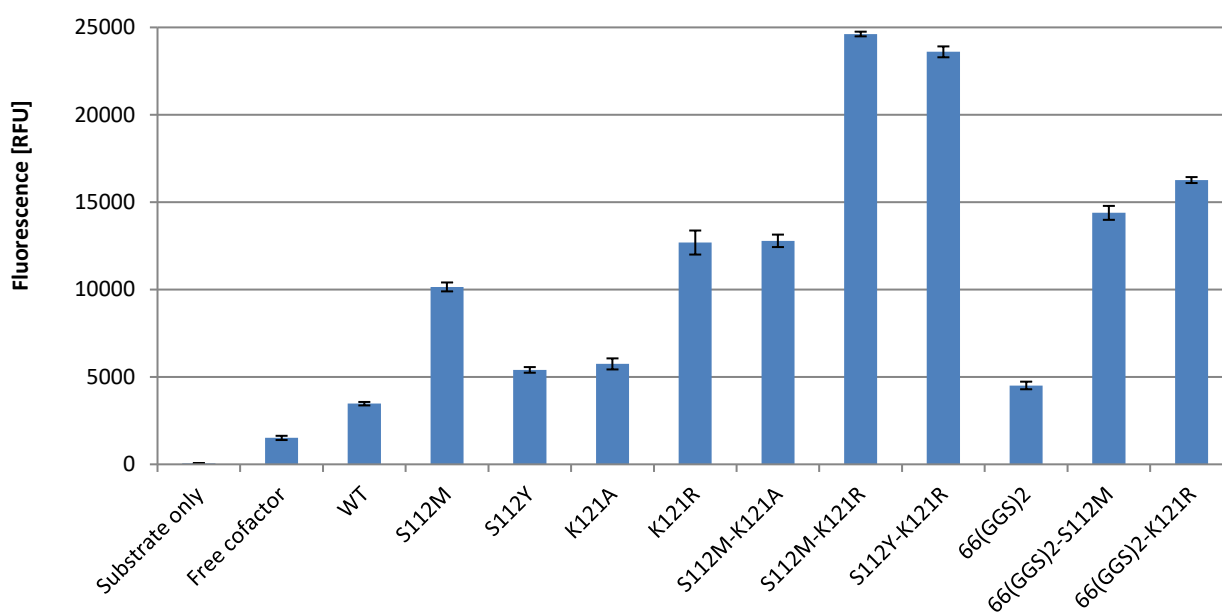


**Figure 12: Rescreening of the best streptavidin mutants for the uncaging of coumarin 1.**

Reaction: see Scheme 6. Reaction conditions: see Figure 11. Error bars =  $\pm 1$  standard deviation of a triplicate measurement.

## 2.3 Catalysis on the surface of *E. coli* cells

Engineered *E. coli* cells, displaying selected proteins on their surface, are applied, amongst others, in whole-cell bio-catalysis<sup>121-123</sup>, in the identification of enantioselective enzymes<sup>124</sup> or in surface-tagging applications.<sup>125</sup> In order to install the proteins of interest on the surface of *E. coli* cells, several outer membrane anchoring systems have been developed.<sup>126</sup> Cell surface display brings along many advantages, in the evolution of enzyme catalysts and their practical application as well as in the development of cascade reactions. In the first one, it allows to screen large enzyme libraries since the individual members do not have to be extracted and purified in a time consuming process (e.g. fluorescence activated droplet sorting (FADS): see chapter 2.3.3). Issues along with the uptake of required cofactors and substrates into the cell as well as with the subsequent release of the product cannot occur (see chapter 3: catalysis in the periplasm). The product can be separated by filtration and the catalyst (*E. coli* cells) can potentially be recycled. Cell surface displayed non-natural enzymes can also be combined with natural enzymes to engineer cascade reactions. Furthermore, by having a compartmentalization between one enzyme outside (e.g. an artificial metalloenzyme) and a potential cascade partner inside the cell, also two incompatible (artificial) enzymes can be combined (see chapter 3: cascade reactions).

### 2.3.1 Design of a surface displayed streptavidin construct

Streptavidin surface display on *E. coli* cells, using the autotransporter domain AIDA-I (adhesin involved in diffuse adherence), was reported by Pyun *et al.*<sup>127</sup> The presence of streptavidin on the surface of *E. coli* was confirmed by SDS-PAGE analysis of the outer membrane proteins as well as by flow cytometry analysis of cells labeled with a biotinylated fluorophore. The expression level was estimated to be  $\sim 1.6 \cdot 10^5$  molecules/cell, which would correspond to a streptavidin concentration of  $\sim 0.26 \mu\text{M}$  at a cell density of  $\text{OD}_{600} = 1$ , assuming that 1 ml of a cell solution at  $\text{OD}_{600} = 1$  contains  $\sim 10^9$  cells.<sup>128</sup>

Herein, we designed a surface displayed streptavidin variant based on the Lpp-ompA anchoring system.<sup>129-130</sup> The used construct is based on the work of Georgiou *et al.*<sup>131</sup> The empty pBAD33 plasmid (provided by Prof. Dehio, University of Basel), containing a Para promoter and an araO operon, was equipped with the gene-cassette Lpp-ompA-T7-Sav (Lpp-ompA provided by Dr. Pinheiro, University College London) to express and translocate the surface-displayed streptavidin (Figure 13). This cassette is composed of the Lpp signal peptide, followed by the first 9 amino acids of the *E. coli* lipoprotein Lpp and a truncated version (amino acids 46 to 159) of the outer-membrane protein ompA. Via a glycine linker, the full-length streptavidin (amino acids 13 to 159; codon optimized DNA-sequence<sup>132</sup>) bearing an N-terminal T7 solubility tag is attached. The expression of this construct is induced by addition of L-arabinose (L-ara). The cloned plasmid was transformed into *E. coli* TOP10(DE3) cells for expression and catalysis. The presence of the designed streptavidin construct on the surface of *E. coli* cells was evaluated by i) labelling of the cells with a biotinylated fluorescent dye and ii) staining of the cells with a fluorescent streptavidin antibody system.

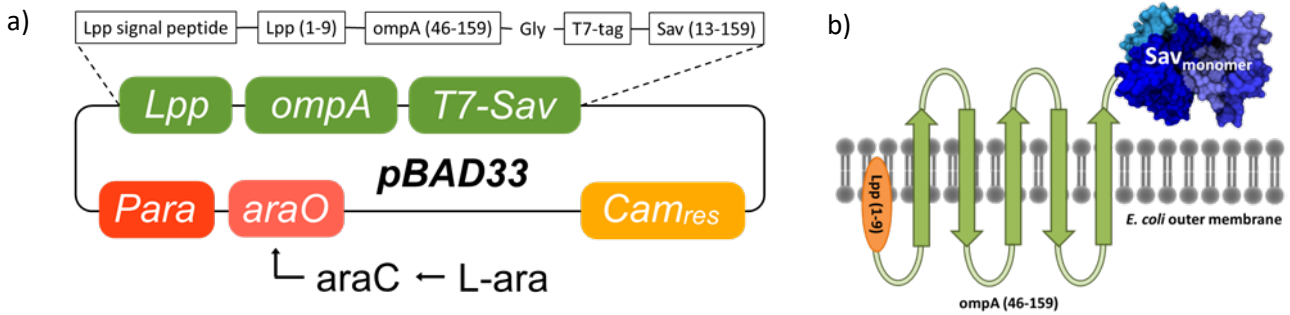


**Figure 13: pBAD33 plasmid map and location of the Lpp-ompA-T7-Sav surface construct on the outer membrane of *E. coli*.**

a) Schematic map of the pBAD33 plasmid containing the Para promoter, the araO operon, the Lpp-ompA-T7-Sav gene cassette as well as an antibiotic resistance against chloramphenicol (Cam<sub>res</sub>). The empty pBAD33 plasmid was provided by the research group of Prof. Dehio (University of Basel). The Lpp-ompA gene was provided by Dr. Vitor Bernardes Pinheiro (University College London). Cloning was carried out by Dipl.-Biol. Juliane Klehr and Dr. Tillmann Heinisch (Ward group, University of Basel). b) Location of the Lpp-ompA anchor in the outer membrane of *E. coli* with the T7-Sav pointing towards the medium.

In the first method, cells expressing the surface streptavidin were incubated with a biotinylated Atto-dye (Atto-565-biotin), washed and analyzed by flow cytometry (Figure 14). Induced cells, both Sav-WT and mutant S112M-K121A, displayed a highly increased fluorescence compared to non-induced cells or cells containing an empty pBAD33 plasmid. This indicates that the Lpp-ompA-T7-Sav construct is indeed expressed and can bind to a biotinylated fluorophore. However, this finding did not completely establish the presence of the streptavidin construct on the surface of *E. coli*, since the applied fluorophore also tends to enter the periplasmic space.<sup>64</sup> At this point, testing the integrity of the outer membrane is also crucial.<sup>129</sup>

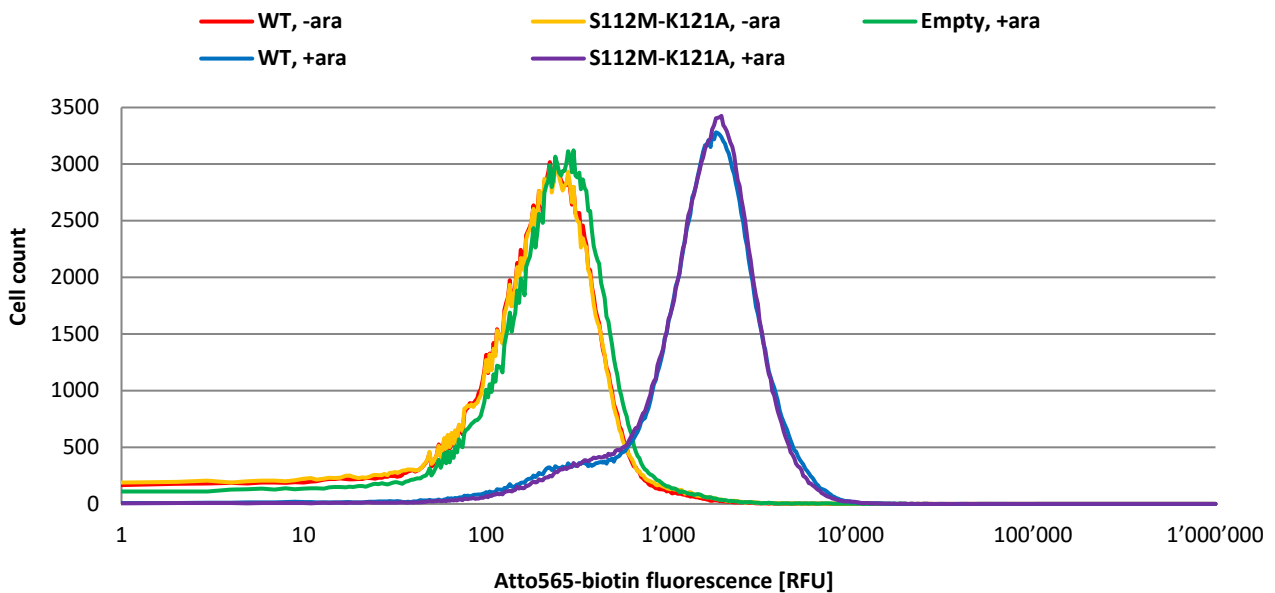


**Figure 14: Atto-565-biotin staining of *E. coli* cells expressing surface-displayed streptavidin.**

Reaction steps: 1) Sav surface expression in *E. coli* TOP10(DE3) cells containing the pBAD33 plasmid (LB-medium, 30 °C, 4 h, induction with 0.2 % L-arabinose (ara)); 2) Incubation with Atto565-biotin (2 μM in PBS-buffer, pH 7.4) for 30 min; 3) 2x washing of cells with PBS-buffer (pH 7.4); 4) Fluorescence analysis of the cells by flow cytometry.



A staining of the cells with a streptavidin antibody, which itself is too big to enter the periplasm, was performed. Cells were first treated with a mouse-anti-streptavidin antibody, followed by labeling with a fluorescein isothiocyanate-tagged goat-anti-mouse antibody. The cells were then analyzed by flow cytometry and fluorescence microscopy (Figure 15). Three types of cells were investigated: cells expressing cytoplasmic streptavidin, cells expressing periplasmic streptavidin and cells containing the surface streptavidin construct. Both, cells with the cytoplasmic streptavidin construct as well as cells with the periplasmic streptavidin construct revealed only a low fluorescence, whereas cells containing the surface-displayed streptavidin were shifted to higher fluorescence intensities in the histogram of the flow cytometry analysis (Figure 15, a). The same result was obtained for the fluorescence microscopy analysis. Cells containing the surface displayed streptavidin glowed, whereas almost no fluorescence was obtained for the periplasmic streptavidin construct (Figure 15, b). These results clearly indicate that the designed Lpp-ompA-T7-Sav construct is expressed and located on the outer membrane of the *E. coli* cells, and that the streptavidin is pointing towards the medium. However, at this point it remains still unclear in which oligomeric state the surface displayed streptavidin is. In the Lpp-ompA-T7-Sav construct, streptavidin is expressed and displayed on the *E. coli* surface as monomer. It is assumed that four of these surface-displayed constructs can be combined to form a streptavidin tetramer. Monomeric streptavidin still shows a moderate affinity for biotin, but its thermal stability is significantly decreased compared to the tetramer (monomeric Sav-V55T-T76R-L109T-W120A-V125R:  $K_d = 123$  nM,  $T_m = 31^\circ\text{C}$ ).<sup>47</sup> The thermal stability as well as the affinity for biotin of the monomeric streptavidin can be increased by introduction of additional stabilizing mutations<sup>47</sup> or by combination with protein sequences from rhizavidin.<sup>133</sup> Mutations, which interrupt the dimer-dimer interface in the tetrameric state (e.g. V55T, T76R, L109T or V125R)<sup>46</sup> could be introduced into our surface-displayed streptavidin construct as well. Obtaining a lower fluorescence intensity in the Atto-565-biotin staining or different results in catalysis might indirectly confirm the hypothesis that the surface-displayed streptavidin construct forms a tetramer. In a different approach, the surface-displayed streptavidin constructs can be crosslinked using bis[sulfosuccinimidyl] suberate<sup>134</sup>, assuming that they are present on the *E. coli* surface as a tetramer. After cell lysis, the oligomeric state of the (crosslinked) surface-displayed constructs can be investigated by SDS-PAGE or Western Blot.<sup>135-136</sup> Alternatively, the proposed tetrameric nature of the surface-displayed streptavidin construct might be investigated by Förster resonance energy transfer (FRET).<sup>137-138</sup>

Based on the positive results obtained in the Sav-antibody staining experiment, catalytic deprotection of the caged coumarin substrate **1**, applying these surface-displayed streptavidin constructs, was tried next. Cells containing the pBAD33 plasmid were cultivated and loaded with the biotinylated ruthenium cofactor [CpRu(QA-Biot)(Sol.)]PF<sub>6</sub> (**27**). Potentially residual cofactor was washed away, caged substrate was added and the cells were incubated overnight. The performance of the Sav-WT construct as well as the activity of the previously identified promising double mutant S112M-K121A (see also Figure 12) was investigated.

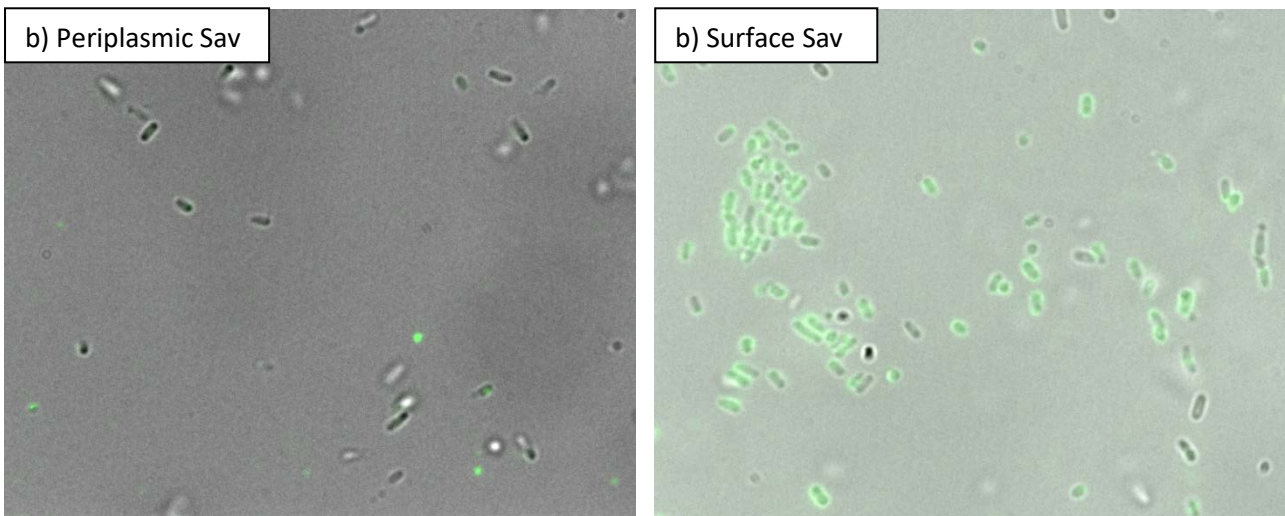
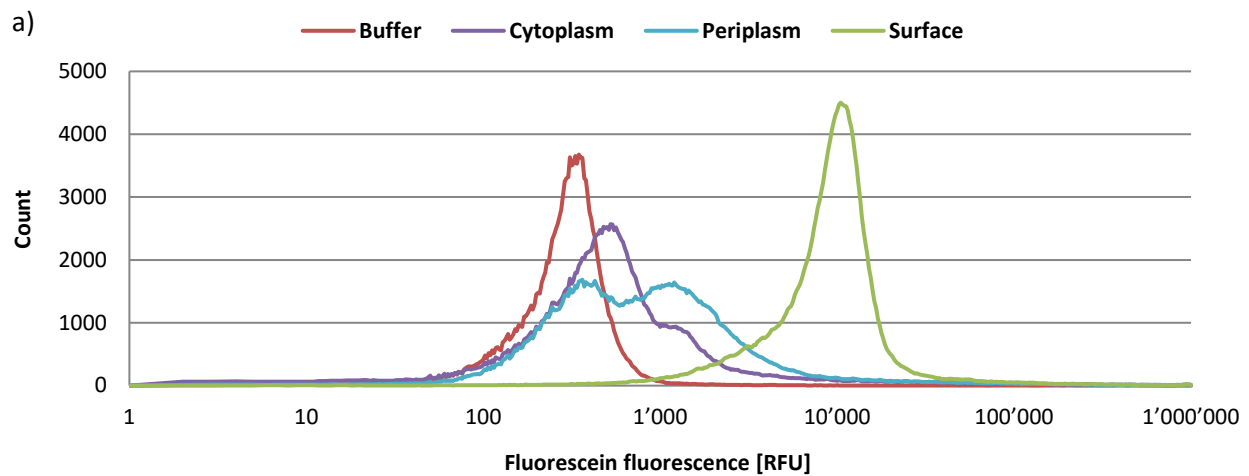


**Figure 15: Sav-antibody staining of *E. coli* cells expressing surface-displayed streptavidin.**

a) Flow cytometry analysis of cytoplasmic, periplasmic and surface-displayed streptavidin in *E. coli* TOP10(DE3). Cells were labelled with a primary mouse-anti-streptavidin antibody in combination with a secondary fluorescein isothiocyanate-tagged goat-anti-mouse antibody. b) Fluorescence microscopy pictures of the cell cultures (merged white-light and fluorescence picture). Baumann and Kleanthous *et al.* found, that outer-membrane proteins tend to accumulate at the poles of the cells when they are expressed.<sup>139</sup> Antibody staining experiments and fluorescence analysis were performed by Dr. Tillmann Heinisch (Ward group, University of Basel) with the help of Dr. Rosario Vanella (group of Prof. Michael Nash, University of Basel) according to the protocol of Wittrup *et al.*<sup>140</sup>

Cells containing an empty pBAD33 vector and two samples containing purified ArMs were tested as controls (Figure 16). For cells containing an empty pBAD33 plasmid (i.e. they do not contain the Lpp-ompA-T7-Sav gene cassette) as well as for all non-induced samples (-ara; i.e. expression of the surface streptavidin construct is not switched on), only a minimal background fluorescence was observed. For the induced wild-type construct (WT, +ara) a minor fluorescence was determined, whereas the double mutant (S112M-K121A, +ara) revealed a highly increased activity. 12-fold higher fluorescence intensity was determined for mutant S112M-K121A compared to the wild-type construct. Compared to the non-induced double mutant (S112M-K121A, -ara), a >30-fold increase in fluorescence intensity was determined for the induced one (S112M-K121A, +ara), which expressed the surface streptavidin.

The surface displayed double mutant S112M-K121A even exceeded the activity of 1  $\mu\text{M}$  purified wild-type metalloenzyme (1  $\mu\text{M}$  ArM-WT). The determined standard deviations for triplicate measurements are small (<15%), thus indicating a good reproducibility of the assay.

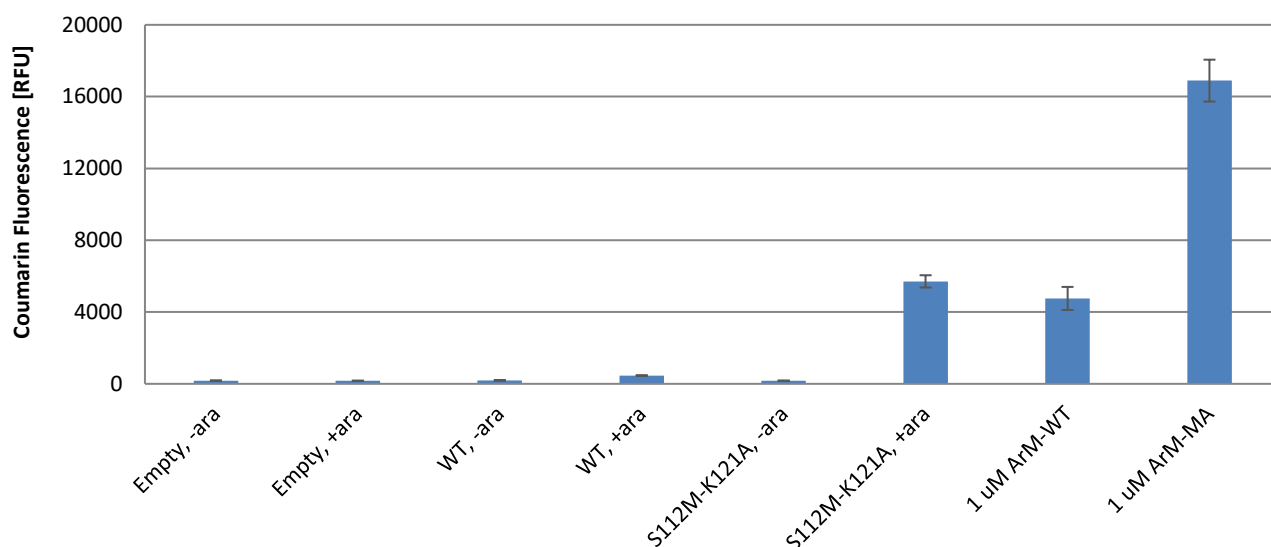


**Figure 16: Deprotection of caged coumarin 1, applying ArMs displayed on the surface of *E. coli* cells.**

Reaction steps: 1) Sav surface expression (see Figure 14); 2) Normalization of the cell density to  $\text{OD}_{600} = 2.0$ ; 3) Exchange of the medium with PBS-buffer (pH 7.4) containing 2  $\mu\text{M}$  ruthenium cofactor  $[\text{CpRu}(\text{QA-Biot})(\text{Sol.})]\text{PF}_6$  (**27**), incubation for 30 min on ice; 4) Exchange of the medium with PBS-buffer (pH 7.4) containing 500  $\mu\text{M}$  allyl-coumarin substrate **1**; 5) Catalysis: 16 h, 30  $^\circ\text{C}$ , 310 rpm shaking, followed by determination of the fluorescence ( $\lambda_{\text{ex.}} = 395 \text{ nm}$ ,  $\lambda_{\text{em.}} = 460 \text{ nm}$ ). Displayed values are corrected for cell density ( $\text{OD}_{600}$ ). Error bars =  $\pm 1$  standard deviation of a triplicate measurement. ara = L-arabinose (inducer), WT = wild-type Sav, MA = mutant S112M-K121A. The screening was performed with the help of Dr. Tillmann Heinisch (Ward group, University of Basel).

The results clearly demonstrated that: i) streptavidin can be expressed and displayed on the outer membrane of *E. coli* bacteria, ii) the surface-displayed streptavidin can bind a biotinylated fluorophore (Atto565-biotin) as well as a biotinylated ruthenium complex ( $[\text{CpRu}(\text{QA-Biot})(\text{Sol.})]\text{PF}_6$  (**27**)), and iii) the surface-displayed ArMs are functional and their activity can be optimized by mutagenesis. Surface-displayed streptavidin constructs are thus suitable for directed evolution of the performance of the designed artificial allylic deallocases. The mutants can be expressed and displayed on the surface of *E. coli* cells without time intensive extraction and purification of the individual streptavidin variants (see chapter 4.2.8). The cofactor and the substrate can be added to the cell cultures and the product formation can be monitored by determination of the fluorescence. This simple experimental setup allows for high-throughput screening in the 96-well plate format. Thus, a library of streptavidin variants containing mutations at several promising positions within the biotin binding vestibule can be examined.

### 2.3.2 Screening of surface-displayed streptavidin libraries

In order to expand the mutant diversity for the deprotection of coumarin substrate **1** using the artificial allylic deallocase Sav · [CpRu(QA-Biot)(Sol.)]PF<sub>6</sub>, potentially promising positions in the biotin binding vestibule of streptavidin were scanned. Beside the previously identified residues S112 and K121 (chapter 2.2.2), especially the loops between the β-barrels of streptavidin were examined. As shown by Jeschek *et al.*<sup>64</sup> and Hesticová *et al.*<sup>63</sup>, an increased loop flexibility in general resulted in a higher catalytic activity of the artificial metalloenzyme. A similar effect was reported by Tezcan *et al.* for an artificial β-lactamase.<sup>141</sup> Crystal structures of catalytically highly active Sav mutants (PDB entries 5F2B<sup>64</sup> and 6ESS<sup>63</sup>) revealed increased B-factors for the loop regions. In order to increase the flexibility of those loops, hydrogen bond networks within the loops were targeted for deletion as well as removal of steric clashes (Figure 17).

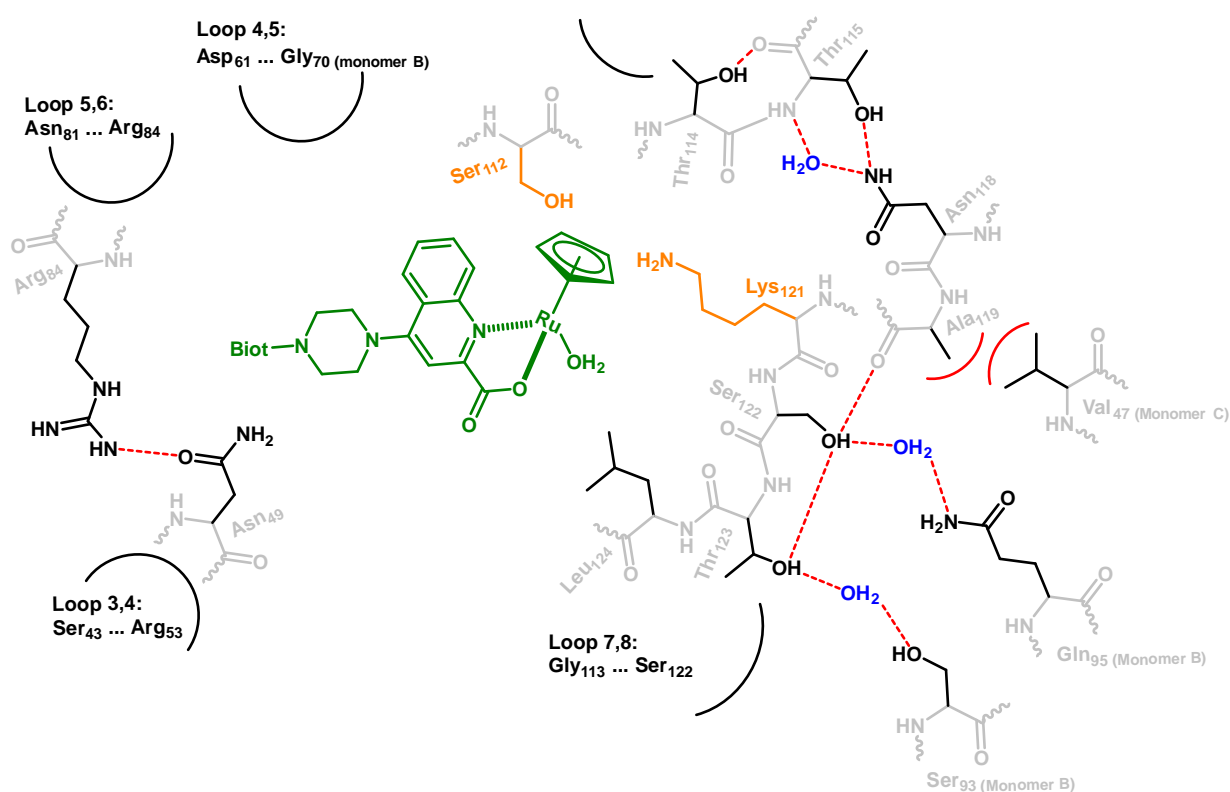


**Figure 17: Hydrogen bond network in the loop regions of streptavidin.**

Hydrogen bonds: dotted red lines, preserved waters: blue, protein backbone: grey, side chains: black, previously identified residues with mayor influence on catalysis (Ser<sub>112</sub>, Lys<sub>121</sub>): orange, biotinylated ruthenium cofactor: green, possible steric clashes: red curves.

With these aims in mind, the following 7 residues were selected for mutagenesis: Val<sub>47</sub> and Ala<sub>119</sub> (minimizing steric clashes), Asn<sub>49</sub> (interrupting hydrogen bond to Arg<sub>84</sub>), Thr<sub>114</sub> and Asn<sub>118</sub> (interrupting hydrogen bonds to Thr<sub>115</sub>), Ser<sub>122</sub> (interrupting extended hydrogen bond network) and Leu<sub>124</sub> (directly located underneath the ruthenium cofactor). Their location in the streptavidin binding vestibule is illustrated in Figure 18.

Single site saturation mutagenesis libraries were created for these 7 residues. Each position was tested independently. The best performing mutants at each position were then combined, hoping for a synergetic effect, resulting in a highly evolved variant.

Alternatively, an iterative saturation mutagenesis approach could have been used, in which the best hit of the first single site library serves as a template for the next (iterative) mutagenesis round.<sup>142</sup> In this strategy, propitious mutations can be identified in a straightforward way. However, this approach does not allow a time-saving parallel screening of the single site libraries.

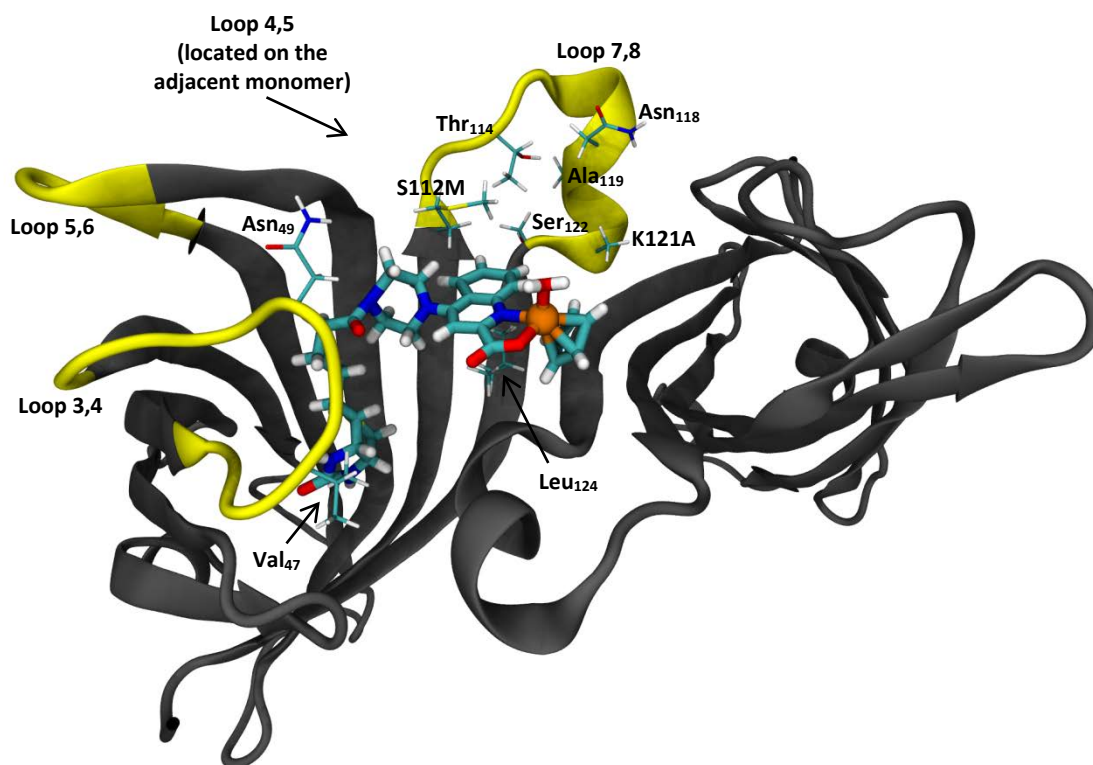


**Figure 18: Selected mutagenesis sites in the artificial allylic deallcose [CpRu(QA-Biot)(H<sub>2</sub>O)]-Sav S112M-K121A.**

The biotinylated cofactor [CpRu(QA-Biot)(H<sub>2</sub>O)] (**27**) was docked into a crystal structure of streptavidin (Protein Database entry: 3PK2).<sup>60</sup> The docking was performed with the dimer of streptavidin (see chapter 4.2.1). Protein represented as grey cartoon. Biotinylated ruthenium complex represented as sticks (elements: H = white, C = cyan, N = blue, O = red, S = yellow, Ru = orange ball). Residues targeted for mutagenesis are highlighted as sticks (Val<sub>47</sub>, Asn<sub>49</sub>, Thr<sub>114</sub>, Asn<sub>118</sub>, Ala<sub>119</sub>, Ser<sub>122</sub> and Leu<sub>124</sub>). Residues targeted in the *in vitro* screening are displayed as well (Ser<sub>112</sub> and Lys<sub>121</sub>). For clarity, only residues from one of the two adjacent binding sites are displayed. Loop regions in close proximity to the ruthenium cofactor are highlighted as yellow tubes. These includes the following loops: loop 3,4: Ser<sub>45</sub>...Arg<sub>53</sub>, loop4,5: Asp<sub>61</sub>...Gly<sub>70</sub> (located on the adjacent monomer), loop 5,6: Asn<sub>81</sub>...Arg<sub>84</sub>, loop 7,8: Gly<sub>113</sub>...Ser<sub>122</sub>. Protein-ligand docking was done by Dr. Vincent Lebrun (University of Basel).

In order to generate the seven single site saturation mutagenesis libraries, PCR primers with degenerate codons were designed. The traditional NNK codon (32 codons/20 amino acids) requires an oversampling of 94 clones to ensure 95% coverage.<sup>143</sup> Alternatively, the so-called “22 codon trick” can be applied.<sup>144</sup> In this method, a mixture of primers with degenerate codons (NDT, VHG and TGG) is used, which reduces the screening effort to 66 clones per single site library. The seven single site saturation mutagenesis libraries were created applying the latter method.

Preparation of the libraries and screening was done by Dr. Tillmann Heinisch and BSc Brett Garabedian (Ward group, University of Basel). Based on the *in vitro* screening results (Figure 11 and Figure 12), the highly active double mutant S112M-K121R was selected as parent for the seven libraries. Thus, all members of these libraries are triple mutants (S112M-K121R + third single mutation).

The quality of each library was verified by analyzing the sequences of 13 randomly picked clones (e.g. analysis of the library S122X stated the following results: 4x wild-type, 8x unique mutant and 1x unclear sequencing result). Sequence analysis revealed a good quality for the libraries V47X, N49X, T114X, A119X, S122X and L124X. For the library at position N118 the PCR did not work satisfactorily. Thus, this library was not included in the screening. Overall, 6 single site saturation libraries with a total of 120 mutants were tested. The screening itself was performed in the 96-well plate format. 88 clones per library were picked, which led to a >95% statistical coverage of all possible mutants. The remaining 8 wells in the 96-well plate contained control samples including i) 2x pure medium to assure a sterile handling of the plates and to exclude any contamination, ii) 2x free biotinylated ruthenium cofactor, iii) 2x streptavidin wild-type, and iv) 2x mutant S112M-K121R. First, a complete 96-well plate only containing the mutant S112M-K121R was prepared. This was done to test the reliability of the screening protocol and to exclude any positional bias on the plate. Cell samples at the edges of a 96-well plate can potentially be better aerated and therefore show a faster proliferation or a higher protein expression. An equal distribution of cell growth and catalytic activity was obtained over the whole plate. A standard deviation of the fluorescence of the coumarin (**2**) of only 9% was determined. Afterwards, the libraries V47X, N49X, T114X, A119X, S122X and L124X were screened. For the library V47X, only clones with decreased activities compared to the S112M-K121R parent were found. The residue V47 is located in the biotin-binding loop and part of the interface between two adjacent monomers. Mutations replacing the valine seem not be tolerated at all. For the remaining 5 libraries (N49X, T114X, A119X, S122X and L124X), a selection of the best performing clones was rescreened. Clones, for which the increased activity compared to the S112M-K121R parent could be confirmed in the rescreening, were sequenced. The 7 best performing clones, displaying activities greater than the one from the parent plus two times the standard deviation, turned out to all contain the mutation S122N. This result clearly demonstrated the reliability of the assay to identify activated mutants. Compared to the parent S112M-K121R, the triple mutant S112M-K121R-S122N performed around 30% better in the *in vivo* screening. This triple mutant will be purified to determine whether the elevated activity is caused by the additional S122N mutation or is just an effect of different expression levels in the *E. coli* surface display. Combinations of this triple mutant with other single site libraries will be further investigated to evaluate any synergetic effects.<sup>118</sup> In addition, crystal structure analysis of the triple mutant S112M-K121R-S122N would be of high interest, since the side chain of the residue at position 122 is pointing away from the biotin-binding site (compare Figure 18). A mutation from serine to asparagine might induce a rearrangement of the backbone of loop 7,8 and thus initiate a structural change of the biotin binding vestibule.

With this screening assay in hand, medium-sized libraries can be investigated in reasonable times. Testing the seven single-site libraries, including preparation of the libraries and rescreening, took about 5 weeks. The working effort can be divided into i) preparation of the libraries including quality control (~2 weeks), ii) screening of the libraries (~2 weeks), and iii) rescreening and sequencing of the best hits (~1 week).

Since the complete assay was performed in 96-well plates (see chapter 4.2.4), it can be easily adapted for automated screening using robots. This would allow to screen up to 10`000 mutants per month. This number can be significantly increased if the screening is performed in micro-droplets in combination with fluorescence activated droplet sorting (FADS).

### 2.3.3 Micro-droplet system for ultrahigh-throughput screening

Fluorescence activated droplet sorting (FADS) is a very powerful tool for the directed evolution of enzymes. It combines compartmentalization, as given in microtiter plates, with the ultrahigh-throughput sorting capacity of conventional fluorescence activated cell sorting (FACS).<sup>145-146</sup> The individual members of a library are separately encapsulated in water-in-oil emulsions, which ensures a genotype-phenotype linkage.<sup>147</sup> The formed monodisperse droplets have diameters in the range of 5-120  $\mu\text{m}$ , which corresponds to internal volumes of approximately 0.05-1000  $\mu\text{L}$ .<sup>146</sup> The droplets can then be sorted based on their fluorescence intensity with frequencies of up to 2000  $\text{s}^{-1}$ .<sup>145</sup> This corresponds to a sorting capacity of up to 7.2 million droplets per hour. A "gedankenexperiment": an enzyme library with simultaneous site-saturation at five positions consists of  $20^5 = 3.2$  million members. This library could be sorted, including oversampling, in a few hours. This clearly demonstrates the potential of this method. FADS was applied, amongst others, in the directed evolution of artificial retro-aldolases<sup>148</sup>, arylsulfatases<sup>149</sup> and horseradish peroxidases.<sup>150</sup>

In this thesis, we aimed for the evolution of an artificial allylic deallocase ([CpRu(QA-Biot)(H<sub>2</sub>O)] (**27**) · Sav) for the deprotection of a caged coumarin substrate using droplet sorting. The formed fluorescent product, coumarin **2**, showed a long residence time (>5 days) inside of the droplets.<sup>120</sup> This is an indispensable requirement to avoid cross-contamination between different droplets. The microfluidic chip for the formation of the droplets was developed, produced and operated by MSc Philipp Rottmann (DBSSE, ETH Zürich), based on the work of Fischlechner and Hollfelder *et al.*<sup>151</sup> *E. coli* TOP10(DE3) cells, expressing the surface-displayed Lpp-OmpA-T7-Sav construct, were incubated with the biotinylated ruthenium cofactor. The excess of non-bound ruthenium complex was washed away. The cells were then, on the microfluidic chip, mixed with a solution of the caged substrate (**1**) and encapsulated in water-in-oil emulsions (Figure 19, a-c). Monodisperse droplets with a diameter of  $\sim 21 \mu\text{m}$  and an internal volume of  $\sim 5 \mu\text{L}$  were formed at a rate of  $\sim 10^4$  droplets per second. The *E. coli* cell solution that was used was diluted to an OD<sub>600</sub> of 0.2, which resulted in a final concentration of  $\sim 0.33$  cells/droplet, assuming that 1 ml of a cell solution at an optical density of OD<sub>600</sub> = 1 contains  $\sim 10^9$  cells.<sup>128</sup>

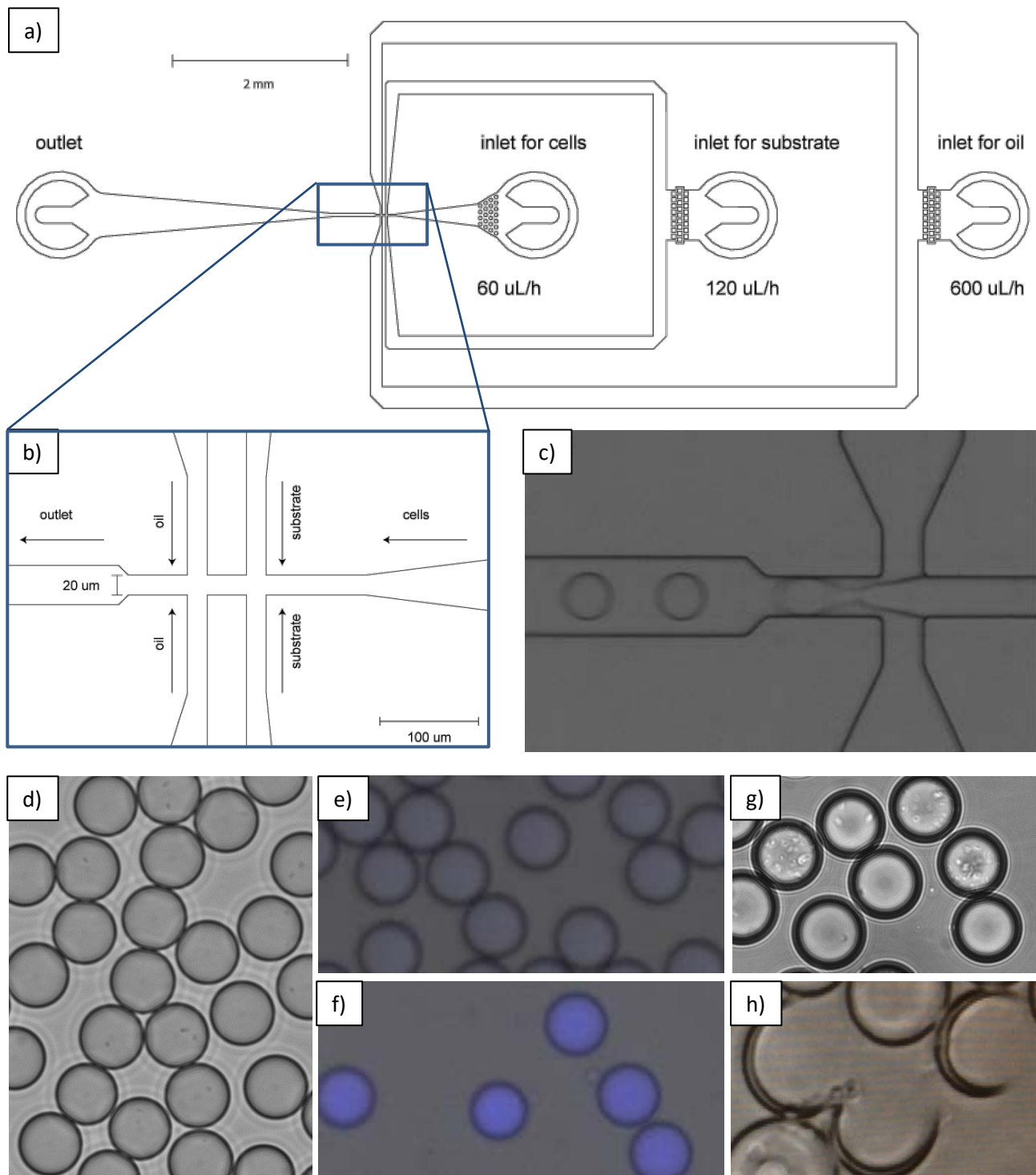


**Figure 19: Production of water-in-oil droplets on a microfluidic device.**

a) Design of the microfluidic chip for the production of water-in-oil emulsions. The chip contains three inlets: i) cell suspension (flow rate =  $60 \mu\text{L/h}$ ), ii) substrate solution (flow rate =  $120 \mu\text{L/h}$ ), and iii) fluorinated oil (flow rate =  $600 \mu\text{L/h}$ ), as well as an outlet for the produced droplets. b) Enlargement of the double junction of the microfluidic chip. Cells get first mixed with the substrate solution (junction at the righthand side) before they are encapsulated in the fluorinated oil (junction at the lefthand side). c) Formation of water-in-oil droplets at the water/oil junction with a rate of  $\sim 10^4$  droplets/second. The produced droplets are monodisperse with a diameter of  $\sim 21 \mu\text{m}$  and an internal volume of  $\sim 5 \text{ pL}$ . d) Water-in-oil droplets right after the production. A part of the droplets contain *E. coli* cells (little black dots). The picture was taken under bright field. e) Fluorescence microscopy picture of droplets containing  $500 \mu\text{M}$  coumarin substrate **1** (no cells), 216 ms exposure time. f) Fluorescence microscopy picture of droplets containing  $500 \mu\text{M}$  coumarin substrate **2** (no cells), 216 ms exposure time. g) Picture of encapsulated cells after overnight incubation. Proliferation of *E. coli* cells (white dots) was obtained. The picture was taken under bright field. h) Double emulsions (water-in-oil-in-water) with an approximate diameter of  $\sim 42 \mu\text{m}$  directly after the production in the microfluidic device. The microfluidic chip for the formation of the droplets was developed, produced and operated by MSc Philipp Rottmann (DBSSE, ETH Zürich), based on the work of Fischlechner and Hollfelder *et al.*<sup>151</sup>



Based on a Poisson distribution with  $\lambda = 0.33$ , 71.9% of the droplets should be empty, 23.7% should contain one cell, 3.9% should contain two cells and 0.4% should contain three or more cells (compare droplets in Figure 19 d). In order to avoid any false positives during the screening, every droplet should only contain one mutant. The cell solution should therefore be further diluted before encapsulation, although this means that a higher number of droplets have to be analyzed. However, the produced droplets were then incubated overnight and analyzed by fluorescence microscopy (Figure 19, e-g). A defined amount of droplets was treated with a surfactant to break the emulsions. The fluorescence intensity of the aqueous phase was then quantitatively determined (Table 5).

**Table 5: Uncaging of coumarin 1 applying *E. coli* surface-displayed artificial allylic deallocases in water-in-oil emulsions.**

Entry	Protein	Ru-cofactor <sup>d</sup>	Washing	Normalized fluorescence <sup>f</sup>
1	Buffer only	-	n.a.	0.67
2	Cells only <sup>b</sup>	-	Yes	1.00
3	Cells only <sup>b</sup>	2 $\mu$ M <sup>e</sup>	Yes	2.33
4	WT	2 $\mu$ M <sup>e</sup>	Yes	4.17
5	S112M-K121A	2 $\mu$ M <sup>e</sup>	Yes	6.50
6	Spiked <sup>c</sup>	2 $\mu$ M	n.a.	49.46

Reaction conditions: LB-medium (50 mM  $\text{NaH}_2\text{PO}_4/\text{Na}_2\text{HPO}_4$ , pH 7.4), 500  $\mu$ M coumarin substrate **1**, 25°C, 19 h. A detailed experimental procedure is given in chapter 4.2.5. <sup>a</sup>This sample did not contain the coumarin substrate. <sup>b</sup>Non-induced cells containing the Sav-WT construct. <sup>c</sup>Sample containing purified artificial metalloenzyme (4  $\mu$ M Sav-S112M-K121A (free biotin binding sites) + 2  $\mu$ M Ru-cofactor). <sup>d</sup>Ru-cofactor =  $[\text{CpRu}(\text{QA-Biot})(\text{H}_2\text{O})]$  (**27**). <sup>e</sup>The non-bound Ru-cofactor was washed away before encapsulation of the cells. <sup>f</sup>A defined amount of droplets was treated with a surfactant to break the emulsions. The fluorescence intensity of the aqueous phase was then analyzed with a plate reader ( $\lambda_{\text{ex.}} = 395 \text{ nm}$ ,  $\lambda_{\text{em.}} = 460 \text{ nm}$ ). The determined fluorescence intensities were normalized to the cellular background (entry 2).

Cells containing Sav-WT showed a 4.17-fold increase in fluorescence compared to the background, whereas the double mutant S112M-K121A revealed a 6.50-fold higher fluorescence intensity (Table 5, entries 4 and 5). For non-induced cells loaded with the ruthenium cofactor, a 2.33-fold increase was determined, which suggests that some of the cofactor unspecifically binds to the cells (Table 5, entry 3). The LB-medium itself also showed a background fluorescence at 460 nm (Table 5, entry 1). Compared to the sample containing purified ArM, the surface-displayed double mutant is not very active (Table 5, entry 6 vs. entry 5). However, these results suggest that catalysis, applying an *E. coli* surface-displayed artificial allylic deallocase, can be performed in micro-droplets.

Encapsulated single cells were able to proliferate inside of the droplets (see Figure 19, g), and thus potentially more surface-displayed streptavidin can be produced over time. Co-encapsulation of an excess of ruthenium cofactor at the beginning might therefore result in a higher concentration of the active artificial metalloenzyme accompanied by a potential increase in catalytic activity. The catalytic efficiency of the system could be improved, assuming that i) the non-bound cofactor is not catalytically very active and ii) the ruthenium cofactor is stable in LB-medium until a high amount of streptavidin is expressed. More important, the difference in the catalytic activity between droplets containing Sav-WT and droplets containing an improved mutant might be increased.

In the current system, the double mutant S112M-K121A led to a 1.6-fold higher fluorescence intensity compared to the wild-type (Table 5, entry 5 vs. entry 4). This difference decreased significantly compared with the catalysis in free solution (12.4-fold difference between Sav-WT and mutant S112M-K121A, see Figure 16). At this point, it should be taken into account that the catalysis in free solution was performed at a cell density of  $OD_{600} = 2.0$ , whereas one cell in a 5 pL droplet approximately corresponds to a density of  $OD_{600} = 0.07$ .

With the applied microfluidic chip, in addition to single emulsions (water-in-oil), also double emulsions (water-in-oil-in-water) can be produced. First single emulsions are produced as described in Figure 19, a-c. The single emulsions are then re-injected (in the former inlet for cells) with a simultaneous swapping of the substrate and the oil channel (Figure 19, a-b; the former substrate channel contains now fluorinated oil and the former oil channel contains now water). In this way, double emulsions with an approximate diameter of 42  $\mu\text{m}$  can be produced (Figure 19, h). This potentially allows to sort the droplets (double emulsions) with a normal FACS setup, rather than sorting the single emulsions directly on the microfluidic chip (FADS).

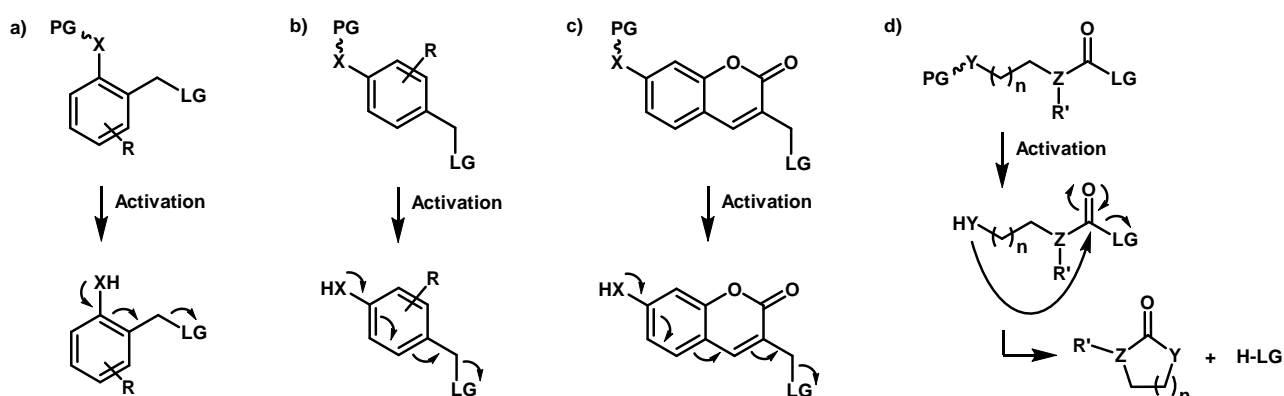
## 2.4 Design of a caged inducer system

In this thesis, IPTG was caged with an *O*-allyl carbamate protective group, which can be cleaved by our designed artificial allylic deallocase (chapter 2.4.3). In this way, the expression of a GFP reporter protein can be regulated by the action of an artificial metalloenzyme (chapter 2.4.4). A closer look at a crystal structure of the lactose operon repressor, the target protein of IPTG, revealed a tight ligand binding including hydrogen bonds between the repressor protein and the 2', 3', 4' and 6'-hydroxy groups of IPTG (PDB ID 1LBH).<sup>152</sup> Attachment of an *O*-allyl carbamate protective group would therefore probably inactivate the function of IPTG. In this way, several caged IPTG derivatives were synthesized and tested in catalysis.

### 2.4.1 Self-immolative linkers

IPTG does not contain any primary amine group, thus no *O*-allyl carbamate protective group can be directly installed. Either one of the alcohol groups of the sugar frame is substituted by a primary amine (chapter 3: 2'-Amino-IPTG substrate) or the allyl function is introduced in the form of an allyl ether or an allyl carbonate. The latter one is not stable in aqueous solutions (chapter 2.4.3) and therefore not suitable for catalysis in the presence of *E. coli* cells. Alternatively, a traceless linker between an alcohol group of IPTG and the *O*-allyl carbamate protective group can be introduced. This can be achieved with the concept of the so-called self-immolative spacers.<sup>153-154</sup> Upon removal of the protective group, an active nucleophilic species is formed, which spontaneously undergoes a self-immolation based on elimination via electronic delocalization or via intramolecular cyclization to liberate the leaving group (Scheme 7).

Applying self-immolative linkers allows to combine a variety of different protective and leaving groups, also those which cannot be introduced directly, as highlighted for IPTG and *O*-allyl-carbamates. This makes the concept of self-immolative linkers to a very powerful tool in catalysis.



**Scheme 7: Self-immolation based on a) 1,4-elimination, b) 1,6-elimination, c) 1,8-elimination or d) intramolecular cyclization.<sup>153</sup>**

PG = protective group (i.e. *O*-allyl carbamate); LG = leaving group (i.e. HO-IPTG); X = O, NH or S; Y = O, NH, NMe or S; Z = CH, O, N; n = 1 or 2.

Self-immolations are generally driven by an increase in entropy and/or the formation of thermodynamically stable products (release of CO<sub>2</sub>, formation of 5- or 6-membered rings). However, the reaction velocity of such self-immolations, after the activation step has taken place, depends on:

- (i) The substituents on the aromatic rings. The reaction is faster with electron-donating groups such as R = OMe or R = NHMe, whereas electron-withdrawing substituents such as R = NO<sub>2</sub> or R = CO<sub>2</sub>Me decrease the reaction speed (Scheme 7 a, b).<sup>153, 155-157</sup>
- (ii) The electronic and steric structure of the aromatic linker. Elimination takes place for a coumarin derivative (Scheme 7 c), whereas no reaction was obtained for the analogous naphthalene and biphenyl derivatives. It is assumed that this is caused by a too high energy barrier to break aromaticity, and by a non-planar structure preventing electron delocalization, respectively.<sup>158</sup>
- (iii) The linker between the aromatic moiety and the leaving group. Carbonate- and carbamate-linked leaving groups were released faster (up to 10<sup>3</sup>-fold shorter half-life times) than their analogues linked via an ether function (Scheme 7 a, b).<sup>153, 155, 159</sup>
- (iv) The acidity of the leaving group. Higher rates were obtained for phenolic leaving groups if their respective pK<sub>a</sub> values decreased (Scheme 7 b).<sup>157</sup> The same effect was determined for self-immolation by cyclization (Scheme 7 d).<sup>160</sup>
- (v) The pH value and the temperature. Higher rates were obtained at high pH and temperature for a self-immolation based on 1,4-elimination (Scheme 7 a).<sup>155</sup>
- (vi) The functional groups Y, Z and the substituent R' (Scheme 7 d). An enhanced intramolecular cyclization rate was obtained for R' = Me, OH or cyclopentyl compared to R' = H in the formation of lactams (Y = NH, Z = CH)<sup>153, 161</sup>, which could be explained by the Thorpe-Ingold effect<sup>162</sup> and/or the reactive rotamer effect.<sup>163-164</sup> In addition, faster cyclizations were obtained for 5-membered rings (n = 1) compared to 6-membered rings (n = 2) in the formation of ureas (Y = NH, Z = N, R' = H or Me).<sup>165</sup>

## 2.4.2 Design and synthesis of caged IPTG substrates

Three substrates containing self-immolative linkers and one substrate with a directly attached *O*-allyl carbonate protective group were designed (Figure 20).

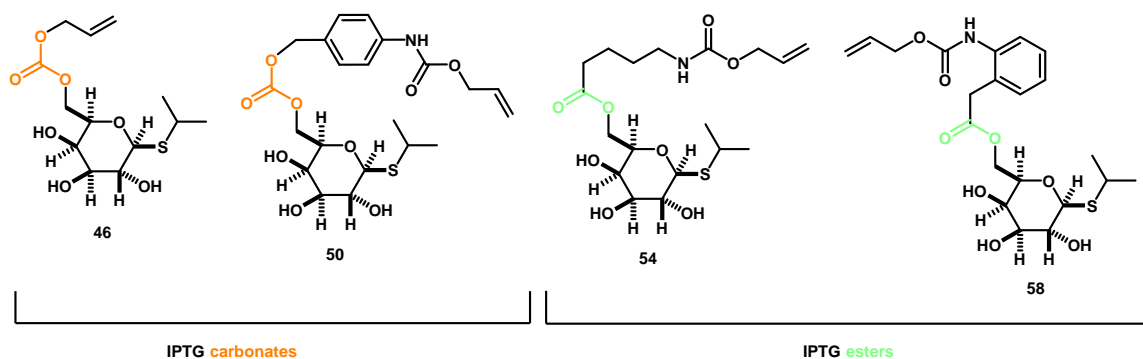
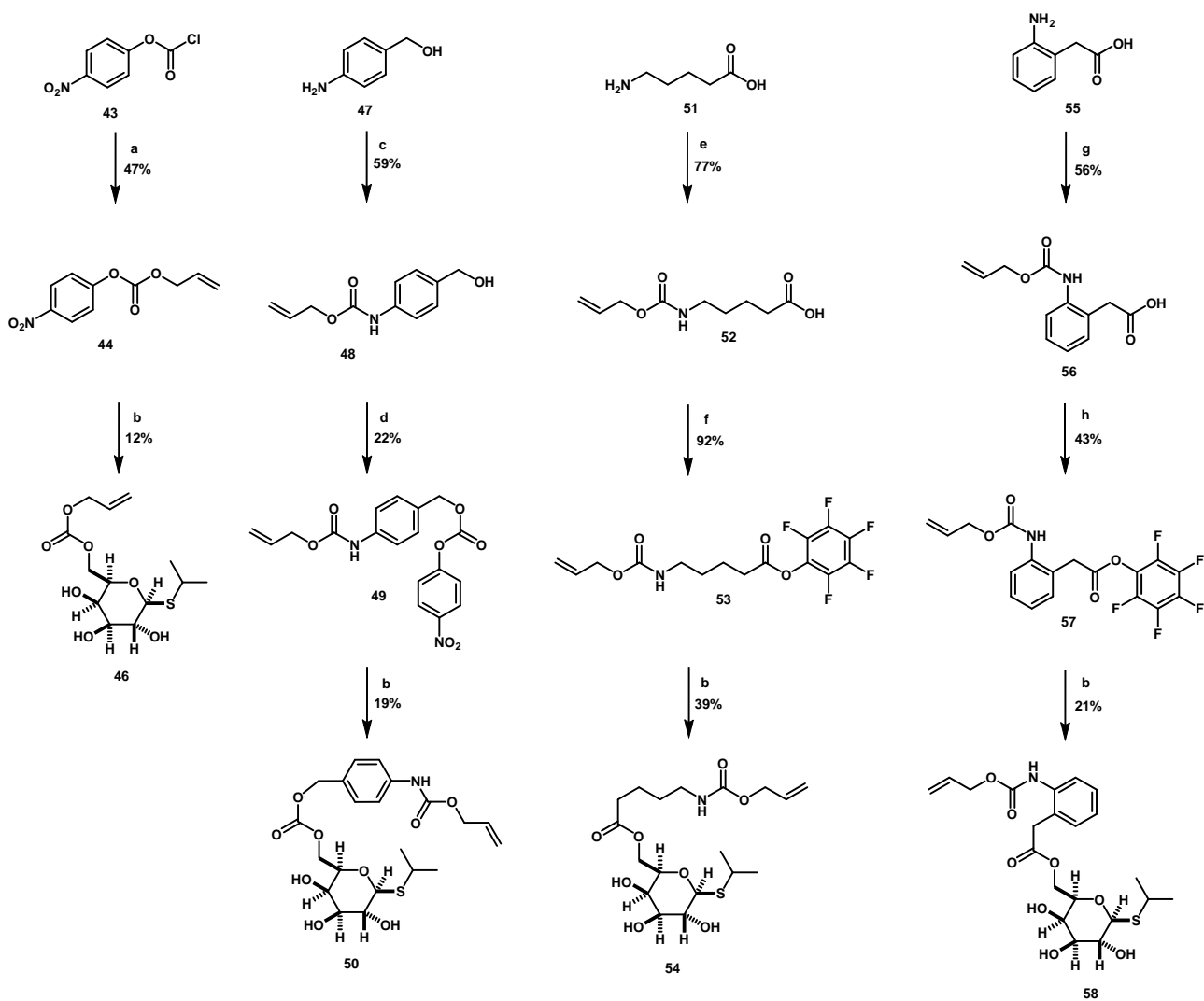


Figure 20: Designed *O*-allyl carbonate/carbamate protected substrates for an artificial allylic deallocase.

Due to its increased nucleophilicity, the primary alcohol at the 6'-position of the IPTG sugar frame offers a suitable anchor for attachment of protective groups and/or self-immolative linkers. In a first version, the protective group was directly attached to this alcohol in the form of an *O*-allyl carbonate (substrate **46**). This concept was then expanded by the installation of a self-immolative linker based on a 1,6-elimination (substrate **50**). Unfortunately, these two carbonate based substrates were not hydrolytically stable in the aqueous reaction medium used (see chapter 2.4.3). Therefore, two substrates containing an ester-linkage were designed. These substrates either contain an aliphatic (substrate **54**) or an aromatic (substrate **58**) self-immolative linker based on intramolecular cyclization. These two substrates displayed an increased stability towards hydrolysis (see chapter 2.4.3). However, to make the caged IPTG substrates even more resistant, the use of a stable carbamate linkage is favorable (see chapter 3).

The synthesis of the two IPTG-carbonates and the two IPTG-esters is summarized in Scheme 8 and can be divided into three parts. First, the linkers were treated with allyl chloroformate or allyl alcohol under basic conditions to attach the *O*-allyl carbamate/carbonate protective groups (compounds **44**, **48**, **52** and **56**). The protected linkers were then activated in the form of *p*-nitrophenyl carbonates (compounds **44** and **49**) or pentafluorophenyl esters (compounds **53** and **57**). Finally, linkage with IPTG was achieved by treatment with 4-(dimethylamino)-pyridine in pyridine (compounds **50**, **54** and **58**). In this process, the secondary alcohols of IPTG were not protected beforehand, which probably led to a decrease in conversion (12% – 39% for the last step).



**Scheme 8: Synthesis of IPTG substrates bearing a caging group at the 6'-OH.**

Reaction conditions: a) Allyl alcohol (1.0 eq.),  $\text{NEt}_3$ , DCM (dry),  $-10^\circ\text{C}$  to r.t., 16 h; b) IPTG (1.0 eq.), DMAP (1.0 eq.), Pyridine, r.t., 18 h; c) Allyl chloroformate (1.1 eq.), Pyridine, DCM, r.t., 3 h; d) 4-nitrophenyl chloroformate (**43**, 1.5 eq.), DIPEA, THF, r.t., 16 h; e) Allyl chloroformate (1.5 eq.), NaOH,  $\text{H}_2\text{O}$ ,  $0^\circ\text{C}$ , 5 h; f) Pentafluorophenyl trifluoroacetate (1.5 eq.),  $\text{NEt}_3$ , DMF,  $0^\circ\text{C}$  to r.t., 3 h. g) Allyl chloroformate (1.50 eq.), NaOH,  $\text{H}_2\text{O}$ ,  $0^\circ\text{C}$  to r.t., 4 h; h) Pentafluorophenyl trifluoroacetate (0.85 eq.),  $\text{NEt}_3$ , DCM,  $0^\circ\text{C}$  to r.t., 4 h.

### 2.4.3 *In vitro* evaluation of the best IPTG substrate

The stability of the *O*-allyl carbonate/carbamate-protected IPTG substrates in the reaction medium at different pH's as well as the performance of different ruthenium complexes and artificial allylic deallocases was investigated (Table 6).

**Table 6: Stability of IPTG substrates and performance of ruthenium complexes/artificial allylic deallocases.<sup>a</sup>**

Entry	Substrate	Complex	Sav	pH	Reaction time	Yield [%]
1	<b>46</b>	-	-	7.4	16 h	54
2	<b>46</b>	[CpRu(QA-NMe <sub>2</sub> )(Allyl)]PF <sub>6</sub> ( <b>7</b> )	-	7.4	16 h	73
3	<b>46</b>	[CpRu(QA-Biot)(Sol.)]PF <sub>6</sub> ( <b>27</b> )	-	7.4	16 h	61
4	<b>46</b>	[CpRu(QA-Biot)(Sol.)]PF <sub>6</sub> ( <b>27</b> )	WT	7.4	16 h	68
5	<b>46</b>	[CpRu(QA-Biot)(Sol.)]PF <sub>6</sub> ( <b>27</b> )	S112Y-K121R	7.4	16 h	79
6	<b>50</b>	-	-	7.4	16 h	57
7	<b>50</b>	[CpRu(QA-NMe <sub>2</sub> )(Allyl)]PF <sub>6</sub> ( <b>7</b> )	-	7.4	16 h	76
8	<b>50</b>	[CpRu(QA-Biot)(Sol.)]PF <sub>6</sub> ( <b>27</b> )	-	7.4	16 h	76
9	<b>50</b>	[CpRu(QA-Biot)(Sol.)]PF <sub>6</sub> ( <b>27</b> )	WT	7.4	16 h	70
10	<b>50</b>	[CpRu(QA-Biot)(Sol.)]PF <sub>6</sub> ( <b>27</b> )	S112Y-K121R	7.4	16 h	79
11	<b>54</b>	-	-	7.4	16 h	4
12	<b>54</b>	[CpRu(QA-NMe <sub>2</sub> )(Allyl)]PF <sub>6</sub> ( <b>7</b> )	-	7.4	16 h	33
13	<b>54</b>	[CpRu(QA-Biot)(Sol.)]PF <sub>6</sub> ( <b>27</b> )	-	7.4	16 h	7
14	<b>54</b>	[CpRu(QA-Biot)(Sol.)]PF <sub>6</sub> ( <b>27</b> )	WT	7.4	16 h	8
15	<b>54</b>	[CpRu(QA-Biot)(Sol.)]PF <sub>6</sub> ( <b>27</b> )	S112Y-K121R	7.4	16 h	13
16	<b>54<sup>b</sup></b>	[CpRu(QA-Biot)(Sol.)]PF <sub>6</sub> ( <b>27</b> )	WT	7.4	22 h	11
17	<b>54<sup>b</sup></b>	[CpRu(QA-Biot)(Sol.)]PF <sub>6</sub> ( <b>27</b> )	S112M	7.4	22 h	12
18	<b>54<sup>b</sup></b>	[CpRu(QA-Biot)(Sol.)]PF <sub>6</sub> ( <b>27</b> )	K121A	7.4	22 h	26
19	<b>54<sup>b</sup></b>	[CpRu(QA-Biot)(Sol.)]PF <sub>6</sub> ( <b>27</b> )	K121F	7.4	22 h	32
20	<b>54<sup>b</sup></b>	[CpRu(QA-Biot)(Sol.)]PF <sub>6</sub> ( <b>27</b> )	L124G	7.4	22 h	27
21	<b>58<sup>c</sup></b>	-	-	7.0	5 h	24
22	<b>58<sup>c</sup></b>	[CpRu(QA-Biot)(Sol.)]PF <sub>6</sub> ( <b>27</b> )	-	7.0	5 h	22
23	<b>58<sup>c</sup></b>	[CpRu(QA-Biot)(Sol.)]PF <sub>6</sub> ( <b>27</b> )	WT	7.0	5 h	26
24	<b>58<sup>c</sup></b>	[CpRu(QA-Biot)(Sol.)]PF <sub>6</sub> ( <b>27</b> )	S112M	7.0	5 h	30
25	<b>58<sup>c</sup></b>	[CpRu(QA-Biot)(Sol.)]PF <sub>6</sub> ( <b>27</b> )	K121F	7.0	5 h	35
26	<b>58<sup>c</sup></b>	[CpRu(QA-Biot)(Sol.)]PF <sub>6</sub> ( <b>27</b> )	L124G	7.0	5 h	40
27	<b>58<sup>c</sup></b>	[CpRu(QA-Biot)(Sol.)]PF <sub>6</sub> ( <b>27</b> )	S112M-K121A	7.0	5 h	61

<sup>a</sup>Reaction conditions: Phosphate-buffer (50 mM NaH<sub>2</sub>PO<sub>4</sub>/Na<sub>2</sub>HPO<sub>4</sub>), 0.9% NaCl, 500 μM substrate, 5 μM ruthenium cofactor, 10 μM Sav (free biotin binding sites), 0.5% DMF (for [CpRu(QA-Biot)(Sol.)]PF<sub>6</sub> (**27**)) or 0.5% DMSO (for [CpRu(QA-NMe<sub>2</sub>)(Allyl)]PF<sub>6</sub> (**7**)), 25°C, shaking (1000 rpm). Yields (concentration of liberated IPTG) were determined by UPLC-MS (see chapter 4.2.3). <sup>b</sup>Complete screening with a variety of Sav mutants at the positions S112X, K121X and L124X: see Table 16. <sup>c</sup>Phosphate buffered LB-medium (50 mM NaH<sub>2</sub>PO<sub>4</sub>/Na<sub>2</sub>HPO<sub>4</sub>, pH 7.0) was used for the catalysis with substrate **58**.

The two IPTG substrates bearing carbonate functions (substrate **46** and **50**) turned out not to be hydrolytically stable in the reaction buffer at pH 7.4. High yields were determined also in the absence of any ruthenium cofactor (Table 6, entries 1 and 6; 54% and 57% yield, respectively). In contrast, substrate **54** bearing an aliphatic ester linker revealed high stability in the reaction buffer (Table 6, entry 11; 4% background hydrolysis). For the non-biotinylated ruthenium cofactor [CpRu(QA-NMe<sub>2</sub>)(Allyl)]PF<sub>6</sub> (**7**) a 33% yield was obtained, whereas the biotinylated ruthenium cofactor [CpRu(QA-Biot)(Sol.)]PF<sub>6</sub> (**27**) led to a conversion of 7% (Table 6, entries 12 and 13).

Incorporated into streptavidin isoforms and upon prolonged reaction times (22 h instead of 16 h), conversions of up to 32% for the mutant K121F were obtained (Table 6, entries 14 – 20; for an extended mutant screening at positions S112X, K121X and L124X: see Table 16). However, the artificial allylic deallocases did not reveal high performances (only 32% yield in 22 h reaction time). Therefore, another substrate (**58**) bearing an aromatic ester linker was tested. This substrate is structurally related to the successfully applied coumarin derivative **1**. Gratifyingly, with this IPTG substrate, higher conversions were obtained with shorter reaction times (5 h instead of 22 h). A set of promising streptavidin mutants from the former aliphatic substrate (**54**) was also applied for this aromatic substrate (**58**). Conversions of up to 61% for the double mutant S112M-K121A were obtained (Table 6, entries 21 - 27). However, this substrate revealed a high hydrolysis background in the reaction medium at pH 7.0 (Table 6, entry 21; 24% yield). Therefore, a pH screening was performed to potentially minimize this background (Table 7).

**Table 7: pH-screening for the deprotection of IPTG substrate 58.<sup>a</sup>**

Entry	Complex	Sav	pH	Yield [%]
1	-	-	6.0	5
2	[CpRu(QA-Biot)(Sol.)]PF <sub>6</sub> ( <b>27</b> )	-	6.0	8
3	[CpRu(QA-Biot)(Sol.)]PF <sub>6</sub> ( <b>27</b> )	WT	6.0	14
4	-	-	7.0	27
5	[CpRu(QA-Biot)(Sol.)]PF <sub>6</sub> ( <b>27</b> )	-	7.0	30
6	[CpRu(QA-Biot)(Sol.)]PF <sub>6</sub> ( <b>27</b> )	WT	7.0	32
7	-	-	8.0	71
8	[CpRu(QA-Biot)(Sol.)]PF <sub>6</sub> ( <b>27</b> )	-	8.0	71
9	[CpRu(QA-Biot)(Sol.)]PF <sub>6</sub> ( <b>27</b> )	WT	8.0	72

Conversions for the substrate alone, the free ruthenium cofactor and the artificial wild type metalloenzyme were determined at different pH's (6.0, 7.0 or 8.0) in phosphate buffer. <sup>a</sup>Reaction conditions: Phosphate-buffer (50 mM NaH<sub>2</sub>PO<sub>4</sub>/Na<sub>2</sub>HPO<sub>4</sub> at pH 6, 7 or 8), 0.9% NaCl, 500 μM IPTG substrate **58**, 5 μM ruthenium cofactor [CpRu(QA-Biot)(Sol.)]PF<sub>6</sub> (**27**), 10 μM Sav (free biotin binding sites), 0.5% DMF, 30°C, shaking (300 rpm), 18 h. Yields (concentration of liberated IPTG) were determined by UPLC-MS analysis (see chapter 4.2.3).

At pH 7.0 and 8.0 high hydrolysis backgrounds (27% and 71%, respectively) were obtained and no protein acceleration could be determined (Table 7, entries 4 – 9). Lowering the pH to 6.0 led to a decrease in background to 5% (Table 7, entry 1). Incorporation of the biotinylated ruthenium cofactor into wild-type streptavidin resulted in an elevated activity (Table 7, entries 2 and 3). Possessing a high stability and an initial activity with the wild-type metalloenzyme ([CpRu(QA-Biot)(Sol.)]PF<sub>6</sub> (**27**)-Sav-WT), this IPTG substrate (**58**) offers an optimal starting point for further optimization. In this perspective, mutants at the positions S112X, K121X and combinations thereof were screened (Figure 21).



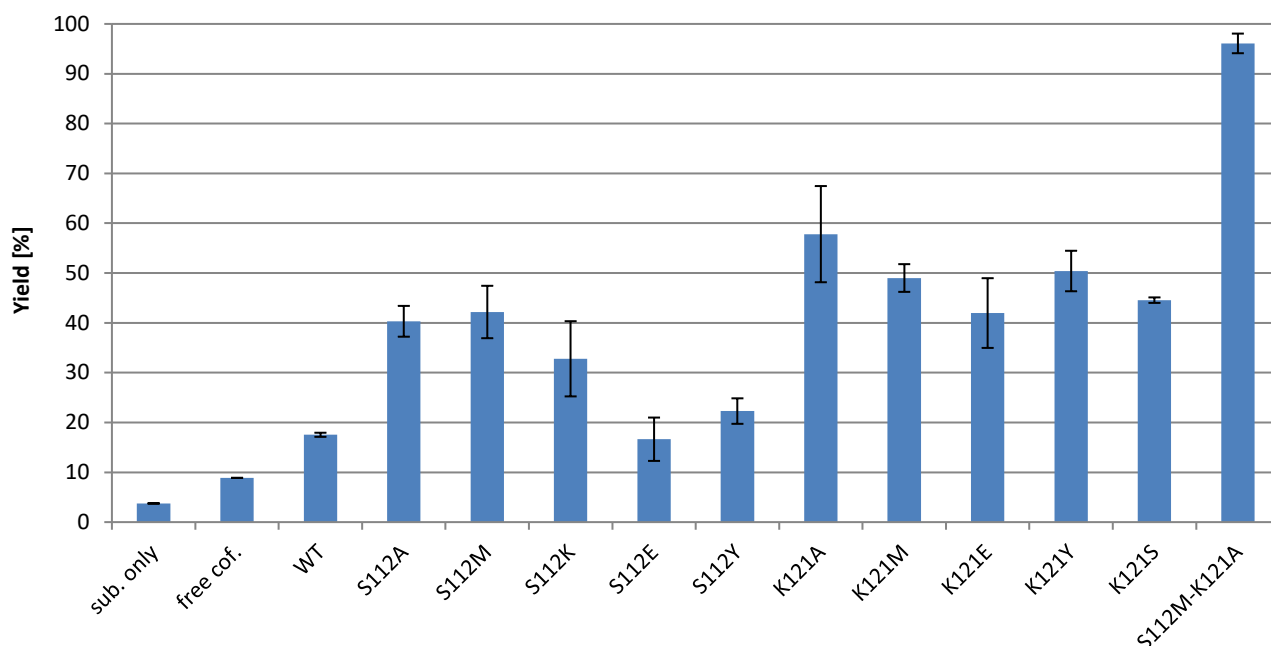


**Figure 21: Screening of Sav isoforms for the deprotection of IPTG 58 using [CpRu(QA-Biot)(Sol.)]PF<sub>6</sub> (27) · Sav.**

The substrate alone (sub. only), the free ruthenium cofactor **27** (free cof.) as well as a selection of artificial metalloenzymes were investigated. Aliphatic (alanine), Lewis base (methionine), charged (lysine and glutamate) and aromatic (tyrosine) mutations at positions S112 and K121 were tested. Reaction conditions: see Table 7. All reactions were performed at pH 6.0. Error bars = ± 1 standard deviation of a triplicate measurement.

A background reaction (hydrolysis of the substrate) of 4% was obtained, whereas the free ruthenium cofactor and the wild-type metalloenzyme yielded 9% and 18% conversion, respectively. The best mutations at both positions (S112M and K121A) were combined, leading to a positive synergetic effect. The double mutant S112M-K121A reached 96% conversion. This corresponded to a 5.5-fold increase in yield compared to the wild-type enzyme and a 10.8-fold increase compared to the free ruthenium cofactor. A crystal structure of the Sav mutant S112M-K121A bearing the ruthenium complex [CpRu(QA-Biot)(H<sub>2</sub>O)]PF<sub>6</sub> is reported in chapter 2.1.4.

#### 2.4.4 Catalysis in the presence of GFP reporter cells

Inspired by the promising results obtained in the *in vitro* screening of streptavidin mutants for the uncaging of IPTG substrate **58** (Figure 21), the performance of the artificial metalloenzyme was tested in the presence of *E. coli* cells. A pCD353 plasmid (provided by the research group of Prof. Dehio, University of Basel)<sup>166</sup> containing a lac-operon<sup>167-168</sup> followed by an GFP gene was transformed into *E. coli* cells (Figure 22).

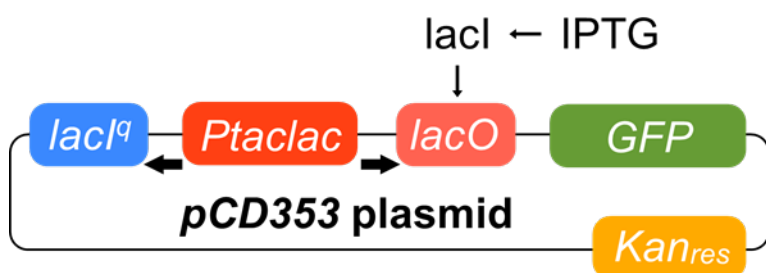
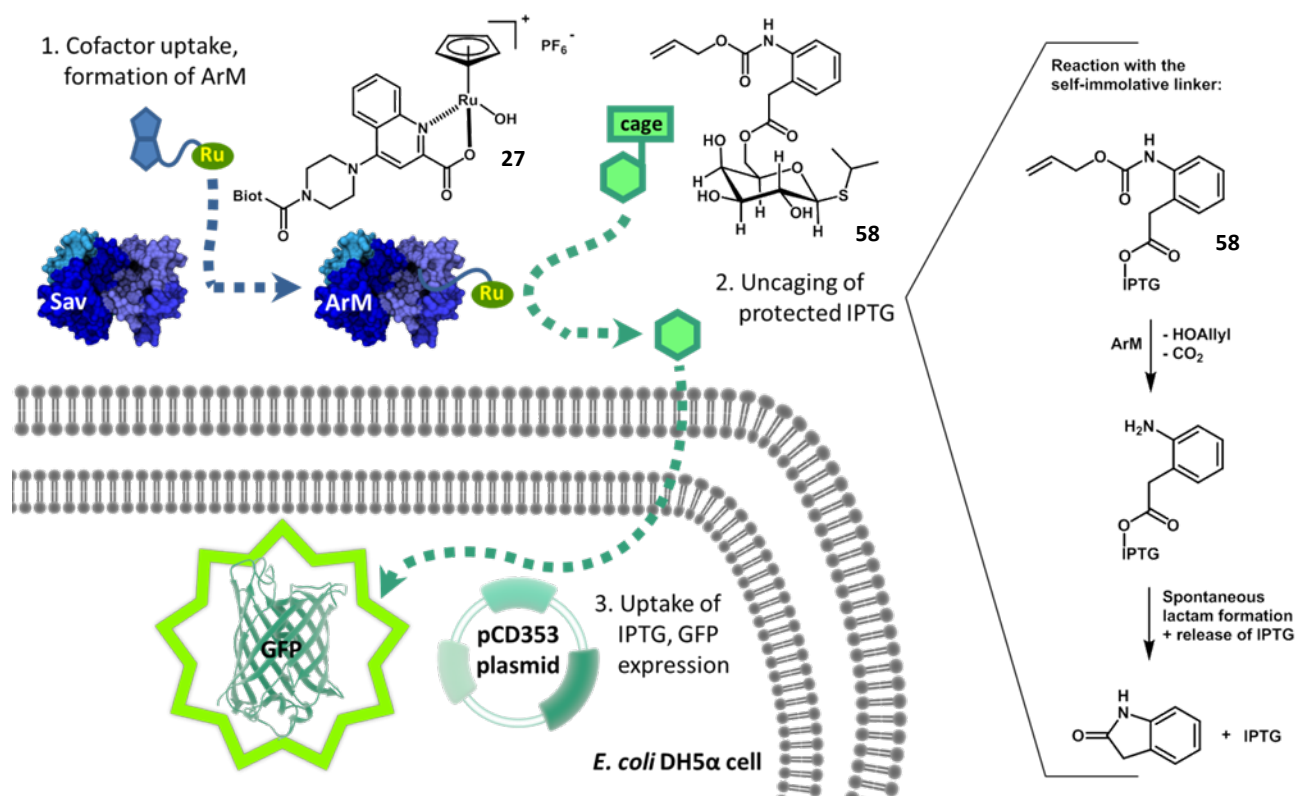


**Figure 22: Schematic map of the pCD353-GFP plasmid.**

The pCD353 plasmid contains the P<sub>t</sub>aclac promoter and the lacI<sup>q</sup> repressor, which binds to the lacO operon. The lacI<sup>q</sup> repressor is released from the lacO operon by binding of the IPTG inducer, which results in the expression of GFP. The plasmid furthermore contains a kanamycin antibiotic resistance (Kan<sub>res</sub>). The pCD353 plasmid was provided by the research group of Prof. Dehio, University of Basel.<sup>166</sup>

The designed system involves three steps: 1) Mixing of purified streptavidin (Sav) with biotinylated ruthenium cofactor ([CpRu(QA-Biot)(Sol.)]PF<sub>6</sub> (**27**)) and subsequent formation of the artificial metalloenzyme (ArM), followed by the addition of the caged substrate and the GFP reporter cells. 2) Deallylation of substrate **58** by the ArM and subsequent release of IPTG via intramolecular cyclization. 3) Uptake of IPTG into the cytoplasm of the *E. coli* cells and expression of the GFP reporter (Scheme 9). The activity of the artificial metalloenzyme, represented in the amount of expressed GFP, can then be determined by fluorescence analysis of the cell culture.



**Scheme 9: Catalysis in the presence of GFP reporter cells.**

Reaction steps: 1) Binding of the biotinylated ruthenium cofactor [CpRu(QA-Biot)(Sol.)]PF<sub>6</sub> (**27**) to streptavidin (Sav) and formation of the artificial metalloenzyme (ArM). 2) Uncaging of the protected IPTG substrate **58** (reaction scheme on the right-hand side). Substrate **58** is deallylated by the ArM with a simultaneous loss of CO<sub>2</sub>. The primary amine spontaneously attacks the neighboring carbonyl to form a lactam and release a molecule of IPTG. 3) Uptake of IPTG into the cytoplasm of *E. coli* DH5α cell and induction of the GFP expression. Finally, the fluorescence of the cells can be determined photospectrometrically.

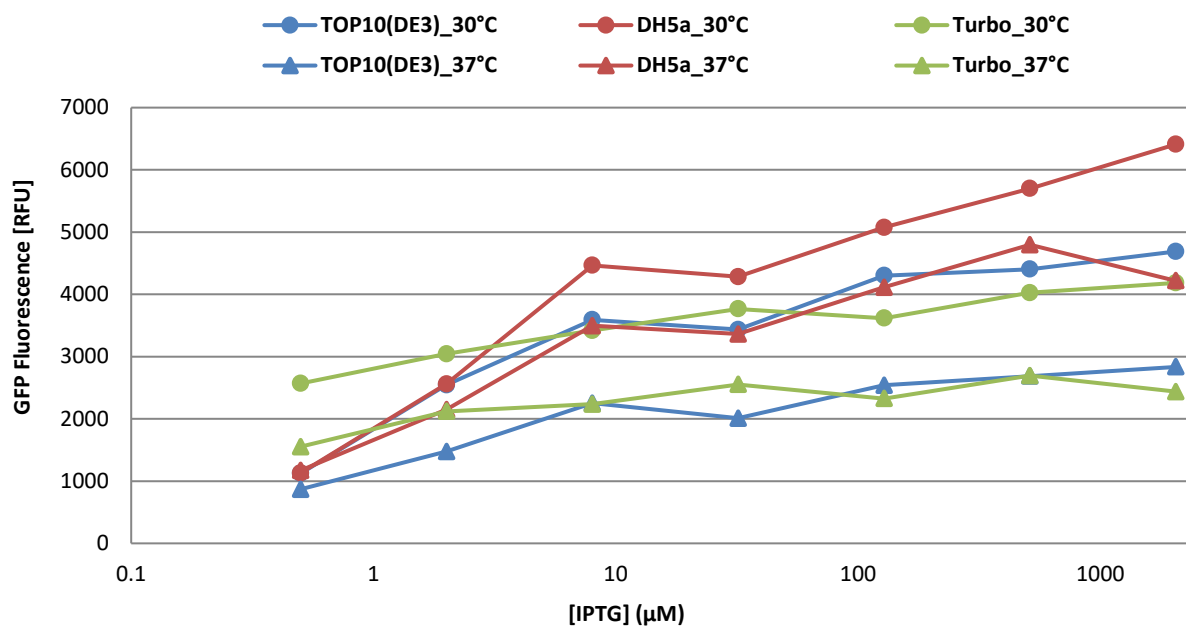


**Figure 23: GFP expression capacities of *E. coli* strains at different inducer concentrations and temperatures.**

Expression conditions: Studier-medium containing 50 μg/ml kanamycin (see chapter 4.2.4), 30°C or 37°C, 16 h, 96-well plate, 1 mL reaction volume, 280 rpm shaking. GFP-fluorescence determined at:  $\lambda_{\text{ex.}} = 475 \text{ nm}$ ,  $\lambda_{\text{em.}} = 509 \text{ nm}$ . The screening was performed by Dr. Tillmann Heinisch (Ward group, University of Basel).

Three *E. coli* strains were tested for their capacity to express GFP at different inducer concentrations and reaction temperatures. It was aimed for a strain which i) expresses high amounts of GFP, ii) reveals a high sensitivity in terms of GFP expression at small IPTG concentrations, and iii) tolerates high amounts of IPTG until the GFP expression reaches saturation. TOP10(DE3), NEB® Turbo and DH5α *E. coli* cells were tested at an IPTG concentration range from 0 – 2 mM and reaction temperatures of 30°C and 37°C, respectively (Figure 23). The *E. coli* strain DH5α, at an expression temperature of 30°C, fulfilled the criteria the best and was therefore selected for the proceeding experiments.

The uncaging reaction using purified artificial allylic deallocases ([CpRu(QA-Biot)(Sol.)]PF<sub>6</sub> (**27**) · Sav) was tested in the presence of *E. coli* DH5α reporter cells, applying the optimized reaction conditions (LB-medium, pH 6, 30°C). The background of the cells and the substrate alone, the activity of the free ruthenium cofactor as well as the performance of various streptavidin mutants was investigated (Figure 24). Thereby two different metal cofactor concentrations were tested: 1 μM and 5 μM.

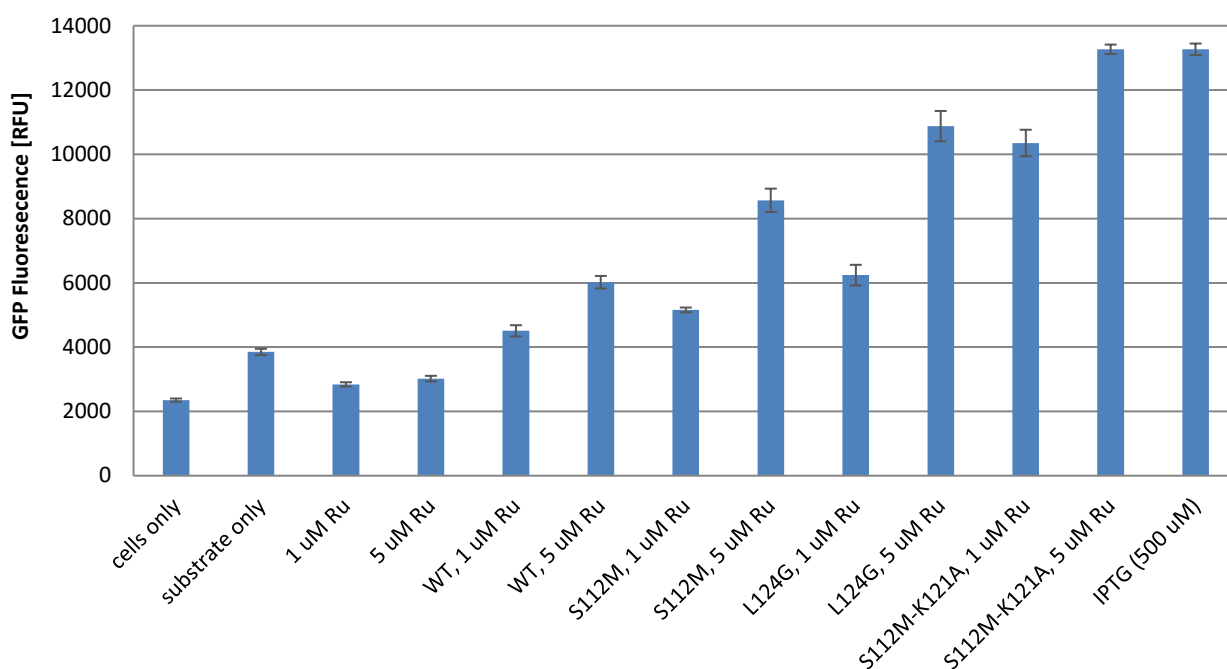


**Figure 24: Performance of ArMs for the uncaging of IPTG substrate 58 in the presence of GFP reporter cells.**

Reaction conditions: Phosphate buffered LB-medium (50 mM Na<sub>2</sub>HPO<sub>4</sub>/NaH<sub>2</sub>PO<sub>4</sub>, pH 6.0), 500 μM IPTG substrate **58**, 1 μM or 5 μM biotinylated ruthenium cofactor [CpRu(QA-Biot)(Sol.)]PF<sub>6</sub> (**27**) in combination with 2 μM or 10 μM streptavidin isoforms (free biotin binding sites), 0.5% DMF, 30°C, reaction time = 15 h, *E. coli* DH5α reporter cells containing the pCD353-GFP plasmid at an initial cell density of OD<sub>600</sub> = 0.7. GFP-fluorescence determined at: λ<sub>ex.</sub> = 475 nm, λ<sub>em.</sub> = 509 nm. The values displayed are corrected for cell density (OD<sub>600</sub>). Error bars are ± 1 standard deviation of a triplicate measurement. The screening was performed with the help of Dr. Tillmann Heinisch (Ward group, University of Basel).

The free biotinylated ruthenium cofactor [CpRu(QA-Biot)(Sol.)]PF<sub>6</sub> (**27**) showed almost no activity above the cellular background, whereas in combination with Sav-WT, an increased fluorescence was observed. For mutants with improved activities in the *in vitro* screening (e.g. S112M, S112M-K121A; Figure 21) higher fluorescence intensities in the presence of GFP reporter cells were observed. This suggests that the catalytic activity of a streptavidin mutant correlates with the amount of expressed GFP.

With a low concentration of artificial metalloenzyme (1  $\mu\text{M}$  ruthenium cofactor in combination with 2  $\mu\text{M}$  streptavidin), mutant S112M-K121A led to a 2.3-fold higher fluorescence intensity compared with Sav-WT and to a 3.6-fold increased intensity compared to the free metal cofactor. With a higher cofactor concentration of 5  $\mu\text{M}$ , the double mutant S112M-K121A reached full conversion, highlighted by a fluorescence intensity identical to the positive control containing 500  $\mu\text{M}$  product (= IPTG).

These experiments clearly demonstrate that i) an IPTG inducer can be protected with an *O*-allyl carbamate group in combination with a self-immolative linker, ii) the designed artificial allylic deallocases [CpRu(QA-Biot)(Sol.)]PF<sub>6</sub> (**27**) · Sav are active *in vitro* as well as in presence of *E. coli* cells, and iii) a biological event (expression of GFP) can be triggered with an artificial metalloenzyme.

#### 2.4.5 Design of a caged DmpR inducer system

In order to extend the diversity of the caged inducer approach, beside the successfully applied caged IPTG/GFP expression system, also another inducer system based on the DmpR regulator was investigated. DmpR is a  $\sigma^{54}$ -dependent regulator of the phenol catabolic pathway in *Pseudomonas sp.* Its function can be activated by the binding of phenols.<sup>169-170</sup> A plasmid containing the DmpR regulator and an sfGFP reporter gene was designed and cloned by Dr. Tsvetan Kardashliev (Panke group, DBSSE ETH Zürich) based on the work from Shingler *et al.*<sup>171</sup> The plasmid was subsequently transformed into *E. coli* DH5 $\alpha$  cells for the evaluation of the induction capacity of different substituted anilines (Table 8). Assuming that these molecules are able to induce the GFP expression as well, they could be protected with an *O*-allyl carbamate function and serve as substrates for the artificial allylic deallocases.

The methyl-, nitro-, chloro- or carboxylic acid-substituted aniline substrates showed no induction capacity (Table 8, entries 4-8). The unsubstituted aniline caused the expression of a small amount of GFP, whereas for the 4-hydroxy-substituted aniline substrate a high GFP fluorescence was obtained (Table 8, entries 3 and 9). Overall, a 76-fold increase in fluorescence intensity in presence of 4-hydroxyaniline compared to the negative control was determined (Table 8, entry 9 vs. entry 1). This represented a significant increase in the induction capacity, but did not completely reach the activity of the positive control (2-methylphenol; >350-fold increase; Table 8, entry 2 vs. entry 1). Based on the increased induction capacity of *para*-hydroxyaniline, the *meta*- and *ortho*-substituted analogues were investigated as well (Table 8, entries 10-13). The *meta*-substituted hydroxyaniline was found to be the most active one, displaying a similar activity than the positive control (2-methylphenol; Table 8, entry 12 vs. entry 10). Therefore, an *O*-allyl carbamate protective group was attached to form the caged substrate **72**.

**Table 8: Induction capacity of various phenols and anilines for a designed DmpR regulator system.**

Entry	Substrate	Incubation time	GFP fluorescence [AU]
1	-	5 h	1100 <sup>a</sup>
2	2-Methylphenol	5 h	405545 <sup>a</sup>
3	Aniline	5 h	5158 <sup>a</sup>
4	2,4,6-Trimethylaniline	5 h	902 <sup>a</sup>
5	3-Methylaniline	5 h	1066 <sup>a</sup>
6	4-Nitroaniline	5 h	905 <sup>a</sup>
7	4-Chloroaniline	5 h	1047 <sup>a</sup>
8	4-Aminobenzoic acid	5 h	1119 <sup>a</sup>
9	4-Hydroxyaniline	5 h	83678 <sup>a</sup>
10	2-Methylphenol	6 h	6213 <sup>b</sup>
11	2-Hydroxyaniline	6 h	2650 <sup>b</sup>
12	3-Hydroxyaniline	6 h	6041 <sup>b</sup>
13	4-Hydroxyaniline	6 h	355 <sup>b</sup>

Reaction steps: 1) *E.coli* DH5 $\alpha$  cells containing the DmpR/sfGFP reporter plasmid were cultivated in LB-medium at 30°C to a cell density of OD<sub>600</sub> = 0.6. 2) Dilution of the cells to OD<sub>600</sub> = 0.05-0.08, followed by the addition of 500  $\mu$ M substrate. 3) Incubation at 30°C, 200 rpm shaking. 4) Analysis of the fluorescence intensity. <sup>a</sup>Fluorescence intensity determined with a TECAN plate reader ( $\lambda_{\text{ex}}$  = 485 nm,  $\lambda_{\text{em}}$  = 510 nm). The GFP fluorescence intensity was normalized to the cell density (OD<sub>600</sub>). <sup>b</sup>Flow cytometry analysis of the cells (median value of the fluorescence intensity is listed). The screening was performed by Dr. Tsvetan Kardashliev (Panke group, DBSSE ETH Zürich).

Based on these results, the activities of artificial allylic deallocases towards the deprotection of caged hydroxyaniline **72** in presence of the DmpR/GFP-reporter cells were investigated. The non-biotinylated ruthenium complex [CpRu(QA-NMe<sub>2</sub>)(Allyl)]PF<sub>6</sub> (**7**), the free biotinylated ruthenium cofactor [CpRu(QA-Biot)(Sol.)]PF<sub>6</sub> (**27**) as well as a variety of artificial allylic deallocases ([CpRu(QA-Biot)(Sol.)]PF<sub>6</sub> (**27**) · Sav) were tested. Thereby, streptavidin mutants which already revealed an elevated activity towards the uncaging of the coumarin and the IPTG substrate (Figure 12 and Figure 24) were selected. The result of this screening is presented in Figure 25. The free biotinylated ruthenium cofactor (**27**) showed almost no activity. Incorporated in streptavidin isoforms, higher activities were obtained. Especially the double mutant S112M-K121A performed well, revealing a 4.9-fold higher fluorescence intensity than the Sav-WT. Compared to the free cofactor (**27**), a 9.2-fold increase was observed. In terms of activity, the double mutant S112M-K121A compares with the non-biotinylated ruthenium complex (**7**), which reached full conversion in 9 h. However, the activity of the artificial allylic deallocase [CpRu(QA-Biot)(Sol.)]PF<sub>6</sub> (**27**) · Sav-S112M-K121A can potentially be further increased by directed evolution.

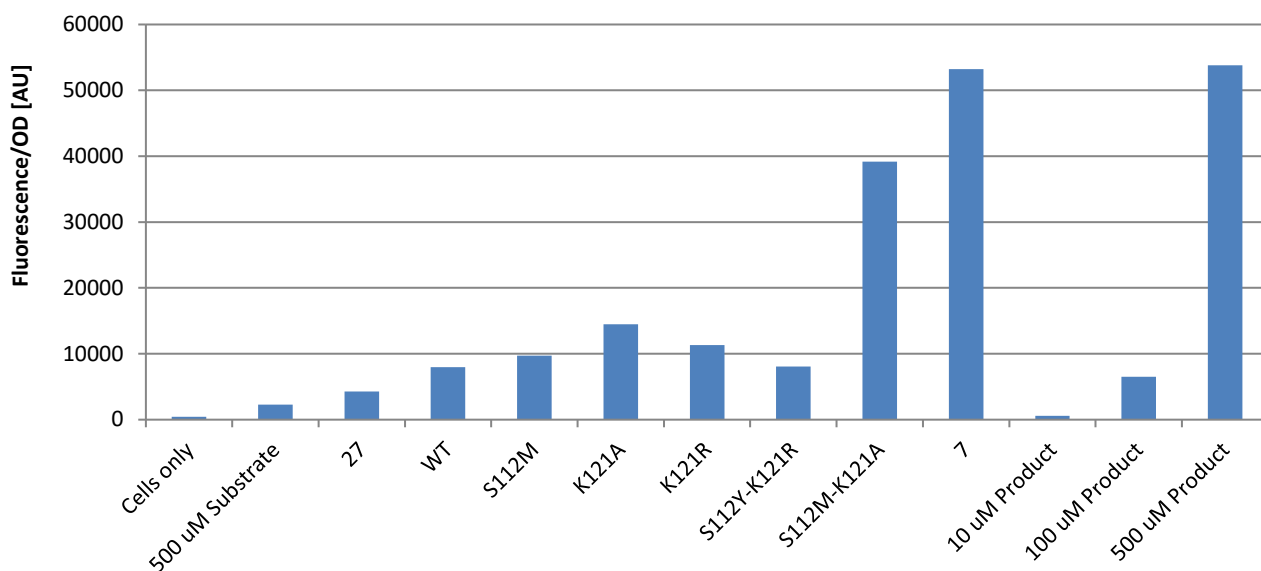


**Figure 25: Screening of artificial allylic deallocases for the deportection of aniline substrate **72**.**

Preparation of DmpR/GFP reporter cells: see Table 8. Reaction conditions: 500  $\mu$ M substrate **72**, 5  $\mu$ M ruthenium complex ([CpRu(QA-NMe<sub>2</sub>)(Allyl)]PF<sub>6</sub> (**7**) in DMSO or [CpRu(QA-Biot)(Sol.)]PF<sub>6</sub> (**27**) in DMF), 10  $\mu$ M streptavidin (free biotin binding sites), 30°C, 9 h, 200 rpm shaking. Cells cultures were analyzed in a TECAN plate reader. The GFP fluorescence intensity was normalized to the cell density (OD<sub>600</sub>). The screening was performed by Dr. Tsvetan Kardashliev (Panke group, DBSSE ETH Zürich).

These experiments clearly demonstrated that i) the DmpR regulator can be activated by the binding of hydroxyanilines, ii) the designed artificial allylic deallocases can catalyse the deallylation of a caged hydroxyaniline substrate (**72**) in the presence of *E. coli* DmpR/GFP reporter cells, and iii) the “caged inducer approach” can be transferred from an IPTG/lac to a hydroxyaniline/DmpR system.

The unsubstituted aniline only showed a modest induction capacity. Thus, a cascade reaction, in which an *O*-allyl carbamate protected aniline substrate gets first deallylated by an artificial metalloenzyme and then hydroxylated by an oxidase (e.g. cytochrome P450), can be envisioned (chapter 3: cascade reactions).<sup>172</sup>

## 2.5 Streptavidin loop mutants

In the Ward research group several streptavidin single site libraries were designed<sup>132</sup>, resulting in artificial metalloenzymes capable of catalyzing a variety of different reactions (see chapter 1.2). To optimize these artificial metalloenzymes, mostly residues within the biotin-binding vestibule in close proximity to the metal cofactor were targeted (i.e. S112, K121 or L124). A look at a crystal structure of such an enzyme revealed that the biotinylated metal-cofactor is exposed to the reaction medium (see chapter 2.1.4). This suggests that one hemisphere of the catalytic reaction space is not influenced by the protein scaffold. This decreases the potential of genetic optimization of ArMs. To increase the control of the reaction environment (i.e. the second coordination sphere<sup>6</sup>), it would be desirable to partially close the biotin binding vestibule. Ideally, lids may be placed on top of the biotin binding site to create a defined reaction environment for the catalytic event. Simultaneously, these lids should be flexible enough to allow the biotinylated catalyst and the substrate to enter the binding pocket. These lids can be composed of unstructured loops (e.g. (GGX)<sub>n</sub> motif<sup>173</sup>), or of more defined secondary structure elements (e.g. antiparallel  $\beta$ -sheets<sup>174</sup>, helix-turn-helix motif<sup>175-177</sup> or coiled coil<sup>178</sup>). The elements to build these streptavidin chimeras<sup>179</sup> can be of natural origin or computationally designed (e.g. Foldit-player design<sup>180</sup>). In addition to fusion proteins, the streptavidin scaffold may also be post-translationally modified.<sup>30, 181</sup> Due to the symmetric structure of the streptavidin tetramer, the introduced elements will appear on both sides of two adjacent binding sites. Thus, these lids may have a significant influence on the second coordination sphere around the biotinylated cofactor. By placing a cysteine residue in the middle of such a lid, a disulfide bond may be created holding two lids together on top of the metal cofactor. In this way, the active site might even be further shielded. However, first suitable positions in the streptavidin sequence for the introduction of these secondary structure elements needed to be identified.

### 2.5.1 Design of streptavidin loop mutants

Streptavidin is a homotetrameric  $\beta$ -barrel protein, in which every monomer consists of eight antiparallel  $\beta$ -sheets with seven interconnecting loops (Figure 26 a; see also chapter 1.2). To ensure the stability of streptavidin, the  $\beta$ -sheets were not targeted for mutagenesis or introduction of the lid structures. From the seven interconnecting loops, five lie in proximity of the biotinylated metal cofactor. These are namely the loops 1,2 (Asn<sub>23</sub>...Ser<sub>27</sub>), 3,4 (Ser<sub>45</sub>...Arg<sub>53</sub>), 4,5 (Asp<sub>61</sub>...Gly<sub>70</sub>, adjacent monomer), 5,6 (Ala<sub>78</sub>...Ala<sub>89</sub>) and 7,8 (Thr<sub>111</sub>...Ser<sub>122</sub>). These loops could potentially function as an anchoring point for introduction of the desired lid structures (Figure 26 a, b). However, there are a number of critical residues involved in biotin binding or tetramer stability, which should not be touched. The strong biotin binding (avidin-biotin complex:  $K_d \approx 10^{-15}$  M)<sup>35</sup> includes several hydrogen bonds (Asn<sub>23</sub>, Ser<sub>27</sub>, Tyr<sub>43</sub>, Ser<sub>45</sub>, Asn<sub>49</sub>, Ser<sub>88</sub>, Thr<sub>90</sub>, Asp<sub>128</sub>) and hydrophobic interactions (Trp<sub>79</sub>, Trp<sub>92</sub>, Trp<sub>108</sub>, Trp<sub>120</sub> (from the adjacent monomer)).<sup>36, 39-41</sup> Furthermore, the loop 3,4 (Ser<sub>45</sub>...Arg<sub>53</sub>) adopts a closed position if biotin is bound.<sup>42</sup>



Indeed, by two point mutations in this loop (Sav S52G-R53D = traptavidin) the off-rate of free biotin was lowered 10-fold.<sup>182</sup> On the other hand, by engineering of the loop 7,8 (Thr<sub>111</sub>...Ser<sub>122</sub>), a streptavidin variant with a reversible biotin binding capability was designed.<sup>183</sup> In terms of tetramer stability, residues in the subunit interfaces (including Val<sub>55</sub>, Thr<sub>76</sub>, Thr<sub>90</sub>, Leu<sub>109</sub>, Trp<sub>120</sub>, Val<sub>125</sub>, His<sub>127</sub> and Asp<sub>128</sub>) play a critical role.<sup>44-47</sup> Furthermore, there is an important inter-subunit salt-bridge between Asp<sub>61</sub> and His<sub>87</sub> (at physiological pH).<sup>48</sup>

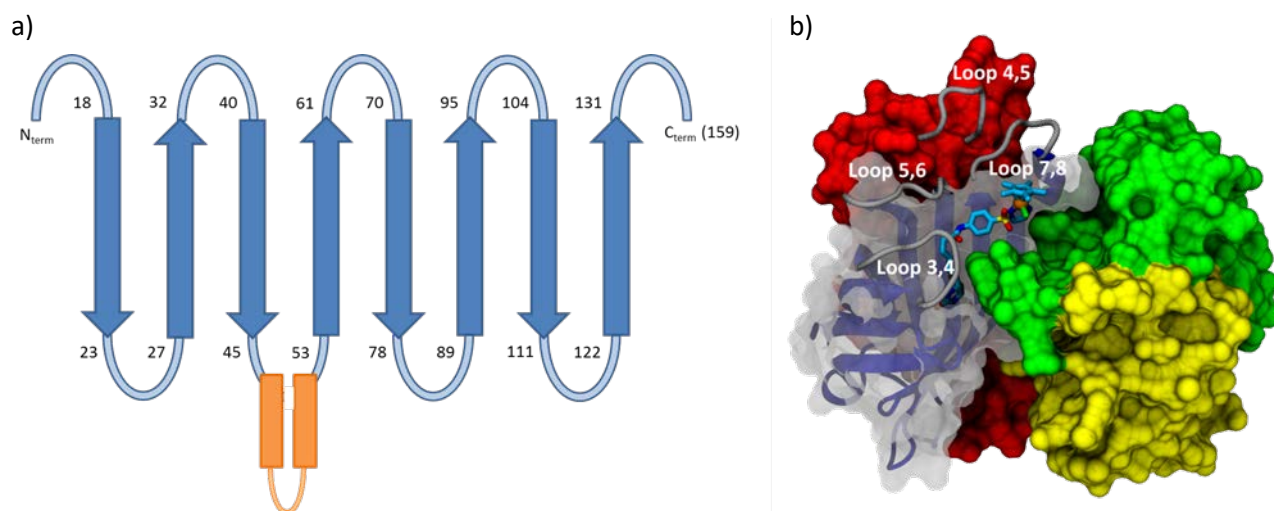


**Figure 26: Design of streptavidin loop mutants.**

a) Schematic representation of full-length streptavidin.  $\beta$ -sheets in dark blue, interconnecting loops in light blue and additional secondary structure elements in orange (here inserted in the loop 3,4 (Ser<sub>45</sub>...Arg<sub>53</sub>)). b) Crystal structure of [Cp\*Ir(biot-*p*-L)Cl] · Sav S112A (PDB ID 3PK2)<sup>60</sup>. Protein in surface representation (monomers displayed in red, green, yellow and translucent grey). Biotinylated iridium cofactor represented as sticks (C = cyan, N = blue, O = red, S = yellow, Cl = green, Ir = orange ball). Loops for insertion of secondary structure elements displayed as grey tubes. These include loop 3,4 (Ser<sub>45</sub>...Arg<sub>53</sub>), loop 4,5 (Asp<sub>61</sub>...Gly<sub>70</sub>, red monomer), loop 5,6 (Ala<sub>78</sub>...Ala<sub>89</sub>) and loop 7,8 (Thr<sub>111</sub>...Ser<sub>122</sub>).

With these limitations in mind, the following positions were selected to insert the secondary structure elements in-between: G<sub>48</sub>...N<sub>49</sub>, T<sub>66</sub>...D<sub>67</sub>, R<sub>84</sub>...N<sub>85</sub> and A<sub>117</sub>...N<sub>118</sub>. Position G<sub>48</sub>...N<sub>49</sub> was selected although it is located in the loop 3,4 (Ser<sub>45</sub>...Arg<sub>53</sub>), and might therefore influence the binding affinity of the biotinylated metal cofactor. The selected positions are all located in the middle of interconnecting loops in proximity of the biotinylated metal cofactor (Figure 26 b). Lid structures introduced at these positions might therefore effectively shield the biotinylated cofactor and influence the catalytic properties of the artificial metalloenzyme. A drawback of this strategy is the necessity that the introduced lids have to adopt a circular structure. The end point of one  $\beta$ -sheet and the starting residue of the next  $\beta$ -sheet are spatially close together. Distances between the C $\alpha$  atoms are as follows: Ser<sub>45</sub>...Arg<sub>53</sub>: 7.92 Å, Asp<sub>61</sub>...Gly<sub>70</sub>: 9.68 Å, Ala<sub>78</sub>...Ala<sub>89</sub>: 4.24 Å and Thr<sub>111</sub>...Ser<sub>122</sub>: 5.46 Å (determined in the crystal structure of [Cp\*Ir(biot-*p*-L)Cl] · Sav S112A (PDB ID 3PK2)<sup>60</sup>). This problem can be avoided by the introduction of a circular permutation into streptavidin. As demonstrated by Stayton and Stenkamp *et al.*<sup>184</sup>, core streptavidin can be circularly permuted at the positions 48/49 or 49/50 with simultaneous connection of the former *N*- and *C*-termini (Ala<sub>13</sub> and Ser<sub>139</sub>, respectively) by a GGGs-linker.

Using such a circularly permuted streptavidin widens the scope of secondary structure elements for the creation of artificial lids on top of the biotin binding vestibule. A further anchoring point for the attachment of such lid structures would be the C-terminus of streptavidin. In the Ward research group full-length streptavidin (159 amino acids) with an N-terminal T7-solubility tag (positions 1-12) is used.<sup>56</sup> Inspection of a crystal structure of apo full-length streptavidin (PDB ID 2BC3)<sup>185</sup> revealed that the C-terminus occupies the biotin-binding site and may therefore be in close proximity to the biotinylated metal cofactor.

### 2.5.2 Expression of streptavidin loop mutants

The tolerance of streptavidin towards the introduction of loop structures on top of the biotin binding site was examined by the insertion of the small and flexible (GGS)<sub>2</sub>-motif at the positions G<sub>48</sub>...N<sub>49</sub>, T<sub>66</sub>...D<sub>67</sub>, R<sub>84</sub>...N<sub>85</sub> and A<sub>117</sub>...N<sub>118</sub> (Table 9, entries 1-4). All four Sav variants were expressed as soluble tetramers. Modelling of their structures revealed that the biotin binding vestibule is narrowed, especially for the 48(GGS)<sub>2</sub> construct (Figure 27). In order to further shield the biotinylated metal cofactor, combinations of these Sav variants were created. These designs bore the (GGS)<sub>2</sub>-motif at two positions simultaneously (Table 9, entries 5-10). The combinations at positions 48+66 and 48+84 could be successfully expressed and purified. In a next step, the inserted loop between the positions G<sub>48</sub>...N<sub>49</sub> was modified. The designed constructs, bearing a (GGX)<sub>n</sub>-motif (n = 2-8), were elongated to contain up to 24 additional amino acids (Table 9, entries 11-18). All constructs were expressed as soluble biotin-binding tetramers, demonstrating the compatibility of streptavidin with an elongated loop 3,4. The structure of Loop2 was modeled applying homology modeling and structure refinement with YASARA (Figure 28 a). This modelling revealed that the biotinylated metal cofactor is most likely not completely shielded when an unstructured (GGX)<sub>n</sub>-motif is applied. A well-defined secondary structure element might better act as a lid on top of the biotin binding vestibule.

Therefore, a 30 amino acid long helix-turn-helix motif from an idealized tetratricopeptide repeat (TPR)<sup>175, 186</sup> was investigated. The TPR motif was inserted between the positions G<sub>48</sub>...N<sub>49</sub>, T<sub>66</sub>...D<sub>67</sub>, R<sub>84</sub>...N<sub>85</sub> and A<sub>117</sub>...N<sub>118</sub>, as well as at the C-terminus of core streptavidin (139TPR) and at the C-terminus of full-length streptavidin (Table 9, entries 19-24). From these six constructs, only the variant bearing the TPR-motif at the C-terminus of the full-length Sav (159TPR) could be expressed and isolated as a soluble biotin-binding tetramer. However, the construct 48TPR, initially obtained as an insoluble tetramer after the expression, was successfully denatured and refolded. The YASARA-modelled structure however suggested that the  $\alpha$ -helices are bent to the back instead than lying on top of the biotin binding site (Figure 28 b). Introduction of a cysteine residue in the middle of the motif, along with the formation of a disulfide bond between two adjacent TPR's, might force the lids to be placed on top of the biotinylated metal cofactor.

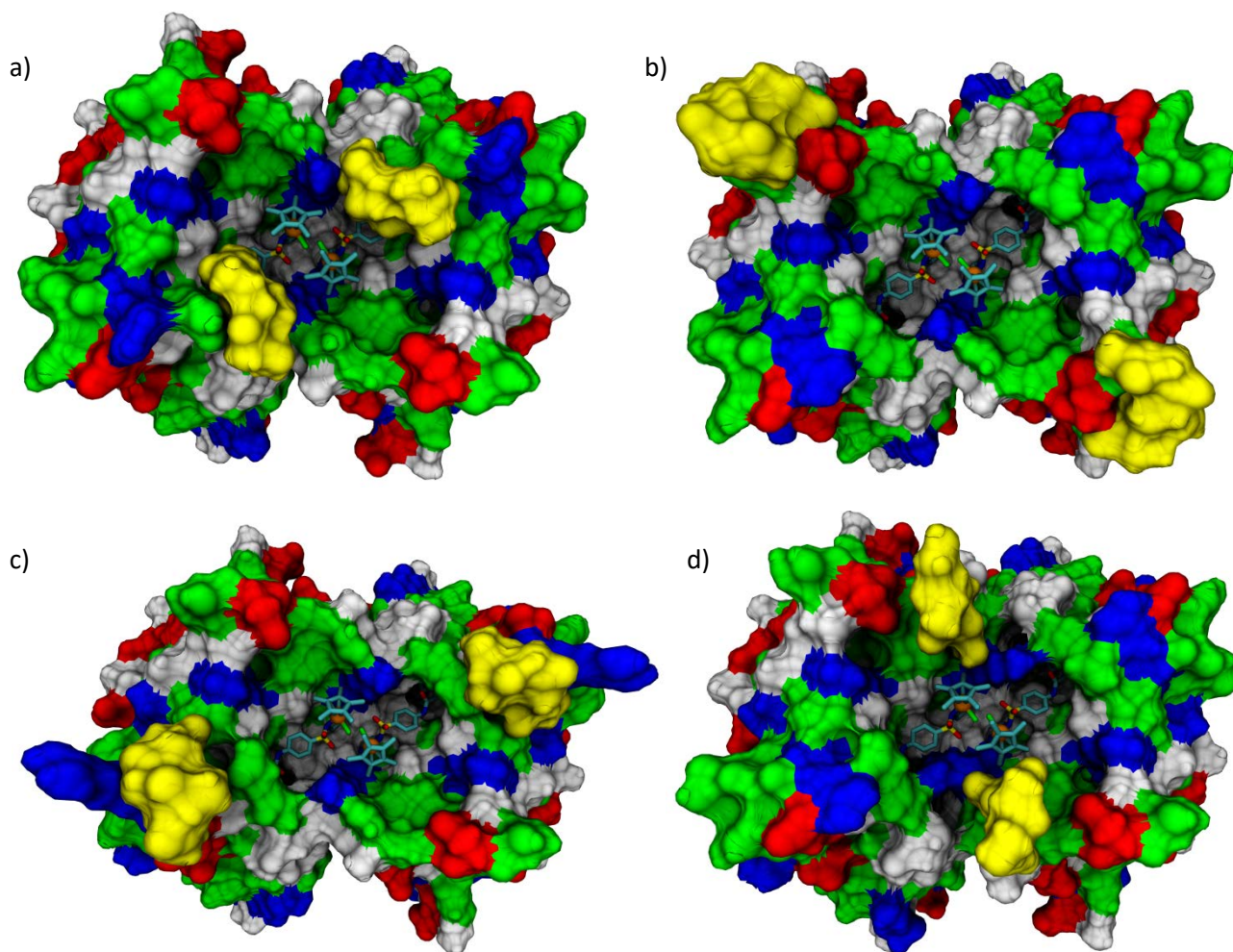


**Figure 27: Modelled structures of elongated Sav loop mutants with (GGG)<sub>2</sub> inserts at the positions G<sub>48</sub>, T<sub>66</sub>, R<sub>84</sub> or A<sub>117</sub>.**

Elongated loop structures were generated from an X-ray crystal structure of homotetrameric Sav S112A bearing the biotinylated iridium cofactor [Cp\*Ir(biot-*p*-L)Cl] (PDB ID 3PK2)<sup>60</sup>, applying homology modeling and structure refinement with YASARA. Protein in surface representation (residues: white = apolar, green = polar, red = acidic, blue = basic), biotinylated iridium complex represented as sticks (elements: H = white, C = cyan, N = blue, O = red, S = yellow, Cl = green, Ir = orange ball). The (GGG)<sub>2</sub> loops are highlighted as yellow surface. (GGG)<sub>2</sub> loops were inserted between the residues a) G<sub>48</sub>...N<sub>49</sub>, b) T<sub>66</sub>...D<sub>67</sub>, c) R<sub>84</sub>...N<sub>85</sub> or d) A<sub>117</sub>...N<sub>118</sub> (see also: Table 9, entries 1-4).

Finally, circular permuted core streptavidin variants were investigated (Table 9, entries 36-40). The circular permutation was performed at the position 64/68 and the former termini were connected with a GGGS-linker (see Table 9 footer for sequences).<sup>184</sup> The new constructs contained a 53 amino acid helix-turn-helix motif designed by Dr. Christine Tinberg in the research group of Prof. David Baker (University of Washington, Seattle). Rosetta calculations suggested that two neighboring motifs can form a four-helix bundle lid on top of the biotin binding site and effectively shield the metal cofactor (Figure 28 c, d). However, these constructs could only be expressed as insoluble inclusion bodies, as before obtained by Stayton and Stenkamp *et al.*<sup>184</sup> for their circular permuted core streptavidin. Initial attempts to refold these Sav variants failed.<sup>184, 187-188</sup> In the meanwhile, a denaturing and refolding procedure was developed and these constructs are applied in catalysis.<sup>179</sup>

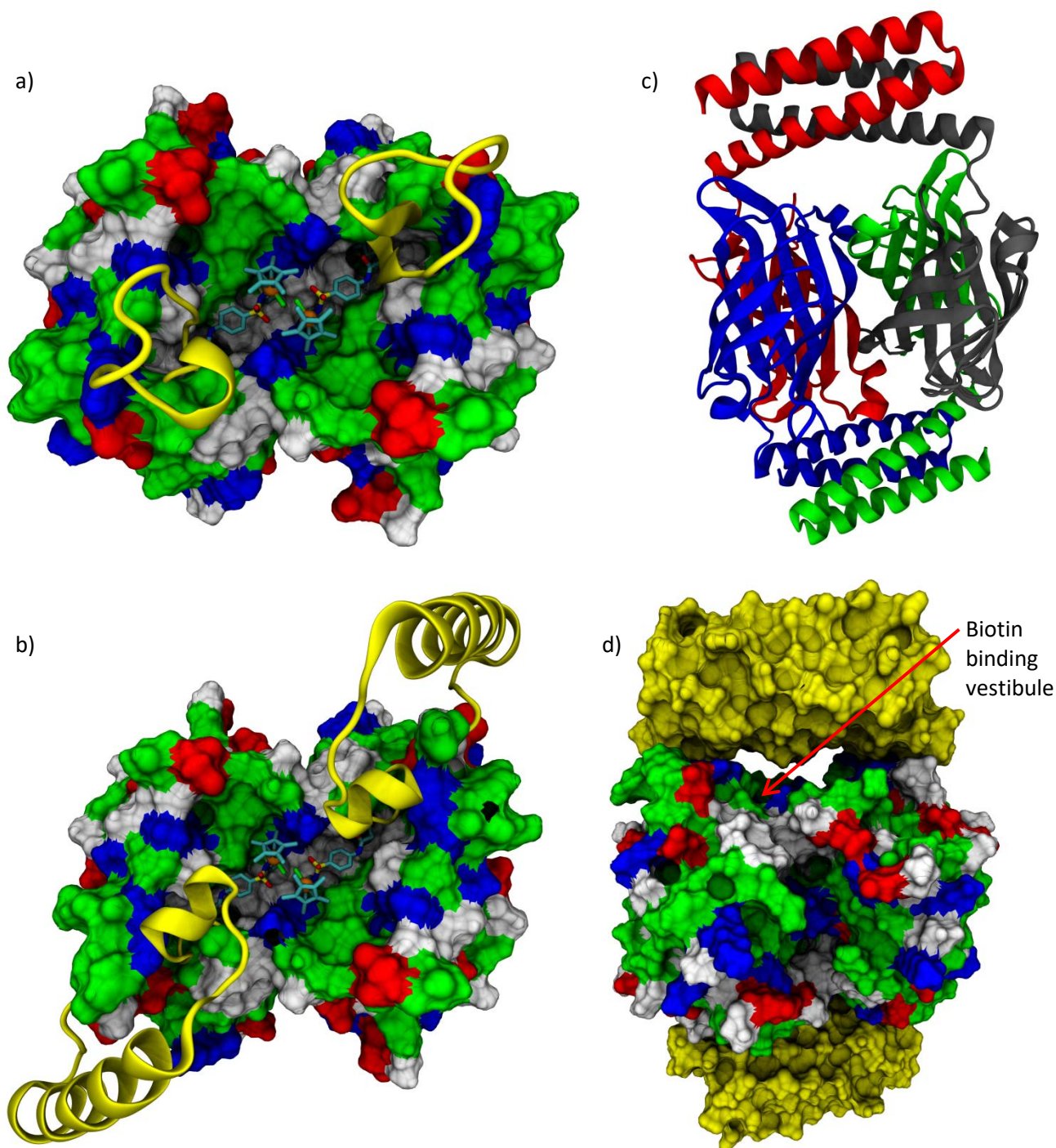


**Figure 28: Designed Sav loop mutants containing defined secondary structure elements.**

a) Elongated (GGX)<sub>5</sub> loop at position G<sub>48</sub>...N<sub>49</sub> (Table 9, entry 12: Loop2). b) Idealized tetratricopeptide repeat<sup>175,186</sup> at position G<sub>48</sub>...N<sub>49</sub> (Table 9, entry 19: 48TPR). c/d) Circularly permuted Sav bearing a helix-turn-helix motif at position P<sub>64</sub> (Table 9, entry 37: Cp1) displayed as cartoon (c) or surface model (d). Elongated loop structures in a) and b) were generated from an X-ray crystal structure of homotetrameric Sav S112A bearing the biotinylated iridium cofactor [Cp\*Ir(biot-*p*-L)Cl] (PDB ID 3PK2)<sup>60</sup>, applying homology modeling and structure refinement with YASARA. The circularly permuted streptavidin in c) and d) was designed by Dr. Christine Tinberg in the research group of Prof. David Baker (University of Washington, Seattle) using Rosetta. a), b), d): Protein in surface representation (residues: white = apolar, green = polar, red = acidic, blue = basic), biotinylated iridium complex represented as sticks (elements: H = white, C = cyan, N = blue, O = red, S = yellow, Cl = green, Ir = orange ball). The inserted secondary structure elements are highlighted in yellow. c): Protein in cartoon representation. The four monomers of streptavidin are highlighted in different colors (blue, grey, green, red).

In summary, 40 streptavidin (loop) mutants were designed, from which 28 could be expressed as soluble biotin binding tetramers. 19 variants were purified and from one (mutant S112M-K121A) a crystal structure with the bound ruthenium cofactor [CpRu(QA-Biot)(H<sub>2</sub>O)]PF<sub>6</sub> (**27**) could be determined (chapter 2.1.4). Some of the loop mutants, especially the 66(GGS)<sub>2</sub> and the 159TPR variants were successfully applied in catalysis (Figure 11 and Figure 12). In general, streptavidin showed a high tolerance towards the introduction of elongated loops. Five positions, suitable for the introduction of lid structures, were identified. These include the positions G48...N49, T66...D67, R84...N85, A117...N118 as well as the C-terminus. Unstructured (small) loops were successfully introduced at those positions. Replacement of these loops with longer well-defined secondary structure elements (e.g. helix-turn-helix motifs)<sup>189-193</sup> might result in the creation of lids on top of the biotin binding site. Thus, the second coordination sphere around the biotinylated metal cofactor can be modified from all sites, potentially resulting in elevated activities and selectivities.

Table 9: Overview of designed and expressed streptavidin (loop) mutants.

Entry	Name	Position(s)	Sequence of insert(s)	Length of insert	Expression host <sup>i</sup>	Solubility and oligomeric state	Mass of monomer <sup>c</sup> [Da]		CFE		Purified protein	
							Calculated	Determined <sup>d</sup>	FBBS <sup>h</sup> [nmol/mg]	Yield <sup>e</sup> [mg/l]	FBBS <sup>i</sup>	Yield <sup>f</sup> [mg/l]
1	48(GGS) <sub>2</sub>	G48...N49	GGSGGS	6	TOP10(DE3)	Soluble tetramer	16827.3	16828.1	2.7	549.6	n.d.	13.8
2	66(GGS) <sub>2</sub>	T66...D67	GGSGGS	6	TOP10(DE3)	Soluble tetramer	16827.3	16827.7	2.7	557.0	n.d.	16.3
3	84(GGS) <sub>2</sub>	R84...N85	GGSGGS	6	TOP10(DE3)	Soluble tetramer	16827.3	16828.0	2.8	529.4	n.d.	13.0
4	117(GGS) <sub>2</sub>	A117...N118	GGSGGS	6	TOP10(DE3)	Soluble tetramer	16827.3	-	2.6	235.4	-	-
5	48+66(GGS) <sub>2</sub>	G48...N49 T66...D67	GGSGGS GGSGGS	6+6	TOP10(DE3)	Soluble tetramer	17229.7	§	6.2	338.0	n.d.	1.5
6	48+84(GGS) <sub>2</sub>	G48...N49 R84...N85	GGSGGS GGSGGS	6+6	TOP10(DE3)	Soluble tetramer	17229.7	§	5.6	489.0	n.d.	0.9
7	48+117(GGS) <sub>2</sub>	G48...N49 A117...N118	GGSGGS GGSGGS	6+6	TOP10(DE3)	Soluble tetramer	17229.7	-	0.2	363.0	-	-
8	66+84(GGS) <sub>2</sub>	T66...D67 R84...N85	GGSGGS GGSGGS	6+6	TOP10(DE3)	Insoluble monomer	17229.7	-	-	-	-	-
9	66+117(GGS) <sub>2</sub>	T66...D67 A117...N118	GGSGGS GGSGGS	6+6	TOP10(DE3)	Soluble tetramer	17229.7	-	0.2	383.0	-	-
10	84+117(GGS) <sub>2</sub>	R84...N85 A117...N118	GGSGGS GGSGGS	6+6	TOP10(DE3)	Insoluble monomer	17229.7	-	-	-	-	-
11	Loop 1	G48...N49	GGDGGNGGSGGLGGC GGS	18	BL21(DE3)	Soluble tetramer	17729.2	-	19.4	678.0	-	-
12	Loop 2	G48...N49	GGNGGNGGGGGVGGG	15	BL21(DE3)	Soluble tetramer	17466.9	17468.3	22.0	580.0	n.d.	55.0
13	Loop 3	G48...N49	GGIGGSGGGGGHGGRG GGGVGGG	24	BL21(DE3)	Soluble tetramer	18131.6	-	12.3	619.0	-	-
14	Loop 4	G48...N49	GGNGGSGGGGGGGGS GGSGGS	21	BL21(DE3)	Soluble tetramer	17800.2	-	12.3	596.0	-	-
15	Loop 5	G48...N49	GGRGGGGHGGCGGV GGS	18	BL21(DE3)	Soluble tetramer	17749.3	-	17.0	1039.0	-	-
16	Loop 7	G48...N49	GGDGGG	6	BL21(DE3)	Soluble tetramer	16855.3	-	15.8	630.0	-	-
17	Loop 8	G48...N49	GGCGGSGGGGGGGG GGCGGS	21	BL21(DE3)	Soluble tetramer	17775.2	-	10.8	544.0	-	-
18	Loop 9	G48...N49	GGCGGIGGS	9	BL21(DE3)	Soluble tetramer	17070.6	-	15.4	519.0	-	-
19	48TPR	G48...N49	TPR motif	36	TOP10(DE3)	Insoluble <sup>a</sup>	20402.1	n.d.	-	-	n.d.	26.4
20	66TPR	T66...D67	TPR motif	36	TOP10(DE3)	Insoluble monomer <sup>b</sup>	20402.1	-	-	-	-	-
21	84TPR	R84...N85	TPR motif	36	TOP10(DE3)	Insoluble monomer	20402.1	-	-	-	-	-
22	117TPR	A117...N118	TPR motif	36	BL21(DE3)	Insoluble monomer	20402.1	-	-	-	-	-
23	139TPR	S139...	TPR motif	36	BL21(DE3)	Insoluble monomer	18396.9	-	-	-	-	-
24	159TPR	Q159...	TPR motif	36	BL21(DE3)	Soluble tetramer	20402.1	20402.0	-	-	n.d.	63.0
25	S112M-K121A	-	-	0	BL21(DE3)	Soluble tetramer	16411.9	16412.6	-	-	3.6	121.2
26	S112M-K121N	-	-	0	BL21(DE3)	Soluble tetramer	16454.9	16455.6	-	-	3.6	19.8

27	S112M-K121R	-	-	0	BL21(DE3)	Soluble tetramer	16497.0	16497.7	-	-	3.9	129.7
28	K121A-L124G	-	-	0	BL21(DE3)	Soluble tetramer	16311.7	16312.0	-	-	2.0	6.7
29	K121N-L124G	-	-	0	BL21(DE3)	Soluble tetramer	16354.7	16355.4	-	-	2.0	11.4
30	K121R-L124G	-	-	0	BL21(DE3)	Soluble tetramer	16396.8	16397.5	-	-	2.2	10.8
31	66(GGS) <sub>2</sub> -S112M	T66...D67	GGSGGS	6	BL21(DE3)	Soluble tetramer	16871.4	16872.2	-	-	3.6	115.1
32	66(GGS) <sub>2</sub> -K121R	T66...D67	GGSGGS	6	BL21(DE3)	Soluble tetramer	16855.3	16856.4	-	-	1.6	115.9
33	Loop2-S112M	G48...N49	GGNGGNGGGGVGGS	15	BL21(DE3)	Soluble tetramer	17511.0	17513.3	-	-	4.0	188.3
34	Loop2-K121R	G48...N49	GGNGGNGGGGVGGS	15	BL21(DE3)	Soluble tetramer	17494.9	17497.5	-	-	3.5	100.4
35	159TPR-K121R	Q159	TPR motif	36	BL21(DE3)	Soluble tetramer	20430.1	20431.8	-	-	3.1	83.9
36	CpSav	-	Circular permutation	-	BL21(DE3)	Insoluble monomer	14191.5	-	-	-	-	-
37	Cp1	P64	Helix-turn-helix motif	57	TOP10(DE3)	Insoluble monomer	20'694.6	-	-	-	-	-
38	Cp2	P64	Helix-turn-helix motif	58	TOP10(DE3)	Insoluble monomer	20'821.9	-	-	-	-	-
39	Cp3	P64	Helix-turn-helix motif	59	TOP10(DE3)	Insoluble monomer	20'965.0	-	-	-	-	-
40	Cp4	P64	Helix-turn-helix motif	59	TOP10(DE3)	Insoluble monomer	20'835.9	-	-	-	-	-

<sup>a</sup>Mostly insoluble monomer with a small B4F-binding insoluble tetrameric fraction. Protein was successfully refolded from insoluble inclusion bodies (detailed procedure described in chapter 4.2.8). The refolded protein bound B4F on the SDS-PAGE. After purification on iminobiotin sepharose beads, the refolded protein precipitated. Thus, no mass spectrum was determined. <sup>b</sup>Refolding of the protein failed. <sup>c</sup>Mass of the streptavidin monomer without the N-terminal methionine. <sup>d</sup>Mass was only determined for purified proteins. <sup>e</sup>Dried cell free extract (CFE) powder per 1 L culture. <sup>f</sup>Isolated purified protein per 1 L culture. <sup>g</sup>Peak corresponding to desired product mass could not be detected in the MS analysis. <sup>h</sup>Amount of free biotin binding sites per weight of dried CFE powder. <sup>i</sup>Free biotin binding sites (FBBS) per streptavidin tetramer. <sup>j</sup>Expression conditions: see chapter 4.2.8.

#### (GGS)<sub>2</sub> motif:

Example sequence of a streptavidin loop mutant with the (GGS)<sub>2</sub> motif between residues G48 and N49 (including T7-tag):

**H<sub>2</sub>N**—ASMTGGQQMGRDQAGITGTWYNQLGSTFIVTAGADGALTGTYESAVG<sub>48</sub>GGSGGS<sub>N49</sub>AESRYVLTGRYDSAPATDGSGTALGWTVAWKNNYRNAHSATTWSGQYVGGAEARINTQWLLTSGTTEANAWKSTLVGHDTFTKVKPSAASIDAACKAGVNNNGNPLDAVQQ—**CO<sub>2</sub>H**

#### TPR motif:

This helix-turn-helix motif is derived from an idealized 30 amino acid tetratricopeptide repeat<sup>175, 186</sup> and is flanked by two short GGS-linkers (example: TPR motif at position 48, including T7-tag):

**H<sub>2</sub>N**—ASMTGGQQMGRDQAGITGTWYNQLGSTFIVTAGADGALTGTYESAVG<sub>48</sub>GSAAEAWYNLGNAYKQGDYDEAIEYQKALELSSGG<sub>N49</sub>AESRYVLTGRYDSAPATDGSGTALGWTVAWKNNYRNAHSATTWSGQYVGGAEARINTQWLLTSGTTEANAWKSTLVGHDTFTKVKPSAASIDAACKAGVNNNGNPLDAVQQ—**CO<sub>2</sub>H**

#### Circular permutation (CpSav):

Circular permutation of T7-core streptavidin at position P64/G68, using a GGG linker<sup>184</sup>:

**H<sub>2</sub>N**—ASMTGGQQMGG<sub>68</sub>SGTALGWTVAWKNNYRNAHSATTWSGQYVGGAEARINTQWLLTSGTTEANAWKSTLVGHDTFTKVKPSAAS<sub>139</sub>GGGSA<sub>13</sub>EAGITGTWYNQLGSTFIVTAGADGALTGTYESAVGNAESRYVLTGRYDSAP<sub>64</sub>—**CO<sub>2</sub>H**

#### Circularly permuted Sav with an additional helix-turn-helix motif (Cp1-4), designed by Dr. Christine Tinberg in the research group of Prof. David Baker (University of Washington, Seattle):

Circular permutation of T7-core streptavidin at position P64/G68, using a GGG linker.<sup>184</sup> At the new C-terminus a 53 amino acid long helix-turn-helix motif is attached via different linkers:

**Cp1:** **H<sub>2</sub>N**—ASMTGGQQMGG<sub>68</sub>SGTALGWTVAWKNNYRNAHSATTWSGQYVGGAEARINTQWLLTSGTTEANAWKSTLVGHDTFTKVKPSAAS<sub>139</sub>GGGSA<sub>13</sub>EAGITGTWYNQLGSTFIVTAGADGALTGTYESAVGNAESRYVLTGRYDSAP<sub>64</sub>SSTDQEKALNMFIRSQTLTLLLEKLNELDAEQADIAESLHDHADELYRSVLARF—**CO<sub>2</sub>H**

**Cp2:** **H<sub>2</sub>N**—ASMTGGQQMGG<sub>68</sub>SGTALGWTVAWKNNYRNAHSATTWSGQYVGGAEARINTQWLLTSGTTEANAWKSTLVGHDTFTKVKPSAAS<sub>139</sub>GGGSA<sub>13</sub>EAGITGTWYNQLGSTFIVTAGADGALTGTYESAVGNAESRYVLTGRYDSAP<sub>64</sub>PSMTTQEKALNMFIRSQTLTLLLEKLNELDAEQADIAESLHDHADELYRSVLARF—**CO<sub>2</sub>H**

**Cp3:** **H<sub>2</sub>N**—ASMTGGQQMGG<sub>68</sub>SGTALGWTVAWKNNYRNAHSATTWSGQYVGGAEARINTQWLLTSGTTEANAWKSTLVGHDTFTKVKPSAAS<sub>139</sub>GGGSA<sub>13</sub>EAGITGTWYNQLGSTFIVTAGADGALTGTYESAVGNAESRYVLTGRYDSAP<sub>64</sub>GWNMTAQEKALNMFIRSQTLTLLLEKLNELDAEQADIAESLHDHADELYRSVLARF—**CO<sub>2</sub>H**

**Cp4:** **H<sub>2</sub>N**—ASMTGGQQMGG<sub>68</sub>SGTALGWTVAWKNNYRNAHSATTWSGQYVGGAEARINTQWLLTSGTTEANAWKSTLVGHDTFTKVKPSAAS<sub>139</sub>GGGSA<sub>13</sub>EAGITGTWYNQLGSTFIVTAGADGALTGTYESAVGNAESRYVLTGRYDSAP<sub>64</sub>GGNMTAQEKALNMFIRSQTLTLLLEKLNELDAEQADIAESLHDHADELYRSVLARF—**CO<sub>2</sub>H**

### 2.5.3 3D-model printing

The 3D-printing market has made a big leap forward in the past years, both in terms of technical innovation and economy. Nowadays, a wide range of three dimensional models, from small molecules up to large protein complexes, can be rapidly and cost-effectively printed in full colors. Several guidelines describe the preparation process of such models, starting from crystal structures.<sup>194-198</sup> These models can help to visualize extended three dimensional structures and are used for educational purposes.<sup>199-201</sup>

Herein, we built a 3D-model of an artificial metalloenzyme to visualize its binding pocket and residues in close proximity of the metal cofactor, which could be considered for mutagenesis. The 3D-print model was prepared based on a crystal structure of homotetrameric Sav S112A bearing the biotinylated iridium cofactor [Cp\*Ir(biot-*p*-L)Cl] (PDB ID 3PK2).<sup>60</sup> The C $\alpha$ -trace of the protein backbone was rendered in ball-and-stick style. The biotinylated iridium cofactor was displayed as van-der-Waals spheres. 28 residues in close proximity of the metal cofactor were highlighted as sticks.<sup>132</sup> In order to increase the rigidity of the model, stabilizing artificial connections between the  $\beta$ -sheets within one monomer and between the four monomers were introduced. Additionally, the hydrogen bonds between the protein and the biotin moiety of the metal complex were included to attach the cofactor to the streptavidin. The complete model was prepared in VMD (version 1.9.1)<sup>202</sup> and exported as an OBJ geometry definition file (Figure 29 a). Labels for selected residues (e.g. "48>") were created in Blender (version 2.70) and combined with the protein model using Meshlab (version 1.3.4)<sup>203</sup> (Figure 29 b). "Water tightness" of the fused structure was checked and the model was printed with the help of Dr. Stefan Imseng (Biozentrum, University of Basel) (Figure 29 c). The printed 3D-structure was finally cleaned and chemically treated to obtain a smooth shiny surface (Figure 29 d). The overall production process, from the initial PDB file to the printed 3D-model, covered around one week of working time. This work can be divided into three phases: i) preparation of the model in VMD (~2.5 days), ii) finalize the model in Meshlab (~1 day) and iii) printing and refinement of the model (~1.5 days).



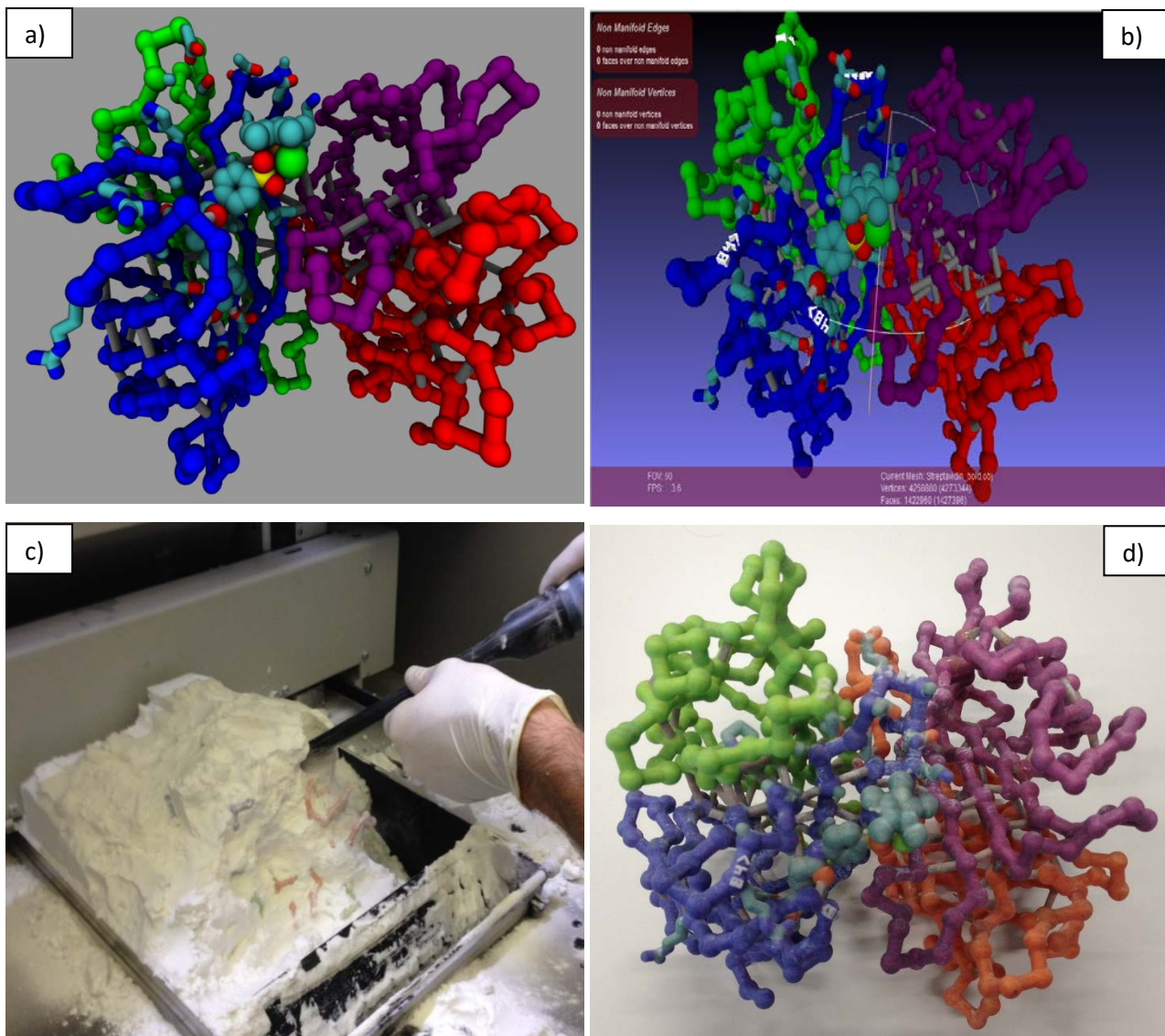


**Figure 29: Printing of a 3D-model of streptavidin.**

a) Preparation of the 3D-model (crystal structure from PDB ID 3PK2)<sup>60</sup> in VMD.<sup>202</sup> Monomers of streptavidin highlighted as C $\alpha$ -trace in blue, green, pink and red. Biotinylated iridium cofactor displayed as van-der-Waals spheres. Selected residues displayed as stick. Artificial stabilizing bonds displayed as grey cylinders. Hydrogen bonds between the protein and the cofactor displayed as white cylinders. b) Fusion of the protein structure and the residue numbering (e.g. "48>") performed in Meshlab.<sup>203</sup> Additionally, the model was checked for "water tightness". c) Printing of the 3D-model in a full-color powder-printer. Printing was performed with the help of Dr. Stefan Imseng (Biozentrum, University of Basel). d) Finalized model after cleaning and chemical treatment of the surface.

### 3 Conclusion and Outlook

In the course of this thesis, an artificial allylic deallocase based on the biotin-streptavidin technology was designed, engineered and applied in catalysis. The artificial metalloenzyme [CpRu(QA-Biot)(H<sub>2</sub>O)]PF<sub>6</sub> (**27**) · Sav was formed by covalent attachment of a biotin anchor to the previously reported ruthenium complex [CpRu(QA-NMe<sub>2</sub>)(Allyl)]PF<sub>6</sub> (**7**)<sup>94</sup> with subsequent incorporation into streptavidin (Sav) isoforms. Different strategies for the synthesis of this biotinylated ruthenium complex were explored and the complex was analyzed by detailed NMR studies (chapters 2.1.1 and 2.1.2). An X-ray crystal structure of the artificial metalloenzyme [CpRu(QA-Biot)(H<sub>2</sub>O)]PF<sub>6</sub> · Sav-S112M-K121A was solved (chapter 2.1.4). The designed artificial allylic deallocase was applied in catalysis towards the deprotection of a pro-fluorescent *O*-allyl-carbamate caged coumarin derivative (**1**). 86 purified streptavidin mutants (point mutations and elongated loop constructs) were tested *in vitro*. High protein acceleration could be determined for some of them. Mutant S112M-K121R revealed a 7.1-fold higher activity than the wild-type and a 16.3-fold increased activity compared to the free biotinylated ruthenium cofactor (chapter 2.2).<sup>118</sup>

In a next step, the artificial allylic deallocases were applied in an *in vivo* catalysis assay. Streptavidin isoforms were expressed and displayed on the surface of *E. coli* cells, using an ompA-Lpp outer-membrane anchoring system.<sup>131</sup> The presence of streptavidin on the outer-membrane of *E. coli* was confirmed by selective labelling of the cells with a biotinylated fluorophore as well as by an assay applying a fluorescently labelled streptavidin antibody system (chapter 2.3.1). Performing catalysis on the surface of *E. coli* cells allows a faster screening of a streptavidin mutant library, since the extraction and purification of the proteins is not required. In this spirit, seven single site saturation mutagenesis libraries with a total of 140 mutants were investigated (chapter 2.3.2; in collaboration with Dr. Tillmann Heinisch and BSc Brett Garabedian, Ward group, University of Basel).<sup>118</sup> Thereby, the activated double mutant S112M-K121R was selected as parent and the residues at the positions V47, N49, T114, N118, A119, S122 and L124 were separately saturated. The triple mutant S112M-K121R-S122N revealed a 30% higher activity in the *in vivo* catalysis than the respective parent S112M-K121R. Screening of these seven libraries was performed in the 96-well plate format with a medium throughput rate. However, the developed assay can be adapted to an automated screening with robots, thus increasing the throughput rate to ~ 10'000 mutants per month.

In order to further increase this number, a screening assay based on microfluidics was implemented (in collaboration with MSc Philipp Rottmann, Panke group, DBSSE ETH Zürich). *E. coli* cells displaying surface-anchored streptavidin were loaded with biotinylated ruthenium cofactor and encapsulated in single emulsions (water-in-oil) together with the coumarin substrate (**1**). The fluorescence intensity of droplets containing either Sav-WT or mutant S112M-K121A was analyzed after overnight incubation. Unfortunately, the elevated activity of the double mutant compared to the wild-type dramatically decreased from 12.4-fold in the 96-well plate to 1.6-fold in the droplets (chapter 2.3.3).

However, libraries possessing only small differences in fluorescence intensity between their members can potentially be enriched for activated mutants applying several rounds of catalysis and sorting.<sup>204</sup>

In a related project, caged small inducer molecules bearing an *O*-allyl-carbamate protective group were developed (chapter 2.4). This allowed us to control the expression of a GFP reporter protein by the action of the designed artificial allylic deallocases. First, the IPTG/lac-system was selected as biogenetic switch. Different caged IPTG derivatives, bearing self-immolative linkers, were synthesized and tested in catalysis. IPTG derivative **58** was selected as substrate for further experiments, due to its high stability against hydrolysis in the aqueous reaction medium. In the *in vitro* catalysis, [CpRu(QA-Biot)(H<sub>2</sub>O)]PF<sub>6</sub> (**27**) · Sav-S112M-K121A led to a 5.5-fold and a 10.8-fold higher conversion compared to the wild-type enzyme and the free cofactor, respectively (chapter 2.4.3). In the presence of GFP reporter cells (*E. coli* DH5α containing the pCD353 reporter plasmid), the purified artificial metalloenzyme [CpRu(QA-Biot)(H<sub>2</sub>O)]PF<sub>6</sub> (**27**) · Sav-S112M-K121A led to a 2.3-fold and a 3.6-fold higher GFP-fluorescence intensity compared to the wild-type enzyme and the free cofactor, respectively (chapter 2.4.4). It could be clearly demonstrated that the expression of a protein of interest in *E. coli* can be switched on by the action of an artificial metalloenzyme. In order to generalize the concept of the caged inducers, another system based on the DmpR regulator was investigated (in collaboration with Dr. Tsvetan Kardashliev, Panke group, DBSSE ETH Zürich; chapter 2.4.5). A caged hydroxyaniline derivative (**72**) was deprotected by our artificial allylic deallocase and subsequently successfully induced the expression of a GFP reporter protein.

In parallel to these projects, the biotin binding vestibule of streptavidin was genetically engineered. It was tested for the construction of a lid-like structure on top of the binding site, which may partially shield the active ruthenium cofactor (chapter 2.5). In this way, the reaction environment (i.e. the second coordination sphere around the ruthenium cofactor<sup>6</sup>) may be influenced by genetic modification of the host protein. This potentially increases the activity and selectivity of the artificial metalloenzyme. Five positions, suitable for the introduction of lid structures, were identified. Small loops (Gly-Gly-Ser-Gly-Gly-Ser) were introduced at these positions. In total, 40 streptavidin (loop) mutants were designed, from which 28 could be expressed as soluble biotin binding tetramers (chapter 2.5.2). 19 variants were purified and from one (mutant S112M-K121A) a crystal structure with the bound ruthenium cofactor [CpRu(QA-Biot)(H<sub>2</sub>O)]PF<sub>6</sub> (**27**) could be determined (PDB ID 6FH8).<sup>118</sup> Some of the loop mutants, especially the 66(GGS)<sub>2</sub> and the 159TPR variants displayed promising catalytic activities. However, a streptavidin variant containing a lid-like structure, which spans the whole biotin binding vestibule, could not be successfully expressed.

Finally, a three-dimensional model of the artificial metalloenzyme [Cp\*Ir(biot-*p*-L)Cl] · Sav-S112A (PDB ID: 3PK2)<sup>60</sup> was prepared and printed (chapter 2.5.3).

In summary, the initial aims of the thesis were (mostly) successfully fulfilled (chapter 1.6). An artificial allylic deallocase based on a ruthenium complex and the biotin-streptavidin technology was designed, synthesized and characterized. The new artificial metalloenzyme was evolved and applied in catalysis (*in vitro* as well as *in vivo*). Nevertheless, the designed artificial allylic deallocase can be further optimized, including:

- Modification of the ruthenium cofactor and the host protein (e.g. ligand and mutant screening)
- Expansion of the substrate scope (e.g. defined transfer of an allyl group)
- Implementation of cascade reactions (e.g. combination of an ArM with a natural enzyme)
- Expansion of the reaction space (e.g. catalysis in the periplasm of *E. coli*)
- Transfer of the ArM to other cells (e.g. mammalian cells or algae)

Concerning the modification of the ruthenium cofactor, the biotin anchor could be attached to the cyclopentadienyl ligand instead of the 2-quinolinecarboxylate ligand (see Figure 3b). Biotinylated cyclopentadiene could be mixed with  $[(C_6H_6)RuCl_2]_2$  and base, followed by treatment with acetonitrile and UV-light to form the complex  $[(Biot-Cp)Ru(MeCN)_3]PF_6$ .<sup>205</sup> The weak acetonitrile ligands can be simply exchanged by other ligands in order to form more active complexes.<sup>95</sup> A similar strategy was successfully applied in the formation of highly active artificial transfer hydrogenases.<sup>62</sup> Beside the biotinylated ruthenium cofactor, also the host protein could be further engineered – by single point mutations as well as by introduction and modification of loops.<sup>206</sup> Typically, large numbers of clones need to be tested in order to further evolve a variant which already shows an increased activity. Microfluidics in combination with droplet sorting provides the required ultrahigh-throughput capacity. Encapsulation of individual mutants in double emulsions (water-in-oil-in-water) combined with fluorescence activated cell sorting potentially allows to screen up to 2000 mutants per second (see chapter 2.3.3).<sup>145</sup> Thus, a library containing five simultaneously saturated single sites ( $20^5 = 3.2$  million mutants) may be screened in reasonable times.<sup>148</sup> At this point, the different proliferation rates of the cells and the expression levels of the mutants should be considered. Droplets containing mutants with a high expression level but a low activity will also show high fluorescence intensities. Thus, these droplets will be sorted too, leading to a higher number of false positives. Ideally, the expression level of a mutants and its activity would be determined simultaneously. This might be achieved by the split-GFP method<sup>207</sup> or the split-HRP method.<sup>208</sup>

Beside the biotinylated ruthenium cofactor and the streptavidin host, also the used substrates could be further engineered. The applied caged IPTG **58** revealed a certain level of unwanted background reaction, caused by hydrolysis of the ester function in the linker (chapters 2.4.2 and 2.4.3). Replacement of the ester by a carbamate would potentially increase the stability of the IPTG substrates. In this manner, an IPTG derivative (**62**) with a directly attached O-allyl carbamate protective group was designed (Figure 30). Since the sugar scaffold of this IPTG derivative was modified (the 2'-OH group was replaced by an  $NH_2$ ), the induction capacity of the uncaged product (**63**) would need to be evaluated first.

In addition, the preliminary test substrate **66** was designed. Possessing two carbamate groups, this substrate should be very stable towards hydrolysis. In order to increase the intramolecular cyclization rate after removal of the *O*-allyl carbamate caging group, an *N,N'*-dimethylethylenediamine core was selected.<sup>165</sup> Simultaneously with the formation of the urea (1,3-dimethyl-2-imidazolidinone), *para*-nitrophenol is released as a leaving group, which can be traced photospectrometrically. In a later stage, the *para*-nitrophenol leaving group will be replaced by an IPTG molecule. The stability and the performance of these two substrates in catalysis will be tested.

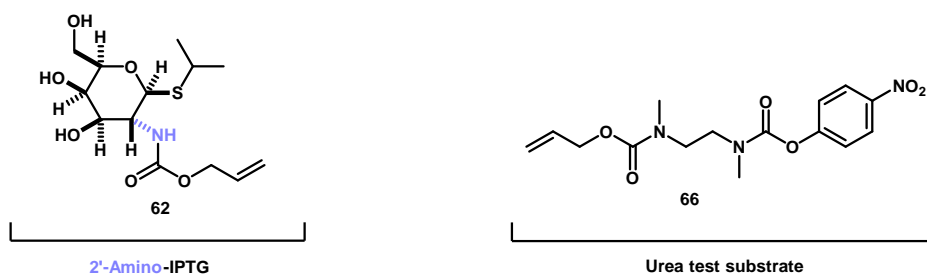
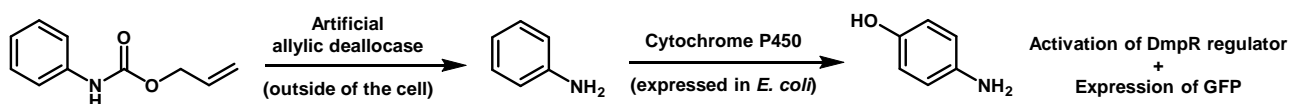


Figure 30: Designed *O*-allyl carbamate protected substrates for an artificial allylic deallocase.

In this thesis, we dealt with the deallylation of *O*-allyl carbamate protected substrates. The focus was set on the liberation of a fluorescent product (**2**) or inducer molecules (**45**, **67**), rather than to which nucleophilic species the allyl fragment was transferred (see Scheme 3). The catalysis reactions were performed in complex medium, containing a variety of potential nucleophiles. A substrate, which contains itself a nucleophile, would potentially allow the transfer of an allyl group in an intramolecular fashion. The overall reaction rate might therefore be higher compared to an intermolecular reaction involving an external nucleophile. Furthermore, a substrate containing two *O*-allyl carbamates or a mixture of different substrates could be used in catalysis in order to evolve a regio- and substrate selectivity of the artificial allylic deallocase. The application of two caged coumarin derivatives, which possess different fluorescence spectra may be envisaged. The substrate selectivity of the artificial metalloenzyme could be determined by the ratio of the two fluorescence intensities.

In addition, the developed artificial allylic deallocase could be applied in a cascade reaction. Based on the obtained results with the caged DmpR regulator system (chapter 2.4.5), we envisioned the combination of our artificial allylic deallocase with a cytochrome P450. The purified artificial metalloenzyme can deprotect an *O*-allyl carbamate-caged aniline. The generated aniline can be hydroxylated by a cytochrome P450<sup>209-210</sup> to generate a small molecule inducer (*para*-hydroxyaniline), which can switch on the expression of a GFP-reporter protein (Scheme 10).



**Scheme 10: Cascade reaction of an artificial allylic deallocase with a cytochrome P450 to activate a biogenetic switch.**

Artificial metalloenzymes are also functional in the periplasmic space of *E. coli*<sup>211</sup>, as shown by Ward *et al.* for an artificial metathase<sup>64</sup> or by Tezcan *et al.* for a designed  $\beta$ -lactamses.<sup>23</sup> Periplasmatic streptavidin was expressed in *E. coli* cell cultures at levels of up to 2  $\mu\text{M}$  at an optical density of  $\text{OD}_{600} = 1$  (unpublished data of the Ward group). These expression levels are up to 8-fold higher than the typical expression level of a surface-displayed streptavidin construct (chapter 2.3.1).<sup>127</sup> Thus, higher conversions might be achieved with artificial metalloenzymes in the periplasm compared to their analogues on the surface of *E. coli* cells. Furthermore, an ultrahigh-throughput screening using FACS techniques could be performed without encapsulation of the cells in micro-droplets, assuming that the formed product (e.g. IPTG) does not diffuse out of the cell. However, first the uptake of the biotinylated ruthenium cofactor and the substrate into the periplasmic space must be ensured. Installation of an engineered FhuA pore in the outer membrane<sup>212-214</sup> or application of an osmotic shock<sup>215-216</sup> might increase the uptake efficiency.

Finally, the designed artificial allylic deallocase was applied in cell cultures other than *E. coli*. Dr. Yasunori Okamoto (Ward group, University of Basel) designed a gene switch in mammalian cells, which can be triggered with the artificial metalloenzyme.<sup>217</sup> In combination with a biotinylated cell-penetrating peptide, the artificial allylic deallocase can enter the mammalian cell. In a cascade reaction with an esterase, an *O*-allyl carbamate caged inducer is deprotected and can then switch on the gene of interest.

MSc Mathieu Szponarski (Gademann group, University of Zürich) performed catalysis with our designed artificial allylic deallocases anchored to the surface of *Chlamydomonas reinhardtii*.<sup>218</sup> The property, that the swimming direction of such algae can be controlled by light irradiation<sup>219</sup> might be used to design a reaction set-up, in which the algae cells as a carrier of an active artificial metalloenzyme can be conducted to a desired place. In this way, the action of an artificial metalloenzyme could be spatially controlled.

## 4 Experimental part

### 4.1 Instruments and material

All commercially available chemicals were purchased from Sigma-Aldrich, ABCR, TCI Europe, Acros Organics, Alfa Aesar, Fluka, Fluorochem, Merck or Ukrorgsyntez Ltd. and used without further purification. FluoroSurfactant was purchased from RAN Biotechnologies. Deuterated solvents were purchased from Cambridge Isotope Laboratories Inc. or Armar Chemicals. Solvents for UPLC-MS measurements were purchased from Romil. The water was purified with a Milli-Q-system (Millipore). Antibiotics were purchased from Applichem GmbH, DNase I was from Roche Diagnostics AG, IPTG was from Apollo Scientific, biotin-4-fluorescein was from ANAWA Trading SA, Atto-565-biotin was from Atto-Tec GmbH and Agarose/SDS-PAGE markers were from New England BioLab® Inc. Restriction enzymes, DNA polymerases and ligases were purchased from New England BioLab® Inc. Primers were ordered from Microsynth AG. DNA string fragments (GeneArt® Strings™ DNA Fragments) were purchased from invitrogen™ by life technologies™. The mouse-anti-streptavidin antibody (ab10020) was purchased from Abcam and the fluorescein isothiocyanate-tagged goat-anti-mouse antibody (f-2761) was purchased from ThermoFisher. Thin layer chromatography (TLC) was performed on Merck TLC Silica gel 60 F254 plates, using a UV-detector (254 nm or 360 nm). Basic KMnO<sub>4</sub> solution or DACA solution (0.1% 4-(dimethylamino)-cinnamaldehyde and 1% H<sub>2</sub>SO<sub>4</sub> in EtOH) was used for the staining. Column chromatography was performed using silica gel (Merck Silica gel 60 (0.040-0.063 mm)) or basic aluminium oxide (Fluka (0.05-0.15 mm)). NMR spectra were measured on a 400 MHz and 500 MHz Bruker Advance spectrometer at room temperature and evaluated with MestReNova. Chemical shifts ( $\delta$ ) are quoted in parts per million (ppm) and referenced to the residual solvent peaks. Scalar coupling (J) is reported in Hertz (Hz). HRMS analysis was performed by Dr. Heinz Nadig (University of Basel) on a Bruker maXis 4G. Mass-spectral analysis of the expressed streptavidin mutants was performed on a Bruker Daltonics, ESI/micrOTOF MS. UPLC-MS analysis was performed on a Water Acquity UPLC® equipped with an SQ Detector 2 mass spectrometer. Details are given in the corresponding sections. Fluorescence/Absorption spectroscopy was performed on a TECAN infinite M1000 Pro. PCR reactions were performed with an Eppendorf Mastercycler Gradient. DNA sequencing (Sanger cycle sequencing/capillary electrophoresis) was performed by Microsynth AG. *E. coli* DH5 $\alpha$  cells were purchased from ThermoFisher, *E. coli* NEB® Turbo cells were from New England BioLab® Inc., *E. coli* BL21(DE3) were from Stratagene (Agilent) and *E. coli* TOP10(DE3) cells were a gift from Dr. Markus Jeschek (Panke group, DBSSE ETH Zürich). Cells were chemically treated by Dipl.-Biol. Juliane Klehr (Ward group, University of Basel) according to the Hanahan method using RbCl. Affinity column chromatography (purification of the expressed streptavidin mutants) was performed on an Äktaprime Plus chromatography system, using 2-iminobiotin sepharose column. Flow cytometry analysis was performed on an Attune NxT acoustic focusing cytometer (life technologies™) with the help of Dr. Emeline Sautron.

## 4.2 Methods

### 4.2.1 Protein-ligand docking

All docking simulations were performed with GOLD (version 5.4), using the graphical interface Hermes 1.8.0 with a method similar to that described by Robles *et al.*<sup>220</sup> The method consists of (i) preparation of the catalyst structure file including the linker, (ii) preparation of the host structure file, and (iii) docking of the catalyst into a biotin-loaded streptavidin crystal structure by covalent linkage of the catalyst to the biotin anchor.

The structure of the non-biotinylated ruthenium catalyst [CpRu(QA)(Allyl)]PF<sub>6</sub> (**5**) was extracted from a crystal structure reported by Kitamura *et al.* (Cambridge Structural Database Refcode: NAJLUG).<sup>85</sup> Afterwards, where applicable, the allyl ligand was replaced by a water molecule giving to the oxygen atom the coordinates of the barycenter of the carbon atoms of the former allyl ligand. In order to preserve the structure of the ruthenium complex, the metal-ligand bonds were explicitly manually added to the structure file (text format), thereby constraining the ruthenium complex during the following docking. Using the building tool of UCSF Chimera<sup>221</sup>, the piperazine linker of [CpRu(QA-piperazine)(Allyl/H<sub>2</sub>O)]PF<sub>6</sub> was constructed (the linker for the complex [(Biot-Cp)Ru(QA-NMe<sub>2</sub>)(Allyl)]PF<sub>6</sub> (**17**) was constructed in the same way). The hydrogen atom of the secondary amine of the piperazine was then removed in order to allow later attachment of the biotin anchor. The structure of the receptor consisted of a dimer of streptavidin generated from a crystal structure reported by Dürrenberger *et al.* (PDB entry: 3PK2).<sup>60</sup> In this homotetrameric structure, streptavidin contains the biotinylated iridium complex [Cp\*Ir(Biot-*p*-L)Cl] (Figure 31). Using UCSF Chimera, two facing monomers, the solvent molecules and the salts were deleted. In the resulting dimer both [Cp\*Ir(Biot-*p*-L)Cl] cofactors were deleted except for one biotin (including the N<sub>Am</sub> atom, Figure 31). Using the mutation tool of Chimera, the two monomers of streptavidin were mutated to yield a dimer of Sav S112M-K121A. As an initial starting point, the chains were set to adopt the conformation which is most frequently observed in crystal structures. During the docking procedure, a covalent restraint was set: the secondary amine N-atom of the piperazine linker of [CpRu(QA-piperazine)(Allyl/H<sub>2</sub>O)] was set to coincide with the N<sub>Am</sub> of the biotin in the streptavidin dimer (Figure 31). The 6 residues with the smallest distance to the catalyst, namely N118, S112M and L124 of both streptavidin monomers, were kept flexible. Thus a library of rotamers was generated. The final rotamer having the highest ChemScore was selected and the coordinates of the atoms of both the biotin and the docked ruthenium cofactor were pooled in a single file to reconstruct the entire biotinylated ruthenium complex [CpRu(QA-Biot)(Allyl/H<sub>2</sub>O)] with the minimized docked conformation.



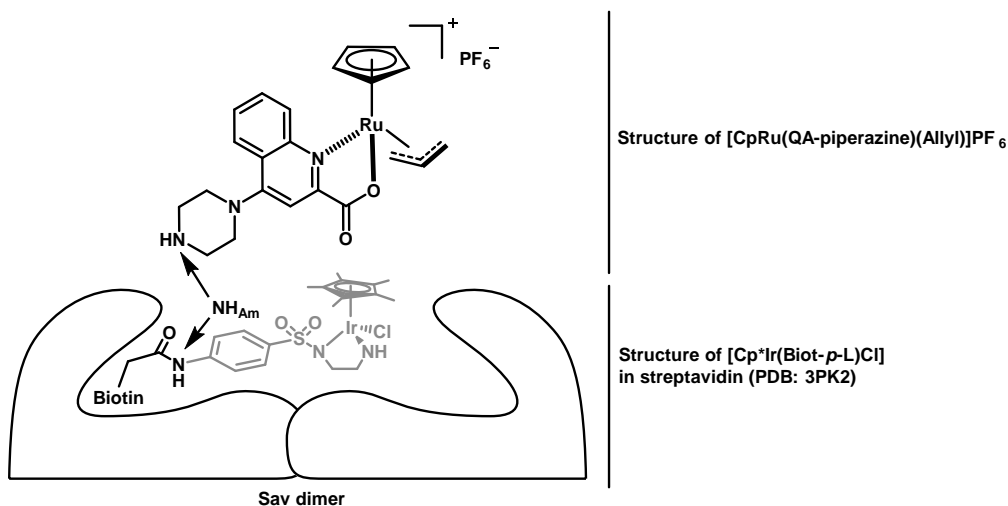


**Figure 31: Covalent docking of a biotinylated ruthenium complex into a streptavidin dimer.**

The amide nitrogen ( $\text{N}_{\text{Am}}$ ) serves as anchoring atom. The part of the original biotinylated iridium complex  $[\text{Cp}^*\text{Ir}(\text{Biot-}p\text{-L})\text{Cl}]$ , which was replaced during the docking process, is depicted in grey.

#### 4.2.2 HABA titration

Stock solutions:

- Phosphate buffer (20 mM  $\text{NaH}_2\text{PO}_4/\text{Na}_2\text{HPO}_4$ , pH 7.4)
- Streptavidin wild-type (8  $\mu\text{M}$  tetramer) in phosphate buffer
- D-Biotin (0.96 mM) in phosphate buffer/DMF (80:20)
- Ligand **26** (0.96 mM) in phosphate buffer/DMF (80:20)
- Complex **27** (0.96 mM, prepared from a 1:1 mixture of  $[\text{CpRu}(\text{MeCN})_3]\text{PF}_6$  and Ligand **26** in DMF) in phosphate buffer/DMF (80:20)
- HABA (9.6 mM) in phosphate buffer

Titration:

A blank sample (phosphate buffer only) was first determined. HABA stock solution (300  $\mu\text{l}$ ) was mixed with protein stock solution (2.4 ml) in a cuvette ( $d = 1 \text{ cm}$ ), incubated for 5 min at room temperature and absorption at 506 nm was determined. D-biotin, ligand or complex stock solution was titrated in steps of 5  $\mu\text{l}$  (= 0.25 eq. biotinylated compound vs. streptavidin tetramer) and absorption was determined.

### 4.2.3 Catalysis procedure for the coumarin substrate

#### Catalysis reactions with coumarin substrate **1** and purified streptavidin:

Stock solutions:

- PBS buffer (1x, pH 7.4) containing 50 mM Na<sub>2</sub>HPO<sub>4</sub>/NaH<sub>2</sub>PO<sub>4</sub> and 0.9% NaCl
- Streptavidin (2 mM free biotin binding sites in water)
- Ruthenium cofactors (1 mM in organic co-solvent)
- Substrate **1** (10 mM in water)

Catalysis reactions were performed in flat 96-well plates at a reaction volume of 200  $\mu$ l and a substrate concentration of 500  $\mu$ M. Other conditions are indicated in Table 4, Figure 11 or Figure 12. PBS buffer was filled into a 96-well plate followed by the addition of streptavidin and ruthenium cofactor. This solution was incubated at room temperature for 10 min (streptavidin can bind the biotinylated cofactor). Substrate was added and the plate was sealed with an aluminum cover and incubated at the given conditions. An aliquot of the reaction mixture (3  $\mu$ l) was then diluted with water (147  $\mu$ l) in a new flat black 96-well plate. Fluorescence of the product **2** was determined in a plate reader at  $\lambda_{\text{ex.}} = 395 \text{ nm}$  /  $\lambda_{\text{em.}} = 460 \text{ nm}$  and compared with a standard curve of the product (Figure 32).

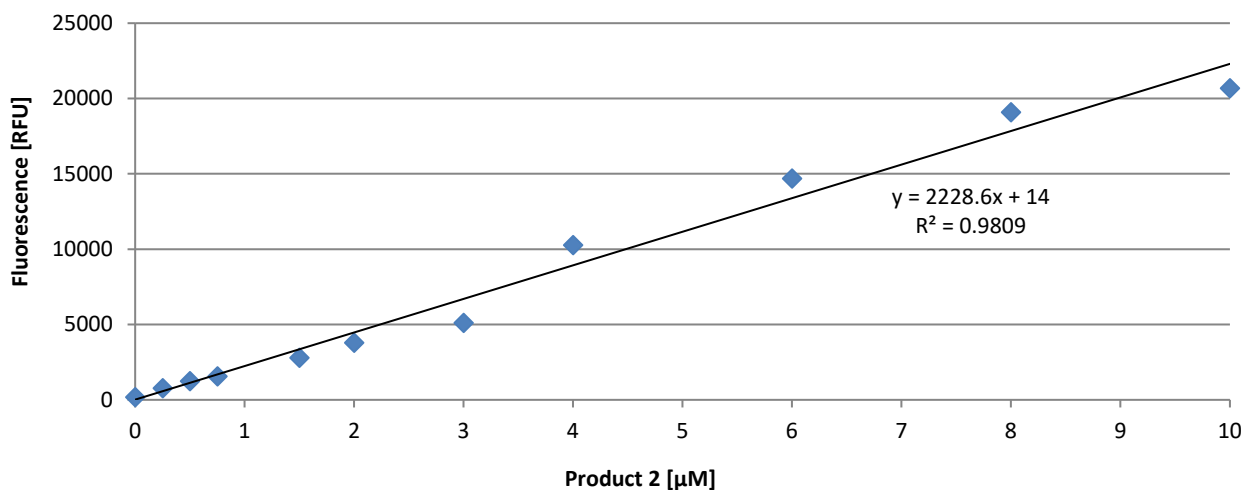


Figure 32: Standard curve of coumarin product **2** in water.

#### 4.2.4 Screening of *E. coli* surface Sav libraries

##### Creation of libraries:

PCR<sup>222</sup> was performed applying the 22-codon trick<sup>144</sup>, in which a 12:9:1 mixture of primers containing the NDT, VHG or TGG codon, respectively, is used. The forward and reverse primers for the 7 mutagenesis positions are listed in Table 10.

**Table 10: Primers for site saturation mutagenesis at the positions V47, N49, T114, N118, A119, S122 and L124.**

Position	Primer	Sequence
V47	NDT_fw	GCGCAndtGGTAATGCAGAAAGC
	VHG_rv	GCGCAvhgGGTAATGCAGAAAGC
	TGG_fw	GCGCAtggGGTAATGCAGAAAGC
	AHN_rv	CTGCATTACCahnTGCgCTTTCATAC
	CDB_rv	CTGCATTACCcdbTGCgCTTTCATAC
	CCA_rv	CTGCATTACCccaTGCgCTTTCATAC
N49	NDT_fw	GGTndtGCAGAAAGCCGTTATGTTT
	VHG_rv	GGTvvhgGCAGAAAGCCGTTATGTTT
	TGG_fw	GGTtggGCAGAAAGCCGTTATGTTT
	AHN_rv	CGGCTTTCTGCahnACCAACTGC
	CDB_rv	CGGCTTTCTGCcdbACCAACTGC
	CCA_rv	CGGCTTTCTGCccaACCAACTGC
T114	NDT_fw	GGGCndtACCGAAGCAAATGCCTGG
	VHG_rv	GGGCvhgACCGAAGCAAATGCCTGG
	TGG_fw	GGGCtggACCGAAGCAAATGCCTGG
	AHN_rv	CATTTGCTTCGGTahnGCCCATGGTCAG
	CDB_rv	CATTTGCTTCGGTcdbGCCCATGGTCAG
	CCA_rv	CATTTGCTTCGGTccaGCCCATGGTCAG
N118	NDT_fw	GCAAndtGCCTGGCGCAGCACCCCTGG
	VHG_rv	GCAAvhgGCCTGGCGCAGCACCCCTGG
	TGG_fw	GCAAtggGCCTGGCGCAGCACCCCTGG
	AHN_rv	GGTGCTGCGCCAGGCahnTGCTTCGGTG
	CDB_rv	GGTGCTGCGCCAGGCcdbTGCTTCGGTG
	CCA_rv	GGTGCTGCGCCAGGCccaTGCTTCGGTG
A119	NDT_fw	CAAATndtTGGCGCAGCACCCCTGGTTG
	VHG_rv	CAAATvhgTGGCGCAGCACCCCTGGTTG
	TGG_fw	CAAATtggTGGCGCAGCACCCCTGGTTG
	AHN_rv	CAGGGTGCTGCGCCAahnATTTGCTTCG
	CDB_rv	CAGGGTGCTGCGCCAcdbATTTGCTTCG
	CCA_rv	CAGGGTGCTGCGCCAccaATTTGCTTCG
S122	NDT_fw	GCGCndtACCCTGGTTGGTCATGATAC
	VHG_rv	GCGCvhgACCCTGGTTGGTCATGATAC
	TGG_fw	GCGCtggACCCTGGTTGGTCATGATAC
	AHN_rv	CATGACCAACCAGGGTahnGCGCCAG
	CDB_rv	CATGACCAACCAGGGTcdbGCGCCAG
	CCA_rv	CATGACCAACCAGGGTccaGCGCCAG
L124	NDT_fw	CTGGAAAAGCACcndtGTTGGTCATG
	VHG_rv	CTGGAAAAGCACvhgGTTGGTCATG
	TGG_fw	CTGGAAAAGCACctggGTTGGTCATG
	AHN_rv	CAACahnGGTGCTGCGCCAGGCATTTGC
	CDB_rv	CAACcdbGGTGCTGCGCCAGGCATTTGC
	CCA_rv	CAACccaGGTGCTGCGCCAGGCATTTGC

PCR mixture:

5 µl Q5-buffer (5x), 1 µl template DNA of Sav mutant S112M-K121R (25 ng/µl), 5 µl forward primers (1 µM; mixture of NDT/VHG/TGG = 12:9:1), 5 µl reverse primers (1 µM; mixture of AHN/CDB/CCA = 12:9:1), 0.5 µl dNTP's (10 mM), 0.5 µl DMSO, 7.75 µl water, 0.25 µl Q5 Hot start HF DNA polymerase (2 U/µl).

PCR program:

95°C for 2 min; 95°C for 30 s, 70 °C for 15 s, 72°C for 5 min (14 cycles); 72°C for 10 min.

PCR products were digested (DpnI, 37°C, 90 min) and transformed into chemically competent *E. coli* TOP10(DE3) cells (50 µl competent cells + 2 µl digested PCR product; heat-shock for 30 s at 42°C; incubation in LB-medium for 1 h at 37°C prior to plating). Colonies were grown on LB-agar plates containing 34 µg/ml chloramphenicol (37°C, overnight). 88 colonies per library were picked and overnight cultures were prepared (LB-medium with 34 µg/mL chloramphenicol, 37°C, 310 rpm). Cells were harvested, plasmids (13 clones per library) were isolated<sup>223</sup> and analysed by Sanger DNA sequencing.<sup>224-225</sup> Glycerol stocks (15% glycerol) were prepared.

#### Catalysis activity assay:

Stock solutions:

- PBS-buffer (1x, pH 7.4)
- L-arabinose (5% (wt/vol) in water)
- Ruthenium cofactor stock (2 mM [CpRu(QA-Biot)(Sol.)] (**27**) in DMF)
- Coumarin substrate stock (5 mM coumarin **1** in PBS-buffer)
- Reaction-buffer: 22.5 ml PBS-buffer + 2.5 ml coumarin substrate stock + 25 µl ruthenium cofactor stock → final concentrations: 500 µM coumarin **1**, 2 µM [CpRu(QA-Biot)(Sol.)] (**27**)

Studier medium:

1x M-stock (25 mM Na<sub>2</sub>HPO<sub>4</sub>, 25 mM KH<sub>2</sub>PO<sub>4</sub>, 50 mM NH<sub>4</sub>Cl, 5 mM Na<sub>2</sub>SO<sub>4</sub>) + MgSO<sub>4</sub> (2 mM) + glycerol (0.5%) + tryptone (15 g/L) + yeast extract (10 g/L).

In a 96-deep well plate, LB-medium containing 34 µg/ml chloramphenicol (300 µl per well) was inoculated from glycerol stocks of the designed libraries (88 clones per library) or the corresponding controls (2x Sav-WT and 2x Sav-S112M-K121R). The plate was incubated overnight (37°C, 200 rpm shaking). In a new 96-deep well plate, Studier-medium (34 µg/ml chloramphenicol, 240 µl per well) was inoculated with pre-culture (10 µl) and incubated for 3.5 h (37°C, 310 rpm shaking). L-arabinose (10 µl) was added and the plate was incubated for 4 h (25°C, 280 rpm shaking).

Cells were centrifuged (3200 g, 8°C, 5 min), supernatant was discarded and the cells were resuspended in reaction-buffer (250 µl). The plate was then incubated for 16 h (30°C, 310 rpm shaking). Finally, the cell density (150 µl PBS-buffer + 50 µl reaction mixture, OD<sub>600</sub>) and the coumarin fluorescence (245 µl PBS-buffer + 5 µl reaction mixture, λ<sub>ex.</sub> = 395 nm, λ<sub>em.</sub> = 460 nm) were determined in a TECAN plate reader.

#### 4.2.5 Microfluidics and droplet production

##### Stock solutions:

- PBS-buffer (1x, pH 7.4)
- Phosphate buffered LB-medium (50 mM Na<sub>2</sub>HPO<sub>4</sub>/NaH<sub>2</sub>PO<sub>4</sub>, pH 7.4)
- L-arabinose (10% in water)
- Ruthenium cofactor stock (2 mM [CpRu(QA-Biot)(Sol.)] (**27**) in DMF)
- Coumarin substrate stock (0.75 mM coumarin **1** in buffered LB-medium (pH 7.4))
- Artificial metalloenzyme (200 µM Sav-S112M-K121A (free biotin binding sites) + 100 µM ruthenium cofactor)
- Fluorinated oil: HFE-7500 3M™ Novec™ Engineered fluid (Fluorochem) +1% FluoroSurfactant (RAN Biotechnologies)

##### Protein expression:

A preculture of *E. coli* TOP10(DE3) cells containing the pBAD33-Lpp-ompA-T7-Sav plasmid was prepared in LB-medium (34 µg/ml chloramphenicol) and incubated overnight (37°C, 210 rpm shaking). Studier medium (see chapter 4.2.4) was inoculated with the preculture to a starting OD<sub>600</sub> of 0.05. The main culture was incubated for 3 h (37°C, 210 rpm shaking). A part of the culture was induced with L-arabinose (final concentration: 0.2%) and incubated for 4 h (25°C, 210 rpm shaking). The remaining cells were kept on ice.

##### Catalyst uptake:

A defined amount of cells (2 ml culture at OD<sub>600</sub> = 2.0) was transferred to an Eppendorf tube and centrifuged (11'000 g, 2 min, 8°C). The supernatant was discarded and the pellet resuspended in 2 ml PBS-buffer (1x, pH 7.4). The sample was then centrifuged (11'000 g, 2 min, 8°C). The supernatant was discarded and the pellet resuspended in 2 ml PBS-buffer (1x, pH 7.4) containing 2 µM ruthenium cofactor. The sample was incubated for 30 min on ice. The sample was then centrifuged (11'000 g, 2 min, 8°C). The supernatant was discarded and the pellet resuspended in 2 ml phosphate buffered LB-medium (pH 7.4) → cells are now at a concentration of OD<sub>600</sub> = 0.2.

**Droplet production:**

Substrate mixture was prepared as follows: ruthenium cofactor stock (1.5  $\mu$ l) + L-arabinose stock (30  $\mu$ l) + substrate stock (750  $\mu$ l) + phosphate buffered LB-medium (218.5  $\mu$ l). This led to the following concentrations: ruthenium cofactor (3  $\mu$ M), L-arabinose (0.3%), substrate (750  $\mu$ M).

The microfluidic chip was operated at the following flow rates:

Cells: 60  $\mu$ l/h; Substrate mixture: 120  $\mu$ l/h; Fluorinated oil: 600  $\mu$ l/h

Droplets of each sample were produced for exactly 15 min. The droplets were then incubated in Eppendorf tubes for 19 h (25°C, gentle mixing).

**Droplet breaking and fluorescence determination:**

The oil at the bottom of the Eppendorf tube was carefully removed. 400  $\mu$ l PBS-buffer (1x, pH 7.4) was added to the sample, followed by the addition of surfactant (1H,1H,2H,2H-perfluorooctan-1-ol, 100  $\mu$ l). The sample was vortexed for 20 seconds and quickly centrifuged. 150  $\mu$ l of the supernatant were transferred into a flat-black 96-well plate and the fluorescence was determined in a plate reader ( $\lambda_{\text{ex.}}$  = 395 nm,  $\lambda_{\text{em.}}$  = 460 nm).

#### 4.2.6 Catalysis procedure for caged IPTG substrates

***In vitro* catalysis:**

General procedure for the *in vitro* catalysis with the IPTG substrates **58**, **46**, **50** and **54**. Further details are given in the relevant sections and in Table 6, Table 7 and Figure 21.

Stock solutions:

- Phosphate buffer (50 mM Na<sub>2</sub>HPO<sub>4</sub>/NaH<sub>2</sub>PO<sub>4</sub>, various pH's, containing 0.9% NaCl)
- Streptavidin (2 mM free biotin binding sites in water)
- Ruthenium cofactors (1 mM in organic co-solvent)
- IPTG substrate (5 mM in water)

Catalysis reactions were performed in flat 96-well plates in a reaction volume of 200  $\mu$ l. Buffer (178  $\mu$ l) was filled into a 96-well plate followed by the addition of streptavidin (1  $\mu$ l) and ruthenium cofactor (1  $\mu$ l). This solution was incubated at room temperature for 10 min (to allow streptavidin to bind to the biotinylated cofactor). Substrate (20  $\mu$ l) was added and the plate was sealed with an aluminum cover and incubated at the given conditions. Aliquots of the reaction mixtures (50  $\mu$ l) were then diluted with methanol (200  $\mu$ l) and incubated at room temperature for 10 min (precipitation of the protein).

Samples were then centrifuged (21'000 g, 20°C, 5 min). Supernatants (5  $\mu$ l) were diluted with MilliQ-water (995  $\mu$ l) and subjected to UPLC-MS analysis (Figure 33).

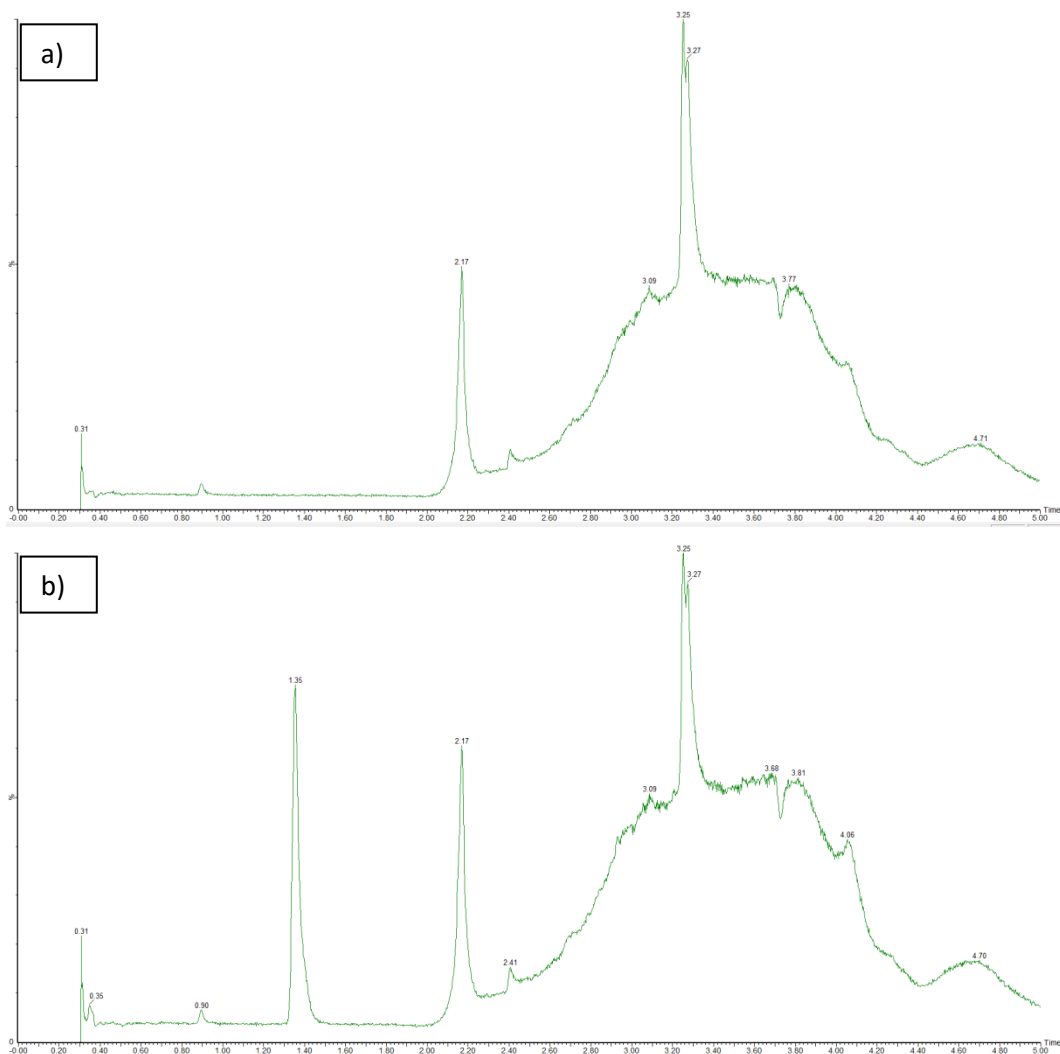


**Figure 33: UPLC-MS chromatograms (single ion recording) of IPTG samples.**

Blank sample. b) Sample containing 0.5 μM IPTG. UPLC-MS conditions: Solvents: MilliQ-water + 0.1% HCOOH (Solvent C), MeCN + 0.1% HCOOH (Solvent D); Column: ACQUITY UPLC® HSS T3 1.8 μm, 2.1x100 mm; Oven temperature: 40°C; Flow rate: 0.6 ml/min, Run time: 5.0 min; Gradient: 0 min (5% D), 1.0 min (5% D), 2.0 min (95% D), 3.0 min (5% D), 5.0 min (5% D); Injection volume: 5 μl; Cone voltage: 40 V; Single ion recording at 261 m/z (= [IPTG+Na]<sup>+</sup>); Retention time IPTG: 1.35 min.

## 4.2.7 Cloning of Sav loop mutants

### Sav gene constructs:

The gene sequences for the streptavidin variants bearing an additional secondary structure element were ordered as double stranded DNA-string fragments (GeneArt® Strings™ DNA Fragments, invitrogen™ by life technologies™), containing a four-base pair overhang (**ATAT**, **TATA**) at both ends (Table 11).

**Table 11: DNA sequences of streptavidin variants with an additional secondary structure element.**

Entry	Name	Sequence (5' to 3')
1	48(GGS) <sub>2</sub>	<b>ATAT</b> CATATGGCAAGCATGACGGGTGCCAGCAGATGGGTCGTGATCAGGCAGGTATTACCGGCACCTGGTATAATCAGCTGGGTAGCACCTTTATTGTTACCGCGGGCGCAGATGGTGCCTGACCGGCACGTACGAAAGCGCAGTTGGTGGC GGCAGCGGCGGCAGCAATGCAGAAAGCCGTTATGTTCTGACCGGTCGTTATGATAGCGCACCGGCAACCGATGGTAG CGGTACCGCACTGGGTTGGACCGTTGCATGGAAAAATAACTATCGTAATGCACATAGCGCAACCACGTGGTCAGGTCA GTATGTTGGTGGTGCAGAAAGCACGCATTAACACCCAGTGGCTGCTGACCAGCGGCACCACCGAAGCAAATGCCTGGA AAAGCACCTGGTTGGTCATGATACCTTTACCAAAGTTAAACCGAGCGCAGCATCAATTGATGCAGCAAAAAAAGCCG GTGTGAATAATGGTAATCCGCTGGATGCAGTTCAGCAGTAATAGGGATCCTATA
2	66(GGS) <sub>2</sub>	<b>ATAT</b> CATATGGCAAGCATGACGGGTGCCAGCAGATGGGTCGTGATCAGGCAGGTATTACCGGCACCTGGTATAATCAGCTGGGTAGCACCTTTATTGTTACCGCGGGCGCAGATGGTGCCTGACCGGCACGTACGAAAGCGCAGTTGGTAAT GCAGAAAGCCGTTATGTTCTGACCGGTCGTTATGATAGCGCACCGGCAACCGGCGGCAGCGGCGGCAGCGATGGTAG CGGTACCGCACTGGGTTGGACCGTTGCATGGAAAAATAACTATCGTAATGCACATAGCGCAACCACGTGGTCAGGTCA GTATGTTGGTGGTGCAGAAAGCACGCATTAACACCCAGTGGCTGCTGACCAGCGGCACCACCGAAGCAAATGCCTGGA AAAGCACCTGGTTGGTCATGATACCTTTACCAAAGTTAAACCGAGCGCAGCATCAATTGATGCAGCAAAAAAAGCCG GTGTGAATAATGGTAATCCGCTGGATGCAGTTCAGCAGTAATAGGGATCCTATA
3	84(GGS) <sub>2</sub>	<b>ATAT</b> CATATGGCAAGCATGACGGGTGCCAGCAGATGGGTCGTGATCAGGCAGGTATTACCGGCACCTGGTATAATCAGCTGGGTAGCACCTTTATTGTTACCGCGGGCGCAGATGGTGCCTGACCGGCACGTACGAAAGCGCAGTTGGTAAT GCAGAAAGCCGTTATGTTCTGACCGGTCGTTATGATAGCGCACCGGCAACCGATGGTAGCGGTACCGCACTGGGTTGG ACCGTTGCATGGAAAAATAACTATCGTGGCGGCAGCGGCGCAGCAATGCACATAGCGCAACCACGTGGTCAGGTCA GTATGTTGGTGGTGCAGAAAGCACGCATTAACACCCAGTGGCTGCTGACCAGCGGCACCACCGAAGCAAATGCCTGGA AAAGCACCTGGTTGGTCATGATACCTTTACCAAAGTTAAACCGAGCGCAGCATCAATTGATGCAGCAAAAAAAGCCG GTGTGAATAATGGTAATCCGCTGGATGCAGTTCAGCAGTAATAGGGATCCTATA
4	117(GGS) <sub>2</sub>	<b>ATAT</b> CATATGGCAAGCATGACGGGTGCCAGCAGATGGGTCGTGATCAGGCAGGTATTACCGGCACCTGGTATAATCAGCTGGGTAGCACCTTTATTGTTACCGCGGGCGCAGATGGTGCCTGACCGGCACGTACGAAAGCGCAGTTGGTAAT GCAGAAAGCCGTTATGTTCTGACCGGTCGTTATGATAGCGCACCGGCAACCGATGGTAGCGGTACCGCACTGGGTTGG ACCGTTGCATGGAAAAATAACTATCGTAATGCACATAGCGCAACCACGTGGTCAGGTCAAGTATGTTGGTGGTGCAGAA GCACGCATTAACACCCAGTGGCTGCTGACCAGCGGCACCACCGAAGCAGGCGGCAGCGGCGGCAGCAATGCCTGGAA AAGCACCTGGTTGGTCATGATACCTTTACCAAAGTTAAACCGAGCGCAGCATCAATTGATGCAGCAAAAAAAGCCGG TGTGAATAATGGTAATCCGCTGGATGCAGTTCAGCAGTAATAGGGATCCTATA
5	48TPR	<b>ATAT</b> CATATGGCAAGCATGACGGGTGCCAGCAGATGGGTCGTGATCAGGCAGGTATTACCGGCACCTGGTATAATCAGCTGGGTAGCACCTTTATTGTTACCGCGGGCGCAGATGGTGCCTGACCGGCACGTACGAAAGCGCAGTTGGTGGC GGCAGCGCGGAAGCGTGGTATAACCTGGGCAACGCGTATTATAAACAGGGCGATTATGATGAAGCGATTGAATATTA TCAGAAAGCGCTGGAAGTGAAGCGGCAATGCAGAAAGCCGTTATGTTCTGACCGGTCGTTATGATAGCGCACCGG CAACCGATGGTAGCGGTACCGCACTGGGTTGGACCGTTGCATGGAAAAATAACTATCGTAATGCACATAGCGCAACCA CGTGGTCAGGTCAAGTATGTTGGTGGTGCAGAAAGCACGCATTAACACCCAGTGGCTGCTGACCAGCGGCACCACCGAA GCAAATGCCTGGAAAAGCACCTGGTTGGTCATGATACCTTTACCAAAGTTAAACCGAGCGCAGCATCAATTGATGCA GCAAAAAAAGCCGGTGTGAATAATGGTAATCCGCTGGATGCAGTTCAGCAGTAATAGGGATCCTATA
6	66TPR	<b>ATAT</b> CATATGGCAAGCATGACGGGTGCCAGCAGATGGGTCGTGATCAGGCAGGTATTACCGGCACCTGGTATAATCAGCTGGGTAGCACCTTTATTGTTACCGCGGGCGCAGATGGTGCCTGACCGGCACGTACGAAAGCGCAGTTGGTAAT GCAGAAAGCCGTTATGTTCTGACCGGTCGTTATGATAGCGCACCGGCAACCGGCGGCAGCGGGAAGCGTGGTATAA CCTGGGCAACGCGTATTATAAACAGGGCGATTATGATGAAGCGATTGAATATTATCAGAAAGCGCTGGAAGTGAAGCG GCGCGATGGTAGCGGTACCGCACTGGGTTGGACCGTTGCATGGAAAAATAACTATCGTAATGCACATAGCGCAACC ACCTGGTCAGGTCAAGTATGTTGGTGGTGCAGAAAGCACGCATTAACACCCAGTGGCTGCTGACCAGCGGCACCACCGA AGCAAATGCCTGGAAAAGCACCTGGTTGGTCATGATACCTTTACCAAAGTTAAACCGAGCGCAGCATCAATTGATGC AGCAAAAAAAGCCGGTGTGAATAATGGTAATCCGCTGGATGCAGTTCAGCAGTAATAGGGATCCTATA
7	84TPR	<b>ATAT</b> CATATGGCAAGCATGACGGGTGCCAGCAGATGGGTCGTGATCAGGCAGGTATTACCGGCACCTGGTATAATCAGCTGGGTAGCACCTTTATTGTTACCGCGGGCGCAGATGGTGCCTGACCGGCACGTACGAAAGCGCAGTTGGTAAT GCAGAAAGCCGTTATGTTCTGACCGGTCGTTATGATAGCGCACCGGCAACCGATGGTAGCGGTACCGCACTGGGTTGG ACCGTTGCATGGAAAAATAACTATCGTGGCGGCAGCGGGAAGCGTGGTATAACCTGGGCAACGCGTATTATAACA GGGCGATTATGATGAAGCGATTGAATATTATCAGAAAGCGCTGGAAGTGAAGCGGCGGCAATGCACATAGCGCAACCA CGTGGTCAGGTCAAGTATGTTGGTGGTGCAGAAAGCACGCATTAACACCCAGTGGCTGCTGACCAGCGGCACCACCGAA GCAAATGCCTGGAAAAGCACCTGGTTGGTCATGATACCTTTACCAAAGTTAAACCGAGCGCAGCATCAATTGATGCA GCAAAAAAAGCCGGTGTGAATAATGGTAATCCGCTGGATGCAGTTCAGCAGTAATAGGGATCCTATA



8	117TPR	<b>ATATCATATGGCAAGCATGACGGGTGGCCAGCAGATGGGTCTGTGATCAGGCAGGTATTACCGGCACCTGGTATAATCAGCTGGGTAGCACCTTTATTGTTACCGCGGGCGCAGATGGTGCCTGACCGGCACGTACGAAAGCGCAGTTGGTAATGCAGAAAAGCCGTTATGTTCTGACCGGTCTTATGATAGCGCACCGGCAACCGATGGTAGCGGTACCGCACTGGGTTGGACCGCATTAAACCCAGTGGCTGCTGACCAGCGGCACCACCGAAGCAGGCGGCGGAAAGCGTGGTATAACCTGGGCAACCGCTATTATAAACAGGGCGATTATGATGAAGCGATTGAATATTATCAGAAAAGCGCTGGAAGCTGAGCGGCGGCAATGCCTGGAAAAGCACCTGGTTGGTATGATACCTTTACCAAAGTTAAACCGAGCGCAGCATCAGGCGGCAGCGCGGAAGCGTGGTATAACCTGGGCAACCGCTATTATAAACAGGGCGATTATGATGAAGCGATTGAATATTATCAGAAAAGCGCTGGAAGCTGAGCGGCGGCTAATAGGGATCCTATA</b>
9	139TPR	<b>ATATCATATGGCAAGCATGACGGGTGGCCAGCAGATGGGTCTGTGATCAGGCAGGTATTACCGGCACCTGGTATAATCAGCTGGGTAGCACCTTTATTGTTACCGCGGGCGCAGATGGTGCCTGACCGGCACGTACGAAAGCGCAGTTGGTAATGCAGAAAAGCCGTTATGTTCTGACCGGTCTTATGATAGCGCACCGGCAACCGATGGTAGCGGTACCGCACTGGGTTGGACCGCATTAAACCCAGTGGCTGCTGACCAGCGGCACCACCGAAGCAAATGCCTGGAAAAGCACCTGGTTGGTATGATACCTTTACCAAAGTTAAACCGAGCGCAGCATCAGGCGGCAGCGCGGAAGCGTGGTATAACCTGGGCAACCGCTATTATAAACAGGGCGATTATGATGAAGCGATTGAATATTATCAGAAAAGCGCTGGAAGCTGAGCGGCGGCTAATAGGGATCCTATA</b>
10	159TPR	<b>ATATCATATGGCAAGCATGACGGGTGGCCAGCAGATGGGTCTGTGATCAGGCAGGTATTACCGGCACCTGGTATAATCAGCTGGGTAGCACCTTTATTGTTACCGCGGGCGCAGATGGTGCCTGACCGGCACGTACGAAAGCGCAGTTGGTAATGCAGAAAAGCCGTTATGTTCTGACCGGTCTTATGATAGCGCACCGGCAACCGATGGTAGCGGTACCGCACTGGGTTGGACCGCATTAAACCCAGTGGCTGCTGACCAGCGGCACCACCGAAGCAAATGCCTGGAAAAGCACCTGGTTGGTATGATACCTTTACCAAAGTTAAACCGAGCGCAGCATCAATTGATGCAGCAAAAAAGCCGGTGTGAATAATGGTAATCCGCTGGATGCAGTTCAGCAGGGCGGCAGCGCGGAAGCGTGGTATAACCTGGGCAACCGCTATTATAAACAGGGCGATTATGATGAAGCGATTGAATATTATCAGAAAAGCGCTGGAAGCTGAGCGGCGGCTAATAGGGATCCTATA</b>
11	CpSav	<b>ATATCATATGGCAAGCATGACGGGTGGCCAGCAGATGGGTGGTAGCGGTACCGCACTGGGTTGGACCGTTGCATGGA AAAATAACTATCGTAATGCACATAGCGCAACCACGTGGTGCAGTTCAGTATGTTGGTGGTGCAGAAAGCACGCATTAACA CCCAGTGGCTGCTGACCAGCGGCACCACCGAAGCAAATGCCTGGAAAAGCACCTGGTTGGTATGATACCTTTACCA AAGTTAAACCGAGCGCAGCATCAGGCGGGCGGCAGCGCGGAAGCAGGTATTACCGGCACCTGGTATAATCAGCTGGGT AGCACCTTTATTGTTACCGCGGGCGCAGATGGTGCCTGACCGGCACGTACGAAAGCGCAGTTGGTAATGCAGAAAAG CCGTTATGTTCTGACCGGTCTTATGATAGCGCACCGCTAATAGGGATCCTATA</b>
12	Cp1	<b>ATATCATATGGCAAGCATGACGGGTGGCCAGCAGATGGGTGGTAGCGGTACCGCACTGGGTTGGACCGTTGCATGGA AAAATAACTATCGTAATGCACATAGCGCAACCACGTGGTGCAGTTCAGTATGTTGGTGGTGCAGAAAGCACGCATTAACA CCCAGTGGCTGCTGACCAGCGGCACCACCGAAGCAAATGCCTGGAAAAGCACCTGGTTGGTATGATACCTTTACCA AAGTTAAACCGAGCGCAGCATCAGGCGGGCGGCAGCGCGGAAGCAGGTATTACCGGCACCTGGTATAATCAGCTGGGT AGCACCTTTATTGTTACCGCGGGCGCAGATGGTGCCTGACCGGCACGTACGAAAGCGCAGTTGGTAATGCAGAAAAG CCGTTATGTTCTGACCGGTCTTATGATAGCGCACCGGAGCAGCACCGATCAGGAAAAACCGCGCTGAACATGGCGCG TTTTATTCGTAGCCAGACCCTGACCCTGCTGGAAAAGTGAACGAACTGGATGCGGATGAACAGGCGGATATTGCGGA AAGCTGCATGATCATGCGGATGAACTGTATCGTAGCGTGTGGCGCGTTTTTAATAGGGATCCTATA</b>
13	Cp2	<b>ATATCATATGGCAAGCATGACGGGTGGCCAGCAGATGGGTGGTAGCGGTACCGCACTGGGTTGGACCGTTGCATGGA AAAATAACTATCGTAATGCACATAGCGCAACCACGTGGTGCAGTTCAGTATGTTGGTGGTGCAGAAAGCACGCATTAACA CCCAGTGGCTGCTGACCAGCGGCACCACCGAAGCAAATGCCTGGAAAAGCACCTGGTTGGTATGATACCTTTACCA AAGTTAAACCGAGCGCAGCATCAGGCGGGCGGCAGCGCGGAAGCAGGTATTACCGGCACCTGGTATAATCAGCTGGGT AGCACCTTTATTGTTACCGCGGGCGCAGATGGTGCCTGACCGGCACGTACGAAAGCGCAGTTGGTAATGCAGAAAAG CCGTTATGTTCTGACCGGTCTTATGATAGCGCACCGGAGCAGTACCACCCAGGAAAAAACCGCGCTGAACATGGC GCGTTTTATTGTTAGCCAGACCCTGACCCTGCTGGAAAAGTGAACGAACTGGATGCGGATGAACAGGCGGATATTGC GGAAGCCTGCATGATCATGCGGATGAACTGTATCGTAGCGTGTGGCGCGTTTTTAATAGGGATCCTATA</b>
14	Cp3	<b>ATATCATATGGCAAGCATGACGGGTGGCCAGCAGATGGGTGGTAGCGGTACCGCACTGGGTTGGACCGTTGCATGGA AAAATAACTATCGTAATGCACATAGCGCAACCACGTGGTGCAGTTCAGTATGTTGGTGGTGCAGAAAGCACGCATTAACA CCCAGTGGCTGCTGACCAGCGGCACCACCGAAGCAAATGCCTGGAAAAGCACCTGGTTGGTATGATACCTTTACCA AAGTTAAACCGAGCGCAGCATCAGGCGGGCGGCAGCGCGGAAGCAGGTATTACCGGCACCTGGTATAATCAGCTGGGT AGCACCTTTATTGTTACCGCGGGCGCAGATGGTGCCTGACCGGCACGTACGAAAGCGCAGTTGGTAATGCAGAAAAG CCGTTATGTTCTGACCGGTCTTATGATAGCGCACCGGGCTGGAACATGACCGCGCAGGAAAAAACCGCGCTGAACAT GGGCGGTTTTATTGTTAGCCAGACCCTGACCCTGCTGGAAAAGTGAACGAACTGGATGCGGATGAACAGGCGGATAT TGGGAAAAGCCTGCATGATCATGCGGATGAACTGTATCGTAGCGTGTGGCGCGTTTTTAATAGGGATCCTATA</b>
15	Cp4	<b>ATATCATATGGCAAGCATGACGGGTGGCCAGCAGATGGGTGGTAGCGGTACCGCACTGGGTTGGACCGTTGCATGGA AAAATAACTATCGTAATGCACATAGCGCAACCACGTGGTGCAGTTCAGTATGTTGGTGGTGCAGAAAGCACGCATTAACA CCCAGTGGCTGCTGACCAGCGGCACCACCGAAGCAAATGCCTGGAAAAGCACCTGGTTGGTATGATACCTTTACCA AAGTTAAACCGAGCGCAGCATCAGGCGGGCGGCAGCGCGGAAGCAGGTATTACCGGCACCTGGTATAATCAGCTGGGT AGCACCTTTATTGTTACCGCGGGCGCAGATGGTGCCTGACCGGCACGTACGAAAGCGCAGTTGGTAATGCAGAAAAG CCGTTATGTTCTGACCGGTCTTATGATAGCGCACCGGGCGGCAACATGACCGCGCAGGAAAAAACCGCGCTGAACAT GGGCGGTTTTATTGTTAGCCAGACCCTGACCCTGCTGGAAAAGTGAACGAACTGGATGCGGATGAACAGGCGGATAT TGGGAAAAGCCTGCATGATCATGCGGATGAACTGTATCGTAGCGTGTGGCGCGTTTTTAATAGGGATCCTATA</b>

For the expression and purification of these constructs see also Table 9.

In case of the (GGG)<sub>2</sub>-constructs (Table 11, entries 1-4), new unique restriction sites were introduced into the gene sequences before and after each (GGG)<sub>2</sub>-motif (Figure 34). This allows a simple subsequent shuffling/combination of the loops (i.e. streptavidin mutants containing two (GGG)<sub>2</sub>-inserts at different positions; Table 9, entries 5-10).

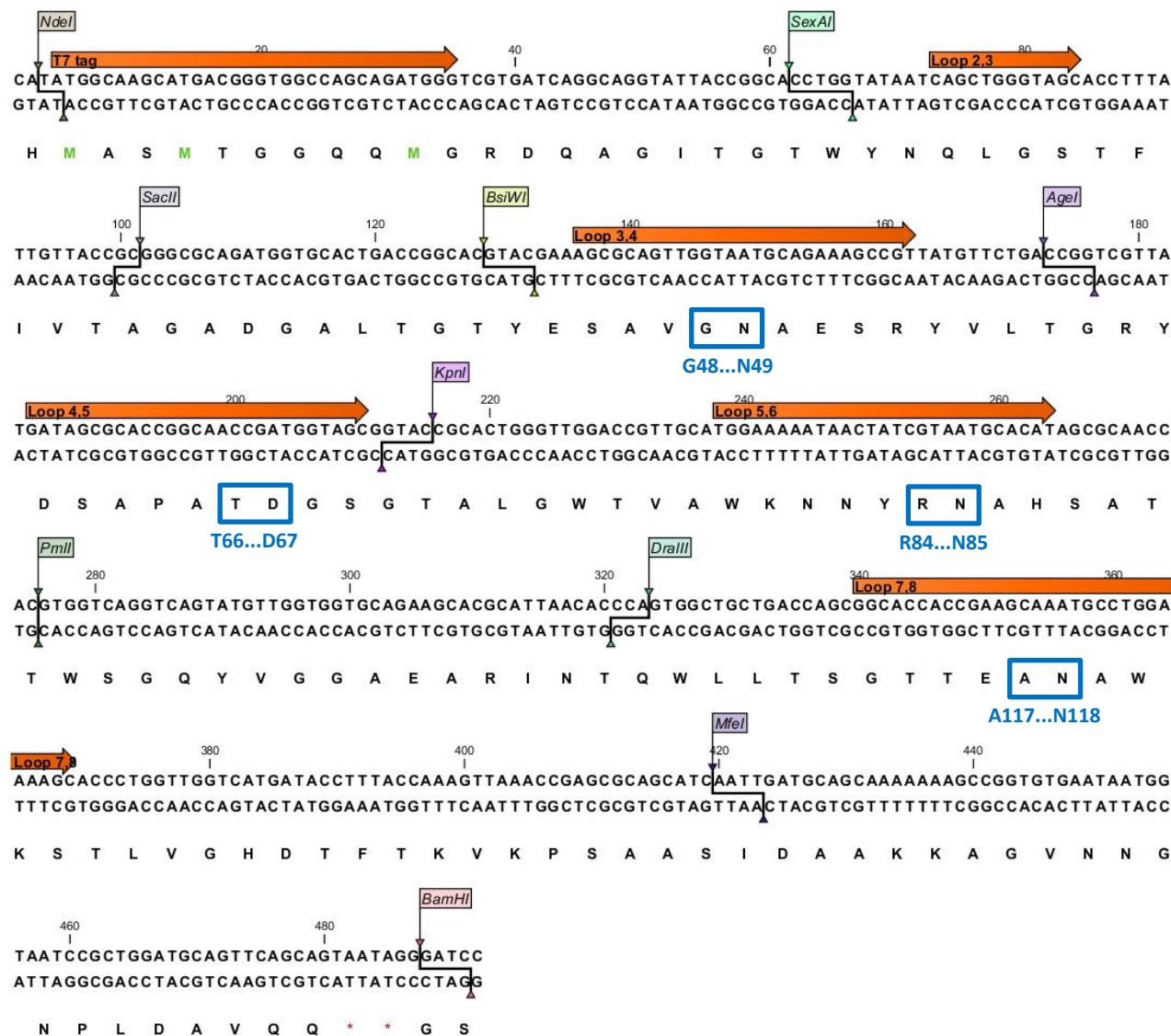


Figure 34: Designed streptavidin sequence containing unique restriction sites before and after the loops.

Streptavidin sequence: double stranded DNA (upper line), amino acids (lower line). Streptavidin loops are displayed as orange arrows. Positions for (GGG)<sub>2</sub>-inserts are labelled in blue.

### General cloning procedure:

PCR<sup>222</sup> and site-directed mutagenesis performed in this thesis are based on the protocol of the QuikChange<sup>TM</sup> site-directed mutagenesis kit from Stratagene<sup>226</sup>, modified by Zheng *et al.*<sup>227</sup> Melting temperatures of primers were calculated according to the nearest neighbor method<sup>228</sup> using the OligoCalc tool.<sup>229</sup> The sequences in Table 11 were amplified by PCR applying the following conditions:

Forward primer (5' to 3'):

General: ATATCATATGGCAAGCATGACGGGTGGCC

Reverse primers (5' to 3'):

General: TATAGGATCCCTATTACTGCTGAACTGCATCC

Cp1-4: TATAGGATCCCTATTA AAAACGCGCCAGCACG

139/159TPR: TATAGGATCCCTATTAGCCGCGCTCAG

CpSav: TATAGGATCCCTATTACGGTGCCTATCATAACG

PCR mixture:

20 µl Q5-buffer (5x), 0.5 µl template DNA (100 ng/µl), 2 µl primers (10 µM), 2 µl dNTP's (10 mM), 4 µl DMSO, 68 µl water, 1 µl Q5 Hot start HF DNA polymerase (2 U/µl).

PCR program:

98°C for 30 s; 98°C for 20 s, 70 °C for 30 s, 72°C for 30 s (30 cycles); 72°C for 8 min.

Amplified DNA was purified by precipitation from ethanol:

- 1) 1 ml ethanol (100 %) and 100 µl sodium acetate (3M, pH 4.8) were added to the PCR product.
- 2) The sample was mixed, centrifuged (21'000 g, 4°C, 15 min) and the supernatant was carefully removed.
- 3) The pellet was resuspended in 500ul cold ethanol (70%).
- 4) The sample was centrifuged (21'000 g, 20°C, 5 min) and the supernatant was carefully removed.
- 5) The pellet was resuspended in sterile MilliQ-water.

The purified plasmids were digested with restriction enzymes (NdeI + BamHI-HF, 37°C, 60 min; removal of the ATAT/TATA overhangs). Simultaneously, an empty pET30a vector (Novagen)<sup>230</sup> was digested applying the same conditions. All digested samples were loaded onto an agarose gel (1% agarose) and the desired bands were cut out and purified.<sup>223</sup> The inserts were then ligated into the digested pET30a vector (T4-DNA Ligase, 16°C, overnight, 10-fold molar excess of insert compared to vector). Ligated products were transformed into electro-competent TOP10 (DE3) *E. coli* cells (50 µl competent cells + 5 µl ligation product; electro-shock for 5.6 ms at 1.8 kV; incubation in SOB-medium for 1 h at 37°C prior to plating) and plated onto LB-agar plates containing kanamycin (50 µg/ml). Colonies were picked and overnight cultures were prepared (LB-medium with 50 µg/ml kanamycin, 37°C, 210 rpm shaking). Cells were harvested, plasmids were isolated<sup>223</sup> and analysed by Sanger DNA sequencing.<sup>224-225</sup> Glycerol stocks (15% glycerol) were prepared from the correct clones. The plasmids were then, where applicable, transformed into chemically competent BL21(DE3) *E. coli* cells (50 µl competent cells + 1 µl purified plasmid; heat-shock for 30 s at 42°C; incubation in LB-medium for 1 h at 37°C prior to plating).

### Cloning of Sav variants containing two (GGG)<sub>2</sub>-motifs:

In order to introduce two (GGG)<sub>2</sub> loops into the same gene (Table 9, entries 5-10), the previously obtained single (GGG)<sub>2</sub> loop mutants were digested applying different restriction enzymes (Figure 34, Table 12). The digested backbones and inserts were combined in the desired way followed by re-ligation. The ligation products were then transformed and sequenced as described for the single (GGG)<sub>2</sub> mutants.

Table 12: Digestion of streptavidin loop sequences applying different restriction enzymes.

Entry	(GGG) <sub>2</sub> loop at position	Restriction enzyme 1	Restriction enzyme 2	Used fragment
1	G48...N49	AgeI	BamHI	backbone
2	T66...D67	AgeI	BamHI	insert
3	R84...N85	AgeI	BamHI	insert
4	A117...N118	AgeI	BamHI	insert
5	T66...D67	KpnI	BamHI	backbone
6	R84...N85	KpnI	BamHI	insert
7	A117...N118	KpnI	BamHI	insert
8	A117...N118	Pm1I	NdeI	backbone
9	R84...N85	Pm1I	NdeI	insert

### Cloning of Sav (GGX)<sub>n</sub>-constructs:

In order to expand the diversity of the streptavidin (GGG)<sub>2</sub> mutants, the first serine residue in the loop ...G<sub>48</sub>-G-G-S-G-G-S-N<sub>49</sub>... was selected for mutagenesis. A primer containing the degenerate “NDT” codon was used, which can encode for 12 different amino acids including aliphatic, aromatic, charged, small and large residues (Phe, Leu, Ile, Val, Tyr, His, Asn, Asp, Cys, Arg, Gly and Ser). PCR was performed applying the following conditions:

Forward primer (5' to 3'): GGTGGCGGCNDTGGCGGCAG

Reverse primer (5' to 3'): CTGCCGCAHNACCGCCACC

PCR mixture:

5 µl Q5-buffer (5x), 0.25 µl template DNA (200 ng/µl), 1.25 µl primers (10 µM), 0.5 µl dNTP's (10 mM), 0.75 µl DMSO, 15.8 µl water, 0.25 µl Phusion Hot start HF DNA polymerase (2 U/µl).

PCR program:

98°C for 2 min; 98°C for 10 s, 68 °C for 20 s, 72°C for 3.5 min (30 cycles); 72°C for 8 min.

PCR products were digested (DpnI, 37°C, 90 min) and mutants were analysed as described for the single (GGG)<sub>2</sub> mutants. Due to the high GC-content of the streptavidin sequence and the similarity of the GGX and the GGS motif, primers likely annealed at a different position (3 amino acids shifted), leading to an elongation of the loop (Table 9, entries 11-18).

### **Cloning of Sav double mutants and Sav loop combinations:**

Various Sav double mutants and combinations of single mutants with loops (Table 9, entries 25-35) were produced, applying the following PCR conditions:

Forward primers (5' to 3'):

S112M\_fw: GACCATGGGCACCACCGAAGCAAATGC  
K121A-L124G\_fw: CCTGGGCAAGCACCGGGTTGGTCATGATACC  
K121R-L124G\_fw: CCTGGCGCAGCACCGGGTTGGTCATGATACC  
K121R\_fw: CCTGGCGCAGCACCCCTGGTTGGTCATGATACC

Reverse primers (5' to 3'):

S112M\_rv: GTGCCCATGGTCAGCAGCCACTGG  
K121A\_rv: GTGCTTGCCAGGCATTTGCTTCGGTGG  
K121R\_rv: GTGCTGCGCCAGGCATTTGCTTCGGTGG

PCR mixture:

5 µl Q5-buffer (5x), 0.5 µl template DNA (25 ng/µl), 0.5 µl primers (10 µM), 0.5 µl dNTP's (10 mM), 1 µl DMSO, 16.5 µl water, 0.5 µl Q5 Hot start HF DNA polymerase (2 U/µl).

PCR program:

95°C for 2 min; 95°C for 15 s, 60 °C for 20 s, 72°C for 5 min (17 cycles); 72°C for 10 min.

PCR products were digested (DpnI, 37°C, 90 min) and mutants were analysed as described for the single (GGS)<sub>2</sub> mutants. Mutants S112M-K121A, S112M-K121N and K121N-L124G were produced by other members of the Ward research group.

#### 4.2.8 Expression and purification of Sav mutants

The recombinant expression of streptavidin in *E. coli* cells used in this thesis relies on a pET expression system.<sup>230-231</sup>

##### **Expression in TOP10(DE3) *E. coli* cells:**

Pre-culture (10 mL LB-medium containing 50 µg/mL kanamycin) was inoculated from a glycerol stock and incubated overnight (37°C, 200 rpm shaking). The main culture (1 L LB-rich medium containing: 5.35 g/L yeast extract, 10.70 g/L bactotryptone, 1.77 g/L Na<sub>2</sub>HPO<sub>4</sub>, 1.70 g/L KH<sub>2</sub>PO<sub>4</sub>, 1.34 g/L NH<sub>4</sub>Cl, 0.36 g/L Na<sub>2</sub>SO<sub>4</sub>, 0.24 g/L MgSO<sub>4</sub>, 0.5 g/L glucose, 6.31 g/L glycerol and 50 µg/mL kanamycin) was inoculated with pre-culture to a starting OD<sub>600</sub> of 0.1 and incubated for 2.5 h (37°C, 200 rpm shaking). The temperature was set to 20°C and the culture was incubated for 1 h. At an OD<sub>600</sub> of 1.0, the main culture was induced with IPTG (final concentration: 40 µM) and incubated for additional 20 h (20°C, 200 rpm shaking). The cell culture was centrifuged (3200 g, 8°C, 10 min). The cell pellet was resuspended in 50 ml lysis buffer (PBS buffer (1x, pH 7.4) containing 0.5 mg/ml DNase, 1.0 mg/ml Lysozyme and 1 mM PMSF) and incubated for 1 h (37°C, 200 rpm shaking). Sample was freeze-thawed once and incubated for another 3 h (25°C, 180 rpm shaking).

##### **Expression in BL21(DE3) *E. coli* cells:**

The pre-culture (25 ml LB-medium containing 50 µg/mL kanamycin) was inoculated from a glycerol stock and incubated overnight (37°C, 200 rpm shaking). The main culture (1 L Auto-induction medium (ZYP-5052)<sup>232</sup> containing 50 µg/mL kanamycin) was inoculated with pre-culture (20 mL) and incubated for 24 h (30°C, 180 rpm shaking). Cells were harvested and treated as described for the expression in *E. coli* TOP10(DE3).

##### **SDS-PAGE analysis:**

The solubility and oligomeric state of the expressed Sav loop mutants was analyzed by SDS-PAGE.<sup>233</sup> 200 µl cell lysate was centrifuged (21'000 g, 8°C, 10 min), the supernatant (= soluble fraction) was separated and the cell pellet (= insoluble fraction) was dissolved in 200 µl urea (8 M). Both fractions (19 µl each) were mixed with 1 µl B4F (0.04 mM in DMSO) and 10 µl loading buffer (3x) and applied to the polyacrylamide gel. The analysis of selected Sav loop mutants is displayed in Figure 35.

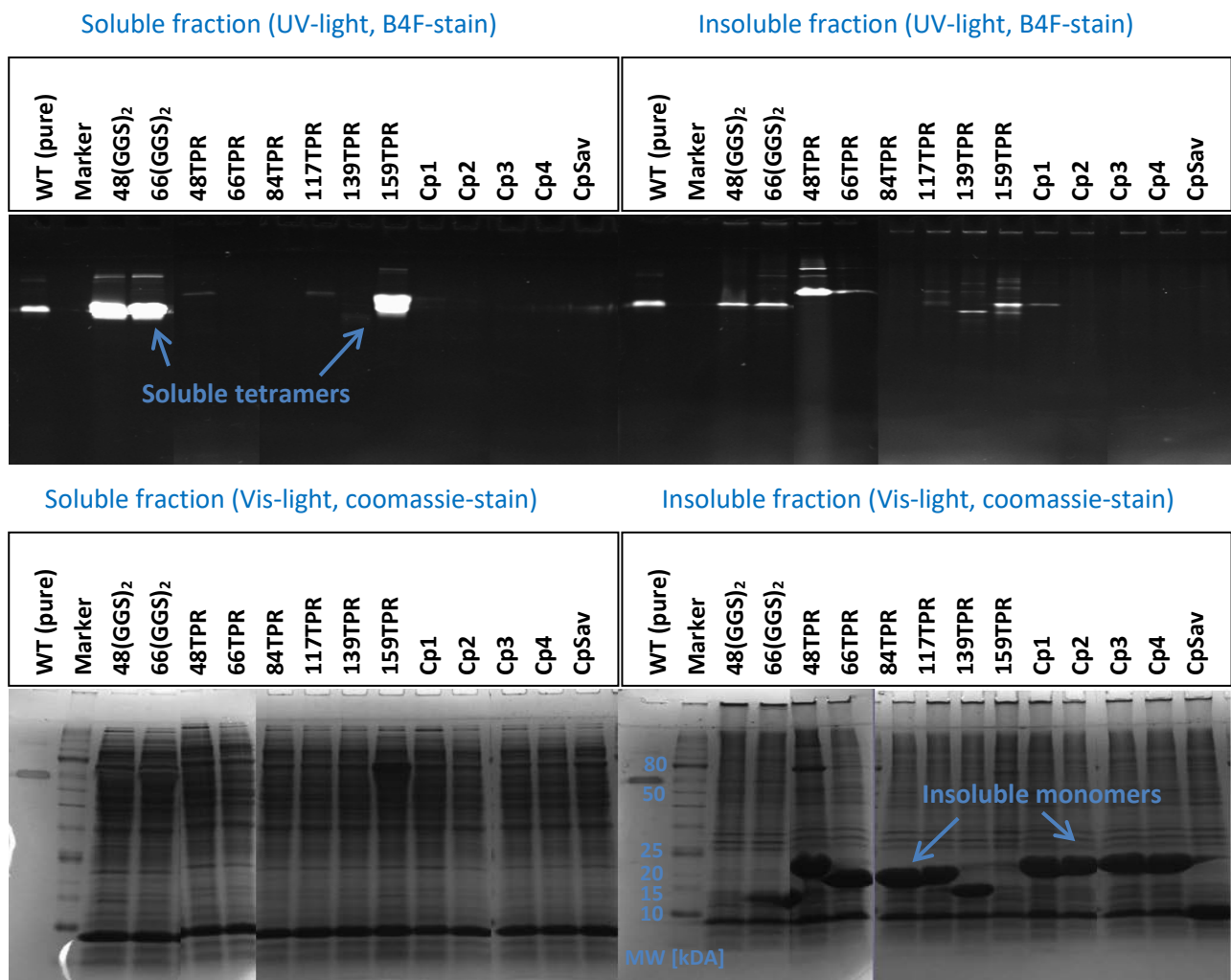


Figure 35: SDS-PAGE analysis of selected Sav loop mutants.

#### Purification of cell lysate:

The cell lysate was filled into dialysis bags (6-8 kDa MWCO) and dialyzed against guanidinium hydrochloride (6 M, pH set to 1.5 with HCl, 12 h), followed by dialysis in Tris-HCl (20 mM, pH 7.4, 12 h) and iminobiotin-binding buffer (50 mM NaHCO<sub>3</sub>, 500 mM NaCl, pH 9.8, 12 h). The sample was centrifuged (3200 g, 10°C, 45 min) and filtered (0.2 μm filter). The sample was purified by affinity column chromatography (AKTAp<sup>prime</sup> Plus chromatography system equipped with a 2-iminobiotin sepharose column). The eluate was neutralized with Tris-HCl (pH 7.4, final concentration: 20 mM), followed by dialysis in MilliQ-water (4 x 12 h) and lyophilisation.

### Refolding of streptavidin loop mutants:

The refolding procedure for the streptavidin constructs 48TPR and 66TPR was adapted from methods reported by Howarth and Ting *et al.*<sup>187-188</sup> Recently Ward *et al.* reported a detailed refolding procedure for chimeric streptavidin constructs.<sup>179</sup>

Buffers:

GuHCl (denaturing): Guanidinium hydrochloride (45.84 g) in 80 ml MilliQ-water. pH set with HCl to 1.5. → final conc.: guanidinium hydrochloride (6 M).

PBS-buffer (refolding): NaCl (32 g) + KCl (0.8 g) + Na<sub>2</sub>HPO<sub>4</sub> · 12 H<sub>2</sub>O (14.32 g) + KH<sub>2</sub>PO<sub>4</sub> (0.96 g) filled up with MilliQ-water to 4 L. pH set with HCl to 7.4. → final conc.: NaCl (137 mM), KCl (2.7 mM), Na<sub>2</sub>HPO<sub>4</sub> (10 mM), KH<sub>2</sub>PO<sub>4</sub> (1.76 mM).

The cell lysate was centrifuged (3200 g, 10°C, 45 min). The supernatant was discarded and the pellet was dissolved in GuHCl (80 ml) and heated to 95°C for 10min. The solution was then added dropwise to PBS-buffer (4 L), whereupon a white precipitate was formed. The resulting mixture was stirred at 8°C overnight. The mixture was centrifuged (3200 g, 8°C, 10 min) and the supernatant, where applicable, was purified by affinity column chromatography (AKTA<sub>prime</sub> Plus chromatography system equipped with a 2-iminobiotin sepharose column). An SDS-PAGE analysis of the refolded streptavidin constructs is illustrated in Figure 36.

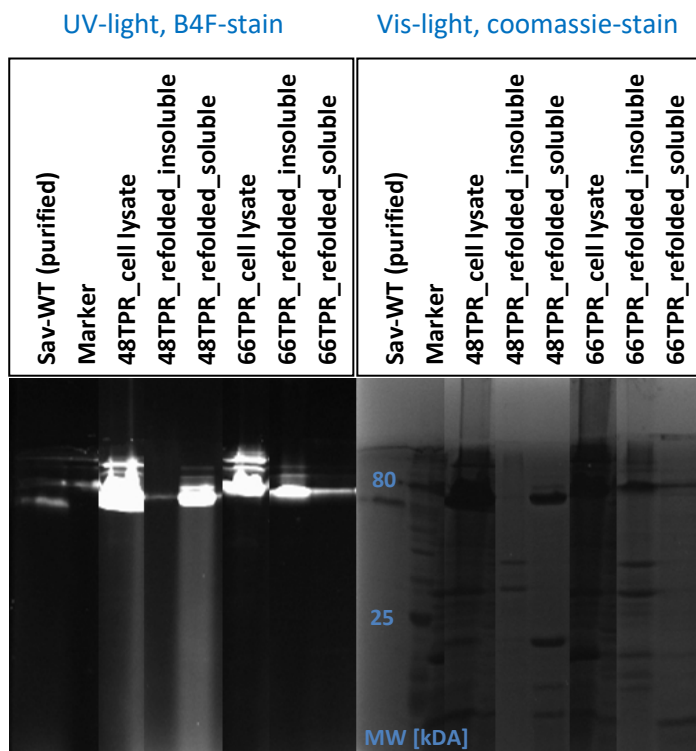


Figure 36: SDS-PAGE analysis of the refolded streptavidin loop constructs 48TPR and 66TPR.



### Free biotin binding sites:

The number of free biotin binding sites per tetramer of the purified streptavidin loop mutants was determined by a B4F-test.<sup>55</sup> BSA-buffer (5 mg BSA in 50 ml phosphate buffer (0.1 M NaH<sub>2</sub>PO<sub>4</sub>/Na<sub>2</sub>HPO<sub>4</sub>, pH 7.0)) was prepared. Solutions of streptavidin (2 μM Sav-tetramer in BSA-buffer) and B4F (40 μM in BSA-buffer) were prepared and mixed at different ratios. The samples were incubated for 5 min at 25°C and the fluorescence ( $\lambda_{\text{ex.}} = 485 \text{ nm}$ ,  $\lambda_{\text{em.}} = 520 \text{ nm}$ ) was determined. The number of free biotin binding sites per streptavidin tetramer was determined at the intersection of the two linear segments in the titration profile. The titration profile of the Sav loop mutant Loop2-K121R (Table 9, entry 34) is displayed in Figure 37.

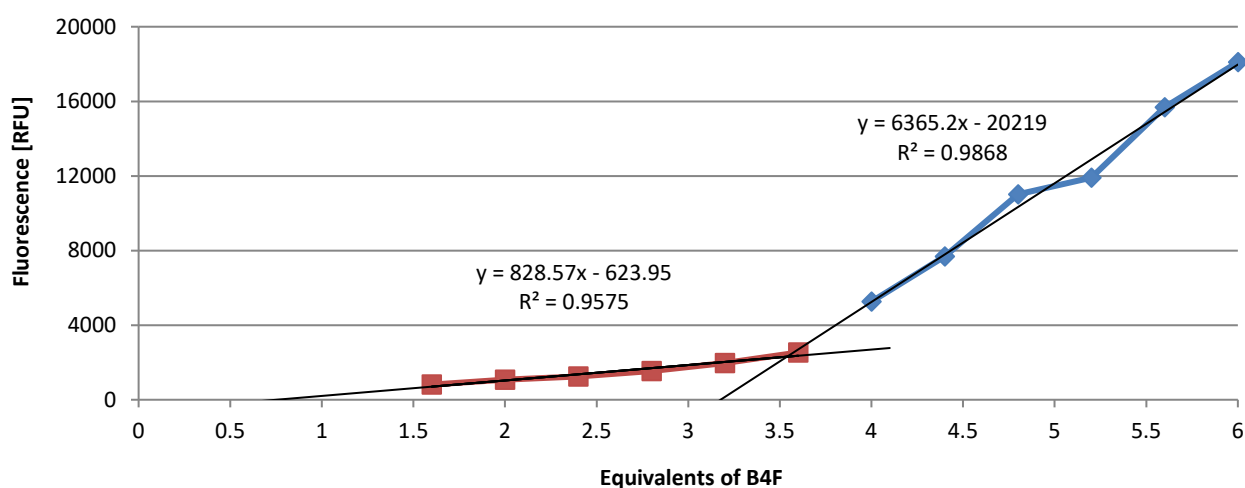


Figure 37: B4F-test with the streptavidin mutant Loop2-K121R.

At the intersection of the two linear segments obtained by linear regression (for the red and blue dots) the number of free biotin binding sites per streptavidin tetramer can be calculated. For the mutant Loop2-K121R displayed, a value of 3.5 was determined.

### MS-analysis:

The mass of the expressed and purified Sav variants was determined by ESI-TOF mass spectrometry. Annex spectra on pages 210-213.

#### 4.2.9 Preparation of a 3D-printing model

##### Protocol for the preparation of a 3D-protein model:

A crystal structure of [Cp\*Ir(biot-*p*-L)Cl] · Sav-S112A (PDB ID 3PK2)<sup>60</sup> was loaded into VMD (version 1.9.1).<sup>202</sup> Table 13 shows the list of “Representations” which were drawn in VMD. The material selection was set to AO Edgy. The resolution was set to 50.

**Table 13: Structure elements of the 3D-model drawn in VMD.**

Entry	Selection	Draw style	Size (radius)	Comment
1	protein	trace	0.8	Protein backbone
2	type CA	licorice	1.2	C $\alpha$ -atoms of the backbone
3	resid 400	CPK	3.0	Biotinylated ligand
4	resid 48 50 53 84 85 86 87 98 110 111 112 113 114 115 116 117 118 119 121 122 123 124 and chain A and not type C N O and not altloc B	licorice	0.6	Side chains of selected residues in monomer A
5	resid 65 67 68 69 and chain D and not type C N O	licorice	0.6	Side chains of selected residues in monomer A
6	resid 64 and chain D and not type C O	licorice	0.6	Pro <sub>64</sub> of monomer D
7	resid 23 27 43 45 90 128 and chain A and not type C N O	licorice	0.6	Biotin binding residues (H-bonds)
8	resid 49 and chain A and not sidechain	licorice	0.6	Asn <sub>49</sub> of monomer A

2) In order to stabilize the protein structure, additional artificial bonds were inserted (grey cylinders). Residues to install these bonds were selected by visual inspection of the protein structure. A list of all stabilizing bonds is given in Table 14. In addition, the H-bonds between the protein and the biotinylated metal cofactor were drawn (white cylinders). The coordinates of the corresponding atoms were extracted from the pdb file using the TkConsole in VMD. The following commands were typed:

```
set sel [atomselect 0 "resid 18 and name CA and chain A"] //selects Ca of residue 18 of chain A
set sel [atomselect 0 "index 84"] //selects the atom with the index 84
atomselect0 get {x y z} //gets coordinates of the selected atoms
atomselect0 writepdb test.pdb //saves selection in pdb file named "test"
```

A grey cylinder between two atoms with the coordinates (X1 Y1 Z1) and (X2 Y2 Z2) was drawn by typing the following commands into the VMD TkConsole:

```
graphics top color 2 //sets the color to grey
graphics top cylinder {X1 Y1 Z1} {X2 Y2 Z2} radius 0.5 resolution 30 filled 1 //draws the cylinder
```

Table 14: Artificial bonds to stabilize the 3D-protein model.

Chain	Residue	↔	Chain	Residue	Chain	Residue	↔	Chain	Residue
A	Tyr22		A	Thr131	A	Ala78		D	Tyr60
A	Thr106		A	Asp128	A	Thr76		D	Gly58
A	Arg103		A	Thr131	A	Gly58		D	Thr57
A	Leu109		A	Val125	A	Ser88		D	Ala72
A	Ala112		A	Ser122	A	Thr91		D	Gly74
A	Gly98		A	Ala102	A	Gly74		D	Thr76
A	Tyr96		A	Ile104	A	Tyr60		D	Ala78
A	Ser93		A	Gln107	A	Thr71		D	Gly113
A	Thr90		A	Leu110	A	Leu73		D	Ala89
A	Ser88		A	Ala112	A	Gly94		D	Thr111
A	Ala78		A	Ala89	A	Thr111		D	Gly94
A	Thr76		A	Thr91	A	Thr91		D	Thr91
A	Ala72		A	Gln95					
A	Asp61		A	Ala72	B	Leu124		D	Leu124
A	Gly58		A	Trp75	B	Trp120		D	Gly126
A	Thr42		A	Val55	B	Lys121		D	Leu124
A	Leu39		A	Gly58	B	Thr123		D	Val125
A	Ala33		A	Leu39					
A	Ile30		A	Thr42	D	Asn23:ND2		Ir400	O1
A	Thr28		A	Glu44	D	Ser27:OG		Ir400	O1
A	Trp21		A	Phe29	D	Ser45:OG		Ir400	N2
A	Thr18		A	Thr32	D	Tyr43:OH		Ir400	O1
					D	Thr90:OG1		Ir400	S1
					D	Asp128:OD2		Ir400	N1
					D	Asn49:N		Ir400	O2

In green: Bonds within the same monomer (here shown for monomer A) were created in the other monomers (B-D) as well. In red: Bonds between two adjacent monomers (here shown for monomer A and D) were created for the other pair of monomers (B and C) as well. In blue: Bonds between two opposite monomers (here shown for monomer B and D) were created for the other pair of monomers (A and C) as well. In pink: Hydrogen bonds between the protein (here monomer D) and the biotinylated metal cofactor.

3) The final structure in VMD was exported as an .OBJ file.

4) The residue numbers (e.g. "48") were drawn in Blender (version 2.70) by adding a new object "Add object (Text)". The text was modified in the "Edit Mode" using the following settings: Scale (X,Y,Z): 0.060; Extrude: 0.200; Resolution: 30; Offset: 0.035; Spacing Letter: 1.50; Font Regular: MW-QUOIN. The labels were exported as .x3d files.

5.) The protein structure from VMD and the residue labels from Blender were both imported into Meshlab (version 1.3.4). The labels were moved to the right place using the "Manipulators tool". When required, the labels can be rescaled using the following command in the menu bar:

*Filters --> Normals, Curvatures and Orientation --> Transform: Scale*

*If color got lost, then press: Render --> Color --> Color per Face*

The labels and the protein structure were fused together:

*Filters --> Mesh layer --> Flatten visible layers (only select "Merge only visible layers")*

*If color got lost, then press: Filters --> Sampling --> Vertex Attribute Transfer (select "Transfer color")*

*Render --> Color --> Per Vertex*

The fused model was then checked for non-manifold edges and vertices:

*Render --> Show Non Manif Edges*

*Render --> Show Non Manif Vertices*

The model was then checked for "water tightness":

*View --> Show layer dialog*

*Filters --> Quality, Measure and computation --> Compute Geometric Measures*

Finally, the model was exported as .x3d file (Vert=Color, Faces=Normal)

6.) The model was printed on a ProJet 4500 printer from 3dsystems with the help of Dr. Stefan Imseng (Biozentrum, University of Basel).

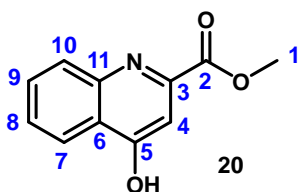
7.) The cleaned model was sprayed with a mixture of isopropanol/chloroform 1:1 to get a smooth and shiny surface.

## 4.3 Synthesis

### 4.3.1 Biotinylated ruthenium cofactor: main synthesis route

The synthesis of the biotinylated ligand **26** described in this chapter will be published elsewhere.<sup>118</sup>

#### Compound 20:



The synthesis was performed similarly to Manfredini *et al.*<sup>234</sup>

Kynurenic acid (**19**, 5.00 g, 26.4 mmol, 1.0 eq.) was dispersed in dry methanol (50 ml, 39.6 g, 1240 mmol, 47 eq.). Concentrated sulfuric acid (3.0 ml, 5.5 g, 56.3 mmol, 2.1 eq.) was added, whereupon the mixture got clear. The solution was heated to reflux for 20 h under an N<sub>2</sub> atmosphere. The solution was evaporated to dryness, yielding a yellow oil. Water (100 ml) and saturated aqueous NaHCO<sub>3</sub> (100 ml) were added, whereupon an off-white solid precipitated. The solid was filtered, washed with diethyl ether (50 ml) and dried to yield the product as a white solid (**20**, 4.53 g, 22.3 mmol, 84% yield).

Annex spectra on page 173.

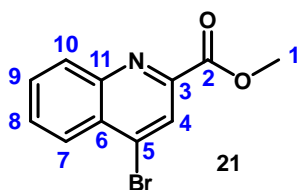
**Appearance:** White solid

**<sup>1</sup>H NMR** (400 MHz, DMSO-*d*<sub>6</sub>, δ/ppm): 12.09 (s, 1H, **OH**), 8.08 (dd, *J* = 8.1, 1.5 Hz, 1H, **7**), 7.94 (d, *J* = 8.4 Hz, 1H, **10**), 7.71 (ddd, *J* = 8.5, 7.0, 1.6 Hz, 1H, **9**), 7.38 (ddd, *J* = 8.1, 7.0, 1.1 Hz, 1H, **8**), 6.66 (s, 1H, **4**), 3.96 (s, 3H, **1**). Solvents: Water (3.37), DMSO (2.50). Standard: TMS (0.01).

**<sup>13</sup>C NMR** (101 MHz, DMSO-*d*<sub>6</sub>, δ/ppm): 162.85 (1C, **2**), 140.45 (1C, **11**, extrapolated from HMBC spectrum), 132.48 (1C, **9**), 125.80 (1C, **6**), 124.59 (1C, **7**), 124.10 (1C, **8**), 120.00 (1C, **10**), 109.90 (1C, **4**), 53.46 (1C, **1**). Solvents: DMSO (40.15, 39.94, 39.73, 39.52, 39.31, 39.10, 38.89). Standard: TMS (0.10). The signals for the quaternary carbons **3** and **5** could not be resolved.

**HRMS** (ESI-MS, pos.) *m/z*: [M+H]<sup>+</sup> calculated for C<sub>11</sub>H<sub>10</sub>NO<sub>3</sub>: 204.0655, found: 204.0655.

### Compound 21:



The synthesis was performed similarly to Kato *et al.*<sup>235</sup>

A mixture of methyl ester **20** (2.30 g, 11.3 mmol, 1.0 eq.), P<sub>2</sub>O<sub>5</sub> (3.55 g, 24.9 mmol, 2.2 eq.) and Bu<sub>4</sub>NBr (4.02 g, 12.4 mmol, 1.1 eq.) in toluene (80 ml) was heated at 90°C for 1 h with vigorous stirring. After cooling to room temperature, the resulting upper toluene layer was collected. The organic phase was washed with saturated NaHCO<sub>3</sub> (150 ml), brine (150 ml) and water (150 ml), dried over Na<sub>2</sub>SO<sub>4</sub> and concentrated under reduced pressure to yield a yellow solid (**21**, 1.10 g, 4.12 mmol, 36% yield). This crude product was used for the next synthesis step without further purification.

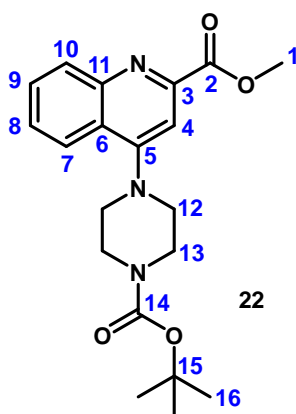
Annex spectra on page 174.

**Appearance:** Yellow solid

**<sup>1</sup>H NMR** (400 MHz, DMSO-*d*<sub>6</sub>, δ/ppm): 8.38 (s, 1H, **4**), 8.23 (s (broad), 1H, **7 or 10**), 8.21 (s (broad), 1H, **7 or 10**), 8.01 – 7.94 (m, 1H, **8 or 9**), 7.94 – 7.88 (m, 1H, **8 or 9**), 3.97 (s, 3H, **1**). Solvents: Toluene (7.24, 7.17, 2.29), Water (3.35), DMSO (2.50).

**<sup>13</sup>C NMR** (101 MHz, DMSO-*d*<sub>6</sub>, δ/ppm): 164.17 (1C, **2**), 147.52 (1C), 147.30 (1C), 134.29 (1C), 131.80 (1C), 130.63 (1C), 130.60 (1C), 127.94 (1C), 126.31 (1C), 124.52 (1C), 52.90 (1C, **1**). Solvents: Toluene (137.32, 128.87, 128.18, 125.29, 21.03), DMSO (40.15, 39.94, 39.73, 39.52, 39.31, 39.10, 38.89). Impurities: 29.04, 23.37.

**UPLC-MS** (ESI-MS, pos.) *m/z*: [M+H]<sup>+</sup> calculated for C<sub>12</sub>H<sub>8</sub><sup>79</sup>BrNO<sub>2</sub>: 265.98, found: 266.02; calculated for C<sub>12</sub>H<sub>8</sub><sup>81</sup>BrNO<sub>2</sub>: 267.98, found: 267.97.

**Compound 22:**

Under an N<sub>2</sub> atmosphere, methyl 4-bromoquinoline-2-carboxylate (**21**, 1.00 g, 3.76 mmol, 1.0 eq.), *tert*-butyl piperazine-1-carboxylate (707 mg, 3.76 mmol, 1.0 eq.), Pd<sub>2</sub>(dba)<sub>3</sub> (196 mg, 0.23 mmol, 0.06 eq.), *rac*. BINAP (135 mg, 0.23 mmol, 0.06 eq.) and CsCO<sub>3</sub> (2.74 g, 8.41 mmol, 2.2 eq.) were mixed in dry 1,4-dioxane (30 ml) and heated to reflux for 15 h. The red mixture was filtered and the clear solution evaporated to dryness. The resulting red oil was taken up in ethyl acetate and purified by flash column chromatography (SiO<sub>2</sub>, ethyl acetate/cyclohexane 1:2 → 1:1). The fractions were concentrated and dried under reduced pressure to yield the product as a yellow-orange solid (**22**, 409 mg, 1.10 mmol, 29% yield).

Annex spectra on page 175.

**Appearance:** Yellow-orange solid

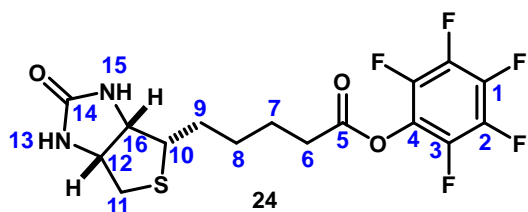
**TLC:** Ethyl acetate/cyclohexane 2:3; *R<sub>f</sub>* = 0.30

**<sup>1</sup>H NMR** (400 MHz, CDCl<sub>3</sub> δ/ppm): 8.26 (ddd, *J* = 8.5, 1.3, 0.6 Hz, 1H, **10**), 8.04 (ddd, *J* = 8.4, 1.5, 0.6 Hz, 1H, **7**), 7.73 (ddd, *J* = 8.5, 6.8, 1.4 Hz, 1H, **9**), 7.67 (s, 1H, **4**), 7.59 (ddd, *J* = 8.2, 6.8, 1.3 Hz, 1H, **8**), 4.06 (s, 3H, **1**), 3.78 – 3.69 (m, 4H, **13**), 3.30 – 3.19 (m, 4H, **12**), 1.50 (s, 9H, **16**). Solvents: Chloroform (7.26), DCM (5.29). Standard: TMS (0.00).

**<sup>13</sup>C NMR** (101 MHz, CDCl<sub>3</sub> δ/ppm): 166.49 (1C, **2**), 158.01 (1C, **5**), 154.86 (1C, **14**), 149.14 (1C, **11**), 148.59 (1C, **3**), 131.60 (1C, **10**), 130.04 (1C, **9**), 127.61 (1C, **8**), 124.47 (1C, **6**), 123.49 (1C, **7**), 109.14 (1C, **4**), 80.37 (1C, **15**), 53.38 (1C, **1**), 52.26 (2C, **12**), 43.63 (2C, **13**, extrapolated from HMQC spectrum), 28.57 (3C, **16**). Solvents: Chloroform (77.48, 77.16, 76.84). Standard: TMS (0.00).

**HRMS** (ESI-MS, pos.) *m/z*: [M+H]<sup>+</sup> calculated for C<sub>20</sub>H<sub>26</sub>N<sub>3</sub>O<sub>4</sub>: 372.1918, found: 372.1923.

## Compound 24:



The synthesis was performed according to Thompson *et al.*<sup>236</sup>

To a dispersion of D-biotin (**23**, 1.00 g, 4.08 mmol, 1.0 eq.) in DMF (25 ml), triethylamine (1.00 ml, 0.73 g, 7.17 mmol, 1.8 eq.) was added at 0°C. Pentafluorophenyl trifluoroacetate (1.00 ml, 1.63 g, 5.81 mmol, 1.4 eq.) was slowly added, which led to the formation of a pink solution. The reaction mixture was allowed to warm up to room temperature and was further stirred for 2 h, whereupon a white precipitate formed. Diethyl ether (80 ml) was added, the precipitate was filtered, washed with diethyl ether (80 ml) and dried at reduced pressure to yield the product as a white solid (**24**, 998 mg, 2.43 mmol, 60% yield).

Annex spectra on page 176.

**Appearance:** White solid

<sup>1</sup>H NMR (400 MHz, DMSO-*d*<sub>6</sub> δ/ppm): 6.45 (s, 1H, **15**), 6.37 (s, 1H, **13**), 4.36 – 4.27 (m, 1H, **12**), 4.19 – 4.11 (m, 1H, **16**), 3.17 – 3.08 (m, 1H, **10**), 2.87 – 2.81 (m, 1H, **11**), 2.79 (t, *J* = 7.6 Hz, 2H, **6**), 2.58 (d, *J* = 12.4 Hz, 1H, **11**), 1.78 – 1.34 (m, 6H, **7 + 8 + 9**). Solvents: Water (3.32), DMSO (2.50).

<sup>13</sup>C NMR (101 MHz, DMSO-*d*<sub>6</sub> δ/ppm): 169.51 (1C, **5**), 162.67 (1C, **14**), 61.02 (1C, **16**), 59.17 (1C, **12**), 55.25 (1C, **10**), 39.78 (1C, **11**, extrapolated from HMQC spectrum), 32.30 (1C, **6**), 27.92 (1C, **9**), 27.68 (1C, **8**), 24.30 (1C, **7**). Solvents: DMSO (40.15, 39.94, 39.73, 39.52, 39.31, 39.10, 38.89). The signals for the quaternary carbons **1 – 4** could not be resolved.

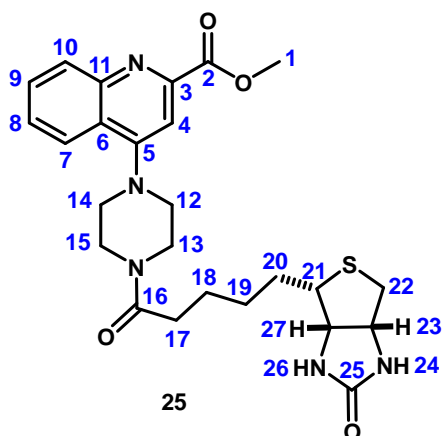
<sup>19</sup>F NMR (376 MHz, DMSO-*d*<sub>6</sub> δ/ppm): -153.59 (d, *J* = 19.1 Hz, 2F, **3**), -158.12 (t, *J* = 23.1 Hz, 1F, **1**), -162.63 (dd, *J* = 23.3, 19.1 Hz, 2F, **2**).

NMR spectra are in good accordance with the results from Neier *et al.*<sup>237</sup>

**HRMS** (ESI-MS, pos.) *m/z*: [M+Na]<sup>+</sup> calculated for C<sub>16</sub>H<sub>15</sub>N<sub>2</sub>O<sub>3</sub>SF<sub>5</sub>Na: 433.0616, found: 433.0616.



## Compound 25:



The synthesis was performed similarly to Kajetanowicz *et al.*<sup>238</sup>

Methyl 4-(4-(tert-butoxycarbonyl)piperazin-1-yl)quinoline-2-carboxylate (**22**, 0.40 g, 1.09 mmol, 1.0 eq.) and triisopropylsilane (0.44 ml, 0.35 g, 2.18 mmol, 2.0 eq., scavenger for carbocations) were dissolved in DCM (2 ml) and treated with concentrated trifluoroacetic acid (2 ml). The red solution was stirred for 1 h at room temperature and then evaporated to dryness. The orange oil was dissolved in DCM (2 ml). Addition of diethyl ether (20 ml) led to the formation of a yellow precipitate which was filtered, washed with diethyl ether (2 x 10 ml) and dried under reduced pressure to afford an off-white solid (0.52 g). This solid was dissolved in DMF (5 ml), followed by the addition of *N,N*-diisopropylethylamine (0.95 ml, 0.70 g, 5.44 mmol, 5.0 eq.) and D-biotin pentafluorophenyl ester (**24**, 0.44 g, 1.09 mmol, 1.0 eq.). The reaction mixture was stirred for 24 h at room temperature (until no more D-biotin pentafluorophenyl ester was detectable on TLC (DCM/MeOH 10:1, DACA-stain) and evaporated to dryness to obtain a brown oil. Addition of diethyl ether (20 ml) led to the precipitation of an off-white solid, which was filtered and washed with diethyl ether (4 x 50 ml). The solid was then dissolved in DCM (20 ml), washed with saturated NaHCO<sub>3</sub> (20 ml) and water (20 ml). The organic fraction was dried over Na<sub>2</sub>SO<sub>4</sub>. The solvent was evaporated under reduced pressure to yield the product as a pale yellow solid (**25**, 224 mg, 0.85 mmol, 78% yield).

Annex spectra on page 177.

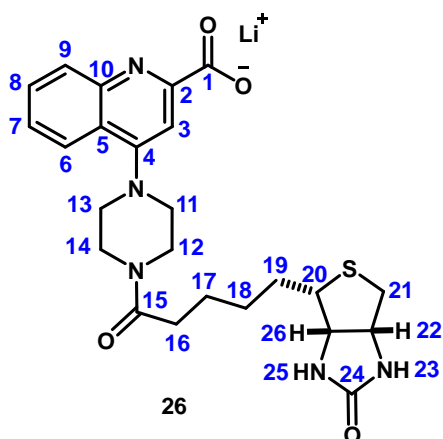
**Appearance:** Pale yellow solid

<sup>1</sup>H NMR (400 MHz, Methanol-*d*<sub>4</sub> δ/ppm): 8.18 (dd, *J* = 5.6, 0.8 Hz, 1H, **7**), 8.16 (dd, *J* = 5.4, 0.6 Hz, 1H, **10**), 7.79 (ddd, *J* = 8.5, 6.9, 1.4 Hz, 1H, **9**), 7.68 (ddd, *J* = 8.2, 6.8, 1.2 Hz, 1H, **8**), 7.67 (s, 1H, **4**), 4.50 (ddd, *J* = 7.9, 5.0, 1.0 Hz, 1H, **23**), 4.32 (dd, *J* = 7.9, 4.4 Hz, 1H, **27**), 4.03 (s, 3H, **1**), 3.92 (t, *J* = 4.8 Hz, 2H, **13 or 15**), 3.88 (t, *J* = 5.0 Hz, 2H, **13 or 15**), 3.39 – 3.33 (m, 2H, **12 or 14**), 3.30 – 3.27 (m, 2H, **12 or 14**), 3.23 (ddd, *J* = 8.8, 5.9, 4.4 Hz, 1H, **21**), 2.93 (dd, *J* = 12.8, 5.0 Hz, 1H, **22**), 2.71 (d, *J* = 12.6 Hz, 1H, **22**), 2.51 (t, *J* = 7.4 Hz, 2H, **17**), 1.83 – 1.59 (m, 4H, **18 + 20**), 1.56 – 1.45 (m, 2H, **19**). Solvents: DCM (5.49), Water (4.86), DMF (7.97, 2.99, 2.86). Standard: TMS (0.00). Acidic protons **24** and **26** are due to proton-deuterium exchange with the solvent methanol-*d*<sub>4</sub> not visible in the <sup>1</sup>H spectrum.

<sup>13</sup>C NMR (101 MHz, Methanol-*d*<sub>4</sub> δ/ppm): 174.24 (1C, **16**), 167.04 (1C, **2**), 166.14 (1C, **25**), 159.64 (1C, **5**), 149.97 (1C, **11**), 149.48 (1C, **3**), 131.56 (1C, **9**), 131.15 (1C, **10**), 128.86 (1C, **8**), 125.46 (1C, **6**), 125.03 (1C, **7**), 109.78 (1C, **4**), 63.41 (1C, **27**), 61.68 (1C, **23**), 57.08 (1C, **21**), 53.48 (1C, **1**), 53.41 (1C, **12 or 14**), 53.15 (1C, **12 or 14**), 46.88 (1C, **13 or 15**), 42.83 (1C, **13 or 15**), 41.09 (1C, **22**), 33.75 (1C, **17**), 29.94 (1C, **19**), 29.60 (1C, **20**), 26.41 (1C, **18**). Solvents: Methanol (49.68, 49.46, 49.25, 49.04, 48.82, 48.61, 48.40). Standard: TMS (0.00).

HRMS (ESI-MS, pos.) m/z: [M+H]<sup>+</sup> calculated for C<sub>25</sub>H<sub>32</sub>N<sub>5</sub>O<sub>4</sub>S: 498.2170, found: 498.2178.

## Compound 26:



The methyl ester **25** (100 mg, 0.20 mmol, 1.0 eq.) was dissolved in MeOH (2 ml) and treated with LiOH·H<sub>2</sub>O (16 mg, 0.40 mmol, 2.0 eq.). The reaction mixture was stirred for 22 h at room temperature (until no more starting material was detected on TLC (DCM/MeOH 10:1)). The mixture was filtered to remove the excess of insoluble LiOH. Addition of diethyl ether (5 ml) led to the formation of an off-white precipitate, which was washed with diethyl ether (3 x 5 ml) and dried under reduced pressure to obtain the product as an off-white solid (**26**, 80.9 mg, 0.17 mmol, 83% yield).

Annex spectra on page 178.

**Appearance:** Off-white solid

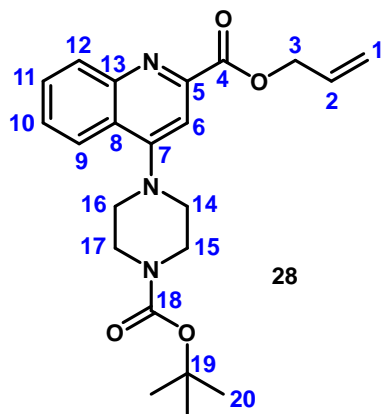
<sup>1</sup>H NMR (400 MHz, Methanol-*d*<sub>4</sub> δ/ppm): 8.14 (dd, *J* = 8.4, 0.8 Hz, 1H, **6**), 8.07 (dd, *J* = 8.6, 0.9 Hz, 1H, **9**), 7.72 (ddd, *J* = 8.4, 6.8, 1.4 Hz, 1H, **8**), 7.66 (s, 1H, **3**), 7.59 (ddd, *J* = 8.3, 6.8, 1.2 Hz, 1H, **7**), 4.50 (ddd, *J* = 7.9, 5.0, 0.9 Hz, 1H, **22**), 4.32 (dd, *J* = 7.9, 4.4 Hz, 1H, **26**), 3.91 (t, *J* = 5.4 Hz, 2H, **12 or 14**), 3.88 (t, *J* = 4.7 Hz, 2H, **12 or 14**), 3.39 – 3.32 (m, 2H, **11 or 13**), 3.30 – 3.23 (m, 2H, **11 or 13**), 3.27 – 3.18 (m, 1H, **20**), 2.93 (dd, *J* = 12.7, 5.0 Hz, 1H, **21**), 2.71 (d, *J* = 12.7 Hz, 1H, **21**), 2.52 (t, *J* = 7.4 Hz, 2H, **16**), 1.84 – 1.58 (m, 4H, **17 + 19**), 1.57 – 1.45 (m, 2H, **18**). Solvents: Water (4.87), diethyl ether (3.49 + 1.17). Standard: TMS (0.00). Acidic protons **23** and **25** are due to proton-deuterium exchange with the solvent methanol-*d*<sub>4</sub> not visible in the <sup>1</sup>H spectrum.

<sup>13</sup>C NMR (101 MHz, Methanol-*d*<sub>4</sub> δ/ppm): 174.24 (1C, **15**), 173.04 (1C, **1**), 166.15 (1C, **24**), 159.12 (1C, **4**), 157.23 (1C, **2**), 149.54 (1C, **10**), 130.78 (1C, **8**), 130.66 (1C, **9**), 127.53 (1C, **7**), 124.80 (1C, **5 or 6**), 124.79 (1C, **5 or 6**), 109.87 (1C, **3**), 63.41 (1C, **26**), 61.69 (1C, **22**), 57.05 (1C, **20**), 53.37 (1C, **11 or 13**), 53.35 (1C, **11 or 13**), 46.99 (1C, **12 or 14**), 42.93 (1C, **12 or 14**), 41.08 (1C, **21**), 33.76 (1C, **16**), 29.92 (1C, **18**), 29.58 (1C, **19**), 26.42 (1C, **17**). Solvents: Methanol (49.68, 49.46, 49.25, 49.04, 48.82, 48.61, 48.40). Standard: TMS (0.00).

**HRMS** (ESI-MS, pos.) *m/z*: [M+H<sub>2</sub>]<sup>+</sup> calculated for C<sub>24</sub>H<sub>30</sub>N<sub>5</sub>O<sub>4</sub>S: 484.2013, found: 484.2014.

### 4.3.2 Biotinylated ruthenium cofactor: alternative synthesis routes

#### Compound 28:



The synthesis was performed similarly to Meggers *et al.*<sup>94</sup>

The methyl ester **22** (100 mg, 0.27 mmol, 1.0 eq.) was dissolved in MeOH (5 ml) and treated with LiOH·H<sub>2</sub>O (22.4 mg, 0.54 mmol, 2.0 eq.). The reaction mixture was stirred at room temperature for 48 h (until no more methyl ester **22** was detected on TLC (cyclohexane/ethyl acetate 1:1)). The mixture was filtered to remove the excess of insoluble LiOH·H<sub>2</sub>O. The solvent was evaporated and the residue dried under reduced pressure to yield a yellow-orange solid (94 mg, lithium salt of the carboxylic acid). This solid and sodium bicarbonate (36 mg, 0.44 mmol, 1.7 eq.) were dispersed in dry DMF (10 ml) and treated with allyl bromide (48 μl, 67 mg, 0.54 mmol, 2.0 eq.). The mixture was stirred at 50°C for 18 h. Water (25 ml) was added and the reaction mixture was extracted with DCM (3 x 25 ml). The organic phase was dried over Na<sub>2</sub>SO<sub>4</sub> and the solvent evaporated to obtain a yellow oil. This oil was purified by flash column chromatography (SiO<sub>2</sub>, cyclohexane/ethyl acetate 5:2). The fractions were concentrated and dried under reduced pressure to yield the product as a yellow solid (**28**, 66 mg, 0.17 mmol, 64% yield).

Annex spectra on page 179.

**Appearance:** Yellow solid

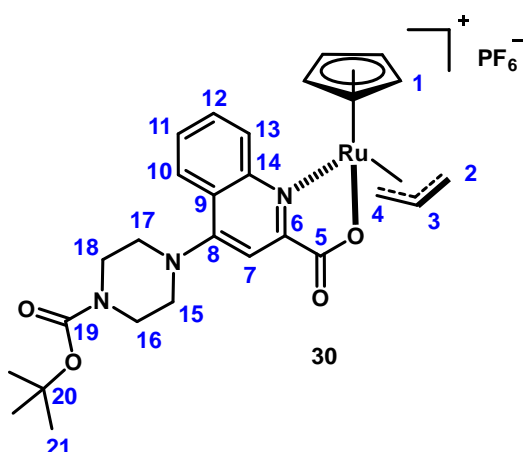
**TLC:** Ethyl acetate/cyclohexane 1:2; *R<sub>f</sub>* = 0.45

**<sup>1</sup>H NMR** (500 MHz, Chloroform-*d* δ/ppm): 8.27 (ddd, *J* = 8.6, 1.3, 0.6 Hz, 1H, **12**), 8.04 (ddd, *J* = 8.4, 1.5, 0.6 Hz, 1H, **9**), 7.73 (ddd, *J* = 8.4, 6.8, 1.4 Hz, 1H, **11**), 7.66 (s, 1H, **6**), 7.59 (ddd, *J* = 8.2, 6.8, 1.3 Hz, 1H, **10**), 6.12 (ddt, *J* = 17.1, 10.4, 5.9 Hz, 1H, **2**), 5.47 (dq, *J* = 17.2, 1.5 Hz, 1H, **1**), 5.34 (dq, *J* = 10.4, 1.2 Hz, 1H, **1**), 4.98 (dt, *J* = 6.0, 1.3 Hz, 2H, **3**), 3.78 – 3.69 (m, 4H, **15 + 17**), 3.30 – 3.21 (m, 4H, **14 + 16**), 1.51 (s, 9H, **20**). Solvents: DMF (8.02, 2.95, 2.88), chloroform (7.27), ethyl acetate (4.12, 2.05, 1.26), water (1.72), cyclohexane (1.43). Standard: TMS (0.00).

**<sup>13</sup>C NMR** (126 MHz, Chloroform-*d* δ/ppm): 165.51 (1C, **4**), 157.82 (1C, **7**), 154.72 (1C, **18**), 149.06 (1C, **13**), 148.54 (1C, **5**), 131.90 (1C, **2**), 131.56 (1C, **12**), 129.83 (1C, **11**), 127.46 (1C, **10**), 124.32 (1C, **8**), 123.30 (1C, **9**), 119.25 (1C, **1**), 109.02 (1C, **6**), 80.23 (1C, **19**), 66.84 (1C, **3**), 52.09 (2C, **14 + 16**), 43.65 (2C, **15 + 17**, extrapolated from HMQC spectrum), 28.43 (3C, **20**). Solvents: Chloroform (77.28, 77.03, 76.77). Standard: TMS (0.00).

**HRMS** (ESI-MS, pos.) m/z: [M+H]<sup>+</sup> calculated for C<sub>22</sub>H<sub>28</sub>N<sub>3</sub>O<sub>4</sub>: 398.2074, found: 398.2080.

### Compound 30:



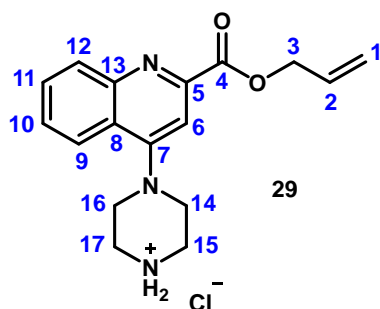
The synthesis was performed similarly to Meggers *et al.*<sup>94</sup>

Under a nitrogen atmosphere, [CpRu(MeCN)<sub>3</sub>]PF<sub>6</sub> (12.8 mg, 0.03 mmol, 1.0 eq.) was dissolved in dry acetone (1 ml), yielding a yellow solution. A solution of ligand **28** (12.0 mg, 0.03 mmol, 1.0 eq.) in dry acetone (1 ml) was added. The resulting orange solution was stirred at room temperature for 45 min. The solvent was evaporated under a stream of nitrogen, yielding an orange-brown residue. This residue was washed with dry cold acetone (1 ml) to obtain the product as a yellow solid (**30**, 4.1 mg, 5.8 μmol, 20% yield).

Annex spectrum on page 180.

**Appearance:** Yellow solid

<sup>1</sup>H NMR (400 MHz, Acetonitrile-*d*<sub>3</sub> δ/ppm): 8.17 (dd, *J* = 8.5, 1.3 Hz, 1H, **10 or 13**), 7.96 (ddd, *J* = 8.6, 6.9, 1.5 Hz, 1H, **11 or 12**), 7.76 (ddd, *J* = 8.3, 6.9, 1.1 Hz, 1H, **11 or 12**), 7.72 (d, *J* = 8.8 Hz, 1H, **10 or 13**), 7.47 (s, 1H, **7**), 6.12 (s, 5H, **1**), 4.64 – 4.49 (m, 2H, **2 or 3 or 4**), 4.37 (d, *J* = 10.1 Hz, 1H, **2 or 3 or 4**), 4.29 (dd, *J* = 6.0, 2.7 Hz, 1H, **2 or 3 or 4**), 4.08 (dd, *J* = 5.8, 2.9 Hz, 1H, **2 or 3 or 4**), 3.77 – 3.60 (m, 4H, **15 + 17 or 16 + 18**), 3.57 – 3.38 (m, 4H, **15 + 17 or 16 + 18**), 1.47 (s, 9H, **21**). Solvents: Water (2.16), acetone (2.09), acetonitrile (1.94).

**Compound 29:**

Allyl ester **28** (25 mg, 63  $\mu$ mol, 1.0 eq.) was dissolved in dry 1,4-dioxane (2 ml) and treated with HCl (4 M in 1,4-dioxane, 157  $\mu$ l, 630  $\mu$ mol, 10.0 eq.). The resulting yellow solution was stirred at room temperature for 2.5 h, whereby a yellow precipitate formed. The precipitate was filtered, washed with diethyl ether (3 x 5 ml) and dried to yield the crude product as a yellow solid (**29**, 15.7 mg, 47  $\mu$ mol, 75% yield). UPLC-MS analysis stated the presence of a small fraction of the educt (**28**). However, the obtained crude product was used for the next synthesis step without further purification.

Annex spectra on page 181.

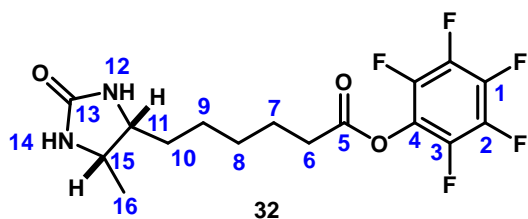
**Appearance:** Yellow solid

**<sup>1</sup>H NMR** (400 MHz, Methanol-*d*<sub>4</sub>  $\delta$ /ppm): 8.33 – 8.25 (m, 2H, **9 – 12**), 8.05 (t, *J* = 7.7 Hz, 1H, **9 – 12**), 7.88 – 7.82 (m, 1H, **9 – 12**), 7.81 (s, 1H, **6**), 6.16 (ddt, *J* = 16.5, 11.1, 5.8 Hz, 1H, **2**), 5.53 (d, *J* = 17.2 Hz, 1H, **1**), 5.40 (d, *J* = 10.4 Hz, 1H, **1**), 5.05 (d, *J* = 6.0 Hz, 2H, **3**), 4.07 (t, *J* = 4.8 Hz, 4H, **14 + 16 or 15 + 17**), 3.62 (t, *J* = 5.0 Hz, 4H, **14 + 16 or 15 + 17**). Solvents: Water (4.88), methanol (3.31). Impurities: 3.79, 2.03, 1.51.

**UPLC-MS** (ESI-MS, pos.) *m/z*: Product **29**: [M-Cl]<sup>+</sup> calculated for C<sub>17</sub>H<sub>20</sub>N<sub>3</sub>O<sub>2</sub>: 298.16, found: 298.15.  
Educt **28**: [M-H]<sup>+</sup> calculated for C<sub>22</sub>H<sub>28</sub>N<sub>3</sub>O<sub>4</sub>: 398.21, found: 398.14.

**Solubility:** Product **29** is soluble in DMSO, MeOH and insoluble in acetone, MeCN, DCM, THF.

### Compound 32:



The synthesis was performed similarly to Thompson *et al.*<sup>236</sup>

To a solution of desthiobiotin (**31**, 0.20 g, 0.93 mmol, 1.0 eq.) in DMF (4 ml), triethylamine (0.23 ml, 0.17 g, 1.68 mmol, 1.8 eq.) was added at room temperature. Pentafluorophenyl trifluoroacetate (0.22 ml, 0.36 g, 1.30 mmol, 1.4 eq.) was slowly added. The reaction mixture was stirred at room temperature for 2 h. The solvent was evaporated and the resulting residue was washed with diethyl ether (3 x 5 ml) and dried under reduced pressure to obtain the product as a white solid (**32**, 100 mg, 0.26 mmol, 28% yield).

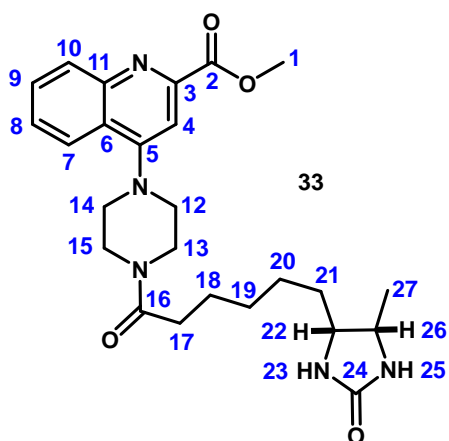
Annex spectra on page 182.

**Appearance:** White solid

<sup>1</sup>H NMR (400 MHz, DMSO-*d*<sub>6</sub> δ/ppm): 6.31 (s, 1H, **12 or 14**), 6.12 (s, 1H, **12 or 14**), 3.67 – 3.56 (m, 1H, **11 or 16**), 3.49 (td, *J* = 7.7, 4.8 Hz, 1H, **11 or 16**), 2.78 (t, *J* = 7.3 Hz, 2H, **6**), 1.67 (p, *J* = 7.2 Hz, 2H, **10**), 1.47 – 1.15 (m, 6H, **7 – 9**), 0.96 (d, *J* = 6.4 Hz, 3H, **16**). Solvents: Water (3.33), DMSO (2.50).

<sup>19</sup>F NMR (376 MHz, DMSO-*d*<sub>6</sub> δ/ppm): -153.68 (d, *J* = 19.3 Hz, 2F, **3**), -158.14 (t, *J* = 23.2 Hz, 1F, **1**), -162.64 (dd, *J* = 23.2, 19.0 Hz, 2F, **2**).



**Compound 33:**

The synthesis was performed similarly to Kajetanowicz *et al.*<sup>238</sup>

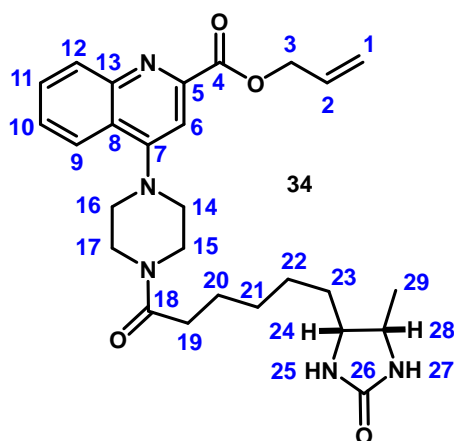
Methyl 4-(4-(tert-butoxycarbonyl)piperazin-1-yl)quinoline-2-carboxylate (**22**, 74 mg, 0.20 mmol, 1.0 eq.) and triisopropylsilane (82  $\mu$ l, 64 mg, 0.40 mmol, 2.0 eq., scavenger for carbocations) were dissolved in DCM (2 ml) and treated with concentrated trifluoroacetic acid (2 ml). The resulting red solution was stirred at room temperature for 2 h. The solvent was evaporated and the yellow residue was dissolved in DMF (3 ml), followed by the addition of *N,N*-diisopropylethylamine (0.35 ml, 0.26 g, 2.00 mmol, 10.0 eq.) and desthiobiotin pentafluorophenyl ester (**32**, 76 mg, 0.20 mmol, 1.0 eq.). The reaction mixture was stirred at room temperature for 24 h (until no more desthiobiotin pentafluorophenyl ester was visible on TLC (DCM/MeOH 10:1, DACA-stain) and then evaporated to dryness. The resulting red-brown oil was taken up in DCM (10 ml), washed with saturated  $\text{NaHCO}_3$  (10 ml) and water (10 ml) and dried over  $\text{Na}_2\text{SO}_4$ . The solvent was evaporated under reduced pressure to afford the crude product as a yellow-orange solid (**33**, 85.5 mg, 0.18 mmol, 92% yield). This crude product was used for the next synthesis step without further purification.

Annex spectra on page 183.

**Appearance:** Yellow-orange solid

**$^1\text{H NMR}$**  (400 MHz, Methanol- $d_4$   $\delta$ /ppm): 8.16 – 8.08 (m, 2H, **7 + 10**), 7.77 (ddd,  $J = 8.4, 6.8, 1.4$  Hz, 1H, **8 or 9**), 7.65 (ddd,  $J = 8.3, 6.8, 1.3$  Hz, 1H, **8 or 9**), 7.59 (s, 1H, **4**), 4.02 (s, 3H, **1**), 3.93 – 3.77 (m, 5H, **13 + 15 + 22 or 26**), 3.75 – 3.65 (m, 1H, **22 or 26**), 3.31 – 3.17 (m, 4H, **12 + 14**), 2.48 (t,  $J = 7.5$  Hz, 2H, **17**), 1.74 – 1.60 (m, 2H, **21**), 1.55 – 1.24 (m, 6H, **18 – 20**), 1.11 (d,  $J = 6.5$  Hz, 3H, **27**). Solvents: DMF (7.98, 2.99, 2.86), DCM (5.50), Water (4.87), Methanol (3.32). Impurities: 4.12, 1.15, 1.13, 1.04. Acidic protons **23** and **25** are due to proton-deuterium exchange with the solvent methanol- $d_4$  not visible in the  $^1\text{H}$  spectrum.

**UPLC-MS** (ESI-MS, pos.)  $m/z$ :  $[\text{M}+\text{H}]^+$  calculated for  $\text{C}_{25}\text{H}_{34}\text{N}_5\text{O}_4$ : 468.26, found: 468.2;  $[\text{M}+\text{Na}]^+$  calculated for  $\text{C}_{25}\text{H}_{33}\text{N}_5\text{O}_4\text{Na}$ : 490.24, found: 490.2.

**Compound 34:**

The synthesis was performed similarly to Meggers *et al.*<sup>94</sup>

The methyl ester **33** (85 mg, 0.18 mmol, 1.0 eq.) was dissolved in MeOH (2 ml) and treated with LiOH·H<sub>2</sub>O (15 mg, 0.36 mmol, 2.0 eq.). The reaction mixture was stirred at room temperature for 24 h (until no more methyl ester **33** was detected on TLC (DCM/MeOH 20:1, DACA-stain)). The mixture was filtered to remove the excess of insoluble LiOH·H<sub>2</sub>O. The obtained yellow solution was evaporated to dryness to yield a yellow-orange solid (83 mg, lithium salt of the carboxylic acid). This solid and sodium bicarbonate (25 mg, 0.30 mmol, 1.7 eq.) were dispersed in dry DMF (2 ml) and treated with allyl bromide (31 μl, 43 mg, 0.36 mmol, 2.0 eq.). The mixture was stirred at 50°C for 18 h. Water (10 ml) was added and the reaction mixture was extracted with DCM (3 x 10 ml). The organic phase was dried over Na<sub>2</sub>SO<sub>4</sub> and concentrated to obtain a yellow oil. This oil was purified by flash column chromatography (SiO<sub>2</sub>, DCM/MeOH 25:1 → 15:1, product spot on TLC stained with DACA-stain). The fractions were concentrated and dried under reduced pressure to yield the crude product as a yellow solid (**34**, 5.0 mg, 0.01 mmol, 6% yield). According to NMR and UPLC-MS analysis the obtained product also contained parts (~15%) of the initial methyl ester **33**. However, the obtained crude product was used for the next synthesis step without further purification.

Annex spectra on page 184.

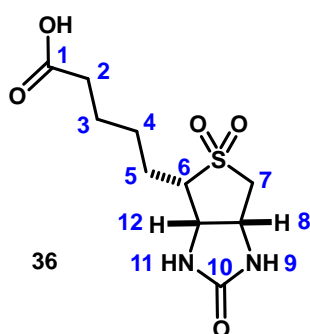
**Appearance:** Yellow solid

**TLC:** DCM/MeOH 15:1; *R<sub>f</sub>* = 0.40

<sup>1</sup>H NMR (400 MHz, Acetone-*d*<sub>6</sub> δ/ppm): 8.26 – 8.19 (m, 1H, **9 or 12**), 8.16 – 8.08 (m, 1H, **9 or 12**), 7.80 (ddd, *J* = 8.4, 6.9, 1.4 Hz, 1H, **10 or 11**), 7.68 (ddd, *J* = 8.3, 6.9, 1.3 Hz, 1H, **10 or 11**), 7.64 (s, 1H, **6**), 6.13 (ddt, *J* = 17.2, 10.5, 5.6 Hz, 1H, **2**), 5.54 – 5.44 (m, 1H, **1**), 5.35 – 5.27 (m, 1H, **1**), 4.91 (dt, *J* = 5.6, 1.5 Hz, 2H, **3**), 3.92 – 3.85 (m, 4H, **15 + 17**), 3.83 – 3.73 (m, 1H, **24 or 28**), 3.71 – 3.63 (m, 1H, **24 or 28**), 3.40 – 3.23 (m, 4H, **14 + 16**), 2.47 (t, *J* = 7.4 Hz, 2H, **19**), 1.73 – 1.47 (m, 8H, **20 – 23**), 1.10 (d, *J* = 6.4 Hz, 3H, **29**). Solvents: DCM (5.62), water (2.82), acetone (2.05), “grease” (1.29, 0.87).

**UPLC-MS** (ESI-MS, pos.) *m/z*: Product **34**: [M+H]<sup>+</sup> calculated for C<sub>27</sub>H<sub>36</sub>N<sub>5</sub>O<sub>4</sub>: 494.28, found: 494.2; [M+Na]<sup>+</sup> calculated for C<sub>27</sub>H<sub>35</sub>N<sub>5</sub>O<sub>4</sub>Na: 516.26, found: 516.2. Impurity (methyl ester **33**) [M+H]<sup>+</sup> calculated for C<sub>25</sub>H<sub>34</sub>N<sub>5</sub>O<sub>4</sub>: 468.26, found: 468.3.

### Compound 36:



The synthesis was performed as described by Alves *et al.*<sup>239</sup>

D-Biotin (**23**, 1.00 g, 4.10 mmol, 1.0 eq.) was suspended in glacial acetic acid (12 ml) and treated with aq. H<sub>2</sub>O<sub>2</sub> (30% v/v, 4.30 ml, 41.00 mmol, 10.0 eq.). The mixture was stirred at room temperature for 24 h, whereupon a white precipitate formed. The precipitate was filtered, washed with diethyl ether (3 x 10 ml) and dried at reduced pressure to yield the product as a white solid (**36**, 932 mg, 3.37 mmol, 82% yield).

Annex spectra on page 185.

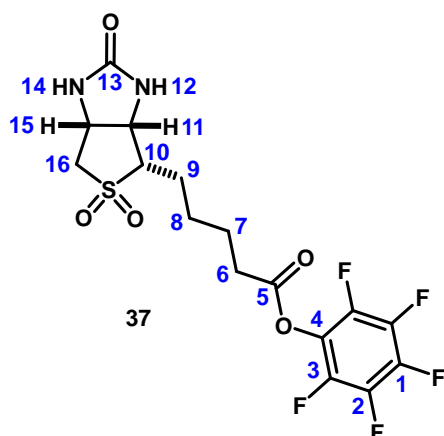
**Appearance:** White solid

<sup>1</sup>H NMR (500 MHz, DMSO-*d*<sub>6</sub> δ/ppm): 12.02 (s, 1H, **COOH**), 6.70 (s, 1H, **11**), 6.60 (s, 1H, **9**), 4.46 – 4.39 (m, 1H, **8**), 4.39 – 4.35 (m, 1H, **12**), 3.32 – 3.27 (m, 1H, **7**), 3.21 – 3.13 (m, 1H, **6**), 3.02 (d, *J* = 13.8 Hz, 1H, **7**), 2.24 – 2.20 (m, 2H, **2**), 1.72 – 1.59 (m, 2H, **5**), 1.58 – 1.49 (m, 2H, **3**), 1.46 – 1.37 (m, 2H, **4**). Solvents: DMSO (2.50).

<sup>13</sup>C NMR (126 MHz, DMSO-*d*<sub>6</sub> δ/ppm): 174.37 (1C, **1**), 161.60 (1C, **10**), 60.25 (1C, **6**), 54.19 (1C, **7**), 53.47 (1C, **12**), 48.96 (1C, **8**), 33.37 (1C, **2**), 25.55 (1C, **4**), 24.40 (1C, **3**), 21.14 (1C, **5**). Solvents: DMSO (40.02, 39.85, 39.69, 39.52, 39.35, 39.19, 39.02).

**HRMS** (ESI-MS, pos.) *m/z*: [M+Na]<sup>+</sup> calculated for C<sub>10</sub>H<sub>16</sub>N<sub>2</sub>O<sub>5</sub>SNa: 299.0672, found: 299.0675.

### Compound 37:



The synthesis was performed similarly to Thompson *et al.*<sup>236</sup>

To a dispersion of D-biotin sulfone (**36**, 0.50 g, 1.81 mmol, 1.0 eq.) in DMF (8 ml), triethylamine (0.44 ml, 0.32 g, 3.19 mmol, 1.76 eq.) was slowly added at 0°C. Pentafluorophenyl trifluoroacetate (0.45 ml, 0.73 g, 2.56 mmol, 1.43 eq.) was then added dropwise. The pink mixture was stirred at 0°C for 1 h and then at room temperature for 4 h. Diethyl ether (100 ml) was added, which led to the formation of a white precipitate. The white solid was filtered, washed with diethyl ether (4 x 20 ml) and dried under reduced pressure to yield the product as a white solid (**37**, 587 mg, 1.33 mmol, 73% yield).

Annex spectra on page 186.

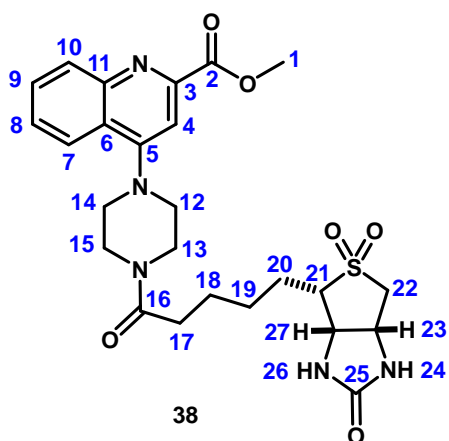
**Appearance:** White solid

**<sup>1</sup>H NMR** (400 MHz, DMSO-*d*<sub>6</sub> δ/ppm): 6.73 (s, 1H, **12 or 14**), 6.62 (s, 1H, **12 or 14**), 4.59 – 4.19 (m, 2H, **11 + 15**), 3.41 – 3.28 (m, 1H, **16**), 3.27 – 3.15 (m, 1H, **10**), 3.15 – 3.01 (m, 1H, **16**), 2.93 – 2.73 (m, 2H, **6**), 1.93 – 1.61 (m, 4H, **7 + 9**), 1.61 – 1.43 (m, 2H, **8**). Solvents: DMSO (2.50). Standard: TMS (0.00).

**<sup>13</sup>C NMR** (101 MHz, DMSO-*d*<sub>6</sub> δ/ppm): 169.46 (1C, **5**), 161.58 (1C, **13**), 60.16 (1C, **10**), 54.19 (1C, **16**), 53.43 (1C, **11 or 15**), 48.96 (1C, **11 or 15**), 32.19 (1C, **6**), 25.20 (1C, **7 or 8**), 24.14 (1C, **7 or 8**), 21.00 (1C, **9**). Solvents: DMSO (40.15, 39.94, 39.73, 39.52, 39.31, 39.10, 38.90). The signals for the quaternary carbons **1 – 4** could not be resolved.

**<sup>19</sup>F NMR** (376 MHz, DMSO-*d*<sub>6</sub> δ/ppm): -153.37 – -153.65 (m, 2F, **3**), -157.95 – -158.27 (m, 1F, **1**), -162.48 – -162.84 (m, 2F, **2**).

**HRMS** (ESI-MS, pos.) *m/z*: [M+Na]<sup>+</sup> calculated for C<sub>16</sub>H<sub>15</sub>N<sub>2</sub>O<sub>5</sub>F<sub>5</sub>SNa: 465.0514, found: 465.0518.

**Compound 38:**

The synthesis was performed similarly to Kajetanowicz *et al.*<sup>238</sup>

Methyl 4-(4-(tert-butoxycarbonyl)piperazin-1-yl)quinoline-2-carboxylate (**22**, 0.13 g, 0.35 mmol, 1.0 eq.) and triisopropylsilane (0.14 ml, 0.11 g, 0.70 mmol, 2.0 eq., scavenger for carbocations) were dissolved in DCM (3.5 ml) and treated with concentrated trifluoroacetic acid (3.5 ml). The resulting orange solution was stirred at room temperature for 2 h. The reaction mixture was concentrated under reduced pressure. The obtained residue was dissolved in DMF (5 ml), followed by the addition of *N,N*-diisopropylethylamine (0.61 ml, 0.46 g, 3.50 mmol, 10.0 eq.) and D-biotin sulfone pentafluorophenyl ester (**37**, 0.15 g, 0.35 mmol, 1.0 eq.). The reaction mixture was stirred at room temperature for 20 h, whereupon a white precipitate was formed. The solvent was evaporated and the white residue was mixed with DCM (50 ml). This mixture was washed with saturated NaHCO<sub>3</sub> (50 ml) and water (50 ml). The organic phase was concentrated under reduced pressure. The obtained white solid was washed with methanol (2 x 10 ml) and diethyl ether (2 x 10 ml) and dried under reduced pressure to yield the product as a white solid (**38**, 156 mg, 0.29 mmol, 84% yield).

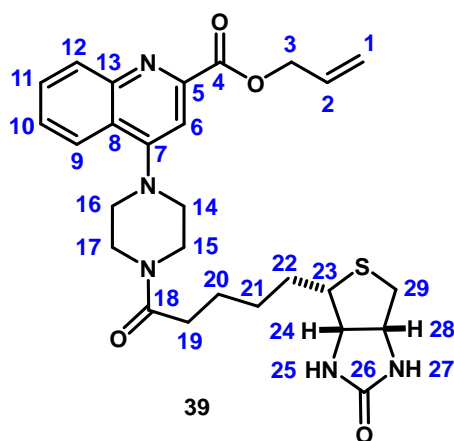
Annex spectra on page 187.

**Appearance:** White solid

<sup>1</sup>H NMR (400 MHz, DMSO-*d*<sub>6</sub> δ/ppm): 8.14 (dd, *J* = 8.4, 1.3 Hz, 1H, **7**), 8.10 (dd, *J* = 8.5, 1.2 Hz, 1H, **10**), 7.82 (ddd, *J* = 8.3, 6.8, 1.4 Hz, 1H, **9**), 7.70 (ddd, *J* = 8.3, 6.8, 1.3 Hz, 1H, **8**), 7.54 (s, 1H, **4**), 6.72 (s, 1H, **26**), 6.61 (s, 1H, **24**), 4.46 – 4.41 (m, 1H, **23**), 4.41 – 4.35 (m, 1H, **27**), 3.94 (s, 3H, **1**), 3.77 (t, *J* = 5.0 Hz, 4H, **13 + 15**), 3.36 – 3.29 (m, 1H, **22**), 3.29 – 3.20 (m, 4H, **12 + 14**), 3.20 – 3.15 (m, 1H, **21**), 3.03 (d, *J* = 14.2 Hz, 1H, **22**), 2.41 (t, *J* = 7.4 Hz, 2H, **17**), 1.78 – 1.63 (m, 2H, **20**), 1.63 – 1.54 (m, 2H, **18**), 1.51 – 1.41 (m, 2H, **19**). Solvents: DMF (7.95, 2.89, 2.73), DCM (5.76), water (3.33), DMSO (2.50).

**<sup>13</sup>C NMR** (Peaks assigned from HMQC and HMBC spectra, DMSO-*d*<sub>6</sub> δ/ppm): 170.65 (1C, **16**), 165.58 (1C, **2**), 161.45 (1C, **25**), 157.11 (1C, **5**), 148.23 (1C, **11**), 130.33 (1C, **10**), 130.01 (1C, **9**), 127.37 (1C, **8**), 123.64 (1C, **7**), 123.28 (1C, **6**), 108.16 (1C, **4**), 60.16 (1C, **21**), 54.05 (1C, **22**), 53.33 (1C, **27**), 52.42 (1C, **1**), 51.56 (2C, **12 + 14**), 48.80 (1C, **23**), 44.70 (1C, **13 or 15**), 40.81 (1C, **13 or 15**), 31.93 (1C, **17**), 25.59 (1C, **19**), 24.53 (1C, **18**), 21.04 (1C, **20**). The signal for the quaternary carbon **3** could not be resolved. A proper <sup>13</sup>C NMR spectrum could not be measured due to limited solubility of the compound in DMSO.

**HRMS** (ESI-MS, pos.) m/z: [M+H]<sup>+</sup> calculated for C<sub>25</sub>H<sub>32</sub>N<sub>5</sub>O<sub>6</sub>S: 530.2068, found: 530.2076.

**Compound 39:**

The synthesis was performed similarly to Meggers *et al.*<sup>94</sup>

The lithium salt of biotinylated acid **26** (75 mg, 0.15 mmol, 1.0 eq.) and sodium bicarbonate (22 mg, 0.26 mmol, 1.7 eq.) were suspended in dry DMF (2 ml) and treated with allyl bromide (20  $\mu$ l, 28 mg, 0.23 mmol, 1.5 eq.). The mixture was stirred at 50°C for 15 h. Water (10 ml) was added and the reaction mixture was extracted with DCM (3 x 10 ml). The organic phase was dried over Na<sub>2</sub>SO<sub>4</sub> and concentrated to obtain a yellow oil. This oil was purified by flash column chromatography (SiO<sub>2</sub>, pure acetone, product spot on TLC stained with DACA-stain). The fractions were concentrated and dried under reduced pressure to yield the product as a light yellow solid (**39**, 66.9 mg, 0.12 mmol, 83% yield).

Annex spectra on page 188.

**Appearance:** Light yellow solid

**TLC:** Pure acetone;  $R_f$  = 0.20

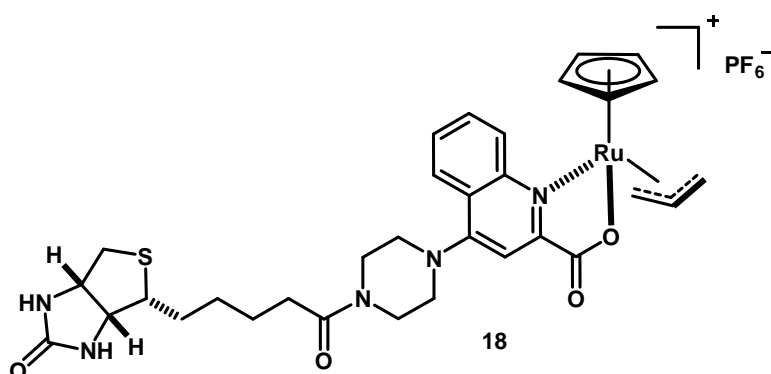
**<sup>1</sup>H NMR** (500 MHz, Chloroform-*d*  $\delta$ /ppm): 8.28 (ddd,  $J$  = 8.5, 1.3, 0.6 Hz, 1H, **12**), 8.05 (ddd,  $J$  = 8.5, 1.5, 0.6 Hz, 1H, **9**), 7.74 (ddd,  $J$  = 8.4, 6.8, 1.4 Hz, 1H, **11**), 7.67 (s, 1H, **6**), 7.61 (ddd,  $J$  = 8.3, 6.8, 1.3 Hz, 1H, **10**), 6.12 (ddt,  $J$  = 17.2, 10.4, 5.9 Hz, 1H, **2**), 5.99 (s, 1H, **25**), 5.47 (dq,  $J$  = 17.2, 1.5 Hz, 1H, **1**), 5.36 (s, 1H, **27**), 5.34 (dq,  $J$  = 10.4, 1.2 Hz, 1H, **1**), 4.98 (dt,  $J$  = 5.9, 1.4 Hz, 2H, **3**), 4.52 (ddt,  $J$  = 7.5, 5.0, 1.1 Hz, 1H, **28**), 4.33 (ddd,  $J$  = 7.8, 4.6, 1.5 Hz, 1H, **24**), 4.00 – 3.85 (m, 2H, **15 or 17**), 3.85 – 3.73 (m, 2H, **15 or 17**), 3.35 – 3.29 (m, 2H, **14 or 16**), 3.29 – 3.23 (m, 2H, **14 or 16**), 3.19 (ddd,  $J$  = 8.1, 6.8, 4.6 Hz, 1H, **23**), 2.92 (dd,  $J$  = 12.8, 5.0 Hz, 1H, **29**), 2.75 (d,  $J$  = 12.7 Hz, 1H, **29**), 2.44 (td,  $J$  = 7.7, 2.4 Hz, 2H, **19**), 1.82 – 1.66 (m, 4H, **20 + 22**), 1.55 – 1.46 (m, 2H, **21**). Solvents: Chloroform (7.27), water (1.94), "grease" (1.26, 0.88). Standard: TMS (0.00).

**<sup>13</sup>C NMR** (126 MHz, Chloroform-*d*  $\delta$ /ppm): 171.72 (1C, **18**), 165.49 (1C, **4**), 163.58 (1C, **26**), 157.45 (1C, **7**), 149.04 (1C, **13**), 148.53 (1C, **5**), 131.85 (1C, **2**), 131.59 (1C, **12**), 129.96 (1C, **11**), 127.65 (1C, **10**), 124.26 (1C, **8**), 123.20 (1C, **9**), 119.33 (1C, **1**), 109.13 (1C, **6**), 66.89 (1C, **3**), 61.89 (1C, **24**), 60.16 (1C, **28**), 55.41 (1C, **23**), 52.32 (1C, **14 or 16**), 52.10 (1C, **14 or 16**), 45.62 (1C, **15 or 17**), 41.58 (1C, **15 or 17**), 40.56 (1C, **29**), 32.62 (1C, **19**), 28.35 (1C, **21**), 28.30 (1C, **20 or 22**), 25.06 (1C, **20 or 22**). Solvents: Chloroform (77.29, 77.03, 76.78). Standard: TMS (0.00).

**HRMS** (ESI-MS, pos.)  $m/z$ :  $[M+H]^+$  calculated for C<sub>27</sub>H<sub>34</sub>N<sub>5</sub>O<sub>4</sub>S: 524.2326, found: 524.2333.



**Compound 18:**



The synthesis was performed similarly to Meggers *et al.*<sup>94</sup>

The synthesis was carried out in the glove-box with oven dried glass equipment. Ligand (**39**, 6.1 mg, 11.5 μmol, 1.0 eq.) was dissolved in dry DCM (2.0 ml), yielding a yellow solution. A solution of [CpRu(MeCN)<sub>3</sub>]PF<sub>6</sub> (5.0 mg, 11.5 μmol, 1.0 eq.) in dry DCM (2.0 ml) was added dropwise over a time period of 15 min, with a simultaneous color change from yellow to orange and the formation of an orange precipitate. This residue was filtered, washed with dry DCM (3 x 1 ml) and dried to obtain a yellow-orange solid.

Annex spectra on page 189.

**Appearance:** Yellow-orange solid

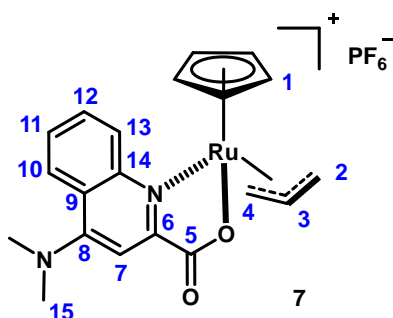
**<sup>1</sup>H NMR** (600 MHz, Acetonitrile-d<sub>3</sub> δ/ppm): Assignment of signals: see chapter 2.1.2

**<sup>19</sup>F NMR** (565 MHz, Acetonitrile-d<sub>3</sub> δ/ppm): -72.95 (d, *J* = 706.4 Hz, PF<sub>6</sub>).

**HRMS** (ESI-MS, pos.) *m/z*: [M-PF<sub>6</sub>]<sup>+</sup> calculated for C<sub>32</sub>H<sub>38</sub>N<sub>5</sub>O<sub>4</sub>Sru: 690.1690, found: 690.1697.

### 4.3.3 Non-biotinylated ruthenium complex

#### Compound 7:



The synthesis of allyl 4-(dimethylamino)quinoline-2-carboxylate (**42**) was performed as described by Meggers *et al.*<sup>94</sup> The starting material used, 4-(dimethylamino)quinoline-2-carboxylic acid (**41**), was purchased from Ukrorgsintez Ltd. The synthesis of [CpRu(QA-NMe<sub>2</sub>)(Allyl)]PF<sub>6</sub> (**7**) was performed as described by Meggers *et al.*<sup>94</sup>

Annex spectra on page 190.

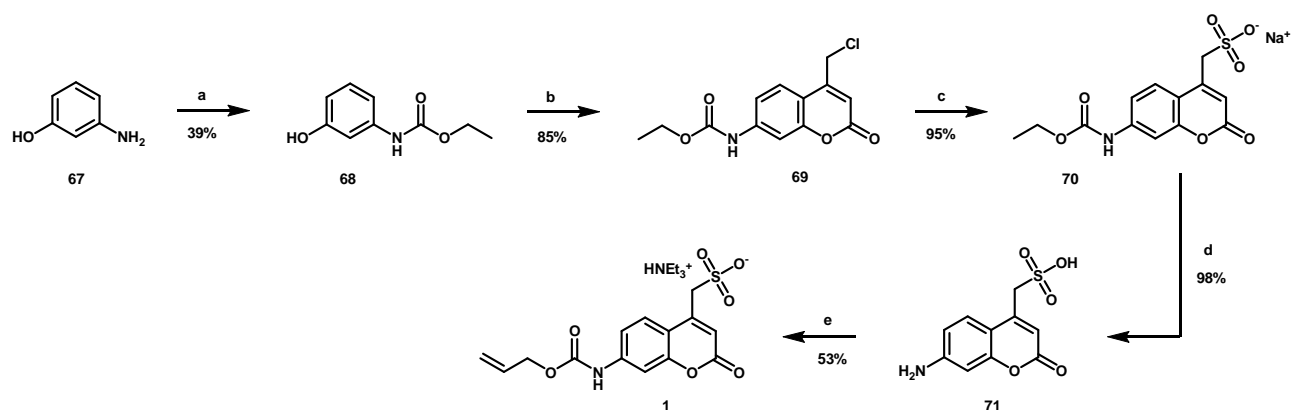
**Appearance:** Yellow solid

<sup>1</sup>H NMR (400 MHz, Acetone-d<sub>6</sub> δ/ppm): 8.38 – 8.31 (m, 1H, **10**), 8.01 – 7.89 (m, 2H, **12 + 13**), 7.72 (ddd, J = 8.3, 5.9, 2.1 Hz, 1H, **11**), 7.32 (s, 1H, **7**), 6.46 (s, 5H, **1**), 4.83 (d, J = 10.7 Hz, 1H, **2 or 4**), 4.73 (tt, J = 10.7, 6.2 Hz, 1H, **3**), 4.60 (d, J = 10.9 Hz, 1H, **2 or 4**), 4.32 (dd, J = 6.2, 2.9 Hz, 1H, **2 or 4**), 4.23 (dd, J = 6.2, 2.9 Hz, 1H, **2 or 4**), 3.41 (s, 6H, **15**). Solvents: Water (2.81), acetone (2.05). Standard: TMS (0.00).

**HRMS** (ESI-MS, pos.) m/z: [M-PF<sub>6</sub>]<sup>+</sup> calculated for C<sub>20</sub>H<sub>21</sub>N<sub>2</sub>O<sub>2</sub>Ru: 423.0646, found: 423.0651.

### 4.3.4 Caged coumarin substrate

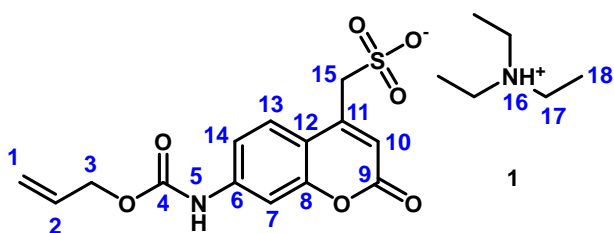
The caged coumarin substrate **1** was synthesized following literature procedures from Kanaoka *et al.*<sup>119</sup>, Griffiths and Ryckelynck *et al.*<sup>120</sup> and Meggers *et al.*<sup>94</sup> 3-Aminophenol (**67**) was treated with ethyl chloroformate to afford carbamate **68**, which was converted to coumarin **69** using a Pechmann condensation. In the next step, sulfonate **70** was formed. The ethyl carbamate group was then cleaved by treatment with a mixture of boiling sulfuric/acetic acid. Amine **71** was then converted into the *O*-allyl carbamate protected coumarin substrate **1** by treatment with allyl chloroformate in triethylammonium bicarbonate buffer. An overview of the synthesis is given in Scheme 11.



**Scheme 11: Synthesis procedure of an allyl carbamate protected coumarin substrate (1).**

Reaction conditions: a) Ethyl chloroformate (2.0 eq.), diethyl ether/THF 5:1 (dry), r.t., 2 h; b) 1.) Ethyl 4-chloroacetoacetate (1.1 eq.), aq. H<sub>2</sub>SO<sub>4</sub> (70%), 0°C to r.t., 16 h. 2.) Water, 0°C, 30 min; c) Na<sub>2</sub>SO<sub>3</sub> (5.0 eq.), acetone/water (3:2), reflux, 24 h; d) H<sub>2</sub>SO<sub>4</sub>/acetic acid 1:1, 100°C, 16 h; e) Allyl chloroformate (5.0 eq.), triethylammonium bicarbonate buffer (1 M, pH 8.5), 0°C to r.t., 3.5 h.

## Compound 1:



The synthesis of 7-aminocoumarin-4-methansulfonic acid (**71**, Scheme 11) was performed as described by Kanaoka *et al.*<sup>119</sup> and Griffiths and Ryckelynck *et al.*<sup>120</sup>

The synthesis of compound **1** was performed as described by Meggers *et al.*<sup>94</sup>

7-aminocoumarin-4-methansulfonic acid (**71**, 102 mg, 0.40 mmol, 1.0 eq.) was dispersed in triethylammonium bicarbonate buffer (1 M, pH 8.5, 4.0 ml, 4.0 mmol, 10.0 eq.). Allyl chloroformate (215  $\mu$ l, 244 mg, 1.96 mmol, 5.0 eq.) was added dropwise at 0°C. The mixture was stirred for 1.5 h at 0°C and then for 2 h at room temperature. The resulting brownish solution was acidified with glacial acetic acid (0.5 ml) to pH 4 and then filtered. The filtrate was purified by preparative reverse phase HPLC (XSELECT™ CSH™ Prep C18 5  $\mu$ m OBD™ 19 x 150 mm, water/acetonitrile containing 5 mM triethylamine and 5 mM acetic acid). The resulting fractions were finally lyophilized to obtain the product as a white solid (**1**, 46.8 mg, 0.11 mmol, 53% yield).

Annex spectra on page 191.

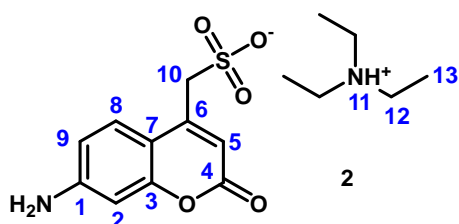
**Appearance:** White solid

**<sup>1</sup>H NMR** (400 MHz, DMSO-*d*<sub>6</sub>  $\delta$ /ppm): 10.21 (s, 1H, **5**), 7.85 (d, *J* = 8.8 Hz, 1H, **13**), 7.54 (d, *J* = 2.1 Hz, 1H, **7**), 7.33 (dd, *J* = 8.8, 2.1 Hz, 1H, **14**), 6.24 (s, 1H, **10**), 6.00 (ddt, *J* = 17.2, 10.9, 5.5 Hz, 1H, **2**), 5.39 (dq, *J* = 17.2, 1.6 Hz, 1H, **1**), 5.26 (dq, *J* = 10.5, 1.3 Hz, 1H, **1**), 4.65 (dt, *J* = 5.5, 1.4 Hz, 2H, **3**), 3.99 (s, 2H, **15**), 3.08 (q, *J* = 7.3 Hz, 6H, **17**), 1.17 (t, *J* = 7.3 Hz, 9H, **18**). Solvents: Water (3.32), DMSO (2.50). Standard: TMS (0.00).

**<sup>13</sup>C NMR** (101 MHz, DMSO-*d*<sub>6</sub>  $\delta$ /ppm): 160.25 (1C, **9**), 154.08 (1C, **8**), 153.01 (1C, **4**), 149.99 (1C, **11**), 142.30 (1C, **6**), 132.97 (1C, **2**), 127.74 (1C, **13**), 117.94 (1C, **1**), 113.96 (1C, **10 or 12 or 14**), 113.91 (1C, **10 or 12 or 14**), 113.78 (1C, **10 or 12 or 14**), 104.19 (1C, **7**), 65.09 (1C, **3**), 53.14 (1C, **15**), 45.71 (3C, **17**), 8.62 (3C, **18**). Solvents: DMSO (40.15, 39.94, 39.73, 39.52, 39.31, 39.10, 38.89).

**HRMS** (ESI-MS, neg.) *m/z*: [M-HNEt<sub>3</sub>]<sup>-</sup> calculated for C<sub>14</sub>H<sub>12</sub>NO<sub>7</sub>S: 338.0340, found: 338.0342.

## Compound 2:



The synthesis of compound **2** was performed as described by Meggers *et al.*<sup>94</sup>

7-aminocoumarin-4-methansulfonic acid (**71**, 100 mg, 0.40 mmol, 1.0 eq.) was dispersed in triethylammonium bicarbonate buffer (1 M, pH 8.5, 4.0 ml, 4.0 mmol, 10.0 eq.). The resulting yellowish solution was acidified with glacial acetic acid (0.5 ml) to pH 4 and then filtered. The filtrate was purified by preparative reverse phase HPLC (XSELECT™ CSH™ Prep C18 5 μm OBD™ 19 x 150 mm, water/acetonitrile containing 5 mM triethylamine and 5 mM acetic acid). The obtained fractions were then lyophilized to obtain the product as a light yellow solid (**2**, 39.0 mg, 0.11 mmol, 28% yield).

Annex spectra on page 192.

**Appearance:** Light yellow solid

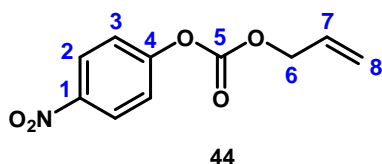
<sup>1</sup>H NMR (500 MHz, DMSO-*d*<sub>6</sub> δ/ppm): 8.86 (s, 1H, **11**), 7.55 (d, *J* = 8.7 Hz, 1H, **8**), 6.51 (dd, *J* = 8.7, 2.2 Hz, 1H, **9**), 6.38 (d, *J* = 2.2 Hz, 1H, **2**), 6.04 (s, 2H, NH<sub>2</sub>), 5.92 (s, 1H, **5**), 3.86 (s, 2H, **10**), 3.08 (q, *J* = 7.2 Hz, 6H, **12**), 1.17 (t, *J* = 7.3 Hz, 9H, **13**). Solvents: Water (3.32), DMSO (2.50).

<sup>13</sup>C NMR (126 MHz, DMSO-*d*<sub>6</sub> δ/ppm): 160.95 (1C, **4**), 155.75 (1C, **1** or **3**), 152.66 (1C, **1** or **3**), 150.51 (1C, **6**), 127.88 (1C, **8**), 110.84 (1C, **9**), 109.24 (1C, **5**), 108.60 (1C, **7**), 98.26 (1C, **2**), 53.32 (1C, **10**), 45.75 (1C, **12**), 8.66 (1C, **13**). Solvents: DMSO (40.02, 39.85, 39.69, 39.52, 39.35, 39.19, 39.02).

**HRMS** (ESI-MS, neg.) *m/z*: [M]<sup>-</sup> calculated for C<sub>10</sub>H<sub>8</sub>NO<sub>5</sub>S: 254.0129, found: 254.0132.

### 4.3.5 Caged IPTG substrates

#### Compound 44:



The synthesis was performed as described by Craig *et al.*<sup>240</sup>

Under an N<sub>2</sub> atmosphere, *p*-nitrophenyl chloroformate (**43**, 2.00 g, 9.92 mmol, 1.1 eq.) was dissolved in dry DCM (10 ml) and the solution was cooled to -10°C. Allyl alcohol (0.62 ml, 0.53 g, 9.02 mmol, 1.0 eq.) was slowly added, followed by the dropwise addition of triethylamine (5.0 ml, 3.63 g, 36.08 mmol, 4.0 eq.). The resulting yellow mixture was stirred for 30 min at -10°C and then allowed to warm up to room temperature with further stirring for 16 h. The residue was mixed with ethyl acetate (40 ml) and washed with sat. aq. NH<sub>4</sub>Cl (4 x 40 ml) and water (40 ml). The organic phase was dried over Na<sub>2</sub>SO<sub>4</sub>, the solvent was evaporated and the residue purified by flash column chromatography (SiO<sub>2</sub>, cyclohexane/ethyl acetate 9:1). The fractions were concentrated and dried under reduced pressure to yield the product as a white crystalline solid (**44**, 938 mg, 4.20 mmol, 47% yield).

Annex spectra on page 193.

**Appearance:** White crystalline solid

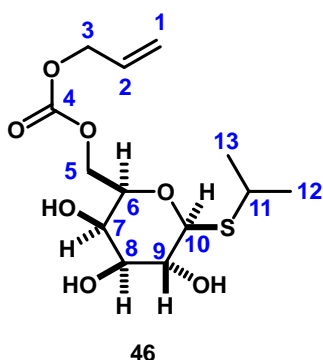
**TLC:** Ethyl acetate/cyclohexane 1:9; *R<sub>f</sub>* = 0.40

**<sup>1</sup>H NMR** (400 MHz, Chloroform-*d* δ/ppm): 8.32 – 8.25 (m, 2H, **2**), 7.43 – 7.36 (m, 2H, **3**), 6.01 (ddt, *J* = 17.2, 10.4, 5.9 Hz, 1H, **7**), 5.46 (dq, *J* = 17.2, 1.4 Hz, 1H, **8**), 5.37 (dq, *J* = 10.4, 1.1 Hz, 1H, **8**), 4.78 (dt, *J* = 5.9, 1.3 Hz, 2H, **6**). Solvents: Chloroform (7.26), water (1.55). Standard: TMS (0.00).

**<sup>13</sup>C NMR** (101 MHz, Chloroform-*d* δ/ppm): 155.52 (1C, **4**), 152.30 (1C, **5**), 145.42 (1C, **1**), 130.58 (1C, **7**), 125.31 (2C, **2**), 121.78 (2C, **3**), 120.19 (1C, **8**), 69.76 (1C, **6**). Solvents: Chloroform (77.33, 77.02, 76.70). Standard: TMS (0.00).

**HRMS** (ESI-MS, pos.) *m/z*: [M+Na]<sup>+</sup> calculated for C<sub>10</sub>H<sub>9</sub>NO<sub>5</sub>Na: 246.0373, found: 246.0374.

**Compound 46:**



The synthesis was performed similarly to Ito and Abe *et al.*<sup>112</sup>

Isopropyl  $\beta$ -D-1-thiogalactopyranoside (**45**, 210 mg, 0.90 mmol, 1.0 eq), 4-dimethylaminopyridine (110 mg, 0.90 mmol, 1.0 eq) and *para*-nitrophenyl allyl carbonate (**44**, 200 mg, 0.90 mmol, 1.0 eq.) were dissolved in pyridine (10 ml). The yellow solution was stirred at room temperature for 18 h. The solvent was evaporated and the residue purified by flash column chromatography (SiO<sub>2</sub>, DCM/MeOH 50:1  $\rightarrow$  25:1). The fractions were concentrated and dried under reduced pressure to yield the product as a white solid (**46**, 34.2 mg, 0.11 mmol, 12% yield).

Annex spectra on page 194.

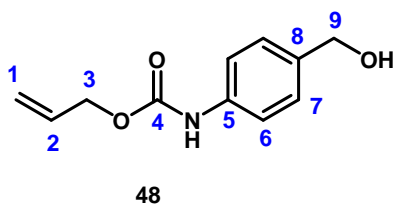
**Appearance:** White solid

**TLC:** DCM/MeOH 50:1;  $R_f$  = 0.20

**<sup>1</sup>H NMR** (400 MHz, Chloroform-*d*  $\delta$ /ppm): 5.93 (ddt,  $J$  = 17.2, 10.4, 5.8 Hz, 1H, **2**), 5.36 (dq,  $J$  = 17.2, 1.5 Hz, 1H, **1**), 5.28 (dq,  $J$  = 10.4, 1.2 Hz, 1H, **1**), 4.63 (dt,  $J$  = 5.8, 1.4 Hz, 2H, **3**), 4.43 – 4.40 (m, 1H, **5**), 4.40 – 4.37 (m, 1H, **10**), 4.37 – 4.32 (m, 1H, **5**), 4.00 (s (broad), 1H, **7**), 3.76 (ddd,  $J$  = 6.9, 5.7, 1.2 Hz, 1H, **6**), 3.69 – 3.60 (m, 2H, **8 + 9**), 3.30 (s (broad), 1H, **OH**), 3.21 (p,  $J$  = 6.8 Hz, 1H, **11**), 2.95 (s (broad), 1H, **OH**), 2.89 (s (broad), 1H, **OH**), 1.34 (d,  $J$  = 6.1 Hz, 3H, **12 or 13**), 1.33 (d,  $J$  = 5.8 Hz, 3H, **12 or 13**). Solvents: Chloroform (7.26), water (1.71). Standard: TMS (0.00).

**<sup>13</sup>C NMR** (101 MHz, Chloroform-*d*  $\delta$ /ppm): 154.97 (1C, **4**), 131.32 (1C, **2**), 119.17 (1C, **1**), 85.91 (1C, **10**), 75.85 (1C, **6**), 74.39 (1C, **8 or 9**), 70.40 (1C, **8 or 9**), 68.78 (1C, **3**), 68.48 (1C, **7**), 66.31 (1C, **5**), 35.91 (1C, **11**), 24.20 (1C, **12 or 13**), 23.98 (1C, **12 or 13**). Solvents: Chloroform (77.33, 77.02, 76.70). Standard: TMS (0.00).

**HRMS** (ESI-MS, pos.)  $m/z$ : [M+Na]<sup>+</sup> calculated for C<sub>13</sub>H<sub>22</sub>O<sub>7</sub>SNa: 345.0978, found: 345.0985.

**Compound 48:**

4-Aminobenzyl alcohol (**47**, 2.00 g, 16.24 mmol, 1.0 eq.) was dissolved in a mixture of pyridine (20 ml) and DCM (30 ml). Allyl chloroformate (1.90 ml, 2.15 g, 17.82 mmol, 1.1 eq.) in DCM (8 ml) was added dropwise and the resulting orange mixture was stirred for 3 h at room temperature. The mixture was diluted with DCM (100 ml) and washed with water (3 x 100 ml). The organic phase was dried over Na<sub>2</sub>SO<sub>4</sub> and the solvent was evaporated. The residue was purified by flash column chromatography (SiO<sub>2</sub>, cyclohexane/ethyl acetate 2:1). The fractions were concentrated and dried under reduced pressure to yield the product as a light yellow crystalline solid (**48**, 1.97 g, 9.51 mmol, 59% yield).

Annex spectra on page 195.

**Appearance:** Light yellow crystalline solid

**TLC:** Ethyl acetate/cyclohexane 1:2; *R<sub>f</sub>* = 0.30

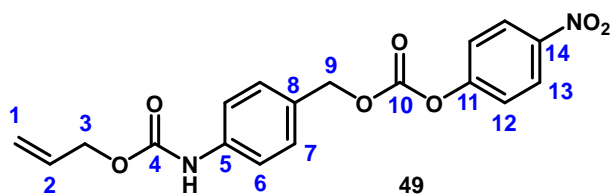
**<sup>1</sup>H NMR** (500 MHz, Chloroform-*d* δ/ppm): 7.35 (d, *J* = 8.2 Hz, 2H, **6**), 7.30 – 7.26 (m, 2H, **7**), 6.84 (s (broad), 1H, **NH**), 5.96 (ddt, *J* = 17.2, 10.4, 5.7 Hz, 1H, **2**), 5.36 (dq, *J* = 17.2, 1.5 Hz, 1H, **1**), 5.26 (dq, *J* = 10.4, 1.3 Hz, 1H, **1**), 4.66 (dt, *J* = 5.7, 1.4 Hz, 2H, **3**), 4.61 (s, 2H, **9**), 2.00 (s (broad), 1H, **OH**). Solvents: Chloroform (7.26). Standard: TMS (0.00).

**<sup>13</sup>C NMR** (126 MHz, Chloroform-*d* δ/ppm): 153.32 (1C, **4**), 137.25 (1C, **5**), 136.04 (1C, **8**), 132.39 (1C, **2**), 127.93 (2C, **7**), 118.85 (2C, **6**), 118.29 (1C, **1**), 65.89 (1C, **3**), 64.86 (1C, **9**). Solvents: Chloroform (77.29, 77.04, 76.79). Standard: TMS (0.00).

**HRMS** (ESI-MS, pos.) *m/z*: [M+Na]<sup>+</sup> calculated for C<sub>11</sub>H<sub>13</sub>NO<sub>3</sub>Na: 230.0788, found: 230.0787.



### Compound 49:



The synthesis was performed similarly to Hay *et al.*<sup>241</sup>

The benzyl alcohol derivative **48** (1.50 g, 7.24 mmol, 1.0 eq.) was dissolved in THF (80 ml) followed by the dropwise addition of *N,N*-diisopropylethylamine (1.60 ml, 1.22 g, 9.41 mmol, 1.3 eq.). A solution of 4-nitrophenyl chloroformate (2.19 g, 10.86 mmol, 1.5 eq.) in THF (20 ml) was then slowly added and the resulting yellow mixture was stirred at room temperature for 16 h. The solvent was evaporated and the residue was taken up in ethyl acetate (100 ml). The organic fraction was washed with water (2 x 50 ml) and brine (50 ml), dried over Na<sub>2</sub>SO<sub>4</sub> and evaporated to dryness. The residue was purified by flash column chromatography (SiO<sub>2</sub>, DCM/cyclohexane 3:1 → pure DCM). The fractions were concentrated and dried under reduced pressure to yield the crude product as a light yellow crystalline solid (**49**, 586 mg, 22% yield). NMR analysis stated the presence of *para*-nitrophenol as an impurity. However, the isolated sample was used for the next synthesis step without further purification.

Annex spectra on page 196.

**Appearance:** Light yellow crystalline solid

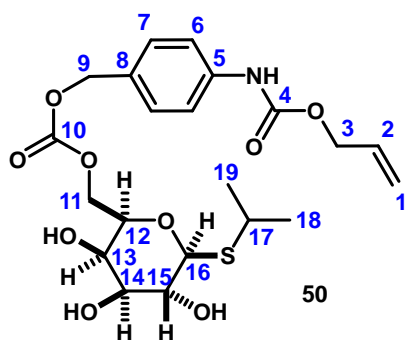
**TLC:** DCM/cyclohexane 3:1; *R<sub>f</sub>* = 0.20

<sup>1</sup>H NMR (500 MHz, Chloroform-*d* δ/ppm): 8.29 – 8.24 (m, 2H, **13**), 7.46 – 7.41 (m, 2H, **6**), 7.41 – 7.38 (m, 2H, **7**), 7.38 – 7.35 (m, 2H, **12**), 6.78 (s (broad), 1H, **NH**), 5.97 (ddt, *J* = 17.2, 10.4, 5.7 Hz, 1H, **2**), 5.37 (dq, *J* = 17.2, 1.5 Hz, 1H, **1**), 5.28 (dq, *J* = 10.4, 1.3 Hz, 1H, **1**), 5.25 (s, 2H, **9**), 4.68 (dt, *J* = 5.7, 1.4 Hz, 2H, **3**). Impurity: *Para*-nitrophenol (8.17 – 8.12 (m, 2H, H<sub>Ar</sub>yl), 6.92 – 6.87 (m, 2H, H<sub>Ar</sub>yl), 6.68 (s (broad), 1H, OH)). Solvents: Chloroform (7.26), Water (1.73). Standard: TMS (0.00).

<sup>13</sup>C NMR (126 MHz, Chloroform-*d* δ/ppm): 155.52 (1C, **11**), 153.23 (1C, **4**), 152.46 (1C, **10**), 145.38 (1C, **14**), 138.55 (1C, **5**), 132.16 (1C, **2**), 129.95 (2C, **7**), 129.21 (1C, **8**), 125.30 (2C, **13**), 121.79 (2C, **12**), 118.83 (2C, **6**), 118.52 (1C, **1**), 70.67 (1C, **9**), 66.10 (1C, **3**). Impurity: *Para*-nitrophenol (161.64 (1C), 141.48 (1C, extrapolated from HMBC spectrum), 126.19 (2C), 115.63 (2C)). Solvents: Chloroform (77.28, 77.03, 76.78). Standard: TMS (0.00).

**HRMS** (ESI-MS, pos.) *m/z*: [M+Na]<sup>+</sup> calculated for C<sub>18</sub>H<sub>16</sub>N<sub>2</sub>O<sub>7</sub>Na: 395.0850, found: 395.0852.

## Compound 50:



The synthesis was performed similarly to Ito and Abe *et al.*<sup>112</sup>

Isopropyl  $\beta$ -D-1-thiogalactopyranoside (**45**, 320 mg, 1.34 mmol, 1.0 eq.), 4-dimethylaminopyridine (166 mg, 1.34 mmol, 1.0 eq.) and *para*-nitrophenyl carbonate **49** (500 mg, 1.34 mmol, 1.0 eq.) were dissolved in pyridine (10 ml). The resulting yellow solution was stirred at room temperature for 16 h. The solvent was evaporated and the residue was purified by flash column chromatography (SiO<sub>2</sub>, DCM/MeOH 20:1  $\rightarrow$  15:1). The fractions were concentrated and dried under reduced pressure to yield the product as a white solid (**50**, 118 mg, 0.17 mmol, 19% yield).

Annex spectra on page 197.

**Appearance:** White solid

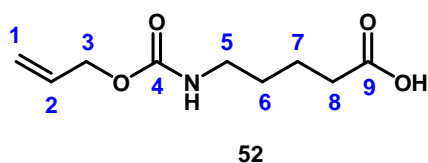
**TLC:** DCM/MeOH 15:1;  $R_f$  = 0.35

**<sup>1</sup>H NMR** (400 MHz, Methanol-*d*<sub>4</sub>  $\delta$ /ppm): 7.45 (d,  $J$  = 8.6 Hz, 2H, **6**), 7.31 (d,  $J$  = 8.6 Hz, 2H, **7**), 6.00 (ddt,  $J$  = 17.2, 10.8, 5.5 Hz, 1H, **2**), 5.36 (dq,  $J$  = 17.2, 1.6 Hz, 1H, **1**), 5.23 (dq,  $J$  = 10.5, 1.4 Hz, 1H, **1**), 5.09 (s, 2H, **9**), 4.63 (dt,  $J$  = 5.4, 1.5 Hz, 2H, **3**), 4.42 – 4.38 (m, 1H, **16**), 4.38 – 4.33 (m, 1H, **11**), 4.22 (dd,  $J$  = 11.3, 4.3 Hz, 1H, **11**), 3.84 (dd,  $J$  = 3.0, 1.1 Hz, 1H, **13**), 3.78 – 3.73 (m, 1H, **12**), 3.58 – 3.49 (m, 1H, **14 or 15**), 3.47 (d,  $J$  = 3.2 Hz, 1H, **14 or 15**), 3.14 (p,  $J$  = 6.7 Hz, 1H, **17**), 1.28 (d,  $J$  = 1.5 Hz, 3H, **18 or 19**), 1.26 (d,  $J$  = 1.6 Hz, 3H, **18 or 19**). Solvents: Water (4.86), methanol (3.31). Alcohol groups of the sugar frame are most likely due to proton-deuterium exchange with the solvent methanol-*d*<sub>4</sub> not visible in the <sup>1</sup>H spectrum.

**<sup>13</sup>C NMR** (101 MHz, Methanol-*d*<sub>4</sub>  $\delta$ /ppm): 156.55 (1C, **10**), 155.56 (1C, **4**), 140.62 (1C, **5**), 134.20 (1C, **2**), 131.37 (1C, **8**), 130.32 (1C, **7**), 119.63 (1C, **6**), 117.87 (1C, **1**), 87.05 (1C, **16**), 77.51 (1C, **12**), 75.97 (1C, **14 or 15**), 71.43 (1C, **14 or 15**), 70.42 (1C, **9 or 13**), 70.39 (1C, **9 or 13**), 68.45 (1C, **11**), 66.45 (1C, **3**), 36.20 (1C, **17**), 24.55 (1C, **18 or 19**), 24.20 (1C, **18 or 19**). Solvents: Methanol (49.64, 49.43, 49.21, 49.00, 48.79, 48.57, 48.36).

**HRMS** (ESI-MS, pos.)  $m/z$ : [M+Na]<sup>+</sup> calculated for C<sub>21</sub>H<sub>29</sub>NO<sub>9</sub>SNa: 494.1455, found: 494.1464.

## Compound 52:



The synthesis was performed similarly to Taylor *et al.*<sup>242</sup>

5-aminovaleric acid (**51**, 2.00 g, 17.07 mmol, 1.0 eq.) and NaOH (2.46 g, 61.46 mmol, 3.6 eq.) were dissolved in water (150 ml) and cooled to 0°C. Allyl chloroformate (2.72 ml, 3.09 g, 25.61 mmol, 1.5 eq.) was slowly added and the resulting mixture was stirred at 0°C for 5 h. The mixture was washed with diethyl ether (100 ml). The aqueous phase was acidified with HCl (1M, 20 ml) to pH 2 and extracted with ethyl acetate (3 x 80 ml). The organic phase was dried over Na<sub>2</sub>SO<sub>4</sub> and evaporated under reduced pressure to obtain the product as a white solid (**52**, 2.63 g, 13.08 mmol, 77% yield).

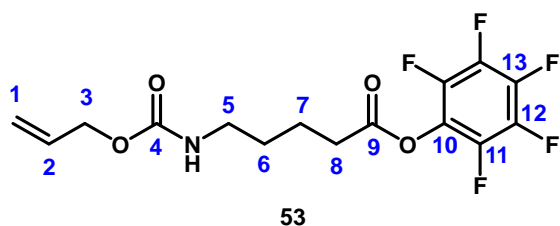
Annex spectra on page 198.

**Appearance:** White solid

**<sup>1</sup>H NMR** (500 MHz, Chloroform-*d* δ/ppm): 5.91 (ddt, *J* = 16.4, 10.9, 5.6 Hz, 1H, **2**), 5.30 (d, *J* = 17.3 Hz, 1H, **1**), 5.21 (d, *J* = 10.4 Hz, 1H, **1**), 4.88 (s (broad), 1H, **NH**), 4.56 (d, *J* = 5.6 Hz, 2H, **3**), 3.26 – 3.14 (m, 2H, **5**), 2.38 (t, *J* = 7.2 Hz, 2H, **8**), 1.73 – 1.63 (m, 2H, **7**), 1.62 – 1.51 (m, 2H, **6**). Solvents: Chloroform (7.27). Standard: TMS (0.00).

**<sup>13</sup>C NMR** (126 MHz, Chloroform-*d* δ/ppm): 178.85 (1C, **9**), 156.39 (1C, **4**), 132.89 (1C, **2**), 117.70 (1C, **1**), 65.56 (1C, **3**), 40.56 (1C, **5**), 33.49 (1C, **8**), 29.33 (1C, **6**), 21.75 (1C, **7**). Solvents: Chloroform (77.30, 77.04, 76.79). Standard: TMS (0.00).

**HRMS** (ESI-MS, pos.) *m/z*: [M+Na]<sup>+</sup> calculated for C<sub>9</sub>H<sub>15</sub>NO<sub>4</sub>Na: 224.0893, found: 224.0892.

**Compound 53:**

The synthesis was performed similarly to Thompson *et al.*<sup>236</sup>

Acid **52** (1.00 g, 4.97 mmol, 1.0 eq.) was dissolved in DMF (20 ml) and cooled to 0°C. Triethylamine (1.24 ml, 0.90 g, 8.95 mmol, 1.8 eq.) was added dropwise, followed by the addition of pentafluorophenyl trifluoroacetate (1.28 ml, 2.09 g, 7.45 mmol, 1.5 eq.). The resulting pink solution was allowed to warm up to room temperature, followed by further stirring for 3 h. The solvent was evaporated and the residue was purified by flash column chromatography (SiO<sub>2</sub>, cyclohexane/ethyl acetate 5:1). The fractions were concentrated and dried under reduced pressure to yield the product as a light yellow solid (**53**, 1.67 g, 92% yield). Due to instability of the activated pentafluorophenyl ester, a small fraction of pentafluorophenol was detected in the obtained product. However, the sample was used for the next synthesis step without further purification.

Annex spectra on page 199.

**Appearance:** Light yellow solid

**TLC:** Ethyl acetate/cyclohexane 1:5; *R<sub>f</sub>* = 0.30

**<sup>1</sup>H NMR** (400 MHz, Chloroform-*d* δ/ppm): 5.92 (ddt, *J* = 16.4, 10.9, 5.7 Hz, 1H, **2**), 5.30 (dq, *J* = 17.2, 1.6 Hz, 1H, **1**), 5.21 (dq, *J* = 10.4, 1.4 Hz, 1H, **1**), 4.80 (s (broad), 1H, **NH**), 4.56 (d, *J* = 5.7 Hz, 2H, **3**), 3.25 (q, *J* = 6.7 Hz, 2H, **5**), 2.71 (t, *J* = 7.3 Hz, 2H, **8**), 1.86 – 1.76 (m, 2H, **7**), 1.69 – 1.59 (m, 2H, **6**). Solvents: Chloroform (7.26). Standard: TMS (0.00).

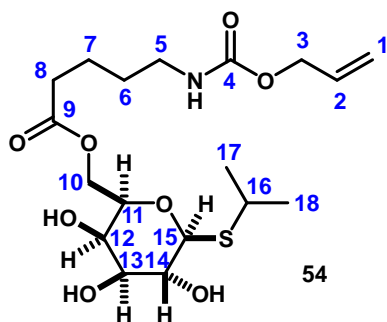
**<sup>13</sup>C NMR** (126 MHz, Chloroform-*d* δ/ppm): 169.25 (1C, **9**), 156.42 (1C, **4**), 132.84 (1C, **2**), 117.75 (1C, **1**), 65.63 (1C, **3**), 40.41 (1C, **5**), 32.84 (1C, **8**), 29.22 (1C, **6**), 21.82 (1C, **7**). Solvents: Chloroform (77.30, 77.04, 76.79). Standard: TMS (0.00). The signals for the quaternary carbons **10** – **13** could not be resolved.

**<sup>19</sup>F NMR** (376 MHz, Chloroform-*d* δ/ppm): -152.84 (d, *J* = 17.8 Hz, 2F, **11**), -158.00 (t, *J* = 21.6 Hz, 1F, **13**), -162.32 (dd, *J* = 22.6, 18.0 Hz, 2F, **12**). Byproduct: Pentafluorophenol (-163.15 (dd, *J* = 17.5, 5.7 Hz), -164.00 – -164.37 (m), -169.15 (tt, *J* = 22.0, 5.8 Hz)).

NMR spectra are in good accordance with the results from Withers *et al.*<sup>243</sup>

**HRMS** (ESI-MS, pos.) *m/z*: [M+Na]<sup>+</sup> calculated for C<sub>15</sub>H<sub>14</sub>NO<sub>4</sub>F<sub>5</sub>Na: 390.0735, found: 390.0739.

### Compound 54:



The synthesis was performed similarly to Ito and Abe *et al.*<sup>112</sup>

Isopropyl β-D-1-thiogalactopyranoside (**45**, 0.65 g, 2.72 mmol, 1.0 eq.), 4-dimethylaminopyridine (0.33 g, 2.72 mmol, 1.0 eq.) and activated pentafluorophenyl ester **53** (1.00 g, 2.72 mmol, 1.0 eq.) were dissolved in pyridine (10 ml). The resulting light-yellow solution was stirred at room temperature for 16 h. The solvent was evaporated and the residue was purified by flash column chromatography (SiO<sub>2</sub>, DCM/MeOH 20:1 → 15:1). The fractions were concentrated and dried under reduced pressure to yield the product as an off-white solid (**54**, 451 mg, 1.07 mmol, 39% yield).

Annex spectra on page 200.

**Appearance:** Off-white solid

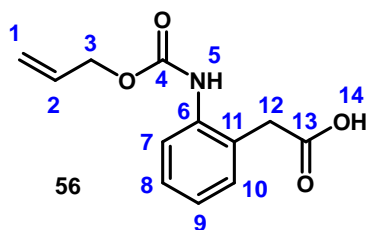
**TLC:** DCM/MeOH 10:1; *R<sub>f</sub>* = 0.55

**<sup>1</sup>H NMR** (400 MHz, Chloroform-*d* δ/ppm): 5.91 (ddt, *J* = 16.4, 10.9, 5.6 Hz, 1H, **2**), 5.30 (dd, *J* = 17.2, 1.5 Hz, 1H, **1**), 5.21 (dd, *J* = 10.4, 1.4 Hz, 1H, **1**), 4.96 (s, 1H, **NH**), 4.55 (d, *J* = 5.7 Hz, 2H, **3**), 4.40 (d, *J* = 9.1 Hz, 1H, **15**), 4.37 – 4.26 (m, 2H, **10**), 3.96 (dd, *J* = 3.0, 1.2 Hz, 1H, **12**), 3.75 – 3.70 (m, 1H, **11**), 3.70 – 3.65 (m, 1H, **14**), 3.65 – 3.63 (m, 1H, **13**), 3.63 – 3.60 (m, 1H, **OH**), 3.27 – 3.21 (m, 1H, **OH**), 3.21 – 3.19 (m, 1H, **16**), 3.19 – 3.11 (m, 2H, **5**), 2.36 (t, *J* = 7.2 Hz, 2H, **8**), 1.74 – 1.60 (m, 2H, **7**), 1.60 – 1.48 (m, 2H, **6**), 1.35 (d, *J* = 6.6 Hz, 3H, **17 or 18**), 1.32 (d, *J* = 6.5 Hz, 3H, **17 or 18**). Solvents: Pyridine (8.60, 7.77, 7.37), chloroform (7.27), methanol (3.49). Standard: TMS (0.00).

**<sup>13</sup>C NMR** (126 MHz, Chloroform-*d* δ/ppm): 173.37 (1C, **9**), 156.44 (1C, **4**), 132.88 (1C, **2**), 117.71 (1C, **1**), 85.88 (1C, **15**), 75.93 (1C, **11**), 74.55 (1C, **13**), 70.37 (1C, **14**), 68.63 (1C, **12**), 65.57 (1C, **3**), 62.99 (1C, **10**), 40.54 (1C, **5**), 35.85 (1C, **16**), 33.59 (1C, **8**), 29.34 (1C, **6**), 24.20 (1C, **17 or 18**), 23.91 (1C, **17 or 18**), 21.89 (1C, **7**). Solvents: Pyridine (148.82, 137.01, 124.18), Chloroform (77.29, 77.03, 76.78), methanol (50.83). Standard: TMS (0.00).

**HRMS** (ESI-MS, pos.) *m/z*: [M+Na]<sup>+</sup> calculated for C<sub>18</sub>H<sub>31</sub>NO<sub>8</sub>SNa: 444.1663, found: 444.1666.

## Compound 56:



The synthesis was performed similarly to Taylor *et al.*<sup>242</sup>

2-aminophenylacetic acid (**55**, 2.50 g, 16.54 mmol, 1.0 eq.) and NaOH (2.38 g, 59.54 mmol, 3.6 eq.) were dissolved in water (150 ml) and cooled to 0°C in an ice bath. Allyl chloroformate (2.64 ml, 2.99 g, 24.81 mmol, 1.5 eq.) was slowly added and the resulting yellow solution was stirred for 2.5 h at 0°C and then for 1.5 h. at room temperature. The reaction mixture was washed with diethyl ether (2 x 50 ml). The aqueous phase was acidified with HCl (1 M, 20 ml) to pH 2 and extracted with ethyl acetate (3 x 80 ml). The organic phase was dried over Na<sub>2</sub>SO<sub>4</sub> and the solvent was evaporated to obtain the crude product as an orange-brown solid (**56**, 2.19 g, 9.30 mmol, 56% yield). This crude product was used for the next synthesis step without further purification.

Annex spectra on page 179.

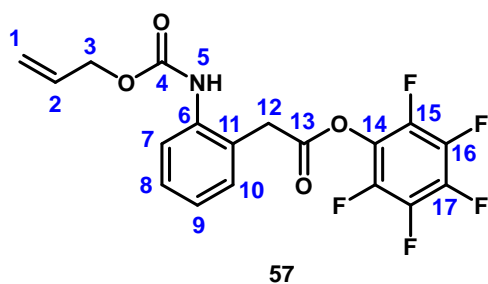
**Appearance:** Orange-brown solid

<sup>1</sup>H NMR (400 MHz, Chloroform-*d* δ/ppm): 10.49 (s (broad), 1H, **14**), 7.63 (s (broad), 2H, **5 + 7**), 7.29 (td (broad), *J* = 7.7, 1.6 Hz, 1H, **8**), 7.21 (dd (broad), *J* = 7.7, 1.7 Hz, 1H, **10**), 7.12 (t (broad), *J* = 7.4 Hz, 1H, **9**), 6.10 – 5.80 (m, 1H, **2**), 5.32 (d (broad), *J* = 17.5 Hz, 1H, **1**), 5.23 (d (broad), *J* = 10.7 Hz, 1H, **1**), 4.66 (dt, *J* = 5.7, 1.4 Hz, 2H, **3**), 3.65 (s, 2H, **12**). Solvents: Chloroform (7.26), ethyl acetate (4.13, 2.04, 1.26). Standard: TMS (0.00).

<sup>13</sup>C NMR (101 MHz, Chloroform-*d* δ/ppm): 176.63 (1C, **13**), 136.23 (1C, **6**), 132.31 (1C, **2**), 130.83 (1C, **10**), 128.54 (1C, **8**), 125.50 (1C, **9**, extrapolated from HMQC spectrum), 124.39 (1C, **7**, extrapolated from HMQC spectrum), 118.29 (1C, **1**), 66.27 (1C, **3**), 38.05 (1C, **12**). Solvents: Ethyl acetate (171.40, 60.50, 21.05, 14.18), chloroform (77.35, 77.03, 76.71). Standard: TMS (0.00). The signals for the quaternary carbons **4** and **11** could not be resolved.

**HRMS** (ESI-MS, pos.) *m/z*: [M+H]<sup>+</sup> calculated for C<sub>12</sub>H<sub>14</sub>NO<sub>4</sub>: 236.0917, found: 236.0915.

### Compound 57:



The synthesis was performed similarly to Thompson *et al.*<sup>236</sup>

To a solution of acid **56** (2.00 g, 8.50 mmol, 1.0 eq.) in DCM (50 ml), triethylamine (2.13 ml, 1.55 g, 15.30 mmol, 1.8 eq.) was slowly added at 0°C, accompanied by the appearance of a red color. Pentafluorophenyl trifluoroacetate (1.24 ml, 2.02 g, 7.23 mmol, 0.85 eq.) was slowly added. The dark yellow solution was allowed to warm up to room temperature, followed by further stirring for 4 h. DCM was removed under reduced pressure and the residue was purified by flash column chromatography (SiO<sub>2</sub>, ethyl acetate/cyclohexane 1:5 → 1:4). The fractions were concentrated and dried under reduced pressure to yield the product as a white crystalline solid (**57**, 1.25 g, 3.12 mmol, 43% yield).

Annex spectra on page 202.

**Appearance:** White crystalline solid

**TLC:** Ethyl acetate/cyclohexane 1:5; *R<sub>f</sub>* = 0.35

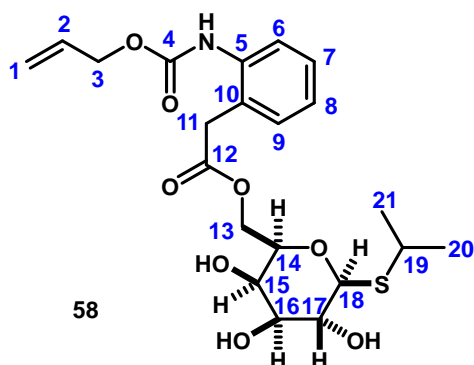
**<sup>1</sup>H NMR** (400 MHz, Chloroform-*d* δ/ppm): 7.88 (d, *J* = 8.2 Hz, 1H, **7**), 7.37 – 7.27 (m, 1H, **8**), 7.30 – 7.23 (m, 1H, **10**), 7.17 (td, *J* = 7.5, 1.1 Hz, 1H, **9**), 6.05 (ddt, *J* = 17.2, 10.5, 5.6 Hz, 1H, **2**), 5.52 (dq, *J* = 17.1, 1.5 Hz, 1H, **1**), 5.35 (dq, *J* = 10.5, 1.3 Hz, 1H, **1**), 4.90 (dt, *J* = 5.6, 1.4 Hz, 2H, **3**), 3.70 (s, 2H, **12**). Solvents: Chloroform (7.26). Standard: TMS (0.00).

**<sup>13</sup>C NMR** (101 MHz, Chloroform-*d* δ/ppm): 172.83 (1C, **13**), 150.66 (1C, **4**), 140.57 (1C, **6**), 131.03 (1C, **2**), 128.25 (1C, **8**), 124.61 (1C, **9**), 124.24 (1C, **10**), 123.25 (1C, **11**), 119.45 (1C, **1**), 115.26 (1C, **7**), 67.58 (1C, **3**), 36.50 (1C, **12**). Solvents: Chloroform (77.36, 77.04, 76.72). Standard: TMS (0.00). The signals for the quaternary carbons **14** – **17** could not be resolved.

**<sup>19</sup>F NMR** (376 MHz, Chloroform-*d* δ/ppm): -163.00 (dd, *J* = 17.4, 5.7 Hz, 2F, **15 or 16**), -164.04 – -164.21 (m, 2F, **15 or 16**), -169.06 (tt, *J* = 22.1, 5.7 Hz, 1F, **17**).

**HRMS** (ESI-MS, pos.) *m/z*: [M-OC<sub>6</sub>F<sub>5</sub>+OCH<sub>3</sub>+H]<sup>+</sup> calculated for C<sub>13</sub>H<sub>16</sub>NO<sub>4</sub>: 250.1074, found: 250.1073.

Trans-esterification of the activated pentafluorophenyl ester to the corresponding methyl ester has most likely taken place in methanol as ESI solvent.

**Compound 58:**

The synthesis was performed similarly to Ito and Abe *et al.*<sup>112</sup>

Isopropyl β-D-1-thiogalactopyranoside (**45**, 0.60 g, 2.49 mmol, 1.0 eq.), 4-dimethylaminopyridine (0.31 g, 2.49 mmol, 1.0 eq.) and activated pentafluorophenyl ester **57** (1.00 g, 2.49 mmol, 1.0 eq.) were dissolved in pyridine (10 ml). The resulting yellow solution was stirred at room temperature for 18 h. The solvent was evaporated and the residue was purified by flash column chromatography (SiO<sub>2</sub>, DCM/MeOH 30:1 → 20:1). The fractions were concentrated and dried under reduced pressure to yield the crude product as a brown solid. This solid was washed with cyclohexane (5 x 5 ml) to yield the product as an off-white solid (**58**, 236 mg, 0.52 mmol, 21% yield).

Annex spectra on page 203.

**Appearance:** Off-white solid

**TLC:** DCM/MeOH 25:1; *R<sub>f</sub>* = 0.20

**<sup>1</sup>H NMR** (400 MHz, Chloroform-*d* δ/ppm): 7.70 (s (broad), 2H, **NH + 6**), 7.30 (td, *J* = 7.8, 1.7 Hz, 1H, **7**), 7.18 (dd, *J* = 7.6, 1.6 Hz, 1H, **9**), 7.10 (td, *J* = 7.4, 1.3 Hz, 1H, **8**), 5.98 (ddt, *J* = 17.4, 10.4, 5.8 Hz, 1H, **2**), 5.36 (dq, *J* = 17.3, 1.5 Hz, 1H, **1**), 5.26 (dq, *J* = 10.5, 1.3 Hz, 1H, **1**), 4.67 (dt, *J* = 5.8, 1.4 Hz, 2H, **3**), 4.40 – 4.34 (m, 1H, **18**), 4.34 – 4.29 (m, 2H, **13**), 3.91 – 3.84 (m, 1H, **14 or 15 or 16 or 17**), 3.71 – 3.66 (m, 1H, **14 or 15 or 16 or 17**), 3.65 (s, 2H, **11**), 3.63 – 3.59 (m, 1H, **14 or 15 or 16 or 17**), 3.59 – 3.54 (m, 1H, **14 or 15 or 16 or 17**), 3.25 – 3.17 (m, 1H, **OH**), 3.17 – 3.09 (m, 1H, **19**), 3.00 – 2.84 (m, 1H, **OH**), 2.80 – 2.75 (m, 1H, **OH**), 1.32 (d, *J* = 7.0 Hz, 3H, **20 or 21**), 1.29 (d, *J* = 6.8 Hz, 3H, **20 or 21**). Solvents: Chloroform (7.26), water (1.70), cyclohexane (1.43). Standard: TMS (0.00).

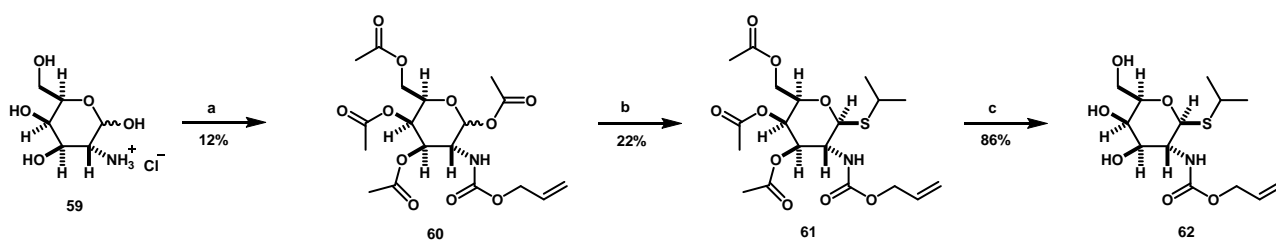
**<sup>13</sup>C NMR** (101 MHz, Chloroform-*d* δ/ppm): 171.81 (1C, **12**), 154.24 (1C, **4**), 136.48 (1C, **5**), 132.52 (1C, **2**), 130.78 (1C, **9**), 128.57 (1C, **7**), 125.83 (1C, **10**, extrapolated from HMBC spectrum), 125.23 (1C, **8**), 124.33 (1C, **6**, extrapolated from HMQC spectrum), 118.28 (1C, **1**), 85.84 (1C, **18**), 75.65 (1C, **14 or 15 or 16 or 17**), 74.35 (1C, **14 or 15 or 16 or 17**), 70.30 (1C, **14 or 15 or 16 or 17**), 68.55 (1C, **14 or 15 or 16 or 17**), 66.09 (1C, **3**), 64.00 (1C, **13**), 38.45 (1C, **11**), 35.80 (1C, **19**), 24.19 (1C, **20 or 21**), 23.96 (1C, **20 or 21**). Solvents: Chloroform (77.33, 77.02, 76.70). Standard: TMS (0.00).

**HRMS** (ESI-MS, pos.) *m/z*: [M+Na]<sup>+</sup> calculated for C<sub>21</sub>H<sub>29</sub>NO<sub>8</sub>SNa: 478.1506, found: 478.1511.



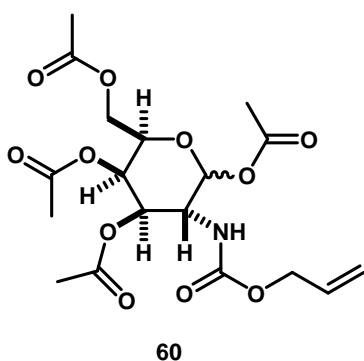
### 4.3.6 Caged 2'-Amino-IPTG substrate

The synthesis of the 2'-amino modified IPTG substrate (**62**, Scheme 12) started from D-(+)-galactosamine hydrochloride (**59**). First, the *O*-allyl carbamate group was introduced by treatment with allyl chloroformate, followed by protection of the alcohols with acetic anhydride (**60**). Next, the isopropyl thioether was introduced using 2-propanethiol and  $\text{BF}_3 \cdot \text{Et}_2\text{O}$  as a Lewis acid (**61**). Finally, the acetyl protecting groups were removed with NaOMe to yield the desired product (**62**).



**Scheme 12: Synthesis procedure of a caged 2'-O-allyl carbamate-IPTG substrate (**62**).**

Reaction conditions: a) 1.) Allyl chloroformate (1.7 eq.),  $\text{NaHCO}_3$ ,  $\text{H}_2\text{O}$ ,  $0^\circ\text{C}$  to r.t., 16 h. 2.) Acetic anhydride (8.0 eq.), pyridine, r.t., 48 h; b) 2-propanethiol (1.5 eq.),  $\text{BF}_3 \cdot \text{Et}_2\text{O}$  (2.6 eq.), DCM (dry), r.t., 3 h; c) NaOMe (4.5 eq.), MeOH, r.t., 2 h.

**Compound 60:**

The synthesis was performed similarly to Spaink *et al.*<sup>244</sup>

D-(+)-Galactosamine hydrochloride (**59**, 1.00 g, 4.64 mmol, 1.00 eq.) and NaHCO<sub>3</sub> (0.97 g, 11.6 mmol, 2.50 eq.) were dissolved in water (100 ml) and cooled to 0°C. Allyl chloroformate (0.84 ml, 0.95 g, 7.89 mmol, 1.70 eq.) was added dropwise and the resulting colorless solution was stirred at room temperature for 16 h. The solution was concentrated under reduced pressure and co-evaporated with toluene (3 x 50 ml). The obtained off-white solid was dissolved in pyridine (15 ml) followed by the slow addition of acetic anhydride (3.51 ml, 3.80 g, 37.12 mmol, 8.0 eq.). The resulting light-yellow mixture was stirred at room temperature for 48 h. The solution was concentrated under reduced pressure and co-evaporated with toluene (3 x 30 ml). The residue was taken up in ethyl acetate (50 ml) and washed with HCl (1 M, 40 ml), water (40 ml) and saturated NaHCO<sub>3</sub> (40 ml). The organic phase was dried over Na<sub>2</sub>SO<sub>4</sub> and concentrated under reduced pressure. The residue was purified by flash column chromatography (SiO<sub>2</sub>, cyclohexane/ethyl acetate 2:1, product spot on TLC stained with KMnO<sub>4</sub>). The fractions were concentrated and dried under reduced pressure to yield the product as a white crystalline solid (**60**, 235 mg, 0.55 mmol, 12% yield). The product was obtained as an anomeric mixture of the sugar. Separation of the required β-anomer was performed at a later step of the synthesis procedure (after introduction of the thioether).

Annex spectra on page 204.

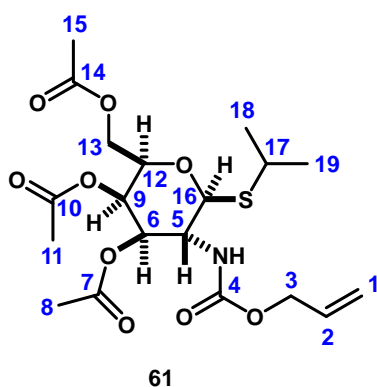
**Appearance:** White crystalline solid

**TLC:** Ethyl acetate/cyclohexane 1:2; *R<sub>f</sub>* = 0.30

**<sup>1</sup>H NMR** (400 MHz, Chloroform-*d* δ/ppm): 6.30 – 6.12 (m, 1H), 5.90 (ddt, *J* = 16.2, 10.8, 5.5 Hz, 1H), 5.71 (d, *J* = 8.8 Hz), 5.41 (ddd, *J* = 16.4, 3.4, 1.2 Hz, 1H), 5.37 – 5.06 (m, 3H), 4.77 – 4.65 (m, 1H), 4.63 – 4.49 (m, 2H), 4.49 – 4.29 (m, 1H), 4.27 – 4.12 (m, 2H), 4.09 – 4.00 (m, 1H), 2.20 – 2.00 (m, 12H, H<sub>Acetyl</sub>). Solvents: Chloroform (7.26), ethyl acetate (4.11, 2.05, 1.26), water (1.59). Standard: TMS (0.00).

**HRMS** (ESI-MS, pos.) *m/z*: [M+Na]<sup>+</sup> calculated for C<sub>18</sub>H<sub>25</sub>NO<sub>11</sub>Na: 454.1320, found: 454.1322.

### Compound 61:



The synthesis was performed similarly to Kong *et al.*<sup>245</sup>

The allyl carbamate/acetyl-protected sugar **60** (0.23 g, 0.53 mmol, 1.0 eq.) was dissolved in dry DCM (10 ml) under an N<sub>2</sub> atmosphere. BF<sub>3</sub>·Et<sub>2</sub>O (48%, 175 μl, 0.20 g, 1.39 mmol, 2.6 eq.) was added dropwise followed by the addition of 2-propanethiol (72 μl, 0.06 g, 0.78 mmol, 1.5 eq.). The obtained orange solution was stirred at room temperature for 3 h. Na<sub>2</sub>CO<sub>3</sub> was added to neutralize the reaction mixture, which was then filtered. The remaining filter cake was extracted with DCM (3 x 20 ml). The combined filtrates were concentrated under reduced pressure and the residue was purified by flash column chromatography (SiO<sub>2</sub>, cyclohexane/ethyl acetate 3:1, product spot on TLC stained with KMnO<sub>4</sub>). The fractions were concentrated and dried under reduced pressure to yield the desired β-anomer of the product as a white solid (**61**, 53 mg, 0.12 mmol, 22% yield). Cross-peaks in the NOESY spectrum between the axial protons **6** – **12**, **6** – **16** and **12** – **16** as well as their non-existence in the spectrum of the α-anomer (the corresponding proton **16'** has only one strong NOE cross-peak to proton **13'**) highlighted the correct spatial geometry of the isolated product. Furthermore, the signal of proton **5** showed a pseudo-quartet splitting in the <sup>1</sup>H NMR spectrum, arising from couplings to protons **6**, **16** and the NH group. The determined coupling constants, all ~10 Hz, are typical for a bi-axial substitution at the sugar scaffold.

Annex spectra on page 205.

**Appearance:** White solid

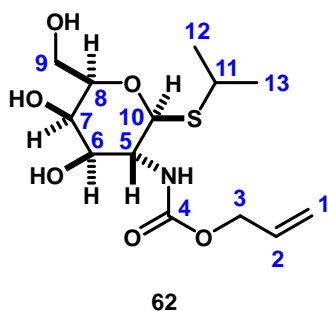
**TLC:** Ethyl acetate/cyclohexane 1:2; *R<sub>f</sub>* (α-anomer) = 0.41, *R<sub>f</sub>* (β-anomer) = 0.27

**<sup>1</sup>H NMR** (500 MHz, Chloroform-*d* δ/ppm): 5.90 (ddt, *J* = 16.2, 10.6, 5.5 Hz, 1H, **2**), 5.40 (dd, *J* = 3.5, 0.7 Hz, 1H, **9**), 5.29 (d (broad), *J* = 17.2 Hz, 1H, **1**), 5.21 (dd, *J* = 10.5, 1.4 Hz, 1H, **1**), 5.18 (s (broad), 1H, **6**), 4.87 – 4.70 (m (broad), 2H, **16** + NH), 4.63 – 4.51 (m, 2H, **3**), 4.17 (dd, *J* = 11.3, 6.9 Hz, 1H, **13**), 4.10 (dd, *J* = 11.3, 6.3 Hz, 1H, **13**), 3.92 (td, *J* = 6.6, 1.1 Hz, 1H, **12**), 3.90 – 3.83 (m, 1H, **5**), 3.20 (hept, *J* = 6.7 Hz, 1H, **17**), 2.15 (s, 3H, **11**), 2.04 (s, 3H, **8** or **15**), 2.01 (s, 3H, **8** or **15**), 1.32 (d, *J* = 2.0 Hz, 3H, **18** or **19**), 1.31 (d, *J* = 1.8 Hz, 3H, **18** or **19**). Solvents: Chloroform (7.27), water (1.65). Standard: TMS (0.00).

**<sup>13</sup>C NMR** (Peaks assigned from HMQC+HMBC spectra, Chloroform-*d* δ/ppm): 170.42 (1C, **7 or 14**), 170.41 (1C, **7 or 14**), 170.30 (1C, **10**), 155.54 (1C, **4**), 132.70 (1C, **2**), 117.64 (1C, **1**), 84.62 (1C, **16**), 74.37 (1C, **12**), 71.19 (1C, **6**), 67.13 (1C, **9**), 65.86 (1C, **3**), 61.85 (1C, **13**), 51.62 (1C, **5**), 35.49 (1C, **17**), 23.79 (1C, **18 or 19**), 23.77 (1C, **18 or 19**), 20.76 (1C, **11**), 20.71 (1C, **8 or 15**), 20.68 (1C, **8 or 15**). Solvents: Chloroform (77.32). Standard: TMS (0.00).

**HRMS** (ESI-MS, pos.) m/z: [M+Na]<sup>+</sup> calculated for C<sub>19</sub>H<sub>29</sub>NO<sub>9</sub>SNa: 470.1455, found: 470.1463.

**Compound 62:**



The synthesis was performed similarly to Kong *et al.*<sup>245</sup>

Protected IPTG derivative **61** (50 mg, 0.11 mmol, 1.0 eq.) was dissolved in MeOH (2 ml). NaOMe (30 mg, 0.50 mmol, 4.5 eq.) in MeOH (1 ml) was slowly added and the mixture was stirred at room temperature for 2 h. The mixture was neutralized with 10% acetic acid in MeOH (1 ml) and concentrated. The residue was purified by flash column chromatography (SiO<sub>2</sub>, DCM/MeOH 10:1, product spot on TLC stained with KMnO<sub>4</sub>). The fractions were concentrated and dried under reduced pressure to yield the product as a white solid (**62**, 31.0 mg, 0.10 mmol, 86% yield).

Annex spectra on page 206.

**Appearance:** White solid

**TLC:** DCM/MeOH 10:1; *R<sub>f</sub>* = 0.30

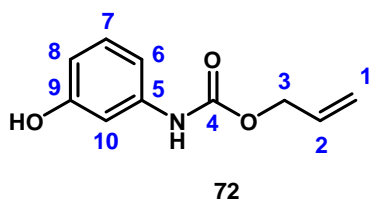
**<sup>1</sup>H NMR** (400 MHz, Methanol-*d*<sub>4</sub> δ/ppm): 5.94 (ddt, *J* = 17.2, 10.5, 5.3 Hz, 1H, **2**), 5.33 (dq, *J* = 17.3, 1.8 Hz, 1H, **1**), 5.17 (dq, *J* = 10.5, 1.5 Hz, 1H, **1**), 4.62 – 4.55 (m, 1H, **10**), 4.55 – 4.46 (m, 2H, **3**), 3.88 (dd, *J* = 3.3, 1.1 Hz, 1H, **6**), 3.78 – 3.69 (m, 2H, **9**), 3.69 – 3.63 (m, 1H, **5**), 3.57 (dd, *J* = 10.2, 3.2 Hz, 1H, **7**), 3.48 (ddd, *J* = 6.7, 5.4, 1.1 Hz, 1H, **8**), 3.20 (p, *J* = 6.8 Hz, 1H, **11**), 1.29 (d, *J* = 6.6 Hz, 3H, **12 or 13**), 1.26 (d, *J* = 6.9 Hz, 3H, **12 or 13**). Solvents: Water (4.86), methanol (3.31).

**<sup>13</sup>C NMR** (126 MHz, Methanol-*d*<sub>4</sub> δ/ppm): 158.81 (1C, **4**), 134.51 (1C, **2**), 117.20 (1C, **1**), 85.94 (1C, **10**), 80.57 (1C, **8**), 74.13 (1C, **7**), 69.85 (1C, **6**), 66.35 (1C, **3**), 62.64 (1C, **9**), 54.72 (1C, **5**), 35.76 (1C, **11**), 24.40 (1C, **12 or 13**), 24.21 (1C, **12 or 13**). Solvents: Methanol (49.51, 49.34, 49.17, 49.00, 48.83, 48.66, 48.49).

**HRMS** (ESI-MS, pos.) *m/z*: [M+Na]<sup>+</sup> calculated for C<sub>13</sub>H<sub>23</sub>NO<sub>6</sub>SNa: 344.1138, found: 344.1143.

### 4.3.7 Caged aniline substrate

#### Compound 72:



The synthesis was performed similarly to Griffiths and Ryckelynck *et al.*<sup>120</sup>

At 0°C, allyl chloroformate (3.90 ml, 4.42 g, 36.7 mmol, 2.0 eq.) was added dropwise to a stirred suspension of 3-aminophenol (**67**, 2.00 g, 18.3 mmol, 1.0 eq.) in a mixture of dry diethyl ether (100 ml) and dry THF (20 ml). A white precipitate (the amine hydrochloride) formed immediately. The reaction mixture was stirred an additional 2 h at room temperature. The hydrochloride was removed by filtration. The filtrate was evaporated under reduced pressure. The obtained brown oil was solubilized in diethyl ether (20 ml) and the resulting organic phase was washed with solutions of HCl (1 M, 20 ml), saturated NaHCO<sub>3</sub> (20 ml) and water (20 ml). The organic phase was dried over Na<sub>2</sub>SO<sub>4</sub> and the solvent was evaporated to yield a brown oil. The residue was purified by flash column chromatography (SiO<sub>2</sub>, ethyl acetate/cyclohexane 1:3) to yield the product as a white crystalline solid (**72**, 792 mg, 4.1 mmol, 22% yield).

Annex spectra on page 207.

**Appearance:** White solid

**TLC:** Ethyl acetate/cyclohexane 1:3; *R<sub>f</sub>* = 0.30

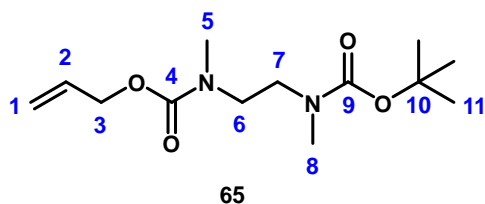
**<sup>1</sup>H NMR** (500 MHz, Chloroform-*d* δ/ppm): 7.30 (s (broad), 1H, **10**), 7.13 (t, *J* = 8.1 Hz, 1H, **7**), 6.81 (s (broad), 1H, **NH**), 6.68 (ddd, *J* = 8.0, 2.1, 0.9 Hz, 1H, **6**), 6.58 (ddd, *J* = 8.1, 2.4, 0.9 Hz, 1H, **8**), 6.52 (s (broad), 1H, **OH**), 5.95 (ddt, *J* = 17.2, 10.4, 5.7 Hz, 1H, **2**), 5.36 (dq, *J* = 17.2, 1.5 Hz, 1H, **1**), 5.26 (dq, *J* = 10.4, 1.3 Hz, 1H, **1**), 4.67 (dt, *J* = 5.7, 1.4 Hz, 2H, **3**). Solvents: Chloroform (7.26), cyclohexane (1.43). Standard: TMS (0.00).

**<sup>13</sup>C NMR** (126 MHz, Chloroform-*d* δ/ppm): 156.77 (1C, **9**), 153.62 (1C, **4**), 138.69 (1C, **5**), 132.07 (1C, **2**), 129.98 (1C, **7**), 118.54 (1C, **1**), 110.86 (1C, **8**), 110.58 (1C, **6**), 106.03 (1C, **10**), 66.17 (1C, **3**). Solvents: Chloroform (77.28, 77.03, 76.77). Standard: TMS (0.00).

**HRMS** (ESI-MS, pos.) *m/z*: [M + H]<sup>+</sup> calculated for C<sub>10</sub>H<sub>12</sub>NO<sub>3</sub>: 194.0812, found: 194.0811.

### 4.3.8 Urea test substrate

#### Compound 65:



The synthesis was performed similarly to Baures *et al.*<sup>246</sup>

*N,N'*-Dimethylethylenediamine (**64**, 7.40 ml, 6.06 g, 68.8 mmol, 1.0 eq.) was dissolved in dry THF (60 ml) and cooled to 0°C. A solution of di-*tert*-butyl dicarbonate (5.00 g, 22.9 mmol, 0.33 eq.) in dry THF (40 ml) was slowly added, whereupon a white precipitate was formed. The reaction mixture was allowed to warm to room temperature and was further stirred for 19 h. The reaction mixture was filtered and the filtrate was concentrated under reduced pressure. The residue was dissolved in ethyl acetate (50 ml) and washed with brine (3 x 50 ml). The organic phase was dried over Na<sub>2</sub>SO<sub>4</sub> and concentrated under reduced pressure to yield a colorless oil (2.938 g, single Boc protected *N,N'*-dimethylethylenediamine = *tert*-butyl methyl(2-(methylamino)ethyl)carbamate). This oil was dissolved in dry THF (30 ml) and cooled to 0°C. Triethylamine (2.17 ml, 1.57 g, 15.6 mmol, 1.1 eq. with respect to the obtained colorless oil) was added. Allyl chloroformate (1.90 ml, 2.15 g, 17.88 mmol, 1.2 eq. with respect to the obtained colorless oil) was added dropwise over 10 min, whereupon a white precipitate formed. The mixture was allowed to warm to room temperature and was further stirred for 3 h. The reaction mixture was concentrated under reduced pressure. The residue was suspended in ethyl acetate (100 ml) and washed with brine (3 x 30 ml). The organic phase was dried over Na<sub>2</sub>SO<sub>4</sub> and concentrated under reduced pressure to yield a slightly yellow oil. The residue was purified by flash column chromatography (SiO<sub>2</sub>, ethyl acetate/cyclohexane 1:3) to yield the product as a colorless oil (**65**, 1920 mg, 7.0 mmol, 33% yield).

Annex spectra on page 208.

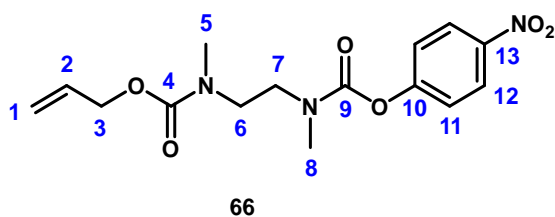
**Appearance:** Colorless oil

**TLC:** Ethyl acetate/cyclohexane 1:3; *R<sub>f</sub>* = 0.30

**<sup>1</sup>H NMR** (500 MHz, Chloroform-*d* δ/ppm): 5.94 (ddt, *J* = 17.3, 10.8, 5.5 Hz, 1H, **2**), 5.30 (dq, *J* = 17.3, 1.7 Hz, 1H, **1**), 5.25 – 5.15 (m, 1H, **1**), 4.62 – 4.55 (m, 2H, **3**), 3.48 – 3.30 (m, 4H, **6 + 7**), 2.95 (s, 3H, **5**), 2.92 – 2.83 (m, 3H, **8**), 1.46 (s, 9H, **11**). Solvents: Chloroform (7.28), water (1.82). Standard: TMS (0.00).

**<sup>13</sup>C NMR** (126 MHz, Chloroform-*d* δ/ppm): 155.95 (1C, **4**), 155.54 (1C, **9**), 133.12 (1C, **2**), 117.59 (1C, **1**), 79.56 (1C, **10**), 66.13 (1C, **3**), 46.71 (2C, **6 + 7**), 35.19 (1C, **5**), 34.53 (1C, **8**), 28.41 (1C, **11**). Solvents: Chloroform (77.31, 77.05, 76.80). Standard: TMS (0.00).

**HRMS** (ESI-MS, pos.) *m/z*: [M+Na]<sup>+</sup> calculated for C<sub>13</sub>H<sub>24</sub>N<sub>2</sub>O<sub>4</sub>Na: 295.1628, found: 295.1632.

**Compound 66:****66**

The synthesis was performed similarly to Hay *et al.*<sup>241</sup>

Boc-protected allyl carbamate **65** (0.91 g, 3.3 mmol, 1.0 eq.) was dissolved in DCM (5 ml) and cooled to 0°C. Triisopropylsilane (1.5 ml, 6.6 mmol, 2.0 eq., scavenger for carbocations) and trifluoroacetic acid (5 ml) were added and the mixture was stirred 30 min at 0°C and then 1.5 h at room temperature. The solvent was evaporated and the residue was dissolved in ethyl acetate (10 ml) and washed with brine (3 x 10 ml). The organic phase was dried over Na<sub>2</sub>SO<sub>4</sub> and concentrated under reduced pressure to yield a yellow oil (0.65 g). This oil was dissolved in dry THF (5 ml). At 0°C, triethylamine (5.30 ml, 3.85 g, 38 mmol, 12 eq.) and *para*-nitrophenyl chloroformate (0.77 g, 3.8 mmol, 1.2 eq.) in dry THF (5 ml) were added dropwise. The mixture was stirred for 30 min at 0°C and then for 2.5 h at room temperature. The solvent was evaporated and the residue taken up in ethyl acetate (20 ml) and washed with brine (3 x 10 ml). The organic phase was dried over Na<sub>2</sub>SO<sub>4</sub> and evaporated under reduced pressure. The crude product was purified by flash column chromatography (aluminum oxide, ethyl acetate/cyclohexane 2:5) to yield the product as a light yellow oil (**66**, 339 mg, 1.00 mmol, 30% yield).

Annex spectra on page 209.

**Appearance:** Light yellow oil

**TLC:** Ethyl acetate/cyclohexane 2:5; *R<sub>f</sub>* = 0.30

**<sup>1</sup>H NMR** (500 MHz, Chloroform-*d* δ/ppm): 8.24 (dd, *J* = 9.3, 2.8 Hz, 2H, **12**), 7.33 – 7.28 (m, 2H, **11**), 6.00 – 5.84 (m, 1H, **2**), 5.37 – 5.25 (m, 1H, **1**), 5.25 – 5.15 (m, 1H, **1**), 4.64 – 4.55 (m, 2H, **3**), 3.61 (dd (broad), *J* = 10.6, 5.7 Hz, **5-8**), 3.55 (s (broad), **5-8**), 3.14 (d (broad), *J* = 14.9 Hz, **5-8**), 3.06 (d (broad), *J* = 14.1 Hz, **5-8**), 2.99 (s (broad), **5-8**). Solvents: Chloroform (7.28), ethyl acetate (4.13, 2.05, 1.26), water (1.74), “grease” (1.26, 0.88). Standard: TMS (0.00).

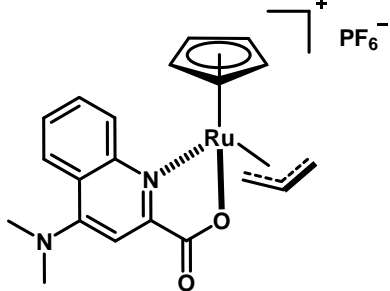
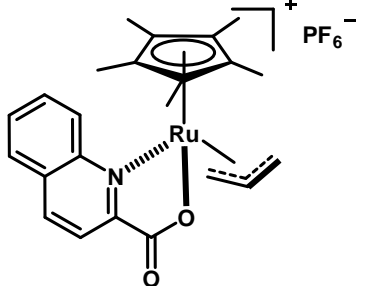
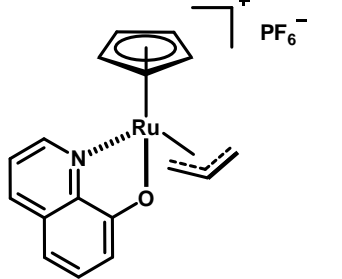
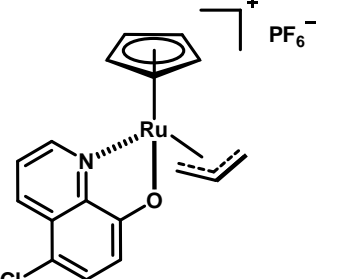
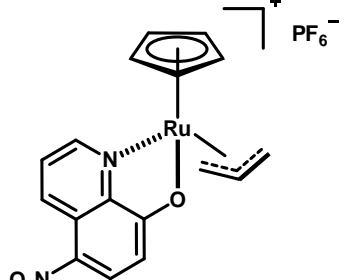
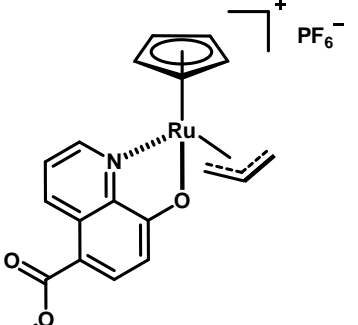
**<sup>13</sup>C NMR** (126 MHz, Chloroform-*d* δ/ppm): 156.34 (1C, **4 or 10**), 155.99 (1C, **4 or 10**), 153.30 (1C, **9**), 144.85 (1C, **13**), 132.82 (1C, **2**), 125.11 (2C, **12**), 122.23 (2C, **11**), 117.60 (1C, **1**), 66.24 (1C, **3**), 46.93 (**5-8**), 46.29 (**5-8**), 35.22 (**5-8**), 34.41 (**5-8**). Solvents: Chloroform (77.32, 77.07, 76.81). Standard: TMS (0.00).

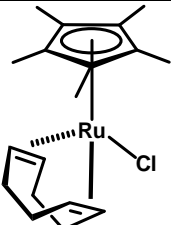
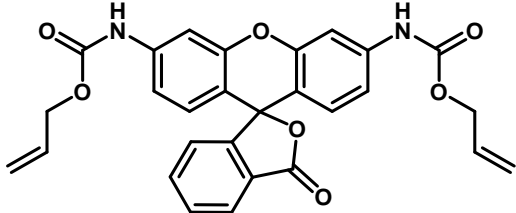
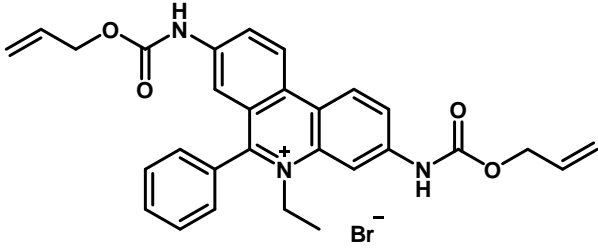
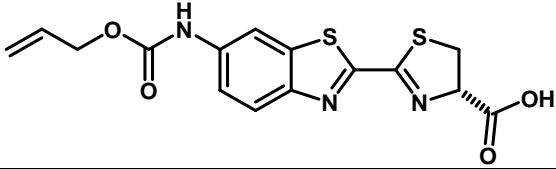
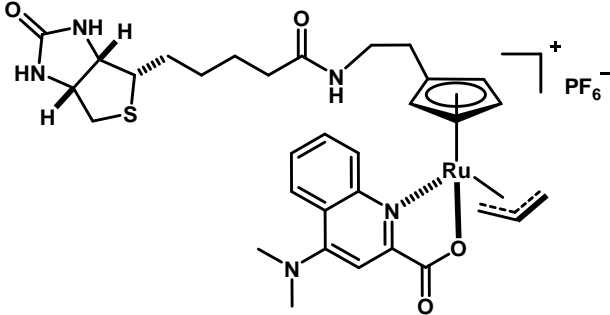
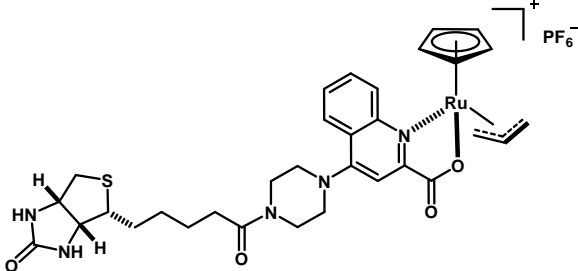
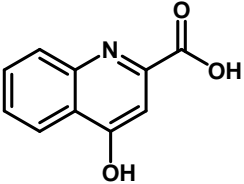
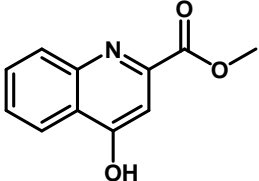
**HRMS** (ESI-MS, pos.) *m/z*: [M+Na]<sup>+</sup> calculated for C<sub>15</sub>H<sub>19</sub>N<sub>3</sub>O<sub>6</sub>Na: 360.1166, found: 360.1171.

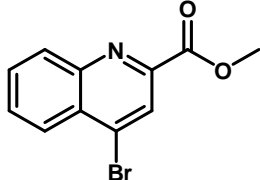
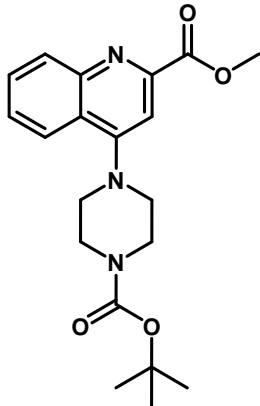
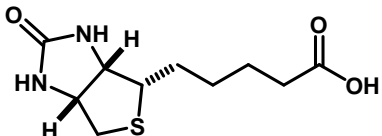
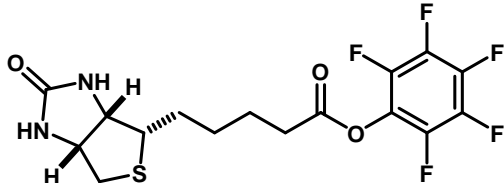
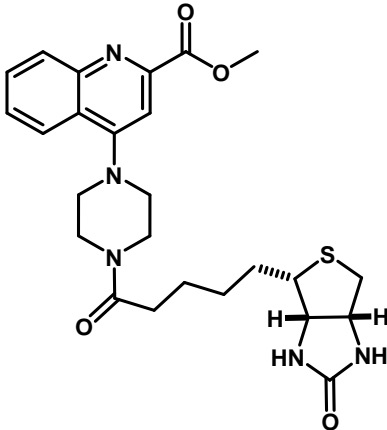
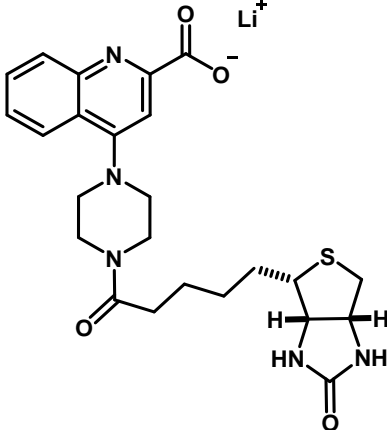


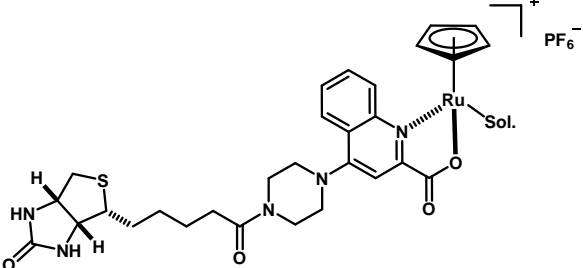
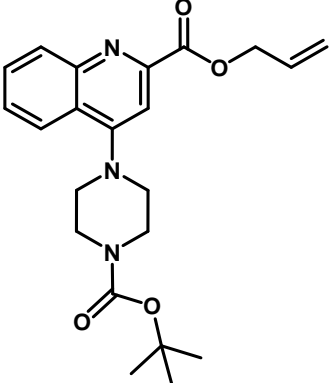
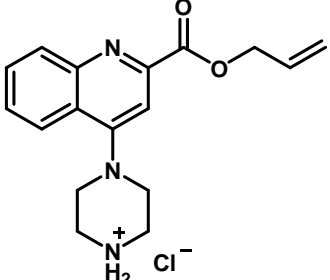
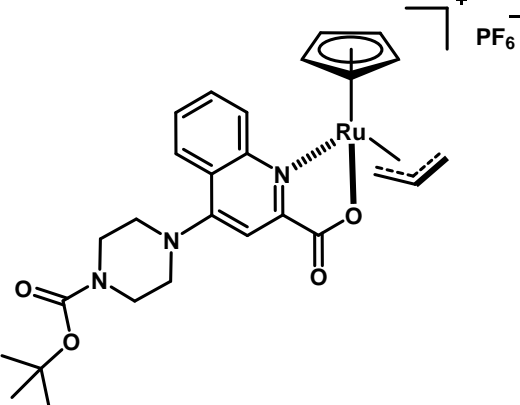
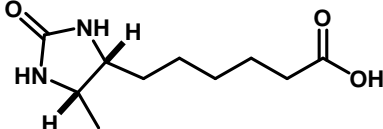
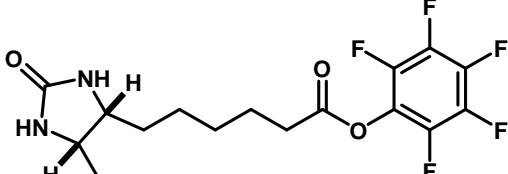
## 4.4 Table of compounds

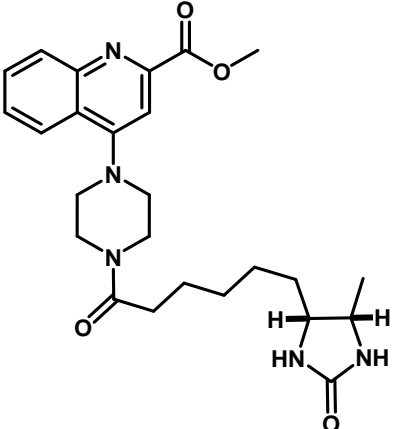
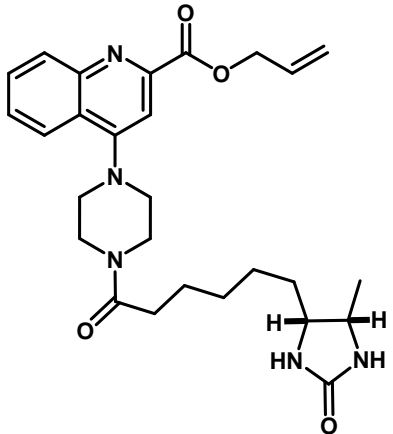
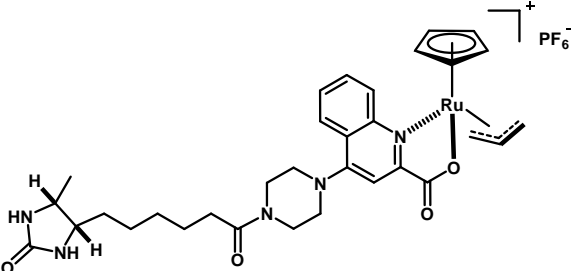
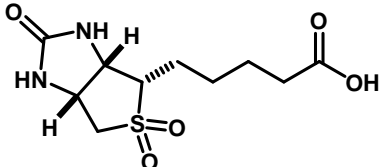
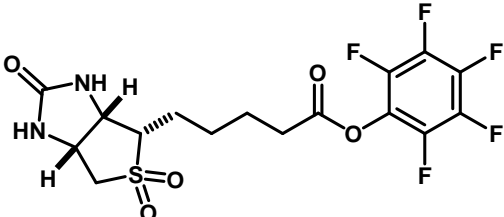
Number	Structure	Name
1		Triethylammonium (7-(((allyloxy)carbonyl)amino)-2-oxo-2H-chromen-4-yl)methanesulfonate
2		Triethylammonium (7-amino-2-oxo-2H-chromen-4-yl)methanesulfonate
3		[CpRu(PA)(Allyl)]PF <sub>6</sub>
4		[Cp*Ru(PA)(Allyl)]PF <sub>6</sub>
5		[CpRu(QA)(Allyl)]PF <sub>6</sub>
6		[CpRu(QA-Ome)(Allyl)]PF <sub>6</sub>

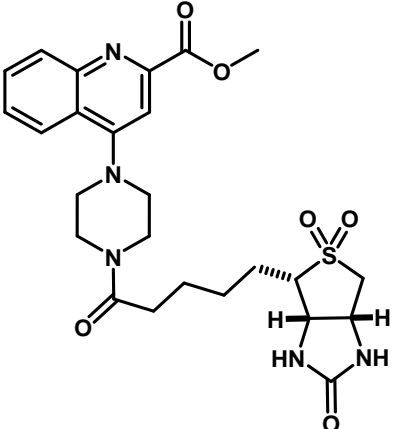
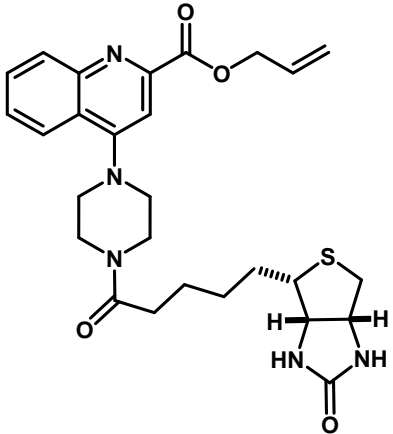
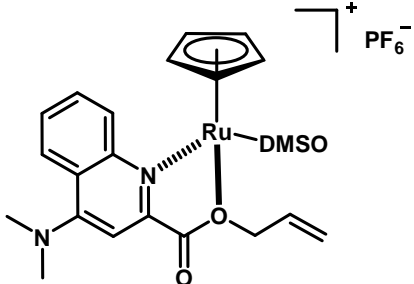
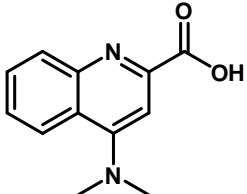
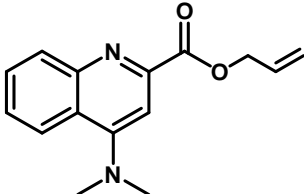
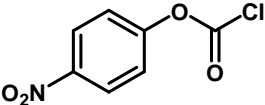
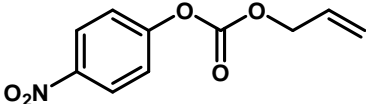
7		[CpRu(QA-NMe <sub>2</sub> )(Allyl)]PF <sub>6</sub>
8		[Cp <sup>*</sup> Ru(QA)(Allyl)]PF <sub>6</sub>
9		[CpRu(HQ)(Allyl)]PF <sub>6</sub>
10		[CpRu(HQ-Cl)(Allyl)]PF <sub>6</sub>
11		[CpRu(HQ-NO <sub>2</sub> )(Allyl)]PF <sub>6</sub>
12		[CpRu(HQ-CO <sub>2</sub> Me)(Allyl)]PF <sub>6</sub>

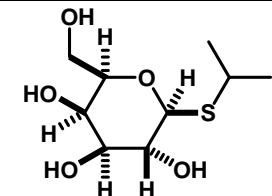
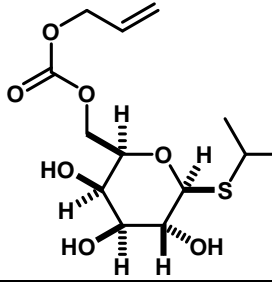
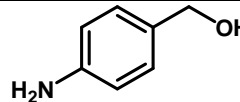
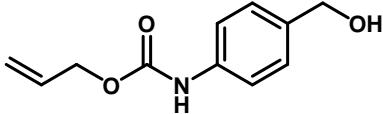
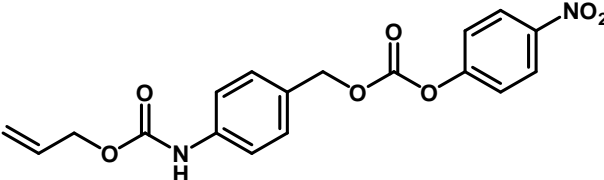
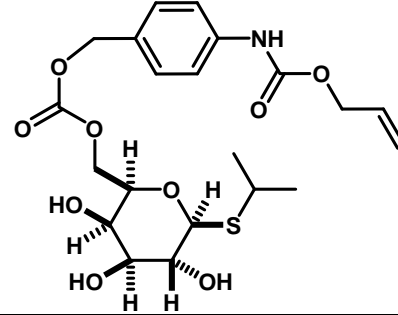
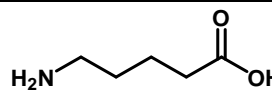
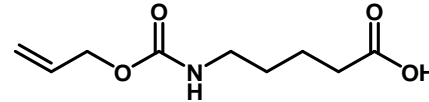
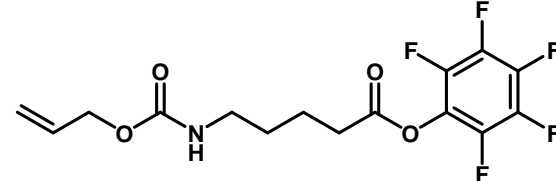
13		[Cp*Ru(cod)Cl]
14		O-allyl-carbamate caged rhodamine 110
15		O-allyl-carbamate caged DNA binding agent
16		O-allyl-carbamate caged D-aminoluciferin
17		[(Cp-Biot)Ru(QA-NMe2)(Allyl)]PF <sub>6</sub>
18		[CpRu(QA-Biot)(Allyl)]PF <sub>6</sub>
19		Kynurenic acid
20		Methyl 4-hydroxyquinoline-2-carboxylate

21		Methyl 4-bromoquinoline-2-carboxylate
22		Methyl 4-(4-(tert-butoxycarbonyl)piperazin-1-yl)quinoline-2-carboxylate
23		D-Biotin
24		D-Biotin pentafluorophenyl ester
25		Methyl 4-(4-(5-((3aS,4S,6aR)-2-oxohexahydro-1H-thieno[3,4-d]imidazol-4-yl)pentanoyl)piperazin-1-yl)quinoline-2-carboxylate
26		Lithium 4-(4-(5-((3aS,4S,6aR)-2-oxohexahydro-1H-thieno[3,4-d]imidazol-4-yl)pentanoyl)piperazin-1-yl)quinoline-2-carboxylate

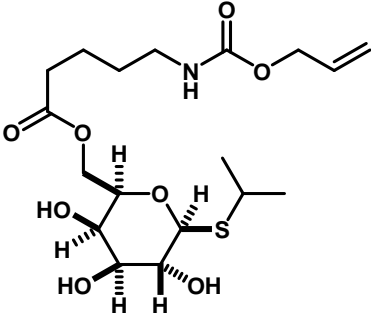
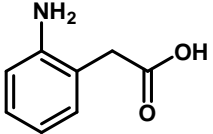
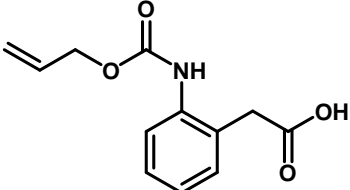
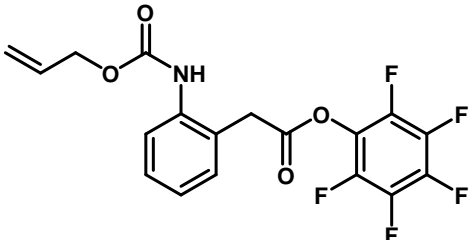
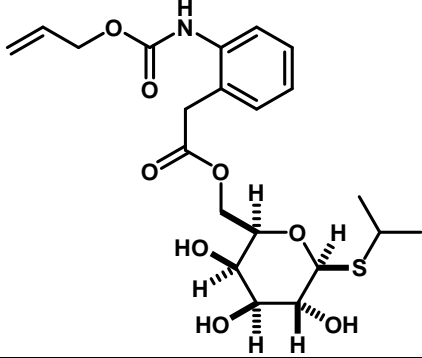
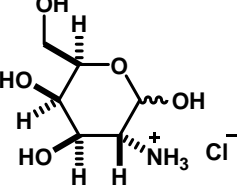
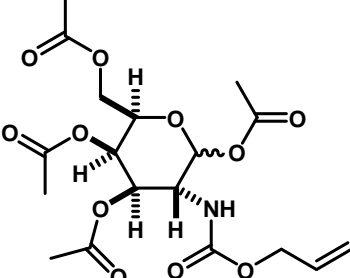
27		[CpRu(QA-Biot)(Sol.)]PF <sub>6</sub>
28		Allyl 4-(4-(tert-butoxycarbonyl)piperazin-1-yl)quinoline-2-carboxylate
29		4-(2-((allyloxy)carbonyl)quinolin-4-yl)piperazin-1-ium chloride
30		[CpRu(QA-Boc)(Allyl)] PF <sub>6</sub>
31		Desthiobiotin
32		Desthiobiotin pentafluorophenyl ester

33		Methyl 4-(4-(6-((4R,5S)-5-methyl-2-oxoimidazolidin-4-yl)hexanoyl)piperazin-1-yl)quinoline-2-carboxylate
34		Allyl 4-(4-(6-((4R,5S)-5-methyl-2-oxoimidazolidin-4-yl)hexanoyl)piperazin-1-yl)quinoline-2-carboxylate
35		[CpRu(QA-Desthiobiot)(Allyl)]PF <sub>6</sub>
36		D-Biotin sulfone
37		D-Biotin sulfone pentafluorophenyl ester

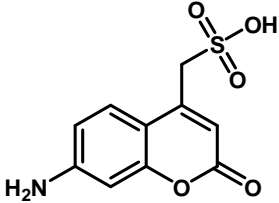
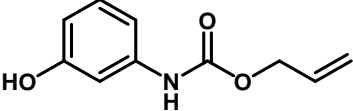
38		Methyl 4-(4-(5-((3aS,4S,6aR)-5,5-dioxido-2-oxohexahydro-1H-thieno[3,4-d]imidazol-4-yl)pentanoyl)piperazin-1-yl)quinoline-2-carboxylate
39		Allyl 4-(4-(5-((3aS,4S,6aR)-2-oxohexahydro-1H-thieno[3,4-d]imidazol-4-yl)pentanoyl)piperazin-1-yl)quinoline-2-carboxylate
40		[CpRu(Allyl-QA-NMe <sub>2</sub> )(DMSO)]PF <sub>6</sub>
41		4-(dimethylamino)quinoline-2-carboxylic acid
42		Allyl 4-(dimethylamino)quinoline-2-carboxylate
43		4-nitrophenyl carbonochloridate
44		Allyl (4-nitrophenyl) carbonate

45		Isopropyl- $\beta$ -D-thiogalactopyranosid (IPTG)
46		Allyl (((2R,3R,4S,5R,6S)-3,4,5-trihydroxy-6-(isopropylthio)tetrahydro-2H-pyran-2-yl)methyl) carbonate
47		(4-aminophenyl)methanol
48		Allyl (4-(hydroxymethyl)phenyl)carbamate
49		Allyl (4-(((4-nitrophenoxy)carbonyl)oxy)methyl)phenyl)carbamate
50		Allyl (4-((((((2R,3R,4S,5R,6S)-3,4,5-trihydroxy-6-(isopropylthio)tetrahydro-2H-pyran-2-yl)methoxy)carbonyl)oxy)methyl)phenyl)carbamate
51		5-aminopentanoic acid
52		5-(((allyloxy)carbonyl)amino)pentanoic acid
53		Perfluorophenyl 5-(((allyloxy)carbonyl)amino)pentanoate



54		((2R,3R,4S,5R,6S)-3,4,5-trihydroxy-6-(isopropylthio)tetrahydro-2H-pyran-2-yl)methyl 5-(((allyloxy)carbonyl)amino)pentanoate
55		2-(2-aminophenyl)acetic acid
56		2-(2-(((allyloxy)carbonyl)amino)phenyl)acetic acid
57		Perfluorophenyl 2-(2-(((allyloxy)carbonyl)amino)phenyl)acetate
58		((2R,3R,4S,5R,6S)-3,4,5-trihydroxy-6-(isopropylthio)tetrahydro-2H-pyran-2-yl)methyl 2-(2-(((allyloxy)carbonyl)amino)phenyl)acetate
59		D-(+)-Galactosamine hydrochloride
60		(3R,4R,5R,6R)-6-(acetoxymethyl)-3-(((allyloxy)carbonyl)amino)tetrahydro-2H-pyran-2,4,5-triyl triacetate

61		(2R,3R,4R,5R,6S)-2-(acetoxymethyl)-5-(((allyloxy)carbonyl)amino)-6-(isopropylthio)tetrahydro-2H-pyran-3,4-diyl diacetate
62		Allyl ((2S,3R,4R,5R,6R)-4,5-dihydroxy-6-(hydroxymethyl)-2-(isopropylthio)tetrahydro-2H-pyran-3-yl)carbamate
63		2-Amino-IPTG
64		<i>N,N'</i> -Dimethylethylenediamine
65		Allyl <i>tert</i> -butyl ethane-1,2-diylbis(methylcarbamate)
66		Allyl (4-nitrophenyl) ethane-1,2-diylbis(methylcarbamate)
67		3-Aminophenol
68		Ethyl (3-hydroxyphenyl)carbamate
69		Ethyl (4-(chloromethyl)-2-oxo-2H-chromen-7-yl)carbamate
70		Sodium (7-((ethoxycarbonyl)amino)-2-oxo-2H-chromen-4-yl)methanesulfonate

71	 <p>The structure shows a coumarin ring system. The benzene ring has an amino group (-NH<sub>2</sub>) at the 7-position. The pyrone ring has a carbonyl group (=O) at the 2-position and a methanesulfonic acid group (-CH<sub>2</sub>SO<sub>3</sub>H) at the 4-position.</p>	7-Aminocoumarin-4-methanesulfonic acid
72	 <p>The structure shows a benzene ring with a hydroxyl group (-OH) at the 3-position. The nitrogen atom of the carbamate group (-NH-CO-O-) is attached to the benzene ring at the 1-position. The oxygen atom of the carbamate group is attached to an allyl group (-CH<sub>2</sub>-CH=CH<sub>2</sub>).</p>	Allyl (3-hydroxyphenyl)carbamate

## 5 Abbreviations

Abbreviation	Name
AIDA	Adhesin involved in diffuse adherence
ArM	Artificial metalloenzyme
B4F	Biotin-4-fluorescein
BINAP	2,2'-bis(diphenylphosphino)-1,1'-binaphthyl
Biot	D-biotin
Boc	<i>tert</i> -butyloxycarbonyl
bpy	2,2'-bipyridine
Bpy-Ala	(2,2'-bipyridin-5-yl) alanine
BSA	Bovine serum albumin
CAP	Catabolite activator protein
CFE	Cell free extract
cod	$\eta^4$ -1,5-cyclooctadiene
COSY	Correlation spectroscopy
Cp	$\eta^5$ -cyclopentadienyl
Cp*	$\eta^5$ -1,2,3,4,5-pentamethyl-cyclopentadienyl
DACA	4-(dimethylamino)-cinnamaldehyde
DCM	Dichloromethane
DIPEA	<i>N,N</i> -Diisopropylethylamine (Hünig's base)
DMAP	4-Dimethylaminopyridine
DMF	<i>N,N</i> -Dimethylformamide
DMSO	Dimethyl sulfoxide
DOSY	Diffusion ordered nuclear magnetic resonance spectroscopy
ESI-TOF MS	Electrospray ionization time of flight mass spectrometry
FACS	Fluorescence activated cell sorting
FADS	Fluorescence activated droplet sorting
FBBS	Free biotin-binding sites
FRET	Förster resonance energy transfer
GFP	Green fluorescent protein
GSH	Glutathione
HABA	2-(4'-hydroxybenzeneazo)benzoic acid
HMBC	Heteronuclear multiple-bond correlation spectroscopy
HMQC	Heteronuclear single-quantum correlation spectroscopy
HPLC	High performance liquid chromatography
HQ	8-hydroxyquinolate
HRMS	High-resolution mass spectrometry
HRP	Horse radish peroxidase
ICP-MS	Inductively coupled plasma mass spectrometry
IPTG	Isopropyl $\beta$ -D-1-thiogalactopyranoside
L-ara	L-arabinose
LB-medium	Lysogeny Broth-medium
MS	Mass spectrometry
MW	Molecular weight
MWCO	Molecular weight cut-off
NMR	Nuclear magnetic resonance spectroscopy
NOESY	Nuclear overhauser enhancement and exchange spectroscopy
OD <sub>600</sub>	Optical density at 600 nm
PA	2-pyridinecarboxylate
PBS	Phosphate buffered saline
PCR	Polymerase chain reaction

<b>Abbreviation</b>	<b>Name</b>
Pd <sub>2</sub> (dba) <sub>3</sub>	Tris(dibenzylideneacetone)dipalladium(0)
PDB	Protein data base
PFP	Pentafluorophenyl ester
PMSF	Phenylmethylsulfonylfluorid
ppm	Parts per million
QA	2-quinolinecarboxylate
rac	Racemic
RFU	Relative fluorescence units
Sav	Streptavidin
SDS-PAGE	Sodium dodecyl sulfate polyacrylamide gel electrophoresis
SOB-medium	Super Optimal Broth-medium
TFA	Trifluoroacetic acid
THF	Tetrahydrofuran
TIS	Triisopropylsilane
TLC	Thin-layer chromatography
TMS	Tetramethylsilane
TPR	Tetratricopeptide repeat
Tris-HCl	Tris(hydroxymethyl)aminomethane hydrochloride
UPLC-MS	Ultra performance liquid chromatography coupled to mass spectrometry
WT	Wild-type

## 6 References

- (1) Schwizer, F.; Okamoto, Y.; Heinisch, T.; Gu, Y.; Pellizzoni, M. M.; Lebrun, V.; Reuter, R.; Köhler, V.; Lewis, J. C.; Ward, T. R., Artificial Metalloenzymes: Reaction Scope and Optimization Strategies, *Chem. Rev.*, **2018**, *118* (1), 142-231.  
DOI: [10.1021/acs.chemrev.7b00014](https://doi.org/10.1021/acs.chemrev.7b00014)
- (2) Ward, T. R., Searchable Web Site on Artificial Metalloenzymes, <http://www.chemie.unibas.ch/~ward/>
- (3) Yu, F.; Cangelosi, V. M.; Zastrow, M. L.; Tegoni, M.; Plegaria, J. S.; Tebo, A. G.; Mocny, C. S.; Ruckthong, L.; Qayyum, H.; Pecoraro, V. L., Protein design: toward functional metalloenzymes, *Chem. Rev.*, **2014**, *114* (7), 3495-3578.  
DOI: [10.1021/cr400458x](https://doi.org/10.1021/cr400458x)
- (4) Dürrenberger, M.; Ward, T. R., Recent achievements in the design and engineering of artificial metalloenzymes, *Curr. Opin. Chem. Biol.*, **2014**, *19*, 99-106.  
DOI: [10.1016/j.cbpa.2014.01.018](https://doi.org/10.1016/j.cbpa.2014.01.018)
- (5) Heinisch, T.; Ward, T. R., Design strategies for the creation of artificial metalloenzymes, *Curr. Opin. Chem. Biol.*, **2010**, *14* (2), 184-199.  
DOI: [10.1016/j.cbpa.2009.11.026](https://doi.org/10.1016/j.cbpa.2009.11.026)
- (6) Rosati, F.; Roelfes, G., Artificial Metalloenzymes, *ChemCatChem*, **2010**, *2* (8), 916-927.  
DOI: [10.1002/cctc.201000011](https://doi.org/10.1002/cctc.201000011)
- (7) Bos, J.; Roelfes, G., Artificial metalloenzymes for enantioselective catalysis, *Curr. Opin. Chem. Biol.*, **2014**, *19*, 135-143.  
DOI: [10.1016/j.cbpa.2014.02.002](https://doi.org/10.1016/j.cbpa.2014.02.002)
- (8) Thomas, C. M.; Ward, T. R., Artificial metalloenzymes: proteins as hosts for enantioselective catalysis, *Chem. Soc. Rev.*, **2005**, *34* (4), 337-346.  
DOI: [10.1039/b314695m](https://doi.org/10.1039/b314695m)
- (9) Qi, D.; Tann, C. M.; Haring, D.; Distefano, M. D., Generation of new enzymes via covalent modification of existing proteins, *Chem. Rev.*, **2001**, *101* (10), 3081-3111.  
DOI: [10.1021/cr000059o](https://doi.org/10.1021/cr000059o)
- (10) Wilson, M. E.; Whitesides, G. M., Conversion of a protein to a homogeneous asymmetric hydrogenation catalyst by site-specific modification with a diphosphinerhodium(I) moiety, *J. Am. Chem. Soc.*, **1978**, *100* (1), 306-307.  
DOI: [10.1021/ja00469a064](https://doi.org/10.1021/ja00469a064)
- (11) Yamamura, K.; Kaiser, E. T., Studies on the oxidase activity of copper(II) carboxypeptidase A, *J. Chem. Soc., Chem. Commun.*, **1976**, (20), 830-831.  
DOI: [10.1039/C39760000830](https://doi.org/10.1039/C39760000830)
- (12) Ward, T. R., Artificial Metalloenzymes Based on the Biotin-Avidin Technology: Enantioselective Catalysis and Beyond, *Acc. Chem. Res.*, **2011**, *44* (1), 47-57.  
DOI: [10.1021/ar100099u](https://doi.org/10.1021/ar100099u)

- (13) Hyster, T. K.; Ward, T. R., Genetic Optimization of Metalloenzymes: Enhancing Enzymes for Non-Natural Reactions, *Angew. Chem., Int. Ed.*, **2016**, *55* (26), 7344-7357.  
DOI: [10.1002/anie.201508816](https://doi.org/10.1002/anie.201508816)
- (14) Renata, H.; Wang, Z. J.; Arnold, F. H., Expanding the Enzyme Universe: Accessing Non-Natural Reactions by Mechanism-Guided Directed Evolution, *Angew. Chem., Int. Ed.*, **2015**, *54* (11), 3351-3367.  
DOI: [10.1002/anie.201409470](https://doi.org/10.1002/anie.201409470)
- (15) Ilie, A.; Reetz, M. T., Directed Evolution of Artificial Metalloenzymes, *Isr. J. Chem.*, **2015**, *55* (1), 51-60.  
DOI: [10.1002/ijch.201400087](https://doi.org/10.1002/ijch.201400087)
- (16) Reetz, M. T., Biocatalysis in Organic Chemistry and Biotechnology: Past, Present, and Future, *J. Am. Chem. Soc.*, **2013**, *135* (34), 12480-12496.  
DOI: [10.1021/ja405051f](https://doi.org/10.1021/ja405051f)
- (17) Bloom, J. D.; Arnold, F. H., In the light of directed evolution: Pathways of adaptive protein evolution, *Proc. Natl. Acad. Sci. U. S. A.*, **2009**, *106* (1), 9995-10000.  
DOI: [10.1073/pnas.0901522106](https://doi.org/10.1073/pnas.0901522106)
- (18) Dydio, P.; Key, H. M.; Nazarenko, A.; Rha, J. Y.; Seyedkazemi, V.; Clark, D. S.; Hartwig, J. F., An artificial metalloenzyme with the kinetics of native enzymes, *Science*, **2016**, *354* (6308), 102-106.  
DOI: [10.1126/science.aah4427](https://doi.org/10.1126/science.aah4427)
- (19) Khare, S. D.; Kipnis, Y.; Greisen, P., Jr.; Takeuchi, R.; Ashani, Y.; Goldsmith, M.; Song, Y.; Gallaher, J. L.; Silman, I.; Leader, H.; Sussman, J. L.; Stoddard, B. L.; Tawfik, D. S.; Baker, D., Computational redesign of a mononuclear zinc metalloenzyme for organophosphate hydrolysis, *Nat. Chem. Biol.*, **2012**, *8* (3), 294-300.  
DOI: [10.1038/nchembio.777](https://doi.org/10.1038/nchembio.777)
- (20) Deuss, P. J.; den Heeten, R.; Laan, W.; Kamer, P. C. J., Bioinspired Catalyst Design and Artificial Metalloenzymes, *Chem. - Eur. J.*, **2011**, *17* (17), 4680-4698.  
DOI: [10.1002/chem.201003646](https://doi.org/10.1002/chem.201003646)
- (21) Ball, Z. T., Designing Enzyme-like Catalysts: A Rhodium(II) Metallopeptide Case Study, *Acc. Chem. Res.*, **2013**, *46* (2), 560-570.  
DOI: [10.1021/ar300261h](https://doi.org/10.1021/ar300261h)
- (22) Zastrow, M. L.; Pecoraro, V. L., Designing functional metalloproteins: From structural to catalytic metal sites, *Coord. Chem. Rev.*, **2013**, *257* (17-18), 2565-2588.  
DOI: [10.1016/j.ccr.2013.02.007](https://doi.org/10.1016/j.ccr.2013.02.007)
- (23) Song, W. J.; Tezcan, F. A., A designed supramolecular protein assembly with *in vivo* enzymatic activity, *Science*, **2014**, *346* (6216), 1525-1528.  
DOI: [10.1126/science.1259680](https://doi.org/10.1126/science.1259680)
- (24) Kaplan, J.; DeGrado, W. F., *De novo* design of catalytic proteins, *Proc. Natl. Acad. Sci. U. S. A.*, **2004**, *101* (32), 11566-11570.  
DOI: [10.1073/pnas.0404387101](https://doi.org/10.1073/pnas.0404387101)
- (25) Faiella, M.; Andreozzi, C.; de Rosales, R. T. M.; Pavone, V.; Maglio, O.; Nistri, F.; DeGrado, W. F.; Lombardi, A., An artificial di-iron oxo-protein with phenol oxidase activity, *Nat. Chem. Biol.*, **2009**, *5* (12), 882-884.  
DOI: [10.1038/nchembio.257](https://doi.org/10.1038/nchembio.257)

- (26) Zastrow, M. L.; Peacock, A. F. A.; Stuckey, J. A.; Pecoraro, V. L., Hydrolytic catalysis and structural stabilization in a designed metalloprotein, *Nat. Chem.*, **2012**, *4*, 118-123.  
DOI: [10.1038/Nchem.1201](https://doi.org/10.1038/Nchem.1201)
- (27) Xiao, H.; Schultz, P. G., At the Interface of Chemical and Biological Synthesis: An Expanded Genetic Code, *Cold Spring Harbor Perspect. Biol.*, **2016**, *8* (9), 1-18.  
DOI: [10.1101/cshperspect.a023945](https://doi.org/10.1101/cshperspect.a023945)
- (28) Lee, H. S.; Schultz, P. G., Biosynthesis of a site-specific DNA cleaving protein, *J. Am. Chem. Soc.*, **2008**, *130* (40), 13194-13195.  
DOI: [10.1021/ja804653f](https://doi.org/10.1021/ja804653f)
- (29) Steinreiber, J.; Ward, T. R., Artificial metalloenzymes as selective catalysts in aqueous media, *Coord. Chem. Rev.*, **2008**, *252* (5-7), 751-766.  
DOI: [10.1016/j.ccr.2007.09.016](https://doi.org/10.1016/j.ccr.2007.09.016)
- (30) Stephanopoulos, N.; Francis, M. B., Choosing an effective protein bioconjugation strategy, *Nat. Chem. Biol.*, **2011**, *7* (12), 876-884.  
DOI: [10.1038/Nchembio.720](https://doi.org/10.1038/Nchembio.720)
- (31) Jing, Q.; Kazlauskas, R. J., Regioselective Hydroformylation of Styrene Using Rhodium-Substituted Carbonic Anhydrase, *ChemCatChem*, **2010**, *2* (8), 953-957.  
DOI: [10.1002/cctc.201000159](https://doi.org/10.1002/cctc.201000159)
- (32) Key, H. M.; Dydio, P.; Clark, D. S.; Hartwig, J. F., Abiological catalysis by artificial haem proteins containing noble metals in place of iron, *Nature*, **2016**, *534* (7608), 534-537.  
DOI: [10.1038/nature17968](https://doi.org/10.1038/nature17968)
- (33) Dydio, P.; Key, H. M.; Hayashi, H.; Clark, D. S.; Hartwig, J. F., Chemoselective, Enzymatic C-H Bond Amination Catalyzed by a Cytochrome P450 Containing an Ir(Me)-PIX Cofactor, *J. Am. Chem. Soc.*, **2017**, *139* (5), 1750-1753.  
DOI: [10.1021/jacs.6b11410](https://doi.org/10.1021/jacs.6b11410)
- (34) Wilchek, M.; Bayer, E. A.; Livnah, O., Essentials of biorecognition: The (strept)avidin–biotin system as a model for protein–protein and protein–ligand interaction, *Immunol. Lett.*, **2006**, *103* (1), 27-32.  
DOI: [10.1016/j.imlet.2005.10.022](https://doi.org/10.1016/j.imlet.2005.10.022)
- (35) Green, N. M., Spectrophotometric determination of avidin and biotin. In *Methods in Enzymology: Vitamins and Coenzymes*, McCormick, D. B.; Wright, L. D., Eds., Elsevier Inc.: Amsterdam, **1970**, Vol. 18, Part A, pp 418-424.  
DOI: [10.1016/0076-6879\(71\)18342-5](https://doi.org/10.1016/0076-6879(71)18342-5)
- (36) Weber, P. C.; Ohlendorf, D. H.; Wendoloski, J. J.; Salemme, F. R., Structural Origins of High-Affinity Biotin Binding to Streptavidin, *Science*, **1989**, *243* (4887), 85-88.  
DOI: [10.1126/science.2911722](https://doi.org/10.1126/science.2911722)
- (37) Hendrickson, W. A.; Pahler, A.; Smith, J. L.; Satow, Y.; Merritt, E. A.; Phizackerley, R. P., Crystal structure of core streptavidin determined from multiwavelength anomalous diffraction of synchrotron radiation, *Proc. Natl. Acad. Sci. U. S. A.*, **1989**, *86* (7), 2190-2194.
- (38) Livnah, O.; Bayer, E. A.; Wilchek, M.; Sussman, J. L., Three-dimensional structures of avidin and the avidin-biotin complex, *Proc. Natl. Acad. Sci. U. S. A.*, **1993**, *90* (11), 5076-5080.



- (39) Weber, P. C.; Wendoloski, J. J.; Pantoliano, M. W.; Salemme, F. R., Crystallographic and Thermodynamic Comparison of Natural and Synthetic Ligands Bound to Streptavidin, *J. Am. Chem. Soc.*, **1992**, *114* (9), 3197-3200.  
DOI: [10.1021/ja00035a004](https://doi.org/10.1021/ja00035a004)
- (40) Freitag, S.; Le Trong, I.; Chilkoti, A.; Klumb, L. A.; Stayton, P. S.; Stenkamp, R. E., Structural studies of binding site tryptophan mutants in the high-affinity streptavidin-biotin complex, *J. Mol. Biol.*, **1998**, *279* (1), 211-221.  
DOI: [10.1006/jmbi.1998.1735](https://doi.org/10.1006/jmbi.1998.1735)
- (41) Laitinen, O. H.; Airene, K. J.; Marttila, A. T.; Kulik, T.; Porkka, E.; Bayer, E. A.; Wilchek, M.; Kulomaa, M. S., Mutation of a critical tryptophan to lysine in avidin or streptavidin may explain why sea urchin fibropellin adopts an avidin-like domain, *FEBS Lett.*, **1999**, *461* (1-2), 52-58.  
DOI: [10.1016/S0014-5793\(99\)01423-4](https://doi.org/10.1016/S0014-5793(99)01423-4)
- (42) Freitag, S.; LeTrong, I.; Klumb, L.; Stayton, P. S.; Stenkamp, R. E., Structural studies of the streptavidin binding loop, *Protein Sci.*, **1997**, *6* (6), 1157-1166.  
DOI: [10.1002/pro.5560060604](https://doi.org/10.1002/pro.5560060604)
- (43) Bansal, N.; Zheng, Z.; Song, L. F.; Pei, J.; Merz, K. M., Jr., The Role of the Active Site Flap in Streptavidin/Biotin Complex Formation, *J. Am. Chem. Soc.*, **2018**, *140* (16), 5434-5446.  
DOI: [10.1021/jacs.8b00743](https://doi.org/10.1021/jacs.8b00743)
- (44) Sano, T.; Vajda, S.; Smith, C. L.; Cantor, C. R., Engineering subunit association of multisubunit proteins: A dimeric streptavidin, *Proc. Natl. Acad. Sci. U. S. A.*, **1997**, *94* (12), 6153-6158.
- (45) Qureshi, M. H.; Wong, S. L., Design, production, and characterization of a monomeric streptavidin and its application for affinity purification of biotinylated proteins, *Protein Expression Purif.*, **2002**, *25* (3), 409-415.  
DOI: [10.1016/S1046-5928\(02\)00021-9](https://doi.org/10.1016/S1046-5928(02)00021-9)
- (46) Wu, S. C.; Wong, S. L., Engineering soluble monomeric streptavidin with reversible biotin binding capability, *J. Biol. Chem.*, **2005**, *280* (24), 23225-23231.  
DOI: [10.1074/jbc.M501733200](https://doi.org/10.1074/jbc.M501733200)
- (47) Lim, K. H.; Huang, H.; Pralle, A.; Park, S., Engineered Streptavidin Monomer and Dimer with Improved Stability and Function, *Biochemistry*, **2011**, *50* (40), 8682-8691.  
DOI: [10.1021/bi2010366](https://doi.org/10.1021/bi2010366)
- (48) Katz, B. A., Binding of biotin to streptavidin stabilizes intersubunit salt bridges between Asp61 and His87 at low pH, *J. Mol. Biol.*, **1997**, *274* (5), 776-800.  
DOI: [10.1006/jmbi.1997.1444](https://doi.org/10.1006/jmbi.1997.1444)
- (49) Määttä, J. A. E.; Eisenberg-Domovich, Y.; Nordlund, H. R.; Hayouka, R.; Kulomaa, M. S.; Livnah, O.; Hytönen, V. P., Chimeric avidin shows stability against harsh chemical conditions—biochemical analysis and 3D structure, *Biotechnol. Bioeng.*, **2011**, *108* (3), 481-490.  
DOI: [10.1002/bit.22962](https://doi.org/10.1002/bit.22962)
- (50) Sano, T.; Pandori, M. W.; Chen, X.; Smith, C. L.; Cantor, C. R., Recombinant core streptavidins. A minimum-sized core streptavidin has enhanced structural stability and higher accessibility to biotinylated macromolecules, *J. Biol. Chem.*, **1995**, *270* (47), 28204-28209.  
DOI: [10.1074/jbc.270.47.28204](https://doi.org/10.1074/jbc.270.47.28204)

- (51) Bayer, E. A.; Ben-Hur, H.; Gitlin, G.; Wilchek, M., An improved method for the single-step purification of streptavidin, *J. Biochem. Biophys. Methods*, **1986**, *13* (2), 103-112.  
DOI: [10.1016/0165-022X\(86\)90022-9](https://doi.org/10.1016/0165-022X(86)90022-9)
- (52) González, M. n.; Argaraña, C. E.; Fidelio, G. D., Extremely high thermal stability of streptavidin and avidin upon biotin binding, *Biomol. Eng.*, **1999**, *16* (1), 67-72.  
DOI: [10.1016/S1050-3862\(99\)00041-8](https://doi.org/10.1016/S1050-3862(99)00041-8)
- (53) González, M.; Bagatolli, L. A.; Echabe, I.; Arrondo, J. L. R.; Argaraña, C. E.; Cantor, C. R.; Fidelio, G. D., Interaction of Biotin with Streptavidin: Thermostability and Conformational Changes upon Binding, *J. Biol. Chem.*, **1997**, *272* (17), 11288-11294.  
DOI: [10.1074/jbc.272.17.11288](https://doi.org/10.1074/jbc.272.17.11288)
- (54) Jones, M. L.; Kurzban, G. P., Noncooperativity of biotin binding to tetrameric streptavidin, *Biochemistry*, **1995**, *34* (37), 11750-11756.  
DOI: [10.1021/bi00037a012](https://doi.org/10.1021/bi00037a012)
- (55) Kada, G.; Falk, H.; Gruber, H. J., Accurate measurement of avidin and streptavidin in crude biofluids with a new, optimized biotin-fluorescein conjugate, *Biochim. Biophys. Acta*, **1999**, *1427* (1), 33-43.  
DOI: [10.1016/S0304-4165\(98\)00178-0](https://doi.org/10.1016/S0304-4165(98)00178-0)
- (56) Sano, T.; Cantor, C. R., Expression of a Cloned Streptavidin Gene in *Escherichia coli*, *Proc. Natl. Acad. Sci. U. S. A.*, **1990**, *87* (1), 142-146.
- (57) Rosano, G. L.; Ceccarelli, E. A., Recombinant protein expression in *Escherichia coli*: advances and challenges, *Front. Microbiol.*, **2014**, *5* (172), 1-17.  
DOI: [10.3389/fmicb.2014.00172](https://doi.org/10.3389/fmicb.2014.00172)
- (58) Laitinen, O. H.; Hytonen, V. P.; Nordlund, H. R.; Kulomaa, M. S., Genetically engineered avidins and streptavidins, *Cell. Mol. Life Sci.*, **2006**, *63* (24), 2992-3017.  
DOI: [10.1007/s00018-006-6288-z](https://doi.org/10.1007/s00018-006-6288-z)
- (59) Laitinen, O. H.; Nordlund, H. R.; Hytonen, V. P.; Kulomaa, M. S., Brave new (strept)avidins in biotechnology, *Trends Biotechnol.*, **2007**, *25* (6), 269-277.  
DOI: [10.1016/j.tibtech.2007.04.001](https://doi.org/10.1016/j.tibtech.2007.04.001)
- (60) Dürrenberger, M.; Heinisch, T.; Wilson, Y. M.; Rossel, T.; Nogueira, E.; Knörr, L.; Mutschler, A.; Kersten, K.; Zimbron, M. J.; Pierron, J.; Schirmer, T.; Ward, T. R., Artificial Transfer Hydrogenases for the Enantioselective Reduction of Cyclic Imines, *Angew. Chem., Int. Ed.*, **2011**, *50* (13), 3026-3029.  
DOI: [10.1002/anie.201007820](https://doi.org/10.1002/anie.201007820)
- (61) Schwizer, F.; Köhler, V.; Dürrenberger, M.; Knörr, L.; Ward, T. R., Genetic Optimization of the Catalytic Efficiency of Artificial Imine Reductases Based on Biotin-Streptavidin Technology, *ACS Catal.*, **2013**, *3* (8), 1752-1755.  
DOI: [10.1021/cs400428r](https://doi.org/10.1021/cs400428r)
- (62) Quinto, T.; Schwizer, F.; Zimbron, J. M.; Morina, A.; Köhler, V.; Ward, T. R., Expanding the Chemical Diversity in Artificial Imine Reductases Based on the Biotin- Streptavidin Technology, *ChemCatChem*, **2014**, *6* (4), 1010-1014.  
DOI: [10.1002/cctc.201300825](https://doi.org/10.1002/cctc.201300825)
- (63) Hesticová, M.; Heinisch, T.; Alonso-Cotchico, L.; Maréchal, J.-D.; Vidossich, P.; Ward, T. R., Directed Evolution of an Artificial Imine Reductase, *Angew. Chem., Int. Ed.*, **2018**, *57* (7), 1863-1868.  
DOI: [10.1002/anie.201711016](https://doi.org/10.1002/anie.201711016)

- (64) Jeschek, M.; Reuter, R.; Heinisch, T.; Trindler, C.; Klehr, J.; Panke, S.; Ward, T. R., Directed evolution of artificial metalloenzymes for *in vivo* metathesis, *Nature*, **2016**, 537 (7622), 661-665.  
DOI: [10.1038/nature19114](https://doi.org/10.1038/nature19114)
- (65) Hyster, T. K.; Knörr, L.; Ward, T. R.; Rovis, T., Biotinylated Rh(III) Complexes in Engineered Streptavidin for Accelerated Asymmetric C-H Activation, *Science*, **2012**, 338 (6106), 500-503.  
DOI: [10.1126/science.1226132](https://doi.org/10.1126/science.1226132)
- (66) Cotelle, Y.; Lebrun, V.; Sakai, N.; Ward, T. R.; Matile, S., Anion- $\pi$  Enzymes, *ACS Cent. Sci.*, **2016**, 2 (6), 388-393.  
DOI: [10.1021/acscentsci.6b00097](https://doi.org/10.1021/acscentsci.6b00097)
- (67) Chatterjee, A.; Mallin, H.; Klehr, J.; Vallapurackal, J.; Finke, A. D.; Vera, L.; Marsh, M.; Ward, T. R., An Enantioselective Artificial Suzukiase based on the Biotin-Streptavidin Technology, *Chem. Sci.*, **2016**, 7 (1), 673-677.  
DOI: [10.1039/c5sc03116h](https://doi.org/10.1039/c5sc03116h)
- (68) Köhler, V.; Mao, J. C.; Heinisch, T.; Pordea, A.; Sardo, A.; Wilson, Y. M.; Knörr, L.; Creus, M.; Prost, J. C.; Schirmer, T.; Ward, T. R., OsO<sub>4</sub> · Streptavidin: A Tunable Hybrid Catalyst for the Enantioselective *cis*-Dihydroxylation of Olefins, *Angew. Chem., Int. Ed.*, **2011**, 50 (46), 10863-10866.  
DOI: [10.1002/anie.201103632](https://doi.org/10.1002/anie.201103632)
- (69) Heinisch, T.; Ward, T. R., Artificial Metalloenzymes Based on the Biotin-Streptavidin Technology: Challenges and Opportunities, *Acc. Chem. Res.*, **2016**, 49 (9), 1711-1721.  
DOI: [10.1021/acs.accounts.6b00235](https://doi.org/10.1021/acs.accounts.6b00235)
- (70) Köhler, V.; Wilson, Y. M.; Dürrenberger, M.; Ghislieri, D.; Churakova, E.; Quinto, T.; Knörr, L.; Häussinger, D.; Hollmann, F.; Turner, N. J.; Ward, T. R., Synthetic cascades are enabled by combining biocatalysts with artificial metalloenzymes, *Nat. Chem.*, **2013**, 5 (2), 93-99.  
DOI: [10.1038/Nchem.1498](https://doi.org/10.1038/Nchem.1498)
- (71) Okamoto, Y.; Köhler, V.; Ward, T. R., An NAD(P)H-Dependent Artificial Transfer Hydrogenase for Multienzymatic Cascades, *J. Am. Chem. Soc.*, **2016**, 138 (18), 5781-5784.  
DOI: [10.1021/jacs.6b02470](https://doi.org/10.1021/jacs.6b02470)
- (72) *Topics in Organometallic Chemistry*, Springer-Verlag: Heidelberg, **2012**, Vol. 38, p 345.  
DOI: [10.1007/978-3-642-22749-3](https://doi.org/10.1007/978-3-642-22749-3)
- (73) Pfaltz, A.; Lautens, M., Allylic Substitution Reactions. In *Comprehensive Asymmetric Catalysis*, Jacobsen, E. N.; Pfaltz, A.; Yamamoto, H., Eds., Springer-Verlag: Heidelberg, **2004**, pp 1-52.
- (74) Sundararaju, B.; Achard, M.; Bruneau, C., Transition metal catalyzed nucleophilic allylic substitution: activation of allylic alcohols via  $\pi$ -allylic species, *Chem. Soc. Rev.*, **2012**, 41 (12), 4467-4483.  
DOI: [10.1039/C2CS35024F](https://doi.org/10.1039/C2CS35024F)
- (75) Butt, N. A.; Zhang, W., Transition metal-catalyzed allylic substitution reactions with unactivated allylic substrates, *Chem. Soc. Rev.*, **2015**, 44 (22), 7929-7967.  
DOI: [10.1039/c5cs00144g](https://doi.org/10.1039/c5cs00144g)
- (76) Lu, Z.; Ma, S., Metal-catalyzed enantioselective allylation in asymmetric synthesis, *Angew. Chem., Int. Ed.*, **2008**, 47 (2), 258-297.  
DOI: [10.1002/anie.200605113](https://doi.org/10.1002/anie.200605113)

- (77) Trost, B. M., Asymmetric allylic alkylation, an enabling methodology, *J. Org. Chem.*, **2004**, *69* (18), 5813-5837.  
DOI: [10.1021/jo0491004](https://doi.org/10.1021/jo0491004)
- (78) Agrofoglio, L. A.; Gillaizeau, I.; Saito, Y., Palladium-assisted routes to nucleosides, *Chem. Rev.*, **2003**, *103* (5), 1875-1916.  
DOI: [10.1021/cr010374g](https://doi.org/10.1021/cr010374g)
- (79) Hartwig, J. F.; Stanley, L. M., Mechanistically driven development of iridium catalysts for asymmetric allylic substitution, *Acc. Chem. Res.*, **2010**, *43* (12), 1461-1475.  
DOI: [10.1021/ar100047x](https://doi.org/10.1021/ar100047x)
- (80) Bruneau, C.; Achard, M., Allylic ruthenium(IV) complexes in catalysis, *Coord. Chem. Rev.*, **2012**, *256* (5), 525-536.  
DOI: [10.1016/j.ccr.2011.10.018](https://doi.org/10.1016/j.ccr.2011.10.018)
- (81) Evans, P. A.; Nelson, J. D., Conservation of Absolute Configuration in the Acyclic Rhodium-Catalyzed Allylic Alkylation Reaction: Evidence for an Enyl ( $\sigma + \pi$ ) Organorhodium Intermediate, *J. Am. Chem. Soc.*, **1998**, *120* (22), 5581-5582.  
DOI: [10.1021/ja980030g](https://doi.org/10.1021/ja980030g)
- (82) Belda, O.; Moberg, C., Molybdenum-catalyzed asymmetric allylic alkylations, *Acc. Chem. Res.*, **2004**, *37* (3), 159-167.  
DOI: [10.1021/ar030239v](https://doi.org/10.1021/ar030239v)
- (83) Malkov, A. V.; Baxendale, I. R.; Dvorak, D.; Mansfield, D. J.; Kocovsky, P., Molybdenum(II)- and Tungsten(II)-Catalyzed Allylic Substitution, *J. Org. Chem.*, **1999**, *64* (8), 2737-2750.  
DOI: [10.1021/jo9821776](https://doi.org/10.1021/jo9821776)
- (84) Castaño, A. M.; Aranyos, A.; Szabó, K. J.; Bäckvall, J.-E., Nucleophilic Attack on ( $\pi$ -allyl)palladium Complexes: Direction of the Attack to the Central or Terminal Carbon Atom by Ligand Control, *Angew. Chem., Int. Ed.*, **1995**, *34* (22), 2551-2553.  
DOI: [10.1002/anie.199525511](https://doi.org/10.1002/anie.199525511)
- (85) Saburi, H.; Tanaka, S.; Kitamura, M., Catalytic dehydrative allylation of alcohols, *Angew. Chem., Int. Ed.*, **2005**, *44* (11), 1730-1732.  
DOI: [10.1002/anie.200462513](https://doi.org/10.1002/anie.200462513)
- (86) Tanaka, S.; Saburi, H.; Ishibashi, Y.; Kitamura, M., CpRu<sup>II</sup>PF<sub>6</sub>/quinaldic acid-catalyzed chemoselective allyl ether cleavage. A simple and practical method for hydroxyl deprotection, *Org. Lett.*, **2004**, *6* (11), 1873-1875.  
DOI: [10.1021/ol0493397](https://doi.org/10.1021/ol0493397)
- (87) Tanaka, S.; Saburi, H.; Murase, T.; Ishibashi, Y.; Kitamura, M., Highly reactive and chemoselective cleavage of allyl esters using an air- and moisture-stable [CpRu(IV)( $\pi$ -C<sub>3</sub>H<sub>5</sub>)(2-quinolinecarboxylato)]PF<sub>6</sub> catalyst, *J. Organomet. Chem.*, **2007**, *692* (1), 295-298.  
DOI: [10.1016/j.jorganchem.2006.03.046](https://doi.org/10.1016/j.jorganchem.2006.03.046)
- (88) Zhang, H.-J.; Demerseman, B.; Toupet, L.; Xi, Z.; Bruneau, C., Novel [Ruthenium(substituted-tetramethylcyclopentadiene) (2-quinolinecarboxylato)(allyl)] Hexafluorophosphate Complexes as Efficient Catalysts for Highly Regioselective Nucleophilic Substitution of Aliphatic Allylic Substrates, *Adv. Synth. Catal.*, **2008**, *350* (10), 1601-1609.  
DOI: [10.1002/adsc.200800135](https://doi.org/10.1002/adsc.200800135)

- (89) Kieseewetter, M. K.; Waymouth, R. M., Kinetics of an Air- and Water-Stable Ruthenium(IV) Catalyst for the Deprotection of Allyl Alcohol in Water, *Organometallics*, **2010**, *29* (22), 6051-6056.  
DOI: [10.1021/om100892v](https://doi.org/10.1021/om100892v)
- (90) Hirakawa, T.; Tanaka, S.; Usuki, N.; Kanzaki, H.; Kishimoto, M.; Kitamura, M., A Magnetically Separable Heterogeneous Deallylation Catalyst: [CpRu( $\eta^3$ -C<sub>3</sub>H<sub>5</sub>)(2-pyridinecarboxylato)]PF<sub>6</sub> Complex Supported on a Ferromagnetic Microsize Particle Fe<sub>3</sub>O<sub>4</sub>@SiO<sub>2</sub>, *Eur. J. Inorg. Chem.*, **2009**, *2009* (6), 789-792.  
DOI: [10.1002/ejoc.200801166](https://doi.org/10.1002/ejoc.200801166)
- (91) Tanaka, S.; Pradhan, P. K.; Maegawa, Y.; Kitamura, M., Highly efficient catalytic dehydrative S-allylation of thiols and thioic S-acids, *Chem. Commun.*, **2010**, *46* (22), 3996-3998.  
DOI: [10.1039/c0cc00096e](https://doi.org/10.1039/c0cc00096e)
- (92) Kondo, T.; Morisaki, Y.; Uenoyama, S.; Wada, K.; Mitsudo, T., First ruthenium-catalyzed allylation of thiols enables the general synthesis of allylic sulfides, *J. Am. Chem. Soc.*, **1999**, *121* (37), 8657-8658.  
DOI: [10.1021/ja991704f](https://doi.org/10.1021/ja991704f)
- (93) Streu, C.; Meggers, E., Ruthenium-induced allylcarbamate cleavage in living cells, *Angew. Chem., Int. Ed.*, **2006**, *45* (34), 5645-5648.  
DOI: [10.1002/anie.200601752](https://doi.org/10.1002/anie.200601752)
- (94) Völker, T.; Dempwolff, F.; Graumann, P. L.; Meggers, E., Progress towards Bioorthogonal Catalysis with Organometallic Compounds, *Angew. Chem., Int. Ed.*, **2014**, *53* (39), 10536-10540.  
DOI: [10.1002/anie.201404547](https://doi.org/10.1002/anie.201404547)
- (95) Völker, T.; Meggers, E., Chemical Activation in Blood Serum and Human Cell Culture: Improved Ruthenium Complex for Catalytic Uncaging of Alloc-Protected Amines, *ChemBioChem*, **2017**, *18* (12), 1083-1086.  
DOI: [10.1002/cbic.201700168](https://doi.org/10.1002/cbic.201700168)
- (96) Tanaka, S. J.; Saburi, H.; Hirakawa, T.; Seki, T.; Kitamura, M., Dehydrative Allylation of Alcohols and Deallylation of Allyl Ethers Catalyzed by [CpRu(CH<sub>3</sub>CN)<sub>3</sub>]PF<sub>6</sub> and 2-Pyridinecarboxylic Acid Derivatives. Effect of  $\pi$ -Accepting Ability and COOH Acidity of Ligand on Reactivity, *Chem. Lett.*, **2009**, *38* (2), 188-189.  
DOI: [10.1246/cl.2009.188](https://doi.org/10.1246/cl.2009.188)
- (97) Trost, B. M.; Toste, F. D.; Pinkerton, A. B., Non-metathesis ruthenium-catalyzed C-C bond formation, *Chem. Rev.*, **2001**, *101* (7), 2067-2096.  
DOI: [10.1021/cr000666b](https://doi.org/10.1021/cr000666b)
- (98) Li, J.; Chen, P. R., Development and application of bond cleavage reactions in bioorthogonal chemistry, *Nat. Chem. Biol.*, **2016**, *12* (3), 129-137.  
DOI: [10.1038/nchembio.2024](https://doi.org/10.1038/nchembio.2024)
- (99) Bai, Y.; Chen, J.; Zimmerman, S. C., Designed transition metal catalysts for intracellular organic synthesis, *Chem. Soc. Rev.*, **2018**, *47* (5), 1811-1821.  
DOI: [10.1039/c7cs00447h](https://doi.org/10.1039/c7cs00447h)
- (100) Sánchez, M. I.; Penas, C.; Vázquez, M. E.; Mascareñas, J. L., Metal-catalyzed uncaging of DNA-binding agents in living cells, *Chem. Sci.*, **2014**, *2014* (5), 1901-1907.  
DOI: [10.1039/c3sc53317d](https://doi.org/10.1039/c3sc53317d)

- (101) Tomas-Gamasa, M.; Martinez-Calvo, M.; Couceiro, J. R.; Mascareñas, J. L., Transition metal catalysis in the mitochondria of living cells, *Nat. Commun.*, **2016**, 7 (12538), 1-10.  
DOI: [10.1038/ncomms12538](https://doi.org/10.1038/ncomms12538)
- (102) Tonga, G. Y.; Jeong, Y.; Duncan, B.; Mizuhara, T.; Mout, R.; Das, R.; Kim, S. T.; Yeh, Y.-C.; Yan, B.; Hou, S.; Rotello, V. M., Supramolecular regulation of bioorthogonal catalysis in cells using nanoparticle-embedded transition metal catalysts, *Nat. Chem.*, **2015**, 7, 597-603.  
DOI: [10.1038/nchem.2284](https://doi.org/10.1038/nchem.2284)
- (103) Wilson, Y. M.; Dürrenberger, M.; Nogueira, E. S.; Ward, T. R., Neutralizing the detrimental effect of glutathione on precious metal catalysts, *J. Am. Chem. Soc.*, **2014**, 136 (25), 8928-8932.  
DOI: [10.1021/ja500613n](https://doi.org/10.1021/ja500613n)
- (104) Hsu, H.-T.; Trantow, B. M.; Waymouth, R. M.; Wender, P. A., Bioorthogonal Catalysis: A General Method To Evaluate Metal-Catalyzed Reactions in Real Time in Living Systems Using a Cellular Luciferase Reporter System, *Bioconjug. Chem.*, **2016**, 27 (2), 376-382.  
DOI: [10.1021/acs.bioconjchem.5b00469](https://doi.org/10.1021/acs.bioconjchem.5b00469)
- (105) Yusop, R. M.; Unciti-Broceta, A.; Johansson, E. M.; Sanchez-Martin, R. M.; Bradley, M., Palladium-mediated intracellular chemistry, *Nat. Chem.*, **2011**, 3 (3), 239-243.  
DOI: [10.1038/nchem.981](https://doi.org/10.1038/nchem.981)
- (106) Li, J.; Yu, J.; Zhao, J.; Wang, J.; Zheng, S.; Lin, S.; Chen, L.; Yang, M.; Jia, S.; Zhang, X.; Chen, P. R., Palladium-triggered deprotection chemistry for protein activation in living cells, *Nat. Chem.*, **2014**, 6 (4), 352-361.  
DOI: [10.1038/nchem.1887](https://doi.org/10.1038/nchem.1887)
- (107) Ritter, C.; Nett, N.; Acevedo-Rocha, C. G.; Lonsdale, R.; Kraling, K.; Dempwolff, F.; Hoebenreich, S.; Graumann, P. L.; Reetz, M. T.; Meggers, E., Bioorthogonal Enzymatic Activation of Caged Compounds, *Angew. Chem., Int. Ed.*, **2015**, 54 (45), 13440-13443.  
DOI: [10.1002/anie.201506739](https://doi.org/10.1002/anie.201506739)
- (108) Brieke, C.; Rohrbach, F.; Gottschalk, A.; Mayer, G.; Heckel, A., Light-Controlled Tools, *Angew. Chem., Int. Ed.*, **2012**, 51 (34), 8446-8476.  
DOI: [10.1002/anie.201202134](https://doi.org/10.1002/anie.201202134)
- (109) Young, D. D.; Deiters, A., Photochemical activation of protein expression in bacterial cells, *Angew. Chem., Int. Ed.*, **2007**, 46 (23), 4290-4292.  
DOI: [10.1002/anie.200700057](https://doi.org/10.1002/anie.200700057)
- (110) Binder, D.; Grunberger, A.; Loeschcke, A.; Probst, C.; Bier, C.; Pietruszka, J.; Wiechert, W.; Kohlheyer, D.; Jaeger, K.-E.; Drepper, T., Light-responsive control of bacterial gene expression: precise triggering of the lac promoter activity using photocaged IPTG, *Integr. Biol.*, **2014**, 6 (8), 755-765.  
DOI: [10.1039/C4IB00027G](https://doi.org/10.1039/C4IB00027G)
- (111) Binder, D.; Bier, C.; Grunberger, A.; Drobiez, D.; Hage-Hulsmann, J.; Wandrey, G.; Buchs, J.; Kohlheyer, D.; Loeschcke, A.; Wiechert, W.; Jaeger, K. E.; Pietruszka, J.; Drepper, T., Photocaged Arabinose: A Novel Optogenetic Switch for Rapid and Gradual Control of Microbial Gene Expression, *ChemBioChem*, **2016**, 17 (4), 296-299.  
DOI: [10.1002/cbic.201500609](https://doi.org/10.1002/cbic.201500609)
- (112) Shibata, A.; Ito, Y.; Abe, H., RNA-templated molecule release induced protein expression in bacterial cells, *Chem. Commun.*, **2013**, 49 (3), 270-272.  
DOI: [10.1039/c2cc37826d](https://doi.org/10.1039/c2cc37826d)

- (113) Chou, C.; Young, D. D.; Deiters, A., Photocaged T7 RNA polymerase for the light activation of transcription and gene function in pro- and eukaryotic cells, *ChemBioChem*, **2010**, *11* (7), 972-977.  
DOI: [10.1002/cbic.201000041](https://doi.org/10.1002/cbic.201000041)
- (114) Pregosin, P. S.; Kumar, P. G. A.; Fernández, I., Pulsed gradient spin-echo (PGSE) diffusion and  $^1\text{H}$ ,  $^{19}\text{F}$  heteronuclear overhauser spectroscopy (HOESY) NMR methods in inorganic and organometallic chemistry: Something old and something new, *Chem. Rev.*, **2005**, *105* (8), 2977-2998.  
DOI: [10.1021/cr0406716](https://doi.org/10.1021/cr0406716)
- (115) Neufeld, R.; Stalke, D., Accurate molecular weight determination of small molecules via DOSY-NMR by using external calibration curves with normalized diffusion coefficients, *Chem. Sci.*, **2015**, *6* (6), 3354-3364.  
DOI: [10.1039/c5sc00670h](https://doi.org/10.1039/c5sc00670h)
- (116) Green, N. M., Avidin and streptavidin. In *Methods in Enzymology: Avidin-Biotin Technology*, Wilchek, M.; Bayer, E. A., Eds., Elsevier Inc.: Amsterdam, **1990**, Vol. 184, pp 51-67.  
DOI: [10.1016/0076-6879\(90\)84259-J](https://doi.org/10.1016/0076-6879(90)84259-J)
- (117) Repo, S.; Paidanius, T. A.; Hytonen, V. P.; Nyholm, T. K. M.; Hailing, K. K.; Huuskonen, J.; Pentikainen, T.; Rissanen, K.; Slotte, J. P.; Airene, T. T.; Salminen, T. A.; Kulomaa, M. S.; Johnson, M. S., Binding properties of HABA-type azo derivatives to avidin and avidin-related protein 4, *Chem. Biol.*, **2006**, *13* (10), 1029-1039.  
DOI: [10.1016/j.chembiol.2006.08.006](https://doi.org/10.1016/j.chembiol.2006.08.006)
- (118) Heinisch, T.; Schwizer, F.; Garabedian, B.; Csibra, E.; Jeschek, M.; Vallapurackal, J.; Pinheiro, V. B.; Marlière, P.; Panke, S.; Ward, T. R., *E. coli* surface display of streptavidin for directed evolution of an allylic deallylase, *Chem. Sci.*, **2018**, Manuscript under revision.
- (119) Sato, E.; Matsuhisa, A.; Sakashita, M.; Kanaoka, Y., New Water-Soluble Fluorogenic Amine: 7-Aminocoumarin-4-methanesulfonic Acid (ACMS) and Related Substrates for Proteinases, *Chem. Pharm. Bull.*, **1988**, *36* (9), 3496-3502.  
DOI: [10.1248/cpb.36.3496](https://doi.org/10.1248/cpb.36.3496)
- (120) Woronoff, G.; El Harrak, A.; Mayot, E.; Schicke, O.; Miller, O. J.; Soumillion, P.; Griffiths, A. D.; Ryckelynck, M., New Generation of Amino Coumarin Methyl Sulfonate-Based Fluorogenic Substrates for Amidase Assays in Droplet-Based Microfluidic Applications, *Anal. Chem.*, **2011**, *83* (8), 2852-2857.  
DOI: [10.1021/ac200373n](https://doi.org/10.1021/ac200373n)
- (121) Schürmann, J.; Quehl, P.; Festel, G.; Jose, J., Bacterial whole-cell biocatalysts by surface display of enzymes: toward industrial application, *Appl. Microbiol. Biotechnol.*, **2014**, *98* (19), 8031-8046.  
DOI: [10.1007/s00253-014-5897-y](https://doi.org/10.1007/s00253-014-5897-y)
- (122) Yang, C.; Zhao, Q.; Liu, Z.; Li, Q.; Qiao, C.; Mulchandani, A.; Chen, W., Cell surface display of functional macromolecule fusions on *Escherichia coli* for development of an autofluorescent whole-cell biocatalyst, *Environ. Sci. Technol.*, **2008**, *42* (16), 6105-6110.  
DOI: [10.1021/es800441t](https://doi.org/10.1021/es800441t)
- (123) Grimm, A. R.; Sauer, D. F.; Polen, T.; Zhu, L.; Hayashi, T.; Okuda, J.; Schwaneberg, U., A Whole Cell *E. coli* Display Platform for Artificial Metalloenzymes: Poly(phenylacetylene) Production with a Rhodium-Nitrobindin Metalloprotein, *ACS Catal.*, **2018**, *8* (3), 2611-2614.  
DOI: [10.1021/acscatal.7b04369](https://doi.org/10.1021/acscatal.7b04369)

- (124) Becker, S.; Höbenreich, H.; Vogel, A.; Knorr, J.; Wilhelm, S.; Rosenau, F.; Jaeger, K.-E.; Reetz, M. T.; Kolmar, H., Single-Cell High-Throughput Screening To Identify Enantioselective Hydrolytic Enzymes, *Angew. Chem., Int. Ed.*, **2008**, *47* (27), 5085-5088.  
DOI: [10.1002/anie.200705236](https://doi.org/10.1002/anie.200705236)
- (125) Peschke, T.; Rabe, K. S.; Niemeyer, C. M., Orthogonal Surface Tags for Whole-Cell Biocatalysis, *Angew. Chem., Int. Ed.*, **2017**, *56* (8), 2183-2186.  
DOI: [10.1002/anie.201609590](https://doi.org/10.1002/anie.201609590)
- (126) van Bloois, E.; Winter, R. T.; Kolmar, H.; Fraaije, M. W., Decorating microbes: surface display of proteins on *Escherichia coli*, *Trends Biotechnol.*, **2011**, *29* (2), 79-86.  
DOI: [10.1016/j.tibtech.2010.11.003](https://doi.org/10.1016/j.tibtech.2010.11.003)
- (127) Park, M.; Jose, J.; Thömmes, S.; Kim, J.-I.; Kang, M.-J.; Pyun, J.-C., Autodisplay of streptavidin, *Enzyme Microb. Technol.*, **2011**, *48* (4), 307-311.  
DOI: [10.1016/j.enzmictec.2010.12.006](https://doi.org/10.1016/j.enzmictec.2010.12.006)
- (128) Volkmer, B.; Heinemann, M., Condition-dependent cell volume and concentration of *Escherichia coli* to facilitate data conversion for systems biology modeling, *PLoS One*, **2011**, *6* (7), e23126 (1-6).  
DOI: [10.1371/journal.pone.0023126](https://doi.org/10.1371/journal.pone.0023126)
- (129) Earhart, C. F., Use of an Lpp-OmpA fusion vehicle for bacterial surface display. In *Methods in Enzymology: Applications of Chimeric Genes and Hybrid Proteins Part A: Gene Expression and Protein Purification*, Thorner, J.; Emr, S. D.; Abelson, J. N., Eds., Elsevier Inc.: Amsterdam, **2000**, Vol. 326, pp 506-516.  
DOI: [10.1016/S0076-6879\(00\)26072-2](https://doi.org/10.1016/S0076-6879(00)26072-2)
- (130) Stathopoulos, C.; Georgiou, G.; Earhart, C. F., Characterization of *Escherichia coli* expressing an Lpp'OmpA(46-159)-PhoA fusion protein localized in the outer membrane, *Appl. Microbiol. Biotechnol.*, **1996**, *45*, 112-119.  
DOI: [10.1007/s002530050657](https://doi.org/10.1007/s002530050657)
- (131) Francisco, J. A.; Earhart, C. F.; Georgiou, G., Transport and anchoring of  $\beta$ -lactamase to the external surface of *Escherichia coli*, *Proc. Natl. Acad. Sci. U. S. A.*, **1992**, *89* (7), 2713-2717.
- (132) Mallin, H.; Hestericová, M.; Reuter, R.; Ward, T. R., Library design and screening protocol for artificial metalloenzymes based on the biotin-streptavidin technology, *Nat. Protoc.*, **2016**, *11* (5), 835-852.  
DOI: [10.1038/nprot.2016.019](https://doi.org/10.1038/nprot.2016.019)
- (133) Lim, K. H.; Huang, H.; Pralle, A.; Park, S., Stable, high-affinity streptavidin monomer for protein labeling and monovalent biotin detection, *Biotechnol. Bioeng.*, **2013**, *110* (1), 57-67.  
DOI: [10.1002/bit.24605](https://doi.org/10.1002/bit.24605)
- (134) DSS and BS<sup>3</sup> Crosslinkers - User Manual, Thermo Fisher Scientific Inc., **2012**, 1-3.
- (135) Rivera, S.; Burns, J. L.; Vansuch, G. E.; Chica, B.; Weinert, E. E., Globin domain interactions control heme pocket conformation and oligomerization of globin coupled sensors, *J. Inorg. Biochem.*, **2016**, *164*, 70-76.  
DOI: [10.1016/j.jinorgbio.2016.08.016](https://doi.org/10.1016/j.jinorgbio.2016.08.016)
- (136) Shi, J.-M.; Pei, J.; Liu, E.-Q.; Zhang, L., Bis(sulfosuccinimidyl) suberate (BS3) crosslinking analysis of the behavior of amyloid- $\beta$  peptide in solution and in phospholipid membranes, *PLoS One*, **2017**, *12*(3) (e0173871), 1-13.  
DOI: [10.1371/journal.pone.0173871](https://doi.org/10.1371/journal.pone.0173871)



- (137) Andreoni, A.; Nardo, L.; Rigler, R., Time-resolved homo-FRET studies of biotin-streptavidin complexes, *J. Photochem. Photobiol. B*, **2016**, *162*, 656-662.  
DOI: [10.1016/j.jphotobiol.2016.07.042](https://doi.org/10.1016/j.jphotobiol.2016.07.042)
- (138) FRET and FLIM techniques. In *Laboratory Techniques in Biochemistry and Molecular Biology*, Gadella, T. W. J.; van der Vliet, P. C.; Pillai, S., Eds., Elsevier Inc.: Amsterdam, **2009**, Vol. 33, pp 1-534.  
DOI: [10.1016/S0075-7535\(08\)00017-X](https://doi.org/10.1016/S0075-7535(08)00017-X)
- (139) Rassam, P.; Copeland, N. A.; Birkholz, O.; Toth, C.; Chavent, M.; Duncan, A. L.; Cross, S. J.; Housden, N. G.; Kaminska, R.; Seger, U.; Quinn, D. M.; Garrod, T. J.; Sansom, M. S.; Piehler, J.; Baumann, C. G.; Kleantous, C., Supramolecular assemblies underpin turnover of outer membrane proteins in bacteria, *Nature*, **2015**, *523* (7560), 333-336.  
DOI: [10.1038/nature14461](https://doi.org/10.1038/nature14461)
- (140) Chao, G.; Lau, W. L.; Hackel, B. J.; Sazinsky, S. L.; Lippow, S. M.; Wittrup, K. D., Isolating and engineering human antibodies using yeast surface display, *Nat. Protoc.*, **2006**, *1* (2), 755-768.  
DOI: [10.1038/nprot.2006.94](https://doi.org/10.1038/nprot.2006.94)
- (141) Song, W. J.; Yu, J.; Tezcan, F. A., Importance of scaffold flexibility/rigidity in the design and directed evolution of artificial metallo- $\beta$ -lactamases, *J. Am. Chem. Soc.*, **2017**, *139* (46), 16772-16779.  
DOI: [10.1021/jacs.7b08981](https://doi.org/10.1021/jacs.7b08981)
- (142) Reetz, M. T.; Carballeira, J. D., Iterative saturation mutagenesis (ISM) for rapid directed evolution of functional enzymes, *Nat. Protoc.*, **2007**, *2* (4), 891-903.  
DOI: [10.1038/nprot.2007.72](https://doi.org/10.1038/nprot.2007.72)
- (143) Reetz, M. T.; Kahakeaw, D.; Lohmer, R., Addressing the numbers problem in directed evolution, *ChemBioChem*, **2008**, *9* (11), 1797-1804.  
DOI: [10.1002/cbic.200800298](https://doi.org/10.1002/cbic.200800298)
- (144) Kille, S.; Acevedo-Rocha, C. G.; Parra, L. P.; Zhang, Z. G.; Opperman, D. J.; Reetz, M. T.; Acevedo, J. P., Reducing Codon Redundancy and Screening Effort of Combinatorial Protein Libraries Created by Saturation Mutagenesis, *ACS Synth. Biol.*, **2013**, *2* (2), 83-92.  
DOI: [10.1021/sb300037w](https://doi.org/10.1021/sb300037w)
- (145) Baret, J. C.; Miller, O. J.; Taly, V.; Ryckelynck, M.; El-Harrak, A.; Frenz, L.; Rick, C.; Samuels, M. L.; Hutchison, J. B.; Agresti, J. J.; Link, D. R.; Weitz, D. A.; Griffiths, A. D., Fluorescence-activated droplet sorting (FADS): efficient microfluidic cell sorting based on enzymatic activity, *Lab Chip*, **2009**, *9* (13), 1850-1858.  
DOI: [10.1039/b902504a](https://doi.org/10.1039/b902504a)
- (146) Guo, M. T.; Rotem, A.; Heyman, J. A.; Weitz, D. A., Droplet microfluidics for high-throughput biological assays, *Lab Chip*, **2012**, *12* (12), 2146-2155.  
DOI: [10.1039/c2lc21147e](https://doi.org/10.1039/c2lc21147e)
- (147) Tawfik, D. S.; Griffiths, A. D., Man-made cell-like compartments for molecular evolution, *Nat. Biotechnol.*, **1998**, *16* (7), 652-656.  
DOI: [10.1038/nbt0798-652](https://doi.org/10.1038/nbt0798-652)
- (148) Obexer, R.; Godina, A.; Garrabou, X.; Mittl, P. R. E.; Baker, D.; Griffiths, A. D.; Hilvert, D., Emergence of a catalytic tetrad during evolution of a highly active artificial aldolase, *Nat. Chem.*, **2017**, *9* (1), 50-56.  
DOI: [10.1038/Nchem.2596](https://doi.org/10.1038/Nchem.2596)

- (149) Kintsjes, B.; Hein, C.; Mohamed, M. F.; Fischlechner, M.; Courtois, F.; Leine, C.; Hollfelder, F., Picoliter Cell Lysate Assays in Microfluidic Droplet Compartments for Directed Enzyme Evolution, *Chem. Biol.*, **2012**, *19* (8), 1001-1009.  
DOI: [10.1016/j.chembiol.2012.06.009](https://doi.org/10.1016/j.chembiol.2012.06.009)
- (150) Agresti, J. J.; Antipov, E.; Abate, A. R.; Ahn, K.; Rowat, A. C.; Baret, J. C.; Marquez, M.; Klibanov, A. M.; Griffiths, A. D.; Weitz, D. A., Ultrahigh-throughput screening in drop-based microfluidics for directed evolution, *Proc. Natl. Acad. Sci. U. S. A.*, **2010**, *107* (9), 4004-4009.  
DOI: [10.1073/pnas.0910781107](https://doi.org/10.1073/pnas.0910781107)
- (151) Zinchenko, A.; Devenish, S. R.; Kintsjes, B.; Colin, P. Y.; Fischlechner, M.; Hollfelder, F., One in a million: flow cytometric sorting of single cell-lysate assays in monodisperse picolitre double emulsion droplets for directed evolution, *Anal. Chem.*, **2014**, *86* (5), 2526-2533.  
DOI: [10.1021/ac403585p](https://doi.org/10.1021/ac403585p)
- (152) Lewis, M.; Chang, G.; Horton, N. C.; Kercher, M. A.; Pace, H. C.; Schumacher, M. A.; Brennan, R. G.; Lu, P., Crystal structure of the lactose operon repressor and its complexes with DNA and inducer, *Science*, **1996**, *271* (5253), 1247-1254.  
DOI: [10.1126/science.271.5253.1247](https://doi.org/10.1126/science.271.5253.1247)
- (153) Alouane, A.; Labruere, R.; Le Saux, T.; Schmidt, F.; Jullien, L., Self-Immolative Spacers: Kinetic Aspects, Structure-Property Relationships, and Applications, *Angew. Chem., Int. Ed.*, **2015**, *54* (26), 7492-7509.  
DOI: [10.1002/anie.201500088](https://doi.org/10.1002/anie.201500088)
- (154) Gnaim, S.; Shabat, D., Quinone-Methide Species, A Gateway to Functional Molecular Systems: From Self-Immolative Dendrimers to Long-Wavelength Fluorescent Dyes, *Acc. Chem. Res.*, **2014**, *47* (10), 2970-2984.  
DOI: [10.1021/ar500179y](https://doi.org/10.1021/ar500179y)
- (155) Alouane, A.; Labruere, R.; Le Saux, T.; Aujard, I.; Dubruille, S.; Schmidt, F.; Jullien, L., Light Activation for the Versatile and Accurate Kinetic Analysis of Disassembly of Self-Immolative Spacers, *Chem. Eur. J.*, **2013**, *19* (35), 11717-11724.  
DOI: [10.1002/chem.201301298](https://doi.org/10.1002/chem.201301298)
- (156) Hay, M. P.; Sykes, B. M.; Denny, W. A.; O'Connor, C. J., Substituent effects on the kinetics of reductively-initiated fragmentation of nitrobenzyl carbamates designed as triggers for bioreductive prodrugs, *J. Chem. Soc., Perkin Trans. 1*, **1999**, (19), 2759-2770.  
DOI: [10.1039/a904067f](https://doi.org/10.1039/a904067f)
- (157) Schmid, K. M.; Jensen, L.; Phillips, S. T., A Self-Immolative Spacer That Enables Tunable Controlled Release of Phenols under Neutral Conditions, *J. Org. Chem.*, **2012**, *77* (9), 4363-4374.  
DOI: [10.1021/jo300400q](https://doi.org/10.1021/jo300400q)
- (158) de Groot, F. M. H.; Loos, W. J.; Koekkoek, R.; van Berkum, L. W. A.; Busscher, G. F.; Seelen, A. E.; Albrecht, C.; de Bruijn, P.; Scheeren, H. W., Elongated multiple electronic cascade and cyclization spacer systems in activatable anticancer prodrugs for enhanced drug release, *J. Org. Chem.*, **2001**, *66* (26), 8815-8830.  
DOI: [10.1021/jo015884](https://doi.org/10.1021/jo015884)
- (159) Lee, H. Y.; Jiang, X.; Lee, D. W., Kinetics of Self-Immolation: Faster Signal Relay over a Longer Linear Distance?, *Org. Lett.*, **2009**, *11* (10), 2065-2068.  
DOI: [10.1021/ol900433g](https://doi.org/10.1021/ol900433g)

- (160) Hanusek, J.; Sedlak, M.; Jansa, P.; Sterba, V., Study of ring closure reaction of substituted phenyl *N*-(2-thiocarbamoylphenyl)carbamates catalysed by methoxide ion, *J. Phys. Org. Chem.*, **2006**, *19* (1), 61-67.  
DOI: [10.1002/poc.999](https://doi.org/10.1002/poc.999)
- (161) Dewit, M. A.; Gillies, E. R., Design, synthesis, and cyclization of 4-aminobutyric acid derivatives: potential candidates as self-immolative spacers, *Org. Biomol. Chem.*, **2011**, *9* (6), 1846-1854.  
DOI: [10.1039/c0ob00890g](https://doi.org/10.1039/c0ob00890g)
- (162) Beesley, R. M.; Ingold, C. K.; Thorpe, J. F., The formation and stability of spiro-compounds. Part I: Spiro-compounds from cyclohexane, *J. Chem. Soc., Trans.*, **1915**, *107*, 1080-1106.  
DOI: [10.1039/ct9150701080](https://doi.org/10.1039/ct9150701080)
- (163) Bruce, T. C.; Pandit, U. K., The Effect of Geminal Substitution Ring Size and Rotamer Distribution on the Intramolecular Nucleophilic Catalysis of the Hydrolysis of Monophenyl Esters of Dibasic Acids and the Solvolysis of the Intermediate Anhydrides, *J. Am. Chem. Soc.*, **1960**, *82* (22), 5858-5865.  
DOI: [10.1021/ja01507a023](https://doi.org/10.1021/ja01507a023)
- (164) Jung, M. E.; Piizzi, G., *gem*-Disubstituent effect: Theoretical basis and synthetic applications, *Chem. Rev.*, **2005**, *105* (5), 1735-1766.  
DOI: [10.1021/cr940337h](https://doi.org/10.1021/cr940337h)
- (165) Saari, W. S.; Schwering, J. E.; Lyle, P. A.; Smith, S. J.; Engelhardt, E. L., Cyclization-Activated Prodrugs - Basic Carbamates of 4-Hydroxyanisole, *J. Med. Chem.*, **1990**, *33* (1), 97-101.  
DOI: [10.1021/jm00163a016](https://doi.org/10.1021/jm00163a016)
- (166) Dehio, M.; Knorre, A.; Lanz, C.; Dehio, C., Construction of versatile high-level expression vectors for *Bartonella henselae* and the use of green fluorescent protein as a new expression marker, *Gene*, **1998**, *215* (2), 223-229.  
DOI: [10.1016/S0378-1119\(98\)00319-9](https://doi.org/10.1016/S0378-1119(98)00319-9)
- (167) Vilar, J. M.; Guet, C. C.; Leibler, S., Modeling network dynamics: the lac operon, a case study, *J. Cell Biol.*, **2003**, *161* (3), 471-476.  
DOI: [10.1083/jcb.200301125](https://doi.org/10.1083/jcb.200301125)
- (168) Bell, C. E.; Lewis, M., The Lac repressor: a second generation of structural and functional studies, *Curr. Opin. Struct. Biol.*, **2001**, *11* (1), 19-25.  
DOI: [10.1016/S0959-440X\(00\)00180-9](https://doi.org/10.1016/S0959-440X(00)00180-9)
- (169) O'Neill, E.; Ng, L. C.; Sze, C. C.; Shingler, V., Aromatic ligand binding and intramolecular signalling of the phenol-responsive  $\sigma^{54}$ -dependent regulator DmpR, *Mol. Microbiol.*, **1998**, *28* (1), 131-141.  
DOI: [10.1046/j.1365-2958.1998.00780.x](https://doi.org/10.1046/j.1365-2958.1998.00780.x)
- (170) Shingler, V.; Moore, T., Sensing of Aromatic-Compounds by the DmpR Transcriptional Activator of Phenol-Catabolizing *Pseudomonas Sp* Strain CF600, *J. Bacteriol.*, **1994**, *176* (6), 1555-1560.  
DOI: [10.1128/jb.176.6.1555-1560.1994](https://doi.org/10.1128/jb.176.6.1555-1560.1994)
- (171) Shingler, V.; Bartilson, M.; Moore, T., Cloning and nucleotide sequence of the gene encoding the positive regulator (DmpR) of the phenol catabolic pathway encoded by pVI150 and identification of DmpR as a member of the NtrC family of transcriptional activators, *J. Bacteriol.*, **1993**, *175* (6), 1596-1604.

- (172) Schwizer, F.; Heinisch, T.; Kardashliev, T.; Vallapurackal, J.; Panke, S.; Ward, T. R., **2018**, Manuscript in preparation.
- (173) Chichili, V. P. R.; Kumar, V.; Sivaraman, J., Linkers in the structural biology of protein-protein interactions, *Prot. Sci.*, **2013**, 22 (2), 153-167.  
DOI: [10.1002/pro.2206](https://doi.org/10.1002/pro.2206)
- (174) Kurochkina, N.; Guha, U., SH<sub>3</sub> domains: modules of protein–protein interactions, *Biophys. Rev.*, **2013**, 5 (1), 29-39.  
DOI: [10.1007/s12551-012-0081-z](https://doi.org/10.1007/s12551-012-0081-z)
- (175) Main, E. R. G.; Xiong, Y.; Cocco, M. J.; D'Andrea, L.; Regan, L., Design of stable  $\alpha$ -helical arrays from an idealized TPR motif, *Structure*, **2003**, 11 (5), 497-508.  
DOI: [10.1016/S0969-2126\(03\)00076-5](https://doi.org/10.1016/S0969-2126(03)00076-5)
- (176) Kramer, M. A.; Wetzel, S. K.; Plückthun, A.; Mittl, P. R. E.; Grütter, M. G., Structural Determinants for Improved Stability of Designed Ankyrin Repeat Proteins with a Redesigned C-Capping Module, *J. Mol. Biol.*, **2010**, 404 (3), 381-391.  
DOI: [10.1016/j.jmb.2010.09.023](https://doi.org/10.1016/j.jmb.2010.09.023)
- (177) Chiu, T. K.; Kubelka, J.; Herbst-Irmer, R.; Eaton, W. A.; Hofrichter, J.; Davies, D. R., High-resolution x-ray crystal structures of the villin headpiece subdomain, an ultrafast folding protein, *Proc. Natl. Acad. Sci. U. S. A.*, **2005**, 102 (21), 7517-7522.  
DOI: [10.1073/pnas.0502495102](https://doi.org/10.1073/pnas.0502495102)
- (178) Coquille, S.; Filipovska, A.; Chia, T.; Rajappa, L.; Lingford, J. P.; Razif, M. F. M.; Thore, S.; Rackham, O., An artificial PPR scaffold for programmable RNA recognition, *Nat. Commun.*, **2014**, 5, 1-9.  
DOI: [10.1038/ncomms6729](https://doi.org/10.1038/ncomms6729)
- (179) Pellizzoni, M. M.; Schwizer, F.; Wood, C. W.; Sabatino, V.; Cotellet, Y.; Matile, S.; Woolfson, D. N.; Ward, T. R., Chimeric Streptavidins as Host Proteins for Artificial Metalloenzymes, *ACS Catal.*, **2018**, 8 (2), 1476-1484.  
DOI: [10.1021/acscatal.7b03773](https://doi.org/10.1021/acscatal.7b03773)
- (180) Eiben, C. B.; Siegel, J. B.; Bale, J. B.; Cooper, S.; Khatib, F.; Shen, B. W.; Players, F.; Stoddard, B. L.; Popovic, Z.; Baker, D., Increased Diels-Alderase activity through backbone remodeling guided by Foldit players, *Nat. Biotechnol.*, **2012**, 30 (2), 190-192.  
DOI: [10.1038/nbt.2109](https://doi.org/10.1038/nbt.2109)
- (181) Hayashi, T.; Hisaeda, Y., New functionalization of myoglobin by chemical modification of heme-propionates, *Acc. Chem. Res.*, **2002**, 35 (1), 35-43.  
DOI: [10.1021/ar000087t](https://doi.org/10.1021/ar000087t)
- (182) Chivers, C. E.; Crozat, E.; Chu, C.; Moy, V. T.; Sherratt, D. J.; Howarth, M., A streptavidin variant with slower biotin dissociation and increased mechanostability, *Nat. Methods*, **2010**, 7 (5), 391-396.  
DOI: [10.1038/Nmeth.1450](https://doi.org/10.1038/Nmeth.1450)
- (183) O'Sullivan, V. J.; Barrette-Ng, I.; Hommema, E.; Hermanson, G. T.; Schofield, M.; Wu, S. C.; Honetschlaeger, C.; Ng, K. K. S.; Wong, S. L., Development of a Tetrameric Streptavidin Mutein with Reversible Biotin Binding Capability: Engineering a Mobile Loop as an Exit Door for Biotin, *Plos One*, **2012**, 7 (4 (e35203)), 1-9.  
DOI: [10.1371/journal.pone.0035203](https://doi.org/10.1371/journal.pone.0035203)

- (184) Le Trong, I.; Chu, V. N.; Xing, Y.; Lybrand, T. P.; Stayton, P. S.; Stenkamp, R. E., Structural consequences of cutting a binding loop: two circularly permuted variants of streptavidin, *Acta Crystallogr., Sect. D: Biol. Crystallogr.*, **2013**, D69, 968-977.  
DOI: [10.1107/S0907444913003855](https://doi.org/10.1107/S0907444913003855)
- (185) Le Trong, I.; Humbert, N.; Ward, T. R.; Stenkamp, R. E., Crystallographic analysis of a full-length streptavidin with its C-terminal polypeptide bound in the biotin binding site, *J. Mol. Biol.*, **2006**, 356 (3), 738-745.  
DOI: [10.1016/j.jmb.2005.11.086](https://doi.org/10.1016/j.jmb.2005.11.086)
- (186) D'Andrea, L. D.; Regan, L., TPR proteins: the versatile helix, *Trends Biochem. Sci.*, **2003**, 28 (12), 655-662.  
DOI: [10.1016/j.tibs.2003.10.007](https://doi.org/10.1016/j.tibs.2003.10.007)
- (187) Howarth, M.; Chinnapen, D. J. F.; Gerrow, K.; Dorrestein, P. C.; Grandy, M. R.; Kelleher, N. L.; El-Husseini, A.; Ting, A. Y., A monovalent streptavidin with a single femtomolar biotin binding site, *Nat. Methods*, **2006**, 3 (4), 267-273.  
DOI: [10.1038/Nmeth861](https://doi.org/10.1038/Nmeth861)
- (188) Howarth, M.; Ting, A. Y., Imaging proteins in live mammalian cells with biotin ligase and monovalent streptavidin, *Nat. Protoc.*, **2008**, 3 (3), 534-545.  
DOI: [10.1038/nprot.2008.20](https://doi.org/10.1038/nprot.2008.20)
- (189) Koga, N.; Tatsumi-Koga, R.; Liu, G.; Xiao, R.; Acton, T. B.; Montelione, G. T.; Baker, D., Principles for designing ideal protein structures, *Nature*, **2012**, 491 (7423), 222-227.  
DOI: [10.1038/nature11600](https://doi.org/10.1038/nature11600)
- (190) Petukhov, M.; Tatsu, Y.; Tamaki, K.; Murase, S.; Uekawa, H.; Yoshikawa, S.; Serrano, L.; Yumoto, N., Design of stable  $\alpha$ -helices using global sequence optimization, *J. Pept. Sci.*, **2009**, 15 (5), 359-365.  
DOI: [10.1002/psc.1122](https://doi.org/10.1002/psc.1122)
- (191) Doig, A. J., The  $\alpha$ -Helix as the Simplest Protein Model: Helix-Coil Theory, Stability, and Design. In *Protein Folding, Misfolding and Aggregation: Classical Themes and Novel Approaches*, Muñoz, V., Ed. The Royal Society of Chemistry: Cambridge, **2008**, pp 1-27.  
DOI: [10.1039/9781847558282-00001](https://doi.org/10.1039/9781847558282-00001)
- (192) Fletcher, J. M.; Boyle, A. L.; Bruning, M.; Bartlett, G. J.; Vincent, T. L.; Zaccai, N. R.; Armstrong, C. T.; Bromley, E. H.; Booth, P. J.; Brady, R. L.; Thomson, A. R.; Woolfson, D. N., A basis set of *de novo* coiled-coil peptide oligomers for rational protein design and synthetic biology, *ACS Synth. Biol.*, **2012**, 1 (6), 240-250.  
DOI: [10.1021/sb300028q](https://doi.org/10.1021/sb300028q)
- (193) Religa, T. L.; Johnson, C. M.; Vu, D. M.; Brewer, S. H.; Dyer, R. B.; Fersht, A. R., The helix–turn–helix motif as an ultrafast independently folding domain: The pathway of folding of Engrailed homeodomain, *Proc. Natl. Acad. Sci. U. S. A.*, **2007**, 104 (22), 9272-9277.  
DOI: [10.1073/pnas.0703434104](https://doi.org/10.1073/pnas.0703434104)
- (194) Chen, T. H.; Lee, S.; Flood, A. H.; Miljanic, O. S., How to print a crystal structure model in 3D, *CrystEngComm*, **2014**, 16 (25), 5488-5493.  
DOI: [10.1039/c4ce00371c](https://doi.org/10.1039/c4ce00371c)

- (195) Rossi, S.; Benaglia, M.; Brenna, D.; Porta, R.; Orlandi, M., Three Dimensional (3D) Printing: A Straightforward, User-Friendly Protocol To Convert Virtual Chemical Models to Real-Life Objects, *J. Chem. Educ.*, **2015**, *92* (8), 1398-1401.  
DOI: [10.1021/acs.jchemed.5b00168](https://doi.org/10.1021/acs.jchemed.5b00168)
- (196) Van Wieren, K.; Taylor, H. N.; Scalfani, V. F.; Merbouh, N., Rapid Access to Multicolor Three-Dimensional Printed Chemistry and Biochemistry Models Using Visualization and Three-Dimensional Printing Software Programs, *J. Chem. Educ.*, **2017**, *94* (7), 964-969.  
DOI: [10.1021/acs.jchemed.6b00602](https://doi.org/10.1021/acs.jchemed.6b00602)
- (197) Scalfani, V. F.; Williams, A. J.; Tkachenko, V.; Karapetyan, K.; Pshenichnov, A.; Hanson, R. M.; Liddie, J. M.; Bara, J. E., Programmatic conversion of crystal structures into 3D printable files using Jmol, *J. Cheminf.*, **2016**, *8* (66), 1-8.  
DOI: [10.1186/s13321-016-0181-z](https://doi.org/10.1186/s13321-016-0181-z)
- (198) Kaminsky, W.; Snyder, T.; Stone-Sundberg, J.; Moeck, P., One-click preparation of 3D print files (\*.stl, \*.wrl) from \*.cif (crystallographic information framework) data using Cif2VRML, *Powder Diffr.*, **2014**, *29* (S2), S42-S47.  
DOI: [10.1017/S0885715614001092](https://doi.org/10.1017/S0885715614001092)
- (199) Wood, P. A.; Sarjeant, A. A.; Bruno, I. J.; Macrae, C. F.; Maynard-Casely, H. E.; Towler, M., The next dimension of structural science communication: simple 3D printing directly from a crystal structure, *CrystEngComm*, **2017**, *19* (4), 690-698.  
DOI: [10.1039/c6ce02412b](https://doi.org/10.1039/c6ce02412b)
- (200) Penny, M. R.; Cao, Z. J.; Patel, B.; dos Santos, B. S.; Asquith, C. R. M.; Szulc, B. R.; Rao, Z. X.; Muwaffak, Z.; Malkinson, J. P.; Hilton, S. T., Three-Dimensional Printing of a Scalable Molecular Model and Orbital Kit for Organic Chemistry Teaching and Learning, *J. Chem. Educ.*, **2017**, *94* (9), 1265-1271.  
DOI: [10.1021/acs4chemect6bC0953](https://doi.org/10.1021/acs4chemect6bC0953)
- (201) Scalfani, V. F.; Vaid, T. P., 3D Printed Molecules and Extended Solid Models for Teaching Symmetry and Point Groups, *J. Chem. Educ.*, **2014**, *91* (8), 1174-1180.  
DOI: [10.1021/ed400887t](https://doi.org/10.1021/ed400887t)
- (202) Humphrey, W.; Dalke, A.; Schulten, K., VMD - Visual Molecular Dynamics, *J. Molec. Graphics*, **1996**, *14* (1), 33-38, <http://www.ks.uiuc.edu/Research/vmd/>.
- (203) MeshLab Visual Computing Lab - ISTI - CNR, <http://meshlab.sourceforge.net/>.
- (204) Griswold, K. E.; Kawarasaki, Y.; Ghoneim, N.; Benkovic, S. J.; Iverson, B. L.; Georgiou, G., Evolution of highly active enzymes by homology-independent recombination, *Proc. Natl. Acad. Sci. U. S. A.*, **2005**, *102* (29), 10082-10087.  
DOI: [10.1073/pnas.0504556102](https://doi.org/10.1073/pnas.0504556102)
- (205) Trost, B. M.; Older, C. M., A Convenient Synthetic Route to [CpRu(CH<sub>3</sub>CN)<sub>3</sub>]PF<sub>6</sub>, *Organometallics*, **2002**, *21* (12), 2544-2546.  
DOI: [10.1021/om020143p](https://doi.org/10.1021/om020143p)
- (206) Romero, P. A.; Arnold, F. H., Exploring protein fitness landscapes by directed evolution, *Nat. Rev. Mol. Cell Biol.*, **2009**, *10* (12), 866-876.  
DOI: [10.1038/nrm2805](https://doi.org/10.1038/nrm2805)

- (207) Santos-Aberturas, J.; Dorr, M.; Waldo, G. S.; Bornscheuer, U. T., In-Depth High-Throughput Screening of Protein Engineering Libraries by Split-GFP Direct Crude Cell Extract Data Normalization, *Chem. Biol.*, **2015**, *22* (10), 1406-1414.  
DOI: [10.1016/j.chembiol.2015.08.014](https://doi.org/10.1016/j.chembiol.2015.08.014)
- (208) Martell, J. D.; Yamagata, M.; Deerinck, T. J.; Phan, S.; Kwa, C. G.; Ellisman, M. H.; Sanes, J. R.; Ting, A. Y., A split horseradish peroxidase for the detection of intercellular protein-protein interactions and sensitive visualization of synapses, *Nat. Biotechnol.*, **2016**, *34* (7), 774-780.  
DOI: [10.1038/nbt.3563](https://doi.org/10.1038/nbt.3563)
- (209) Di Nardo, G.; Fantuzzi, A.; Sideri, A.; Panicco, P.; Sassone, C.; Giunta, C.; Gilardi, G., Wild-type CYP102A1 as a biocatalyst: turnover of drugs usually metabolised by human liver enzymes, *J. Biol. Inorg. Chem.*, **2007**, *12* (3), 313-323.  
DOI: [10.1007/s00775-006-0188-4](https://doi.org/10.1007/s00775-006-0188-4)
- (210) O'Hanlon, J. A.; Ren, X.; Morris, M.; Wong, L. L.; Robertson, J., Hydroxylation of anilides by engineered cytochrome P450<sub>BM3</sub>, *Org. Biomol. Chem.*, **2017**, *15* (41), 8780-8787.  
DOI: [10.1039/c7ob02236k](https://doi.org/10.1039/c7ob02236k)
- (211) Jeschek, M.; Panke, S.; Ward, T. R., Periplasmic Screening for Artificial Metalloenzymes. In *Methods in Enzymology: Peptide, Protein and Enzyme Design*, Pecoraro, V. L., Ed. Elsevier Inc.: Burlington, **2016**, Vol. 580, pp 539-556.  
DOI: [10.1016/bs.mie.2016.05.037](https://doi.org/10.1016/bs.mie.2016.05.037)
- (212) Braun, M.; Killmann, H.; Maier, E.; Benz, R.; Braun, V., Diffusion through channel derivatives of the *Escherichia coli* FhuA transport protein, *Eur. J. Biochem.*, **2002**, *269* (20), 4948-4959.  
DOI: [10.1046/j.1432-1033.2002.03195.x](https://doi.org/10.1046/j.1432-1033.2002.03195.x)
- (213) Krewinkel, M.; Dworeck, T.; Fioroni, M., Engineering of an *E. coli* outer membrane protein FhuA with increased channel diameter, *J. Nanobiotechnol.*, **2011**, *9* (33), 1-8.  
DOI: [10.1186/1477-3155-9-33](https://doi.org/10.1186/1477-3155-9-33)
- (214) Ferguson, A. D.; Hofmann, E.; Coulton, J. W.; Diederichs, K.; Welte, W., Siderophore-mediated iron transport: Crystal structure of FhuA with bound lipopolysaccharide, *Science*, **1998**, *282* (5397), 2215-2220.  
DOI: [10.1126/science.282.5397.2215](https://doi.org/10.1126/science.282.5397.2215)
- (215) Chen, G.; Hayhurst, A.; Thomas, J. G.; Harvey, B. R.; Iverson, B. L.; Georgiou, G., Isolation of high-affinity ligand-binding proteins by periplasmic expression with cytometric screening (PECS), *Nat. Biotechnol.*, **2001**, *19* (6), 537-542.  
DOI: [10.1038/89281](https://doi.org/10.1038/89281)
- (216) Sarkar, C. A.; Dodevski, I.; Kenig, M.; Dudli, S.; Mohr, A.; Hermans, E.; Plückthun, A., Directed evolution of a G protein-coupled receptor for expression, stability, and binding selectivity, *Proc. Natl. Acad. Sci. U. S. A.*, **2008**, *105* (39), 14808-14813.  
DOI: [10.1073/pnas.0803103105](https://doi.org/10.1073/pnas.0803103105)
- (217) Okamoto, Y.; Kojima, R.; Schwizer, F.; Bartolami, E.; Heinisch, T.; Matile, S.; Fussenegger, M.; Ward, T. R., A Cell-Penetrating Artificial Metalloenzyme Regulates a Gene Switch in a Designer Mammalian Cell, *Nat. Commun.*, **2018**, accepted.  
DOI: [10.1038/s41467-018-04440-0](https://doi.org/10.1038/s41467-018-04440-0)
- (218) Szponarski, M.; Schwizer, F.; Ward, T. R.; Gademann, K., **2018**, Manuscript in preparation.

- (219) Ueki, N.; Ide, T.; Mochiji, S.; Kobayashi, Y.; Tokutsu, R.; Ohnishi, N.; Yamaguchi, K.; Shigenobu, S.; Tanaka, K.; Minagawa, J.; Hisabori, T.; Hirono, M.; Wakabayashi, K., Eyespot-dependent determination of the phototactic sign in *Chlamydomonas reinhardtii*, *Proc. Natl. Acad. Sci. U. S. A.*, **2016**, *113* (19), 5299-5304.  
DOI: [10.1073/pnas.1525538113](https://doi.org/10.1073/pnas.1525538113)
- (220) Robles, V. M.; Durrenberger, M.; Heinisch, T.; Lledos, A.; Schirmer, T.; Ward, T. R.; Maréchal, J. D., Structural, Kinetic, and Docking Studies of Artificial imine Reductases Based on Biotin-Streptavidin Technology: An Induced Lock-and-Key Hypothesis, *J. Am. Chem. Soc.*, **2014**, *136* (44), 15676-15683.  
DOI: [10.1021/ja508258t](https://doi.org/10.1021/ja508258t)
- (221) Pettersen, E. F.; Goddard, T. D.; Huang, C. C.; Couch, G. S.; Greenblatt, D. M.; Meng, E. C.; Ferrin, T. E., UCSF chimera - A visualization system for exploratory research and analysis, *J. Comput. Chem.*, **2004**, *25* (13), 1605-1612.  
DOI: [10.1002/jcc.20084](https://doi.org/10.1002/jcc.20084)
- (222) Mullis, K.; Faloona, F.; Scharf, S.; Saiki, R.; Horn, G.; Erlich, H., Specific Enzymatic Amplification of DNA *In Vitro*: The Polymerase Chain Reaction, *Cold Spring Harbor Symp. Quant. Biol.*, **1986**, *51*, 263-273.  
DOI: [10.1101/sqb.1986.051.01.032](https://doi.org/10.1101/sqb.1986.051.01.032)
- (223) Machery-Nagel Plasmid DNA purification: User manual (NucleoSpin Plasmid), Macherey-Nagel, **2012**.
- (224) Sanger, F.; Nicklen, S.; Coulson, A. R., DNA sequencing with chain-terminating inhibitors, *Proc. Natl. Acad. Sci. U. S. A.*, **1977**, *74* (12), 5463-5467.
- (225) Artimo, P.; Jonnalagedda, M.; Arnold, K.; Baratin, D.; Csardi, G.; de Castro, E.; Duvaud, S.; Flegel, V.; Fortier, A.; Gasteiger, E.; Grosdidier, A.; Hernandez, C.; Ioannidis, V.; Kuznetsov, D.; Liechti, R.; Moretti, S.; Mostaguir, K.; Redaschi, N.; Rossier, G.; Xenarios, I.; Stockinger, H., ExpASY: SIB bioinformatics resource portal, *Nucleic Acids Res.*, **2012**, *40* (W1), W597-W603.  
DOI: [10.1093/nar/gks400](https://doi.org/10.1093/nar/gks400)
- (226) QuikChange™ Site-Directed Mutagenesis Kit, Agilent Technologies, Stratagene Products Division, **2010**.
- (227) Zheng, L.; Baumann, U.; Reymond, J. L., An efficient one-step site-directed and site-saturation mutagenesis protocol, *Nucleic Acids Res.*, **2004**, *32* (14 (e115)), 1-5.  
DOI: [10.1093/nar/gnh110](https://doi.org/10.1093/nar/gnh110)
- (228) Breslauer, K. J.; Frank, R.; Blocker, H.; Marky, L. A., Predicting DNA Duplex Stability from the Base Sequence, *Proc. Natl. Acad. Sci. U. S. A.*, **1986**, *83* (11), 3746-3750.
- (229) Kibbe, W. A., OligoCalc: an online oligonucleotide properties calculator, *Nucleic Acids Res.*, **2007**, *35*, W43-W46, <http://basic.northwestern.edu/biotools/OligoCalc.html>.  
DOI: [10.1093/nar/gkm234](https://doi.org/10.1093/nar/gkm234)
- (230) EMD Biosciences Inc. Novagen® pET System Manual, 10<sup>th</sup> Edition, **2003**, 1-68.
- (231) Studier, F. W.; Moffatt, B. A., Use of bacteriophage T7 RNA polymerase to direct selective high-level expression of cloned genes, *J. Mol. Biol.*, **1986**, *189* (1), 113-130.  
DOI: [10.1016/0022-2836\(86\)90385-2](https://doi.org/10.1016/0022-2836(86)90385-2)
- (232) Studier, F. W., Protein production by auto-induction in high density shaking cultures, *Protein Expr. Purif.*, **2005**, *41* (1), 207-234.  
DOI: [10.1016/j.pep.2005.01.016](https://doi.org/10.1016/j.pep.2005.01.016)



- (233) Laemmli, U. K., Cleavage of Structural Proteins during the Assembly of the Head of Bacteriophage T4, *Nature*, **1970**, 227 (5259), 680-685.  
DOI: [10.1038/227680a0](https://doi.org/10.1038/227680a0)
- (234) Manfredini, S.; Vertuani, S.; Pavan, B.; Vitali, F.; Scaglianti, M.; Bortolotti, F.; Biondi, C.; Scatturin, A.; Prasad, P.; Dalpiaz, A., Design, synthesis and *in vitro* evaluation on HRPE cells of ascorbic and 6-bromoascorbic acid conjugates with neuroactive molecules, *Bioorg. Med. Chem.*, **2004**, 12 (20), 5453-5463.  
DOI: [10.1016/j.bmc.2004.07.043](https://doi.org/10.1016/j.bmc.2004.07.043)
- (235) Kato, Y.; Okada, S.; Tomimoto, K.; Mase, T., A facile bromination of hydroxyheteroarenes, *Tetrahedron Lett.*, **2001**, 42 (29), 4849-4851.  
DOI: [10.1016/S0040-4039\(01\)00864-4](https://doi.org/10.1016/S0040-4039(01)00864-4)
- (236) Jones, J. E.; Slack, J. L.; Fang, P. F.; Zhang, X. S.; Subramanian, V.; Causey, C. P.; Coonrod, S. A.; Guo, M.; Thompson, P. R., Synthesis and Screening of a Haloacetamide Containing Library To Identify PAD4 Selective Inhibitors, *ACS Chem. Biol.*, **2012**, 7 (1), 160-165.  
DOI: [10.1021/cb200258q](https://doi.org/10.1021/cb200258q)
- (237) Vallinayagam, R.; Weber, J.; Neier, R., Novel Bioconjugates of Aminolevulinic Acid with Vitamins, *Org. Lett.*, **2008**, 10 (20), 4453-4455.  
DOI: [10.1021/ol801496j](https://doi.org/10.1021/ol801496j)
- (238) Kajetanowicz, A.; Chatterjee, A.; Reuter, R.; Ward, T. R., Biotinylated Metathesis Catalysts: Synthesis and Performance in Ring Closing Metathesis, *Catal. Lett.*, **2014**, 144 (3), 373-379.  
DOI: [10.1007/s10562-013-1179-z](https://doi.org/10.1007/s10562-013-1179-z)
- (239) Jobin, M. L.; Blanchet, M.; Henry, S.; Chaignepain, S.; Manigand, C.; Castano, S.; Lecomte, S.; Burlina, F.; Sagan, S.; Alves, I. D., The role of tryptophans on the cellular uptake and membrane interaction of arginine-rich cell penetrating peptides, *Biochim. Biophys. Acta, Biomembr.*, **2015**, 1848 (2), 593-602.  
DOI: [10.1016/j.bbamem.2014.11.013](https://doi.org/10.1016/j.bbamem.2014.11.013)
- (240) Craig, D.; Lansdell, M. I.; Lewis, S. E., Highly regioselective decarboxylative Claisen rearrangement reactions of diallyl 2-sulfonylmalonates, *Tetrahedron Lett.*, **2007**, 48 (44), 7861-7864.  
DOI: [10.1016/j.tetlet.2007.08.130](https://doi.org/10.1016/j.tetlet.2007.08.130)
- (241) Hay, M. P.; Wilson, W. R.; Denny, W. A., Nitroarylmethylcarbamate prodrugs of doxorubicin for use with nitroreductase gene-directed enzyme prodrug therapy, *Bioorg. Med. Chem.*, **2005**, 13 (12), 4043-4055.  
DOI: [10.1016/j.bmc.2005.03.055](https://doi.org/10.1016/j.bmc.2005.03.055)
- (242) Yadav, S.; Taylor, C. M., Synthesis of Orthogonally Protected (2S)-2-Amino-adipic Acid ( $\alpha$ -AAA) and (2S,4R)-2-Amino-4-hydroxyadipic Acid (Ahad), *J. Org. Chem.*, **2013**, 78 (11), 5401-5409.  
DOI: [10.1021/jo400558t](https://doi.org/10.1021/jo400558t)
- (243) Buchini, S.; Buschiazzo, A.; Withers, S. G., A new generation of specific Trypanosoma cruzi transsialidase inhibitors, *Angew. Chem., Int. Ed.*, **2008**, 47 (14), 2700-2703.  
DOI: [10.1002/anie.200705435](https://doi.org/10.1002/anie.200705435)
- (244) Kamst, E.; Zegelaar-Jaarsveld, K.; van der Marel, G. A.; van Boom, J. H.; Lugtenberg, B. J. J.; Spaik, H. P., Chemical synthesis of N-acetylglucosamine derivatives and their use as glycosyl accepters by the *Mesorhizobium loti* chitin oligosaccharide synthase NodC, *Carbohydr. Res.*, **1999**, 321 (3-4), 176-189.  
DOI: [10.1016/S0008-6215\(99\)00190-1](https://doi.org/10.1016/S0008-6215(99)00190-1)

- (245) Li, A. X.; Kong, F. Z., Concise syntheses of arabinogalactans with  $\beta$ -(1 $\rightarrow$ 6)-linked galactopyranose backbones and  $\alpha$ -(1 $\rightarrow$ 3)- and  $\alpha$ -(1 $\rightarrow$ 2)-linked arabinofuranose side chains, *Bioorg. Med. Chem.*, **2005**, *13* (3), 839-853.  
DOI: [10.1016/j.bmc.2004.10.035](https://doi.org/10.1016/j.bmc.2004.10.035)
- (246) Xu, Z. G.; Wheeler, K. A.; Baures, P. W., Parallel Synthesis of Peptide-Like Macrocycles Containing Imidazole-4,5-dicarboxylic Acid, *Molecules*, **2012**, *17* (5), 5346-5362.  
DOI: [10.3390/molecules17055346](https://doi.org/10.3390/molecules17055346)

## 7 Annexes

### 7.1 Additional screening results

Table 15: Screening of streptavidin mutants for the uncaging of coumarin 1 using [CpRu(QA-Biot)(Sol.)]PF<sub>6</sub>Sav.

Mutant	Fluorescence [RFU]	Mutant	Fluorescence [RFU]
Substrate only	2335	L124H	2018
Free cofactor	1921	L124K	1321
WT	3247	L124N	1786
N49A	3206	L124V	1474
N49Y	4657	L124Y	407
P64G	2903	H127A	3034
A65F	3437	D128A	1219
H87A	3004	S112A-K121A	14491
T114G	1600	S112A-K121G	8031
S112A	6010	S112A-K121L	14771
S112C	1531	S112A-K121N	8960
S112D	1890	S112A-K121T	8497
S112E	840	S112C-K121H	1082
S112F	5099	S112H-K121H	1722
S112G	2646	S112K-L124E	982
S112H	6024	S112M-K121A	26435
S112K	3453	S112M-K121E	12460
S112L	7965	S112M-K121N	15600
S112M	10770	S112M-K121R	35527
S112N	3752	S112N-K121E	1727
S112P	1657	S112Q-K121E	3731
S112Q	3977	S112R-K121E	4345
S112R	4053	S112V-K121E	1664
S112T	4996	S112W-K121E	2599
S112V	8555	S112Y-K121E	10359
S112W	4717	S112Y-K121R	17264
S112Y	6285	N118E-K121E	1384
K121A	10318	N118K-K121E	866
K121C	479	N118L-K121E	2659
K121D	2057	N118S-K121E	1201
K121E	2293	K121N-L124G	1507
K121F	7102	K121R-L124G	3641
K121H	1792	D67V-S112A-K121L	12369
K121L	10423	R84A-S112A-K121A	4931
K121M	4358	48(GGS) <sub>2</sub>	1280
K121N	5638	66(GGS) <sub>2</sub>	4175
K121P	1667	66(GGS) <sub>2</sub> -S112M	13787
K121Q	5412	66(GGS) <sub>2</sub> -K121R	19529
K121R	15224	84(GGS) <sub>2</sub>	2136
K121S	5587	Loop2	1642
K121V	7387	Loop2-S112M	2700
K121W	5844	Loop2-K121R	2780
K121Y	5401	159TPR	1587
L124F	3820	159TPR-K121R	11046
L124G	10154		

Equation: see Scheme 6. Conditions: see Figure 11.

**Table 16: Screening of streptavidin mutants for the uncaging of IPTG substrate 54 using [CpRu(QA-Biot)(Sol.)]PF<sub>6</sub>·Sav.<sup>a</sup>**

Entry	Sav	Yield [%]
1 <sup>b</sup>	-	6
2	-	10
3	WT	11
4	S112A	10
5	S112D	11
6	S112H	11
7	S112K	11
8	S112M	12
9	S112L	11
10	S112N	9
11	S112Y	11
12	K121A	26
13	K121E	12
14	K121F	32
15	K121H	7
16	K121M	20
17	K121R	26
18	K121Y	19
19	K121Q	28
20	L124F	9
21	L124G	27
22	L124H	7
23	L124K	5
24	L124Y	6

<sup>a</sup>Reaction conditions: Phosphate-buffer (50 mM NaH<sub>2</sub>PO<sub>4</sub>/Na<sub>2</sub>HPO<sub>4</sub>, pH 7.4), 0.9% NaCl, 500 μM IPTG substrate **54**, 5 μM ruthenium cofactor [CpRu(QA-Biot)(Sol.)]PF<sub>6</sub> (**27**), 10 μM Sav (free biotin binding sites), 0.5% DMF, 25°C, shaking (1000 rpm), 22 h. Yields (concentration of liberated IPTG) were determined by UPLC-MS (see chapter 4.2.6). <sup>b</sup>No ruthenium cofactor was added.

# 7.2 NMR and mass spectra

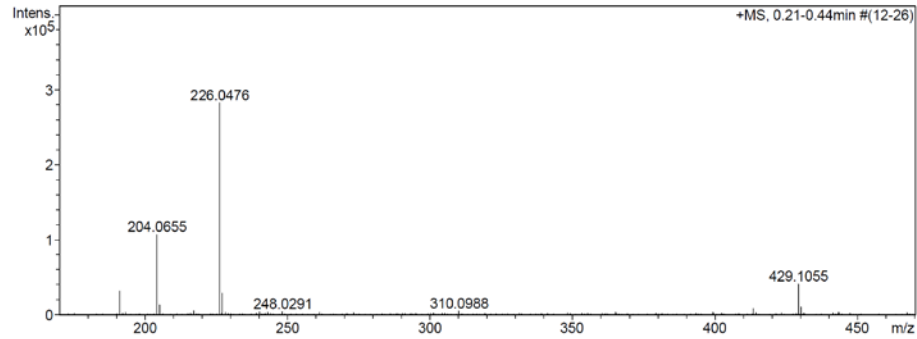
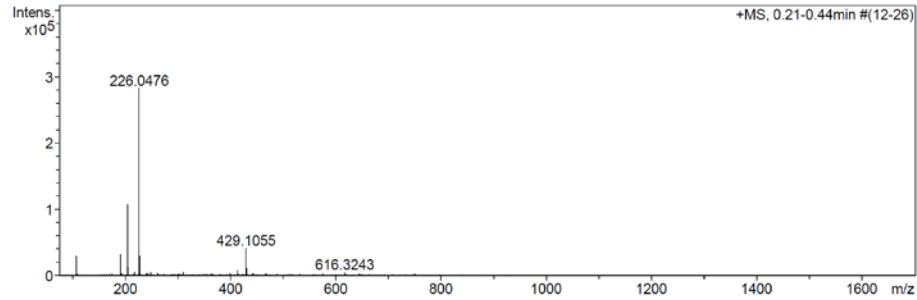
## Annex 1: Compound 20

### Mass Spectrum SmartFormula Report

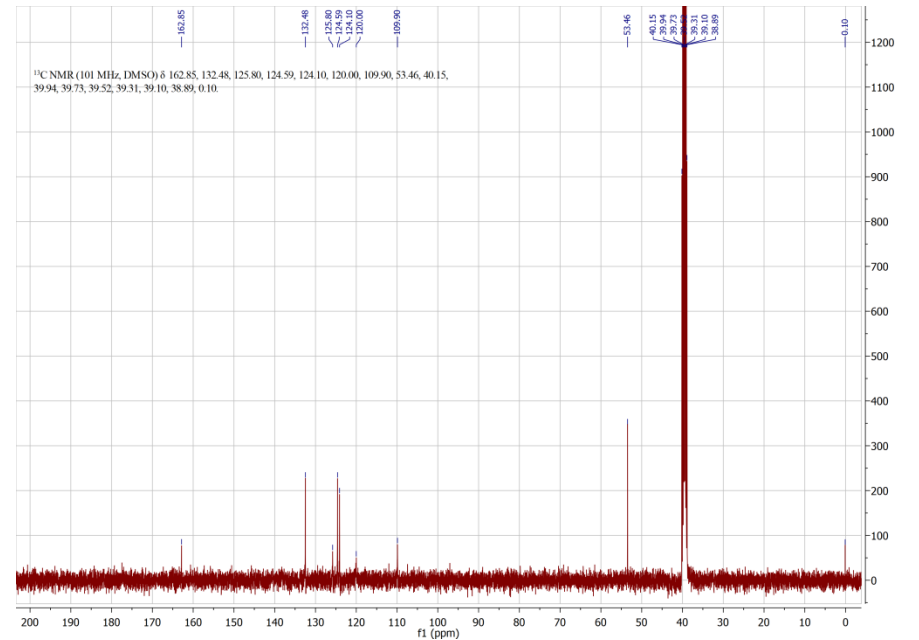
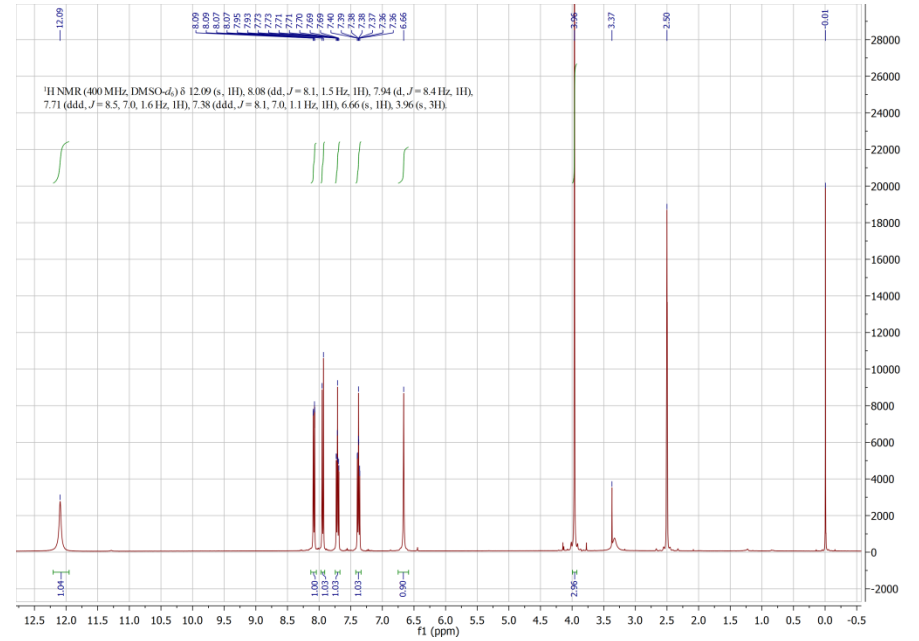
**Analysis Info**  
 Analysis Name: N:\new acq data\FS81 001.d  
 Method: hn Direct\_Infusion\_pos mode\_75-1700 mid 4eV.m  
 Sample Name: Fabian Schwizer  
 Comment: FS81, ca. 5 ug/ml MeOH  
 Acquisition Date: 08.04.2016 09:05:15  
 Operator: hn  
 Instrument / Ser#: maXis 4G 21243

**Acquisition Parameter**

Source Type	ESI	Ion Polarity	Positive	Set Nebulizer	0.4 Bar
Focus	Not active	Set Capillary	3600 V	Set Dry Heater	180 °C
Scan Begin	75 m/z	Set End Plate Offset	-500 V	Set Dry Gas	4.0 l/min
Scan End	1700 m/z	Set Collision Cell RF	350.0 Vpp	Set Ion Energy (MS only)	4.0 eV

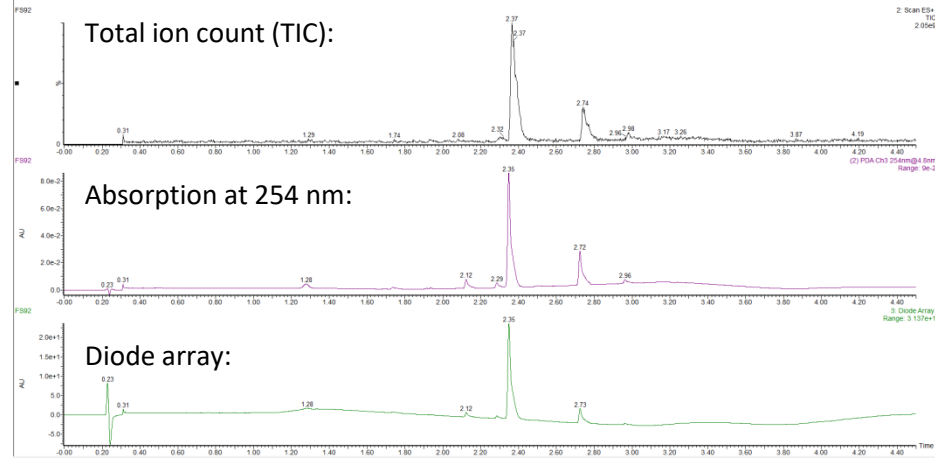


Meas. m/z	#	Formula	Score	m/z	err [mDa]	err [ppm]	mSigma	rdB	e <sup>-</sup> Conf	N-Rule	z
204.0655	1	C 11 H 10 N O 3	100.00	204.0655	-0.0	-0.1	2.7	7.5	even	ok	1+
226.0476	1	C 11 H 9 N Na O 3	100.00	226.0475	-0.2	-0.7	12.0	7.5	even	ok	
429.1055	1	C 22 H 18 N 2 Na O 6	100.00	429.1057	0.2	0.6	7.3	14.5	even	ok	

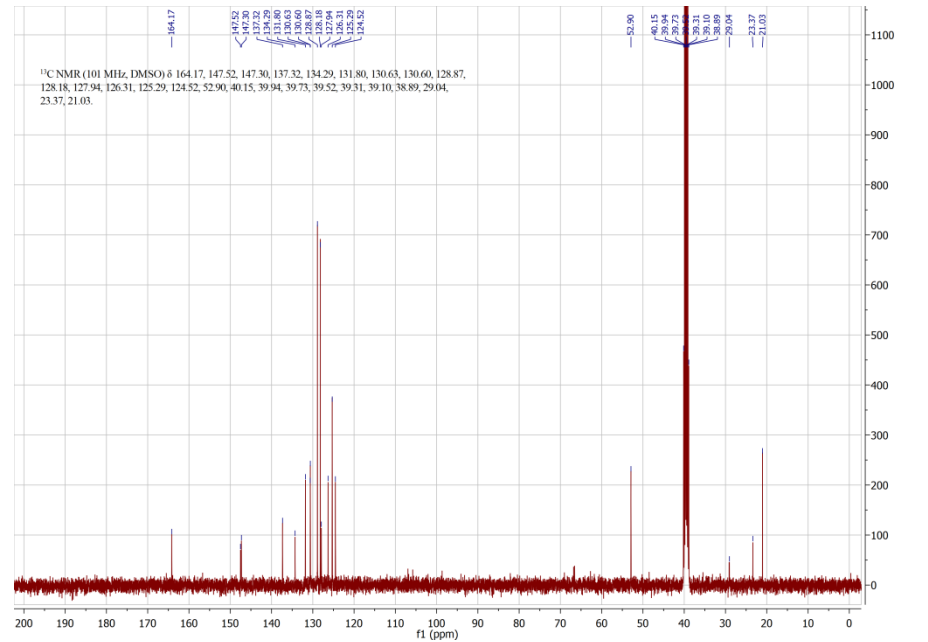
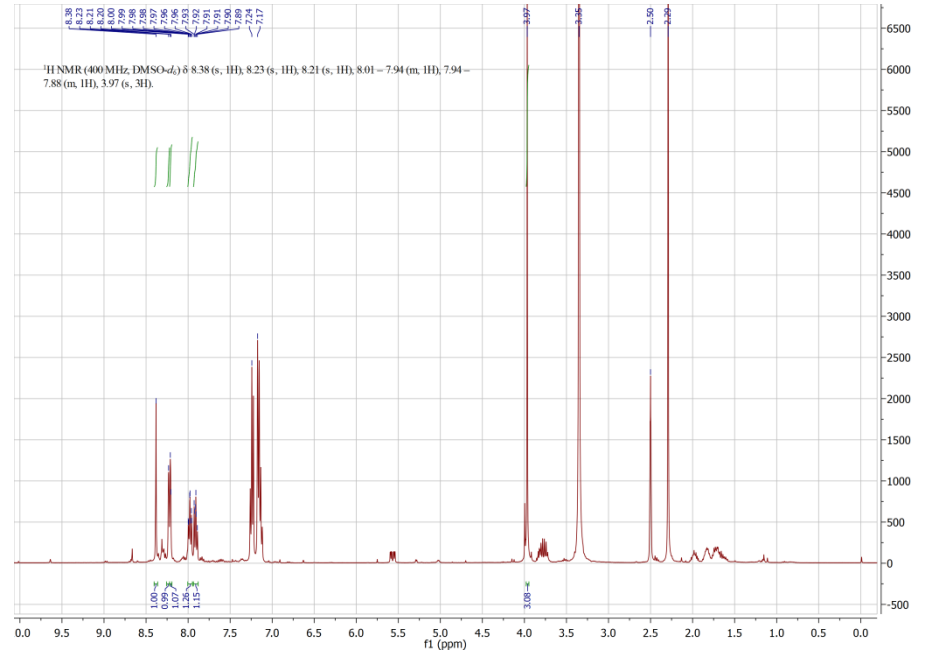
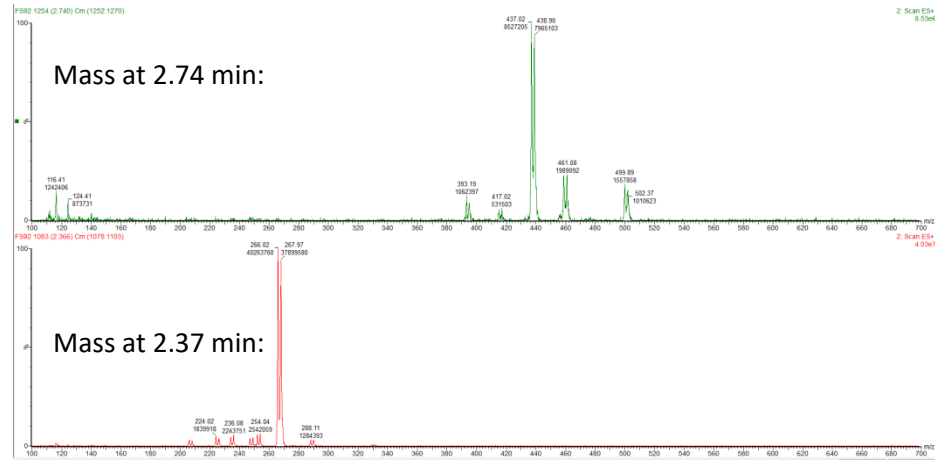


Annex 2: Compound 21

UPLC – trace:



Mass – trace:



Annex 3: Compound 22

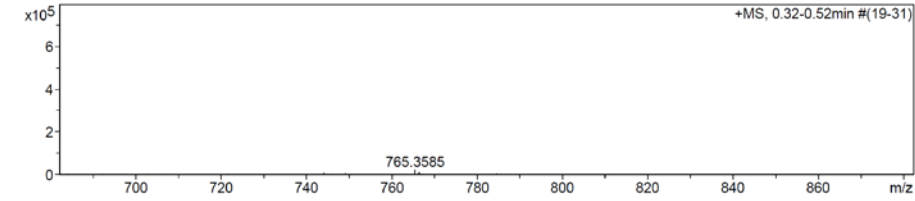
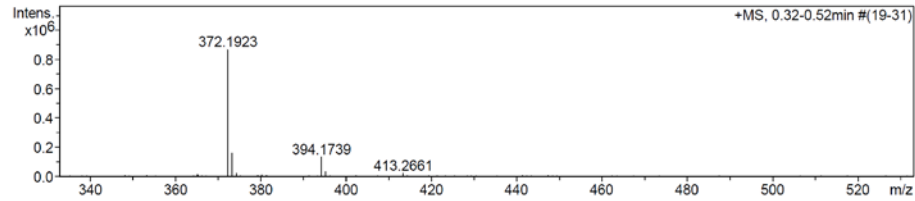
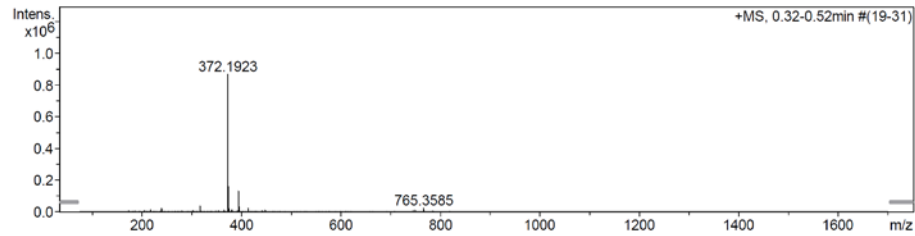
### Mass Spectrum SmartFormula Report

**Analysis Info**

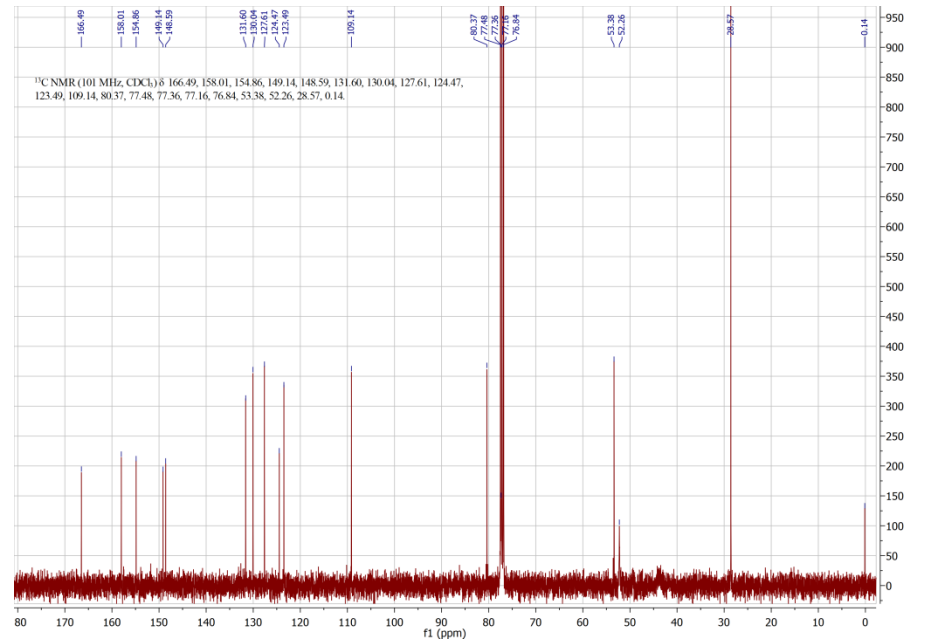
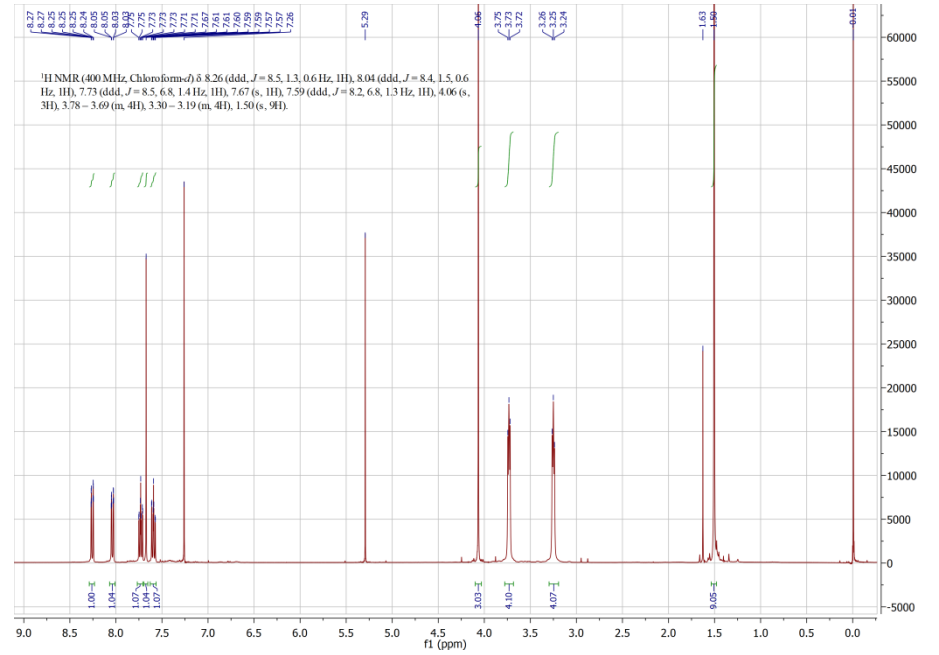
Analysis Name N:\new\_acq\_data\FS93\_001.d Acquisition Date 08.04.2016 10:06:42  
 Method hn Direct\_Infusion\_pos mode\_75-1700 mid 4eV.m Operator hn  
 Sample Name Fabian Schwizer Instrument / Ser# maXis 4G 21243  
 Comment FS93, ca. 5 ug/ml MeOH

**Acquisition Parameter**

Source Type ESI Ion Polarity Positive Set Nebulizer 0.4 Bar  
 Focus Not active Set Capillary 3600 V Set Dry Heater 180 °C  
 Scan Begin 75 m/z Set End Plate Offset -500 V Set Dry Gas 4.0 l/min  
 Scan End 1700 m/z Set Collision Cell RF 350.0 Vpp Set Ion Energy (MS only) 4.0 eV



Meas. m/z	#	Formula	Score	m/z	err [mDa]	err [ppm]	mSigma	rdB	e <sup>-</sup> Conf	N-Rule	z
372.1923	1	C <sub>20</sub> H <sub>26</sub> N <sub>3</sub> O <sub>4</sub>	100.00	372.1918	-0.5	-1.3	26.0	9.5	even	ok	1+
394.1739	1	C <sub>20</sub> H <sub>25</sub> N <sub>3</sub> NaO <sub>4</sub>	100.00	394.1737	-0.2	-0.5	2.9	9.5	even	ok	
765.3585	1	C <sub>40</sub> H <sub>50</sub> N <sub>6</sub> NaO <sub>8</sub>	100.00	765.3582	-0.3	-0.4	10.6	18.5	even	ok	



Annex 4: Compound 24

### Mass Spectrum SmartFormula Report

**Analysis Info**

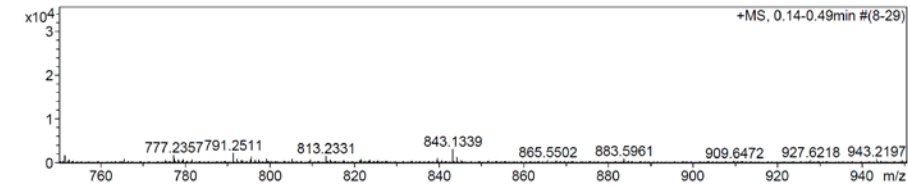
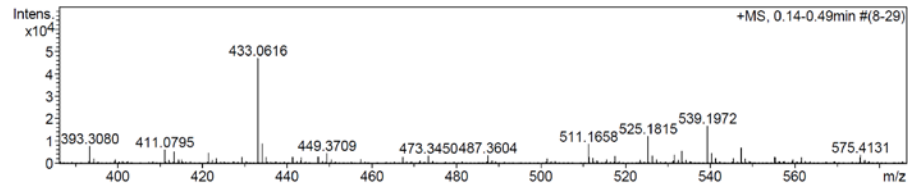
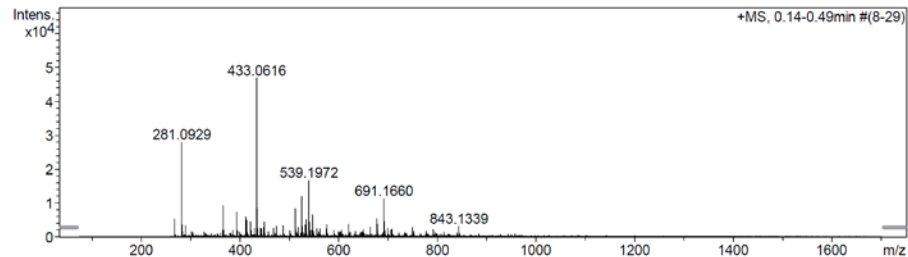
Analysis Name N:\new acq data\FS40 001.d  
 Method hn Direct\_Infusion\_pos mode\_75-1700 mid 4eV.m  
 Sample Name Fabian Schwizer  
 Comment FS40, ca. 5 ug/ml MeOH

Acquisition Date 08.04.2016 10:42:14

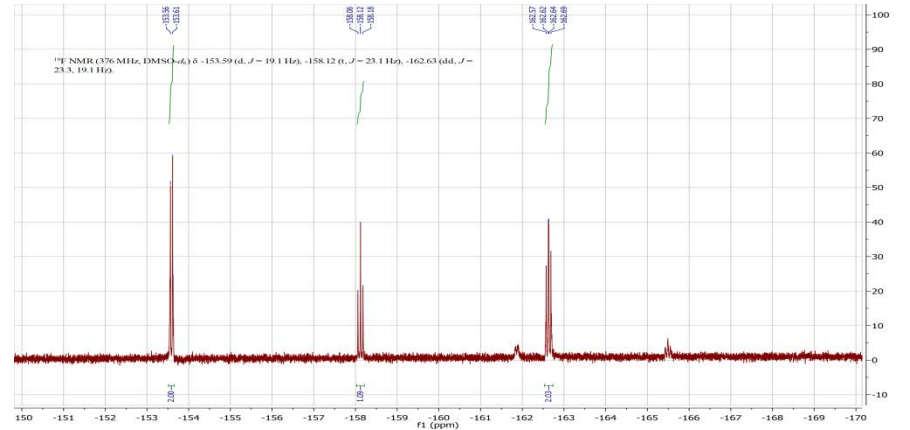
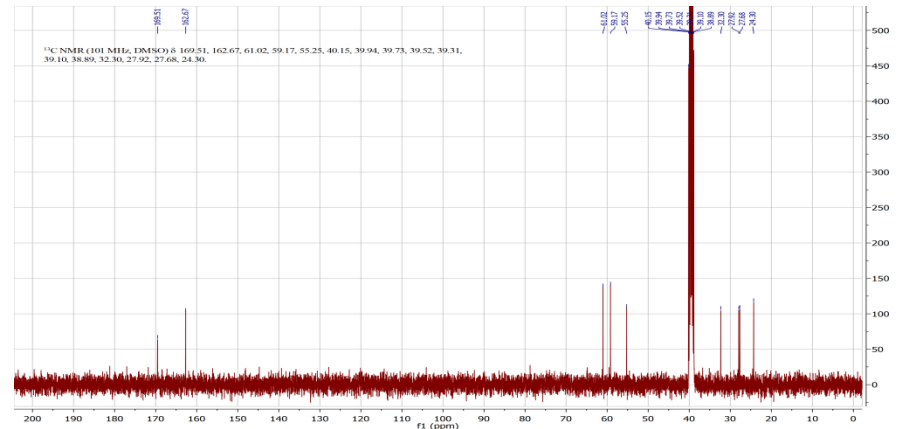
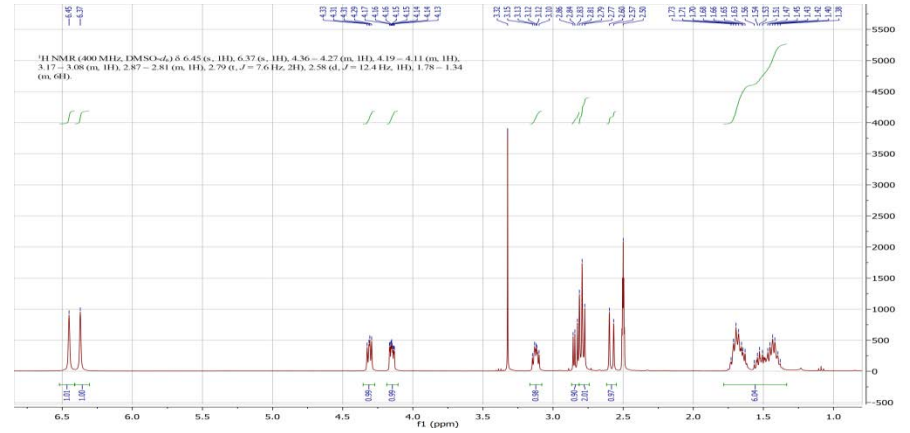
Operator hn  
 Instrument / Ser# maXis 4G 21243

**Acquisition Parameter**

Source Type	ESI	Ion Polarity	Positive	Set Nebulizer	0.4 Bar
Focus	Not active	Set Capillary	3600 V	Set Dry Heater	180 °C
Scan Begin	75 m/z	Set End Plate Offset	-500 V	Set Dry Gas	4.0 l/min
Scan End	1700 m/z	Set Collision Cell RF	350.0 Vpp	Set Ion Energy (MS only)	4.0 eV



Meas. m/z	#	Formula	Score	m/z	err [mDa]	err [ppm]	mSigma	rdB	e <sup>-</sup> Conf	N-Rule	z
433.0616	1	C <sub>16</sub> H <sub>15</sub> F <sub>5</sub> N <sub>2</sub> NaO <sub>3</sub> S	100.00	433.0616	-0.1	-0.2	7.0	7.5	even	ok	1+
843.1339	1	C <sub>32</sub> H <sub>30</sub> F <sub>10</sub> N <sub>4</sub> NaO <sub>6</sub> S <sub>2</sub>	100.00	843.1339	0.0	0.0	15.2	14.5	even	ok	





Annex 5: Compound 25

### Mass Spectrum SmartFormula Report

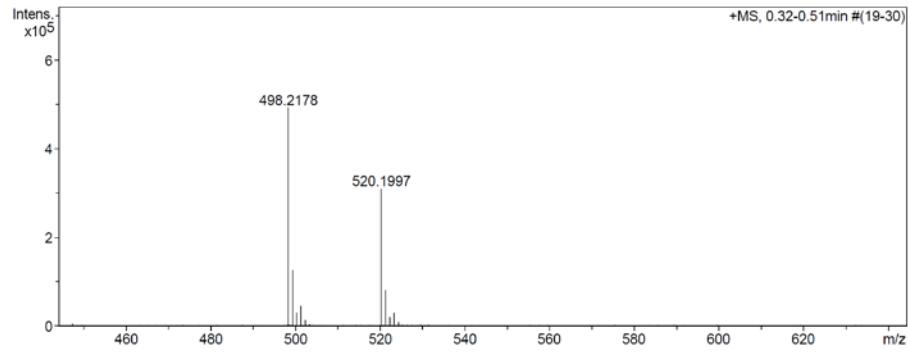
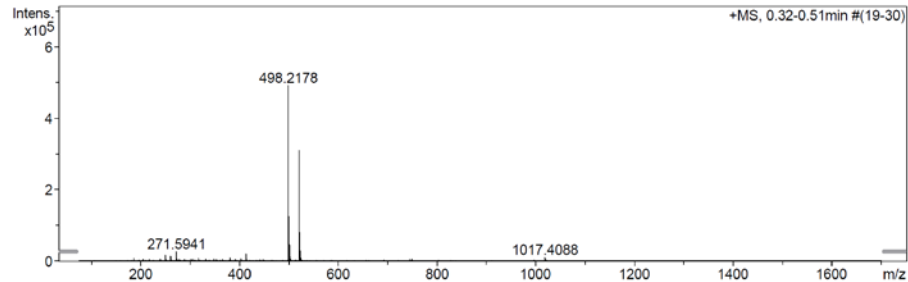
**Analysis Info**

Analysis Name N:\new acq data\FS41 001.d  
 Method hn Direct\_Infusion\_pos mode\_75-1700 mid 4eV.m  
 Sample Name Fabian Schwizer  
 Comment FS41, ca. 5 ug/ml MeOH

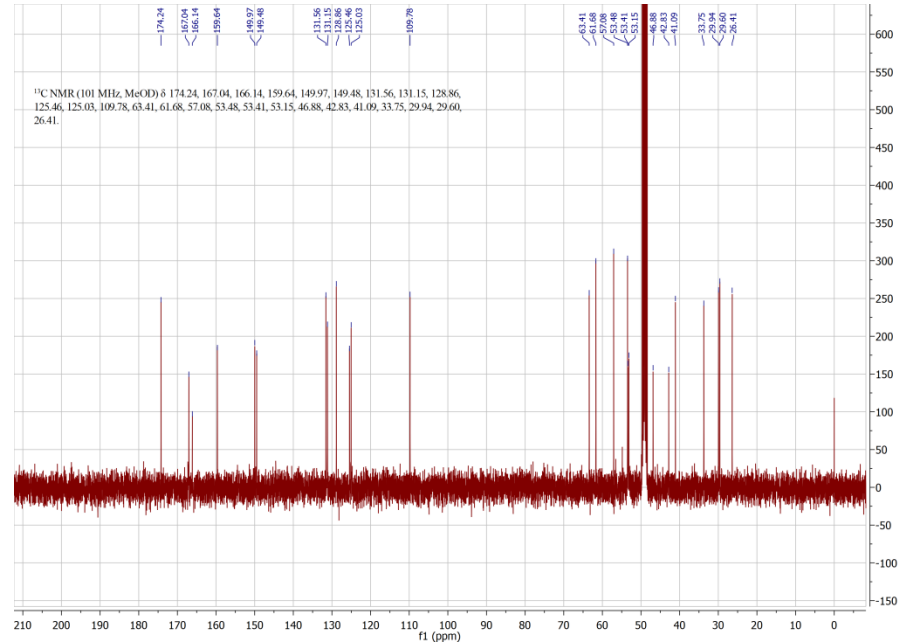
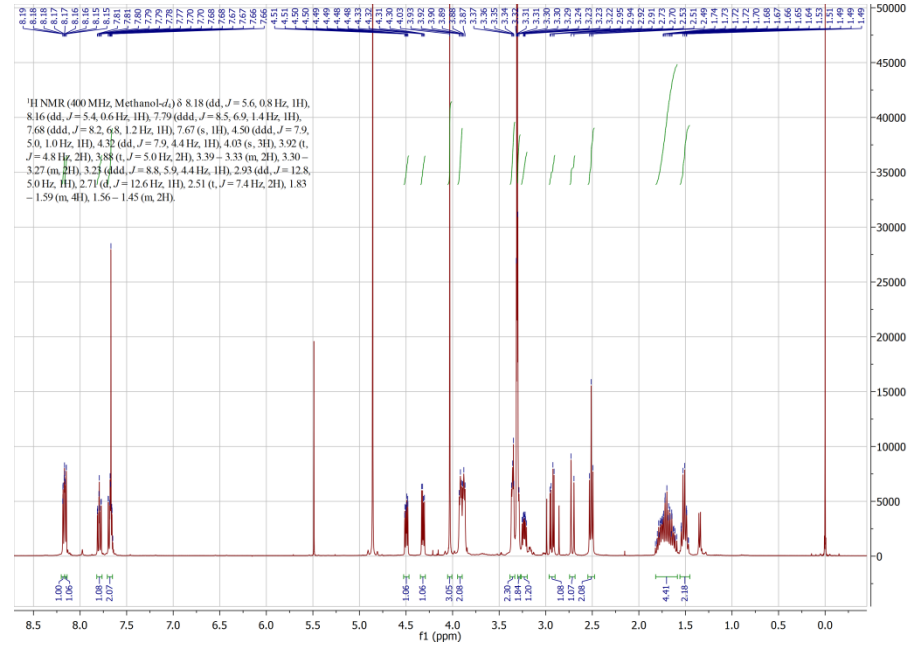
Acquisition Date 08.04.2016 11:09:54  
 Operator hn  
 Instrument / Ser# maXis 4G 21243

**Acquisition Parameter**

Source Type	ESI	Ion Polarity	Positive	Set Nebulizer	0.4 Bar
Focus	Not active	Set Capillary	3600 V	Set Dry Heater	180 °C
Scan Begin	75 m/z	Set End Plate Offset	-500 V	Set Dry Gas	4.0 l/min
Scan End	1700 m/z	Set Collision Cell RF	350.0 Vpp	Set Ion Energy (MS only)	4.0 eV



Meas. m/z	#	Formula	Score	m/z	err [mDa]	err [ppm]	mSigma	rdb	e <sup>-</sup> Conf	N-Rule	z
498.2178	1	C <sub>25</sub> H <sub>32</sub> N <sub>5</sub> O <sub>4</sub> S	100.00	498.2170	-0.8	-1.6	30.8	12.5	even	ok	1+
520.1997	1	C <sub>25</sub> H <sub>31</sub> N <sub>5</sub> NaO <sub>4</sub> S	100.00	520.1989	-0.8	-1.5	28.0	12.5	even	ok	
1017.4088	1	C <sub>50</sub> H <sub>62</sub> N <sub>10</sub> NaO <sub>8</sub> S <sub>2</sub>	100.00	1017.4086	-0.2	-0.2	97.8	24.5	even	ok	



Annex 6: Compound 26

### Mass Spectrum SmartFormula Report

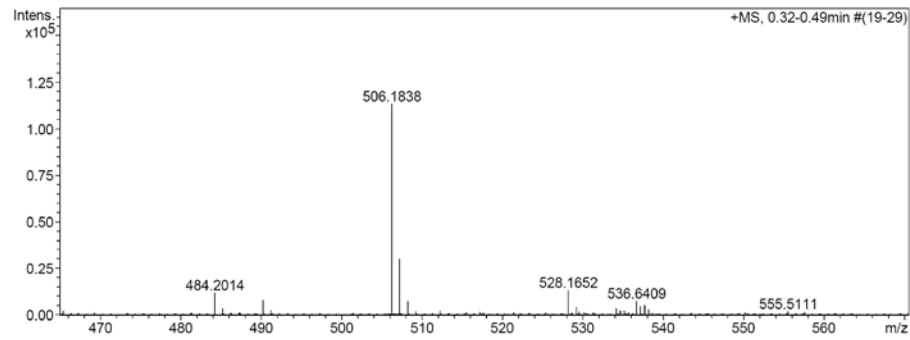
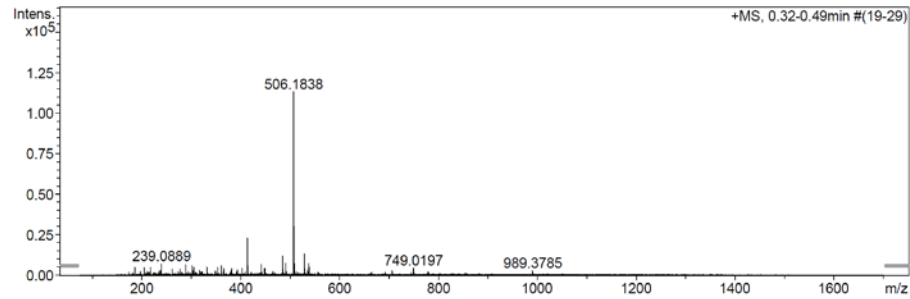
**Analysis Info**

Analysis Name N:\new acq data\FS130 002.d  
 Method hn Direct\_Infusion\_pos mode\_75-1700 mid 4eV.m  
 Sample Name Fabian Schwizer  
 Comment FS130, ca. 5 ug/ml MeOH, wash (MeOH)

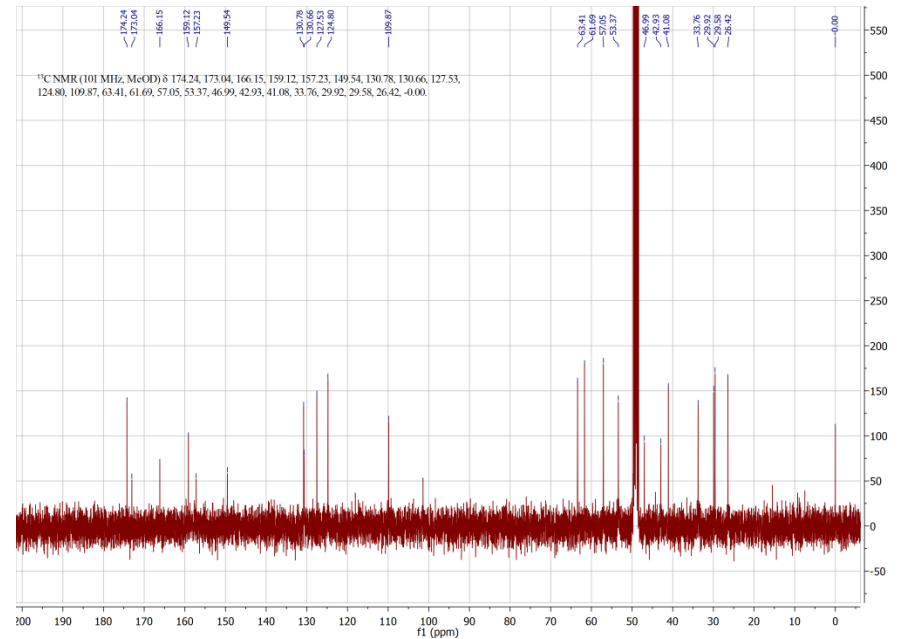
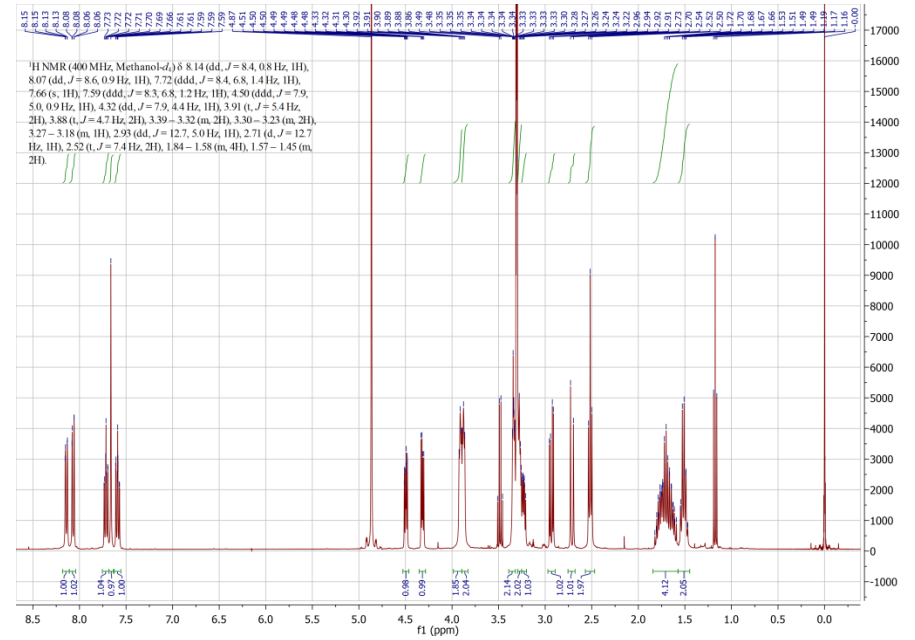
Acquisition Date 08.04.2016 16:13:45  
 Operator hn  
 Instrument / Ser# maXis 4G 21243

**Acquisition Parameter**

Source Type ESI Ion Polarity Positive Set Nebulizer 0.4 Bar  
 Focus Not active Set Capillary 3600 V Set Dry Heater 180 °C  
 Scan Begin 75 m/z Set End Plate Offset -500 V Set Dry Gas 4.0 l/min  
 Scan End 1700 m/z Set Collision Cell RF 350.0 Vpp Set Ion Energy (MS only) 4.0 eV



Meas. m/z	#	Formula	Score	m/z	err [mDa]	err [ppm]	mSigma	rdB	e <sup>-</sup> Conf	N-Rule	z
484.2014	1	C <sub>24</sub> H <sub>30</sub> N <sub>5</sub> O <sub>4</sub> S	100.00	484.2013	-0.1	-0.2	9.1	12.5	even	ok	1+
506.1838	1	C <sub>24</sub> H <sub>29</sub> N <sub>5</sub> NaO <sub>4</sub> S	100.00	506.1832	-0.5	-1.1	17.7	12.5	even	ok	
528.1652	1	C <sub>24</sub> H <sub>28</sub> N <sub>5</sub> Na <sub>2</sub> O <sub>4</sub> S	100.00	528.1652	-0.0	-0.0	7.7	12.5	even	ok	
989.3785	1	C <sub>48</sub> H <sub>58</sub> N <sub>10</sub> NaO <sub>8</sub> S <sub>2</sub>	100.00	989.3773	-1.2	-1.3	33.9	24.5	even	ok	



### Mass Spectrum SmartFormula Report

**Analysis Info**

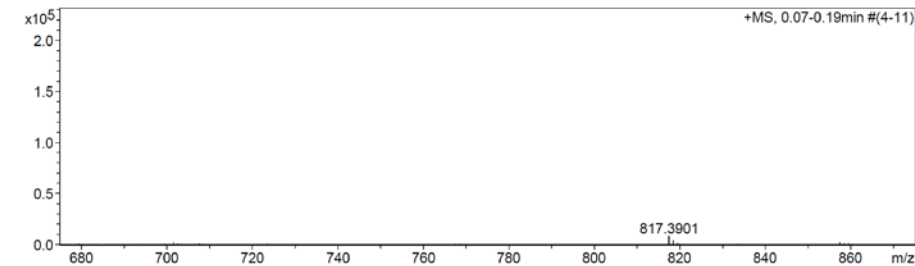
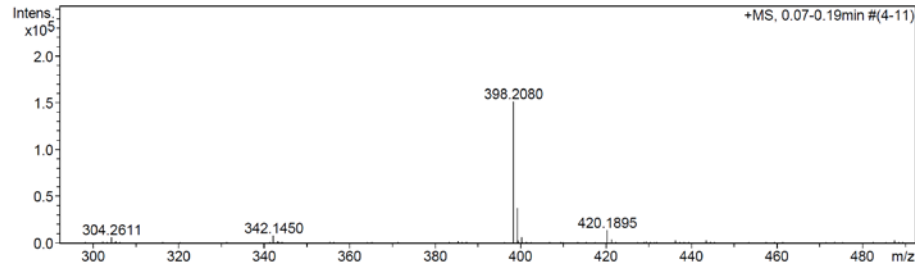
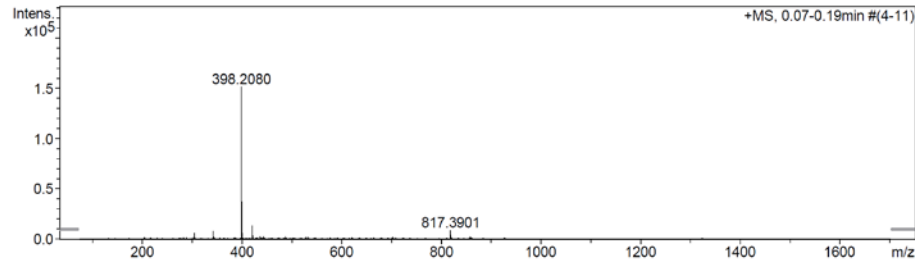
Analysis Name E:\new acq data for data analysis\FS96 001.d  
 Method hn Direct\_Infusion\_pos mode\_75-1700 mid 4eV.m  
 Sample Name Fabian Schwizer  
 Comment FS96, ca. 5 ug/mL MeCN

Acquisition Date 30.03.2017 15:42:55

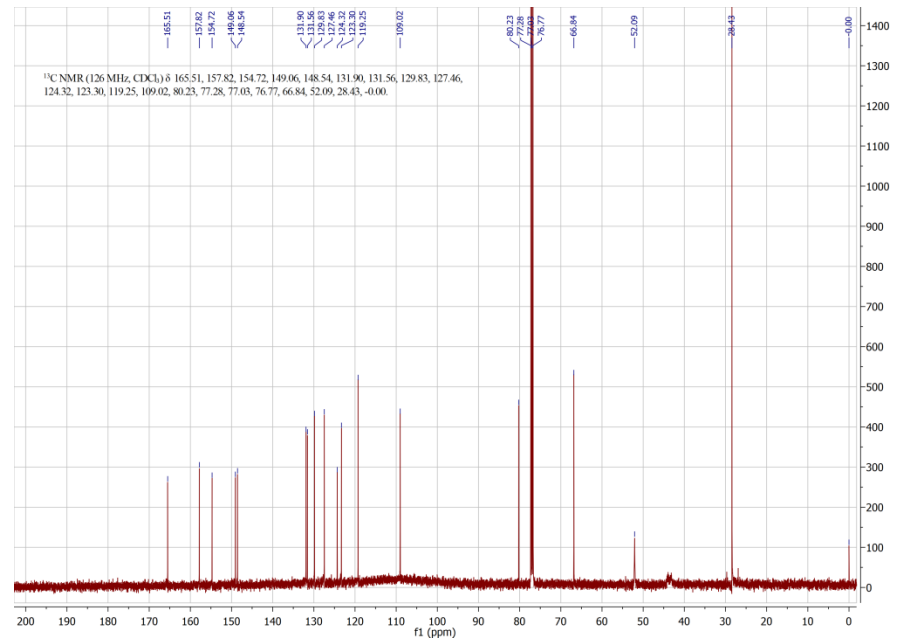
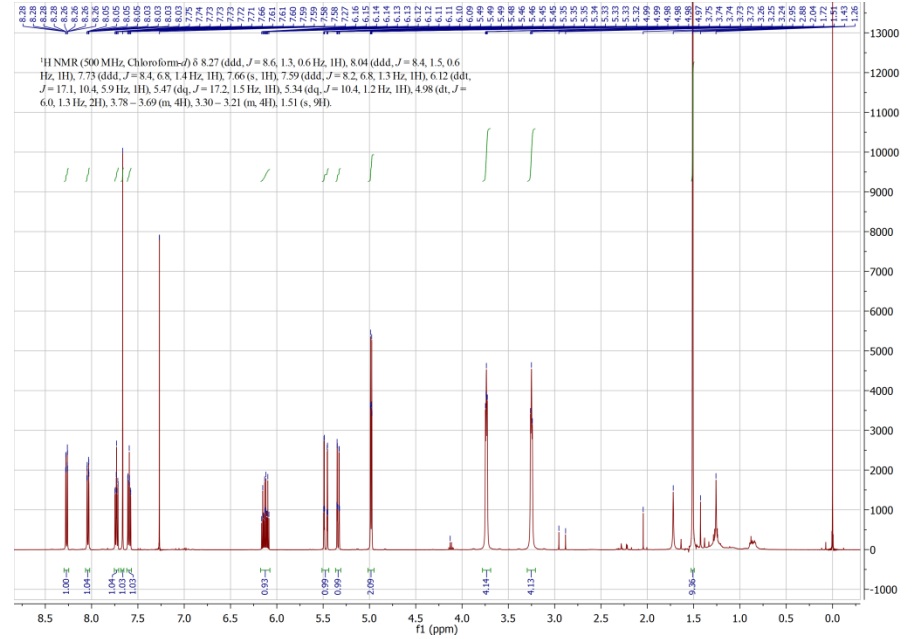
Operator hn  
 Instrument / Ser# maXis 4G 21243

**Acquisition Parameter**

Source Type	ESI	Ion Polarity	Positive	Set Nebulizer	0.4 Bar
Focus	Not active	Set Capillary	3600 V	Set Dry Heater	180 °C
Scan Begin	75 m/z	Set End Plate Offset	-500 V	Set Dry Gas	4.0 l/min
Scan End	1700 m/z	Collision Energy	8.0 eV	Set Ion Energy (MS only)	4.0 eV



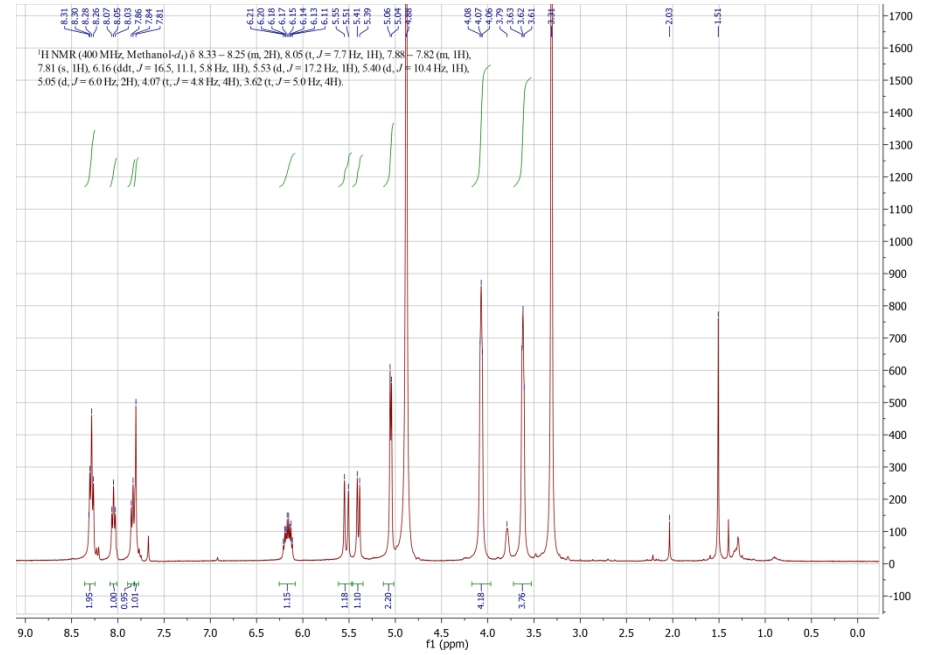
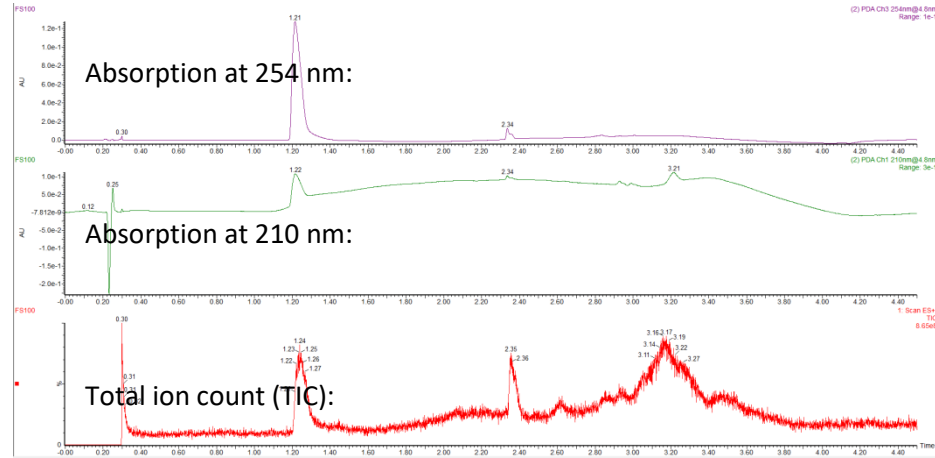
Meas. m/z	#	Formula	Score	m/z	err [mDa]	err [ppm]	mSigma	rdb	e <sup>-</sup> Conf	z
398.2080	1	C 22 H 28 N 3 O 4	100.00	398.2074	-0.6	-1.5	2.6	10.5	even	1+
420.1895	1	C 22 H 27 N 3 Na O 4	100.00	420.1894	-0.1	-0.2	1.5	10.5	even	
817.3901	1	C 44 H 54 N 6 Na O 8	100.00	817.3895	-0.6	-0.7	12.4	20.5	even	



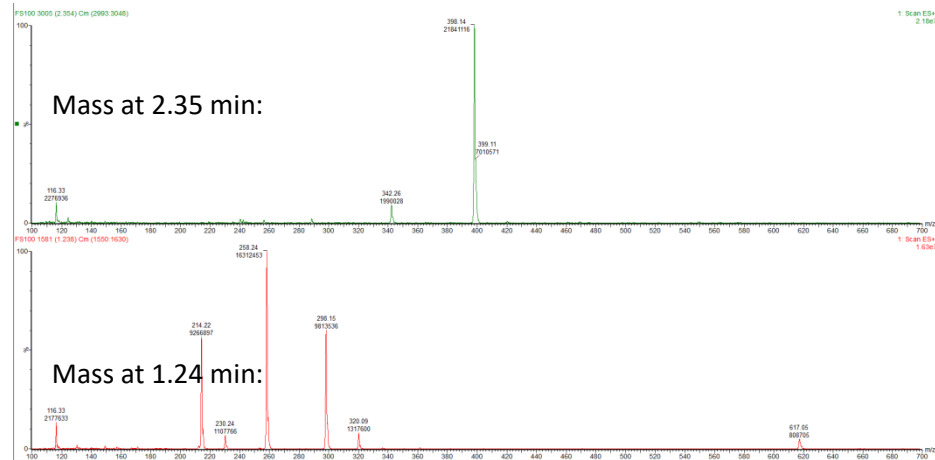


Annex 9: Compound 29

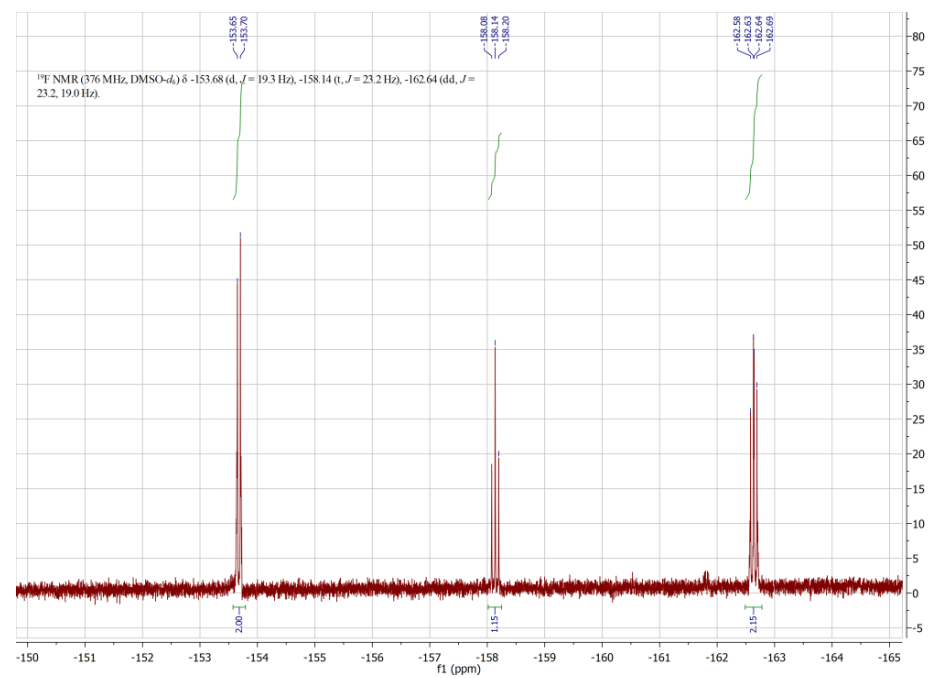
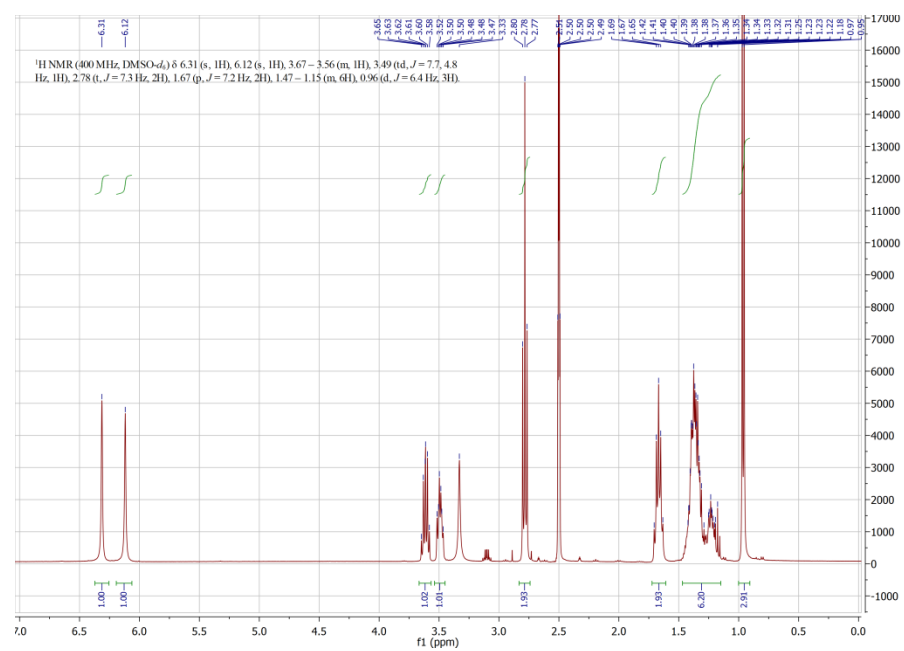
UPLC – trace:



MS – trace:

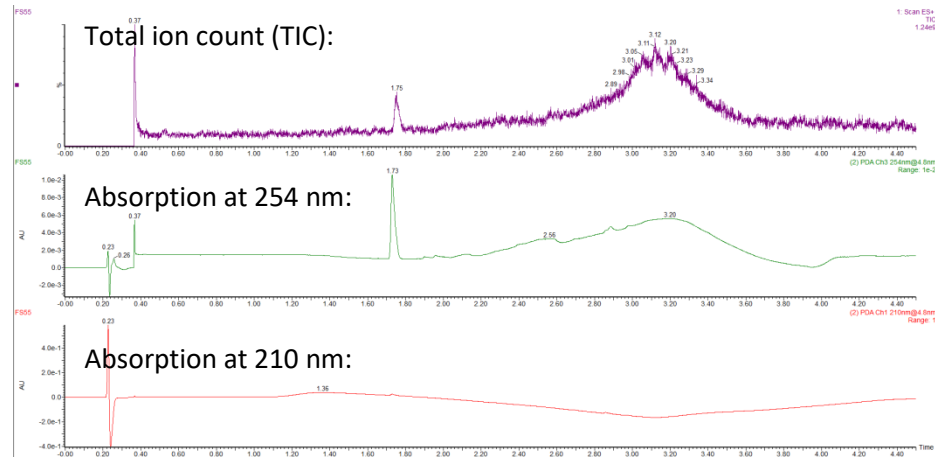


Annex 10: Compound 32

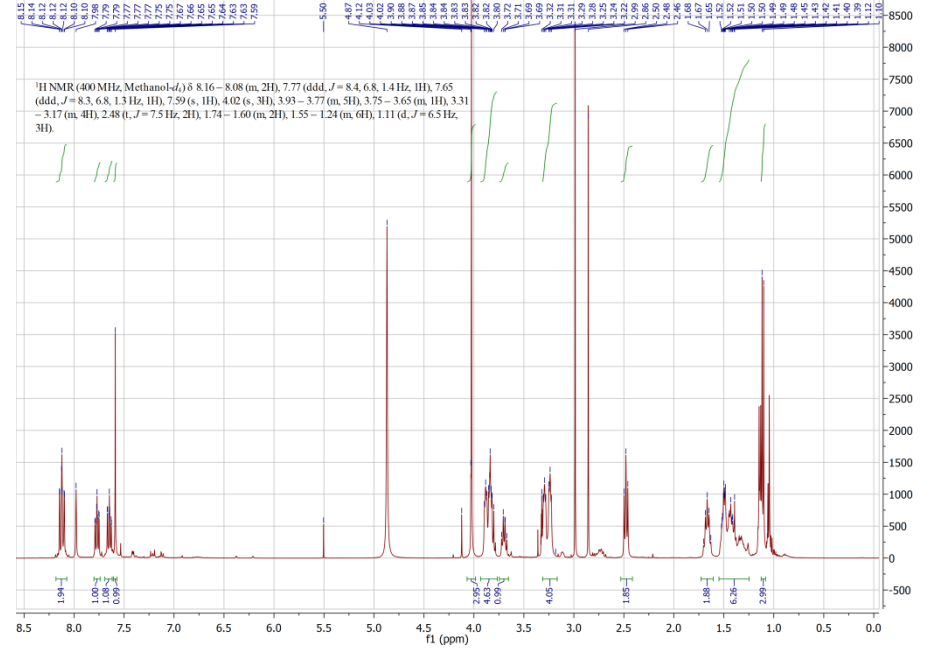
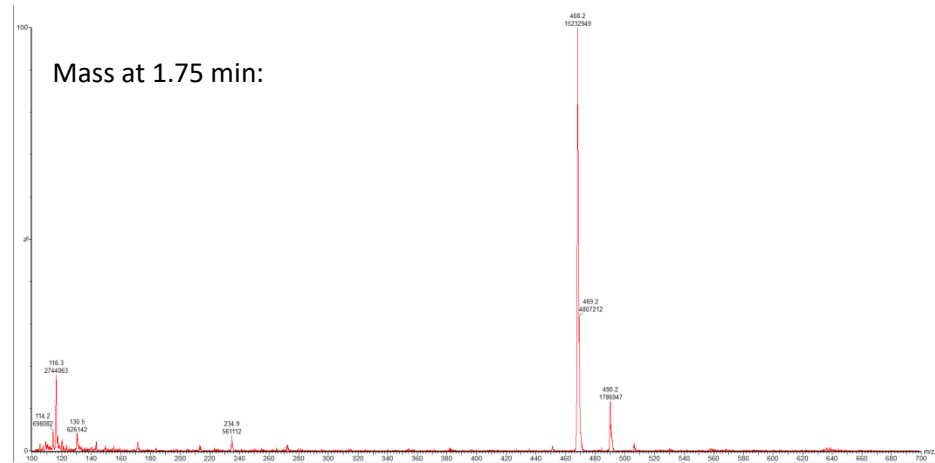


Annex 11: Compound 33

UPLC – trace:

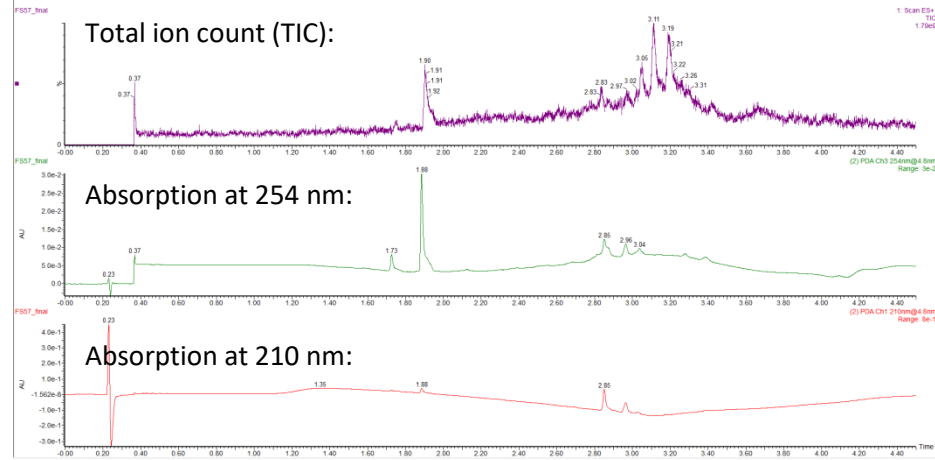


Mass – trace:

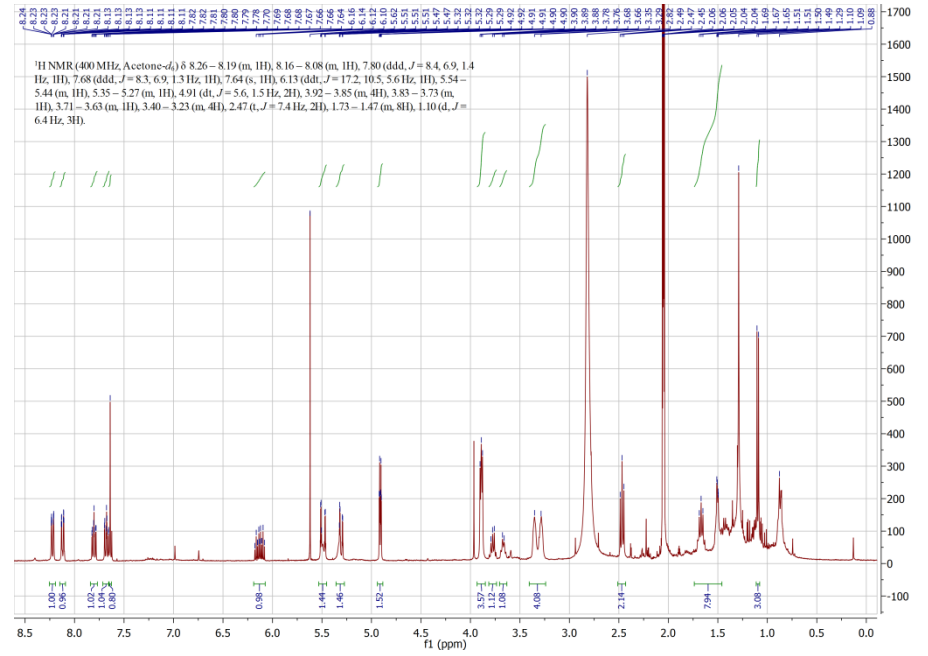
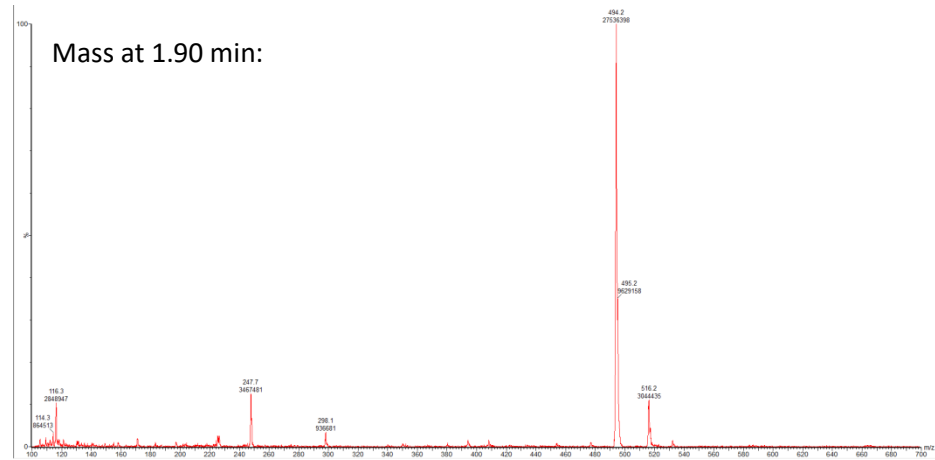


Annex 12: Compound 34

UPLC – trace:



Mass – trace:





Annex 13: Compound 36

### Mass Spectrum SmartFormula Report

**Analysis Info**

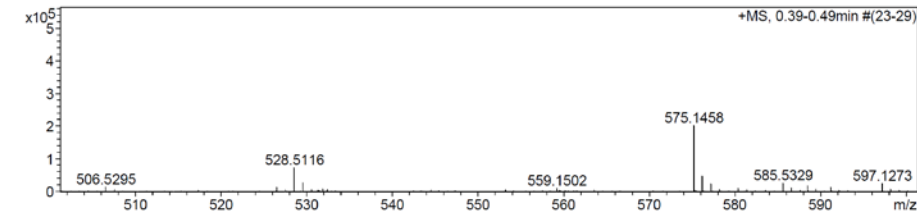
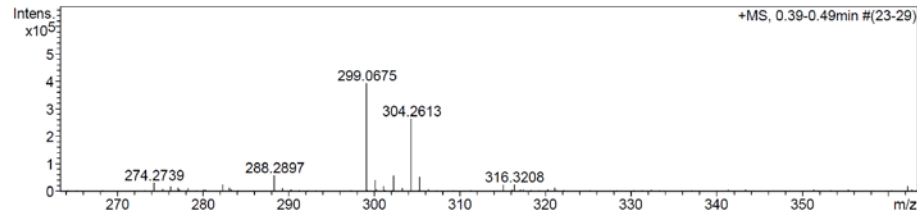
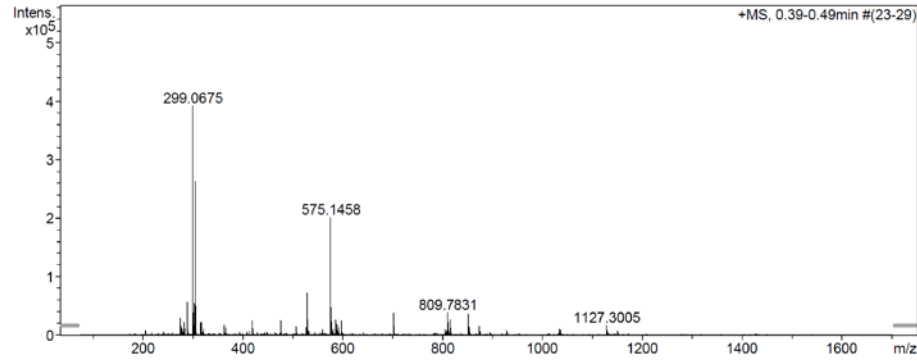
Analysis Name E:\new acq data for data analysis\FS97 001.d  
 Method hn Direct\_Infusion\_pos mode\_75-1700 mid 4eV.m  
 Sample Name Fabian Schwizer  
 Comment FS97, ca. 5 ug/mL MeOH

Acquisition Date 30.03.2017 15:04:52

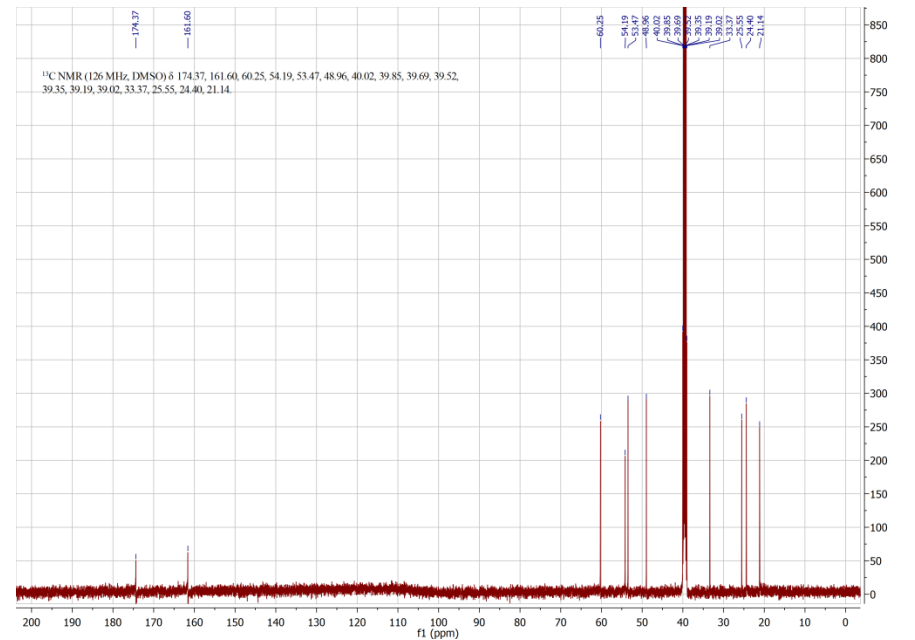
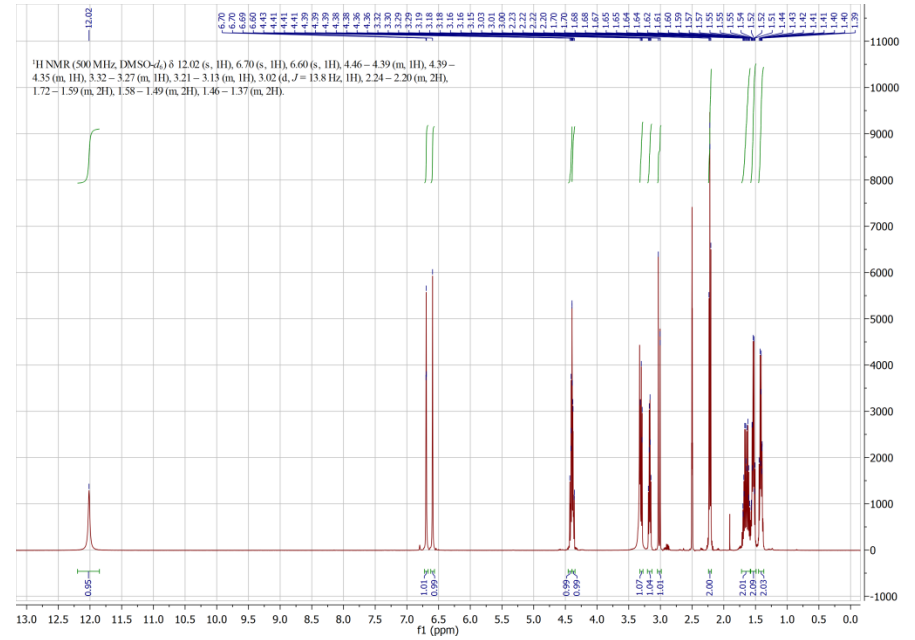
Operator hn  
 Instrument / Ser# maXis 4G 21243

**Acquisition Parameter**

Source Type	ESI	Ion Polarity	Positive	Set Nebulizer	0.4 Bar
Focus	Not active	Set Capillary	3600 V	Set Dry Heater	180 °C
Scan Begin	75 m/z	Set End Plate Offset	-500 V	Set Dry Gas	4.0 l/min
Scan End	1700 m/z	Collision Energy	8.0 eV	Set Ion Energy ( MS only )	4.0 eV



Meas. m/z	#	Formula	Score	m/z	err [mDa]	err [ppm]	mSigma	rdb	e <sup>-</sup> Conf	z
299.0675	1	C 10 H 16 N 2 Na O 5 S	100.00	299.0672	-0.3	-1.1	16.8	3.5	even	1+
575.1458	1	C 20 H 32 N 4 Na O 10 S 2	100.00	575.1452	-0.6	-1.0	17.5	6.5	even	



Annex 14: Compound 37

Mass Spectrum SmartFormula Report

Analysis Info

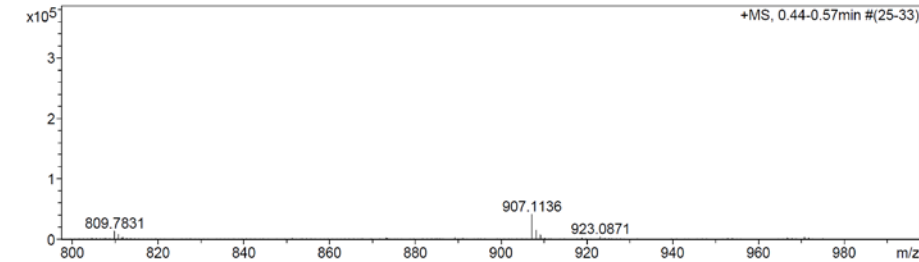
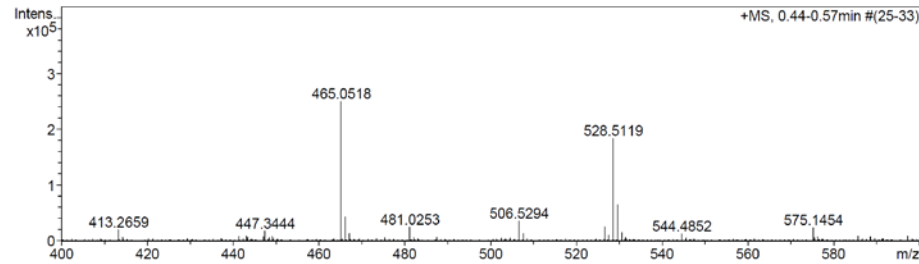
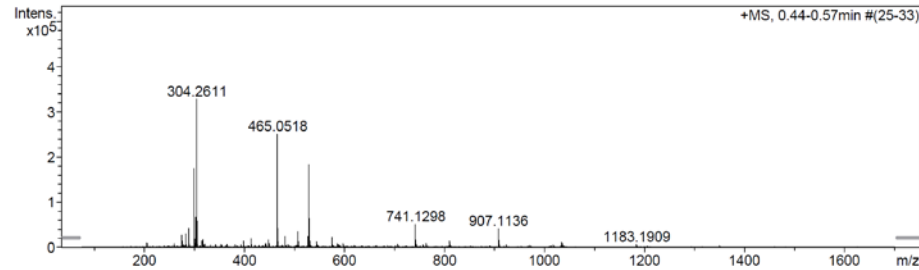
Analysis Name E:\new acq data for data analysis\FS98 001.d  
 Method hn Direct\_Infusion\_pos mode\_75-1700 mid 4eV.m  
 Sample Name Fabian Schwizer  
 Comment FS98, ca. 5 ug/mL MeCN

Acquisition Date 30.03.2017 16:26:21

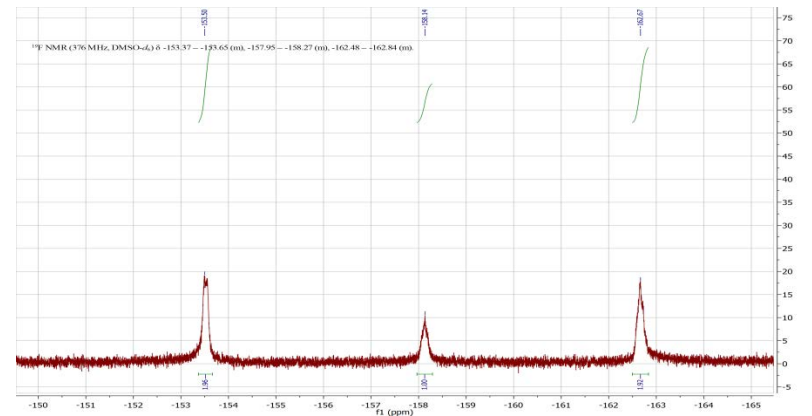
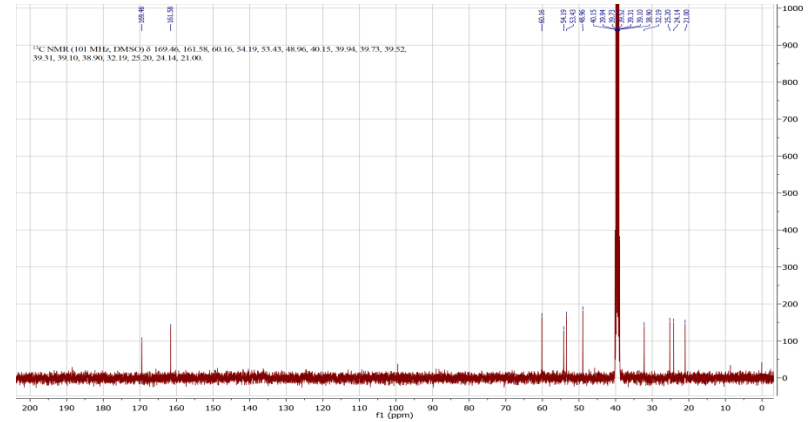
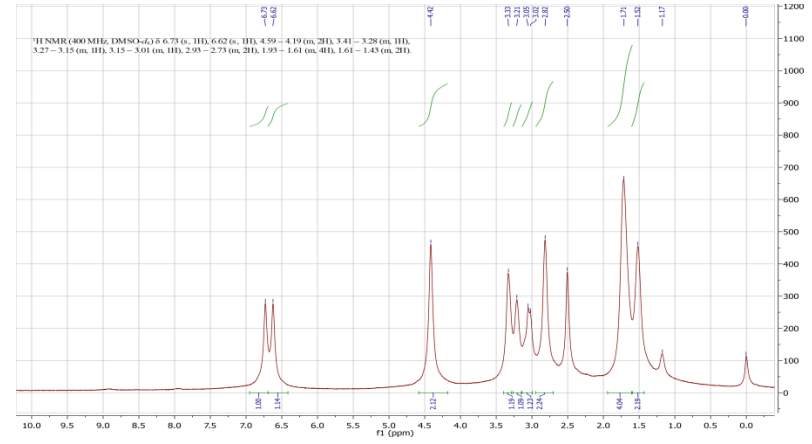
Operator hn  
 Instrument / Ser# maXis 4G 21243

Acquisition Parameter

Source Type ESI Ion Polarity Positive Set Nebulizer 0.4 Bar  
 Focus Not active Set Capillary 3600 V Set Dry Heater 180 °C  
 Scan Begin 75 m/z Set End Plate Offset -500 V Set Dry Gas 4.0 l/min  
 Scan End 1700 m/z Collision Energy 15.0 eV Set Ion Energy ( MS only ) 4.0 eV



Meas. m/z	#	Formula	Score	m/z	err [mDa]	err [ppm]	mSigma	rdB	e <sup>-</sup> Conf	z
465.0518	1	C 16 H 15 F 5 N 2 Na O 5 S	100.00	465.0514	-0.4	-0.8	14.4	7.5	even	1+
481.0253	1	C 16 H 15 F 5 K N 2 O 5 S	100.00	481.0253	0.1	0.1	7.4	7.5	even	
907.1136	1	C 32 H 30 F 10 N 4 Na O 10 S 2	100.00	907.1136	-0.0	-0.0	5.6	14.5	even	



Annex 15: Compound 38

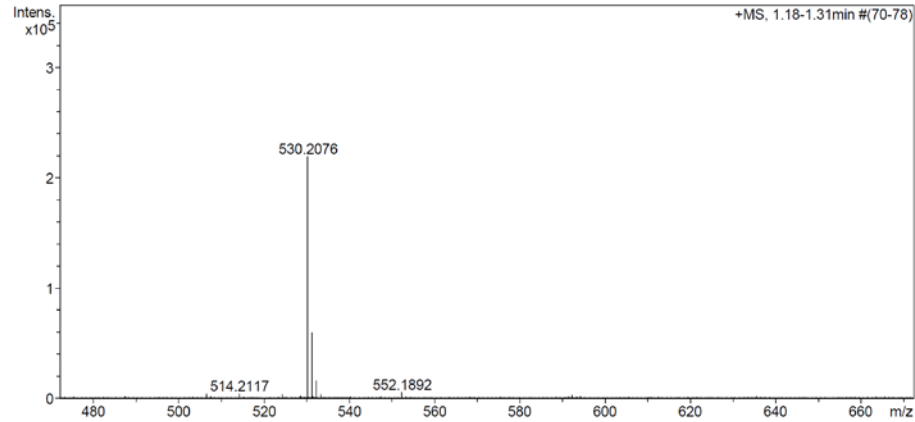
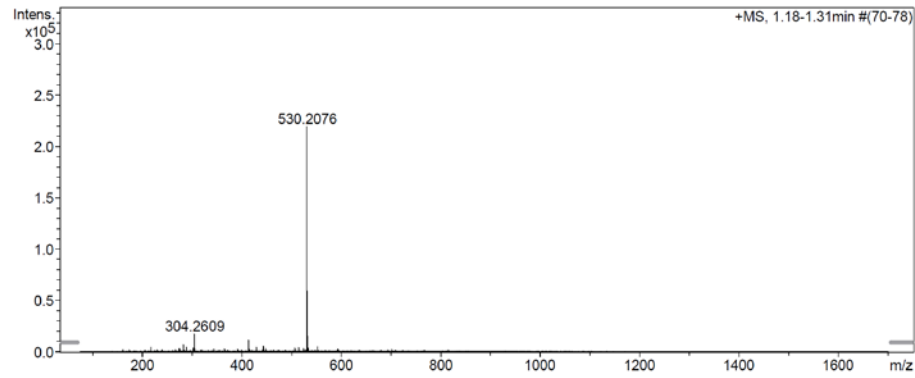
Mass Spectrum SmartFormula Report

**Analysis Info**  
 Analysis Name: E:\new acq data for data analysis\FS102 001.d  
 Method: hn Direct\_Infusion\_pos mode\_75-1700 mid 4eV.m  
 Sample Name: Fabian Schwizer  
 Comment: FS102, ca. 5 ug/mL MeOH

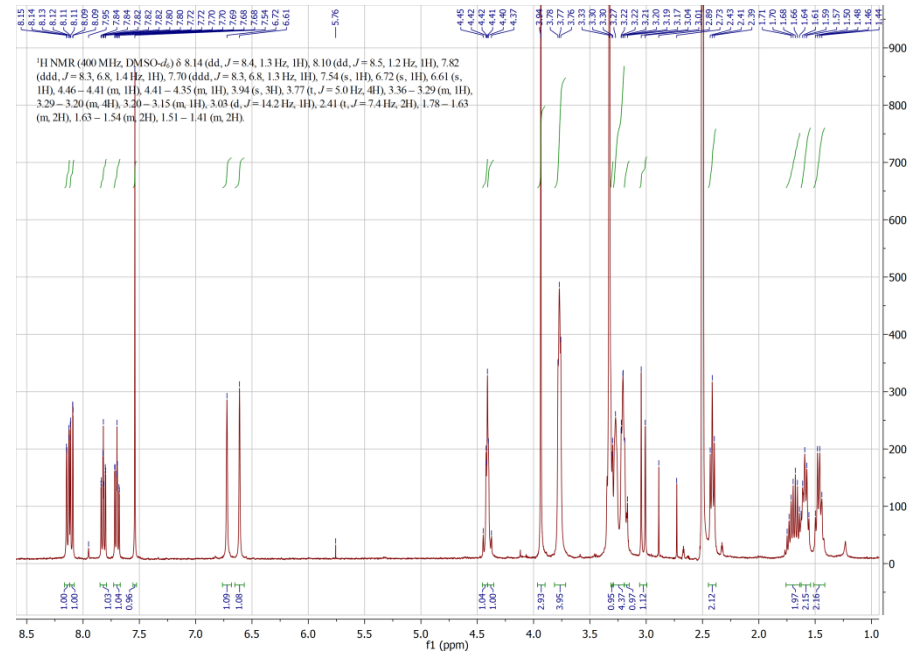
Acquisition Date: 31.03.2017 09:43:27  
 Operator: hn  
 Instrument / Ser#: maXis 4G 21243

**Acquisition Parameter**

Source Type	ESI	Ion Polarity	Positive	Set Nebulizer	0.4 Bar
Focus	Not active	Set Capillary	3600 V	Set Dry Heater	180 °C
Scan Begin	75 m/z	Set End Plate Offset	-500 V	Set Dry Gas	4.0 l/min
Scan End	1700 m/z	Collision Energy	8.0 eV	Set Ion Energy (MS only)	4.0 eV



Meas. m/z	#	Formula	Score	m/z	err [mDa]	err [ppm]	mSigma	rdb	e <sup>-</sup> Conf	z
530.2076	1	C <sub>25</sub> H <sub>32</sub> N <sub>5</sub> O <sub>6</sub> S	100.00	530.2068	-0.8	-1.5	20.6	12.5	even	1+
552.1892	1	C <sub>25</sub> H <sub>31</sub> N <sub>5</sub> NaO <sub>6</sub> S	100.00	552.1887	-0.5	-0.9	13.3	12.5	even	
568.1624	1	C <sub>25</sub> H <sub>31</sub> KN <sub>5</sub> O <sub>6</sub> S	100.00	568.1627	0.2	0.4	33.4	12.5	even	



Annex 16: Compound 39

### Mass Spectrum SmartFormula Report

**Analysis Info**

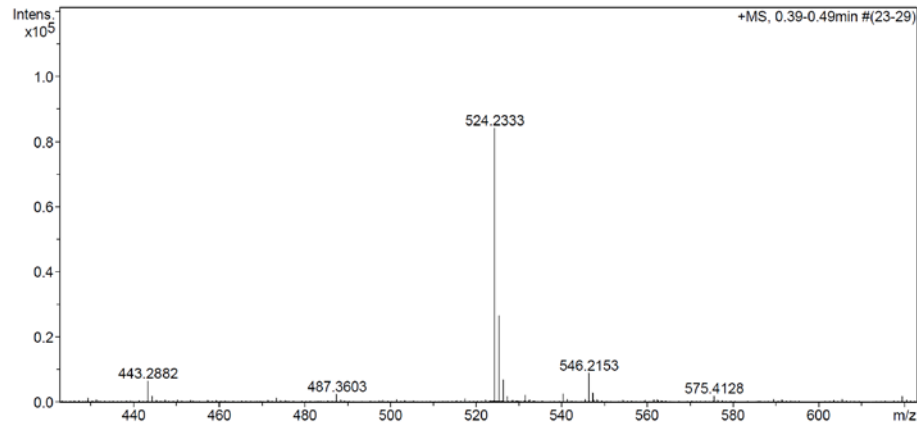
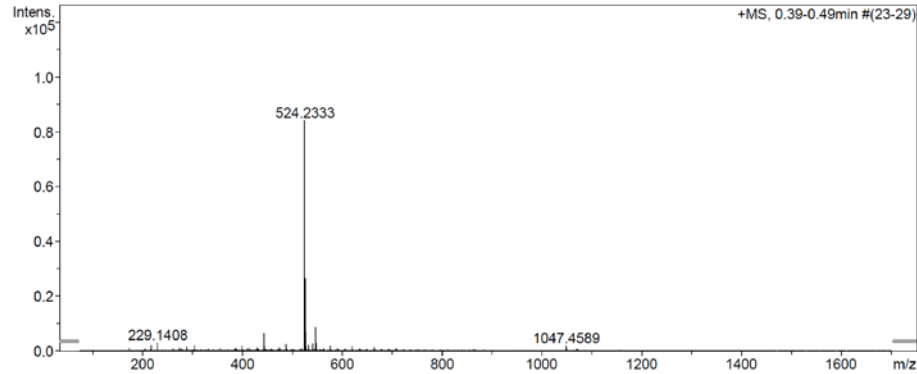
Analysis Name E:\new acq data for data analysis\FS65 002.d  
 Method hn Direct\_Infusion\_pos mode\_75-1700 mid 4eV.m  
 Sample Name Fabian Schwizer  
 Comment FS65, ca. 5 ug/mL MeCN

Acquisition Date 30.03.2017 17:07:01

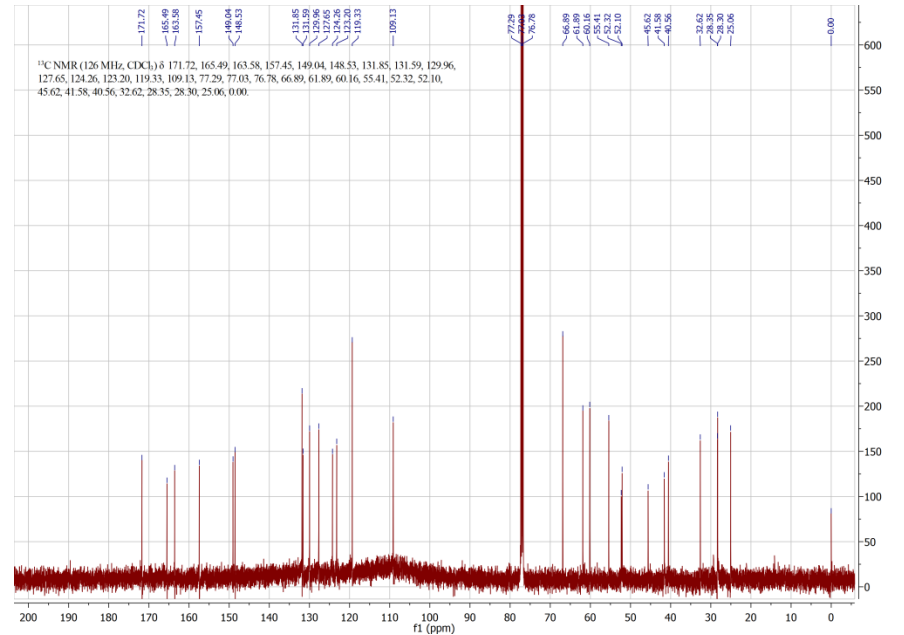
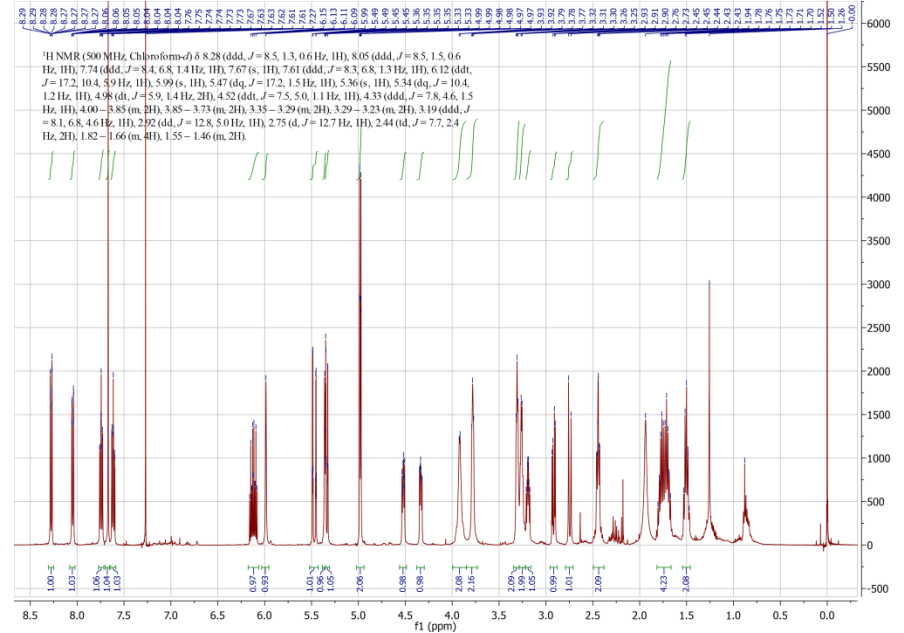
Operator hn  
 Instrument / Ser# maXis 4G 21243

**Acquisition Parameter**

Source Type	ESI	Ion Polarity	Positive	Set Nebulizer	0.4 Bar
Focus	Not active	Set Capillary	3600 V	Set Dry Heater	180 °C
Scan Begin	75 m/z	Set End Plate Offset	-500 V	Set Dry Gas	4.0 l/min
Scan End	1700 m/z	Collision Energy	8.0 eV	Set Ion Energy (MS only)	4.0 eV



Meas. m/z	#	Formula	Score	m/z	err [mDa]	err [ppm]	mSigma	rdb	e <sup>-</sup> Conf	z
524.2333	1	C 27 H 34 N 5 O 4 S	100.00	524.2326	-0.7	-1.4	12.5	13.5	even	1+
546.2153	1	C 27 H 33 N 5 Na O 4 S	100.00	546.2145	-0.8	-1.4	12.8	13.5	even	
1047.4589	1	C 54 H 67 N 10 O 8 S 2	100.00	1047.4579	-1.0	-0.9	29.1	26.5	even	
1069.4402	1	C 54 H 66 N 10 Na O 8 S 2	100.00	1069.4399	-0.3	-0.3	33.4	26.5	even	



Annex 17: Compound 18

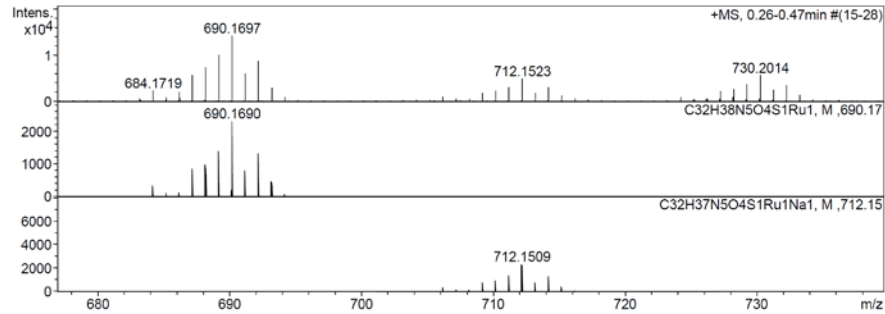
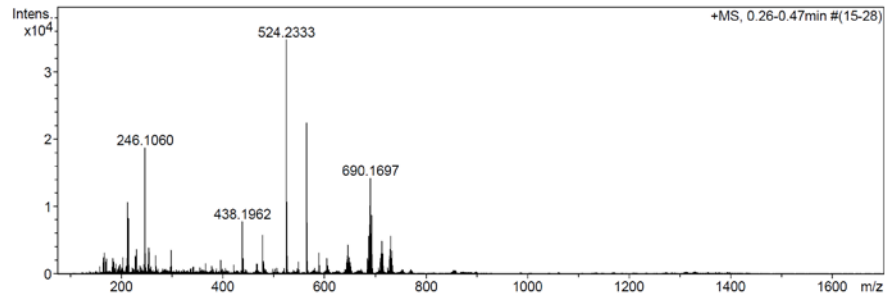
Mass Spectrum SmartFormula Report

**Analysis Info**  
 Analysis Name N:\new acq data\RuBiot 001.d  
 Method hn Direct\_Infusion\_pos mode\_75-1700 mid 4eV.m  
 Sample Name Fabian Schwizer, RuBiot  
 Comment ca. 10 ug/ml ACN

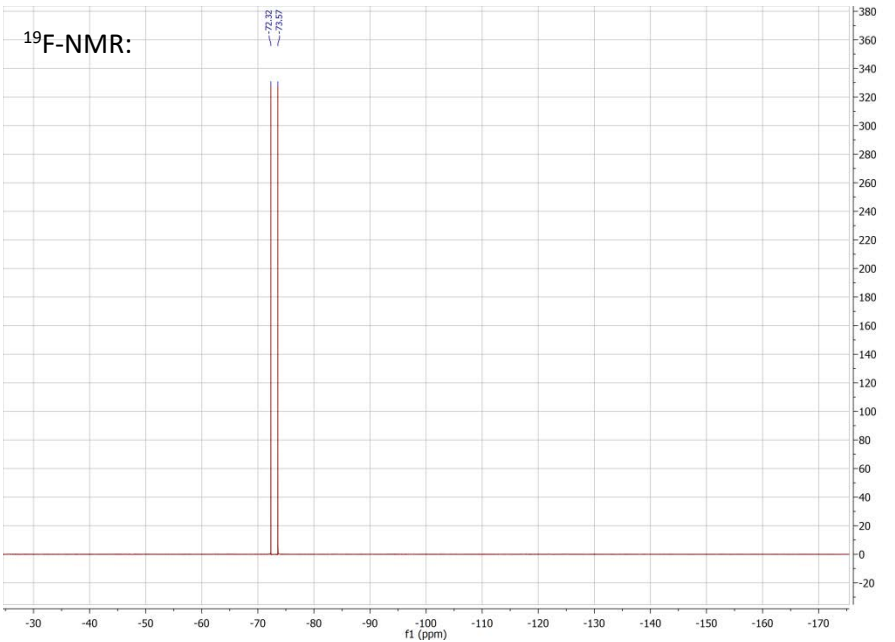
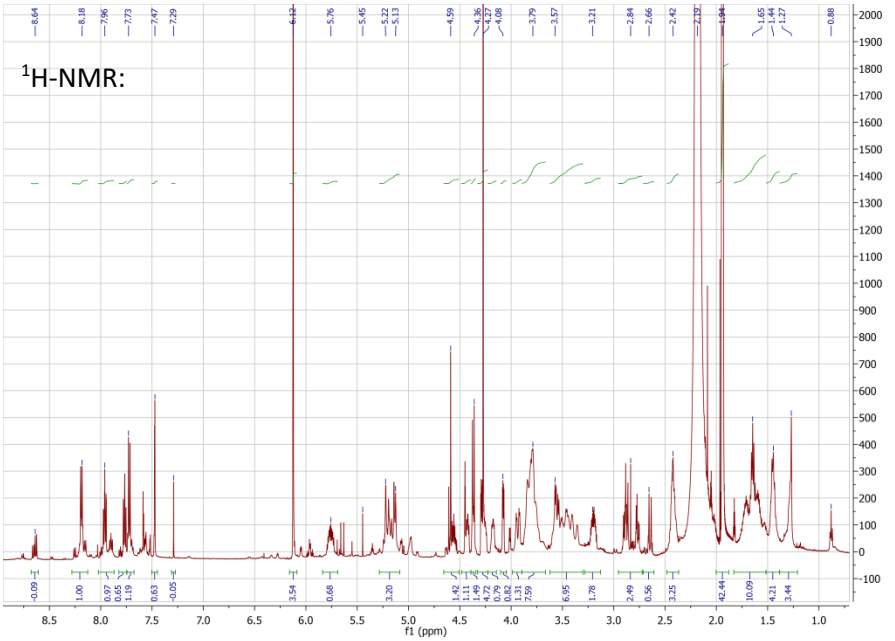
Acquisition Date 13.08.2015 10:22:24  
 Operator hn  
 Instrument / Ser# maXis 4G 21243

**Acquisition Parameter**

Source Type	ESI	Ion Polarity	Positive	Set Nebulizer	0.4 Bar
Focus	Not active	Set Capillary	3600 V	Set Dry Heater	180 °C
Scan Begin	75 m/z	Set End Plate Offset	-500 V	Set Dry Gas	4.0 l/min
Scan End	1700 m/z	Set Collision Cell RF	500.0 Vpp	Set Ion Energy ( MS only )	60.0 eV



Meas. m/z	#	Formula	Score	m/z	err [mDa]	err [ppm]	mSigma	rb	e <sup>-</sup> Conf	N-Rule	z
690.1697	1	C 32 H 38 N 5 O 4 Ru S	100.00	690.1690	-0.7	-1.0	51.8	17.0	odd	-	1+
712.1523	1	C 32 H 37 N 5 Na O 4 Ru S	100.00	712.1509	-1.4	-1.9	32.5	17.0	odd	-	-



Annex 18: Compound 7

### Mass Spectrum SmartFormula Report

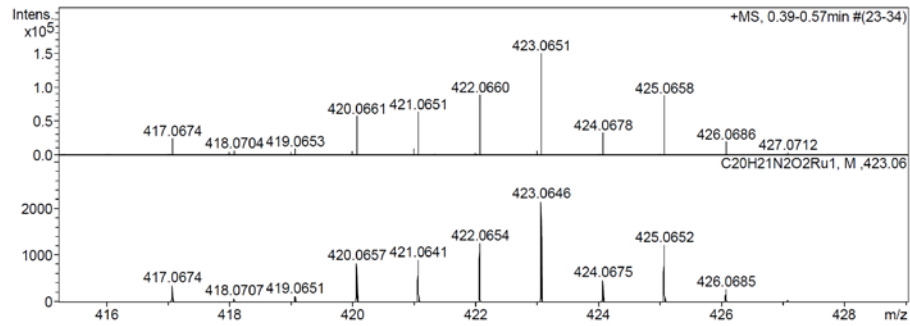
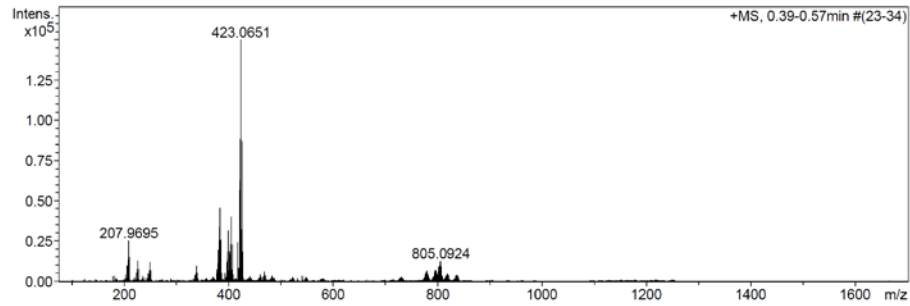
**Analysis Info**

Analysis Name N:\new acq data\RuNMe2 001.d  
 Method hn Direct\_Infusion\_pos mode\_75-1700 mid 4eV.m  
 Sample Name Fabian Schwizer, RuNMe2  
 Comment ca. 10 ug/ml ACN

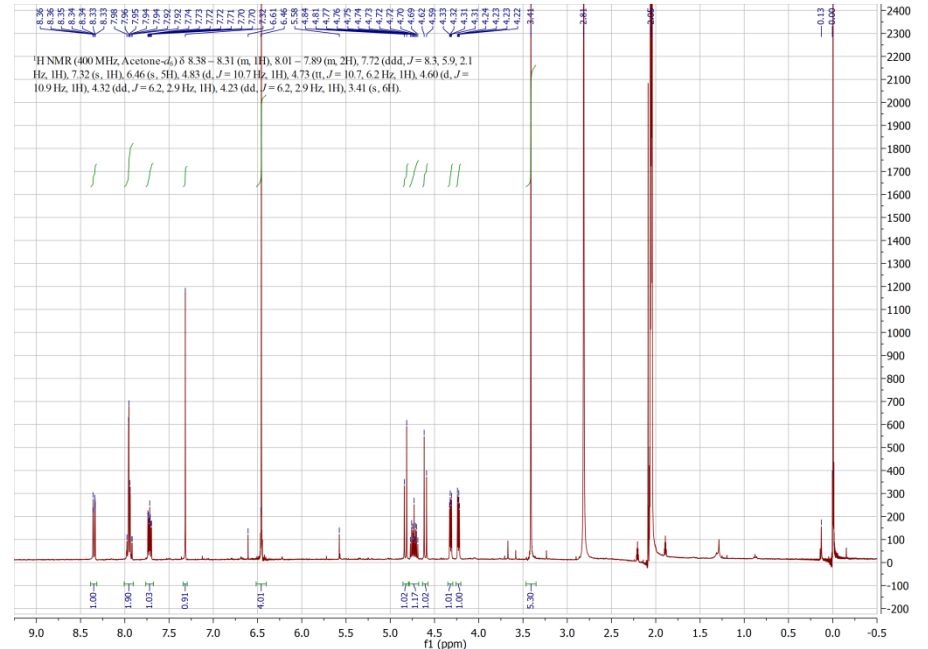
Acquisition Date 13.08.2015 09:38:22  
 Operator hn  
 Instrument / Ser# maXis 4G 21243

**Acquisition Parameter**

Source Type	ESI	Ion Polarity	Positive	Set Nebulizer	0.4 Bar
Focus	Not active	Set Capillary	3600 V	Set Dry Heater	180 °C
Scan Begin	75 m/z	Set End Plate Offset	-500 V	Set Dry Gas	4.0 l/min
Scan End	1700 m/z	Set Collision Cell RF	500.0 Vpp	Set Ion Energy (MS only)	4.0 eV



Meas. m/z	#	Formula	Score	m/z	err [mDa]	err [ppm]	mSigma	rdb	e <sup>-</sup> Conf	N-Rule	z
423.0651	1	C 20 H 21 N 2 O 2 Ru	100.00	423.0646	-0.5	-1.2	13.3	12.0	odd	-	1+



Annex 19: Compound 1

### Mass Spectrum SmartFormula Report

**Analysis Info**

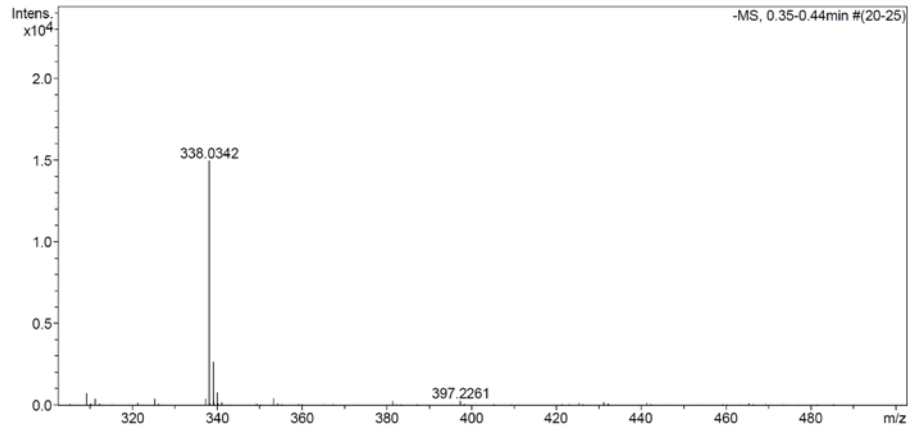
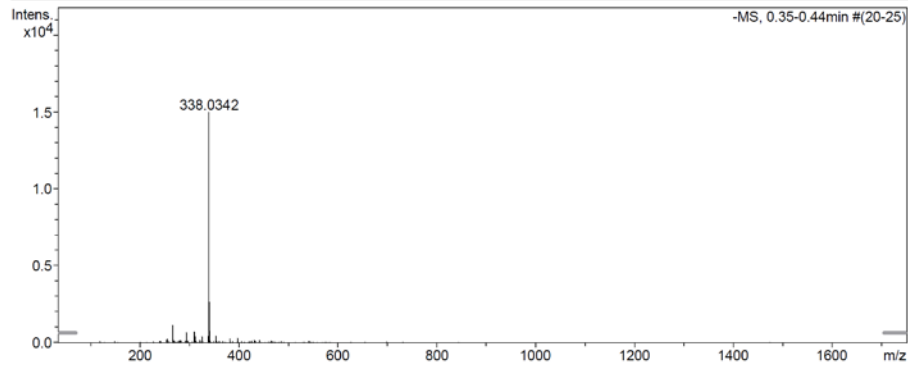
Analysis Name E:\acq data for data analysis\FS90 002.d  
 Method Direct\_neg\_mid.m  
 Sample Name Fabian Schwizer  
 Comment FS90, ca. 5 ug/ml MeCN

Acquisition Date 03.08.2017 10:36:55

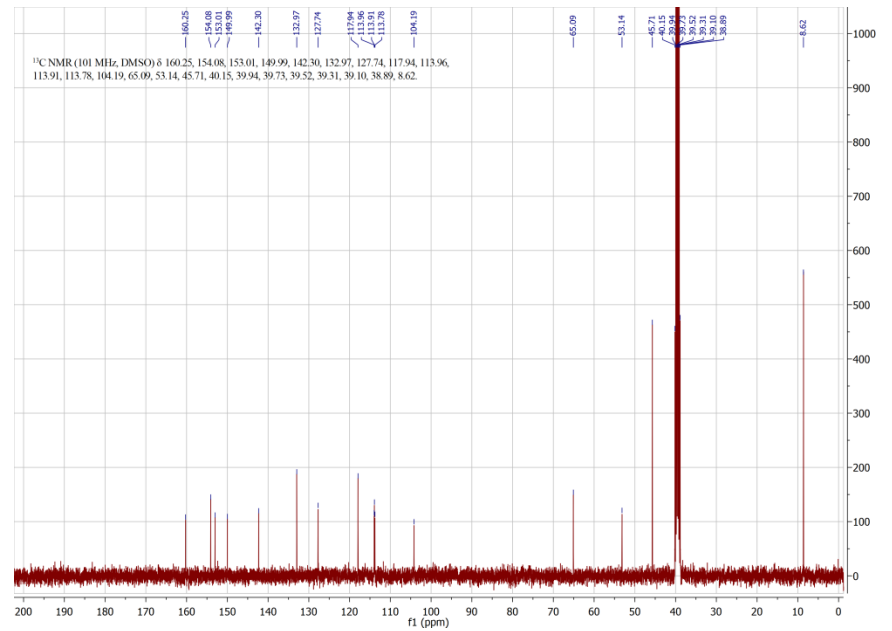
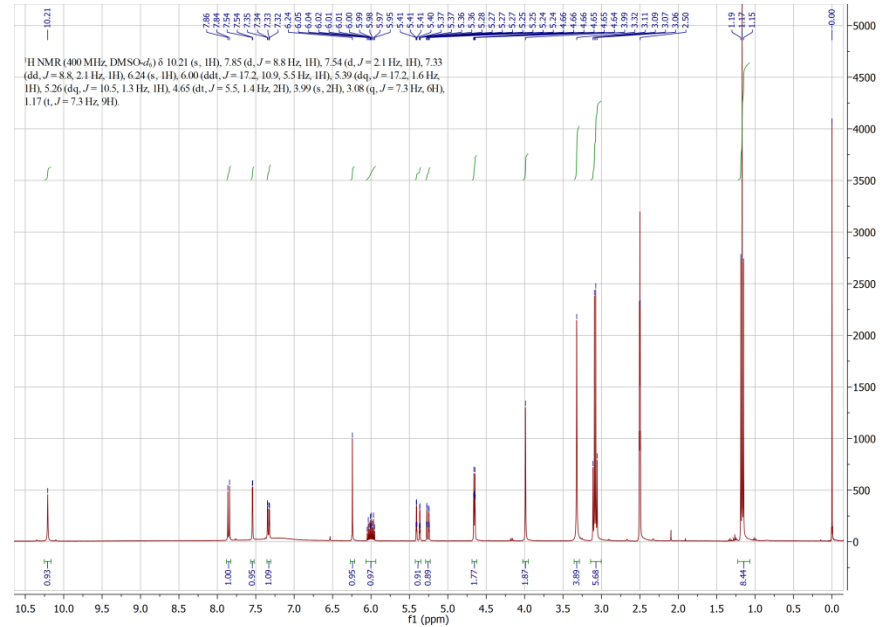
Operator hn  
 Instrument / Ser# maXis 4G 21243

**Acquisition Parameter**

Source Type	ESI	Ion Polarity	Negative	Set Nebulizer	0.4 Bar
Focus	Not active	Set Capillary	4500 V	Set Dry Heater	180 °C
Scan Begin	75 m/z	Set End Plate Offset	-500 V	Set Dry Gas	4.0 l/min
Scan End	1700 m/z	Collision Energy	-10.0 eV	Set Ion Energy (MS only)	-4.0 eV



Meas. m/z	#	Formula	Score	m/z	err [mDa]	err [ppm]	mSigma	rdb	e <sup>-</sup> Conf	z
338.0342	1	C <sub>14</sub> H <sub>12</sub> N <sub>2</sub> O <sub>7</sub> S	100.00	338.0340	-0.2	-0.6	12.6	9.5	even	1-



Annex 20: Compound 2

### Mass Spectrum SmartFormula Report

**Analysis Info**

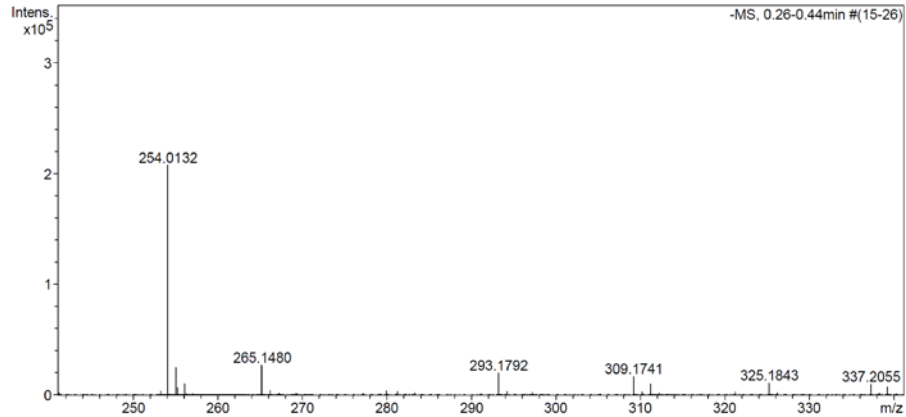
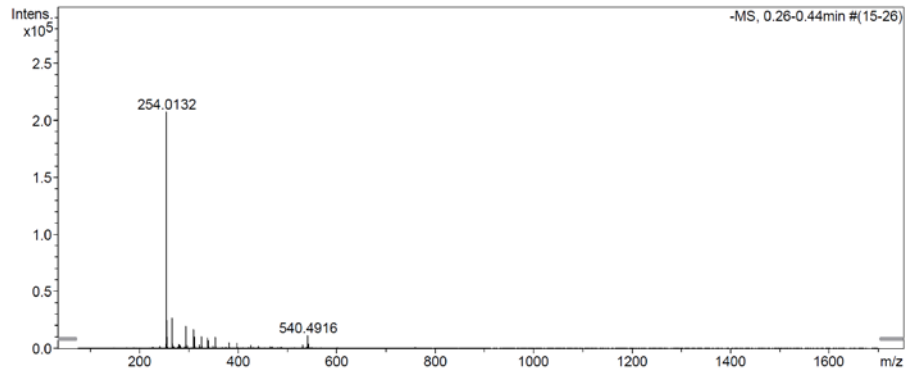
Analysis Name E:\acq data for data analysis\FS89 002.d  
 Method hn Direct\_Infusion\_neg\_mode\_75-1700 mid 4eV.m  
 Sample Name Fabian Schwizer  
 Comment FS89, ca. 5 ug/ml MeCN

Acquisition Date 03.08.2017 10:01:34

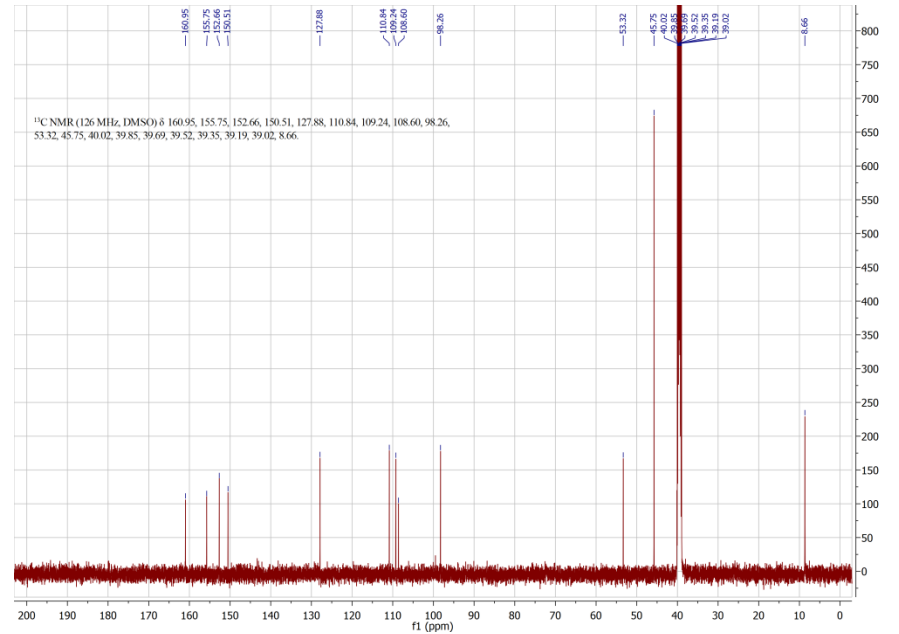
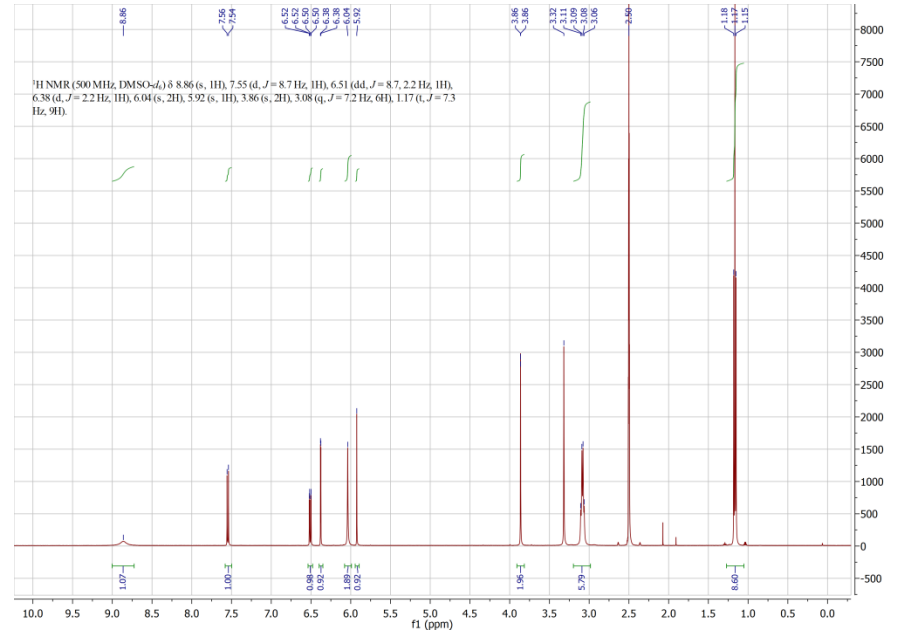
Operator hn  
 Instrument / Ser# maXis 4G 21243

**Acquisition Parameter**

Source Type	ESI	Ion Polarity	Negative	Set Nebulizer	0.4 Bar
Focus	Not active	Set Capillary	4500 V	Set Dry Heater	180 °C
Scan Begin	75 m/z	Set End Plate Offset	-500 V	Set Dry Gas	4.0 l/min
Scan End	1700 m/z	Collision Energy	-10.0 eV	Set Ion Energy (MS only)	-4.0 eV



Meas. m/z	#	Formula	Score	m/z	err [mDa]	err [ppm]	mSigma	rdb	e <sup>-</sup> Conf	z
254.0132	1	C <sub>10</sub> H <sub>8</sub> NO <sub>5</sub> S	100.00	254.0129	-0.3	-1.3	7.6	7.5	even	1-





Annex 21: Compound 44

### Mass Spectrum SmartFormula Report

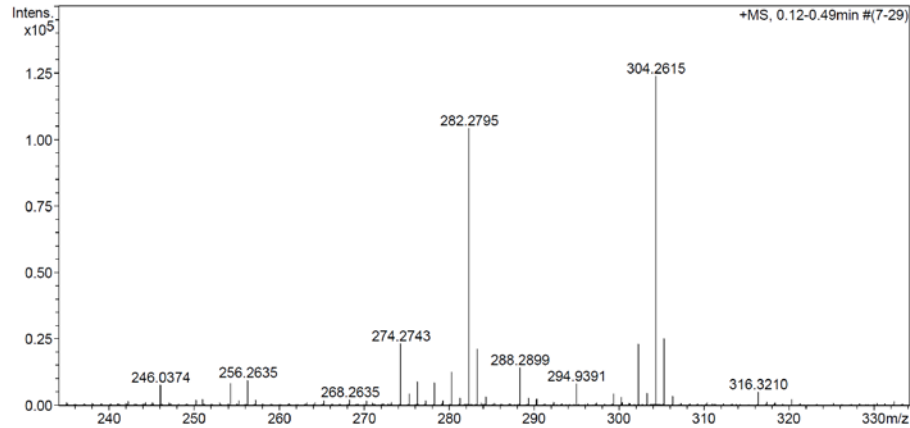
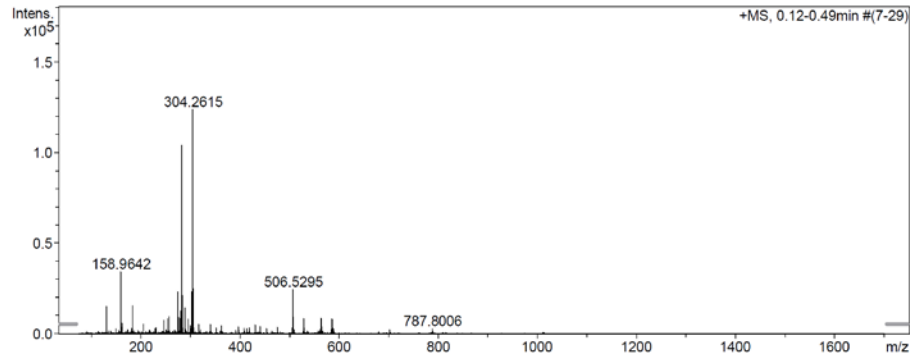
**Analysis Info**

Analysis Name E:\new acq data for data analysis\FS110 001.d  
 Method hn Direct\_Infusion\_pos\_mode\_75-1700 low 4eV.m  
 Sample Name Fabian Schwizer  
 Comment FS110, ca. 5 ug/ml MeOH

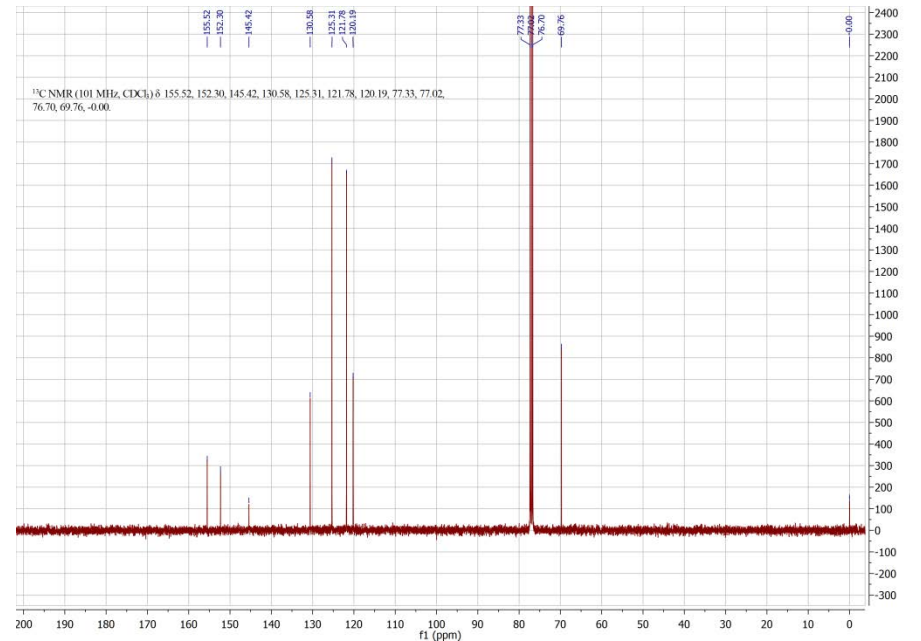
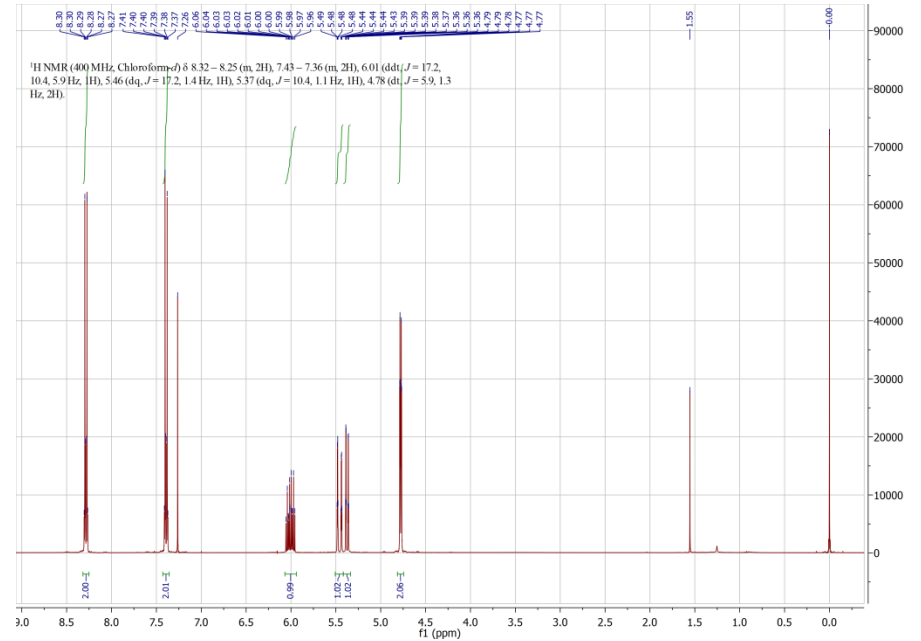
Acquisition Date 02.03.2017 15:10:08  
 Operator hn  
 Instrument / Ser# maXis 4G 21243

**Acquisition Parameter**

Source Type	ESI	Ion Polarity	Positive	Set Nebulizer	0.4 Bar
Focus	Not active	Set Capillary	3600 V	Set Dry Heater	180 °C
Scan Begin	75 m/z	Set End Plate Offset	-500 V	Set Dry Gas	3.0 l/min
Scan End	1700 m/z	Collision Energy	1.0 eV	Set Ion Energy (MS only)	4.0 eV



Meas. m/z	#	Formula	Score	m/z	err [mDa]	err [ppm]	mSigma	rdb	e <sup>-</sup> Conf	z
246.0374	1	C <sub>10</sub> H <sub>9</sub> NNaO <sub>5</sub>	100.00	246.0373	-0.1	-0.6	7.3	6.5	even	1+



Annex 22: Compound 46

### Mass Spectrum SmartFormula Report

**Analysis Info**

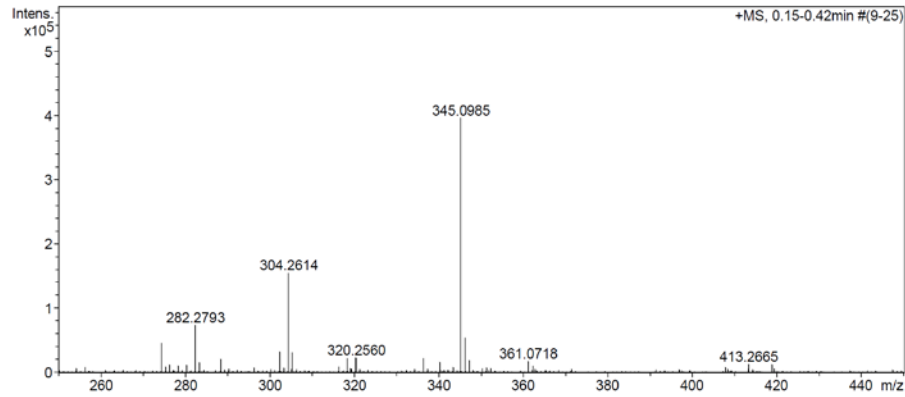
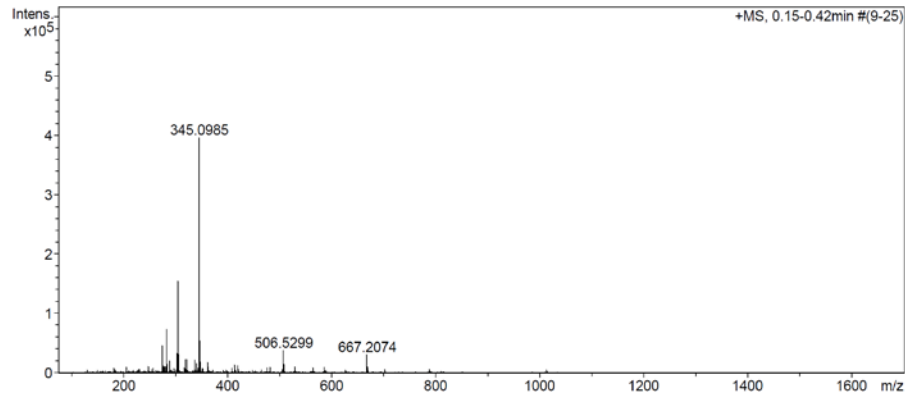
Analysis Name E:\new acq data for data analysis\FS112 002.d  
 Method hn Direct\_Infusion\_pos mode\_75-1700 low 4eV.m  
 Sample Name Fabian Schwizer  
 Comment FS112, ca. 5 ug/ml MeOH

Acquisition Date 02.03.2017 15:50:21

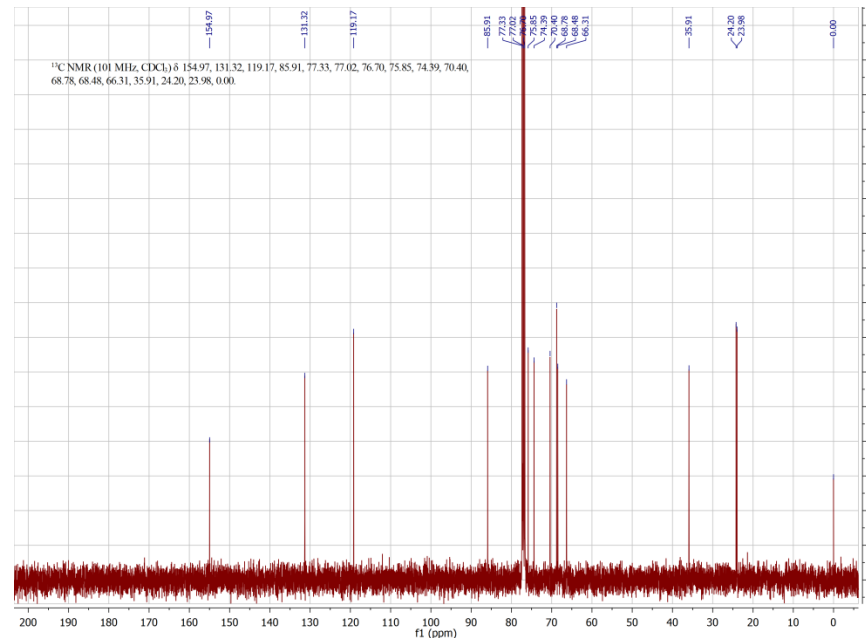
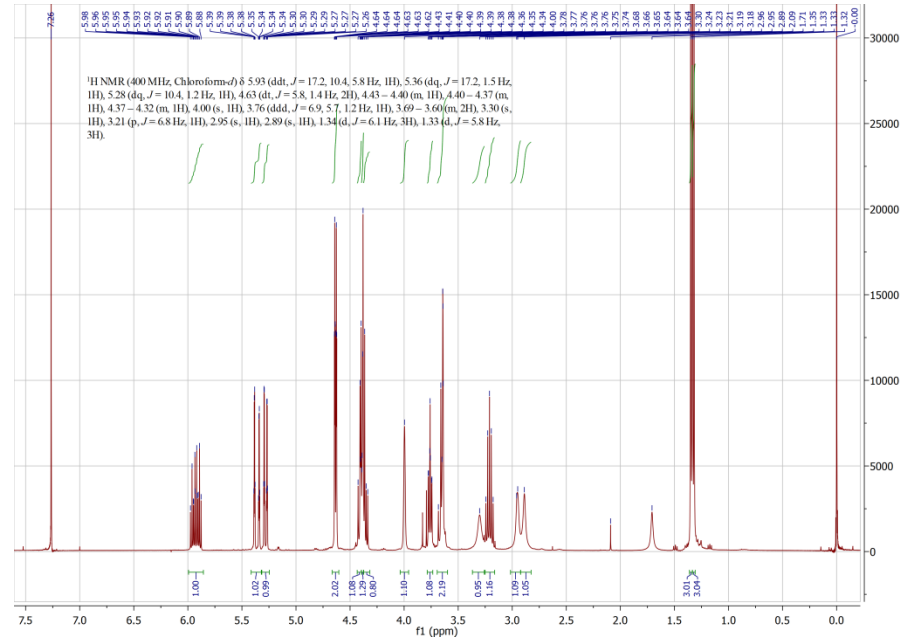
Operator hn  
 Instrument / Ser# maXis 4G 21243

**Acquisition Parameter**

Source Type	ESI	Ion Polarity	Positive	Set Nebulizer	0.4 Bar
Focus	Not active	Set Capillary	3600 V	Set Dry Heater	180 °C
Scan Begin	75 m/z	Set End Plate Offset	-500 V	Set Dry Gas	3.0 l/min
Scan End	1700 m/z	Collision Energy	8.0 eV	Set Ion Energy ( MS only )	4.0 eV



Meas. m/z	#	Formula	Score	m/z	err [mDa]	err [ppm]	mSigma	rdb	e <sup>-</sup> Conf	z
345.0985	1	C 13 H 22 Na O 7 S	100.00	345.0978	-0.6	-1.8	13.5	2.5	even	1+
361.0718	1	C 13 H 22 K O 7 S	100.00	361.0718	0.0	0.0	8.5	2.5	even	
667.2074	1	C 26 H 44 Na O 14 S 2	100.00	667.2065	-0.9	-1.4	9.7	4.5	even	



Annex 23: Compound 48

### Mass Spectrum SmartFormula Report

**Analysis Info**

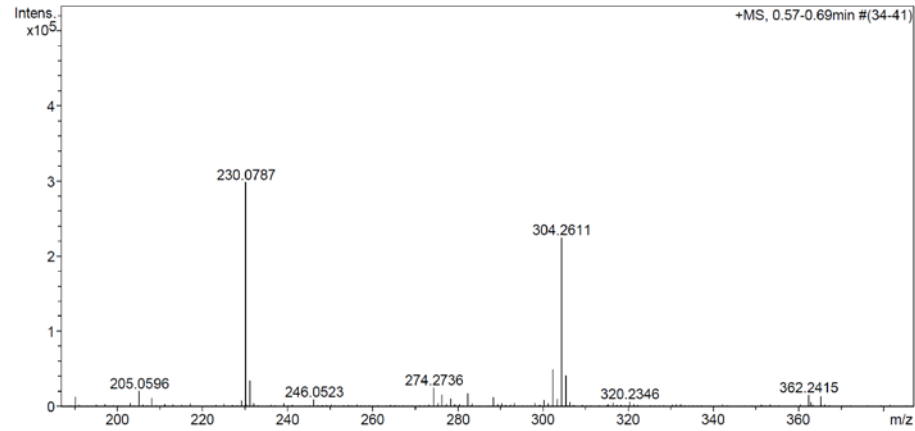
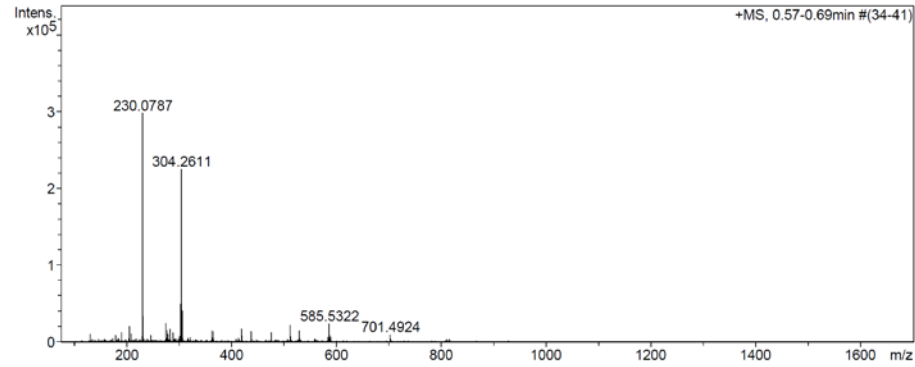
Analysis Name E:\new acq data for data analysis\FS139 002.d.d  
 Method hn Direct\_Infusion\_pos mode\_75-1700 low 4eV.m  
 Sample Name Fabian Schwizer  
 Comment FS139, ca. 5 ug/ml MeOH

Acquisition Date 02.03.2017 14:19:59

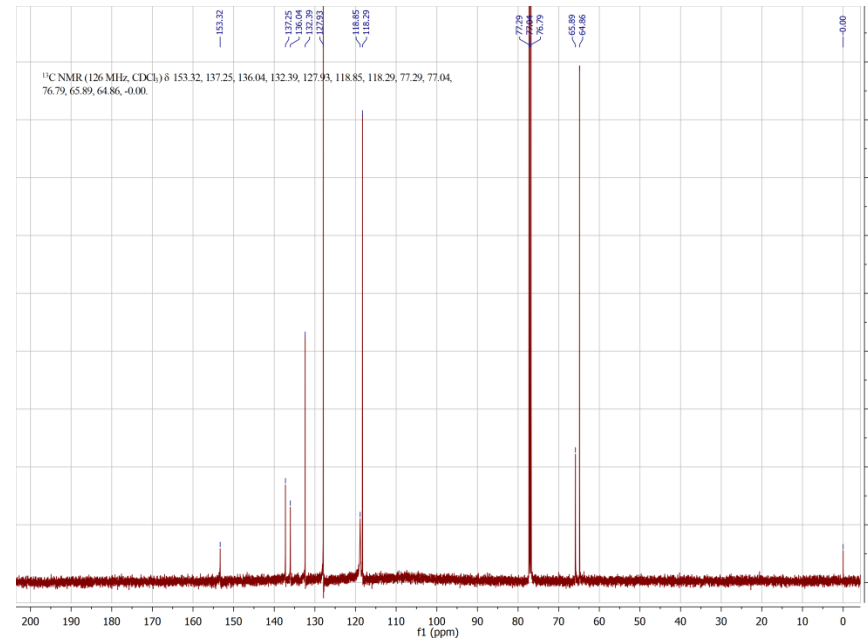
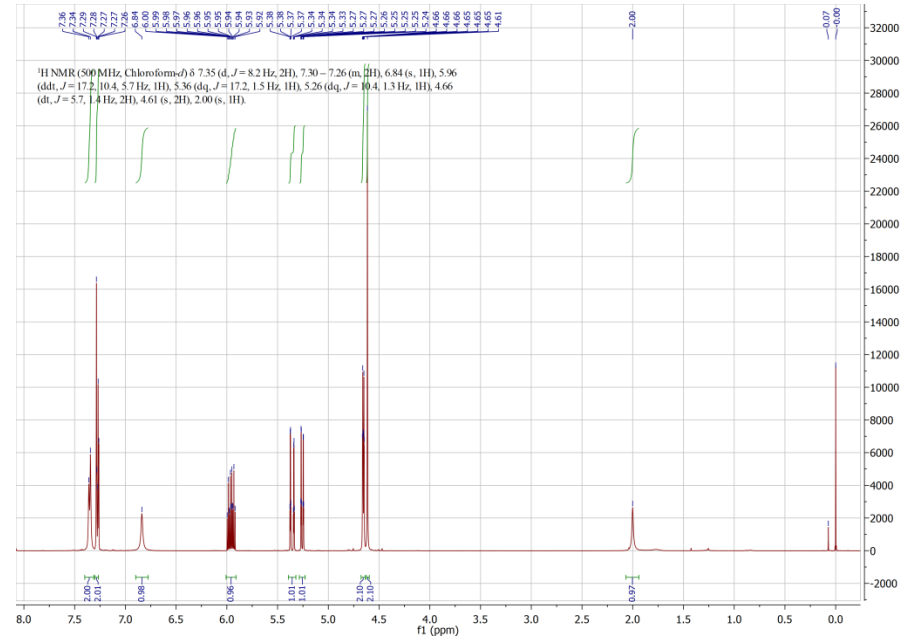
Operator hn  
 Instrument / Ser# maXis 4G 21243

**Acquisition Parameter**

Source Type	ESI	Ion Polarity	Positive	Set Nebulizer	0.4 Bar
Focus	Not active	Set Capillary	3600 V	Set Dry Heater	180 °C
Scan Begin	75 m/z	Set End Plate Offset	-500 V	Set Dry Gas	3.0 l/min
Scan End	1700 m/z	Collision Energy	8.0 eV	Set Ion Energy (MS only)	4.0 eV



Meas. m/z	#	Formula	Score	m/z	err [mDa]	err [ppm]	mSigma	rdb	e <sup>-</sup> Conf	z
230.0787	1	C 11 H 13 N Na O 3	100.00	230.0788	0.1	0.3	5.4	5.5	even	1+



Annex 24: Compound 49

### Mass Spectrum SmartFormula Report

**Analysis Info**

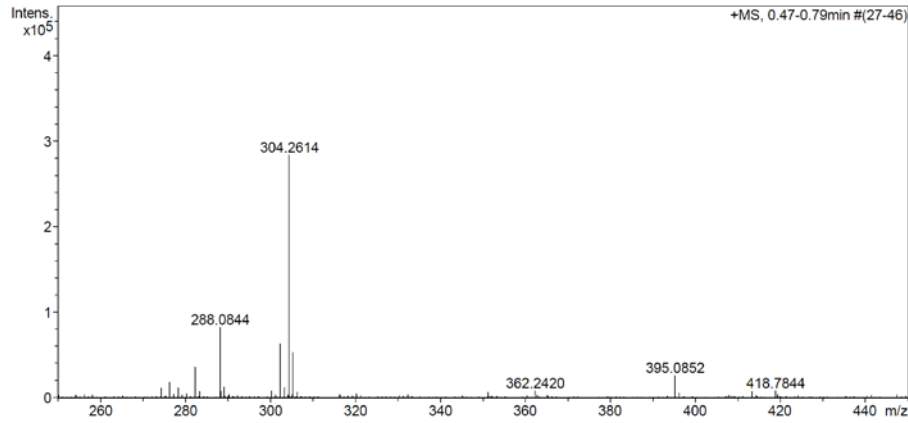
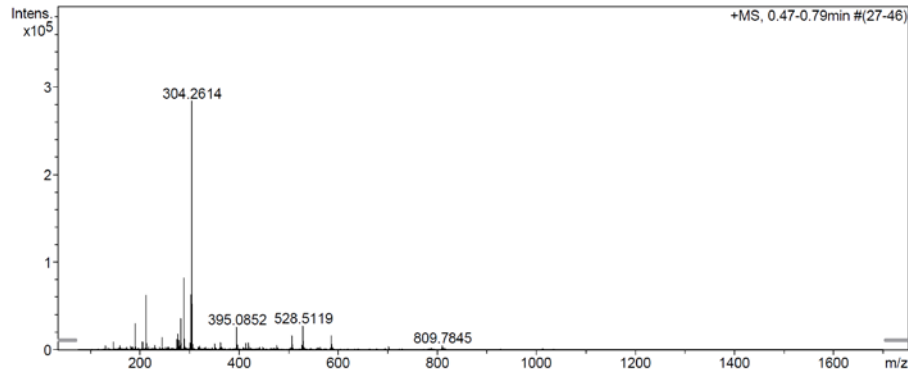
Analysis Name E:\new acq data for data analysis\FS144 002.d  
 Method hn Direct\_Infusion\_pos mode\_75-1700 low 4eV.m  
 Sample Name Fabian Schwizer  
 Comment FS144, ca. 5 ug/ml MeOH

Acquisition Date 02.03.2017 16:33:15

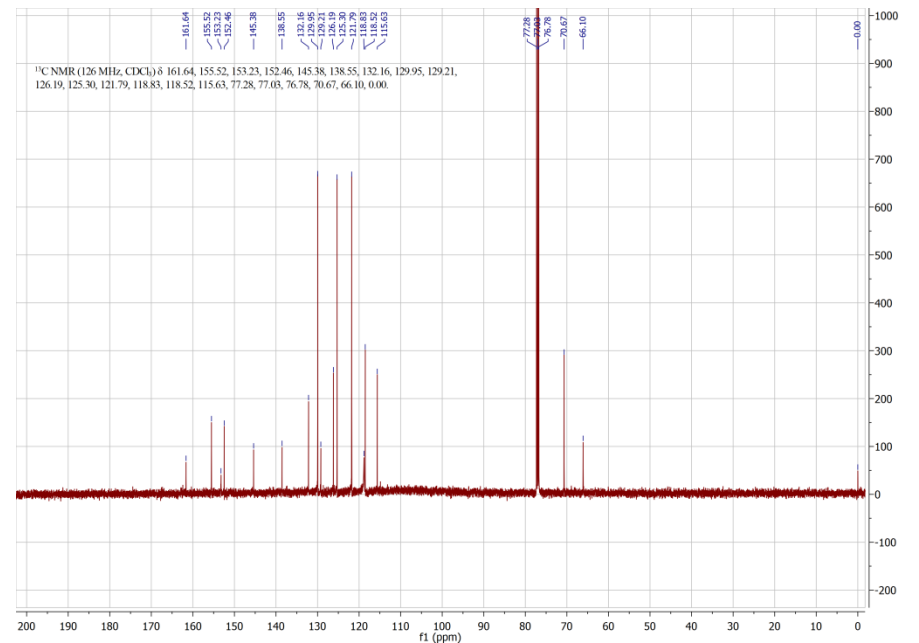
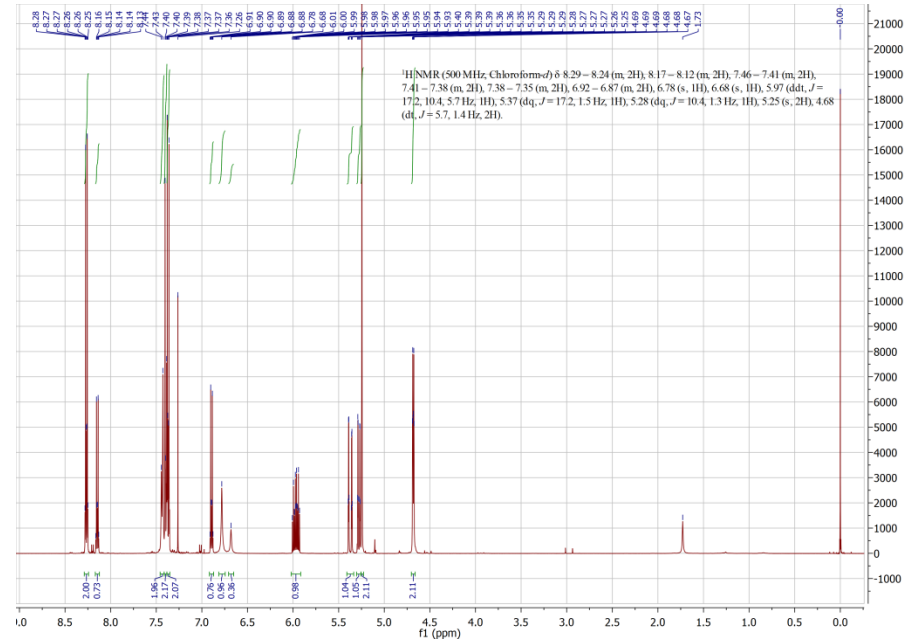
Operator hn  
 Instrument / Ser# maXis 4G 21243

**Acquisition Parameter**

Source Type	ESI	Ion Polarity	Positive	Set Nebulizer	0.4 Bar
Focus	Not active	Set Capillary	3600 V	Set Dry Heater	180 °C
Scan Begin	75 m/z	Set End Plate Offset	-500 V	Set Dry Gas	3.0 l/min
Scan End	1700 m/z	Collision Energy	8.0 eV	Set Ion Energy (MS only)	4.0 eV



Meas. m/z	#	Formula	Score	m/z	err [mDa]	err [ppm]	mSigma	rdb	e <sup>-</sup>	Conf	z
395.0852	1	C <sub>18</sub> H <sub>16</sub> N <sub>2</sub> NaO <sub>7</sub>	100.00	395.0850	-0.3	-0.7	2.8	11.5	even	1+	



Annex 25: Compound 50

### Mass Spectrum SmartFormula Report

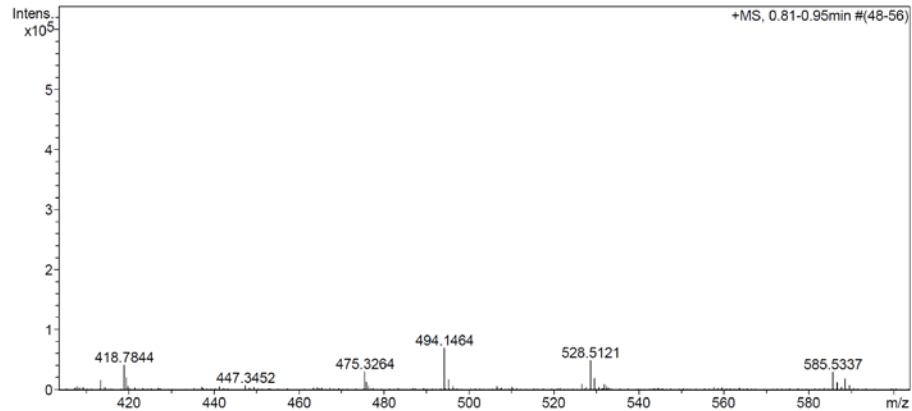
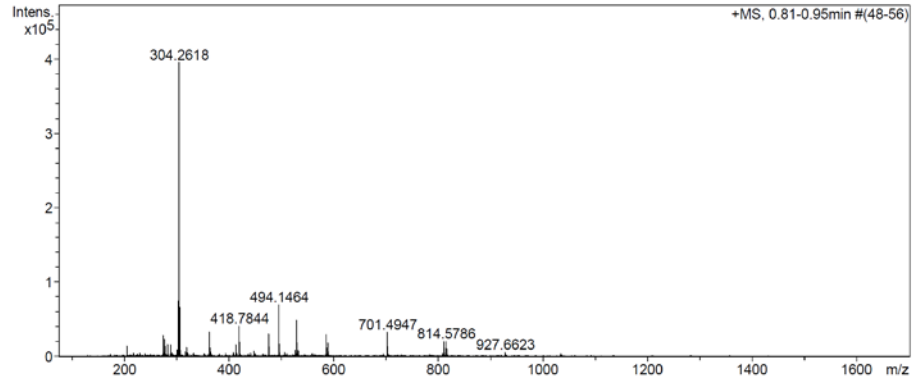
**Analysis Info**

Analysis Name E:\new acq data for data analysis\FS148 004.d  
 Method hn Direct\_Infusion\_pos mode\_75-1700 mid 4eV.m  
 Sample Name Fabian Schwizer  
 Comment FS148. ca. 5 ug/ml MeOH

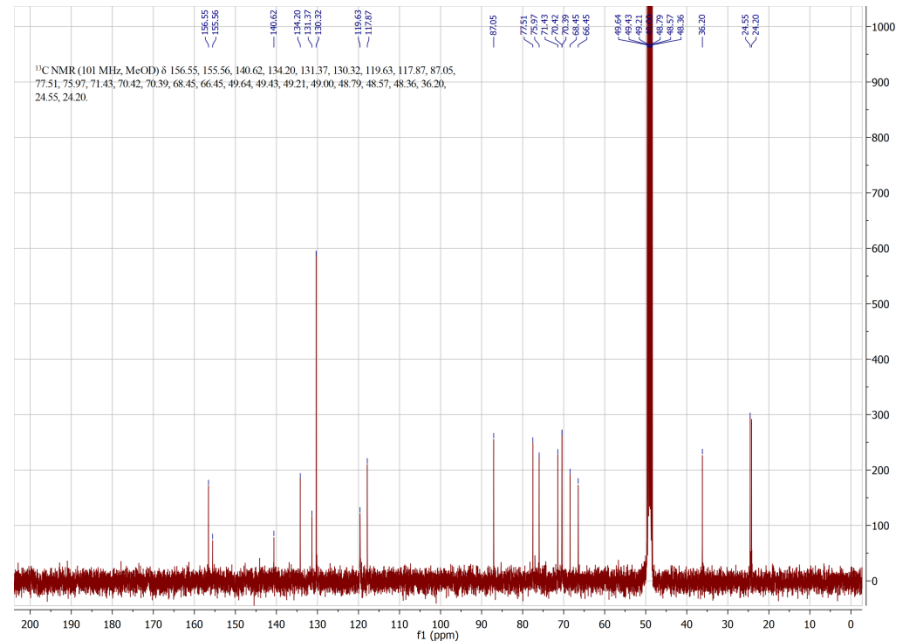
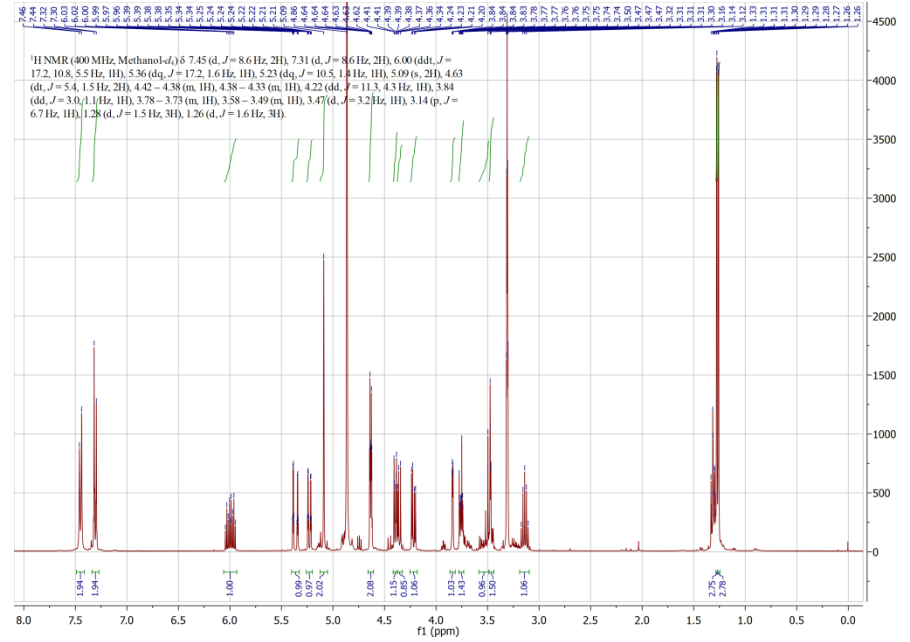
Acquisition Date 03.03.2017 09:41:53  
 Operator hn  
 Instrument / Ser# maXis 4G 21243

**Acquisition Parameter**

Source Type	ESI	Ion Polarity	Positive	Set Nebulizer	0.4 Bar
Focus	Not active	Set Capillary	3600 V	Set Dry Heater	180 °C
Scan Begin	75 m/z	Set End Plate Offset	-500 V	Set Dry Gas	4.0 l/min
Scan End	1700 m/z	Collision Energy	8.0 eV	Set Ion Energy (MS only)	4.0 eV



Meas. m/z	#	Formula	Score	m/z	err [mDa]	err [ppm]	mSigma	rdb	e <sup>-</sup> Conf	z
494.1464	1	C 21 H 29 N Na O 9 S	100.00	494.1455	-0.9	-1.9	9.7	7.5	even	1+



Annex 26: Compound 52

### Mass Spectrum SmartFormula Report

**Analysis Info**

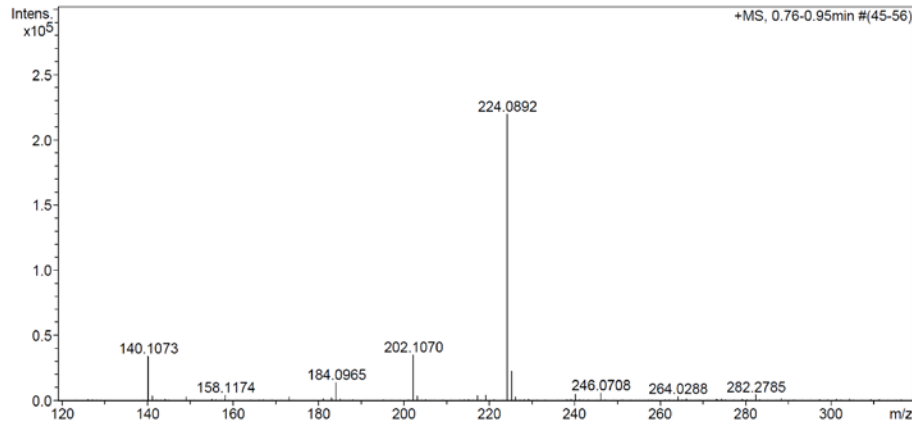
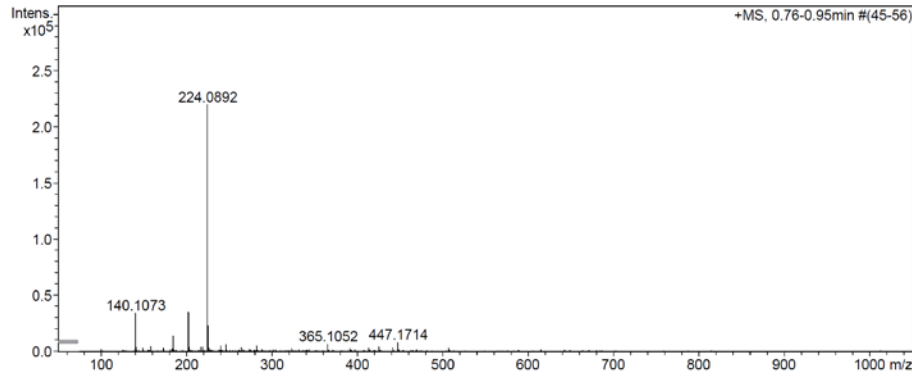
Analysis Name E:\new acq data for data analysis\FS143 001.d  
 Method hn Direct\_Infusion\_pos mode\_75-1700 low 4eV.m  
 Sample Name Fabian Schwizer  
 Comment FS143, ca. 5 ug/ml MeOH

Acquisition Date 13.03.2017 10:04:07

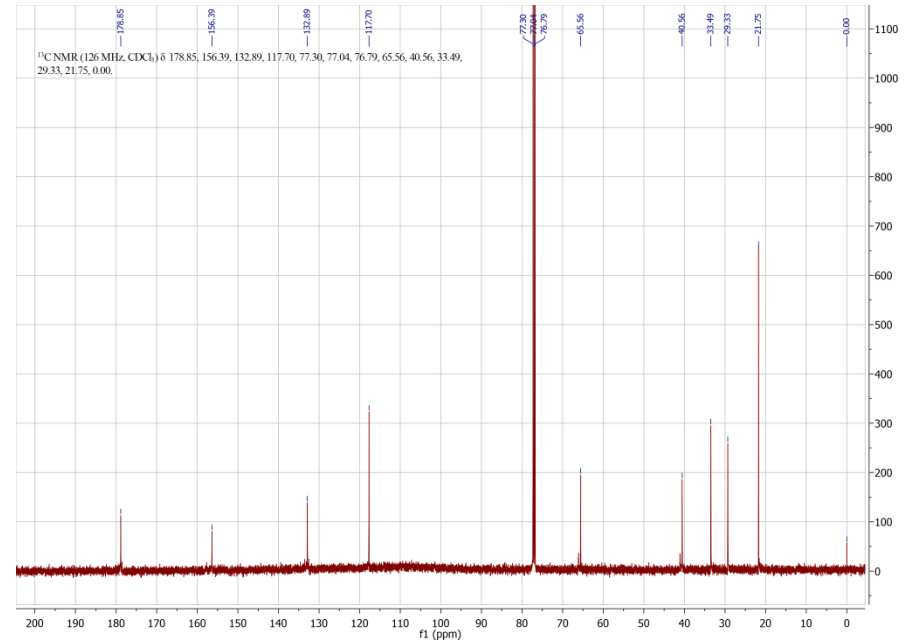
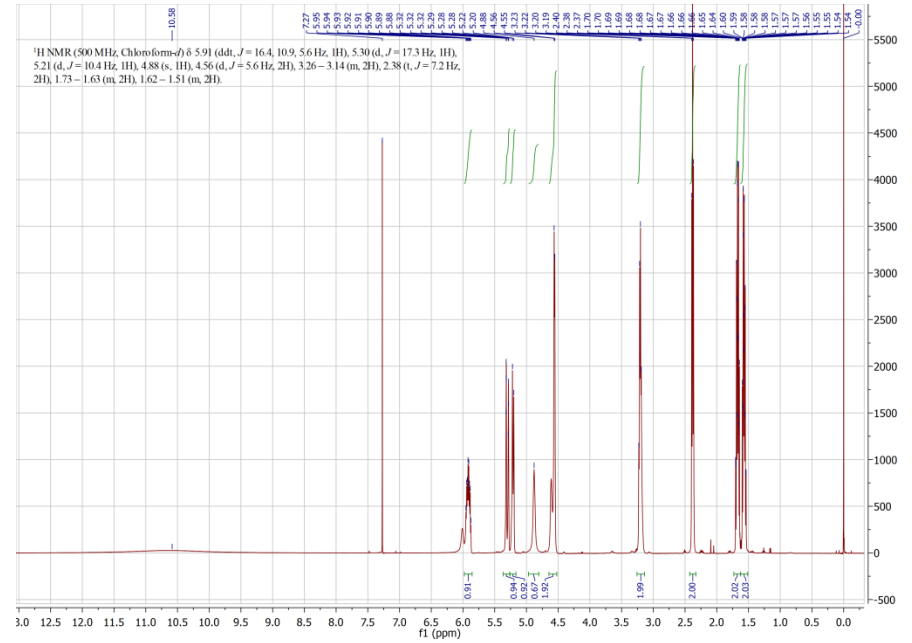
Operator hn  
 Instrument / Ser# maXis 4G 21243

**Acquisition Parameter**

Source Type	ESI	Ion Polarity	Positive	Set Nebulizer	0.4 Bar
Focus	Not active	Set Capillary	3600 V	Set Dry Heater	180 °C
Scan Begin	75 m/z	Set End Plate Offset	-500 V	Set Dry Gas	3.0 l/min
Scan End	1700 m/z	Collision Energy	8.0 eV	Set Ion Energy ( MS only )	4.0 eV



Meas. m/z	#	Formula	Score	m/z	err [mDa]	err [ppm]	mSigma	rdB	e <sup>-</sup> Conf	z
202.1070	1	C <sub>9</sub> H <sub>16</sub> N <sub>2</sub> O <sub>4</sub>	100.00	202.1074	0.3	1.7	3.0	2.5	even	1+
224.0892	1	C <sub>9</sub> H <sub>15</sub> N <sub>2</sub> NaO <sub>4</sub>	100.00	224.0893	0.2	0.8	0.8	2.5	even	
246.0708	1	C <sub>9</sub> H <sub>14</sub> N <sub>2</sub> Na <sub>2</sub> O <sub>4</sub>	100.00	246.0713	0.4	1.8	10.2	2.5	even	



Annex 27: Compound 53

### Mass Spectrum SmartFormula Report

**Analysis Info**

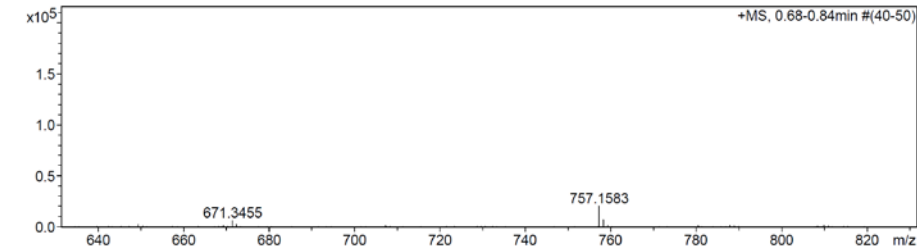
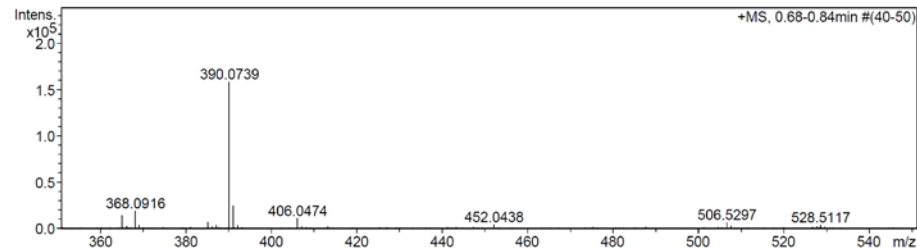
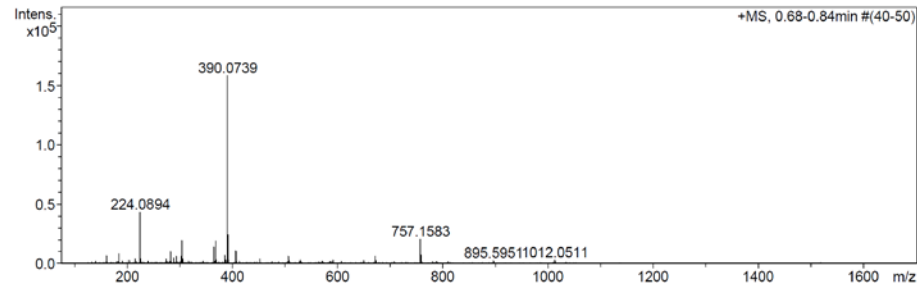
Analysis Name E:\new acq data for data analysis\FS146 001.d  
 Method hn Direct\_Infusion\_pos\_mode\_75-1700 mid 4eV.m  
 Sample Name Fabian Schwizer  
 Comment FS146, ca. 5 ug/ml MeCN

Acquisition Date 13.03.2017 14:12:10

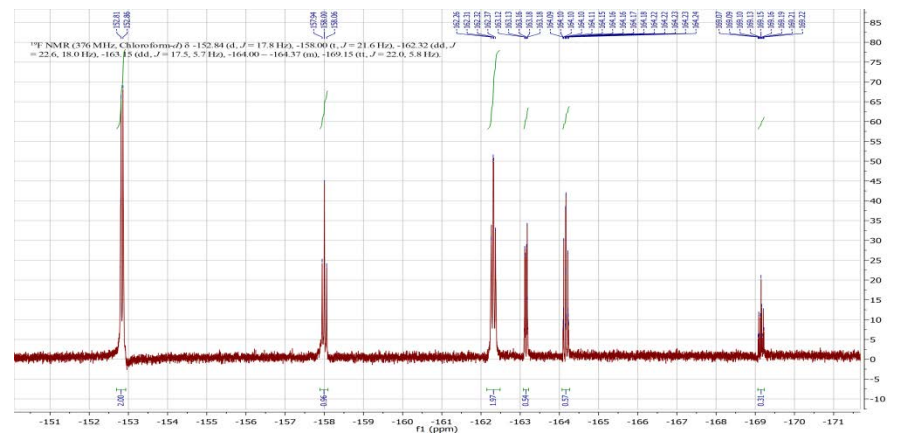
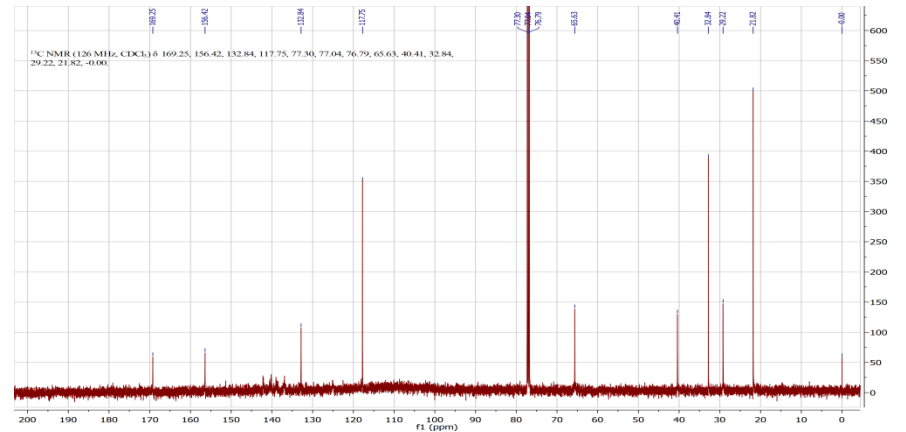
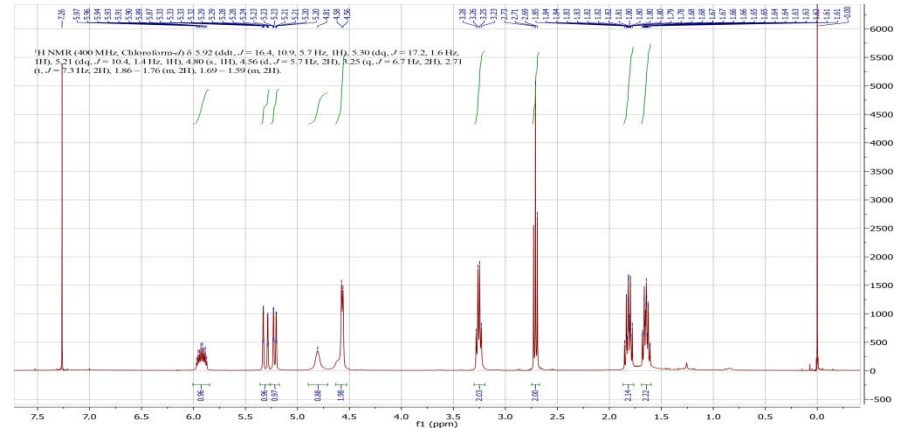
Operator hn  
 Instrument / Ser# maXis 4G 21243

**Acquisition Parameter**

Source Type	ESI	Ion Polarity	Positive	Set Nebulizer	0.4 Bar
Focus	Not active	Set Capillary	3600 V	Set Dry Heater	180 °C
Scan Begin	75 m/z	Set End Plate Offset	-500 V	Set Dry Gas	4.0 l/min
Scan End	1700 m/z	Collision Energy	8.0 eV	Set Ion Energy ( MS only )	4.0 eV



Meas. m/z	#	Formula	Score	m/z	err [mDa]	err [ppm]	mSigma	rdB	e <sup>-</sup> Conf	z
390.0739	1	C 15 H 14 F 5 N Na O 4	100.00	390.0735	-0.4	-1.1	6.9	6.5	even	1+
757.1583	1	C 30 H 28 F 10 N 2 Na O 8	100.00	757.1578	-0.5	-0.6	9.0	12.5	even	



Annex 28: Compound 54

### Mass Spectrum SmartFormula Report

**Analysis Info**

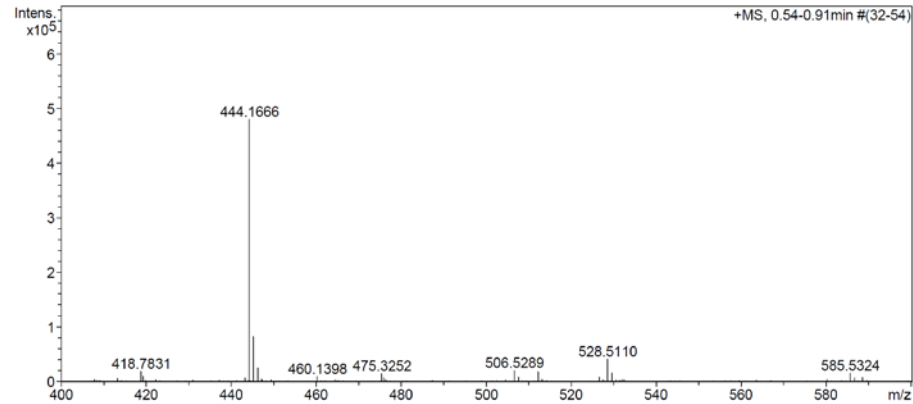
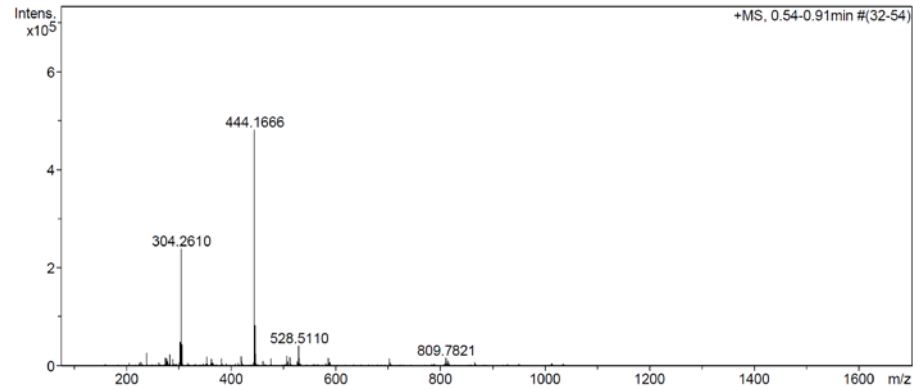
Analysis Name E:\new acq data for data analysis\FS147 002.d  
 Method hn Direct\_Infusion\_pos mode\_75-1700 mid 4eV.m  
 Sample Name Fabian Schwizer  
 Comment FS147, ca. 5 ug/ml MeOH

Acquisition Date 13.03.2017 14:56:38

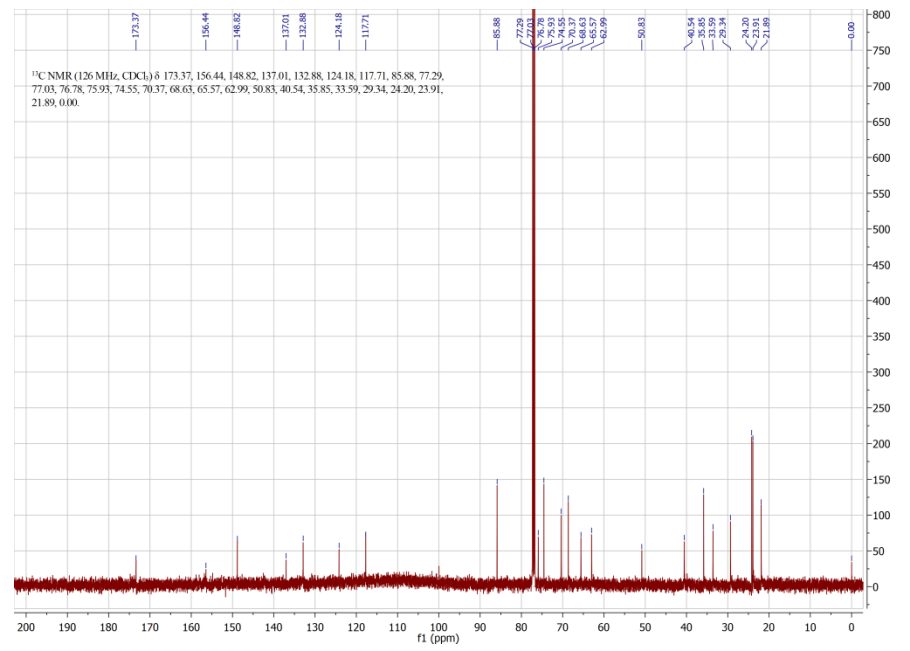
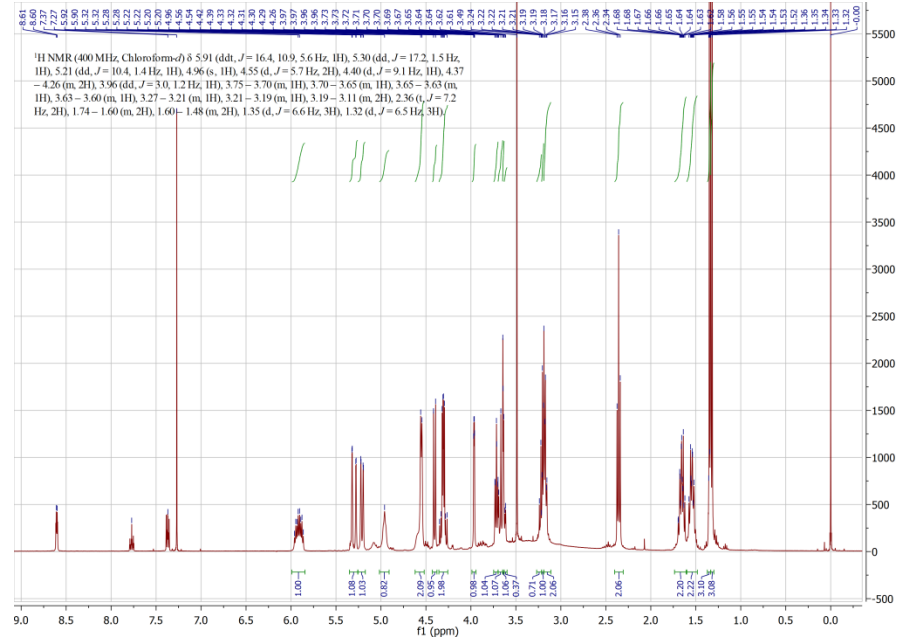
Operator hn  
 Instrument / Ser# maXis 4G 21243

**Acquisition Parameter**

Source Type	ESI	Ion Polarity	Positive	Set Nebulizer	0.4 Bar
Focus	Not active	Set Capillary	3600 V	Set Dry Heater	180 °C
Scan Begin	75 m/z	Set End Plate Offset	-500 V	Set Dry Gas	4.0 l/min
Scan End	1700 m/z	Collision Energy	8.0 eV	Set Ion Energy (MS only)	4.0 eV



Meas. m/z	#	Formula	Score	m/z	err [mDa]	err [ppm]	mSigma	rdb	e <sup>-</sup> Conf	z
444.1666	1	C 18 H 31 N Na O 8 S	100.00	444.1663	-0.3	-0.7	25.0	3.5	even	1+
865.3422	1	C 36 H 62 N 2 Na O 16 S 2	100.00	865.3433	1.1	1.3	7.9	6.5	even	





Annex 29: Compound 56

### Mass Spectrum SmartFormula Report

**Analysis Info**

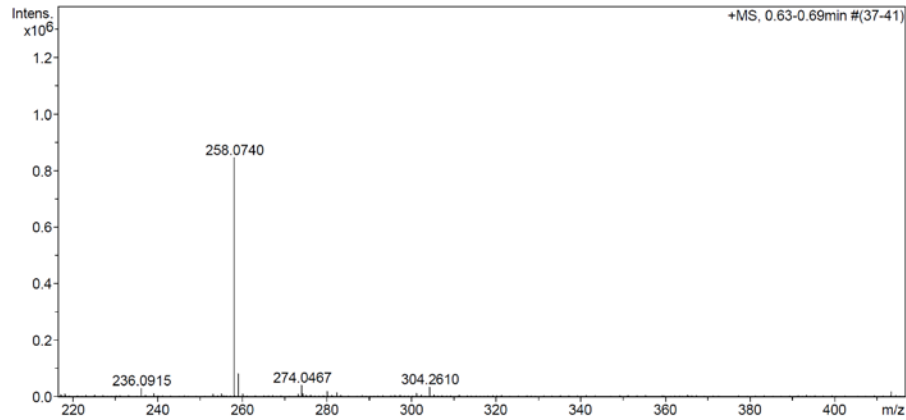
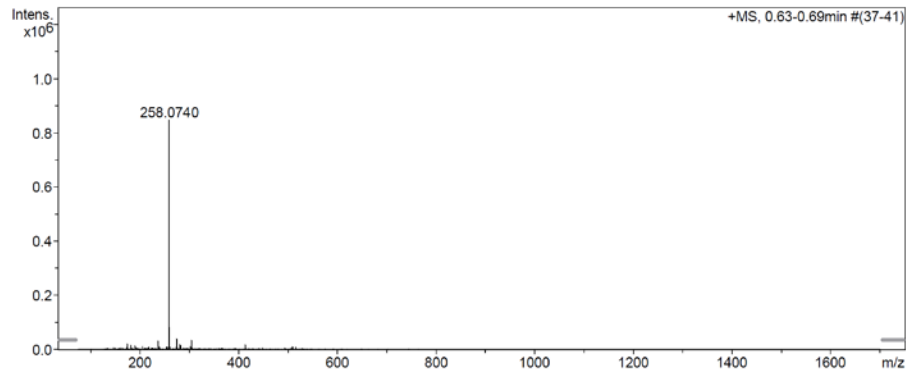
Analysis Name E:\new acq data for data analysis\FS161 001.d  
 Method hn Direct\_Infusion\_pos mode\_75-1700 low 4eV.m  
 Sample Name Fabian Schwizer  
 Comment FS161, ca. 5 ug/ml MeOH

Acquisition Date 24.02.2017 10:08:30

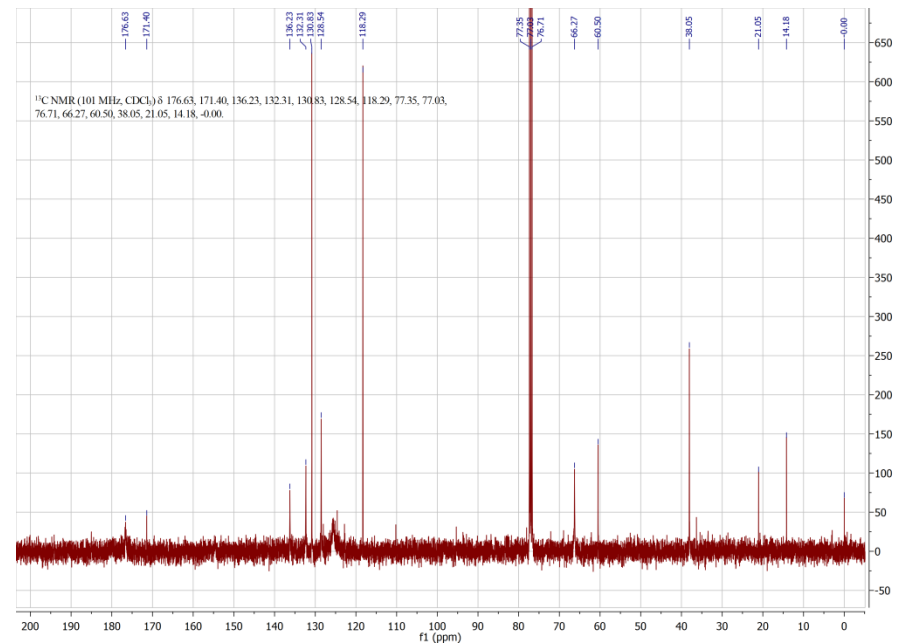
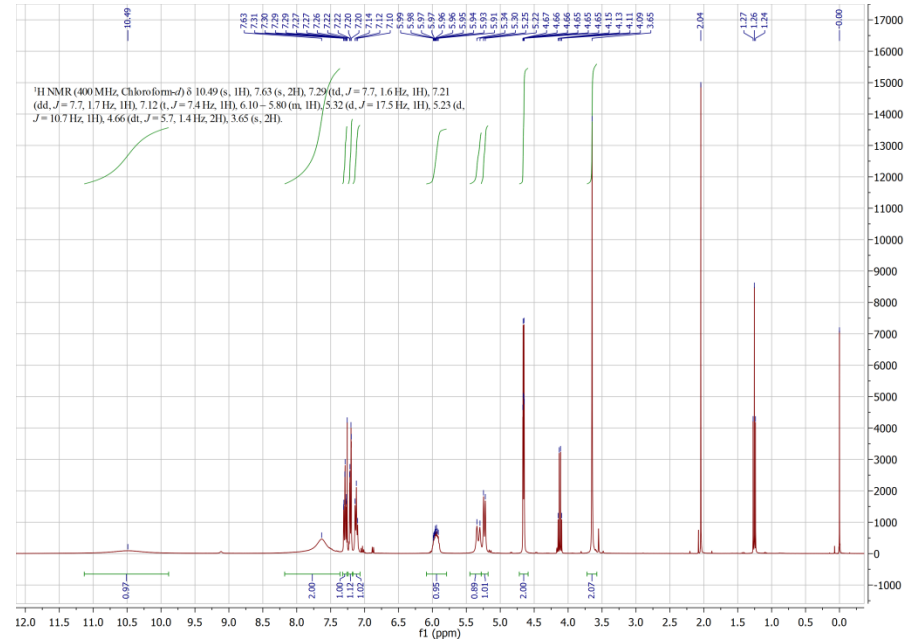
Operator hn  
 Instrument / Ser# maXis 4G 21243

**Acquisition Parameter**

Source Type	ESI	Ion Polarity	Positive	Set Nebulizer	0.4 Bar
Focus	Not active	Set Capillary	3600 V	Set Dry Heater	180 °C
Scan Begin	75 m/z	Set End Plate Offset	-500 V	Set Dry Gas	3.0 l/min
Scan End	1700 m/z	Collision Energy	8.0 eV	Set Ion Energy (MS only)	4.0 eV



Meas. m/z	#	Formula	Score	m/z	err [mDa]	err [ppm]	mSigma	rdb	e <sup>-</sup> Conf	z
236.0915	1	C 12 H 14 N O 4	100.00	236.0917	0.2	0.9	4.2	6.5	even	1+
258.0740	1	C 12 H 13 N Na O 4	100.00	258.0737	-0.3	-1.3	21.7	6.5	even	



### Mass Spectrum SmartFormula Report

**Analysis Info**

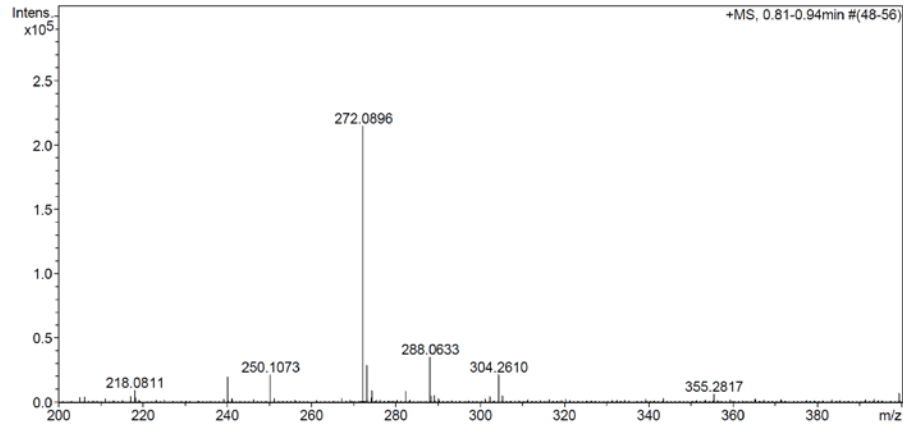
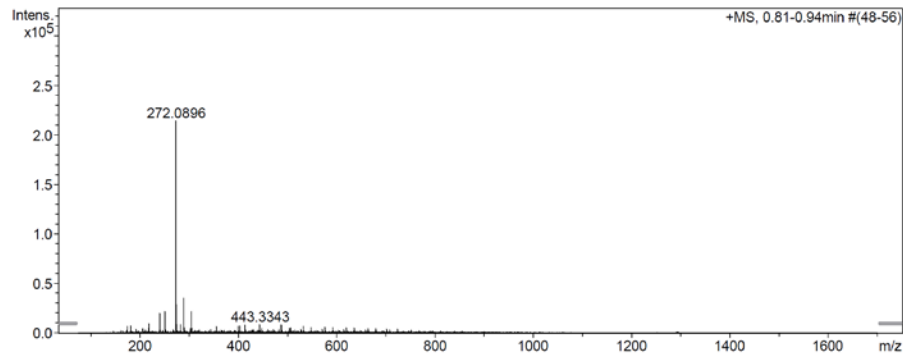
Analysis Name E:\new acq data for data analysis\FS162 001.d  
 Method hn Direct\_Infusion\_pos mode\_75-1700 mid 4eV.m  
 Sample Name Fabian Schwizer  
 Comment FS162, ca. 5 ug/ml MeOH

Acquisition Date 24.02.2017 11:48:34

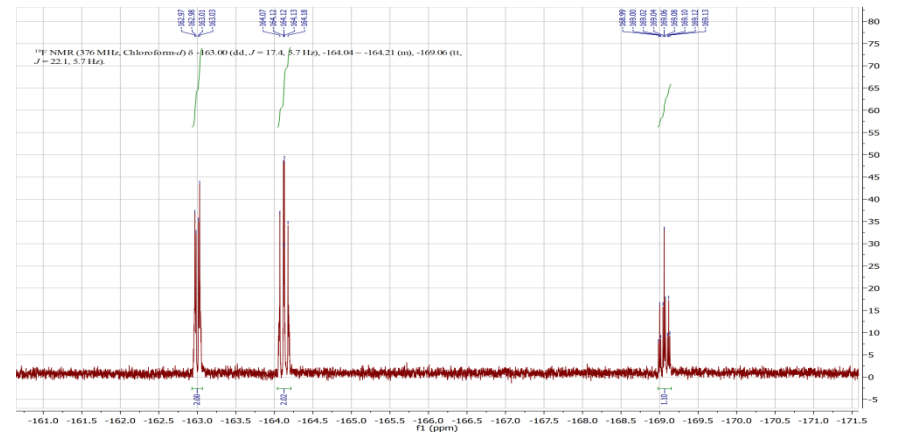
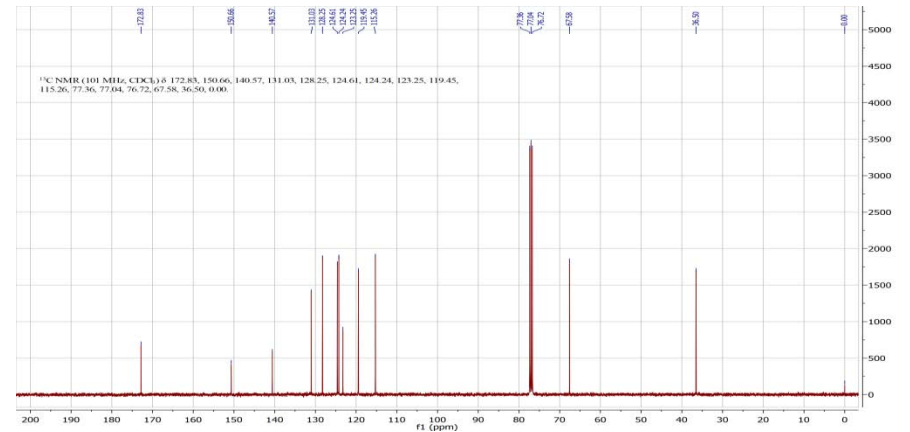
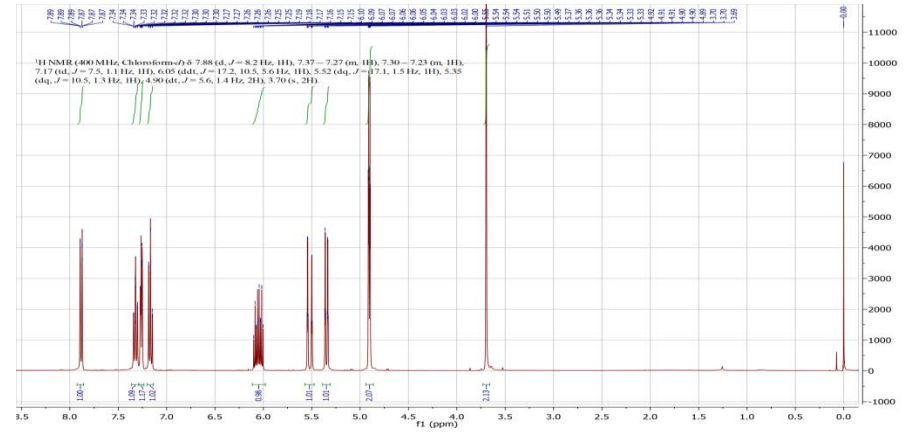
Operator hn  
 Instrument / Ser# maXis 4G 21243

**Acquisition Parameter**

Source Type	ESI	Ion Polarity	Positive	Set Nebulizer	0.4 Bar
Focus	Not active	Set Capillary	3600 V	Set Dry Heater	180 °C
Scan Begin	75 m/z	Set End Plate Offset	-500 V	Set Dry Gas	4.0 l/min
Scan End	1700 m/z	Collision Energy	8.0 eV	Set Ion Energy ( MS only )	4.0 eV



Meas. m/z	#	Formula	Score	m/z	err [mDa]	err [ppm]	mSigma	rdb	e <sup>-</sup> Conf	z
250.1073	1	C 13 H 16 N O 4	100.00	250.1074	0.0	0.1	3.9	6.5	even	1+
272.0896	1	C 13 H 15 N Na O 4	100.00	272.0893	-0.3	-1.2	6.3	6.5	even	
288.0633	1	C 13 H 15 K N O 4	100.00	288.0633	-0.0	-0.1	6.0	6.5	even	



Annex 31: Compound 58

### Mass Spectrum SmartFormula Report

**Analysis Info**

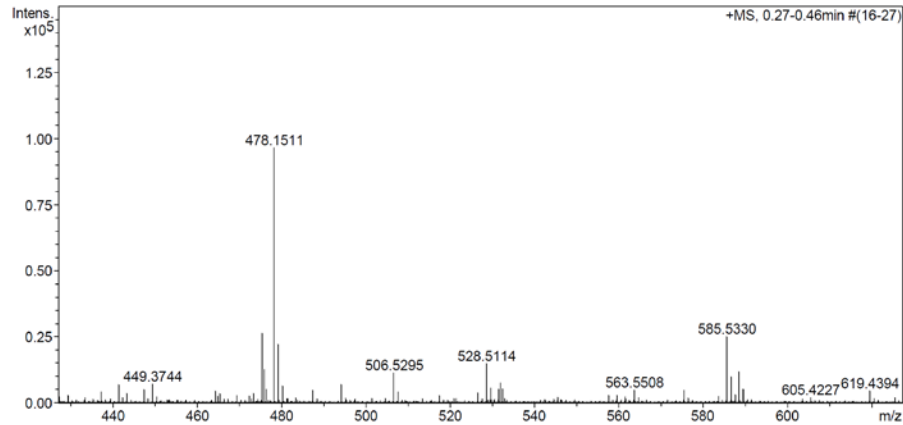
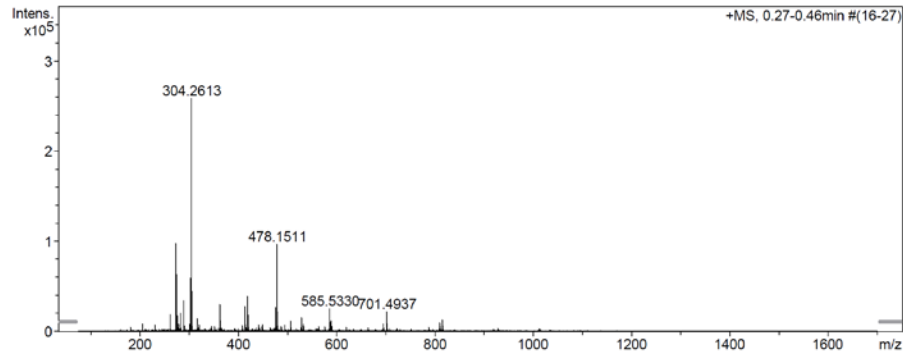
Analysis Name E:\new acq data for data analysis\FS163 002.d  
 Method hn Direct\_Infusion\_pos mode\_75-1700 mid 4eV.m  
 Sample Name Fabian Schwizer  
 Comment FS163, ca. 5 ug/ml MeOH

Acquisition Date 24.02.2017 11:07:52

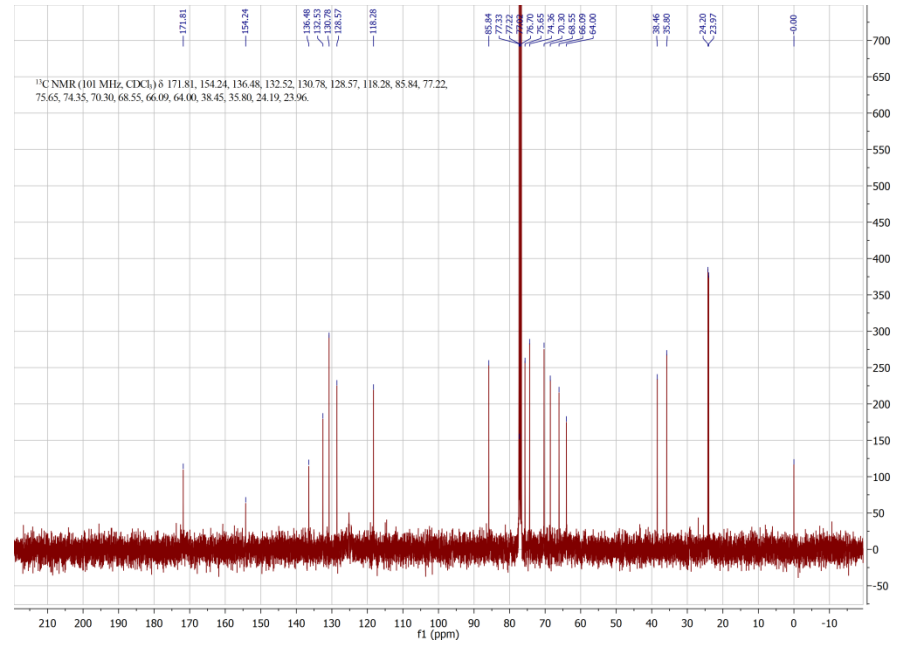
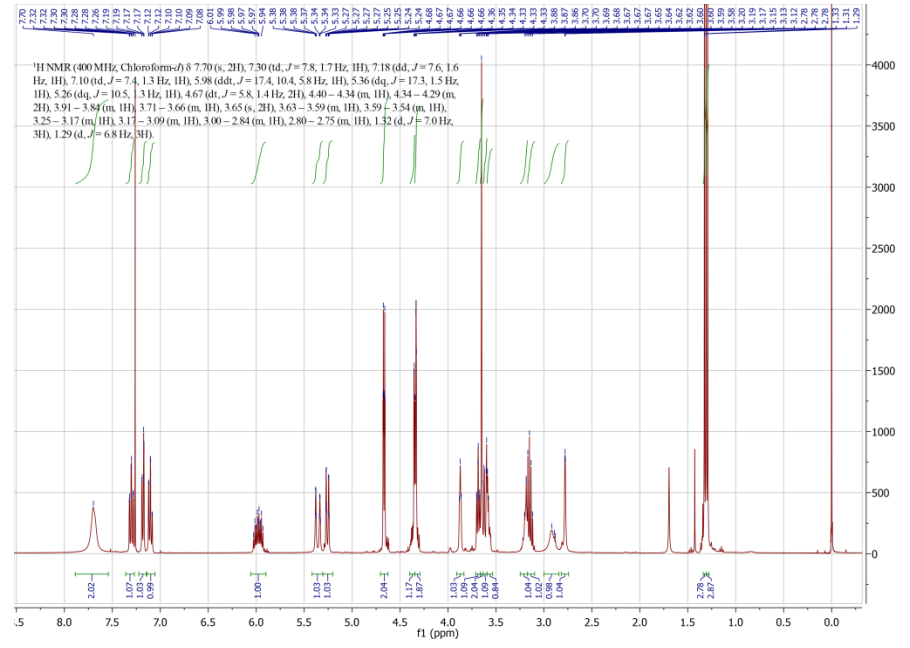
Operator hn  
 Instrument / Ser# maXis 4G 21243

**Acquisition Parameter**

Source Type	ESI	Ion Polarity	Positive	Set Nebulizer	0.4 Bar
Focus	Not active	Set Capillary	3600 V	Set Dry Heater	180 °C
Scan Begin	75 m/z	Set End Plate Offset	-500 V	Set Dry Gas	4.0 l/min
Scan End	1700 m/z	Collision Energy	8.0 eV	Set Ion Energy ( MS only )	4.0 eV



Meas. m/z	#	Formula	Score	m/z	err [mDa]	err [ppm]	mSigma	rdB	e <sup>-</sup>	Conf	z
478.1511	1	C <sub>21</sub> H <sub>29</sub> N Na O <sub>8</sub> S	100.00	478.1506	-0.5	-1.0	12.4	7.5	even	1+	



### Mass Spectrum SmartFormula Report

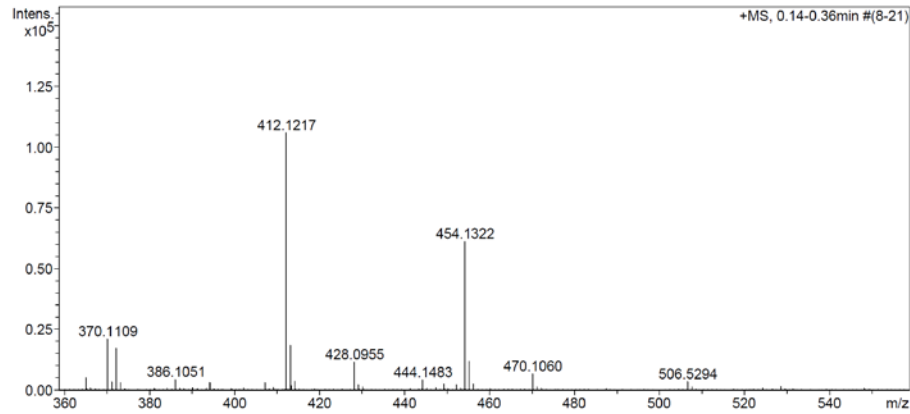
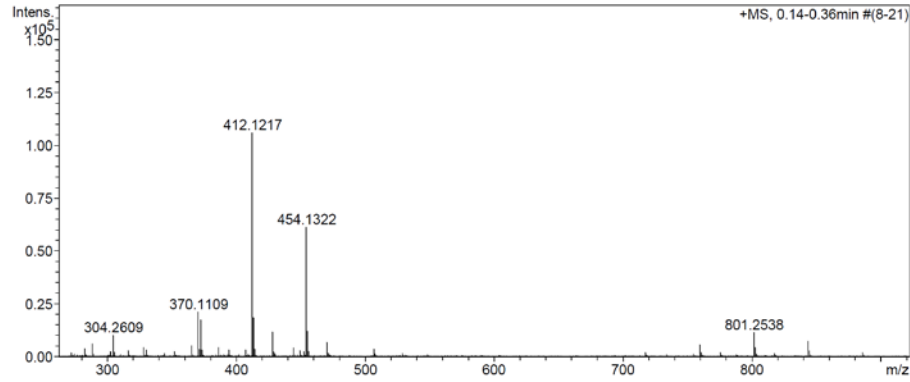
**Analysis Info**

Analysis Name E:\new acq data for data analysis\FS140 001.d  
 Method hn Direct\_Infusion\_pos mode\_75-1700 mid 4eV.m  
 Sample Name Fabian Schwizer  
 Comment FS140, ca. 5 ug/ml MeOH

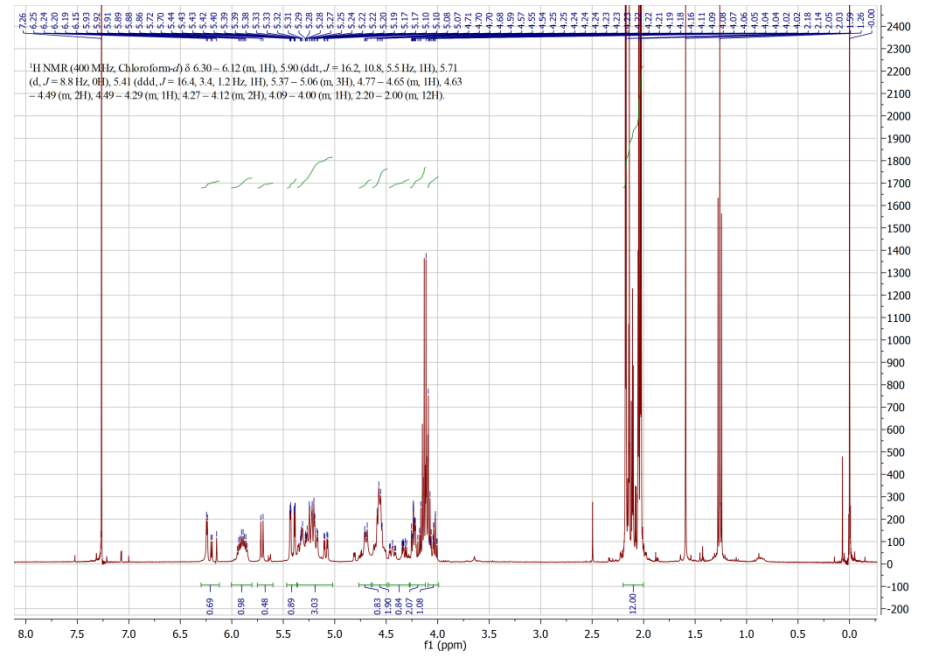
Acquisition Date 13.03.2017 15:31:19  
 Operator hn  
 Instrument / Ser# maXis 4G 21243

**Acquisition Parameter**

Source Type	ESI	Ion Polarity	Positive	Set Nebulizer	0.4 Bar
Focus	Not active	Set Capillary	3600 V	Set Dry Heater	180 °C
Scan Begin	75 m/z	Set End Plate Offset	-500 V	Set Dry Gas	4.0 l/min
Scan End	1700 m/z	Collision Energy	8.0 eV	Set Ion Energy (MS only)	4.0 eV



Meas. m/z	#	Formula	Score	m/z	err [mDa]	err [ppm]	mSigma	rdb	e <sup>-</sup> Conf	z
454.1322	1	C 18 H 25 N Na O 11	100.00	454.1320	-0.2	-0.5	4.2	6.5	even	1+
470.1060	1	C 18 H 25 K N O 11	100.00	470.1059	-0.1	-0.2	5.1	6.5	even	
885.2745	1	C 36 H 50 N 2 Na O 22	100.00	885.2747	0.2	0.3	16.4	12.5	even	



Annex 33: Compound 61

### Mass Spectrum SmartFormula Report

**Analysis Info**

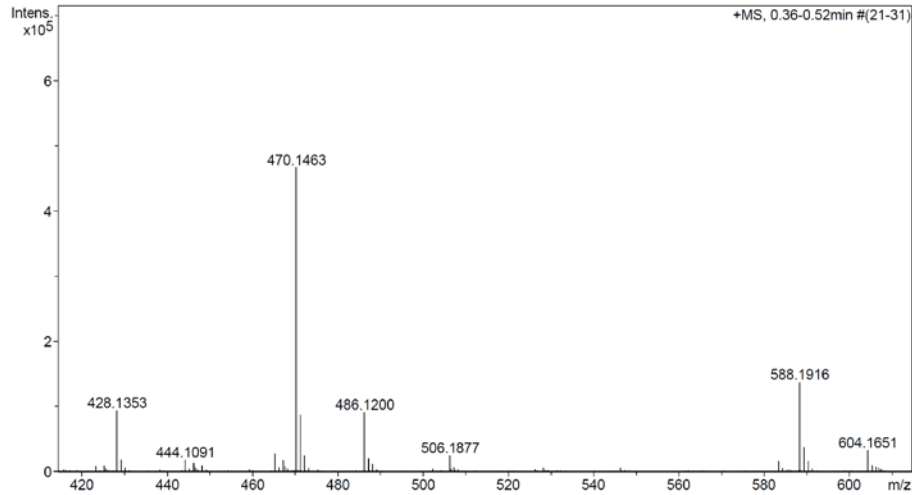
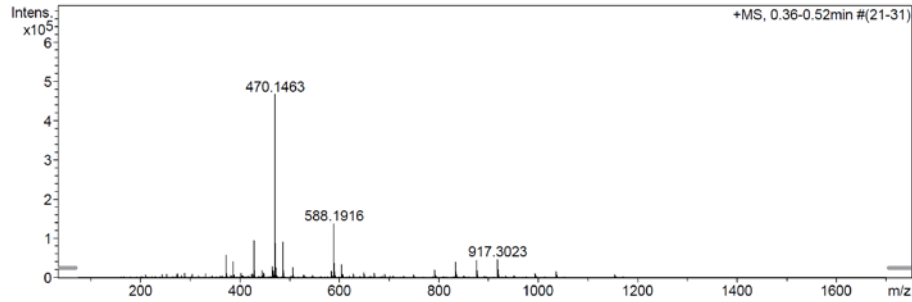
Analysis Name E:\new acq data for data analysis\FS141 001.d  
 Method hn Direct\_Infusion\_pos mode\_75-1700 mid 4eV.m  
 Sample Name Fabian Schwizer  
 Comment FS141, ca. 5 ug/ml MeOH

Acquisition Date 13.03.2017 16:33:32

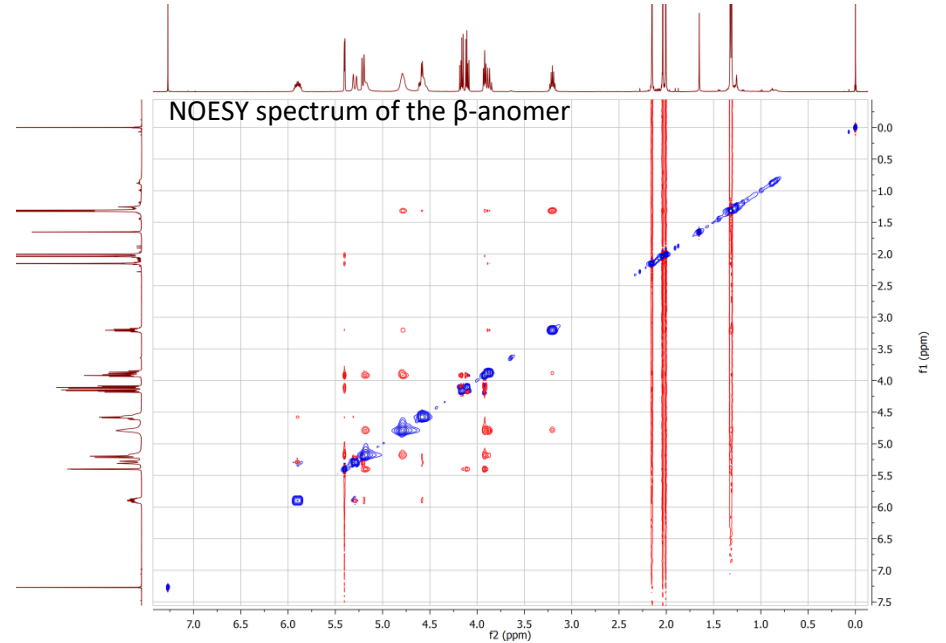
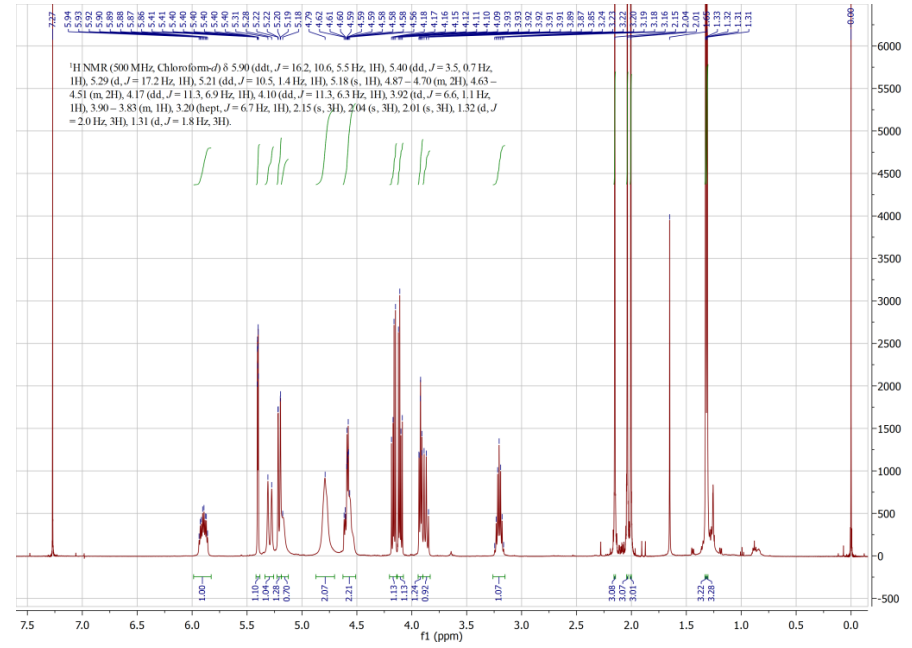
Operator hn  
 Instrument / Ser# maXis 4G 21243

**Acquisition Parameter**

Source Type	ESI	Ion Polarity	Positive	Set Nebulizer	0.4 Bar
Focus	Not active	Set Capillary	3600 V	Set Dry Heater	180 °C
Scan Begin	75 m/z	Set End Plate Offset	-500 V	Set Dry Gas	4.0 l/min
Scan End	1700 m/z	Collision Energy	8.0 eV	Set Ion Energy ( MS only )	4.0 eV



Meas. m/z	#	Formula	Score	m/z	err [mDa]	err [ppm]	mSigma	rdB	e <sup>-</sup> Conf	z
470.1463	1	C 19 H 29 N Na O 9 S	100.00	470.1455	-0.8	-1.7	23.5	5.5	even	1+
486.1200	1	C 19 H 29 K N O 9 S	100.00	486.1195	-0.5	-1.1	15.0	5.5	even	
917.3023	1	C 38 H 58 N 2 Na O 18 S 2	100.00	917.3018	-0.5	-0.5	9.5	10.5	even	



Annex 34: Compound 62

### Mass Spectrum SmartFormula Report

**Analysis Info**

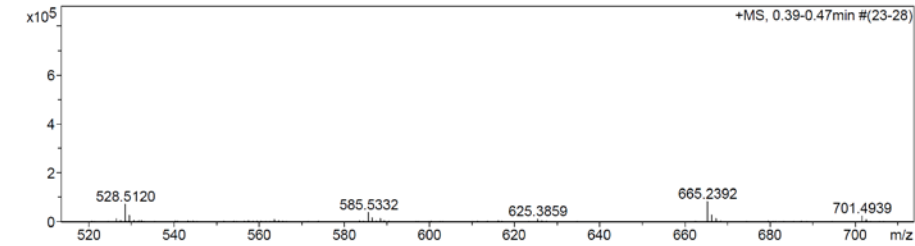
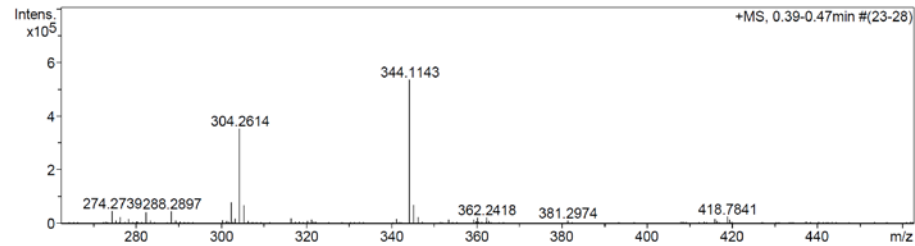
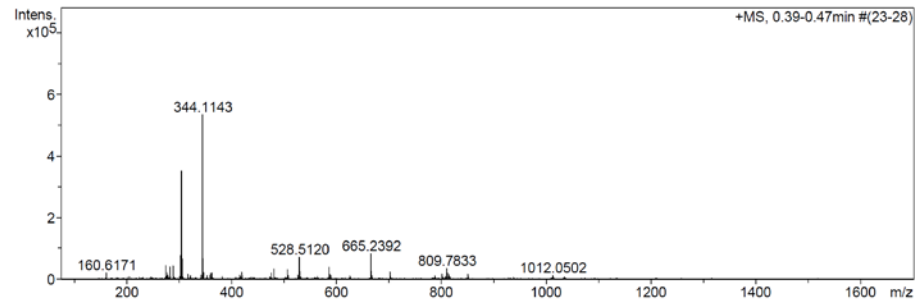
Analysis Name E:\new acq data for data analysis\FS142 001.d  
 Method hn Direct\_Infusion\_pos mode\_75-1700 mid 4eV.m  
 Sample Name Fabian Schwizer  
 Comment FS142, ca. 5 ug/ml MeOH

Acquisition Date 13.03.2017 10:52:16

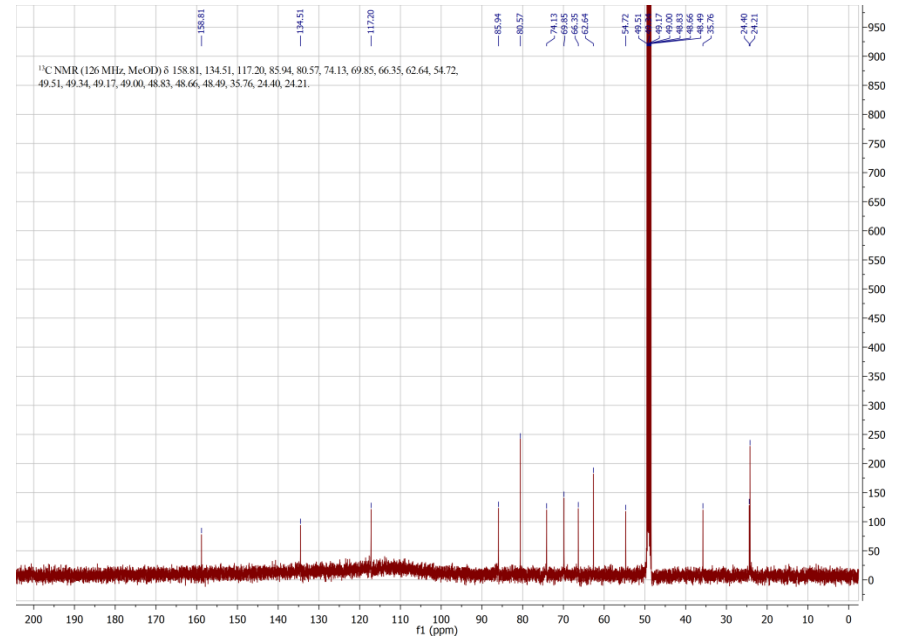
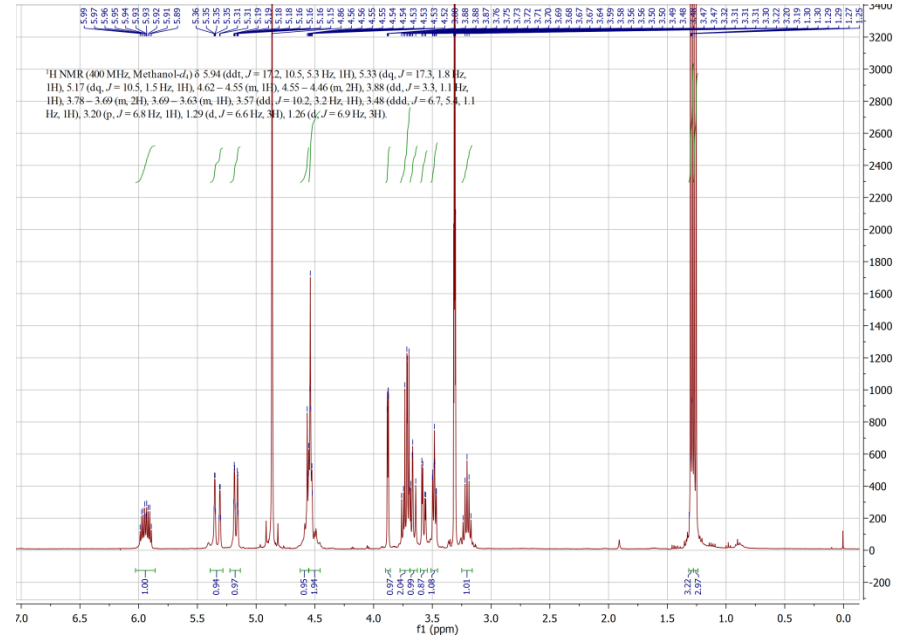
Operator hn  
 Instrument / Ser# maXis 4G 21243

**Acquisition Parameter**

Source Type	ESI	Ion Polarity	Positive	Set Nebulizer	0.4 Bar
Focus	Not active	Set Capillary	3600 V	Set Dry Heater	180 °C
Scan Begin	75 m/z	Set End Plate Offset	-500 V	Set Dry Gas	4.0 l/min
Scan End	1700 m/z	Collision Energy	8.0 eV	Set Ion Energy (MS only)	4.0 eV



Meas. m/z	#	Formula	Score	m/z	err [mDa]	err [ppm]	mSigma	rdb	e <sup>-</sup> Conf	z
344.1143	1	C 13 H 23 N Na O 6 S	100.00	344.1138	-0.5	-1.4	19.5	2.5	even	1+
665.2392	1	C 26 H 46 N 2 Na O 12 S 2	100.00	665.2384	-0.8	-1.2	10.9	4.5	even	



Annex 35: Compound 72

### Mass Spectrum SmartFormula Report

**Analysis Info**

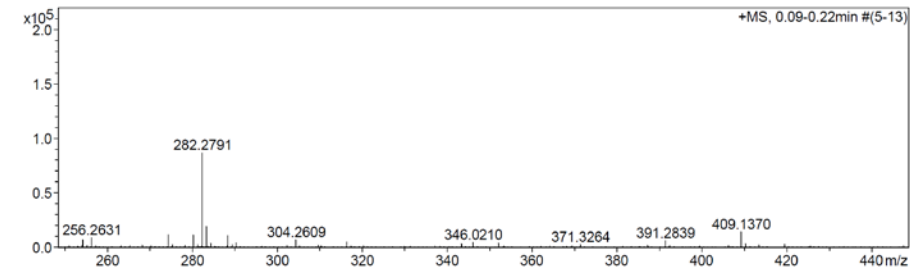
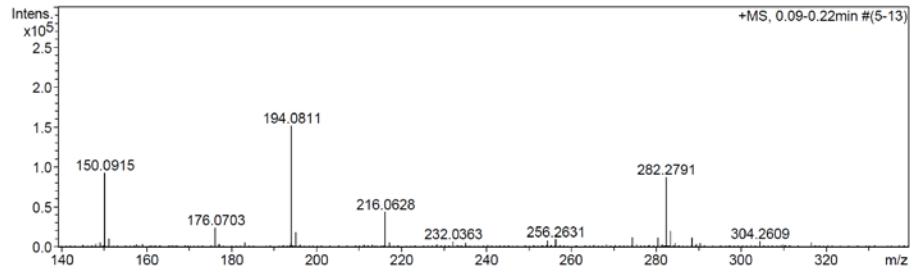
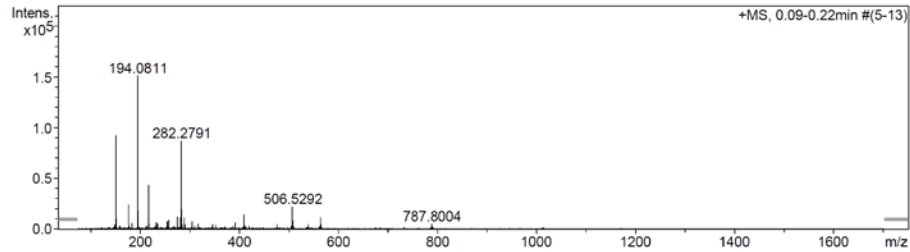
Analysis Name E:\acq data for data analysis\FS208 001.d  
 Method hn Direct\_Infusion\_pos\_mode\_75-1700 low 4eV.m  
 Sample Name Fabian Schwizer  
 Comment FS208, 5 ug/ml MeCN

Acquisition Date 01.06.2017 15:29:43

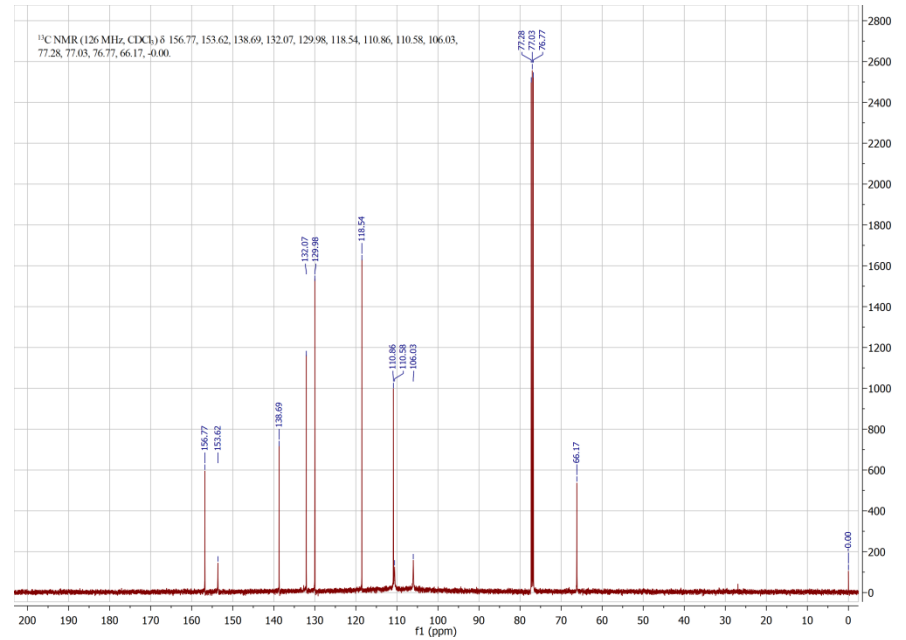
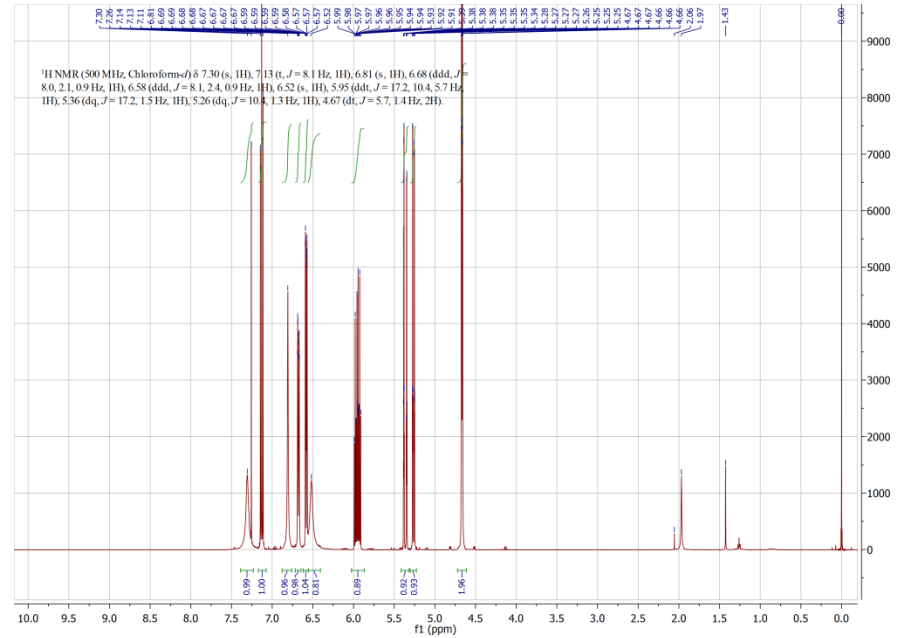
Operator hn  
 Instrument / Ser# maXis 4G 21243

**Acquisition Parameter**

Source Type	ESI	Ion Polarity	Positive	Set Nebulizer	0.4 Bar
Focus	Not active	Set Capillary	3600 V	Set Dry Heater	180 °C
Scan Begin	75 m/z	Set End Plate Offset	-500 V	Set Dry Gas	3.0 l/min
Scan End	1700 m/z	Collision Energy	3.0 eV	Set Ion Energy ( MS only )	4.0 eV



Meas. m/z	#	Formula	Score	m/z	err [mDa]	err [ppm]	mSigma	rdb	e- Conf	z
194.0811	1	C 10 H 12 N O 3	100.00	194.0812	0.1	0.4	1.7	5.5	even	1+
216.0628	1	C 10 H 11 N Na O 3	100.00	216.0631	0.4	1.6	1.5	5.5	even	
387.1560	1	C 20 H 23 N 2 O 6	100.00	387.1551	-0.9	-2.4	20.6	10.5	even	
409.1370	1	C 20 H 22 N 2 Na O 6	100.00	409.1370	0.0	0.1	5.3	10.5	even	



Annex 36: Compound 65

### Mass Spectrum SmartFormula Report

**Analysis Info**

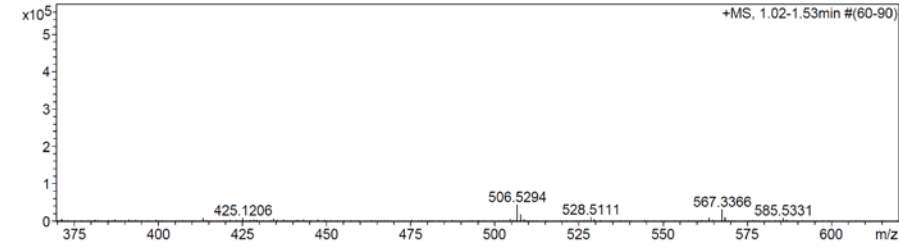
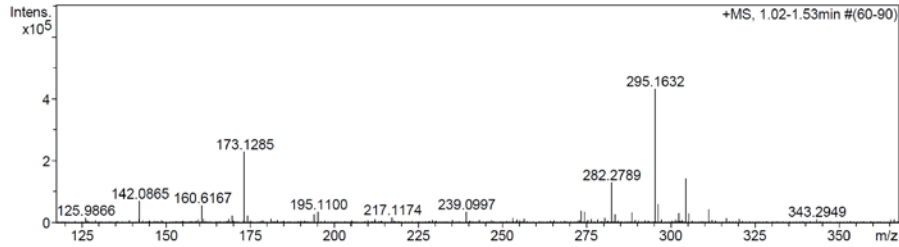
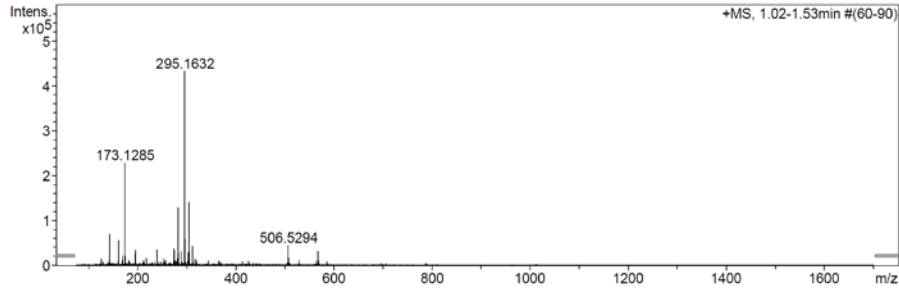
Analysis Name E:\acq data for data analysis\FS205 002.d  
 Method hn Direct\_Infusion\_pos mode\_75-1700 low 4eV.m  
 Sample Name Fabian Schwizer  
 Comment FS205, 5 ug/ml MeCN

Acquisition Date 01.06.2017 16:47:14

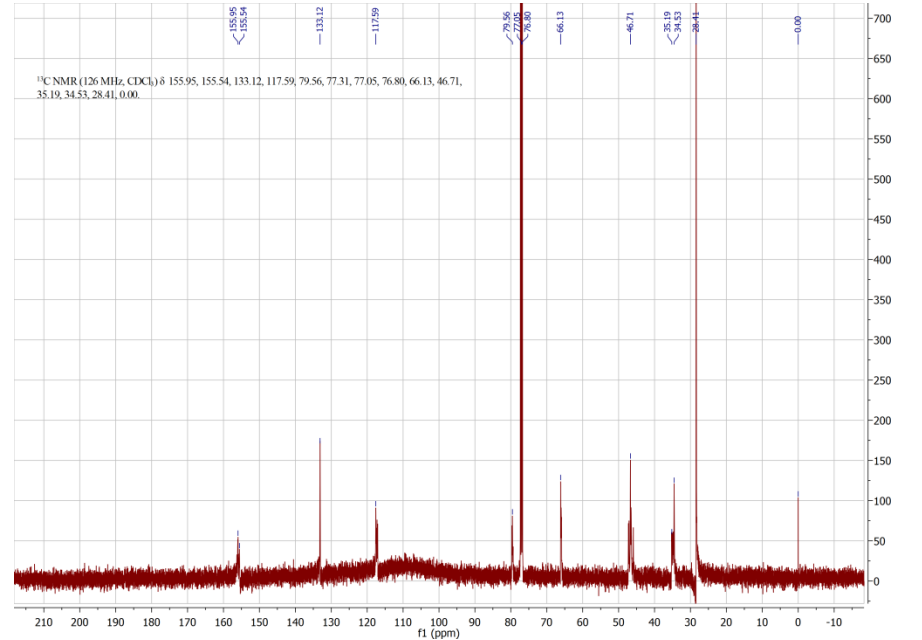
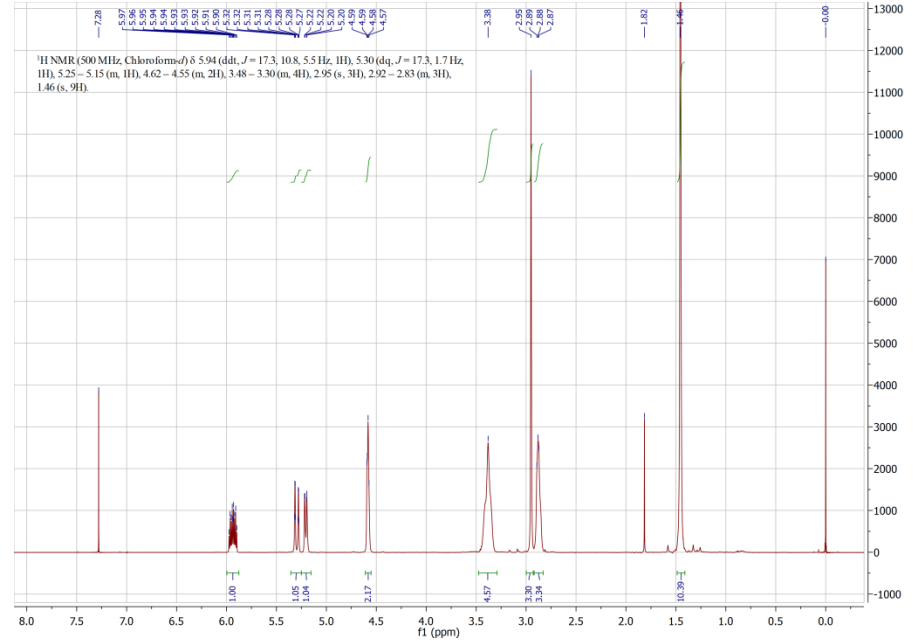
Operator hn  
 Instrument / Ser# maxIs 4G 21243

**Acquisition Parameter**

Source Type	ESI	Ion Polarity	Positive	Set Nebulizer	0.4 Bar
Focus	Not active	Set Capillary	3600 V	Set Dry Heater	180 °C
Scan Begin	75 m/z	Set End Plate Offset	-500 V	Set Dry Gas	3.0 l/min
Scan End	1700 m/z	Collision Energy	8.0 eV	Set Ion Energy ( MS only )	4.0 eV



Meas. m/z	#	Formula	Score	m/z	err [mDa]	err [ppm]	mSigma	rdb	e <sup>-</sup> Conf	z
173.1285	1	C 8 H 17 N 2 O 2	100.00	173.1285	-0.0	-0.2	4.0	1.5	even	1+
273.1805	1	C 13 H 25 N 2 O 4	100.00	273.1809	0.4	1.5	13.9	2.5	even	
295.1632	1	C 13 H 24 N 2 Na O 4	100.00	295.1628	-0.4	-1.3	7.7	2.5	even	
311.1365	1	C 13 H 24 K N 2 O 4	100.00	311.1368	0.3	0.9	11.1	2.5	even	
567.3366	1	C 26 H 48 N 4 Na O 8	100.00	567.3364	-0.2	-0.3	12.9	4.5	even	





Annex 37: Compound 66

Mass Spectrum SmartFormula Report

Analysis Info

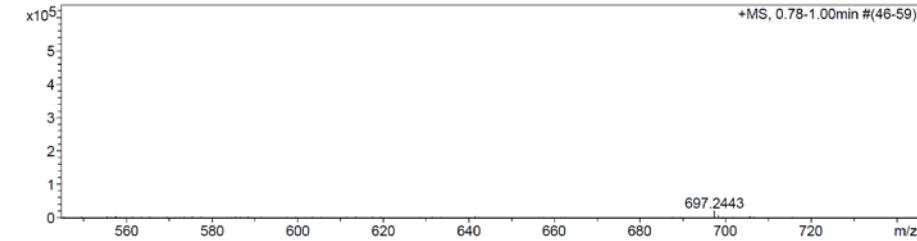
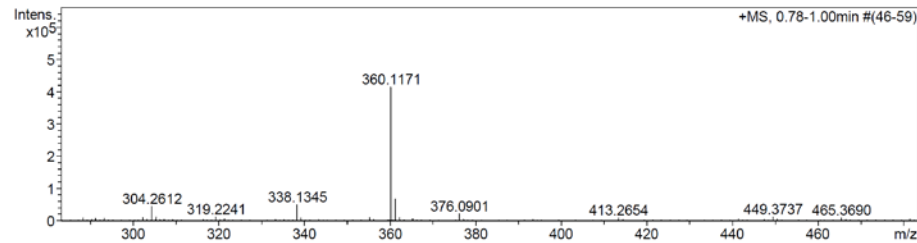
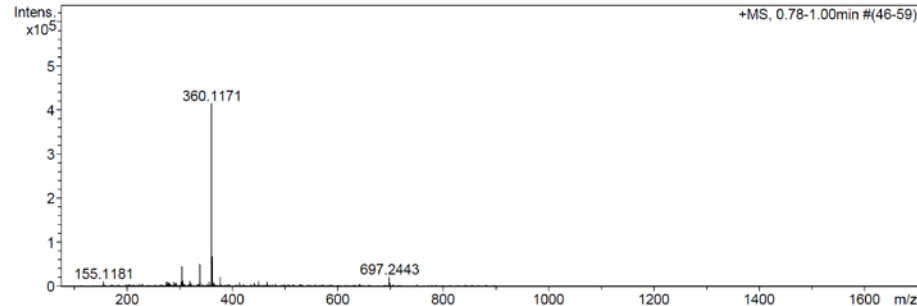
Analysis Name E:\acq data for data analysis\FS206 001.d  
 Method hn Direct\_Infusion\_pos mode\_75-1700 low 4eV.m  
 Sample Name Fabian Schwizer  
 Comment FS206, 5 ug/ml MeCN

Acquisition Date 01.06.2017 17:24:58

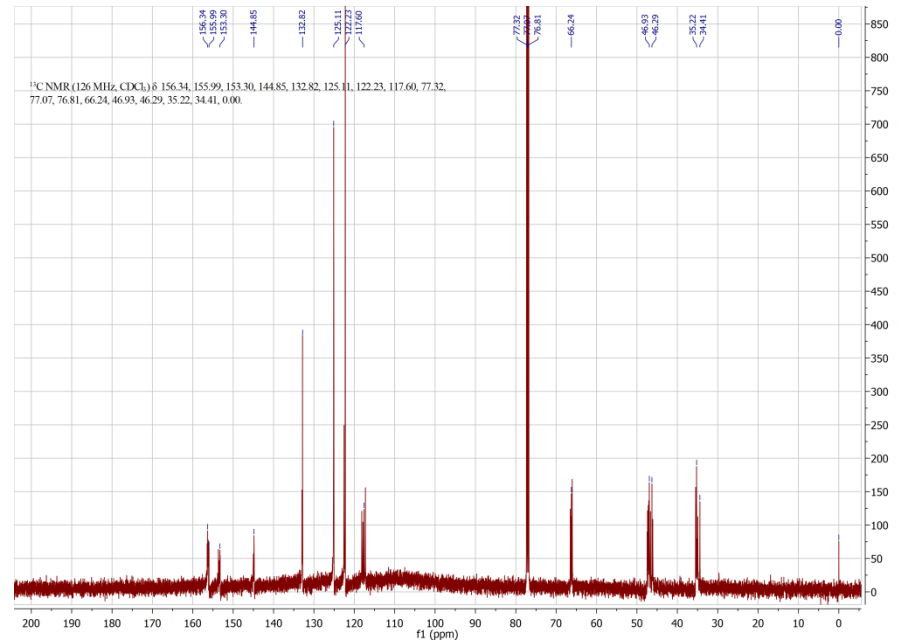
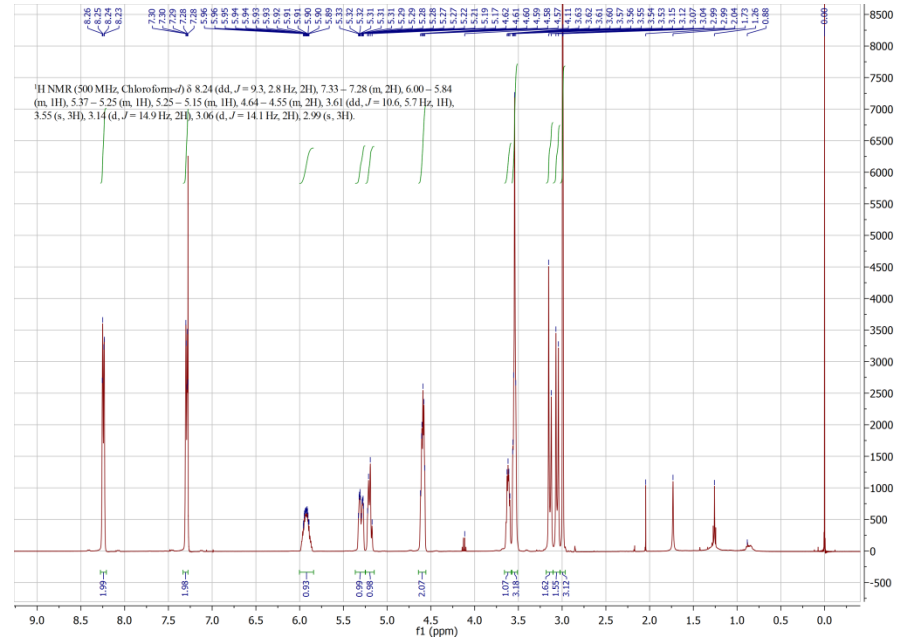
Operator hn  
 Instrument / Ser# maXis 4G 21243

Acquisition Parameter

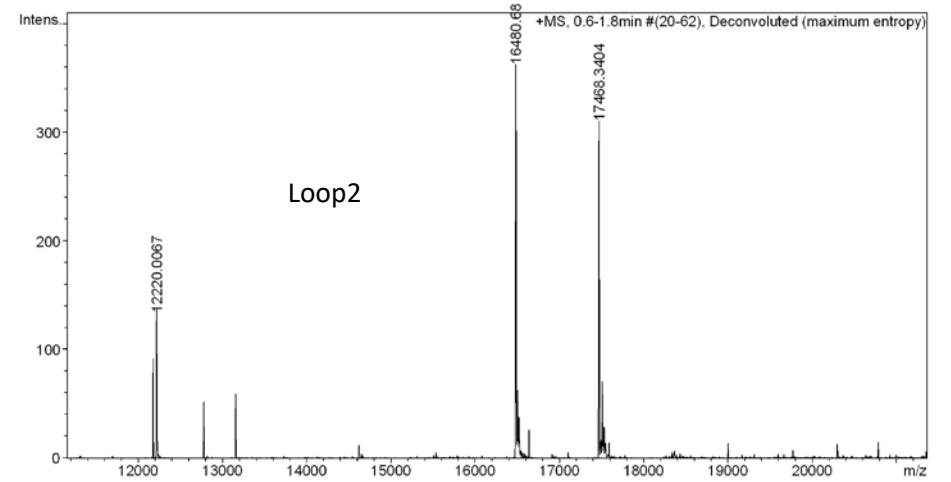
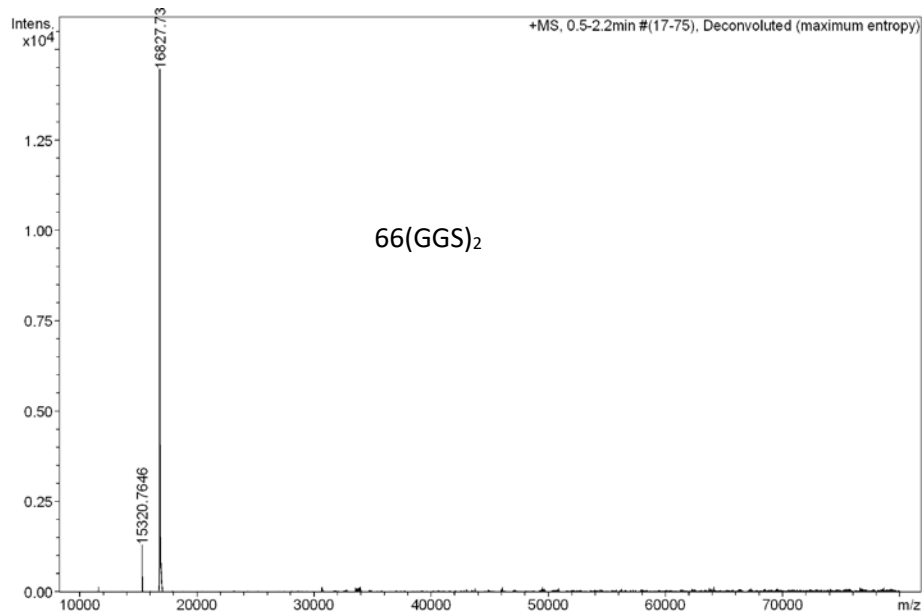
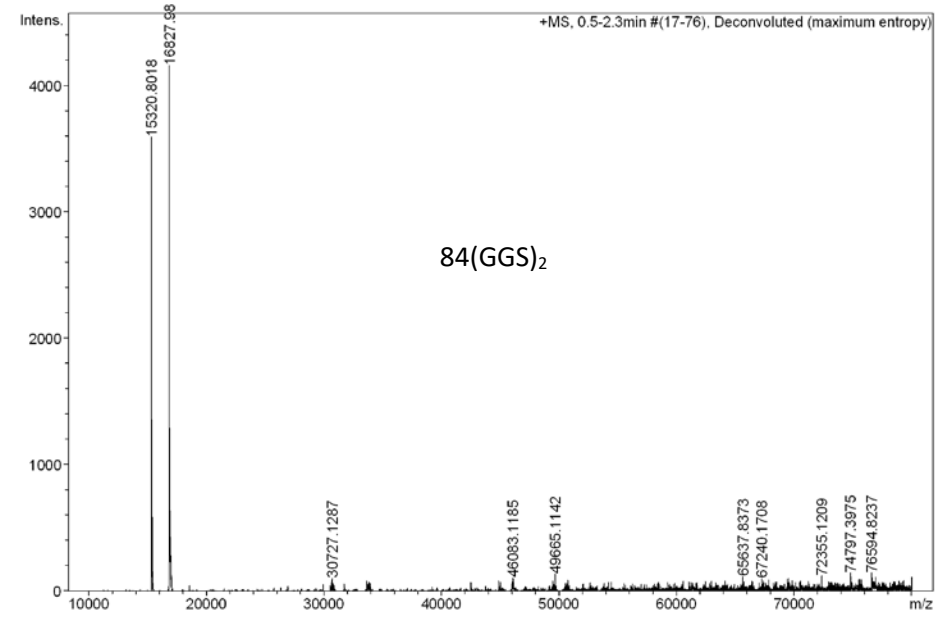
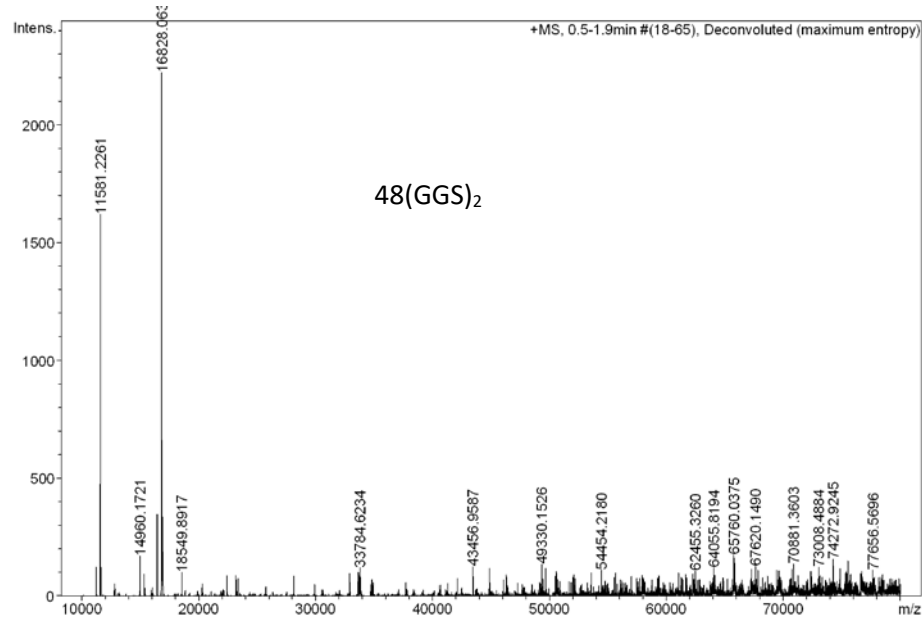
Source Type ESI Ion Polarity Positive Set Nebulizer 0.4 Bar  
 Focus Not active Set Capillary 3600 V Set Dry Heater 180 °C  
 Scan Begin 75 m/z Set End Plate Offset -500 V Set Dry Gas 3.0 l/min  
 Scan End 1700 m/z Collision Energy 8.0 eV Set Ion Energy ( MS only ) 4.0 eV



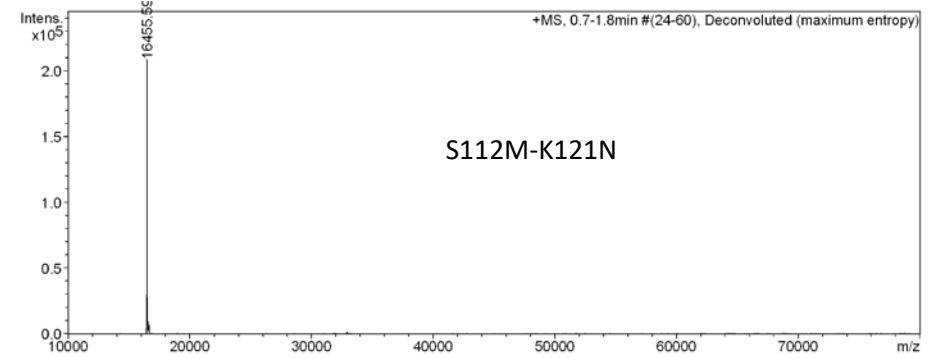
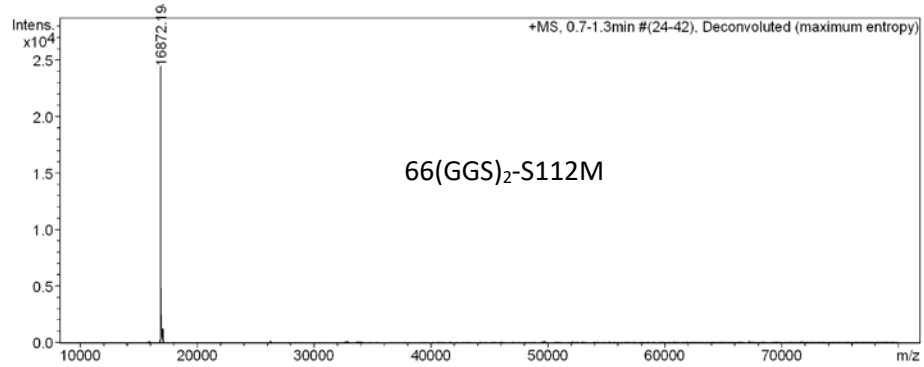
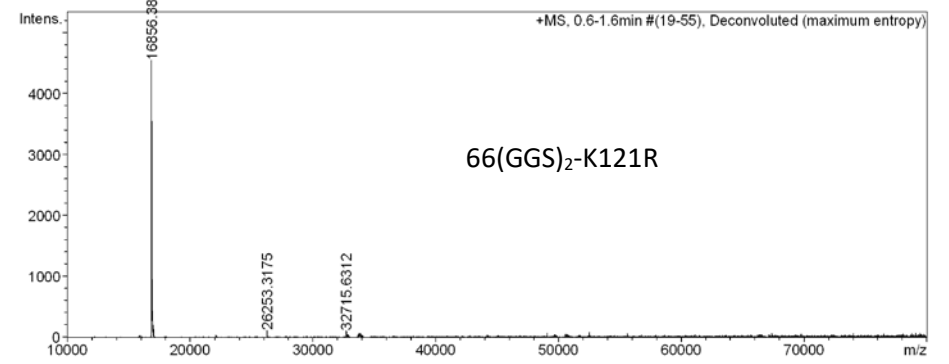
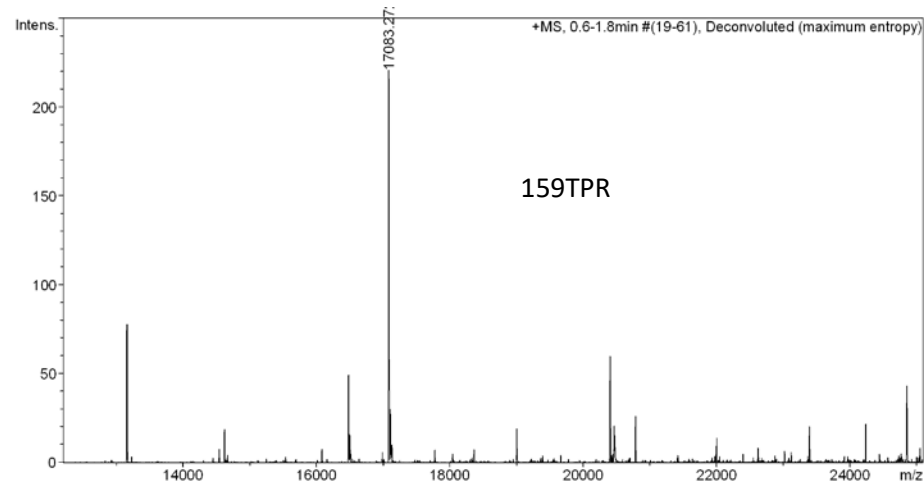
Meas. m/z	#	Formula	Score	m/z	err [mDa]	err [ppm]	mSigma	rdb	e <sup>-</sup> Conf	z
338.1345	1	C 15 H 20 N 3 O 6	100.00	338.1347	0.1	0.4	3.5	7.5	even	1+
360.1171	1	C 15 H 19 N 3 Na O 6	100.00	360.1166	-0.5	-1.4	7.2	7.5	even	
376.0901	1	C 15 H 19 K N 3 O 6	100.00	376.0905	0.5	1.3	7.7	7.5	even	
697.2443	1	C 30 H 38 N 6 Na O 12	100.00	697.2440	-0.3	-0.4	6.5	14.5	even	



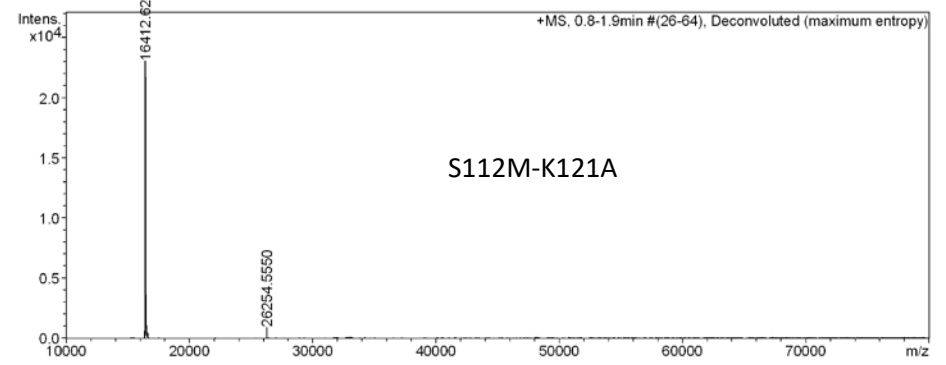
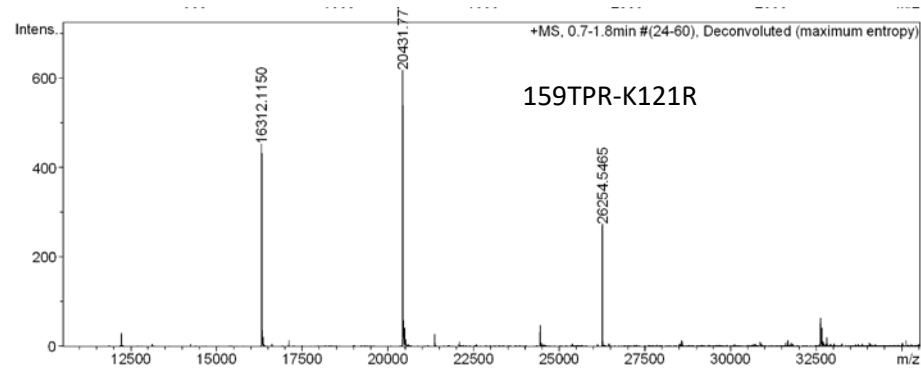
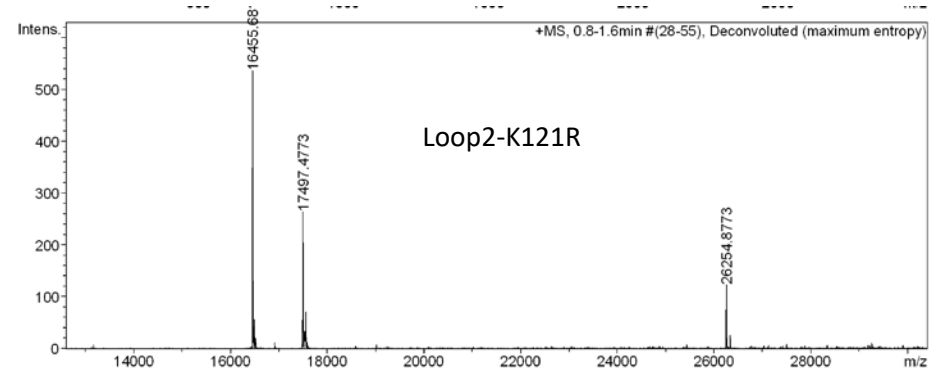
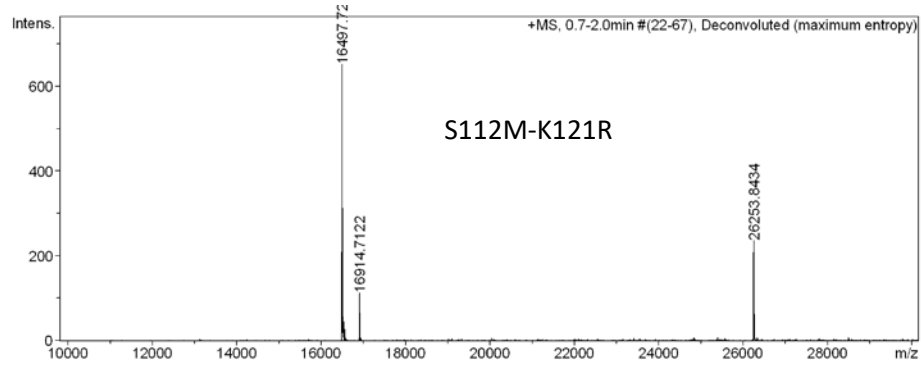
Annex 38: ESI-TOF MS analysis of expressed and purified Sav variants after deconvolution



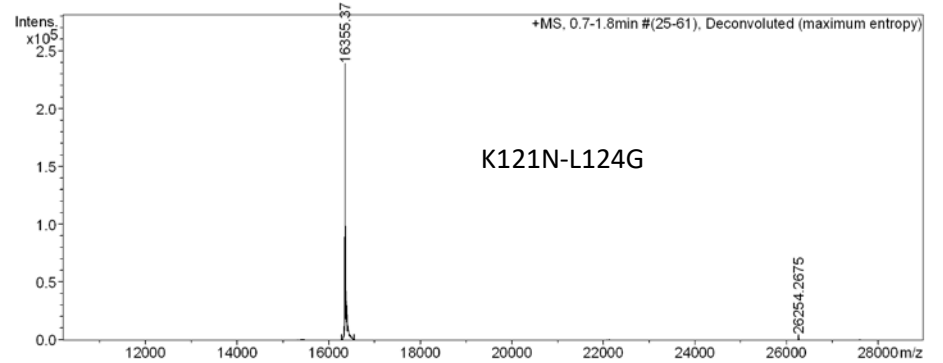
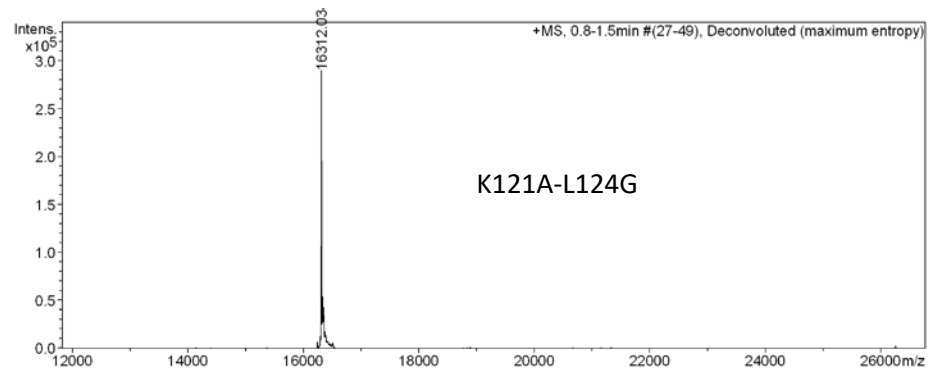
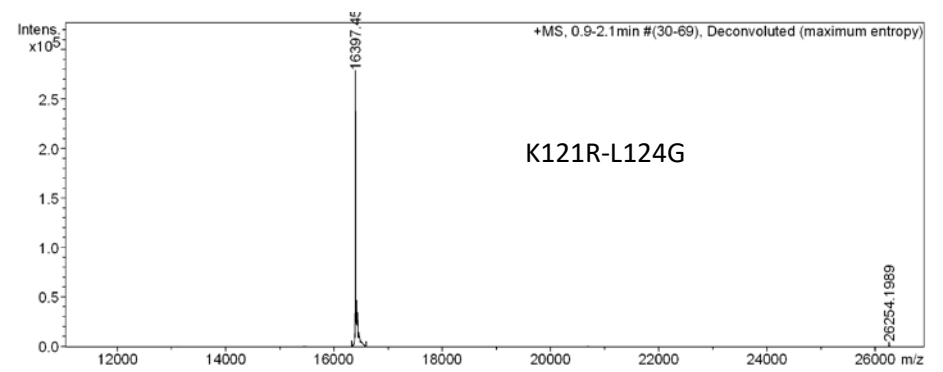
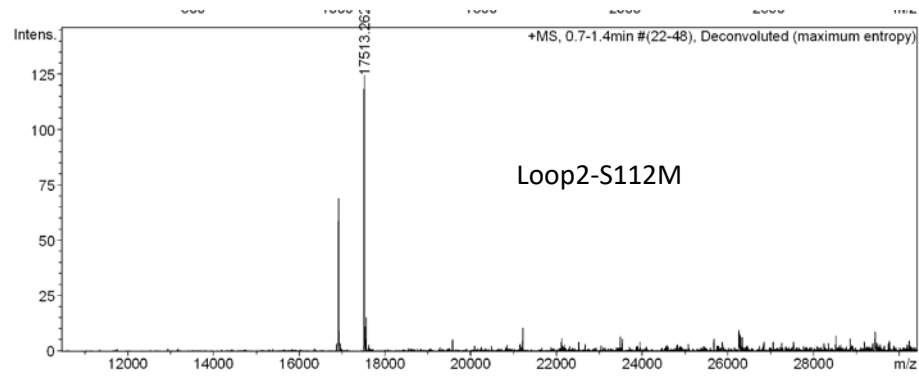
Annex 39: ESI-TOF MS analysis of expressed and purified Sav variants after deconvolution



Annex 40: ESI-TOF MS analysis of expressed and purified Sav variants after deconvolution



Annex 41: ESI-TOF MS analysis of expressed and purified Sav variants after deconvolution



## 8 Curriculum Vitae

### Personal details

Date and place of birth: September 1<sup>st</sup>, 1988, St. Gallen, Switzerland

Nationality: Swiss

### Education

05/2013 – 12/2017 **PhD in Chemistry (summa cum laude)**, University of Basel, Switzerland  
*Evolution of an Artificial Allylic Alkylase based on the Biotin-Streptavidin Technology*

Thesis advisor: Prof. Dr. Thomas R. Ward

Co-Referee: Prof. Dr. Andreas Pfaltz

Results have been published in high-impact, peer-reviewed scientific journal and were presented at numerous international conferences (e.g. Best Poster Award at the SYCA Snow Symposium 2017).

09/2011 – 02/2013 **MSc in Chemistry**, University of Basel, Switzerland  
*Engineering lipophilicity into artificial transfer hydrogenases*

Thesis advisor: Prof. Dr. Thomas R. Ward

09/2008 – 08/2011 **BSc in Chemistry**, University of Basel, Switzerland

07/2007 – 05/2008 Military service

08/2003 – 06/2007 **Matura with main subject Chemistry/Biology**,  
Kantonsschule am Burggraben, St. Gallen, Switzerland

### Teaching

09/2013 – 06/2015 Assistant of the chemistry practicum courses

03/2011 – 12/2016 Private tutor for Chemistry, Biology, Physics and Mathematics at the Studienkreis Mittelland

## Publication record

- 2018 Heinisch, T. ‡; Schwizer, F. ‡; Garabedian, B.; Csibra, E.; Jeschek, M.; Vallapurackal, J.; Pinheiro, V. B.; Marlière, P.; Panke, S.; Ward, T. R., *E. coli* surface display of streptavidin for directed evolution of an allylic deallylase, *Chem. Sci.*, **2018**, Manuscript under revision (‡ equal contribution).
- Okamoto, Y. ‡; Kojima, R. ‡; Schwizer, F. ‡; Bartolami, E.; Heinisch, T.; Matile, S.; Fussenegger, M.; Ward, T. R., A Cell-Penetrating Artificial Metalloenzyme Regulates a Gene Switch in a Designer Mammalian Cell, *Nat. Commun.*, **2018**, accepted (‡ equal contribution).
- DOI: [10.1038/s41467-018-04440-0](https://doi.org/10.1038/s41467-018-04440-0)
- Pellizzoni, M. M.; Schwizer, F.; Wood, C. W.; Sabatino, V.; Cotelle, Y.; Matile, S.; Woolfson, D. N.; Ward, T. R., Chimeric Streptavidins as Host Proteins for Artificial Metalloenzymes, *ACS Catal.*, **2018**, 8, 2, 1476-1484.
- DOI: [10.1021/acscatal.7b03773](https://doi.org/10.1021/acscatal.7b03773)
- Schwizer, F. ‡; Okamoto, Y. ‡; Heinisch, T. ‡; Gu, Y. ‡; Pellizzoni, M. M. ‡; Lebrun, V. ‡; Reuter, R. ‡; Köhler, V. ‡; Lewis, J. C.; Ward, T. R., Artificial Metalloenzymes: Reaction Scope and Optimization Strategies, *Chem. Rev.*, **2018**, 118, 1, 142-231 (‡ equal contribution).
- DOI: [10.1021/acs.chemrev.7b00014](https://doi.org/10.1021/acs.chemrev.7b00014)
- 2016 Keller, S. G.; Pannwitz, A.; Schwizer, F.; Klehr, J.; Wenger, O. S.; Ward, T. R., Light-driven electron injection from a biotinylated triarylamine donor to [Ru (diimine)<sub>3</sub>]<sup>2+</sup>-labeled streptavidin, *Org. Biomol. Chem.*, **2016**, 14, 30, 7197-7201.
- DOI: [10.1039/c6ob01273f](https://doi.org/10.1039/c6ob01273f)
- 2014 Quinto, T.; Schwizer, F.; Zimbron, J. M.; Morina, A.; Köhler, V.; Ward, T. R., Expanding the chemical diversity in artificial imine reductases based on the biotin–streptavidin technology, *ChemCatChem*, **2014**, 6, 4, 1010-1014.
- DOI: [10.1002/cctc.201300825](https://doi.org/10.1002/cctc.201300825)
- Publication with back cover graphic (DOI: [10.1002/cctc.201490026](https://doi.org/10.1002/cctc.201490026)).
- 2013 Schwizer, F.; Köhler, V.; Dürrenberger, M.; Knörr, L.; Ward, T. R., Genetic optimization of the catalytic efficiency of artificial imine reductases based on biotin–streptavidin technology, *ACS Catal.*, **2013**, 3, 8, 1752-1755.
- DOI: [10.1021/cs400428r](https://doi.org/10.1021/cs400428r)
- Publication with front cover graphic (<https://pubs.acs.org/toc/accacs/3/8>).